

Some pages of this thesis may have been removed for copyright restrictions.

If you have discovered material in Aston Research Explorer which is unlawful e.g. breaches copyright, (either yours or that of a third party) or any other law, including but not limited to those relating to patent, trademark, confidentiality, data protection, obscenity, defamation, libel, then please read our [Takedown policy](#) and contact the service immediately (openaccess@aston.ac.uk)

TOOL DESIGN AND THE MECHANICS OF HYDRODYNAMIC
LUBRICATION IN TUBE-DRAWING

by

THIAM BENG LIM

Submitted in fulfilment of the requirements
for the degree of

DOCTOR OF PHILOSOPHY

Faculty of Engineering

Department of Production Technology and Production Management

The University of Aston in Birmingham

January 1984

Supervisor: Professor D H Sansome

Flap design
Flap-attachment
Hydrodynamic lubrication
Pick-up

TOOL DESIGN AND THE MECHANICS OF HYDRODYNAMIC

LUBRICATION IN TUBE-DRAWING

Submitted in fulfilment of the requirements
for the Degree of Doctor of Philosophy

Author: THIAM BENG LIM

Year: 1984

Summary

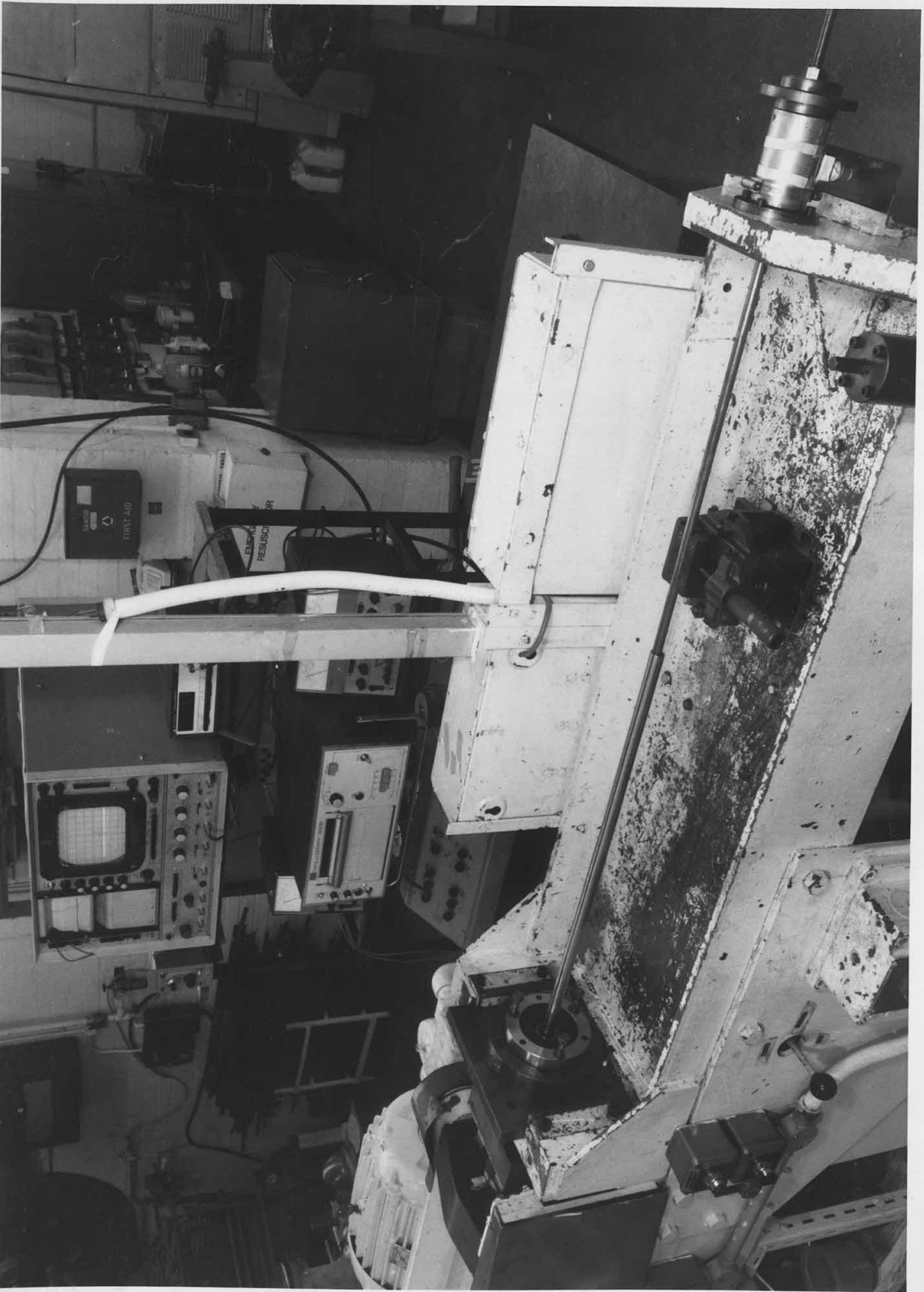
Although fixed-plug tube-drawing has been an industrial practice for many years, difficulties remain in the lubrication of the bore. High friction, pick-up and chatter are the major problems. Preventive measures by surface roughening to entrap the lubricant or the use of a suitable coating render the process route long, cumbersome and costly. This research project is the first to be undertaken to develop a new technique of bore lubrication without recourse to surface treatment, which is likely to reduce production costs.

The new technique involved generating a high lubricant pressure at entry to the metal deformation zone, based on the concept of induced hydrodynamic action, by fitting an attachment to the plug. This pressure increased the lubricant throughput, thus improving lubrication. Friction, or the plug force, decreased substantially with increasing lubricant pressures. Stainless steel tubes, which had not been roughened, were drawn successfully without the occurrence of pick-up or chatter. This was not otherwise possible. A lustrous finish obtained on the bore surface deteriorated, comparatively, with higher lubricant pressures. A new plug design eliminated the risk of pick-up initiating at the start of drawing.

External lubrication using Christopherson tubes was considered also. Experimental observations, at a draw speed of 15 ft min^{-1} , with straight-parallel plug-attachments and Christopherson tubes compared well with theoretical predictions. The theories extended to consider such devices having straight-tapered, composite and stepped profiles. The lubricant pressure and film thickness varied directly with the draw speed, lubricant viscosity and length of these devices, and inversely with the radial clearance. Thus, a practical tool design demands a compromise among these factors. A "quasi-hydrodynamic" lubrication regime obtained under experimental conditions. Full hydrodynamic lubrication is achievable at higher draw speeds and/or lubricant viscosities.

The new plug and the plug-attachment lubrication technique are now being discussed for a UK patent application.

Keywords: Tube-drawing
 Plug design
 Plug-attachment
 Hydrodynamic lubrication
 Pick-up



Frontispiece

C O N T E N T S

Page No

Page No

List of Figures	9
List of Tables	13
List of Photographs	13
Acknowledgements	14
Notation	15

CHAPTER 1

GENERAL INTRODUCTION

CHAPTER 2

REVIEW OF THE LITERATURE

2.1	Introduction	30
2.2	Theory of friction and lubrication	31
2.2.1	Mechanism of dry friction	31
2.2.2	Boundary lubrication	34
2.2.3	Hydrodynamic lubrication	35
2.2.4	Elasto-hydrodynamic lubrication	38
2.3	Theory of lubrication in metal-forming	40
2.3.1	Representation of friction in metal-forming	44
2.3.1.1	Coulomb coefficient of friction	45
2.3.1.2	Constant friction factor	46
2.3.1.3	Hydrodynamic lubrication	47
2.3.2	Hydrodynamic lubrication theories	48
2.4	Promotion of hydrodynamic lubrication	56
2.4.1	Hydrodynamic lubricating systems	58

2.5	Variation of lubricant viscosity with temperature and pressure	66
2.5.1	Viscosity-temperature relationships	66
2.5.2	The influence of pressure on the viscosity of lubricants	68
2.5.3	Viscosity-pressure relationships	70
2.5.4	Viscosity-temperature-pressure relationships	72
2.6	Basic theories of metal-drawing	73
2.6.1	Equilibrium approach in drawing	75
2.6.1.1	Axisymmetric wire or bar-drawing	75
2.6.1.2	Axisymmetric tube-drawing	77
2.6.2	Kinematically admissible approach	79
2.6.2.1	Slip-line field solutions	80
2.6.2.2	Upper-bound solutions	81
2.6.3	Energy approach	87
2.7	Determination of friction in drawing	92
2.7.1	Die-rotation	93
2.7.2	Split-die	96
2.7.3	Measurement of die pressure	98
2.7.4	Optimum die-angle	99
2.7.5	Estimation of redundant work	100
2.7.6	Back-pull	101

CHAPTER 3

THEORETICAL ANALYSIS OF THE PROMOTION OF HYDRODYNAMIC

LUBRICATION IN THE TUBE-DRAW PROCESS

3.1	Introduction	102
3.2	Promotion of hydrodynamic lubrication at the die-tube interface	103

3.2.1	Hydrodynamic analysis of the plastic deformation zone	105
3.2.2	Lubricant film thickness at entry to the plastic deformation zone	108
3.2.3	Analysis of Christopherson tubes	111
3.2.3.1	Straight-parallel Christopherson tube	113
3.2.3.2	Straight-tapered Christopherson tube	114
3.2.4	Analysis of two-zone Christopherson tubes	115
3.2.4.1	Stepped Christopherson tube	115
3.2.4.2	Composite Christopherson tube	118
3.3	Determination of the hydrodynamic pressure and lubricant film thickness	119
3.4	Promotion of hydrodynamic lubrication at the plug-tube interface	120
3.4.1	Hydrodynamic analysis of the sink zone	124
3.4.2	Lubricant film thickness at entry to the plug-tube interface	127
3.4.3	Analysis of plug-attachments	129
3.4.3.1	Straight-parallel plug-attachment	130
3.4.3.2	Straight-tapered plug-attachement	130
3.4.4	Analysis of two-zone plug-attachments	132
3.4.4.1	Stepped plug-attachment	132
3.4.4.2	Composite plug-attachment	135
3.5	Solution of the hydrodynamic pressure and lubricant film thickness generated by the plug-attachments	136
3.6	Application to plug-attachment design	138
3.6.1	The computer programme for tool design	139
3.6.3	Determination of the optimum die semi-angle	173
3.6.4	Preparatory experiments with plug-attachments	173
3.6.4.1	Initial experiments with straight-parallel and composite plug-attachments	181

CHAPTER 4DESCRIPTION OF EXPERIMENTAL EQUIPMENTAND MATERIALS

4.1	Introduction	148
4.2	The draw-bench	148
4.3	Load cells	149
4.3.1	The draw load cell	149
4.3.2	The plug load cell	151
4.4	Hydrodynamic pressure measurement	151
4.5	Draw speed measurement	154
4.6	Dies and plugs	154
4.7	Tools for promoting hydrodynamic lubrication	158
4.8	Tube material	158
4.9	Lubricants	159

CHAPTER 5EXPERIMENTAL PROGRAMME

5.1	Introduction	165
5.2	Experimental technique	166
5.3	Preparatory experiments	169
5.3.1	Assessment of basic drawing parameters	169
5.3.2	Experiments on the effect of the plug-tube contact length	174
5.3.3	Determination of the optimum die semi-angle	177
5.3.4	Preparatory experiments with plug-attachments	178
5.3.4.1	Initial experiments with straight-parallel and composite plug-attachments	181

5.3.4.2	Elimination of plug chatter	186
5.3.4.3	Measurement of hydrodynamic pressure	186
5.4	Tool design	191
5.4.1	Design of plugs	191
5.4.2	Design of plug-attachments	196
5.5	Experiments with new plugs and plug-attachments	199
5.6	Experiments with Christopherson tubes	204

CHAPTER 6

APPENDICES

A1	Supporting paper	320
	<u>DISCUSSION OF RESULTS</u>	
6.1	Introduction	209
6.2	Observations	210
6.2.1	The effect of the curve-profiled plug	211
6.2.2	Hydrodynamic lubricant pressure, plug force and draw stress	213
6.2.3	Surface finish	217
6.3	Discussion of the experimental results	219
6.3.1	Experimental results of plug-attachments	219
6.3.1.1	Length of the plug-attachments	220
6.3.1.2	Radial clearance	221
6.3.1.3	Lubricant viscosity	222
6.3.2	Experimental results of Christopherson tubes	223
6.4	Discussion of the theoretical results	225
6.4.1	Comparison between experimental and theoretical results	226
6.4.2	Theoretical results of plug-attachments	229
6.4.3	Theoretical results of Christopherson tubes	234
6.5	Graphical results	237

CHAPTER 7CONCLUSIONS

309

LIST OF FIGURES

Figure No

CHAPTER 8

316

SUGGESTIONS FOR FURTHER WORKAPPENDICES

A1	Supporting paper	320
A2	Tabulated experimental results	340
A3	Tabulated theoretical results	355
A4	Computer programmes	366
A5	Theoretical analysis of tube-drawing - an upper-bound approach	381
A6	Mechanical drawings and sample surface topography of undrawn tubes	392
A7	Calibration charts	410
A8	Specifications of the equipment and instrumentation	414

LIST OF REFERENCES

418

LIST OF FIGURES

<u>Figure No</u>	<u>Title</u>	<u>Page No</u>
1.1	Typical tube-drawing processes	20
1.2	Tube-drawing with new plugs	27
2.1	Idealized coefficient of friction-temperature diagram (after Bowden and Tabor ⁽¹⁴⁾)	36
2.2	Generalised process with rigid-plastic deformation zone (after Wilson and Walowit ⁽⁹³⁾)	50
2.3	Elasto-plasto-hydrodynamic lubrication in drawing (after Dowson et al ^(94,95,96))	50
2.4	The relation between lubricant film thickness and wire speed at die entry for a range of entry oil viscosities and die semi-angles (after Dowson et al ⁽⁹⁵⁾)	53
2.5	Plasto-hydrodynamic lubrication in drawing considering thermal effects on lubricant film profile (after Wilson et al ^(99,100,101))	53
2.6	The Christopherson tube in wire-drawing (after Christopherson et al ^(4,5))	59
2.7	External pressurization in hydrodynamic lubrication in wire drawing (after Butler ⁽⁹⁾)	59
2.8	Industrial hydrodynamic lubrication unit (after Avitzur ⁽⁸⁸⁾)	65
2.9	Plane strain extrusion through wedge-shaped die (after Johnson ⁽¹²⁾)	84
2.10	Tube-drawing on a floating-plug (after Smith and Bramley ⁽⁸⁹⁾)	85
2.11	Spherical velocity field in axisymmetric drawing (after Avitzur ^(92,159))	88
2.12	Spherical velocity field in tube-sinking (after Avitzur ⁽¹⁶⁰⁾)	88

<u>Figure No</u>	<u>Title</u>	<u>Page No</u>
2.13	Area under true stress-strain curve showing the three forms of energy expended in a drawing process (after Basily and Sansome ⁽⁸¹⁾)	91
2.14	Representation of forces in axisymmetric drawing (after Rothman and Sansome ⁽⁷⁸⁾)	94
2.15	Velocity and friction vectors with die rotation at 'F' viewed from 'q' (after Rothman and Sansome ⁽⁷⁸⁾)	95
2.16	Forces in wire-drawing with split-die (after Wiestreich ⁽⁷⁵⁾)	97
3.1	Details of lubricant film geometry	106
3.2	Analysis of Christopherson tubes	112
3.3	Analysis of two-zone Christopherson tubes	116
3.4	Computing procedure for the theoretical results of the Christopherson tubes	121
3.5	Possible positions of plug-attachment within the sink zone	122
3.6	Details of the sink zone	125
3.7	Analysis of plug-attachments	131
3.8	Analysis of two-zone plug-attachments	133
3.9	Computer flow-chart for the solution of hydrodynamic pressure and lubricant film thickness	137
3.10	Computer flow-chart for tool design	140-142
3.11	Equivalent lengths of a stepped plug-attachment to develop the same pressure on entry to the sink zone	145
3.12	Equivalent lengths of a composite plug-attachment to develop the same pressure on entry to the sink zone	146
4.1	Circuit diagram of the tag load cells	150
4.2	Circuit diagram of the plug load cell	150
4.3	Schematic arrangement of the pressure transducer and instrumentation	152

<u>Figure No</u>	<u>Title</u>	<u>Page No</u>
4.4	Stress-strain relation of annealed tube material (Austenitic stainless steel, AISI 347)	160
4.5	Viscosity-temperature relation of EP50	163
5.1	Variation of draw stress with homogeneous strain for different lubricants	171
5.2	Variation of drawn tube temperature with homogeneous strain for different lubricants	172
5.3	Calibration chart for the plug-bar	175
5.4	Variation of plug force and draw stress with plug-tube contact length	176
5.5	Variation of draw stress with homogeneous strain for different die semi-angles	179
5.6	Variation of draw stress with die semi-angle for different values of homogeneous strain	180
5.7	Plug-attachment	182
5.8	Arrangement of the tools and pressure transducers in the preliminary experiments	183
5.9	Force traces obtained when drawing with plug-attachment	184
5.10	Force traces obtained when drawing without plug-attachment	184
5.11	Bore surface topography of drawn tubes	187
5.12-5.14	Traces of hydrodynamic lubricant pressure and plug force	189
5.15	Position of conventional plug at the start of drawing	192
5.16	Position of proposed plug at the start of drawing	192
5.17	Experimental tube-drawing plug	194
5.18	Assembly of the new plug and plug-attachment	197
5.19	Experimental set-up for bore surface lubrication	200
5.20	Experimental programme for straight-parallel plug-attachments	203

<u>Figure No</u>	<u>Title</u>	<u>Page No</u>
5.21	Experimental set-up for external surface lubrication	206
6.1 - 6.41	Graphical experimental results	237-272
6.42-6.44	Comparison between theoretical results predicted by present theory with Christopherson et al's ⁽⁵⁾ experimental results in wire-drawing	273-275
6.45-6.77	Graphical theoretical results	276-308
A5.1	Proposed straight line velocity discontinuities	382
A5.2	Hodograph associated with Figure (A5.1)	382
A6.1	Tag load cell	392
A6.2	Tag load cell calibrating adaptor	393
A6.3	Tag load cell - Denison adaptor	394
A6.4	Tag load cell - Denison adaptors	395
A6.5	Plug load cell	396
A6.6	Tube-drawing die	397
A6.7	Tube-drawing plug	398
A6.8a	Plug-attachment No.1	399
A6.8b	Plug-attachment No.2	400
A6.8c	Plug-attachment No.3	401
A6.9	Christopherson tube	402
A6.10	Inlet-guide	403
A6.11	Lock-flange	404
A6.12	Die sleeve	405
A6.13,A6.14	Typical surface topographies of undrawn tubes	406-409
A7.1	Calibration chart of the load cell at the tag holder	410
A7.2,A7.3	Calibration charts of the plug load cell	411-412
A7.4	Calibration chart of the pressure transducer	413

LIST OF TABLES

<u>Table No</u>	<u>Title</u>	<u>Page No</u>
2.1	Typical measured values of lubricant film thickness	41
2.2	Typical theoretical values of lubricant film thickness	55
4.1	Dimensions of the tools used in the preparatory experiments	157
A2.1 - A2.29	Tabulated experimental results	340-354
A3.1 - A3.21	Tabulated theoretical results	355-365

LIST OF PHOTOGRAPHS

<u>Plate No</u>	<u>Title</u>	<u>Page No</u>
	Frontispiece	2
4.1	Dies and conventional plugs available for tube-drawing	155
5.1	Experimental tube-drawing plugs and pressure transducer	195
5.2	Assembly of the experimental plugs and plug-attachments	198
5.3	Arrangement of the plug-attachment technique during drawing	201
5.4	Arrangement of the plug in conventional tube-drawing practice	202
5.5	Experimental set-up of the Christopherson tube technique for external lubrication	207

ACKNOWLEDGEMENTS

I am grateful to the University of Aston in Birmingham and the Committee of Vice-Chancellors and Principals of the Universities in the United Kingdom (CVCP) for the award of this research scholarship, and to Fine Tubes Limited of Plymouth for their support in providing the funds, tools, tubes and lubricants for the experimental work. To my supervisor, Professor D H Sansome, I owe special thanks for his continued interest and counsel throughout the course of the research.

The technical staff of the Department of Production Technology and Production Management, especially Messrs G M Jones, T Rudge and P McGuire of the George Alexander Laboratory, deserve special acknowledgements for their co-operation and assistance. My gratitude goes also to Mrs Jeanette Neale and Mrs Maureen Creighton for their efforts and patience in typing the thesis.

I should like also to record my appreciation of the friendship and company of the staff and students of the University, especially fellow researchers of the Laboratory, whom I have the opportunity to meet during my time at the University. To my family, in particular my parents, and friends in Singapore, I would like to extend my especial gratitude for their unfailing support and encouragement.

It is said that "in the beginning there is no mountain, in the middle there is no mountain, but in the end there is the mountain", and without the above mentioned persons I know there will always be some mountain. Once again, I thank them all.

NOTATION

A	Area
A_1	initial cross-sectional area
A_2	final cross-sectional area
A_s	cross-sectional area of tube after sinking
B	$(e^{-\phi P_2} - e^{-\phi Y})$ in the analysis of Christopherson tubes
B_1	$(e^{-\phi P_3} - e^{-\phi P_4})$ in the analysis of plug-attachments
c	circumference of tube
D	diameter
D_1	initial diameter
D_2	final diameter
e	natural logarithm base = 2.7183
h	lubricant film thickness
h_m	constant in integrated Reynolds equation (equals lubricant film thickness at maximum pressure)
K	$\frac{h_1}{h_2} - 1$
k	shear yield stress
L_d	length of the land of the die
L_p	length of contact between the plug and the tube
l	length of Christopherson tube or plug-attachment
l_o	overall length of plug-attachment = $l_1 + l_2$

l_r	length ratio of plug-attachment = $\frac{l_2}{l_1}$
m	friction factor
m_d	friction factor at the die-tube interface
m_p	friction factor at the plug-tube interface
n	strain hardening exponent
P	lubricant pressure
q	volume rate of lubricant flow per unit circumference of tube
R	radius of tube in deformation zone
R_i	initial internal radius of tube
R_{if}	final internal radius of tube
R_o	initial external radius of tube
R_{of}	final external radius of tube
R_p	radius of plug
r	reduction in cross-sectional area
T	temperature
t	wall thickness of tube
t_1	initial wall thickness of tube
t_2	final wall thickness of tube
U	velocity
U_s	velocity of tube during sinking

\dot{V}	rate of volume of material deformed
\dot{W}	rate of plastic working
\dot{W}_T	total rate of plastic working
w	$\frac{R_p}{\tan \alpha}$
x_1, x_2	horizontal distances from the origins defined in Figures (3.1) and (3.6)
Y	yield stress in uniaxial tension
Y_m	mean yield stress
z	$\frac{z_2}{z_1} = \frac{R_i}{R_{if}}$
z_1	distance from the end of sinking to the virtual apex defined in Figure (3.6)
z_2	distance from the start of sinking to the virtual apex defined in Figure (3.6)
α	die semi-angle
ϵ	logarithmic strain
$\bar{\epsilon}$	equivalent strain
ϵ_s	homogeneous strain in sinking
η	dynamic viscosity of lubricant at any pressure P
η_0	dynamic viscosity of lubricant at atmospheric pressure
μ	Coulomb coefficient of friction
ζ_1	$(1 + \frac{R_p}{h_3})$
ζ_2	$(1 + \frac{R_p}{h_4})$

σ	draw stress or true stress
σ^r	strength coefficient in empirical stress-strain relationship
$\bar{\sigma}$	effective stress
σ_b	back-pressure or back-pull stress
σ_n	normal pressure or die pressure
τ	shear stress or frictional stress
τ_s	shear stress in pure shear
ϕ	viscosity-pressure coefficient

Subscript

1,2,3,4	refer to the corresponding zones of the Christopherson tubes or plug-attachments
---------	--

CHAPTER 1: GENERAL INTRODUCTION

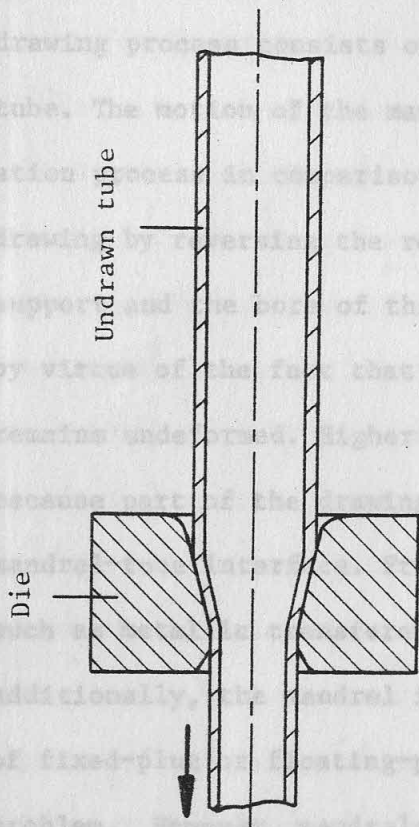
Tubes are common engineering materials which are used extensively in applications ranging from simple structures to chemical engineering, aerospace and nuclear industries. There are two basic types of tubes, namely, fabricated and seamless. Fabricated tubes are formed from strips or plates and welded along the joints. Most seamless tubes are formed by rolling solid billets; thus a die or sleeve shapes the external profile while the bore is formed by a punch or mandrel. Although the tubes are often used in the fabricated or pierced conditions, most of these are however further processed once or many times at room temperature by an operation called cold-drawing. The drawing operation elongates the tube while reducing its diameter and, usually, its wall thickness. Stainless steel hypodermic needles, for example, which may be smaller than one hundredth of an inch in outside diameter are produced by drawing. Apart from providing a good dimensional accuracy, cold-drawing also improves the surface finish of the tube.

The cold-drawing of tubes is performed by one of four methods, namely; sinking, fixed-plug drawing, floating-plug drawing and moving-mandrel drawing, as illustrated in Figure (1.1). The operations consist of pulling the tube through a die, the size of which determines the outside diameter of the drawn tube. In the sinking process the tube is drawn without internal support in the bore, resulting in a

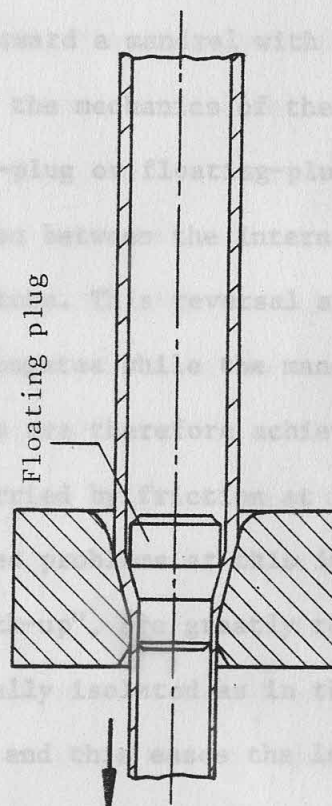
CHAPTER 1: GENERAL INTRODUCTION

Tubes are common engineering materials which are used extensively in applications ranging from simple structures to chemical engineering, aerospace and nuclear industries. There are two basic types of tubes, namely, fabricated and seamless. Fabricated tubes are formed from strips or plates and welded along the joints. Most seamless tubes are produced by punch or rotary piercing solid billets; thus a die or sleeve shapes the external profile while the bore is formed by a punch or mandrel. Although the tubes are often used in the fabricated or pierced conditions, most of these are however further processed once or many times at room temperature by an operation called cold-drawing. The drawing operation elongates the tube while reducing its diameter and, usually, its wall thickness. Stainless steel hypodermic needles, for example, which may be smaller than one hundredth of an inch in outside diameter are produced by drawing. Apart from providing a good dimensional accuracy, cold-drawing also improves the surface finish of the tube.

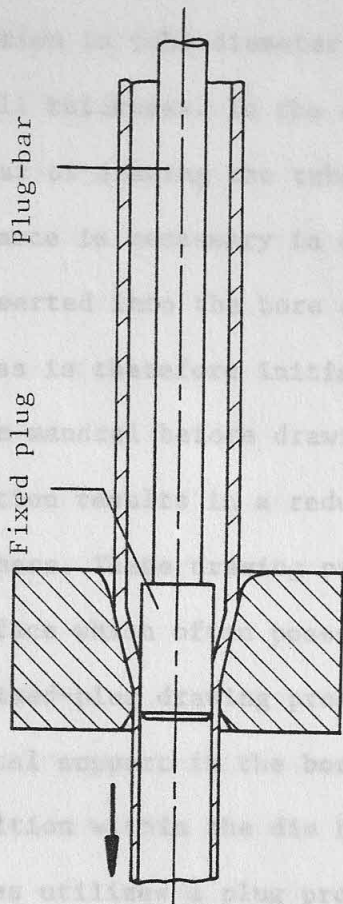
The cold-drawing of tubes is performed by one of four methods, namely; sinking, fixed-plug drawing, floating-plug drawing and moving-mandrel drawing, as illustrated in Figure (1.1). The operations consist of pulling the tube through a die, the size of which determines the outside diameter of the drawn tube. In the sinking process the tube is drawn without internal support in the bore, resulting in a



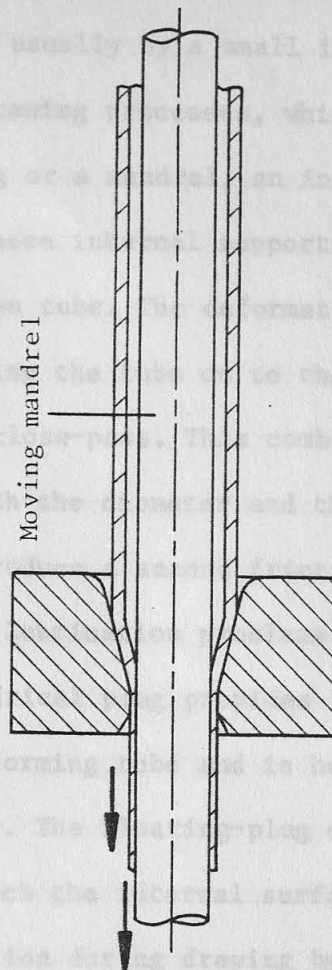
(a) Tube sinking



(c) Floating-plug drawing



(b) Fixed-plug drawing



(d) Moving-mandrel drawing

Figure (1.1) Typical tube-drawing processes

reduction in tube diameter accompanied usually by a small increase in wall thickness. In the other tube-drawing processes, which consist of drawing the tube over a plug or a mandrel, an initial clearance is necessary in order that these internal supports can be inserted into the bore of the undrawn tube. The deformation process is therefore initiated by sinking the tube on to the plug or the mandrel before drawing it in a close-pass. This combined operation results in a reduction of both the diameter and the wall thickness. These drawing processes introduce a second friction interface which often poses additional lubrication problems. In the fixed-plug drawing process a cylindrical plug provides the internal support in the bore of the deforming tube and is held in a position within the die by a plug-bar. The floating-plug drawing process utilizes a plug profiled to match the internal surface of the deforming tube and is held in position during drawing by the equilibrium of the normal and friction forces. The moving-mandrel drawing process consists of pulling forward a mandrel with the tube. The motion of the mandrel alters the mechanics of the deformation process in comparison with fixed-plug or floating-plug tube-drawing by reversing the relative motion between the internal support and the bore of the deforming tube. This reversal arises by virtue of the fact that the tube elongates while the mandrel remains undeformed. Higher deformations are therefore achievable because part of the drawing load is carried by friction at the mandrel-tube interface. Friction related problems at this interface such as metallic transference i.e. "pick-up", are greatly reduced. Additionally, the mandrel is not thermally isolated as in the case of fixed-plug or floating-plug drawing and this eases the lubrication problem. However, mandrels are expensive, cumbersome to handle, need careful usage and storage, and they must be removed from

the drawn tubes by a reeling process. *can reconsidered.*

The effect of friction in tube-drawing and indeed in any metal-forming operation is fairly complex and its importance may be seen in that a significant proportion of the total energy requirement has to be expended in overcoming friction - which would not otherwise be necessary. The higher the friction, therefore, the greater the energy required to impose a particular deformation. This, however, is not the main concern, but the elimination of metallic transference between the workpiece and the tools resulting from poor lubrication is of major importance. Thus, the principal industrial requirements of tube-drawing lubricating systems are to facilitate a high reduction per pass, long tool life and the provision of suitable surface finishes together with an absence of pick-up or chatter. Apart from the presence of "foreign particles", the failure of a lubricating system is directly indicated by high forces and pick-up between the tube and the tools. Clearly, there are two surfaces to be considered, namely, the die-tube and the plug-tube interfaces. On both surfaces there arises a conflict between the need to reduce tool wear and to improve surface finish since the former suggests a need for minimum contact between the tools and the tube, whereas the latter implies some burnishing of the tube surfaces and hence intimate contact between the tools and the tube. Generally a compromise solution to the problem of meeting these requirements is achieved economically by the selection of the appropriate tool material, die-angle, lubricant, surface treatment and heat treatment of the undrawn tube and drawing conditions such as draw speed and the reduction of area. However, as there is a continuing and an increasing need to reduce costs, i.e. to draw at higher speeds and at higher reductions and to eliminate surface treatments and the changing of tools frequently, methods

of solving lubrication problems have been reconsidered.

Investigation of friction, wear and lubrication in metal-forming processes has been largely directed along two lines. The first is the selection of a suitable tool material which, in itself, has good friction and wear properties and secondly, the use of appropriate lubricant films and/or surface treatments. One of the best known lubricating systems employs soap or oil as the drawing lubricant together with another low shear strength coating such as lead, copper, phosphate, lime or complex oxalate or zinc compounds. A review of the developments in the use of chemical conversion coatings to facilitate better lubrication in metal-forming operations has been presented by James and Haynes⁽¹⁾. In slow-speed bar-drawing, Lancaster and Rowe^(2,3) have shown that entrapping the lubricant by grit-blasting the undrawn bar surface enabled higher reductions to be made without the danger of burnishing and pick-up. Smaller die-angles⁽²⁾ were shown to encourage contribution to lubrication from the hydrodynamic action induced by the motion of the bar, thus increasing the lubricant throughput. There is, however, a restriction on the size of this angle since it is desirable to draw with the optimum die-angle at which the total work done including frictional and redundant work is minimal. However, surface coatings and surface treatments may be expensive and cumbersome to apply, and the removal and disposal of the effluents of such coatings may be difficult particularly when the number of passes required is taken into consideration. Consequently the cost becomes prohibitively high.

The promotion of hydrodynamic lubrication which introduces, between the tool and the deforming material, a sufficiently thick or tenacious lubricant film would therefore alleviate the lubrication problem significantly. Under favourable drawing conditions, for

example, when drawing at sufficiently high speeds using dies of small semi-angles, a degree of hydrodynamic lubrication is likely to exist at the die-tube interface. The possibility is enhanced particularly when the external surface of the undrawn tube has been roughened since this surface of the tube is caused to extend during deformation, thus entrapping a larger quantity of lubricant. True hydrodynamic lubrication however may be achieved by supplying the lubricant to the die entry at an elevated pressure using the Christopherson tube technique developed by Christopherson and Naylor^(4,5) in the wire-drawing process. The necessary pressure was generated by causing the undrawn wire to approach the die through a tube filled with a viscous lubricant at atmospheric pressure, sealed to the entry side of the die and having a diameter slightly larger than the wire diameter. The motion of the undrawn wire generated a pressure in the lubricant by the classical mechanism of hydrodynamic lubrication, thereby introducing a thick lubricant film between the deforming wire and the die. This resulted in significant reductions in the draw force and the die wear. The idea has aroused considerable interest^(6,7,8) and industrially viable hydrodynamic lubricators^(9,10,11) have been developed for the wire-drawing process. No such provision appears to have been made on lubrication in the bore of the tube in tube-drawing and the high pressures involved in the deformation process preclude the possibility of hydrodynamic lubrication so that boundary lubrication prevails; the nearest lubricating system has consisted of entrapping the lubricant in a roughened bore surface. In the case of drawing stainless steel tubes the difficulty is aggravated by their propensity to work harden rapidly.

In some companies fixed-plug tube-drawing practice consists of a process route which is considered to be long, cumbersome and

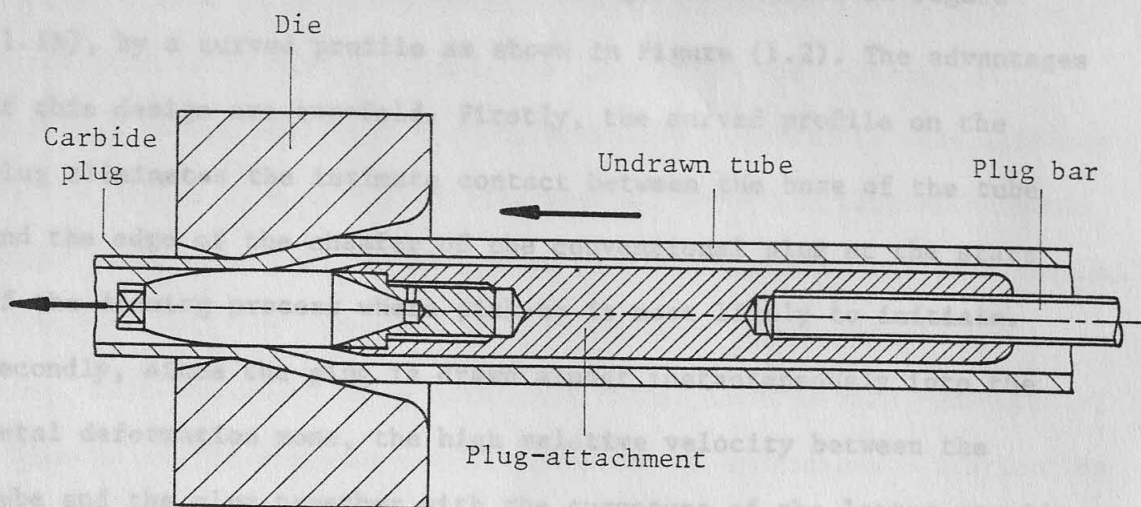
costly. This arises as a result of the difficulties experienced in the lubrication of the bore i.e. the plug-tube interface. Pick-up on the plug which damages the bore surface is the major problem. Essentially the bore surface of the undrawn tube is roughened by grit-blasting or pickling before each pass in order to entrap the lubricant and also to provide a more effective surface for the adhesion of a plastic coating which is sometimes necessary when drawing some of the stainless steel materials. However, when it is considered that the residual lubricant must be removed before annealing in preparation for the subsequent pass, grit-blasting or pickling, washing and drying, it becomes apparent that the ultimate solution has not been obtained. Clearly a cost effective process route would be the elimination of the surface treatment and the related cleaning operations and hence the ability to draw immediately after annealing. In response to these considerations, the present research project was undertaken to improve the bore lubrication and at the same time explore the possibility of drawing stainless steel tubes without recourse to bore surface treatment such as grit-blasting or pickling.

A comprehensive review of the literature was made of the subjects which were considered relevant to the promotion of hydrodynamic lubrication in metal-forming. This included the theories of friction and lubrication both in general and with reference to metal-forming, particularly metal-drawing processes. The influences of temperature and pressure on the lubricant viscosity, which affect the promotion of hydrodynamic lubrication during metal deformation, were considered also. The review included the basic theories of metal-drawing and the techniques of determining friction associated with the process.

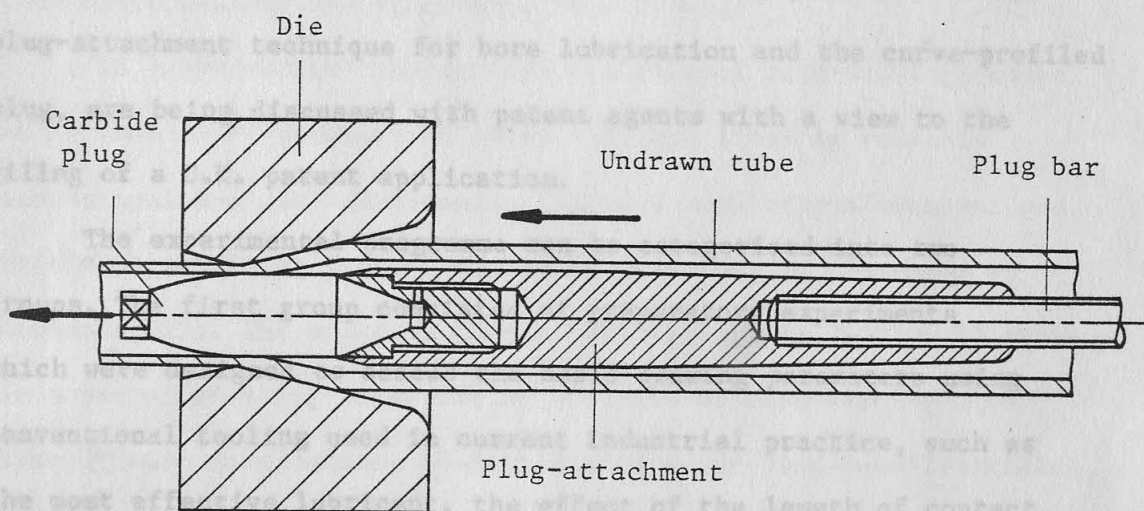
In the present work it was proposed to promote hydrodynamic

lubrication of the bore, based on the concept of induced hydrodynamic action, by fitting to the plug an attachment having a diameter slightly smaller than the bore of the undrawn tube. The arrangement is illustrated in Figure (1.2). The motion of the undrawn tube and the viscosity of the lubricant pull the lubricant into the small annular space between the attachment and the bore of the undrawn tube. A high pressure is thus generated at the entry to the deformation zone by the classical mechanism of hydrodynamic lubrication. This pressure increased the separation of the surfaces and the flow of lubricant into the deformation zone, thereby improving lubrication at this interface. Additionally, hydrodynamic lubrication at the die-tube interface was considered using the Christopherson tube technique developed in the wire-drawing process. The theoretical analyses of the mechanics of lubricant pressure generation, by induced hydrodynamic action to promote hydrodynamic lubrication, using the Christopherson tube technique and the newly developed plug-attachment technique for the tube-drawing process are presented in Chapter 3. The influence, on the generation of hydrodynamic pressure, of the geometrical features of these lubricant pressurizing devices, such as their lengths and radial clearances between them and the undrawn tube, and drawing conditions such as draw speed and lubricant viscosity, were considered. Such pressurizing devices having straight-parallel and straight-tapered profiles were studied initially and extended to include a second parallel or tapered portion, thus forming a stepped or composite profile. For a desired lubricant pressure the theory was utilized to calculate, with the aid of a computer, the required lengths of the four designs of plug-attachments for a range of drawing conditions and radial clearances. This enabled a direct comparison of the practicability of the design of these tools.

In addition to the use of the plug-attachment to promote



(a) Straight-parallel plug-attachment



(b) Composite plug-attachment

Figure (1.2) Tube-drawing with new plugs

hydrodynamic lubrication, it was proposed to replace the chamfer at the fore end of the conventional plug, illustrated in Figure (1.1b), by a curved profile as shown in Figure (1.2). The advantages of this design are two-fold. Firstly, the curved profile on the plug eliminates the intimate contact between the bore of the tube and the edge of the chamfer of the conventional plug at the start of the drawing process where pick-up is most likely to initiate. Secondly, since the plug is drawn almost instantaneously into the metal deformation zone, the high relative velocity between the tube and the plug together with the curvature of the latter provide conditions which are favourable for a better lubrication during the initial stage of the drawing process, by hydrodynamic action. Thus, during drawing, lubrication is aided by the hydrodynamic action of the plug-attachment.

These new developments in the tube-drawing process i.e. the plug-attachment technique for bore lubrication and the curve-profiled plug, are being discussed with patent agents with a view to the filing of a U.K. patent application.

The experimental programme can be categorised into two groups. The first group consisted of preparatory experiments which were designed to assess the basic drawing parameters using conventional tooling used in current industrial practice, such as the most effective lubricant, the effect of the length of contact between the plug and the tube and the determination of the optimum die semi-angle. Within this group initial experiments were conducted with a straight-parallel and a composite plug-attachment. These experiments were investigative in nature and designed to test the efficacy of the plug-attachment in promoting hydrodynamic lubrication of the bore of the deforming tube and also to develop a practicable method of measuring the generated lubricant pressure.

The draw force, plug force, lubricant pressure and the resulting surface finish of the bore which are all indicative of the lubrication efficiency were measured. The experience and information acquired in the course of these preparatory experiments were utilized in the design of a series of experimental plugs and plug-attachments. These tools were used in the second group of tests in the experimental programme i.e. the promotion of hydrodynamic lubrication of the bore. Christopherson tubes were used in conjunction with conventional plugs in the experiments on the promotion of hydrodynamic lubrication at the die-tube interface. The observations made in this group of experiments enabled the validity of the theories developed in Chapter 3 to be verified. The use of plug-attachments in drawing tubes in which the bore surface had not been grit-blasted or pickled indicated directly the possibility of eliminating such bore surface treatments without the occurrence of pick-up.

An "upper-bound" theoretical analysis of tube-drawing, based on Johnson's⁽¹²⁾ proposal of using straight lines as velocity discontinuities and additionally included both circumferential and thickness straining in the deformation process, is presented in Appendix (A5). The solution to the theoretical analysis would serve as a useful starting point for an analysis of tube-drawing with hydrodynamic lubrication, at both die-tube and plug-tube interfaces, by induced hydrodynamic action.

CHAPTER 2: REVIEW OF THE LITERATURE

also. The review includes the basic theories of metal-drawing and the techniques of determining friction associated with the process.

2.2 THEORY OF FRICTION AND LUBRICATION

Although the present work is not aimed directly at achieving an understanding of the mechanics of friction, but rather at

CHAPTER 2: REVIEW OF THE LITERATURE

2.1 INTRODUCTION

Mankind has experienced friction and recognised the need for lubrication since the earliest civilizations. Today, friction and lubrication are vital elements of science, technology and engineering practice. The importance of these may be seen in the fact that a substantial proportion of the economy is expended annually in overcoming frictional losses and that additional expenditure are incurred through poor lubrication practice and design. Extensive research and development, both in general engineering practice and in metal-forming processes, have been documented in the strive to solve this persisting problem.

It is the objective of this chapter to present a review of the literature. However, it is not intended, nor is it desirable, to take full account of the voluminous publications but rather to concentrate on those which are relevant to, or which would contribute towards a better understanding of the present work. It covers the postulated mechanisms of friction and lubrication in general and extends to consider metal-forming operations, with particular reference to metal-drawing. The influences of temperature and pressure on the lubricant viscosity, which affect the promotion of hydrodynamic lubrication during metal deformation, are considered

also. The review includes the basic theories of metal-drawing and the techniques of determining friction associated with the process.

2.2 THEORY OF FRICTION AND LUBRICATION

Although the present work is not aimed directly at achieving an understanding of the mechanics of friction, but rather at means of promoting lubrication, it is useful and appropriate to take account of the very considerable quantity of work which had been done on friction phenomena in general.

2.2.1 Mechanism of dry friction

The pioneers in the study of friction were notably Leonardo da Vinci (1452-1519), Amontons (1699) and Coulomb (1781). Early theories regarded the coefficient of friction, μ , as being independent of the applied load, the apparent area of contact and sliding velocity. Amontons proposed that metallic friction can be attributed to the mechanical interlocking of surface roughness elements. Friction was regarded as the force required to lift the asperities of one surface over those of the other. Tomlinson⁽¹³⁾ considered a molecular theory in which friction forces were attributed to energy dissipation when the atoms of one material were forced out of the attractive range of their counterparts on the mating surface. Electrostatic forces were also suggested in which friction was regarded as the force required to separate the surfaces held together by electrostatic attraction.

Such theories have largely been abandoned in the light of a better understanding of the physical, chemical and mechanical fundamentals. The mechanism of friction on surfaces in dry contact is explained in a variety of ways, the most popular being the welding theory of Bowden and Tabor⁽¹⁴⁾ also reported by Cameron⁽¹⁵⁾

wherein the junctions formed between asperities of surfaces in stationary contact, welded, under the action of high local pressure. Friction was attributed to the shearing of such junctions, and together with a degree of surface ploughing, could result in metallic transference or pick-up. An alternative theory by Hardy⁽¹⁶⁾ proposed that local plastic deformation caused the surfaces to conform and welding of the asperities may occur. Edwards and Halling^(17,18), working with model asperities, showed that junction growth was only slight as one asperity slid across another provided that reference planes within the bulk remained at constant separation. An interface was formed at the face angle of the asperities which, on sliding, rotated until it was tangential to the direction of sliding and then it sheared. Tensile forces between the two surfaces were recorded. However, these model asperities were large and their behaviour may be atypical due to size effects. The work hardening effect of the asperities was also considered^(17,19), but it is generally accepted that this is insignificant compared with the influence of junction growth.

With the presence of a contaminant film on the surfaces, Rabinowicz and Tabor⁽²⁰⁾ showed that the coefficient of friction and metallic transference were dramatically reduced. The influence of the contaminant film was to interpose between the sliding surfaces a film of low shear strength capable of reducing the amount of metallic interaction. That such a film may be provided by the metallic oxide, formed naturally on the surfaces and only of several molecular layers thick, was demonstrated by Bowden et al.^(21,22) in their experiments with unoxidized surfaces in a vacuum. It was impossible for the denuded specimens to slide over each other; gross seizure occurred, junction growth was noted and the specimens adhered with the bulk strength of the metal. Under

normal conditions adhesion did not occur at the oxide surface, but if this was not penetrated, shearing occurred within the oxide itself since it reduced the effective shear strength at the interface below the yield shear strength of the metal. The puncture of the oxide was accompanied by an increase in metallic interaction, friction and hence metallic transference. Whitehead⁽²³⁾ and Wilson⁽²⁴⁾ showed that the rupture of the oxide film is determined primarily by the relative physical properties of the oxide and the substrate. In observing that friction is a function of the mechanical and geometrical properties of the oxide film, Rabinowicz^(25,26) suggested that the adhesion theory due to Bowden and Tabor⁽¹⁴⁾ may be inadequate in describing friction. The theory of metallic compatibility was proposed. This states that if two metals in sliding contact are compatible, in some way analogous to that in which a metal is compatible relative to itself, friction and wear will be high. Several criteria of compatibility have been proposed based on the solubility of one metal of the rubbing pair in the other, both of which may be in either the liquid or solid state; the tendency to form solutions is associated with high friction^(27,28,29).

The effect of the rise in temperature due to friction on the formation of the oxide film was demonstrated by the work of Welsh⁽³⁰⁾, wherein the reduction in the wear rate of steel, which was observed at higher loads, was attributed to the interaction with the atmospheric nitrogen at the temperatures generated which formed a harder surface layer. The temperature of surfaces in sliding contact was studied theoretically and experimentally by Bowden et al.^(31,32). This was shown to be a function of the load, sliding speed, coefficient of friction and thermal conductivity of the materials. Surface temperatures of 1200°C in steel on

steel pairs were recorded although the mass of the metal did not show a significant rise in temperature.

2.2.2 Boundary lubrication

The theories of boundary lubrication may be considered as an extension of the theory of dry friction where the additional variables of surface contamination are recognised and included. The lubricant interposes between the sliding surfaces, by reaction or absorption, a film of low shear strength, several molecular layers thick. Thus the objective of boundary lubrication is to reduce friction by reducing the shear strength of the junction interfaces.

It has been known for sometime that fatty acids, the ingredient common to animal, vegetable and marine fats, play a dominant role in reducing friction under boundary conditions^(33,34,35). The action of these acids, which possess long hydrocarbon chain polar molecules, is generally agreed to be one of molecular adherence. Chemisorption, physisorption or chemical reaction, which produces a metallic soap film that is chemically bound to the metal surface, are popularly postulated mechanisms of film adhesion⁽¹⁴⁾. This has also been described as being likened to the piles of a carpet. The longer the hydrocarbon chain, therefore, the more effective would be the separation.

This was demonstrated by Hardy and Doubleday⁽³⁶⁾ who found that there is an inverse relationship between the molecular length and the coefficient of friction. A similar conclusion was also reached by Campbell⁽³⁷⁾ in his experiments on the effect of the molecular weight of paraffin hydrocarbons and fatty acids on the coefficient of friction. In general the metallic soaps have appreciably higher melting points than the parent fatty acids⁽¹⁴⁾.

These have been found to be less susceptible to thermal influences and improve lubrication considerably⁽³⁸⁾.

Metallic soaps, however, tend to decompose at elevated temperatures⁽³⁹⁾ such as those encountered in severe working conditions. Chlorine and sulphur have been proven to be effective in forming thermal stable films with mineral oil. The mechanism of these films has been investigated by Gregory⁽⁴⁰⁾ and Greenhill⁽⁴¹⁾. Phosphorous was also considered and these lubricants are generally classified as "Extreme Pressure" (EP) lubricants. These additives function by reacting with the surface at elevated temperatures to form the metal chloride, sulphide or phosphide in situ, thus protecting the underlying materials up to their melting points or decomposition temperatures. Thus, the addition of a fatty acid in addition to the EP additives provides a most effective form of lubrication over a wider range of temperatures. An idealized diagram showing frictional behaviour of various lubricants as a function of temperature⁽¹⁴⁾ is presented in Figure (2.1).

Low strength solids form another group of boundary lubricants. The most common of these are graphite and molybdenum disulphide whose lamellar crystal structures are easily sheared. Their efficacy is apparent from the work of Boyd and Robertson⁽⁴²⁾. Recently Loh⁽⁴³⁾ has also successfully applied graphite to the hot drawing of steel wires. Non-ferrous metals such as indium, tin, lead and copper have also been proven to be good solid lubricants^(39,44).

2.2.3 Hydrodynamic lubrication

As distinct from boundary lubrication, hydrodynamic lubrication endeavours to maintain a lubricant film sufficiently thick to prevent the surfaces from making intimate contact. In

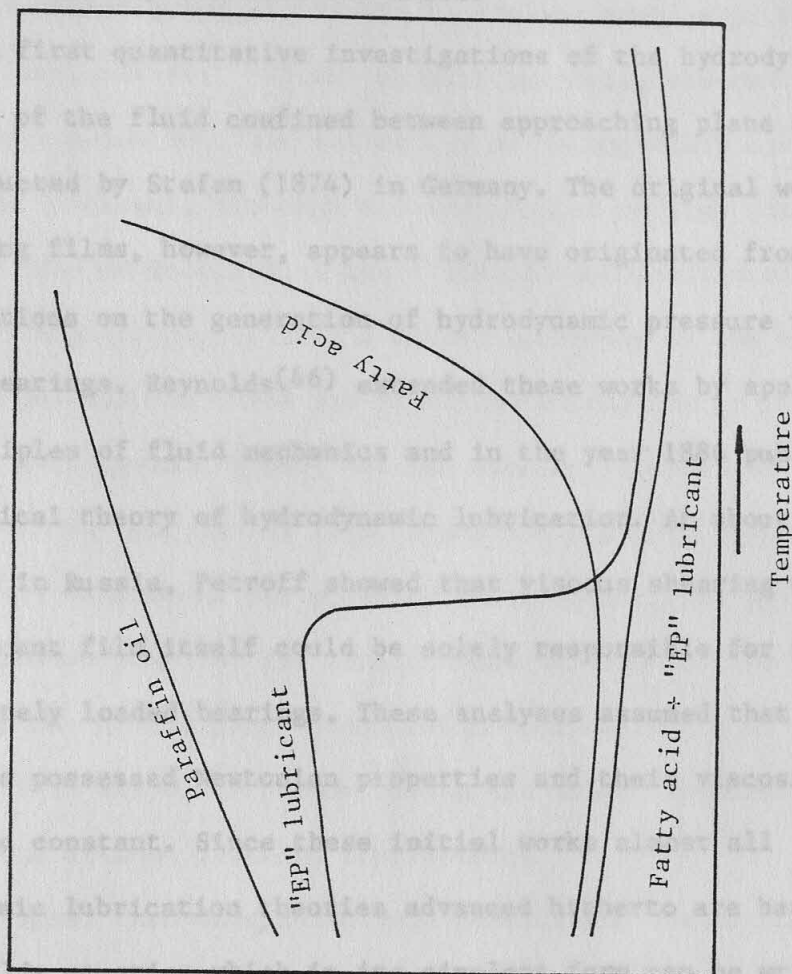


Figure (2.1) Idealized coefficient of friction - temperature diagram
[after Bowden and Tabor (14)]

general, hydrodynamic lubrication is said to occur when the mean thickness of the lubricating film is large compared with the height of the asperities of the surfaces. This phenomenon implies that a pressure is generated within the lubricating film itself and which is a function of the relative velocity of sliding, the lubricant viscosity and film thickness.

The first quantitative investigations of the hydrodynamic behaviour of the fluid confined between approaching plane surfaces were conducted by Stefan (1874) in Germany. The original work on lubricating films, however, appears to have originated from Tower's(45) investigations on the generation of hydrodynamic pressure in journal bearings. Reynolds(46) extended these works by applying the principles of fluid mechanics and in the year 1886 published his classical theory of hydrodynamic lubrication. At about the same time in Russia, Petroff showed that viscous shearing within the lubricant film itself could be solely responsible for friction in moderately loaded bearings. These analyses assumed that the lubricants possessed Newtonian properties and their viscosity was considered constant. Since these initial works almost all hydrodynamic lubrication theories advanced hitherto are based on the Reynolds equation which in its simplest form can be written:

$$\frac{dP}{dx} = 6\eta_0 U \frac{h - h_m}{h^3} \quad (2.1)$$

The general trend appears to be the gradual refinements and extensions to the original theory. A good example is the treatment of the lubricant viscosity as being a function of temperature and/or pressure according to some empirical relations. (See Section (2.5)). More significantly, this has led to the current theories of elastohydrodynamic lubrication.

2.2.4 Elastohydrodynamic lubrication

It has long been recognised that heavily loaded contacts such as gears, roller contact bearings and cams frequently behave as though they are hydrodynamically lubricated. The early theoretical analysis by Martin⁽⁴⁷⁾, using an extended form of the standard Reynolds solution, in the equivalent problem of two loaded rolling discs, however, did not support operating observations. Martin had considered rigid solids and an incompressible, isoviscous lubricant, although the application of high contact loads can lead to substantial local elastic deformation of the solids and high pressures have a marked influence on the viscosity of liquid lubricants. These are important extensions to the classical hydrodynamic theory and can substantially alter the geometry of the lubricating film. Since the shape of the lubricant film in turn determines the pressure distribution, the elastohydrodynamic problem requires the simultaneous solution of two equations; one giving the hydrodynamic pressures corresponding to an unknown lubricant film shape, the other giving the solid contours in terms of the unknown pressure distribution.

The first theoretical analysis postulating the existence of a hydrodynamic lubricant film appeared to be that of Grubin and Vinogradova⁽⁴⁸⁾, whose work allowed for the combined effects of elastic distortion and the viscosity-pressure characteristics of the lubricant. The approximate film thickness equation for highly loaded elastic contacts predicted film thicknesses which were orders of magnitude greater than the corresponding predictions of the Martin theory, and consistent with the formation of satisfactory fluid films in gear contacts. Like the many other proposals which were to appear later in the literature^(49,50), the method

of analysis was by the simultaneous solution of Reynolds equation, in which the constant viscosity term was replaced by some law relating viscosity to pressure, and the Hertz contact stress equation. Two approaches were adopted in the technique of solution, both yielded equally satisfactory results. The first of these assumed that the surfaces of the boundary solids would adopt the shape produced by a Hertzian contact zone and then determine its pressure distribution. The other, notably that of Dowson and Higginson⁽⁵¹⁾, used an iterative procedure by first assuming a pressure distribution and then to determine the consequent deformation on the basis of the elastic equation and the hydrodynamic equation. The iteration continued until the deformed shapes predicted by the two equations agreed.

The analysis of thermal effects in contacts exhibiting mixed rolling and sliding has been extended by Cheng and Sternlicht⁽⁵²⁾. These authors considered the difficult mathematical problem presented by the requirement for a solution of the Reynolds, elasticity, energy and heat transfer equations for a cylindrical contact. The results indicated that the basic features of the elastohydrodynamic contact shown by isothermal theory were also evident in solutions for sliding conditions. The calculated film thickness was not appreciably influenced by the oil film temperature generated in sliding.

The majority of the workers in this area relied on electrical methods, namely oil film resistance and capacitance, in measuring the lubricant film thickness^(53,54,55). Other reported methods included measuring the oil flow⁽⁵³⁾ and an X-ray transmission technique⁽⁵⁶⁾. Of these, the capacitance method as employed by Crook⁽⁵³⁾ appears to be the most reliable. Typical film thickness in the region of 40 μin were measured and these were consistent

with theoretical predictions.

2.3 THEORY OF LUBRICATION IN METAL-FORMING

When a metal is deforming plastically under the action of external forces on a contacting platen or die, relative motion must normally occur between the plastic and non-plastic contacting surfaces. Additionally, the plastic surface extends in area as deformation progresses. It may be supposed that the mechanism of friction and lubrication is essentially that discussed previously, where, even up to very high pressures, it has been shown that such friction is proportional to the applied pressure. It would therefore seem reasonable to conclude that the coefficient of friction in cold-working processes would be in the range found in the usual dynamic tests. However, comparison between the coefficients of friction deduced from the slider tests, in which any bulk deformation must invariably be elastic in nature, and those deduced from operations involving bulk plastic deformation suggests that friction is generally lower in the latter⁽⁵⁷⁾. That the friction is low might imply that while boundary friction will generally occur, fluid film conditions may occasionally exist^(2,58-61) and that the concept, due to Bowden and Tabor⁽¹⁴⁾, of boundary friction between bodies in bulk elastic contact is only of limited application.

Considerable experimental evidence exists to suggest that the quantity of lubricant throughput across the metal deformation zone is of an order much higher than can be accounted for by the boundary lubrication theory, which in terms of thickness usually ranges from mono-molecular to several molecular layers. Table (2.1) shows typical measured lubricant film thickness from a number of sources.

Source	Process	Die-semi-angle (degree)	Condition	Lubricant film thickness (μ in)
Bowden and Tabor (14)	Sliding	-	-	0.4-2
Ranger and Wistreich(62)	Wire-drawing	1.9-5.3	Lubricant: soap powder Speed: 0-5000 ft min ⁻¹ Surface: smooth	4-120
Lancaster and Rowe(2)	Bar-drawing		Lubricant: radioactive soap solution Speed: 0-0.5 ft min ⁻¹ Surface: hand ground Surface: grit-blasted	20-40 20-180
Isupor, Smetanina and Mashura(63)	Rod-drawing	4-20	Lubricant: oil Speed: 0.2-49 ft min ⁻¹ Surface: as rolled and as drawn	56-212
Lancaster(64)	Wire-drawing	presumably 0-15	Lubricant: oil Speed: 0-5900 ft min ⁻¹	40-320
Fowler and Lancaster(65)	Wire-drawing	presumably 0-15	Lubricant: oil Speed: 0-5900 ft min ⁻¹	8-240

Table (2.1) Typical measured values of lubricant film thickness.

The methods adopted in these measurements were varied. Most of them depended on the examination of a sample of the drawn material by, for example, noting its weight before and after removing the residual lubricant⁽⁶³⁾, immersing it in a solvent and then determining the concentration of lubricant in the solvent^(64,65) and measuring the level of radiation in the case of the radioactive lubricant⁽²⁾. However, the electrical method adopted by Ranger and Wistreich⁽⁶²⁾ in measuring the resistance of the lubricant film during actual drawing seems more realistic in view of the absence of such possible interfering factors as elastic recovery at the die exit. An alternative to this method is to measure the capacitance of the lubricant film^(53,54).

Under strict boundary lubrication conditions, during bulk plastic deformation, the deforming surface will attempt to match the contour of the contacting tool. However, if a film of lubricant is present at the interface then conditions might be expected to be quite different. The deforming surface will tend to resist conformation to the die surface and the lubricant film, which bears the pressure, will tend to modify the grain structure at the interface. In consequence, the surface appearance of the deformed material may be matt or dull. A number of investigators^(2,58-61,66) in various metal-forming processes have observed this effect under supposedly boundary lubrication conditions. Recent works by Butler⁽⁶⁷⁻⁶⁹⁾ in simple compression tests appear to have solved this seemingly ambiguous role of the lubricant in metal-forming processes. It was shown that with no lubricant, or with one of very low viscosity, the deforming surface became virtually a replica of the die surface, but as the viscosity increased, the resemblance between the topographies of the metal and die surface became less well marked. This is in apparent contradiction to the boundary

lubrication theory in which viscosity is generally believed to be unimportant. Furthermore, there was a striking similarity in appearance, one of surface finish deterioration, between deformed surfaces obtained by mechanically entrapping a light lubricant and those obtained by using a viscous lubricant between originally parallel faces. Also, the presence of boundary additives was demonstrated to reduce the coefficient of friction while producing a lustrous finish on the deformed material. This was attributed to the formation, by chemical reaction or physical absorption, of minute but firmly adherent surface films. It was concluded that deformation proceeded mainly via the film at the interface and that its presence offered an explanation for the low coefficient of friction, and for the observed modifications to the surface appearance. In bar-drawing Lancaster and Rowe⁽³⁾ demonstrated that friction can be reduced considerably and that the reduction in area per pass can be increased when the steel bars were grit-blasted before drawing. The effect of grit-blasting was to provide a regular pattern of pockets on the bar surface to entrap the lubricant such that more lubricant was present in the deformation zone. These tests were conducted at slow drawing speeds and with dies of large entry angles in order to discourage contributions to lubrication by hydrodynamic action.

The foregoing evidence suggests that the mechanism of friction and boundary lubrication proposed by Bowden and Tabor⁽¹⁴⁾ for slider experiments between elastic bodies is not wholly tenable for the regime of lubrication in metal-forming, particularly in drawing processes where conditions favour the hydrodynamic phenomenon. Obviously, the friction would be dependent upon the roughness of the die and the workpiece surfaces to a great extent because the continually deforming surface will attempt to fit itself into the asperities on the die, and these will tend to plough their way

through the deforming metal. If a lubricant is present between the surfaces, it will be entrapped between the asperities, and intense pressures which result in the film during deformation will tend to prevent interfacial contact. While boundary additives will continue to be active, the die semi-angle, surface roughness, drawing speed and lubricant viscosity proved to be significant factors governing the film formation. That the film thickness is greater than several molecular layers, as shown in Table (2.1), suggests that a regime of hydrodynamic or quasi-hydrodynamic lubrication may exist, provided the conditions are favourable.

2.3.1 Representation of friction in metal-forming

Metal-forming theories present the working load for an operation in terms of the geometrical parameters of the process, the yielding characteristics of the material being worked, and a means of representing the frictional boundary conditions. A complete analysis of any process should consider the frictional losses between the sliding surfaces as a variable. This is immediately justified when one considers the state of stress acting on the material within the deformation zone. Although the fundamentals of this phenomenon have been much studied, very little that is known would facilitate formulation of the exact functional relationship between friction and its related variables such as surface roughness, lubricant viscosity and the rate of deformation. Consequently, in practically all proposed metal-forming theories it is necessary to assume that friction remains constant during deformation and that the use of a mean value suffices so that the differential equations are amenable to relatively simple analytical solutions. Thus, it is legitimate to assume that flow against a constant friction and at constant shear stress occurs on surfaces adjacent to one another, divided

by a sharp line of demarcation. Three mathematical descriptions of friction in common use are discussed here.

2.3.1.1 Coulomb coefficient of friction

The Coulomb law of friction, which has long been substantiated for moderately loaded sliders, describes the frictional stress τ at any point on that surface as being proportional to the normal pressure σ_n between the two bodies and is directed opposite to the relative motion between these bodies. The coefficient of friction is taken as a constant for a given pair of surfaces and is said to be independent of the velocity. Thus, assuming that the stresses are uniform over a small element of area δA , total surface area A , then a mean coefficient of friction may be written as:

$$\mu = \frac{\int_0^A \tau \, dA}{\int_0^A \sigma_n \, dA} \quad (2.2)$$

for a given set of working conditions.

The nature of metal-forming demands that the material is caused to flow plastically through a constricting die only once as opposed to experimental studies of friction and wear, where model sliders are made to slide over one another repeatedly. In this context, many workers⁽⁷⁰⁻⁷³⁾ have expressed their doubts as to the compatibility of the conditions prevalent in the two distinctively different cases and hence the applicability of Coulomb's Law to metal-forming. It would appear that Hockett's⁽⁷⁴⁾ call for a redefinition of the coefficient of friction in terms of surface conditions, and materials and lubricant properties seems in many ways justifiable. Fortunately, in spite of the difficulties in determining precise and meaningful values of μ in metal-forming

operations by, for example, the split-die^(75,76,77), rotating-die^(70,78,79), simulative⁽⁸⁰⁾, or semi-analytical techniques^(81,82,83), experimental results have shown that mean values of μ are adequate for most purposes in predicting loads and stresses. These techniques are discussed in greater detail in Section (2.7).

In general the coefficients of friction in cold-drawing processes are less than 0.1. It is difficult to postulate the precise values or range of values inasmuch as the experimental data will tend to vary with the method and the conditions of derivation. However, Wistreich⁽⁵⁸⁾ has suggested that likely ranges of μ are 0.01 to 0.05 for soap and 0.08 to 0.15 for oil; but since then more data has become available and taking account of the shortcomings of many of the methods of derivation, Rothman⁽⁷⁰⁾ suggested corresponding ranges of 0.02 to 0.05 and 0.06 to 0.12. In tube-drawing, the values of the coefficient of friction generally fall within the range 0.01 to 0.08⁽⁸⁴⁻⁸⁷⁾.

2.3.1.2 Constant-friction factor

While the vast majority of the investigations on friction have been concentrated on the Coulomb model, some workers prefer to assume a constant shear stress irrespective of the pressure between die and material. In this model the von Mises' yield criterion is assumed for the deforming material. The frictional stress at any point on the interface is written:

$$\tau = m \frac{Y}{\sqrt{3}} \quad (2.3)$$

or $\tau = mk$

where m = friction factor

Y = yield stress of material in uniaxial tension

k = shear yield stress of material

The friction factor is taken as constant for a given die and material under constant surface and temperature conditions. It is also considered to be independent of velocity. In the absence of friction, $m = 0$. The limiting shear strength of a material according to von Mises' yield criterion is $\frac{Y}{\sqrt{3}}$ or k . It therefore follows that the limits for m are $0 \leq m \leq 1$.

Experimental data on the typical values of m are scarce. However, Loke⁽⁸⁴⁾ has obtained reasonably consistent correlation between experimental and theoretical predictions of draw stress in bimetal tube-drawing by ascribing values of 0.01 and 0.02 to m . Avitzur⁽⁸⁸⁾ using a value of $m = 0.02$ has also predicted draw stresses in good agreement with the experimental results obtained by Wistreich⁽⁷⁵⁾. Smith and Bramley⁽⁸⁹⁾, drawing tubes on a floating-plug, have reported reasonable consistency between theoretical and experimental results for $m = 0.02$.

2.3.1.3 Hydrodynamic lubrication

There is an increasing evidence that conditions of hydrodynamic lubrication often exist during many metal-forming processes. A full hydrodynamic regime, however, does not normally prevail, as evidenced by the burnished surface of the deformed product and tool wear, provided the process is aided by means of special devices. This is very much a specialized field and deserved a more detailed discussion in Section (2.4).

Under conditions of a full hydrodynamic lubrication regime, a thick lubricant film separates the deforming material from the surface of the tool. Consequently, friction is characterized by the viscous properties of the lubricant. The basic assumptions associated with this model are that the lubricant has Newtonian properties and that its flow is laminar. Friction is then described by:

$$\tau = \eta \frac{U}{h} \quad (2.4)$$

where η = lubricant viscosity

U = velocity of deforming material

h = lubricant film thickness in deformation zone

It is at once apparent that the exact solution to this equation is extremely complex if not impossible. Firstly, the viscosity of liquids is a strong function of temperature and pressure; both being pertinent features of any metal-forming process. Secondly, the velocity term and lubricant film thickness are variables in the deformation zone. Although the velocity term can be accommodated quite easily, additional difficulties arise since the lubricant film thickness is in turn a function of its viscosity.

The analysis of metal-forming processes with hydrodynamic lubrication is scarce. However, the available literature shows that further assumptions are necessary so that the differential equations are amenable to some approximate solutions, for example, by assuming the process to be isothermal or that the lubricant obeys some empirical viscosity-temperature-pressure relationships. These theories are reviewed in the following section.

2.3.2 Hydrodynamic lubrication theories

That a consideration of hydrodynamic lubrication is justified is shown by Table (2.1), illustrating the typical measured values of the thickness of the lubricant film remaining on the wire after drawing. Experiments in hydrostatic extrusion by fluid pressure⁽⁹⁰⁾ have also shown that friction at the billet-container and billet-die interfaces can be eliminated or significantly reduced and, in particular, the existence of a film of lubricant on the extruded parts.

Perhaps one of the earliest analysis of hydrodynamic lubrication in metal-forming was proposed by Hillier⁽⁹¹⁾ for hydrostatic extrusion. The analysis assumed isothermal conditions and a pressure coefficient of viscosity according to equation (2.17). The lubricant film thickness, which was assumed to be constant, was estimated by the use of a minimum work technique⁽⁹²⁾. Hydrodynamic lubrication was shown to be associated with high velocities, viscosities, pressure coefficients of viscosity and high pressure in the lubricant, which was in turn a function of the die angle and extrusion ratio. The analysis considered only the metal deformation zone.

A generalised isothermal hydrodynamic lubrication theory for hydrostatic extrusion and drawing processes with conical dies was presented by Wilson and Walowit⁽⁹³⁾. The comprehensive analysis, in addition to the deformation zone, in which the equation of plastic equilibrium was adopted, included the inlet and outlet zones, as shown in Figure (2.2). Equations relating to the lubricant pressure, film thickness and friction were developed for the three zones. The conclusions reached were essentially those reported by Hillier⁽⁹¹⁾. Additionally, it was shown that a high hydrostatic extrusion pressure promoted the formation of a thick lubricant film. A positive augmentation stress tended to reduce the film thickness. On the other hand, a negative augmentation stress could result in a substantial increase in film thickness and offered a partial explanation for the use of back-pull in wire-drawing to reduce friction and die-wear^(58,60,83). Using an entering wire speed of 1.8 ft min^{-1} and representative data, the theory predicted a film thickness varying from $30 \text{ } \mu\text{in}$ at the die entry to $20 \text{ } \mu\text{in}$ at the die exit.

In the theoretical studies described above a rigid-plastic model has been adopted for the worked material. A variant of the

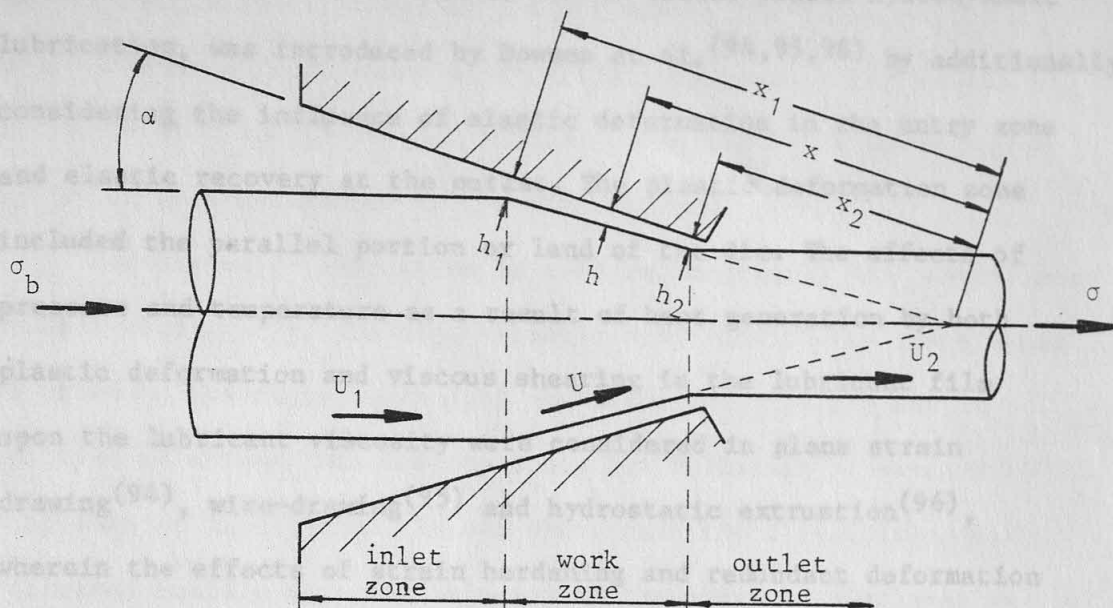
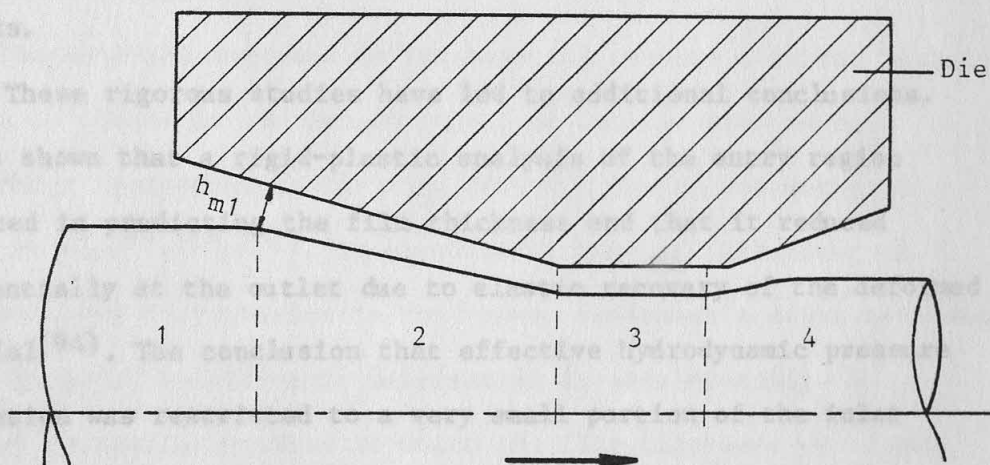


Figure (2.2) Generalised process with rigid-plastic deformation zone

(after Wilson and Walowit⁽⁹³⁾)



- 1 Elasto-hydrodynamic inlet
- 2 Plasto-hydrodynamic deformation
- 3 Plasto-hydrodynamic land
- 4 Elasto-hydrodynamic outlet

Figure (2.3) Elasto-plasto-hydrodynamic lubrication in drawing

(after Dowson et al^(94, 95, 96))

hydrodynamic lubrication regime, termed elasto-plasto-hydrodynamic lubrication, was introduced by Dowson et al.^(94,95,96) by additionally considering the influence of elastic deformation in the entry zone and elastic recovery at the outlet. The plastic deformation zone included the parallel portion or land of the die. The effects of pressure and temperature as a result of heat generation by both plastic deformation and viscous shearing in the lubricant film upon the lubricant viscosity were considered in plane strain drawing⁽⁹⁴⁾, wire-drawing⁽⁹⁵⁾ and hydrostatic extrusion⁽⁹⁶⁾, wherein the effects of strain hardening and redundant deformation were included. A schematic representation of the deformation zone is shown in Figure (2.3). However, the complete analysis requires for its solution, which is iterative in nature, the use of a computer. Although the influence of the various process parameters on lubrication follow the general trend predicted by the isothermal theories^(91,93), the inclusion of the thermal effects must yield more realistic results.

These rigorous studies have led to additional conclusions. It was shown that a rigid-plastic analysis of the entry region sufficed in predicting the film thickness and that it reduced substantially at the outlet due to elastic recovery of the deformed material⁽⁹⁴⁾. The conclusion that effective hydrodynamic pressure generation was restricted to a very small portion of the inlet region appeared to cause some concern⁽⁹⁷⁾ since pressure tubes have been used successfully in promoting hydrodynamic lubrication, (see Section (2.4)). However, the author draws attention to the fact that the theory leading to this conclusion considered the pressure at this region to be the atmospheric pressure. Smaller die semi-angles were shown to increase the film thickness^(94,95), as might be expected. At the same time their influence on friction and redundant deformation

was also mentioned. Isothermal assumptions in the inlet region gave reasonable predictions of the film thickness at low speeds, but in general the isothermal limitation in the deformation region led to an over-estimation of the viscous shear stress.

Hydrodynamic lubrication in cold sheet-drawing was investigated by Kudo et al. (98). The rigid-plastic model considered the effects of pressure and temperature upon the lubricant viscosity and in addition an attempt was made to study the influence of surface roughness on lubrication. It was shown that the film thickness increased rapidly with the velocity of the undrawn sheet when an isothermal theory was used. However, with the thermal analysis, the film thickness decreased with increasing velocity after attaining a maximum value. (See Figure (2.4)). This phenomenon has also been reported elsewhere(95,99) and could be attributed to the rise in temperature associated with increasing speeds which in turn reduced the lubricant viscosity.

The theories reviewed so far have all assumed that the variation of film thickness in the deformation zone was the same as that found under isothermal conditions. However, the recent works of Wilson et al.(99,100,101), in considering thermal influences on film thickness distribution in this zone, represent a major refinement to the study of hydrodynamic lubrication in metal-forming. By contrast to earlier studies in which the film thickness was shown to decrease linearly and gradually in the deformation zone, it was shown that the lubricant film adopted a concave profile exhibiting a maximum value well inside the deformation zone. This is illustrated in Figure (2.5). Comparison between theoretical and experimental film thickness in hydrostatic extrusion showed good agreement. The analyses adopted a rigid-plastic model.

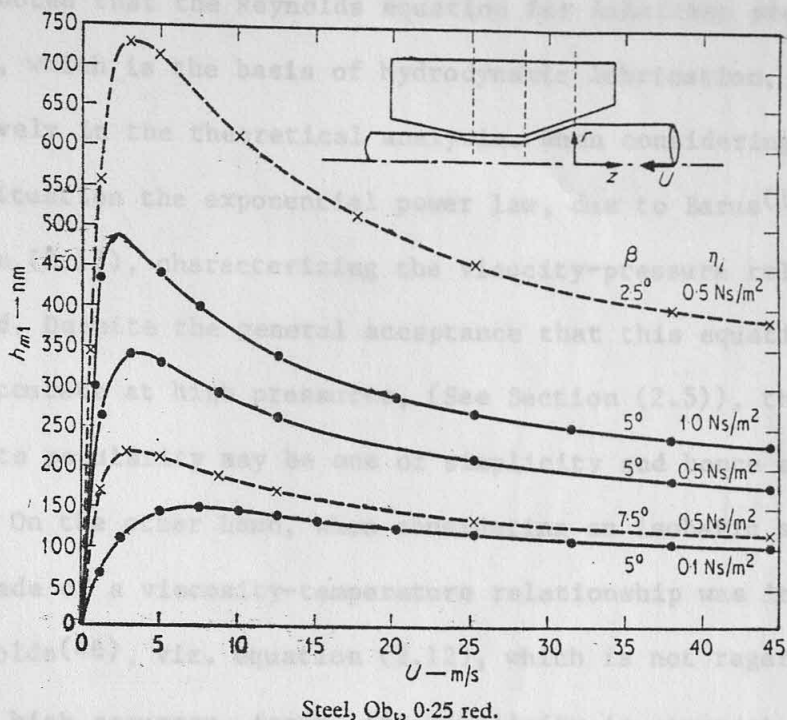


Figure (2.4) The relation between lubricant film thickness and wire speed at die entry for a range of entry oil viscosities and die semi-angles⁽⁹⁵⁾ (after Dowson et al)

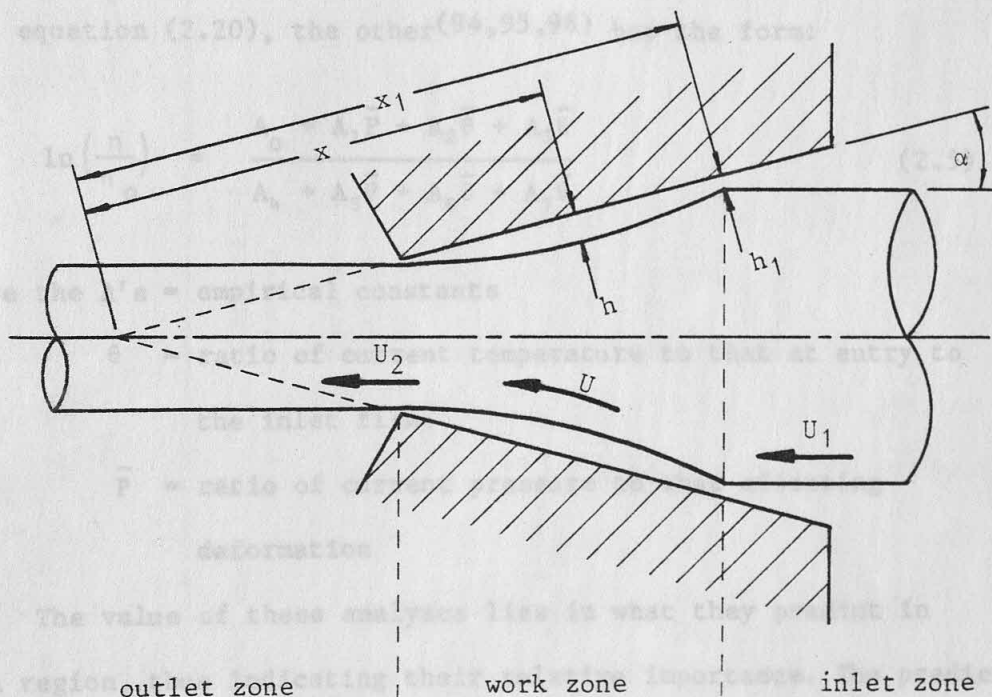


Figure (2.5) Plasto-hydrodynamic lubrication in drawing considering thermal effects on lubricant film profile (after Wilson et al^(99,100,101))

It is noted that the Reynolds equation for lubricant pressure distribution, which is the basis of hydrodynamic lubrication, was used extensively in the theoretical analysis. When considering an isothermal situation the exponential power law, due to Barus(102), viz. equation (2.17), characterizing the viscosity-pressure relationship was used. Despite the general acceptance that this equation may not be accurate at high pressures, (See Section (2.5)), the reason for its popularity may be one of simplicity and hence ease of handling. On the other hand, when considering an isobaric situation, the choice made of a viscosity-temperature relationship was invariably that of Reynolds(46), viz. equation (2.12), which is not regarded to be one of high accuracy. Again, its simplicity is apparent. However, to account for viscosity variation with pressure and temperature simultaneously, there appears to be two choices. While one resorts to combine Barus' isotherm with Reynolds' isobar(98,99), viz. equation (2.20), the other(94,95,96) has the form:

$$\ln\left(\frac{\eta}{\eta_o}\right) = \frac{A_o + A_1\bar{P} + A_2\bar{\theta} + A_3\bar{\theta}}{A_4 + A_5\bar{P} + A_6\bar{\theta} + A_7\bar{\theta}} \quad (2.5)$$

where the A's = empirical constants

$\bar{\theta}$ = ratio of current temperature to that at entry to the inlet film

\bar{P} = ratio of current pressure to that effecting deformation

The value of these analyses lies in what they predict in each region, thus indicating their relative importance. The predicted film thickness from these sources are tabulated in Table (2.2). By comparison with the measured values of Table (2.1), it is apparent that the theoretical values of Table (2.2) are generally smaller. However, this discrepancy may be expected since theoretical analysis

Source	Process	Die semi-angle (degree)	Entry Speed (ft min ⁻¹)	Theoretical Lubricant film thickness (μ in)
Bloor, Dowson and parsons(94)	Plane strain drawing	5	5000	88-68
Wilson and Walowit(93)	Hydrostatic extrusion and drawing	15	1.8	30-20
Dowson, Parsons and Lidgitt(95)	Wire-drawing	5	0-9000	20-10
Sniddle, Parsons and Dowson(96)	Hydrostatic extrusion	15	5	15-6
Wilson and Mahdavian(99)	Hydrostatic extrusion	22	2-19700	240-10
Kudo, Tsubouchi, Takada and Okamura(98)	Sheet-drawing	4	0-200	92-44

Table (2.2) Typical theoretical values of lubricant film thickness.

assumes "perfectly" flat surfaces, while measurement invariably leads to a mean film thickness which includes the lubricant entrapped in between the asperities.

2.4 PROMOTION OF HYDRODYNAMIC LUBRICATION

The discussion, hitherto, has considered metal-forming processes in general. However, in view of the interest of the present work, particular reference will be made to metal-drawing processes from here, although other processes will be mentioned from time to time.

The principal industrial requirements of the lubricating system in metal-drawing processes, and indeed any metal-forming process, can be regarded as being two-fold, namely, the increase in tool life and the maintenance of a suitable surface finish on the drawn product. The provision of a suitable surface finish generally implies some burnishing of the surface and hence intimate contact between the deforming material and the tool or tools, whereas the reduction of tool wear suggests the need for minimum contact between the two, it is apparent that there is some conflict between these two requirements. In practice, however, the engineer is generally able to achieve a compromise solution to the problem of meeting these requirements by selecting appropriate conditions of tool material and geometry, drawing speeds, surface pre-treatment and lubricants. Additionally, a distinction is often made between drawing for "high reduction" and drawing for "suitable surface finish". Productivity, however, is of prime concern to the industrialist. One of the major factors limiting the production rate is the necessity of changing tools rather frequently as a result of excessive wear. Precautionary and corrective measures to prevent and rectify damage to both tool and work can ease the

problem to some degree, but these incur extra cost. Investigation of friction and wear in metal-forming has been largely directed along two lines. The first is the selection of a suitable tool material which, in itself, has good friction and wear properties and secondly, the use of an appropriate lubricant film. It seems that there is a wider scope in this area and in consequence has aroused an increasing interest.

Surface pre-treatment, for example by abrasive blasting or a suitable coating, is popularly employed in metal-drawing industries. A review of the developments in the use of chemical conversion coatings to facilitate metal working has been presented by James and Haynes(1). However, such additional operations are not considered to be the ultimate solution and hence there is a continuing quest for more cost effective methods. Hydrodynamic lubrication falls into this category. Research and development in this area have largely been concentrated on drawing processes, as might be expected, since they lend themselves to the promotion of such a regime of lubrication.

The co-ordinated results of Table (2.1) show that the quantity of lubricant passing through the metal deformation zone is much greater than can be accounted for by the few molecular layers which are required for boundary lubrication. These may suggest that an even thicker lubricant film can be achieved by drawing at higher speeds, and at the same time increase productivity. However, researches(94,99) have shown that this is not to be the case, for the film thickness decreases with velocity after attaining a maximum value. If some other additional actions could be taken to increase still further the flow of lubricant through the metal deformation zone, true fluid lubrication might be established, and very substantial reductions in wear obtained. This may be achieved by supplying

the lubricant to the entry of the deformation zone at high pressures. Indeed, if the pressure is of the same order as the yield stress of the metal, the deformation can be initiated by the fluid pressure only, without any metal-to-metal contact between tool and work⁽⁵⁾.

2.4.1 Hydrodynamic lubricating systems

To supply lubricant at high pressures to the entry of the deformation zone, one intuitively formulates the idea of the utilisation of a hydrostatic pump. However, it was Christopherson et al.^(4,5) who proposed a novel, self-acting scheme for promoting hydrodynamic lubrication in wire-drawing. It was shown that the necessary pressure can be conveniently generated by causing the undrawn wire to approach the die through a tube filled with a viscous lubricant at atmospheric pressure, sealed on to the entry side of the die and of diameter slightly larger than the wire diameter. The motion of the undrawn wire generated a pressure in the lubricant by exactly the classical mechanism of hydrodynamic lubrication by drawing lubricant from a point where the clearance between the moving surfaces is large towards a point of small clearance. A schematic representation of this arrangement is shown in Figure (2.6). The idea was conceived from the work of MacLellan and Cameron⁽¹⁰³⁾ who regarded the device as relevant mainly to the separate question of swarf removal; aqueous lubricants were used in tubes having fairly large clearances, and the pressures generated were of the order of a few atmospheres.

Tubes of up to 40 cm long and of diameters 0.004 in, or less, larger than those of the undrawn wire were employed when drawing copper and mild steel wires at speeds of up to 600 ft min⁻¹. Using an electrical method it was demonstrated that complete separation occurred between the die and the deforming wire. Considerable

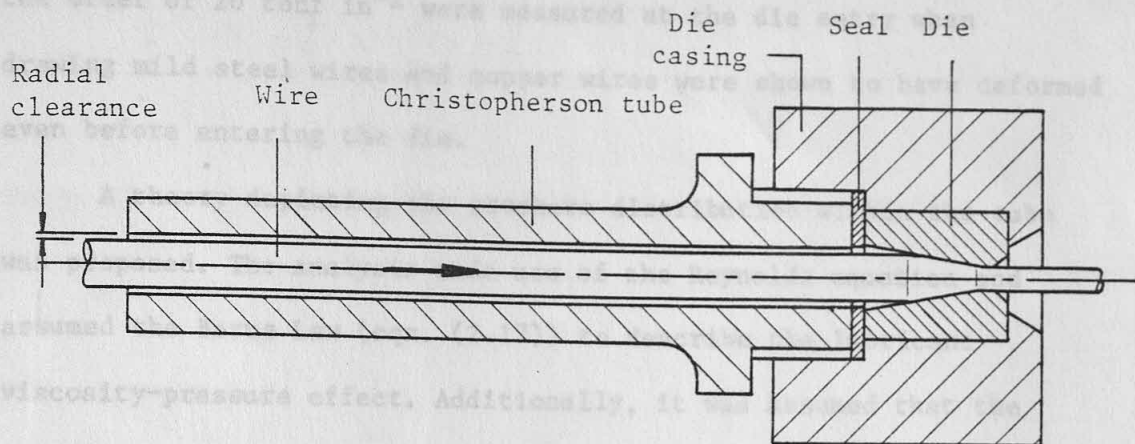


Figure (2.6) The Christopherson tube in wire-drawing
(after Christopherson et al^(4,5))

$$1 - \frac{q}{q_0} = \frac{6\eta U(1 - \epsilon^2)}{b^2} \int_0^1 \frac{1}{(1 + \frac{3}{2}f^2)} df \quad (2.6)$$

where q = ratio of actual lubricant flow to that of unrestricted flow

ϵ = eccentricity

The viscous is described by:

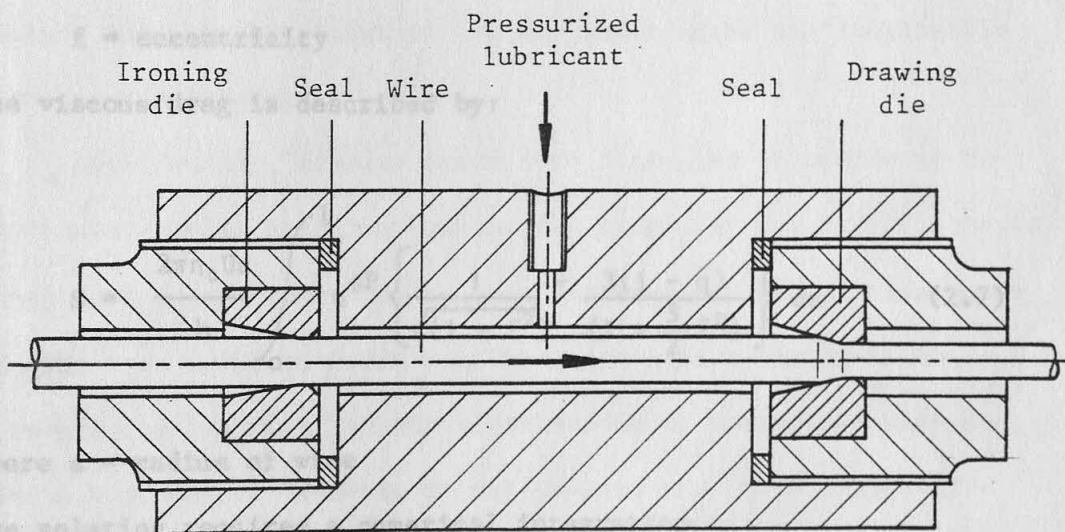


Figure (2.7) External pressurization in hydrodynamic lubrication in wire-drawing
(after Butler⁽⁹⁾)

reductions in draw force and die wear were observed. Pressures of the order of 20 tonf in⁻² were measured at the die entry when drawing mild steel wires and copper wires were shown to have deformed even before entering the die.

A theory depicting the pressure distribution within the tube was proposed. The analysis made use of the Reynolds equation and assumed the Barus Law (eqn. (2.17)) to describe the lubricant viscosity-pressure effect. Additionally, it was assumed that the wire within the tube would take up that position associated with a minimum viscous drag. The pressure generated is given below by:

$$1 - e^{-\phi P} = \frac{6\eta_0 U(1-q)\phi}{h^2} \int_0^1 \frac{1}{(1 + \frac{3}{2} f^2)} dx \quad (2.6)$$

where q = ratio of actual lubricant flow to that of unrestricted flow

f = eccentricity

The viscous drag is described by:

$$S = \frac{2\pi\eta_0 Ua}{h} \int_0^1 e^{\phi P} \left\{ \frac{1}{\sqrt{(1-f^2)}} + \frac{3(1-q)}{(1 + \frac{3}{2} f^2)} \right\} dx \quad (2.7)$$

where a = radius of wire

The solution requires a numerical integration.

Tattersall⁽⁶⁾ improved on the inadequacy in Christopherson's theory by considering all regions up to that in which the wire has deformed so that the lubricant flow could be predicted from entirely independent variables. This was expressed in terms of the thickness of the lubricant film remaining on the drawn wire which was then utilized to predict the hydrodynamic pressure generated. The equation

for the lubricant film thickness is written:

$$t = \frac{-(b - \frac{M}{U}) \pm \sqrt{(b - \frac{M}{U})^2 - 4ac}}{2a} \quad (2.8)$$

where f = ratio of initial wire radius to final wire radius

$$a = f^2 \left(\frac{1}{\alpha h^2} - \frac{2l}{h^3} \right) \quad (2.10)$$

$$b = f \left(\frac{1}{h^2} - \frac{1}{\alpha h} \right)$$

$$c = \frac{1}{4\alpha}$$

$$M = \frac{f}{6\eta_0\phi} (1 - e^{-\phi Y})$$

Although the theoretical values of pressures compared well with Christopherson's experimental observations, those of the lubricant flow were higher by a factor of two or three. It was thought that the breakdown of the oil under shear was responsible for this discrepancy.

Additionally, drawing tests were conducted at speeds up to 80 ft min⁻¹ using soap lubricants. The length of the Christopherson tubes used ranged from 0.25 to 1 in and provided radial clearances ranging from 0.003 to 0.050 in. The use of soap lubricants in wire-drawing has more industrial relevance by comparison with oil lubricants. Soaps, however, do not possess Newtonian properties. Consequently, the recorded hydrodynamic pressure and soap film thickness remaining on the drawn wire were used to determine the apparent viscosity of the soaps from the integrated Reynolds equation for the Christopherson tube, given by:

$$P = \frac{12\eta_0 l}{h^3} \left(\frac{U_h}{2} - q \right) \quad (2.9)$$

where P = hydrodynamic pressure at the die entry

$q = fUt$

t = film thickness on drawn wire

Quite interestingly, it was found that the viscosity could be expressed as a single valued function of the wire speed:

$$\eta = \eta_0 e^{(-BU)} \quad (2.10)$$

where η_0 = apparent viscosity at zero wire speed

B = empirical constant

The experimental results showed that high lubricant pressures were associated with the drawn wire having poorer surface finish. The longer the length of the Christopherson tube and the smaller the radial clearance, the higher were the pressure and the lubricant throughput for a given wire speed. However, these increased with speed, rising to their maximum values before decreasing as the speed was further increased. Tattersall attributed this to the negative exponential relation between the wire speed and the apparent viscosity of the soap as in equation (2.10). Later investigators^(95,98,99) using theories which included thermal effects on oil lubricants have predicted similar results for film thickness variation with draw speed. In these cases, the fall of film thickness appeared to be due to the fall in the lubricant viscosity as a result of higher temperatures associated with higher speeds. Consequently, the empirical nature of equation (2.10) may suggest that the speed and thermal effects have been consolidated. Further, that the experimental results of Christopherson et al.⁽⁵⁾, at draw speeds of up to 600 ft min⁻¹, did not exhibit this maximum may be an indication of the thermal stability of the viscosity of soap and oil lubricants.

Using the works of Tattersall⁽⁶⁾, Chu⁽⁷⁾ contributed to the works in this area by presenting practicable charts for the design

of the, by now well known, Christopherson tubes. These endeavoured to correlate the geometrical factors of the Christopherson tube with parameters of lubricant properties, speed, die-angle, and film thickness. An extension was made by Osterle and Dixon⁽⁸⁾ by including pressure and temperature effects on the lubricant viscosity, described by equation (2.20), and strain hardening effects on the wire material.

Recently Fogg and Dafila⁽¹⁰⁴⁾ attempted forced hydrodynamic lubrication in the sinking of thin-walled ($D/t = 70$), soft aluminium tubes by feeding the lubricant at very high pressures through orifices on the conical portion of the die. However, the tubes collapsed due to these pressures and the idea does not appear to be viable.

Since hydrodynamic lubrication in wire-drawing is a collective function of drawing speed, lubricant properties and geometry of the Christopherson tube, there are several criticisms which prevent its industrial application in its original form. While lubricants of high viscosity ensure hydrodynamic lubrication at lower speeds and with shorter tubes, they may be such as to require very high speeds and impracticably long tubes. A series of tubes of various lengths and diameters would therefore be required to meet the requirements of various drawing schedules. Furthermore, the lubricant film would be broken during starting and stopping at the beginning and end of each wire.

Consequently, to overcome such difficulties Butler⁽⁹⁾ and Moseev and Korostilin⁽¹⁰⁾ proposed a method of controlling the lubricant pressure at the die entry, independent of the lubricant viscosity, drawing speed, and process geometry. The method, shown schematically in Figure (2.7), is slightly more sophisticated than Christopherson's original proposal. It relies on the combined

action of external pressurization and hydrodynamic action to effect hydrodynamic lubrication. The central bore in the pressure chamber through which the wire passes is essentially a Christopherson tube. However, its geometry becomes of secondary importance. The ironing die takes a very light pass and acts as a seal for the externally generated hydrostatic oil pressure of up to $15000 \text{ lbf in}^{-2}$. With the higher pressures in the chamber, hydrodynamic lubrication can be accomplished with lower velocities and lower viscosities. The results showed reductions in die wear and drawing force with increase in hydrostatic pressure. There is, however, an upper limit to the value of this radial pressure. Its effect is to increase the effective longitudinal tensile stress in the wire which, in conjunction with the back-tension imposed by the ironing die, can be sufficiently high to neck and break the wire before it enters the drawing die.

An extensive research programme was undertaken by Middlemiss⁽¹¹⁾ to develop an industrially acceptable unit. The observations reported by previous workers^(9,10) were confirmed and it was demonstrated that the use of an ironing die as an inlet seal is impracticable for industrial operation in view of the excessive wear encountered in this component. It is interesting to note that the investigation completed a full circle, leading back to the Christopherson tube. A tungsten carbide tube 2.5 cm (1 in) long and providing a 0.05 mm (0.002 in) radial clearance replaced the ironing die. The hydrostatic pump was used only to prime the system and provide an initial starting pressure. Once full drawing speed had been attained, the pressure could be maintained by the hydrodynamic pressure generated by the motion of the wire through the tube, allowing the pump to be eliminated. It was concluded that when drawing carbon steel wires there was no need for assistance from the pump even during starting-up. This however did not apply when drawing stainless

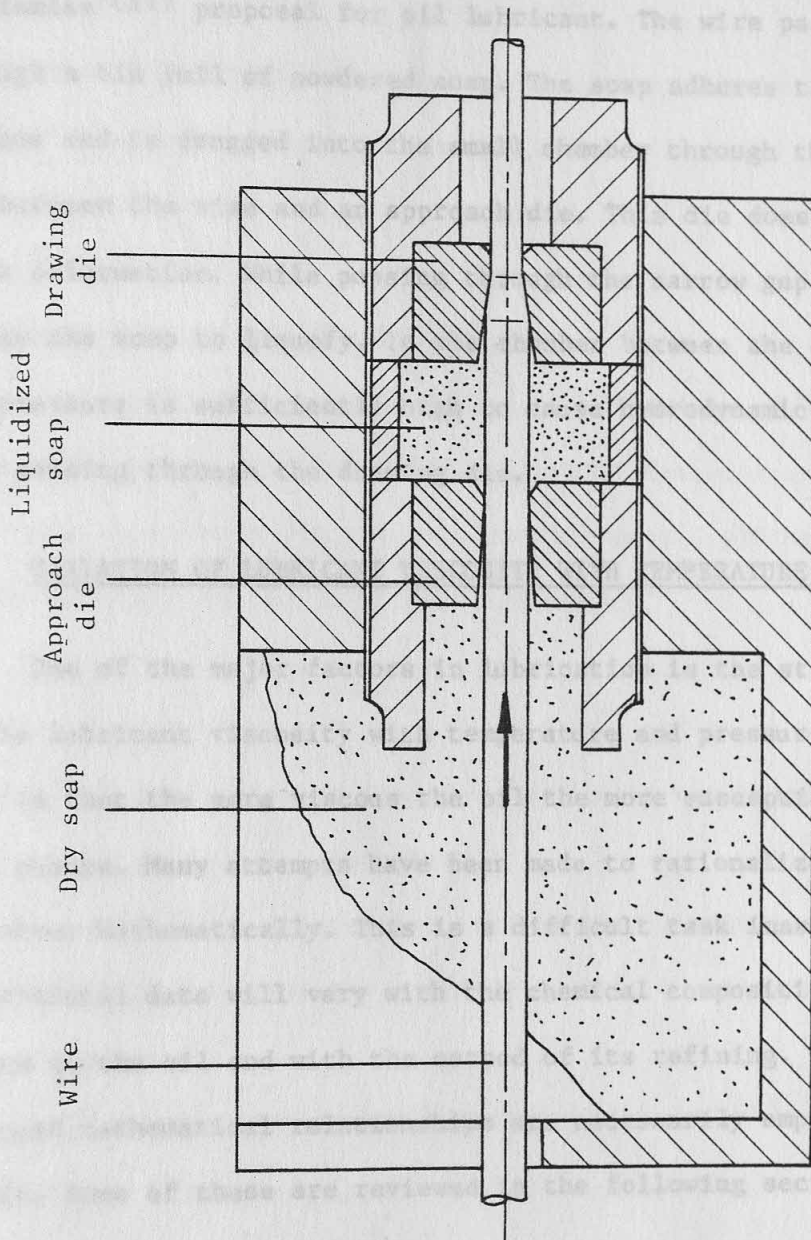


Figure (2.8) Industrial hydrodynamic lubrication unit
(after Avitzur⁽⁸⁸⁾)

steel wires where conditions were obviously more severe.

Avitzur⁽⁸⁸⁾ quoted an industrial hydrodynamic lubricating system using soap as the lubricant, illustrated in Figure (2.8). Except for the absence of the hydrostatic pump, it resembles Middlemiss⁽¹¹⁾ proposal for oil lubricant. The wire passes first through a bin full of powdered soap. The soap adheres to the wire surface and is dragged into the small chamber through the narrow gap between the wire and an approach die. This die does not effect metal deformation. While passing through the narrow gap friction heating causes the soap to liquefy. In the chamber between the two dies, the pressure is sufficiently high to cause hydrodynamic lubrication when passing through the drawing die.

2.5 VARIATION OF LUBRICANT VISCOSITY WITH TEMPERATURE AND PRESSURE

One of the major factors in lubrication is the strong variation of the lubricant viscosity with temperature and pressure. A general rule is that the more viscous the oil the more susceptible it is to this change. Many attempts have been made to rationalize this behaviour mathematically. This is a difficult task inasmuch as the experimental data will vary with the chemical composition and source of the oil and with the method of its refining. Thus, the proposed mathematical relationships are necessarily empirical in nature. Some of these are reviewed in the following sections.

2.5.1 Viscosity-temperature relationships

It has long been recognised⁽¹⁰⁵⁾ that the majority of the viscosity-temperature laws proposed were solutions to the differential equation:

$$\frac{1}{\eta_0} \frac{d\eta_0}{dT} = \frac{1}{(c_1 + c_2 T + c_3 T^2 + \dots + c_n T^n)} \quad (2.11)$$

where η_0 = viscosity at any temperature T under atmospheric pressure
 c 's = empirical constants

Most of the standard equations can be derived by using different numbers of terms in the polynomial on the right-hand side of this equation.

Reynolds' formula⁽⁴⁶⁾ is a two-constant equation obtained if the first term only is retained:

$$\eta_0 = Ae^{-mT} \quad (2.12)$$

where A = viscosity at T = 0

m = empirical constant

This is the simplest of all viscosity-temperature relations, but holds only for a limited temperature range. Slotte⁽¹⁰⁶⁾, using two terms in the polynomial, proposed:

$$\eta_0 = \frac{A}{(T - c)^m} \quad (2.13)$$

where c = pour point or temperature of apparent solidification

A, m = empirical constants

Herschel⁽¹⁰⁷⁾ pointed out that in the Fahrenheit scale c can be equated to zero. The validity of this equation extends over a wider range.

A three-constant equation proposed by Vogel⁽¹⁰⁸⁾ has the form:

$$\eta_0 = Ae^{\frac{A}{(T - c)}} \quad (2.14)$$

where c = pour point or temperature of apparent solidification

A = viscosity at T = ∞

Cameron⁽¹⁰⁹⁾ suggested that when using the Centigrade scale, value of -95 can be assigned to c. This equation usually provides closer fit than the other two.



However, the most widely used formula is probably that due to Walther⁽¹¹⁰⁾. This is an expression for the kinematic viscosity ν in centistokes at an absolute temperature T in degrees Rankine:

$$\log_{10} (\nu + c) = \frac{A}{T^m} \quad (2.15)$$

where A, c, m = empirical constants

In general usage the constant c is maintained at an optimum value over a chosen temperature range. For lubricating oils the value of c is often assumed to be approximately constant, and was considered to have an average value which has been reported successively as 0.8 and 0.6, though a better approximation appeared to be 0.7⁽¹¹¹⁾.

Cornelissen and Waterman⁽¹¹²⁾ introduced the following formula to describe the relationship, at atmospheric pressure, between the kinematic viscosity ν and the absolute temperature T in degrees Kelvin:

$$\log_{10} \nu = \frac{A}{T^x} + B \quad (2.16)$$

where A, B, x = empirical constants

Later Roelands, Vlugter and Waterman⁽¹¹³⁾, showed the formula to be equally valid at higher pressures, generally up to at least 3000 atmospheres, when writing in terms of the dynamic viscosity.

The formulae reviewed above are generally regarded to be the better known ones of the many proposed viscosity-temperature relations. Hersey⁽⁵⁰⁾ have reviewed at least six other published works, and still others can be found in their references.

2.5.2 The influence of pressure on the viscosity of lubricants

While it is well known that the viscosity of liquid lubricants varies inversely with its temperature, less widely appreciated

is the fact that lubricants may show equally large variations in viscosity with pressure. However, it was some years after Barus⁽¹⁰²⁾ who in 1893 published a viscosity-pressure-temperature diagram for marine glue that the study on the influence of high pressure on the behaviour of lubricants began to arouse interest.

The phenomenon of lubricants attaining a plastic condition of "apparent solidification" under high pressure was discovered by Bridgeman⁽¹¹⁴⁾. This observation was also reported a few years later by Hersey⁽¹¹⁵⁾. Needs⁽¹¹⁶⁾ showed similar results in his work on heavily-loaded journal bearings when the coefficient of friction increased with pressure despite the absence of metallic contact. Later Bradbury, Mark and Kleinschmidt⁽¹¹⁷⁾ covering some fifty lubricating oils in pressure ranges up to 150,000 lbf in⁻² recorded increases in viscosity of the order of 10^7 fold. More recent studies by Roelands et al.⁽¹¹³⁾ and Galvin, Naylor and Wilson⁽¹¹⁸⁾ on a considerable number of lubricants at different temperature and pressure ranges have also shown viscosity increases with pressure. Reviews and co-ordinated data by Hersey and Hopkins^(119,120) cover most of the published literature in this field. These references list over twenty other studies which show evidence of the viscosity-pressure effect of a number of lubricants.

Naturally the way of expressing the influence of pressure upon viscosity is by means of a pressure coefficient, or fractional change in viscosity per unit increase of pressure. Earlier studies on the subject defined the pressure coefficient at any pressure as the rate of change of the viscosity with respect to the given pressure at a constant temperature, divided by the viscosity at atmospheric pressure, ie. $(d\eta/dP) (1/\eta_0)$. On this basis Hersey⁽¹¹⁵⁾ and Hyde⁽¹²¹⁾ discovered that mineral oils as a class have pressure coefficients greater than those of lard oils and fatty oils.

Dow(122) on the basis that viscosity is a strong function of the molecular structure in liquids, showed that the pressure coefficient is influenced by the basic chemical composition of hydrocarbon oils, their sources as well as the method of refining. Further investigations(123) showed that in general the pressure coefficients of naphthenic oils are greater than those of paraffinic oils. It can be deduced from the experimental data of the studies by Roelands et al.(113) and Galvin et al.(118) that the pressure coefficient of viscosity is inversely proportional to both the temperature and pressure of the lubricant. In general it has been observed also, in the earlier studies(117,119,120), that higher temperatures reduced the influence of pressure on the lubricant viscosity. Pressures and temperatures up to 140,000 lbf in⁻² and 425°F respectively were considered. Conversely, at higher pressures the influence of temperature on viscosity is reduced, due to the constraining action of the higher pressure on the normal thermal agitation in the liquid.

2.5.3 Viscosity-pressure relationships

It is convenient to express mathematically the behaviour of lubricants under pressure in order to incorporate this effect in the theoretical treatment on lubrication. Attempts to rationalize this behaviour must necessarily be empirical in nature. Barus(102) originally proposed an isothermal equation of the form:

$$\log_{10} \frac{\eta}{\eta_0} = \phi P \quad (2.17)$$

where η = viscosity at any pressure P , although a linear equation proved to fit better(50). The Napierian logarithm is also frequently used in place of the Briggsian logarithm. This relationship is almost universally adopted in theoretical studies of the subject

although it has been recognised that few lubricants in fact conform closely to it over a wide range of pressure. This is evidenced by the slight non-linearity of the graphs of the logarithm of $\eta - P$ isotherms^(113,117,118,124). However, at the temperature range 32°F to about 200°F it appears that the isotherms approximate very closely indeed to straight lines. An exception to this non-conformity is naphthenic oils which Bradbury et al.⁽¹¹⁷⁾ and Chu and Cameron⁽¹²⁴⁾ have shown to fit the Barus equation very well.

Additionally, to account for the deviation from the Barus equation for paraffinic oils as well as recognising the order of the error which could arise when using a value of ϕ calculated at a low pressure to predict viscosities at much higher pressures, Chu and Cameron⁽¹²⁴⁾ proposed a power law, which fitted very well with co-ordinated experimental data, of the form:

$$(\log_{10} \eta)^{3/2} = m(P + a) \quad (2.18)$$

where a, m = empirical constants

For the same reasons Roelands et al.⁽¹¹³⁾ proposed the equation:

$$\log_{10} \log_{10} \frac{\eta}{\eta_0} = m \log_{10} P + \log_{10} a \quad (2.19)$$

where a, m = empirical constants

A graphical method to predict lubricant viscosities at high pressure was proposed by Clark⁽¹²⁵⁾ but this approach, for purposes of theoretical analysis, is not deemed to be as versatile as one in the form of a mathematical equation. There have been other proposals and some of these published literature have been reviewed by Hersey⁽¹²⁶⁾.

2.5.4 Viscosity-temperature-pressure relationships

From the literature already reviewed it is clear that being a property of state, viscosity is a function of temperature and pressure; both of which having the opposite effects. Despite this recognition the majority of investigations in the field of the viscosity variation of liquids is confined to the temperature dependence at atmospheric pressure.

To account for effects of both of these variables simultaneously, the so called "complete viscosity-temperature-pressure" relationship was introduced. One of the most widely used equations is obtained by combining Reynolds' isobar (equation (2.12)) with Barus' isotherm (equation (2.17)), giving rise to the equation:

$$\eta = \eta_0 e^{\phi P - \gamma \theta} \quad (2.20)$$

where γ = empirical temperature coefficient of viscosity

θ = rise in temperature

Sternlicht(127) introduced a third empirical constant and obtained a closer fit by writing:

$$\eta = \eta_0 e^{\left(\phi P + \frac{\beta P}{T} + \frac{\gamma}{T} - \frac{\gamma}{T_0}\right)} \quad (2.21)$$

where T_0 = lubricant solidification temperature

Appeldorns' proposal(128) may be written:

$$\log \frac{\eta}{\eta_0} = a P + (m + cP) \log \frac{T}{T_0} \quad (2.22)$$

where a, c, m = empirical constants

This reduces to Slotte's Fahrenheit isobar (equation (2.13)) when $P = 0$, and to Barus' isotherm when $T = T_0$. Correlations were found among the empirical constants a, c and m by statistical studies of test data such that the number of constants required could be

reduced, depending on the degree of accuracy required.

Lastly Roelands et al.(113) proposed a six-constant equation of the form:

$$\log_{10} \frac{\eta}{\eta_0} = a T^{-x} + b P^y T^{-x} + c P^y + d \quad (2.23)$$

where a, b, c, d, x, y = empirical constants

T = absolute temperature in degrees Kelvin

P = gauge pressure in atmospheric pressure

when $P = 0$, the equation reduces to the Cornelissen-Waterman isobar (equation (2.16)).

2.6 BASIC THEORIES OF METAL-DRAWING

In practice the drawing process, which consists of pulling a workpiece through a die in order to impart geometrical changes, is superficially simple. Indeed, there is evidence of ornamental wire drawing dating back prior to the last millenium B.C., during the days of the affluent ancient civilizations. For many years the technique has been widely used in industry to draw wire, rod, strip, tube, section etc. Theoretical analysis of the mechanics of deformation are, however, complex and it was not until the early 1900's that serious attempts were made to analyse the deformation process. The earliest publications were generally qualitative and empirical in nature, but it was soon recognised that a rational analysis must consider the geometrical parameters of the process, the yielding characteristics of the material being worked, and the friction boundary conditions.

Over the years the theories and practices of drawing processes have been well documented. Reviews, both critical and documentary in nature, have also appeared in the literature, and it would be to some extent repetitive to attempt to construct

such a detailed review here. In view of the fact that this investigation was concerned primarily with the promotion of hydrodynamic lubrication at the boundary interfaces, rather than with the internal mechanics of deformation, such a review also would not be entirely appropriate. Nevertheless, the author feels responsible to present a concise discussion of the above subjects in order that the role of friction, or the lack of it, in the domain of drawing technology may be better appreciated.

Of the early theories, perhaps the most important of which was that due to Sachs(129) who in 1927 proposed a theory for wire-drawing by considering the metal in the deformation zone to be in equilibrium. Later improvements and refinements were made by Davis and Dokos(130), Wistreich(131), Shield(132), MacLellan(76) and Korber and Eichinger(133) to give a more accurate statement of the mechanics of the process. These included the effects of work hardening and redundant work. Substantial reviews of the theory of axisymmetric drawing have been published by MacLellan(77), Johnson and Sowerby(134) and Shaw, Stableford and Sansome(135). Plane strain theories of drawing using the slip-line field technique have been discussed by Hill(136), Hill and Tupper(137), Green and Hill(138) and Pawelski(139). Johnson(12), Kudo(140), Avitzur(88) and Kobayashi(141) simplified Hill's limit load theorem and developed upper bound solutions to both plane strain and axisymmetric forming processes.

Since Sachs' original proposal, drawing theories proliferated very rapidly, and these can be classified broadly under three main headings, namely, the equilibrium approach, the kinematically admissible approach and the energy approach. It is noted that some theories utilize more than one method in their solution. Major difficulties, however, have been encountered in applying

mathematical expressions to practice due to the lack of knowledge of certain process characteristics such as the mean yield stress of the material and the coefficient of friction at the boundary interfaces during the working operation. Research consequently extended in these directions. In addition, such factors as die design and redundant work have also received attention.

2.6.1 Equilibrium approach in drawing

The method is based on the equilibrium of forces and predicts a value of the draw force lower than the actual value. It is a lower-bound solution which neglects redundant work.

2.6.1.1 Axisymmetric wire or bar-drawing

It will be realised that there is no fundamental difference between the processes of wire-drawing and bar-drawing provided that both are axisymmetric. Theoretically, the division between these processes is one of dimension only and the mechanics of deformation are identical. However, in practice they differ considerably with regard to design of the machinery and drawing speeds.

Sachs⁽¹²⁹⁾ presented the first rational solution for wire-drawing through a conical die. It was assumed that plane cross-sections of the workpiece remained plane as they passed through the die, the stress distribution was uniform on such planes, Coulomb friction prevailed and that the friction at the die-workpiece interface did not affect the stress distribution. Thus, by a consideration of the equilibrium of the forces acting on an element within the deformation zone in conjunction with Tresca's yield criterion, an equation for the draw stress for no back tension was derived:

$$\sigma = Y_m \left(\frac{1+B}{B} \right) \left[1 - \left(\frac{D_2}{D_1} \right)^{2B} \right] \quad (2.24)$$

where $B = \mu \cot \alpha$. For the case with back tension^(58,60,75), which is commonly applied to reduce friction and die wear, Sachs' equation is written:

$$\sigma = Y_m \left(\frac{1+B}{B} \right) \left[1 - \left(\frac{D_2}{D_1} \right)^{2B} \right] + \sigma_b \left(\frac{D_2}{D_1} \right)^{2B} \quad (2.25)$$

Davis and Dokos⁽¹³⁰⁾ assumed a linear relationship for the strain-hardening effect of the workpiece of the form:

$$Y = Y_o + \sigma' \ln \left(\frac{D_2}{D_1} \right)^2 \quad (2.26)$$

where σ' is a constant having stress dimensions, and derived the draw stress as:

$$\sigma = Y_o \left(\frac{1+B}{B} \right) \left\{ \left[1 - \left(\frac{D_2}{D_1} \right)^{2B} \right] \left[\left(1 - \frac{\sigma'}{Y_o B} \right) + \frac{\sigma'}{Y_o} \ln \left(\frac{D_2}{D_1} \right)^2 \right] \right\} \quad (2.27)$$

Thus, when $\sigma' = 0$, equation (2.24) for a non-strain hardening material is obtained. Atkins and Caddell⁽¹⁴²⁾ have shown that for the practical range of parameters the error is about 8% when the mean yield stress used is as in equation (2.26) instead of formally including the power law into the differential equation before solution.

Korber and Eichinger⁽¹³³⁾ argued that Sachs' equation neglected shear stress on the vertical surfaces of the elements and proposed an equation for draw stress which included a term sometimes referred to as the Korber and Eichinger effect. Contribution of the parallel portion or land of the die and the effect of speed were considered by MacLellan⁽⁷⁶⁾ and Yang⁽¹⁴³⁾, and Parson, Taylor and Cole⁽¹⁴⁴⁾ respectively. The works of Atkins and Caddell⁽¹⁴⁵⁾, Johnson and Rowe⁽¹⁴⁶⁾, and Siebel⁽¹⁴⁷⁾ incorporated redundant deformation.

2.6.1.2 Axisymmetric tube-drawing

Analyses of tube-drawing in terms of sinking, fixed-plug drawing and mandrel drawing have been well documented by Sachs and his collaborators using the equilibrium approach. Sachs, Lubahn and Tracy⁽¹⁴⁸⁾ derived an equation for the drawing of thin-walled tubing on a moving mandrel to yield the draw stress:

$$\sigma = Y_m \left(\frac{1+B}{B} \right) \left[1 - \left(\frac{t_2}{t_1} \right)^B \right] \quad (2.28)$$

where $B = \frac{\mu_1 - \mu_2}{\tan \alpha_1 - \tan \alpha_2}$

μ_1, μ_2 = Coulomb coefficients of friction at the die-tube and mandrel-tube interfaces respectively

α_1, α_2 = semi-angles of the die and mandrel respectively

t_1, t_2 = initial and final wall thickness respectively

The solution was based on the assumption that the normal stress acting on a transverse section was distributed uniformly over the cross-section, the normal pressures on the die and the mandrel were equal, and that a close-pass prevailed. In practice, however, drawing is always accompanied by a certain amount of sinking.

In the case of plug drawing, friction forces at the die-tube and plug-tube interfaces act in the same direction. The solution is the same as that for mandrel drawing except that the parameter B is now defined by:

$$B = \frac{\mu_1 + \mu_2}{\tan \alpha_1 - \tan \alpha_2} \quad (2.29)$$

An equation for the draw stress in tube-sinking proposed by Sachs and Baldwin⁽¹⁴⁹⁾ was written:

$$\sigma = Y'_m \left(\frac{1+B}{B} \right) \left[1 - \left(\frac{D_2}{D_1} \right)^B \right] \quad (2.30)$$

where $B = \mu \cot \alpha$

$Y'_m = aY_m$ = modified mean yield stress from the von Mises' yield criterion applied to the complex state of stress occurring in tube-sinking. The average value of $a = 1.1$

The method of analysis assumed that a shear stress produced by friction existed on the die-tube interface, transverse sections were free from shear stresses, the normal stress acting on the transverse sections was uniformly distributed over the cross-section and was a principal stress, the wall thickness of the tube was small in comparison with the tube diameter, and that the wall thickness of the tube remained constant throughout the process. This last assumption is not strictly valid since in practice, a slight increase, not exceeding 5% is observed.

Swift⁽¹⁵⁰⁾ and Chung and Swift⁽¹⁵¹⁾ contributed to works in this area by introducing expressions for the prediction of the draw stress and increments in the wall thickness and length of the tube in sinking. An allowance was made for the strain hardening of the tube material by assuming a uniform rate of strain hardening in relation to the principal logarithmic strain. Strictly speaking no such provision exists in Sachs' theories. In all cases, the stress distribution across the tube wall was assumed to remain constant which applies only to thin-walled tubing. A more general method of accounting for the effect of redundancy was proposed by Blazynski and Cole^(86,152) in their investigations of the sinking, fixed-plug and mandrel drawing processes. The semi-empirical method is a modification of Hill and Tupper's⁽¹³⁷⁾ concept of the equivalent total mean stress. The main equations used were those due to Sachs and his collaborators. Green⁽¹⁵³⁾ proposed a correction for redundant work in tube-drawing based on the analogy between strip-drawing and close-pass tube-drawing assuming conditions of

plane strain. The approach, however, is not applicable to tube-sinking.

Young and Meadows⁽⁸⁷⁾ postulated that the redundant work factor in close-pass fixed-plug drawing can be written as:

$$\theta = 0.76 + 0.24 \left(\frac{2-r}{r} \right) \frac{\sin \alpha_1}{2} \quad (2.31)$$

where r = reduction in cross-sectional area. Thus the draw stress, with allowance for a portion of sink, strain hardening and redundant work, was found to be:

$$\sigma = \sigma_s \left(\frac{t_2}{t_1} \right)^B + \theta \left\{ x \left(\frac{1+B}{B} \right) \left[1 - \left(\frac{t_2}{t_1} \right)^B \right] - y \left(\frac{1+B}{B-K'} \right) \left[\left(\frac{t_2}{t_1} \frac{D_2}{D_1} \right)^{K'} - \left(\frac{t_2}{t_1} \right)^B \left(\frac{D_2}{D_1} \right)^{K'} \right] \right\} \quad (2.32)$$

where x, y, K' = stress-strain relation parameters

$$B = \frac{\mu_1 + \mu_2}{\tan \alpha_1 - \tan \alpha_2}$$

$$\sigma_s = 1.1 \bar{Y} \left(\frac{1+B}{B} \right) \left[1 - \left(\frac{D_2}{D_1} \right)^B \right] + 1.1 \bar{Y} \frac{\tan \alpha_1}{2}$$

$$\bar{Y} = \frac{1}{\epsilon_s - \epsilon_0} \int_{\epsilon_0}^{\epsilon_s} Y d\epsilon$$

ϵ_s = natural strain in sink

ϵ_0 = natural strain at plane of entry

2.6.2 Kinematically admissible approach

By its implication, the kinematically admissible approach is concerned with the movement of the material in shear through the deformation zone. In particular, it considers only those

modes of deformation which conform to the external boundaries without violating the incompressibility and continuity criteria, and the primary concern of the approach is the deduction of such admissible velocity fields. Since the velocity of the die is prescribed, if the assumed velocity field has its normal component in the deforming body, matching that of the die and satisfying the above-mentioned criteria, then the velocity field is kinematically admissible. Within this approach there are two main methods of solution in common use, namely, the slip-line field solutions, also known as the method of characteristics, and the upper-bound solutions.

2.6.2.1 Slip-line field solutions

It is well known that the basic mechanism of metal deformation is by shear. A knowledge of the directions of maximum shear can be used, together with the magnitude of the shear yield stress, to determine a working load. This is the basis of slip-line field solutions and is valid only in plane strain deformation. Since shear must always be accompanied by complementary shear of equal magnitude and opposite sense, there exists two sets of shear lines orthogonal to each other but tangential to the directions of maximum shear. Except for certain geometrically convenient situations the method can be extremely laborious, particularly so because the validity of the field cannot be verified until it has been completed. However, once a valid field has been constructed, the working loads may be deduced directly from the associated stress plane. In addition, the solution gives a direct method of determining redundant deformation.

Hill and Tupper⁽¹³⁷⁾ applied the method to plane strain drawing and presented it at that time as a theory of wire-drawing, but it is now known⁽⁷⁵⁾ that such a direct transposition is not valid. Nevertheless, the slip-line field theory does give an

approximate indication of stress distribution for the axisymmetric forming process. Johnson and Mellor⁽¹³⁴⁾ and Johnson, Sowerby and Haddow⁽¹⁵⁵⁾ have presented substantial and comprehensive reviews of the application of the theories to the various plane strain deformation processes.

2.6.2.2 Upper-bound solutions

For many metal-forming operations, no exact solutions to the working loads are available. Upper-bound solutions are, therefore, particularly valuable since they predict a working load which is at least sufficient to perform the operation.

Generally, in a deformation process it is necessary to provide work for internal deformation of the material and for shearing across surfaces of velocity discontinuities, including those at the tool-work interfaces. In some cases, work is also supplied by the predetermined body tractions, e.g. back-tension in drawing. These three categories of work are summed up in Prager and Hodge's⁽¹⁵⁶⁾ upper-bound theorem for the von Mises' rigid-perfectly plastic material to read:

"Among all kinematically admissible strain fields the actual one minimizes the expression:

$$J^* = \frac{2}{\sqrt{3}} \sigma_0 \int_V \sqrt{\frac{1}{2} \dot{\epsilon}_{ij} \dot{\epsilon}_{ij}} dV + \int_{S_T} \tau |\Delta v| dS - \int_{S_t} T_i v_i dS \quad (2.33)$$

where J^* = externally supplied power.

A strain rate field derived from a kinematically admissible velocity field is kinematically admissible.

Hill⁽¹⁵⁷⁾ derived a similar theorem based on his maximum work-rate principle, which can be stated as follows:

$$LU \leq \int_V \frac{\dot{\sigma}}{\sigma \dot{\epsilon}} dV + \int_S \tau_s v dS \quad (2.34)$$

where L = true forming load

U = forming velocity

$\dot{\epsilon}$ = effective strain rate in an element of volume dV

v = relative slip along the surface S

τ_s = shearing stress along a surface

$\bar{\sigma}$ = effective or representative stress

dV = volume of an element of material

One of the earliest papers to appear in the literature after these early works is that due to Johnson⁽¹²⁾, who in 1959, proposed a simplified slip-line field, composed of a series of straight lines along which the velocity discontinuities act. The deforming material in extrusion and coining processes were considered to move between these discontinuity surfaces as a rigid body and all deformation took place by shear at the boundaries. The integral on the right-hand side of equation (2.34) was set to zero, and since straight line discontinuities were considered, no integration on the second term was required, giving:

$$\dot{W} \leq \sum \tau_s v A \quad (2.35)$$

where A = surface area of the velocity discontinuity

v = relative slip along the discontinuity surface

τ_s = shear stress in pure shear

Depending on the sets of straight lines chosen, the upper-bound load will differ accordingly and the best solution is the one which gives the minimum load effected by optimising the geometry. The same approach has been adopted to axisymmetric forming processes by Smith and Bramley⁽⁸⁹⁾ in floating-plug tube-drawing and by Loke⁽⁸⁴⁾ in floating-plug and mandrel bimetal tube-drawing. These

are illustrated in Figures (2.9) and (2.10). Friction at the tool-workpiece interfaces was characterized by a constant friction factor.

A year later in 1960, Kudo⁽¹⁴⁰⁾ introduced the concept of "unit rectangular deforming region" in plane strain forging and extrusion. The workpiece was divided into suitable rectangular regions and each of these was then sub-divided into rigid triangles. As with Johnson's⁽¹²⁾ method, deformation was considered to be by shearing at the boundaries of these triangles. The minimum energy dissipated was calculated for a unit region algebraically or by scale drawing for various unit dimensions and frictional conditions. The optimal geometry for each sub-unit was thus determined for the deforming zone.

The solution under plane strain conditions can be adapted to axial-symmetry by supposing that the diagrams represent diametral sections of the workpiece. Alexander⁽¹⁵⁸⁾ discussed Johnson's⁽¹²⁾ plane strain solutions and extended the method to represent the case of axial-symmetry. The velocity field proposed by Johnson was retained but the deformation zone in this case was a single annular region which appeared triangular in the plane of symmetry. Deformation was considered by shearing at the boundaries in addition to the homogeneous deformation. Thus, using the maximum work principle in conjunction with the von Mises' yield criterion, the rate of internal energy dissipation \dot{W} , was:

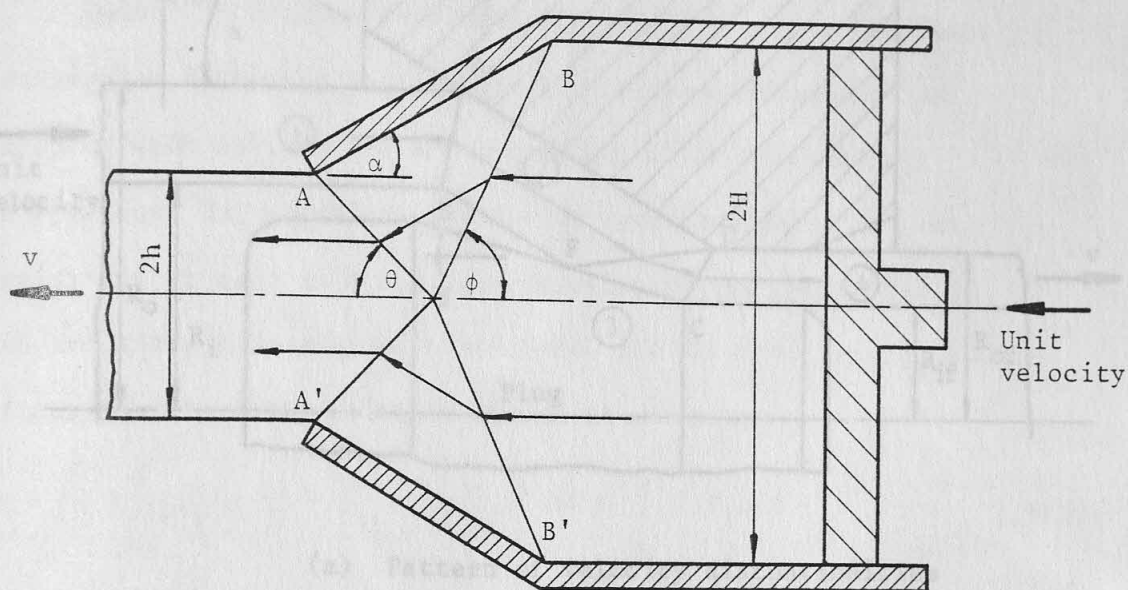
$$\dot{W} = \frac{Y}{\sqrt{3}} \int \Delta v \, dS + Y \int \bar{\epsilon}_p \, dV \quad (2.36)$$

where Y = yield stress in uniaxial tension or compression

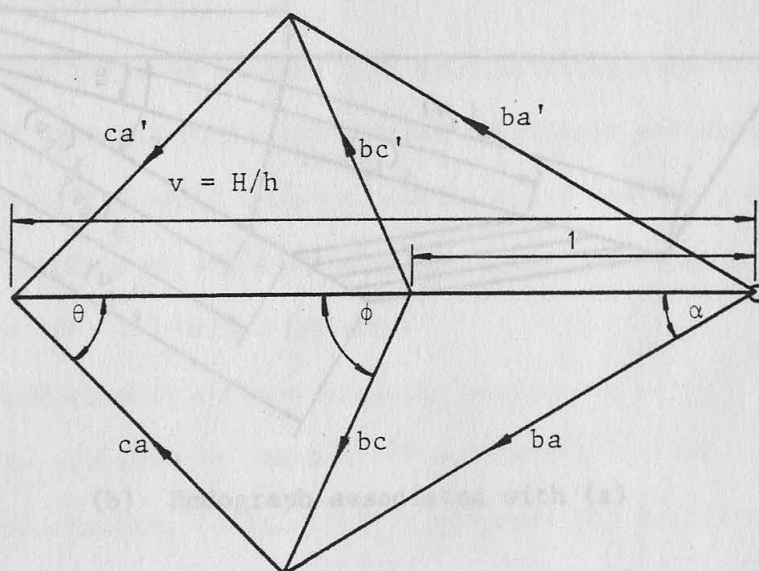
Δv = relative slip along the discontinuity surface S

dV = volume of an element of material

$\bar{\epsilon}_p$ = total plastic strain rate

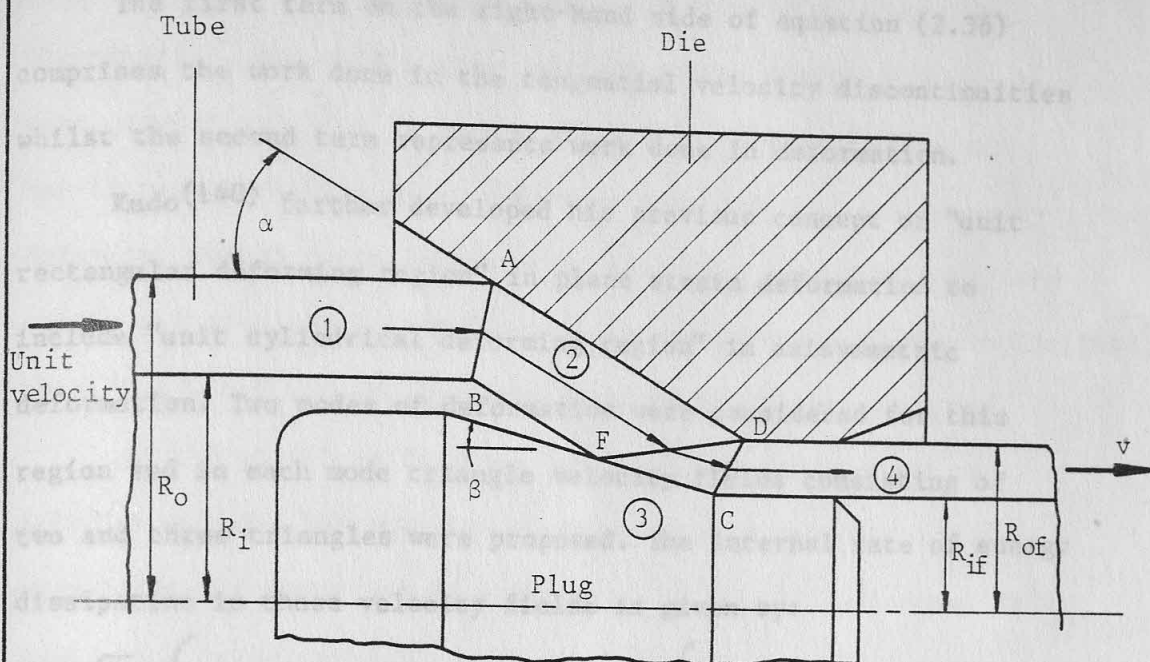


(a) Pattern of velocity discontinuities



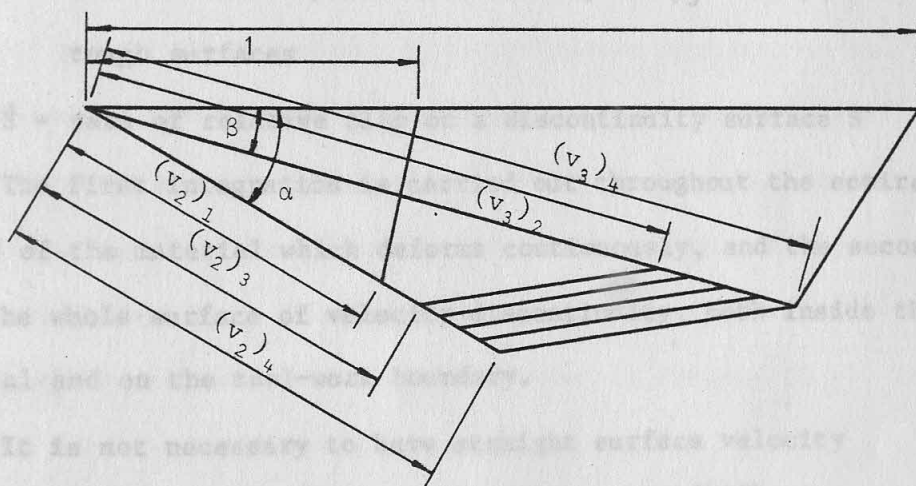
(b) Hodograph associated with (a)

Figure (2.9) Plane strain extrusion through wedge-shaped die (after Johnson⁽¹²⁾)



(a) Pattern of velocity discontinuities

$$v = (R_o^2 - R_i^2) / (R_{of}^2 - R_{if}^2)$$



(b) Hodograph associated with (a)

Figure (2.10) Tube-drawing on a floating-plug
(after Smith and Bramley⁽⁸⁹⁾)

The first term on the right-hand side of equation (2.36) comprises the work done in the tangential velocity discontinuities whilst the second term represents work done in deformation.

Kudo⁽¹⁴⁰⁾ further developed his previous concept of "unit rectangular deforming region" in plane strain deformation to include "unit cylindrical deforming region" in axisymmetric deformation. Two modes of deformation were considered for this region and in each mode triangle velocity fields consisting of two and three triangles were proposed. The internal rate of energy dissipation in these velocity fields is given by:

$$\dot{E} = \sqrt{\frac{2}{3}} Y \int_V (\dot{\epsilon}_r^2 + \dot{\epsilon}_\theta^2 + \dot{\epsilon}_z^2 + \frac{1}{2} \dot{\gamma}_{rz}^2)^{\frac{1}{2}} dV + Y \int_S f \dot{S} dS \quad (2.37)$$

where f = slip-resistance ratio and takes the value of 0 for perfectly lubricated smooth surfaces and according to the von Mises' yield criterion equals $\frac{1}{\sqrt{3}}$ for perfectly rough surfaces

\dot{S} = rate of relative slip on a discontinuity surface S

The first integration is carried out throughout the entire volume of the material which deforms continuously, and the second over the whole surface of velocity discontinuity, both inside the material and on the tool-work boundary.

It is not necessary to have straight surface velocity discontinuity as proposed by Johnson⁽¹²⁾ and Kudo⁽¹⁴⁰⁾. For axisymmetric deformation, Kobayashi⁽¹⁴¹⁾ proposed the replacement of Kudo's⁽¹⁴⁰⁾ straight surface discontinuities in the "unit deforming region" by curved surfaces. In addition, admissible velocity fields for flow through conical dies were proposed. The type of the velocity field for plane strain drawing suggested by Green⁽¹⁵³⁾ was shown to exist also for an axisymmetric flow through conical dies when it was compared with the distorted grid-

line pattern of a lead specimen extruded through conical dies. Consequently, velocity fields consisting of a series of triangles were assumed for flow through conical dies in wire-drawing and bar-extrusion. Unlike plane strain deformation, the continuously deforming region in an axisymmetric situation cannot be described completely by rigid-body motion⁽¹²⁾ in the presence of discontinuities, thus, the first integral term in equation (2.37) was retained.

An important contribution to the upper-bound method of solution was the introduction of the spherical velocity field in axisymmetric deformation by Avitzur^(92,159,160,161). Kinematically admissible velocity fields were developed by assuming a deformation zone lying between spherical surfaces centered on the virtual apex of the die. At any point within this zone of plastic deformation, the material was assumed to move towards this apex. The theory was applied to compute the internal power of deformation, shearing across the spherical velocity discontinuities and the tool-workpiece interfaces in wire-drawing and extrusion^(92,159), and tube-sinking and tube-expanding⁽¹⁶⁰⁾. In addition, the general case of having flow through conical converging dies with hydrodynamic lubrication treated as an adiabatic process was considered⁽¹⁶¹⁾. Typical spherical velocity fields are shown in Figures (2.11) and (2.12).

2.6.3 Energy approach

The energy approach is based on the assumption that the work expended in drawing may be divided into three components of the drawing force. The first component is due to homogeneous deformation, the second component is due to friction at the boundary interfaces, and the third arises from redundant deformation. This approach is a combination of both the lower-bound and the

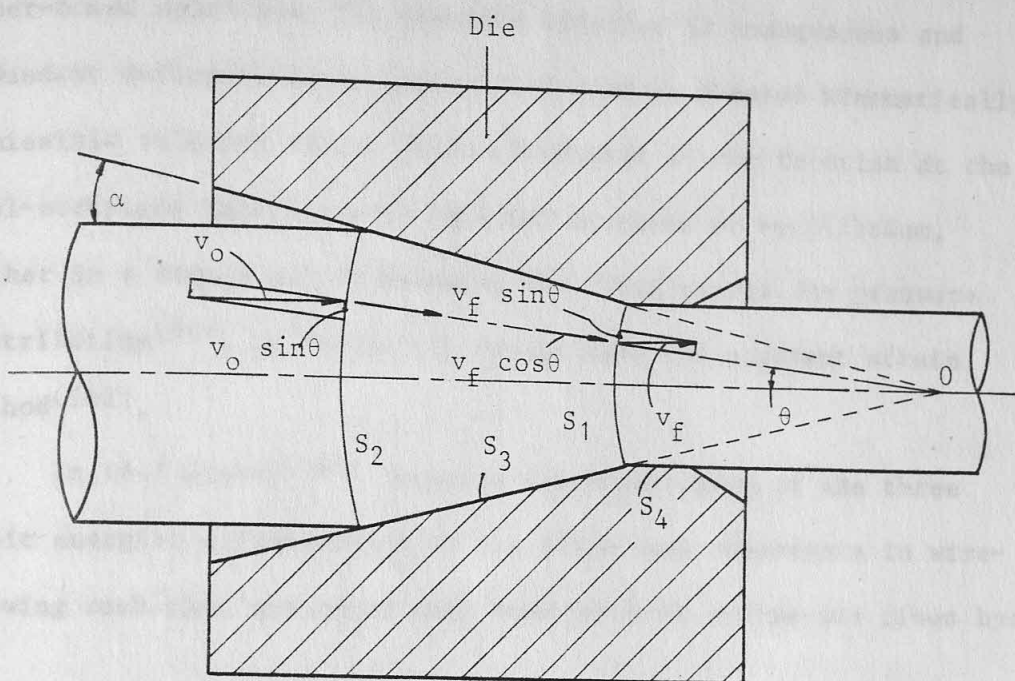


Figure (2.11) Spherical velocity field in axisymmetric drawing
(after Avitzur^(92, 159))

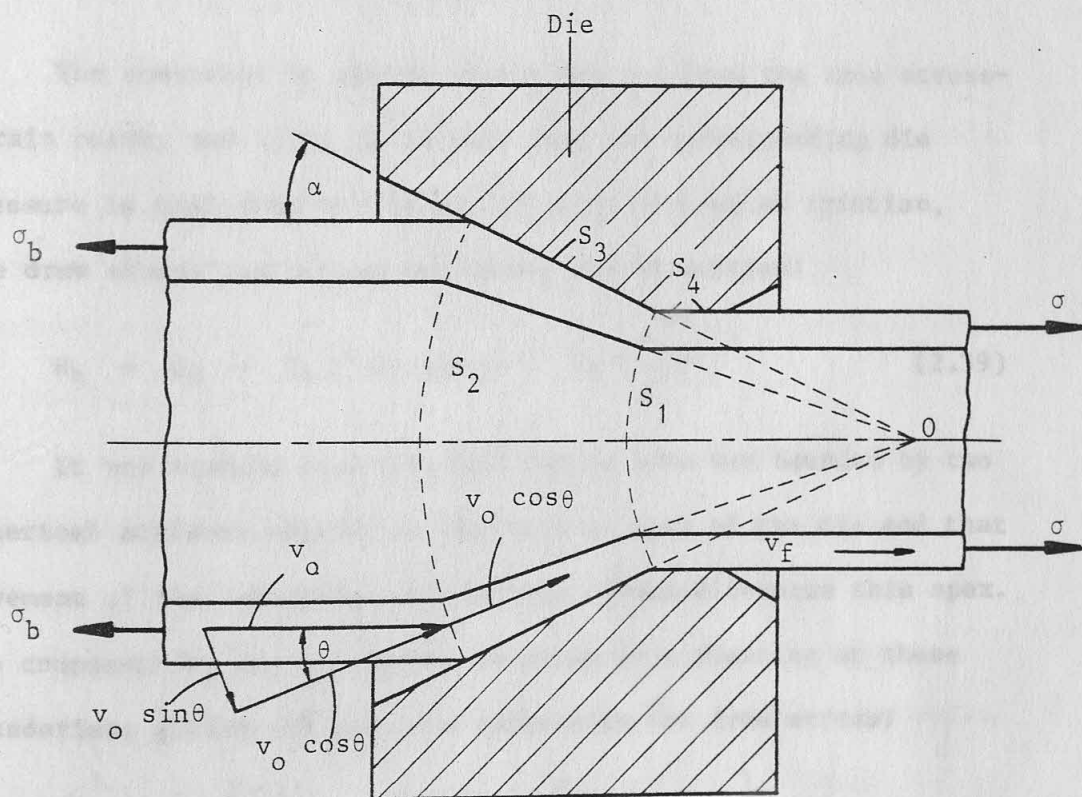


Figure (2.12) Spherical velocity field in tube-sinking
(after Avitzur⁽¹⁶⁰⁾)

upper-bound solutions. The energies expended in homogeneous and redundant deformations are calculated from an assumed kinematically admissible velocity field, while an account of the friction at the tool-workpiece interfaces is obtained by means of equilibrium, either in a direct way by assuming the frictionless die pressure distribution⁽⁸⁸⁾, or indirectly by applying the apparent strain method⁽¹⁶²⁾.

In 1947 Siebel⁽¹⁴⁷⁾ proposed the superposing of the three basic energies corresponding to the three load components in wire-drawing such that the total work done per unit volume was given by:

$$W_t = W_h + W_f + W_r \quad (2.38)$$

where W_h = work done in homogenous deformation

W_f = work done against friction

W_r = work done in redundant deformation

The component W_h may be simply derived from the true stress-strain curve, and if it is assumed that the corresponding die pressure is unaltered by the introduction of Coulomb friction, the draw stress neglecting redundancy may be written:

$$W_h + W_f = Y_m (1 + \mu \cot \alpha) \ln \left(\frac{A_1}{A_2} \right) \quad (2.39)$$

It was assumed that the deformation zone was bounded by two spherical surfaces centred on the virtual apex of the die and that movement of the deforming material was directed towards this apex. The component W_r was considered to arise from shearing at these boundaries, giving the complete expression for draw stress:

$$W_t = Y_m \left[(1 + \mu \cot \alpha) \ln \left(\frac{A_1}{A_2} \right) + \frac{2}{3} \alpha \right] \quad (2.40)$$

noting that work done per unit volume equals the draw stress.

Pugh⁽¹⁶³⁾ considered the energy approach in simple hydrostatic

extrusion and although it was assumed that the homogeneous, frictional and redundant works were additive as in equation (2.38), the analysis was based on a consideration of the mean strains induced in the process. Simple plane cross-section, conical and spherical shear surfaces were considered for the estimation of the redundant work. The extrusion pressure was written:

$$P = \int_0^{\epsilon_3} Y d\epsilon + \frac{\mu r \ln(r)}{(r-1) \sin \alpha} \int_{\epsilon_1}^{\epsilon_2} Y d\epsilon \quad (2.41)$$

where r = extrusion ratio

ϵ_1 = mean strain induced by shearing at the inlet zone

ϵ_2 = mean strain induced after the material has passed through the conical die passage and equals $\epsilon_1 + \ln(r)$

ϵ_3 = mean final strain after the material has left the deformation zone by passing through the outlet shear plane and equals $2 \epsilon_1 + \ln(r)$

The work done across the inlet and outlet shear surfaces were not equal due to work hardening. This did not arise in Siebel's analysis⁽¹⁴⁷⁾ which considered the material to be perfectly plastic. On the basis of the experimental results, Pugh⁽¹⁶³⁾ concluded that the spherical surfaces gave the best estimate of the redundant work.

A variant of the energy approach was considered by Basily and Sansome⁽⁸¹⁾ in the determination of some basic parameters, such as mean coefficient of friction, mean die pressure and mean equivalent strain, for use in section rod-drawing. The basic assumptions were that the three forms of work done in deformation were additive as in equation (2.38), illustrated in Figure (2.13), and that the true stress-strain curve fitted the following parabolic curve:

$$\sigma = \sigma' \epsilon^n \quad (2.42)$$

Hence, the three energy components can be computed by integrating the three sections of the area under the true stress-strain curve given by:

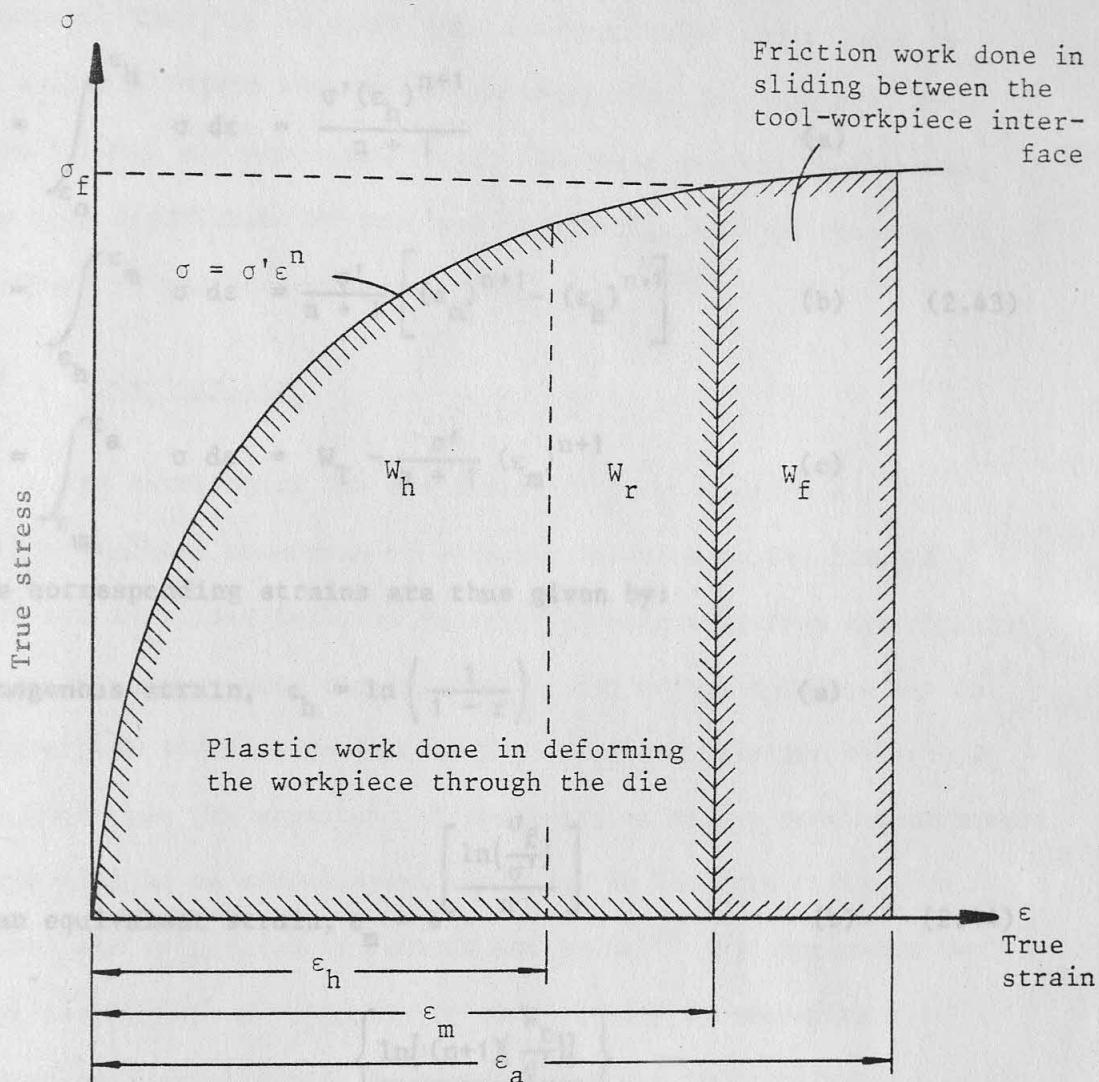


Figure (2.13) Area under true stress-strain curve showing the three forms of energy expended in a drawing process (after Basily and Sansome⁽⁸¹⁾)

Hence, the three energy components can be computed by integrating the three sections of the area under the true stress-strain curve given by:

$$W_h = \int_{\epsilon_0}^{\epsilon_h} \sigma d\epsilon = \frac{\sigma'(\epsilon_h)^{n+1}}{n+1} \quad (a)$$

$$W_T = \int_{\epsilon_h}^{\epsilon_m} \sigma d\epsilon = \frac{\sigma'}{n+1} \left[(\epsilon_m)^{n+1} - (\epsilon_h)^{n+1} \right] \quad (b) \quad (2.43)$$

$$W_f = \int_{\epsilon_m}^{\epsilon_a} \sigma d\epsilon = W_T - \frac{\sigma'}{n+1} (\epsilon_m)^{n+1} \quad (c)$$

The corresponding strains are thus given by:

$$\text{homogenous strain, } \epsilon_h = \ln \left(\frac{1}{1-r} \right) \quad (a)$$

$$\text{mean equivalent strain, } \epsilon_m = e^{\left[\frac{\ln \left(\frac{\sigma_f}{\sigma'} \right)}{n} \right]} \quad (b) \quad (2.44)$$

$$\text{apparent strain, } \epsilon_a = e^{\left\{ \frac{\ln \left[(n+1) \left(\frac{W_t}{\sigma'} \right) \right]}{n+1} \right\}} \quad (c)$$

2.7 DETERMINATION OF FRICTION IN DRAWING

It has been suggested⁽⁷⁰⁻⁷⁴⁾ that the classical concept of Coulomb friction may not be valid in metal-forming processes. However, it is possible, as is commonly practised, to describe friction in terms of μ , provided that it is considered as a ratio of stresses or forces, rather than as an immutable material property. The measurement of friction in drawing represents a considerable problem, since the equilibrium in the axial direction

leaves two unknowns, namely, the shear force and the normal force acting on the tool-workpiece interfaces, in terms of the draw force. Measuring the draw force results in an equation with two unknowns. Thus, it is clear that a second relationship must be established before the two can be separated. Many methods, both experimental and semi-analytical, have been devised to determine the mean coefficient of friction in drawing. Some of these are reviewed in the following sections.

2.7.1 Die-rotation

The rotation of the die during drawing produces a circumferential component of velocity relative to the die, so that its resultant relative velocity diverts away from the virtual apex. In consequence, the friction vector swings round to act in a direction opposite to that of the resultant relative velocity. Provided that the magnitude of the friction vector remains unchanged, there will be an accompanying reduction in the draw force. The method was originated by Linicus and Sachs⁽⁷⁹⁾ who evaluated the mean coefficient of friction in wire-drawing by measuring the reduction in draw force. By rotating the die in bar-drawing, Rothman and Sansome⁽⁷⁸⁾ determined the mean coefficient of friction by a consideration of the reduction in the draw force as well as the torque required for rotating the die, illustrated in Figures (2.14) and (2.15). Thus, the mean coefficients of friction are given by:

$$\mu_p = \frac{F}{Q} = \frac{(p - p_r) \tan \alpha}{(p_r - p \cos \phi)} \quad (2.45)$$

and
$$\mu_T = \frac{F}{Q} = \frac{2T \sin \alpha}{(pD_m \sin \phi - 2T \cos \alpha)} \quad (2.46)$$

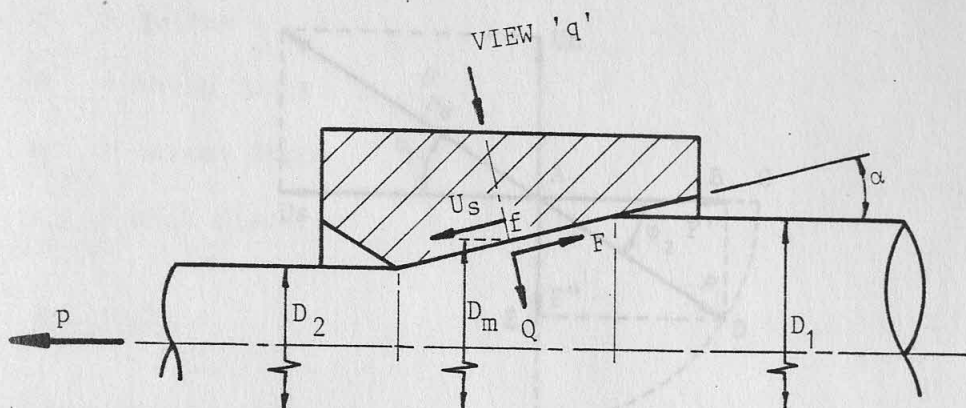


Figure (2.14) Representation of forces in axisymmetric drawing [after Rothman and Sansome(78)]

AC represents the friction vector F without the die rotation. Assuming that $\phi_1 = \phi_2 = \phi$ and that F is unaltered by the rotating motion, there is a reduction in draw force corresponding to the die rotation is given by:

$$p = Q \sin \alpha + F \cos \alpha \quad (2.47)$$

$$p_0 = Q \sin \alpha + F \cos \alpha \cos \phi \quad (2.48)$$

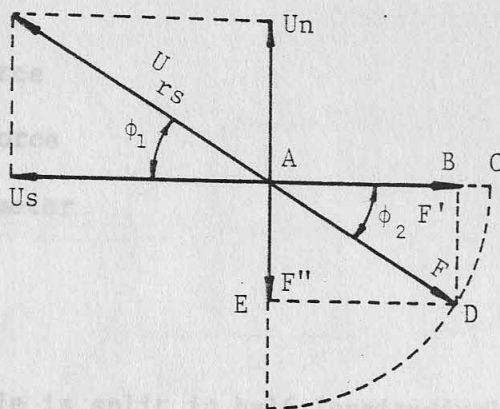
Combining equations (2.47) and (2.48), the mean coefficient of friction is given by equation (2.45).

The rotational torque is given by

$$\begin{aligned} T &= F \cdot \frac{D}{2} \\ &= \frac{F}{2} D \sin \alpha \end{aligned} \quad (2.49)$$

Combining equations (2.47) and (2.49), the mean coefficient of friction is given by equation (2.46).

Us



where μ_p = mean coefficient from consideration of reduced draw force
 μ_T = mean coefficient from consideration of torque
 p = draw force without die rotation
 p_r = draw force with die rotation
 T = torque
 F = shear force
 Q = normal force
 D_m = mean diameter

2.7.2 Split-die

If the drawing die is split in half longitudinally, and the force tending to separate the two halves during drawing is measured concurrently with the draw force, then the mean coefficient of friction and the mean die pressure can be deduced directly from these measurements. The method was originated by MacLellan⁽⁷⁷⁾ in wire-drawing. However, the experimental work did not yield conclusive results⁽⁷⁶⁾. It was postulated that this was due to the penetration of lubricant between the two halves, giving rise to an additional pressure of the unknown magnitude. The method was refined by Wistreich⁽⁷⁵⁾ wherein the two halves of the die were held by a known force which was reduced progressively until separation occurred; at this point the holding force was equated to the die separating force. The arrangement is shown in Figure (2.16). By considering the equilibrium of forces the following relations were derived:

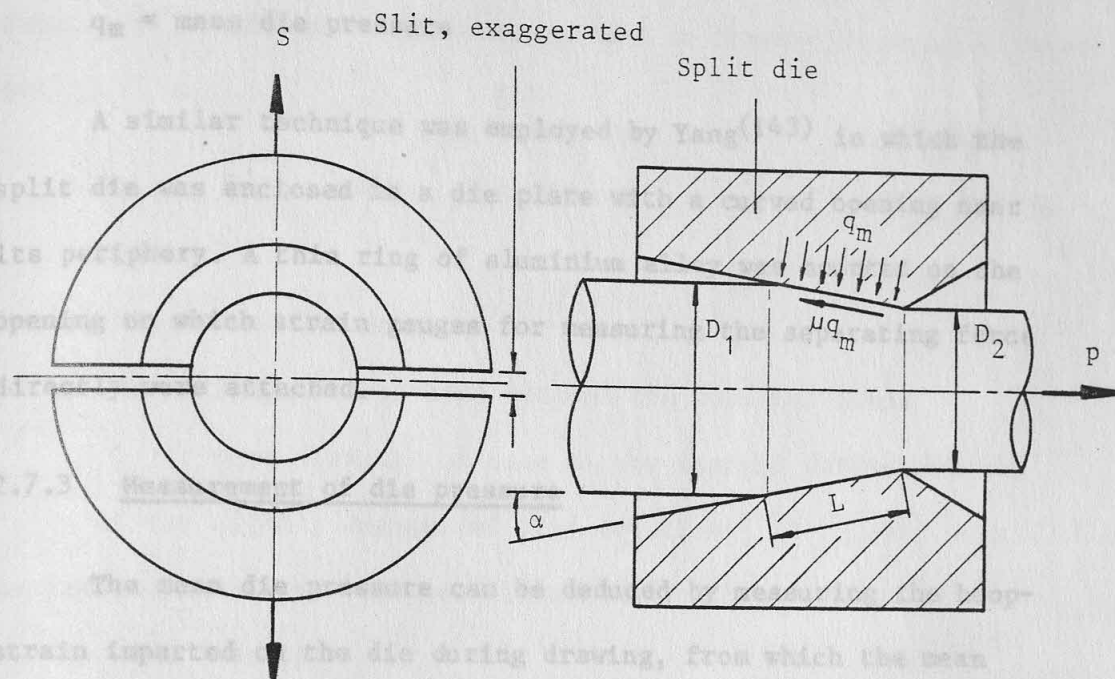
$$\mu = \tan \left(\frac{P}{\pi S} - \alpha \right) \quad (2.50)$$

$$q_m = \frac{\pi S}{(A_1 - A_2) (\cot \alpha - \mu)} \quad (2.51)$$

where p = draw force

S = die separating force

q_m = mean die pressure



S = die separating force

sufficiently wide range of hydrostatic pressures in calibration

Figure (2.16) Forces in wire-drawing with split-die (after Wistreich⁽⁷⁵⁾)

Majors⁽¹⁶⁴⁾ in wire-drawing. By summing up the longitudinal forces

Consideration of the equilibrium of the forces shown in the diagram above yields the following equations:

$$p = (A_1 - A_2)(1 + \mu \cot \alpha) q_m \quad (2.52)$$

$$S = \frac{1}{\pi} (A_1 - A_2)(\cot \alpha - \mu) q_m \quad (2.53)$$

where from which equations (2.50) and (2.51) for μ and q_m were derived.

q_m = mean die pressure

A die semi-angle of 1° was used, and although this eased the problem of calibration, it would seem to render the results unrepresentative.

The technique was adopted by Blazynski and Cole⁽⁸⁶⁾ in wire-drawing on a fixed-plug. The friction work was separated from the

where p = draw force

S = die separating force

q_m = mean die pressure

A similar technique was employed by Yang⁽¹⁴³⁾ in which the split die was enclosed in a die plate with a curved opening near its periphery. A thin ring of aluminium alloy was mounted on the opening on which strain gauges for measuring the separating force directly were attached.

2.7.3 Measurement of die pressure

The mean die pressure can be deduced by measuring the hoop-strain imparted on the die during drawing, from which the mean coefficient of friction may be obtained. However, the need for a sufficiently wide range of hydrostatic pressures in calibration can pose considerable sealing problems, and relying on extrapolation results in a second uncertainty. The technique was proposed by Majors⁽¹⁶⁴⁾ in wire-drawing. By summing up the longitudinal forces in the deformation zone, the following relation was derived:

$$\frac{\frac{\sigma}{\sigma_n}}{\frac{A_1}{A_2} - 1} - 1 = \mu \cot \alpha \quad (2.54)$$

where σ = draw stress

σ_n = mean die pressure

A die semi-angle of 1° was used, and although this eased the problem of calibration, it would seem to render the results unrepresentative.

The technique was adopted by Blazynski and Cole⁽⁸⁶⁾ in tube-drawing on a fixed-plug. The friction work was separated from the

total work done per unit volume using the concept of the "equivalent strain". The mean coefficient of friction was deduced from the frictional component of the drawing load in fixed-plug drawing given by:

$$F = 2 \mu \pi D \int_0^x \sigma_n dx \quad (2.55)$$

where σ_n = mean die pressure

x = length of contact between the tube and tools

D = mean diameter of tube at any instant during drawing

It was rightly emphasised that equation (2.55) gives only an indication of the mean coefficient of friction over the length of the tool bearing.

2.7.4 Optimum die-angle

Theories of metal-forming yield solutions of the general form:

$$\sigma = f(\mu \text{ or } m, A_1, r, Y, \alpha) \quad (2.56)$$

It is well established that for any proposed combination of geometry, material and lubricant, there will be an optimum die semi-angle which gives the minimum draw force. This arises because the redundant and frictional components of the draw force have opposed dependencies on the die semi-angle. Evans and Avitzur⁽⁸²⁾ differentiated the specific forms of equation (2.56) in wire-drawing and extrusion, with respect to α , and set the derivative to zero. The resulting equations express implicitly the relation of the optimum die semi-angle, which minimizes the working stresses, to the other variables. When the optimal angle is found experimentally, these equations serve to compute the mean coefficient of friction.

The results are, however, dependent on the experimental method in determining this exact optimum angle, and also on the effect of changing the die semi-angle which is known to alter lubrication conditions.

2.7.5 Estimation of redundant work

The estimation of redundant work can lead to the determination of friction since the power dissipated in friction would already have been determined. The method has, to some extent, been described in Section (2.6.3) in the elucidation of the energy approach.

If tension tests are conducted on the undrawn material and the resulting true stress-strain curve compared with that obtained for the drawn material, the curve for the drawn material rises above that of the undrawn material. Thus, when the curve for the drawn material is translated in the direction of the increasing strain until the two curves fit, the difference may be taken to represent the redundant strain. The corresponding redundant work W_r is calculated from the displaced area under the curve of the undrawn material (81,145,165). Graphically fitting the two curves is vulnerable to errors, particularly if the material does not work-harden rapidly. Consequently, if the stress-strain is described by equation (2.42), the mean redundant strain and redundant work are deduced analytically by the appropriate substitution of equation (2.44) into equation (2.43), leading to the derivation of W_f . By considering the equilibrium of the horizontal forces of the deformation zone, the total work done per unit volume W_t and the frictional work done per unit volume W_f can be obtained. The procedure provides three equations with two unknowns, namely the mean die pressure and mean coefficient of friction, and thus allowing their solution.

2.7.6 Back-pull

When a back-pull or back-tension is applied to the material being drawn, the required drawing force increases, but it does so by less than the magnitude of the back-pull. The explanation seems to be that the material will deform under lower compressive stresses because the tensile stress has increased and that this in turn reduces the shear stress at the die-workpiece interface. Lunt and MacLellan(83) derived an expression for the "back-pull factor" in wire-drawing from which the coefficient of friction can be deduced:

$$b = (1 + \mu \cot \alpha) r \quad (2.57)$$

However, Wistreich(58) has summarised the weaknesses of the method. The main argument was that when both the geometrical parameters and μ are small, changes in the mode of deformation are negligible, so that the only significant result is a drop in the frictional component of the forward pull. On the other hand, when these parameters are large, the change in the mode of deformation can no longer be ignored; back-pull affects also the deformation component of the pull. Nevertheless, it is worth noting that in general the geometrical parameters and the coefficient of friction in wire-drawing are relatively small and thus in most cases the method is valid.

CHAPTER 3: THEORETICAL ANALYSIS OF THE PROMOTION OF HYDRODYNAMIC LUBRICATION IN THE TUBE-DRAW PROCESS

3.1 INTRODUCTION

The tube-draw process, with the exception of tube-sinking, is unique among all axisymmetric drawing processes in that there are two tool-workpiece interfaces to be lubricated. As noted in

Chapter 1, CHAPTER 3: THEORETICAL ANALYSIS OF THE PROMOTION OF HYDRODYNAMIC LUBRICATION IN THE TUBE-DRAW PROCESS interest in the plug-tube interface.

In the review of the literature it was shown that hydrodynamic lubrication will occur provided that the lubricant pressure at the die entry is sufficiently high.

In this chapter, the analysis of the mechanics of pressure generation by induced hydrodynamic action to promote hydrodynamic lubrication at both the die-tube and plug-tube interfaces is presented. At the die-tube interface, the Christoffersen tube technique developed in the wire-drawing process was employed. The influence, on the generation of hydrodynamic pressure, of geometrical features of the Christoffersen tube, such as its length and the radial clearance between it and the drawn tube, and drawing conditions such as the speed of drawing and lubricant viscosity, were considered. "Christoffersen" tubes having

CHAPTER 3: THEORETICAL ANALYSIS OF THE PROMOTION OF HYDRODYNAMIC
LUBRICATION IN THE TUBE-DRAW PROCESS

3.1 INTRODUCTION

The tube-draw process, with the exception of tube-sinking, is unique among all axisymmetric drawing processes in that there are two tool-workpiece interfaces to be lubricated. As noted in Chapter 1, the present work involves the theoretical and experimental studies on the promotion of hydrodynamic lubrication at both interfaces, with particular interest in the plug-tube interface. In the review of the literature it was shown that hydrodynamic lubrication will occur provided that the lubricant pressure at the die entry is sufficiently high.

In this chapter, the analysis of the mechanics of pressure generation by induced hydrodynamic action to promote hydrodynamic lubrication at both the die-tube and plug-tube interfaces is presented. At the die-tube interface, the Christopherson tube technique developed in the wire-drawing process was employed. The influence, on the generation of hydrodynamic pressure, of geometrical features of the Christopherson tube, such as its length and the radial clearance between it and the undrawn tube, and drawing conditions such as the speed of drawing and lubricant viscosity, were considered. "Christopherson" tubes having

geometrical features other than a straight-parallel internal profile were studied also.

At the plug-tube interface, lubricant pressurisation was by means of the newly developed method of inducing hydrodynamic action by fitting an attachment to the plug. The analysis of the mechanics of pressure generation is similar to that obtained for the external surface; some modifications, however, were necessary. A numerical method was adopted in the solution for the hydrodynamic pressure and lubricant film thickness generated by the plug-attachment. Plug-attachments having a straight-parallel or a straight-tapered profile were considered initially. The analysis was extended to include a second parallel or tapered portion, thus forming a stepped or composite profile. A computer programme was developed to assist in the design of plug-attachments.

3.2 PROMOTION OF HYDRODYNAMIC LUBRICATION AT THE DIE-TUBE INTERFACE

Although a number of investigators, using the Christopherson tube technique to promote hydrodynamic lubrication in wire-drawing, had reported similar experimental observations, their theoretical approaches differed considerably. The original work by Christopherson and Naylor⁽⁵⁾ considered only the surrounding tube and assumed that the undrawn wire within it would take up a position associated with a minimum drag. The use of the Reynolds equation, which is the starting point for the theory of hydrodynamic lubrication, led Christopherson et al. to a fairly complex equation (equation (2.6)) describing the pressure generated within the tube in terms of two unknown variables, namely the volume rate of

lubricant flow and the position of the wire within the tube. Thus, the solution requires a numerical integration. Tattersall's theory⁽⁶⁾ considered, additionally, the metal deformation zone and by expressing the lubricant flow in terms of the thickness of the lubricant film remaining on the drawn wire allowed both the volume rate of lubricant flow and the hydrodynamic pressure generated to be predicted from entirely independent variables. Osterle and Dixon⁽⁸⁾ dismissed Christopherson and Naylor's⁽⁵⁾ minimum drag hypothesis as having no physical basis and proposed a theory which included thermal effects arising from the energy dissipated in the deforming metal and viscous shearing.

In the tube-draw process hydrodynamic lubrication at the die-tube interface can be promoted by exactly the same principles. It is therefore advantageous to analyse the conditions prevailing in tube-drawing and develop equations which can predict the hydrodynamic pressure generated and the lubricant flow rate from entirely independent variables. The theoretical analysis considers three main zones. These are the plastic deformation zone, the zone between the die entry and entry to the plastic deformation zone and the zone or zones comprising the Christopherson tube. It considers first, the lubrication conditions in the plastic deformation zone in which an equation for the constant in the Reynolds equation is derived in terms of the process parameters. An analysis of the die entry zone allows the equations to the rate of lubricant flow and the lubricant film thickness at entry to the plastic deformation zone to be developed. Since the continuity of flow demands that the rate of lubricant flow within the entire arrangement is constant, its knowledge therefore facilitates the development of an equation for the hydrodynamic pressure generated at the die entry.

This equation permits the pressure to be predicted from entirely independent variables. Its validity can be verified by comparing theoretical predictions with experimental observations.

The following assumptions are made in the theoretical analysis:

1. The radial clearance between the undrawn tube and the Christopherson tube is sufficiently small so that the one-dimensional Reynolds equation for a plane wedge can be applied.
2. The lubricant has Newtonian properties.
3. The lubricant obeys the exponential viscosity-pressure law, $\eta = \eta_0 e^{\phi P}$.
4. Isothermal conditions prevail.
5. The die and plug remain rigid.
6. The undrawn tube and the Christopherson tube do not deform.
7. The undrawn tube travels concentrically with respect to the Christopherson tube.
8. Thin-walled tubes are considered.

3.2.1 Hydrodynamic analysis of the plastic deformation zone

With reference to the origin chosen as in Figure (3.1), the integral form of the Reynolds equation is

$$\frac{dP}{dx} = -6\eta U_3 \left(\frac{h - h_m}{h^3} \right) \quad (3.1)$$

Taking into account the exponential viscosity-pressure relationship $\eta = \eta_0 e^{\phi P}$, this may be written as

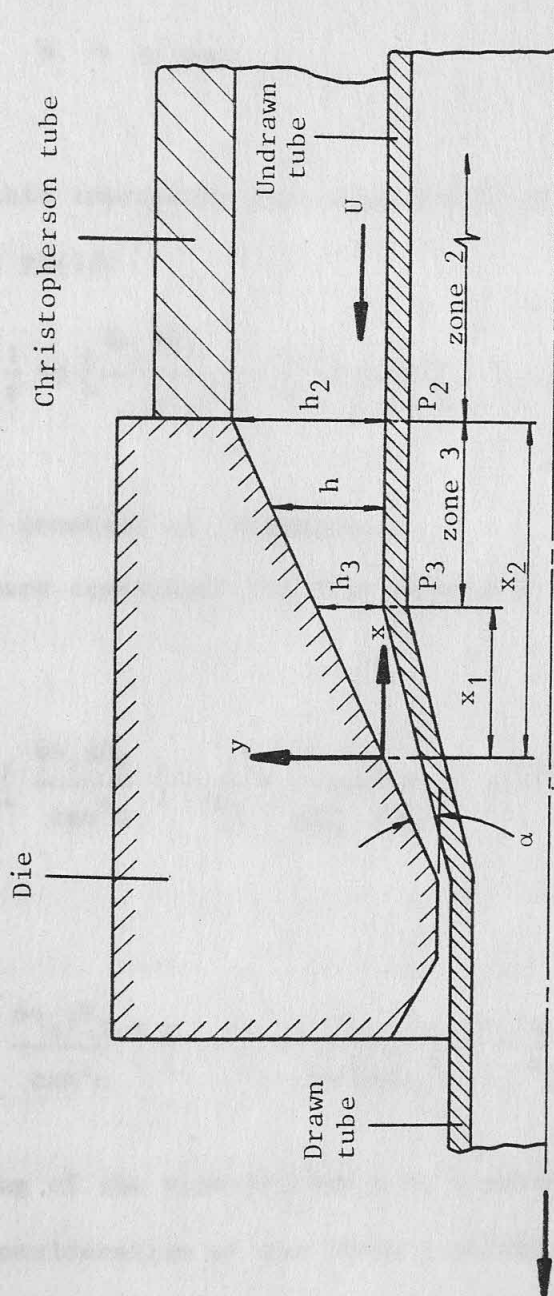


Figure (3.1) Details of lubricant film geometry

$$e^{-\phi P} \frac{dP}{dx} = -6\eta_0 U_3 \left(\frac{h - h_m}{h^3} \right) \quad (3.2)$$

The lubricant film thickness at any point in the die entry zone (zone 3) is given by

$$h = x \tan \alpha \quad (3.3)$$

Substituting this expression into equation (3.2) and upon integration it yields

$$P = -\frac{1}{\phi} \ln \left[\frac{6\eta_0 \phi U_3}{\tan^2 \alpha} \left(-\frac{1}{x} + \frac{h_m}{2x^2 \tan \alpha} \right) - \phi A \right] \quad (3.4)$$

where A is the constant of integration.

The boundary conditions for this equations are $P = P_2$ at $x = x_2$. Thus

$$A = \frac{1}{\phi} \left[\frac{6\eta_0 \phi U_3}{\tan^2 \alpha} \left(-\frac{1}{x_2} + \frac{h_m}{2x_2^2 \tan \alpha} \right) - e^{-\phi P_2} \right] \quad (3.5)$$

and

$$P = -\frac{1}{\phi} \ln \left\{ \frac{6\eta_0 \phi U_3}{\tan^2 \alpha} \left[\left(-\frac{1}{x} + \frac{h_m}{2x^2 \tan \alpha} \right) - \left(-\frac{1}{x_2} + \frac{h_m}{2x_2^2 \tan \alpha} \right) \right] + e^{-\phi P_2} \right\} \quad (3.6)$$

If yielding of the tube initiates at a point where $x = x_1$ and $h = h_3$, by a consideration of the yield criterion, the mean axial stress in the tube, the pressure exerted by the die, and the yield stress of the tube material at this plane may be related by

$$\sigma + P = Y \quad (3.7)$$

However, at this plane the mean axial stress σ is zero. Thus, the lubricant pressure P_3 can be equated to the yield stress of the tube material Y . Substituting these conditions into equation (3.6) gives

$$P_3 = Y = -\frac{1}{\phi} \ln \left\{ \frac{6\eta_0 \phi U_3}{\tan^2 \alpha} \left[\left(-\frac{1}{x_1} + \frac{h_m}{2x_1^2 \tan \alpha} \right) - \left(-\frac{1}{x_2} + \frac{h_m}{2x_2^2 \tan \alpha} \right) \right] + e^{-\phi P_2} \right\} \quad (3.8)$$

This can be rearranged and written as

$$h_m = \frac{2 \tan \alpha (x_1 x_2)}{(x_1 + x_2)} + \frac{\tan^3 \alpha (x_1 x_2)^2}{3\eta_0 \phi U_3 (x_1^2 - x_2^2)} \cdot B \quad (3.9)$$

where $B = (e^{-\phi P_2} - e^{-\phi Y})$

By equation (3.3), $x_1 = \frac{h_3}{\tan \alpha}$ and $x_2 = \frac{h_2}{\tan \alpha}$, hence

$$h_m = \frac{2h_2 h_3}{(h_2 + h_3)} + \frac{\tan \alpha (h_2 h_3)^2}{3\eta_0 \phi U_3 (h_3^2 - h_2^2)} \cdot B \quad (3.10)$$

The derivation of equation (3.10) essentially follows the route suggested by Bloor, Dowson and Parsons⁽⁹⁴⁾, however, it must be emphasized that they were considering plane strain drawing under normal conditions. Thus, the inclusion of the term B in equation (3.10) is an extension which considers contributions from the induced hydrodynamic action.

3.2.2 Lubricant film thickness at entry to the plastic deformation zone

The volume rate of lubricant flow, q , per unit circumference of

the tube in terms of the pressure gradient $\frac{dP}{dx}$ in the Reynolds equation is obtained by

$$q = \frac{U_3 h}{2} + \frac{h^3}{12\eta_0} e^{-\phi P} \frac{dP}{dx} \quad (3.11)$$

Substituting for $e^{-\phi P} \frac{dP}{dx}$ as in equation (3.2), the volume rate of flow per unit circumference of the tube in the die entry zone is given by

$$q_3 = \frac{U_3 h_m}{2} \quad (3.12)$$

At the entry to the plastic deformation zone, the mean axial tensile stress in the tube is equal to the plastic work done per unit volume of the tube material. Thus,

$$\sigma = \int_0^{\epsilon} Y d\epsilon, \quad \frac{d\sigma}{d\epsilon} = Y \quad (3.13)$$

From equations (3.7) and (3.13),

$$\frac{dP_3}{d\epsilon} = \frac{dY}{d\epsilon} - Y \quad (3.14)$$

In the plastic deformation zone

$$dx = dR \cot \alpha \quad (3.15)$$

$$d\epsilon = \frac{2dR}{R} \quad (3.16)$$

where R = radius of tube.

Hence,

$$d\epsilon = \frac{2dx \tan\alpha}{R} \quad (3.17)$$

Substituting for $d\epsilon$ as in equation (3.17) into equation (3.14) and rearranging

$$\frac{dP_3}{dx} = \left(\frac{RdY}{2dx \tan\alpha} - Y \right) \frac{2\tan\alpha}{R} \quad (3.18)$$

When $\alpha \approx 0$ as at the plane considered, $\frac{dP_3}{dx} = 0$. Hence the application of equation (3.11) for the volume rate of lubricant flow reduces to

$$q_3 = \frac{U_3 h_3}{2} \quad (3.19)$$

Alternatively, equation (3.19) may be arrived at by considering the fact that in this zone the second term on the right-hand side of equation (3.11) is negligibly small since $e^{-\phi P_3} = e^{-\phi Y}$ is also negligibly small (of the order of 10^{-10}).

It follows from equations (3.12) and (3.19) that

$$h_m = h_3 \quad (3.20)$$

A good approximation to the lubricant film thickness at the entry to the plastic deformation zone can therefore be obtained by equating h_3 to h_m in equation (3.10). This can be simplified and rearranged as a quadratic in h_3 ,

$$h_3^2 - h_3 \left(2h_2 + \frac{h_2^2 \tan\alpha}{3\eta_0 \phi U_3} \cdot B \right) + h_2^2 = 0 \quad (3.21)$$

Since the lubricant film thickness must take a positive value, it can be shown that the solution of this quadratic equation is

$$h_3 = \left(h_2 + \frac{h_2^2 B \tan \alpha}{6\eta_0 \phi U_3} \right) - \sqrt{\left(\frac{h_2^2 B \tan \alpha}{6\eta_0 \phi U_3} \right)^2 + \frac{2h_2^3 B \tan \alpha}{6\eta_0 \phi U_3}} \quad (3.22)$$

However, the term B contains P_2 , the lubricant pressure at the die entry generated by the Christopherson tube. Consequently, equation (3.22) is amenable to a direct solution provided that the magnitude of P_2 is known. Equation (3.21) can be rearranged to give P_2 as

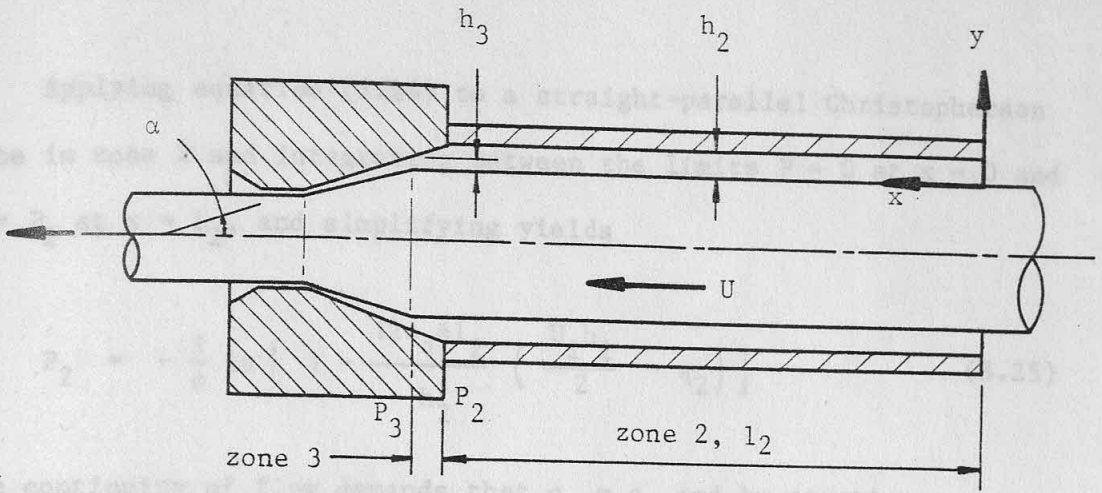
$$P_2 = -\frac{1}{\phi} \ln \left[\frac{(h_3 - h_2)^2}{h_3} \cdot \frac{3\eta_0 \phi U_3}{h_2^2 \tan \alpha} + e^{-\phi Y} \right] \quad (3.23)$$

3.2.3 Analysis of Christopherson tubes

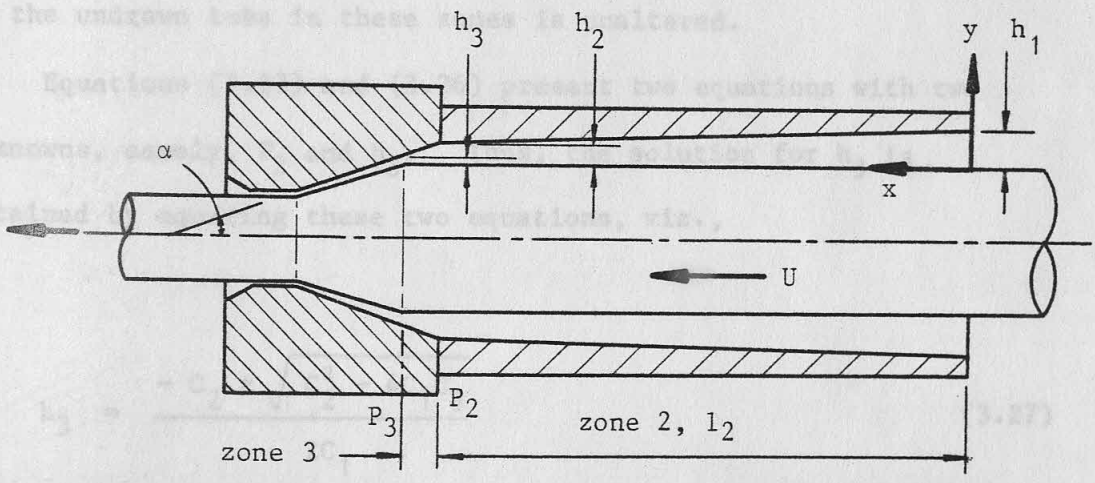
The two basic internal profiles of the Christopherson tubes considered in this section of the theoretical analysis are i) straight-parallel and ii) straight-tapered. These are illustrated in zone 2 of Figure (3.2). The detail analyses of the extensions to these basic profiles, thus forming a stepped or a composite Christopherson tube, are included also.

The origins of the co-ordinate systems are chosen at the beginning of each zone so that the Reynolds equation for the lubricant film pressure gradient at any point, taking into account the increase in viscosity due to pressure can be written as

$$e^{-\phi P} \frac{dP}{dx} = \frac{12\eta_0}{h^3} \left(\frac{Uh}{2} - q \right) \quad (3.24)$$



(a) Straight-parallel Christopherson tube



(b) Straight-tapered Christopherson tube

Figure (3.2) Analysis of Christopherson tubes

3.2.3.1 Straight-parallel Christopherson tube

Applying equation (3.24) to a straight-parallel Christopherson tube in zone 2 and integrating between the limits $P = 0$ at $x = 0$ and $P = P_2$ at $x = l_2$, and simplifying yields

$$P_2 = -\frac{1}{\phi} \ln \left[1 - \frac{12\eta_0 \phi l_2}{h_2^3} \left(\frac{U_2 h_2}{2} - q_2 \right) \right] \quad (3.25)$$

The continuity of flow demands that $q_2 = q_3$ and by equation (3.19), equation (3.25) may be simplified to read

$$P_2 = -\frac{1}{\phi} \ln \left[1 - \frac{6\eta_0 \phi U l_2}{h_2^3} (h_2 - h_3) \right] \quad (3.26)$$

the subscripts for the velocity terms are omitted since the velocity of the undrawn tube in these zones is unaltered.

Equations (3.23) and (3.26) present two equations with two unknowns, namely, P_2 and h_3 . Thus, the solution for h_3 is obtained by equating these two equations, viz.,

$$h_3 = \frac{-C_2 \pm \sqrt{C_2^2 - 4C_1 C_3}}{2C_1} \quad (3.27)$$

where $C_1 = (h_2 - 2l_2 \tan \alpha)$

$$C_2 = 2h_2 \left[l_2 \tan \alpha - h_2 - \frac{h_2^2 \tan \alpha (1 - e^{-\phi Y})}{6\eta_0 \phi U} \right] \quad (3.28)$$

$$C_3 = h_2^3 \quad (3.29)$$

3.2.3.2 Straight-tapered Christopherson tube

The case, is considered, of a straight-tapered Christopherson tube in zone 2. If h is the radial clearance at any point within this zone, by simple geometry

$$h = h_2 \left(1 + K - \frac{K}{l_2} x \right) \quad (3.28)$$

$$\text{where } K = \frac{h_1 - h_2}{h_2} \quad \text{ie. } \frac{h_1}{h_2} = 1 + K$$

Substituting equation (3.28) for h in equation (3.24), the pressure distribution of a straight-tapered Christopherson tube is

$$e^{-\phi P} \frac{dP}{dx} = 12\eta_0 \left[\frac{U_2}{2h_2^2 \left(1 + K - \frac{K}{l_2} x \right)^2} - \frac{q_2}{h_2^3 \left(1 + K - \frac{K}{l_2} x \right)^3} \right] \quad (3.29)$$

Integrating between the limits $P = 0$ at $x = 0$ and $P = P_2$ at $x = l_2$, and simplifying,

$$P_2 = -\frac{1}{\phi} \ln \left\{ 1 - \frac{6\eta_0 \phi l_2}{h_2^3 (1+K)} \left[U_2 h_2 - q_2 \left(\frac{2+K}{1+K} \right) \right] \right\} \quad (3.30)$$

Applying the conditions that $q_2 = q_3$ and $U_2 = U_3 = U$, and by equation (3.19), equation (3.30) may be simplified to read

$$P_2 = -\frac{1}{\phi} \ln \left\{ 1 - \frac{6\eta_0 \phi U l_2^{(2+K)}}{2h_2^3 (1+K)^2} \left[\frac{2(1+K)}{(2+K)} h_2 - h_3 \right] \right\} \quad (3.31)$$

It is noted that equation (3.31) reduces to equation (3.26) for a straight-parallel Christopherson tube when $K = 0$, ie. $h_1 = h_2$.

The solution for h_3 in this case is obtained by equating equation (3.23) to (3.31), viz.,

$$h_3 = \frac{-D_2 \pm \sqrt{D_2^2 - 4D_1 D_3}}{2D_1} \quad (3.32)$$

$$\text{where } D_1 = 2 \left[h_2(1 + K) - l_2 \left(\frac{2 + K}{1 + K} \right) \tan \alpha \right]$$

$$D_2 = 4h_2 \left[l_2 \tan \alpha - h_2(1 + K) - \frac{h_2^2 \tan \alpha (1 + K) (1 - e^{-\phi Y})}{6\eta_0 \phi U} \right]$$

$$D_3 = 2h_2^3 (1 + K)$$

3.2.4 Analysis of two-zone Christopherson tubes

The analysis so far was confined to zone 2 where the Christopherson tube has either a straight-parallel or straight-tapered internal profile. If zone 2 is extended to include zone 1 which is of a different geometry [Figure (3.3)], a two-zone Christopherson tube is formed. This may consist of either a straight-parallel portion resulting in the stepped configuration or a straight-tapered portion to form the composite configuration.

3.2.4.1 Stepped Christopherson tube

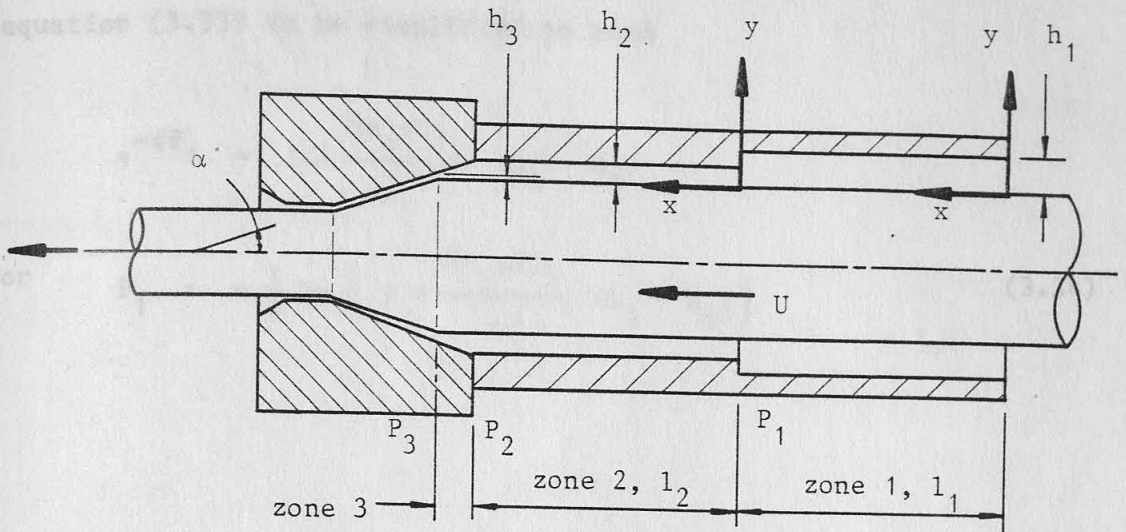
Applying equation (3.24) to the straight-parallel portion in zone 1 and integrating between the limits $P = 0$ at $x = 0$ and $P = P_1$ at $x = l_1$, and simplifying,

$$e^{-\phi P_1} = 1 - \frac{12\eta_0 \phi l_1}{h_1^3} \left(\frac{U_1 h_1}{2} - q_1 \right)$$

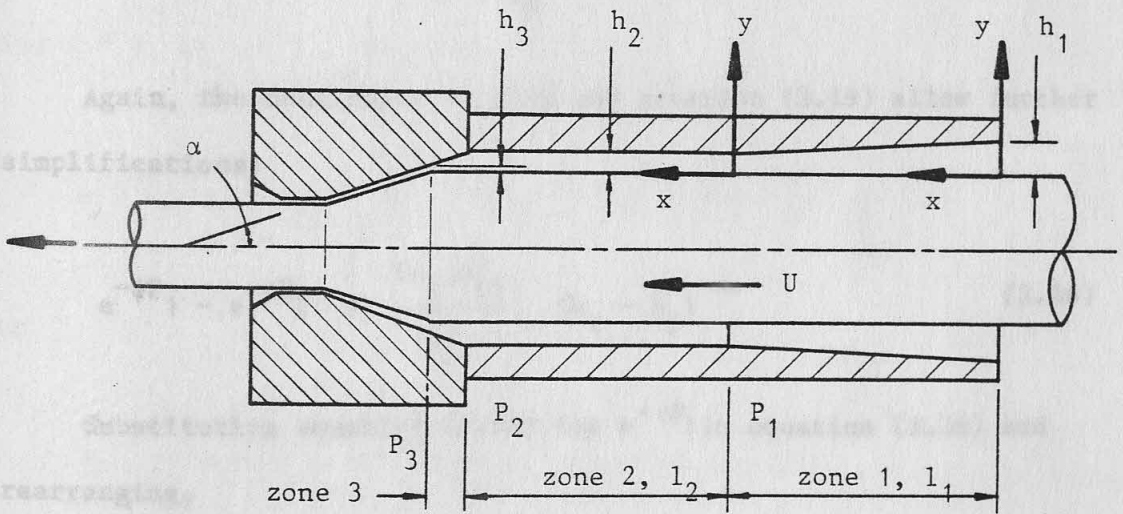
or

(3.33)

$$P_1 = -\frac{1}{\phi} \ln \left[1 - \frac{12\eta_0 \phi l_1}{h_1^3} \left(\frac{U_1 h_1}{2} - q_1 \right) \right]$$



(a) Stepped Christopherson tube



(b) Composite Christopherson tube

Figure (3.3) Analysis of two-zone Christopherson tubes

(3.37) The condition that $q_1 = q_2 = q_3$ and equation (3.19) allow equation (3.33) to be simplified to read

$$e^{-\phi P_1} = 1 - \frac{6\eta_0 \phi U l_1}{h_1^3} (h_1 - h_3) \quad (3.38)$$

or

$$P_1 = -\frac{1}{\phi} \ln \left[1 - \frac{6\eta_0 \phi U l_1}{h_1^3} (h_1 - h_3) \right] \quad (3.34)$$

Integrating equation (3.24) for zone 2 between the limits $P = P_1$ at $x = 0$ and $P = P_2$ at $x = l_2$, and simplifying,

$$-\frac{1}{\phi} e^{-\phi P_2} + \frac{1}{\phi} e^{-\phi P_1} = \frac{12\eta_0 l_2}{h_2^3} \left(\frac{U_2 h_2}{2} - q_2 \right) \quad (3.35)$$

Again, the continuity of flow and equation (3.19) allow further simplifications:

$$e^{-\phi P_1} - e^{-\phi P_2} = \frac{6\eta_0 \phi U l_2}{h_2^3} (h_2 - h_3) \quad (3.36)$$

Substituting equation (3.34) for $e^{-\phi P_1}$ in equation (3.36) and rearranging,

$$e^{-\phi P_2} = 1 - 6\eta_0 \phi U \left[\frac{1}{h_1^3} (h_1 - h_3) + \frac{1}{h_2^3} (h_2 - h_3) \right] \quad (3.37)$$

$$P_2 = -\frac{1}{\phi} \ln \left\{ 1 - 6\eta_0 \phi U \left[\frac{1}{h_1^3} (h_1 - h_3) + \frac{1}{h_2^3} (h_2 - h_3) \right] \right\}$$

The solution for h_3 is obtained by equating equation (3.23) to

(3.37), viz.,

$$h_3 = \frac{-E_2 \pm \sqrt{E_2^2 - 4E_1E_3}}{2E_1} \quad (3.38)$$

where $E_1 = 6\eta_0 \phi U \left(\frac{1}{2h_2^2 \tan \alpha} - \frac{1}{h_1^3} - \frac{1}{h_2^3} \right)$

$$E_2 = - \left\{ 6\eta_0 \phi U \left(\frac{1}{h_2 \tan \alpha} - \frac{1}{h_1^2} - \frac{1}{h_2^2} \right) + (1 - e^{-\phi Y}) \right\}$$

$$E_3 = \frac{3\eta_0 \phi U}{\tan \alpha} \quad (3.41)$$

3.2.4.2 Composite Christopherson tube

Applying equations (3.24) and (3.28) to the straight-tapered portion in zone 1 and integrating between the limits $P = 0$ at $x = 0$ and $P = P_1$ at $x = l_1$, and simplifying,

$$e^{-\phi P_1} = 1 - \frac{6\eta_0 \phi l_1}{h_2^3(1+K)} \left[U_1 h_2 - q_1 \left(\frac{2+K}{1+K} \right) \right]$$

or (3.39)

$$P_1 = -\frac{1}{\phi} \ln \left\{ 1 - \frac{6\eta_0 \phi l_1}{h_2^3(1+K)} \left[U_1 h_2 - q_1 \left(\frac{2+K}{1+K} \right) \right] \right\}$$

Similarly, by the continuity of flow and by equation (3.19), equation (3.39) may be simplified to read

$$e^{-\phi P_1} = 1 - \frac{6\eta_0 \phi U l_1 (2+K)}{2h_2^3 (1+K)^2} \left[\frac{2(1+K)}{(2+K)} h_2 - h_3 \right]$$

or (3.40)

$$P_1 = -\frac{1}{\phi} \ln \left\{ 1 - \frac{6\eta_0 \phi U l_1 (2+K)}{2h_2^3 (1+K)^2} \left[\frac{2(1+K)}{(2+K)} h_2 - h_3 \right] \right\}$$

For the straight-parallel portion in zone 2, equation (3.36) applies. Hence substituting equation (3.40) for $e^{-\phi P_1}$ into equation (3.36) and rearranging,

$$e^{-\phi P_2} = 1 - 3\eta_0 \phi U \left\{ \frac{1}{h_2^3} \frac{(2+K)}{(1+K)^2} \left[\frac{2(1+K)}{(2+K)} h_2 - h_3 \right] + \frac{21_2}{h_2^3} (h_2 - h_3) \right\} \quad (3.41)$$

or

$$P_2 = -\frac{1}{\phi} \ln \left\{ 1 - 3\eta_0 \phi U \left\{ \frac{1}{h_2^3} \frac{(2+K)}{(1+K)^2} \left[\frac{2(1+K)}{(2+K)} h_2 - h_3 \right] + \frac{21_2}{h_2^3} (h_2 - h_3) \right\} \right\}$$

Equating equation (3.23) to (3.41), h_3 is given by

$$h_3 = -F_2 \pm \sqrt{F_2^2 - 4F_1 F_3} \quad (3.42)$$

where $F_1 = \frac{6\eta_0 \phi U}{h_2^2} \left[\frac{2F_1}{2 \tan \alpha} - \frac{1_1(2+K)}{2h_2(1+K)^2} - \frac{1_2}{h_2} \right]$

$$F_2 = - \left\{ \frac{6\eta_0 \phi U}{h_2} \left[\frac{1}{\tan \alpha} - \frac{1_1}{h_2(1+K)} - \frac{1_2}{h_2} \right] + (1 - e^{-\phi Y}) \right\}$$

$$F_3 = \frac{3\eta_0 \phi U}{\tan \alpha}$$

3.3 DETERMINATION OF THE HYDRODYNAMIC PRESSURE AND LUBRICANT FILM THICKNESS

The technique of analysis of the Christopherson tubes has, in each case, provided two equations with two unknown quantities; namely, P_2 the hydrodynamic pressure generated at the die entry and

h_3 the lubricant film thickness at the plane of the initiation of plastic deformation. The theoretical values of these parameters are computed by equating equation (3.23) for P_2 , derived by the analyses of the die entry and plastic deformation zones, to the equations for P_2 derived by the analyses of the Christopherson tubes. Thus, the elimination of P_2 allows computation of the appropriate values of h_3 . The knowledge of h_3 in turn facilitates the computation of the generated hydrodynamic pressure. These are illustrated in the flow-chart in Figure (3.4). Furthermore, the lubricant flow rate is obtained by substituting the value of h_3 into equation (3.19).

3.4 PROMOTION OF HYDRODYNAMIC LUBRICATION AT THE PLUG-TUBE INTERFACE

The mechanics of lubricant pressurization in the bore of the tube by induced hydrodynamic action is analysed in this section. The theoretical approach parallels that adopted in the analysis of the Christopherson tubes, although some fundamental modifications are necessary. Precise close-pass tube-drawing does not exist. Thus, with reference to Figure (3.5), the sink zone is defined as that region in the bore of the deforming tube lying between the plane of the initiation of sinking and that at which the bore surface of the tube comes into contact with the plug. It is therefore possible for the end of the attachment, which is conveniently chamfered at an angle equal to the die semi-angle, to take any of the four positions illustrated in Figures (3.5a - 3.5d). In practice, however, the length of the sink zone is necessarily short. Thus, in the theoretical analysis it is assumed that any

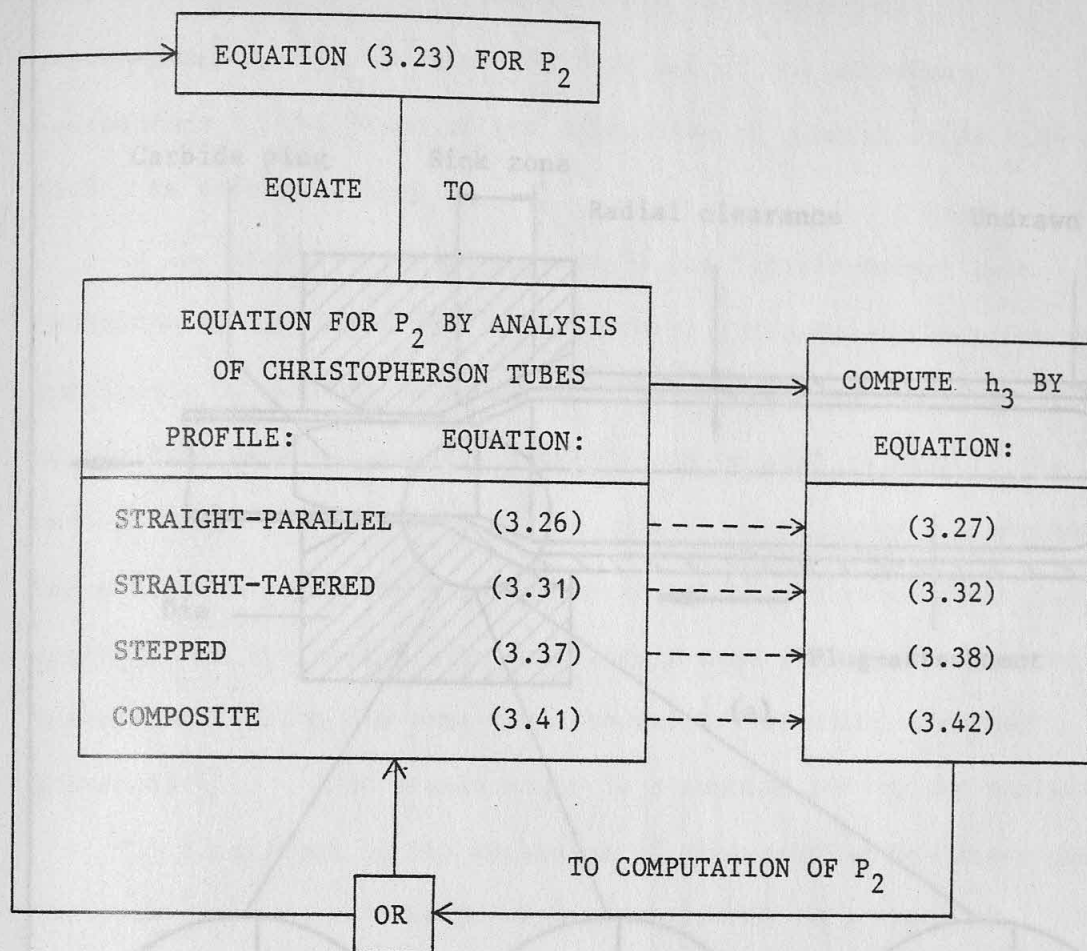
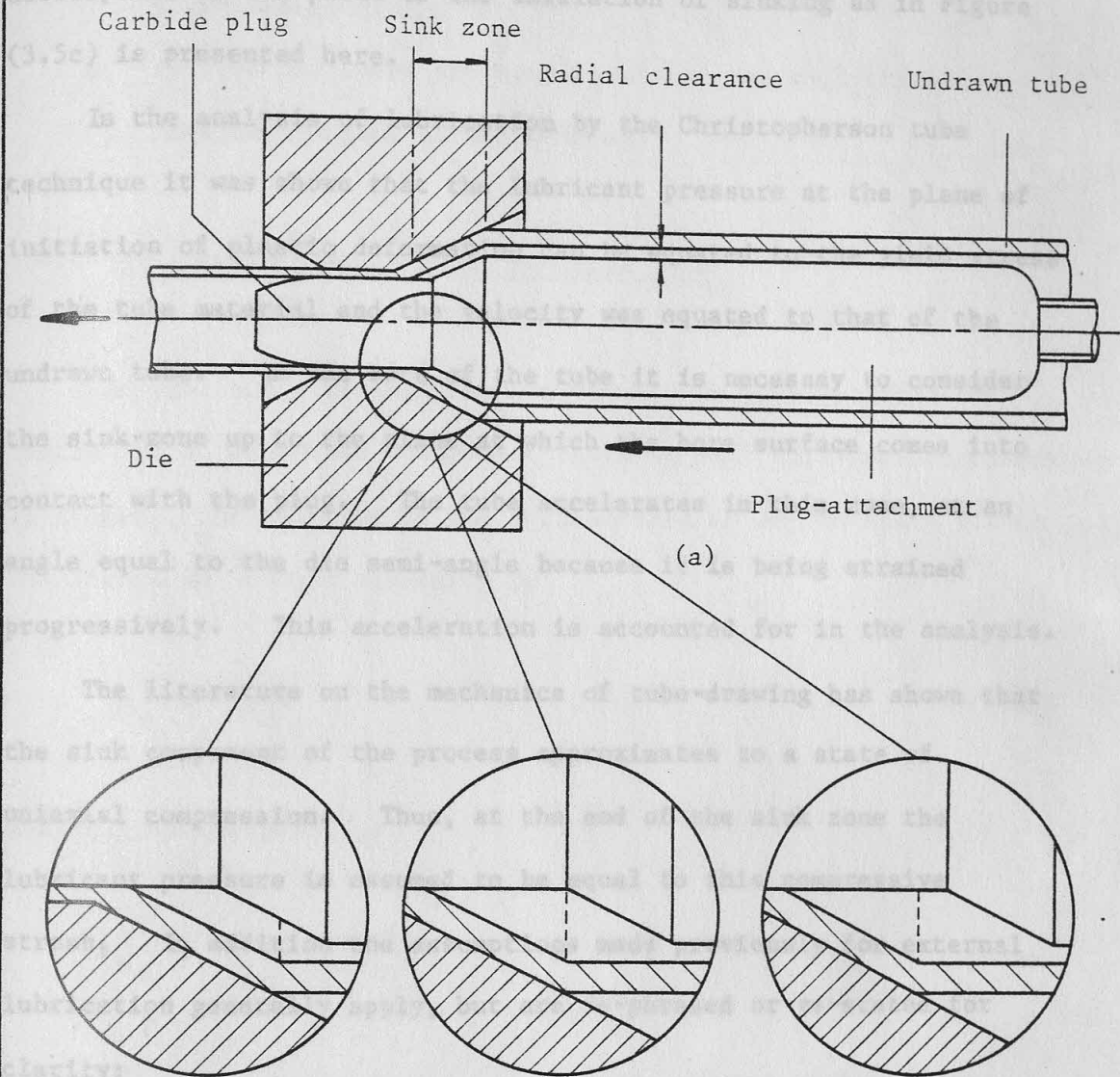


Figure (3.4) Computing procedure for the theoretical results of the Christopherson tubes

differences in these four positions are insignificant. A representative case in which the fore end of the attachment corresponds to the plane of the initiation of sinking as in Figure (3.5c) is presented here.



1. The radial clearance between the bore of the undrawn tube and the attachment is sufficiently small so that the two-dimensional Reynolds equation for a plane wedge can be applied.

2. Figure (3.5) Possible positions of plug-attachment within the sink zone

3. The lubricant obeys the exponential viscosity-pressure law,

$$\eta = \eta_0 e^{\alpha p}$$
4. Isothermal conditions prevail.
5. The plug and die remain rigid.

differences in these four positions are insignificant. A representative case in which the fore end of the attachment corresponds to the plane of the initiation of sinking as in Figure (3.5c) is presented here.

In the analysis of lubrication by the Christopherson tube technique it was shown that the lubricant pressure at the plane of initiation of plastic deformation can be equated to the yield stress of the tube material and the velocity was equated to that of the undrawn tube. In the bore of the tube it is necessary to consider the sink-zone up to the plane at which the bore surface comes into contact with the plug. The tube accelerates in this zone, at an angle equal to the die semi-angle because it is being strained progressively. This acceleration is accounted for in the analysis.

The literature on the mechanics of tube-drawing has shown that the sink component of the process approximates to a state of uniaxial compression. Thus, at the end of the sink zone the lubricant pressure is assumed to be equal to this compressive stress. In addition the assumptions made previously for external lubrication generally apply, but are re-phrased or re-stated for clarity:

1. The radial clearance between the bore of the undrawn tube and the attachment is sufficiently small so that the one-dimensional Reynolds equation for a plane wedge can be applied.
2. The lubricant has Newtonian properties.
3. The lubricant obeys the exponential viscosity-pressure law,
$$\eta = \eta_0 e^{\phi P}.$$
4. Isothermal conditions prevail.
5. The plug and die remain rigid.

6. The undrawn tube and the plug-attachment do not deform.
7. The undrawn tube travels concentrically with respect to the plug-attachment.
8. Thin-walled tubes are considered and the wall thickness remains constant during sinking.

3.4.1 Hydrodynamic analysis of the sink zone

Consider the sink zone (zone 4) in Figure (3.6). From the continuity of workpiece volume and assuming wall thickness constancy in sinking, the velocity of the bore surface at any radius R within the sink-zone changes according to

$$U_s = U \frac{R_i}{R} \quad (3.43)$$

This can be expressed as

$$U_s = U_3 \left(\frac{h_3 + R_p}{h + R_p} \right) \quad (3.44)$$

With the chosen origin for the co-ordinate system, the lubricant film thickness within the sink zone is given by

$$h = x \tan \alpha \quad (3.45)$$

Thus, the velocity of the bore surface in this zone can be written

$$U_s = U \left[\frac{(h_3 + R_p)}{(x \tan \alpha + R_p)} \right] \quad (3.46)$$

Substituting equations (3.45) and (3.46) for the film thickness and

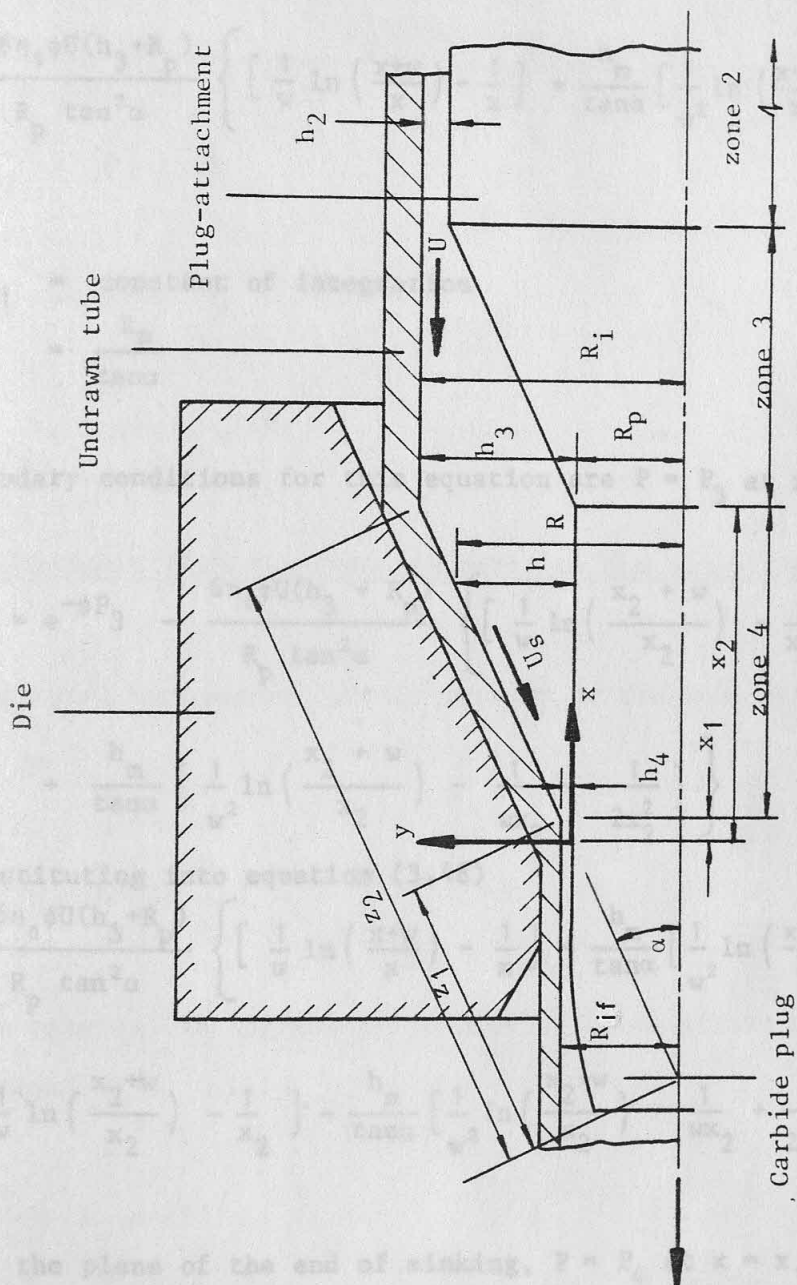


Figure (3.6) Details of the sink zone

the velocity terms respectively into the Reynolds equation as in equation (3.2)

$$e^{-\phi P} \frac{dP}{dx} = -6\eta_0 U \left[\frac{(h_3 + R_p)}{(x \tan \alpha + R_p)} \right] \left[\frac{1}{(x \tan \alpha)^2} - \frac{h_m}{(x \tan \alpha)^3} \right] \quad (3.47)$$

and upon integration it yields

$$e^{-\phi P} = \frac{6\eta_0 \phi U (h_3 + R_p)}{R_p \tan^2 \alpha} \left\{ \left[\frac{1}{w} \ln \left(\frac{x+w}{x} \right) - \frac{1}{x} \right] + \frac{h_m}{\tan \alpha} \left[\frac{1}{w^2} \ln \left(\frac{x+w}{x} \right) - \frac{1}{wx} + \frac{1}{2x^2} \right] \right\} + A_1 \quad (3.48)$$

where A_1 = constant of integration

$$w = \frac{R_p}{\tan \alpha}$$

The boundary conditions for this equation are $P = P_3$ at $x = x_2$.

Thus

$$A_1 = e^{-\phi P_3} - \frac{6\eta_0 \phi U (h_3 + R_p)}{R_p \tan^2 \alpha} \left\{ \left[\frac{1}{w} \ln \left(\frac{x_2 + w}{x_2} \right) - \frac{1}{x_2} \right] + \frac{h_m}{\tan \alpha} \left[\frac{1}{w^2} \ln \left(\frac{x_2 + w}{x_2} \right) - \frac{1}{wx_2} + \frac{1}{2x_2^2} \right] \right\} \quad (3.49)$$

and substituting into equation (3.48)

$$e^{-\phi P} = \frac{6\eta_0 \phi U (h_3 + R_p)}{R_p \tan^2 \alpha} \left\{ \left[\frac{1}{w} \ln \left(\frac{x+w}{x} \right) - \frac{1}{x} \right] + \frac{h_m}{\tan \alpha} \left[\frac{1}{w^2} \ln \left(\frac{x+w}{x} \right) - \frac{1}{wx} + \frac{1}{2x^2} \right] - \left[\frac{1}{w} \ln \left(\frac{x_2 + w}{x_2} \right) - \frac{1}{x_2} \right] - \frac{h_m}{\tan \alpha} \left[\frac{1}{w^2} \ln \left(\frac{x_2 + w}{x_2} \right) - \frac{1}{wx_2} + \frac{1}{2x_2^2} \right] \right\} + e^{-\phi P_3} \quad (3.50)$$

At the plane of the end of sinking, $P = P_4$ at $x = x_1$ and

substituting these conditions into equation (3.50) gives

$$e^{-\phi P_4} = \frac{6\eta_0 \phi U (h_3 + R_p)}{R_p \tan^2 \alpha} \left\{ \left[\frac{1}{w} \ln \left(\frac{x_1 + w}{x_1} \right) - \frac{1}{x_1} \right] + \frac{h_m}{\tan \alpha} \left[\frac{1}{w^2} \ln \left(\frac{x_1 + w}{x_1} \right) - \frac{1}{wx_1} + \frac{1}{2x_1^2} \right] - \left[\frac{1}{w} \ln \left(\frac{x_2 + w}{x_2} \right) - \frac{1}{x_2} \right] - \frac{h_m}{\tan \alpha} \left[\frac{1}{w^2} \ln \left(\frac{x_2 + w}{x_2} \right) - \frac{1}{wx_2} + \frac{1}{2x_2^2} \right] \right\} + e^{-\phi P_3} \quad (3.51)$$

By equation (3.45), $x_1 = \frac{h_4}{\tan \alpha}$ and $x_2 = \frac{h_3}{\tan \alpha}$. Upon substituting these values into equation (3.51), it may be rearranged and simplified to give

$$h_m = \frac{\ln(\zeta_2/\zeta_1) + R_p \left(\frac{1}{h_3} - \frac{1}{h_4} \right)}{\frac{1}{R_p} \ln(\zeta_1/\zeta_2) + \left(\frac{1}{h_4} - \frac{1}{h_3} \right) + \frac{R_p}{2} \left(\frac{1}{h_3^2} - \frac{1}{h_4^2} \right)} + \frac{R_p^2 \tan \alpha B_1}{6\eta_0 \phi U (h_3 + R_p) \left[\frac{1}{R_p} \ln(\zeta_1/\zeta_2) + \left(\frac{1}{h_4} - \frac{1}{h_3} \right) + \frac{R_p}{2} \left(\frac{1}{h_3^2} - \frac{1}{h_4^2} \right) \right]} \quad (3.52)$$

$$\text{where } \zeta_1 = \left(1 + \frac{R_p}{h_3} \right)$$

$$\zeta_2 = \left(1 + \frac{R_p}{h_4} \right)$$

$$B_1 = e^{-\phi P_3} - e^{-\phi P_4}$$

3.4.2 Lubricant film thickness at entry to the plug-tube interface

The total homogeneous strain imposed on the tube as a result of sinking is

$$\epsilon_s = \ln \frac{A_1}{A_s} \quad (3.53)$$

The tube material is assumed to possess a stress-strain relationship of the form

$$\sigma = \sigma' \epsilon^n \quad (3.54)$$

Thus combining equations (3.53) and (3.54), the plug-tube interface can be obtained by equating h_4 to h_m in equation (3.52), but see page 126. However, $\sigma = \sigma' \left(\ln \frac{A_1}{A_s} \right)^n$ (3.55)

Since the sink component approximates to a state of uniaxial compression, σ in equation (3.55) approximates the compressive stress on the plane where sinking terminates. At this plane it is assumed that the radial stress can be equated to the lubricant pressure P_4 . Thus

$$P_4 = \sigma' \left(\ln \frac{A_1}{A_s} \right)^n \quad (3.56)$$

Furthermore, at this plane the bore surface velocity is given by

$$U_s = Uz \quad (3.57)$$

where $z = \frac{z_2}{z_1} = \frac{R_i}{R_{if}}$ since profiles were considered initially. These were the straight-parallel $z_1 = \frac{R_{if}}{\sin \alpha} \approx \frac{R_p}{\sin \alpha}$ profiles. Extensions were made to include a second parallel or tapered portion, thus forming a stepped

$$\text{and } z_2 = \frac{R_i}{\sin \alpha} \quad (3.59)$$

Applying equation (3.19) to the sink zone, the lubricant flow rate in terms of the bore surface velocity by equation (3.57) and the lubricant film thickness at the end of sinking can be written as

$$q_4 = \frac{Uzh_4}{2} \quad (3.60)$$

by equation (3.20) $h_4 = h_m$. Thus, a good approximation to the lubricant film thickness at the entry to the plug-tube interface can be obtained by equating h_4 to h_m in equation (3.52), but see page 136. However, unlike external lubrication, h_4 cannot be separated easily from the other terms, but the equation may be rearranged to

give the hydrodynamic pressure generated at the entry to the sink zone P_3 as

$$P_3 = -\frac{1}{\phi} \ln \left\{ \left[h_4 - \frac{\ln(\zeta_2/\zeta_1) + R_p \left(\frac{1}{h_3} - \frac{1}{h_4} \right)}{\frac{1}{R_p} \ln(\zeta_1/\zeta_2) + \left(\frac{1}{h_4} - \frac{1}{h_3} \right) + \frac{R_p}{2} \left(\frac{1}{h_3^2} - \frac{1}{h_4^2} \right)} \right] \right. \\ \left. \left[\frac{6\eta_0 \phi U (h_3 + R_p) \left[\frac{1}{R_p} \ln(\zeta_1/\zeta_2) + \left(\frac{1}{h_4} - \frac{1}{h_3} \right) + \frac{R_p}{2} \left(\frac{1}{h_3^2} - \frac{1}{h_4^2} \right) \right]}{R_p^2 \tan \alpha} \right] + e^{-\phi P_4} \right\} \quad (3.61)$$

where ζ_1 and ζ_2 are as defined in equation (3.52).

3.4.3 Analysis of plug-attachments

In the theoretical analysis of the plug-attachments, two basic profiles were considered initially. These were the straight-parallel and straight-tapered profiles. Extensions were made to include a second parallel or tapered portion, thus forming a stepped or composite attachment. As in the analysis of Christopherson tubes, the origins of the co-ordinate systems were chosen at the beginning of each zone so that the Reynolds equation as in equation (3.24) applies.

It was mentioned earlier that the length of the sink zone is short. Consequently, the length of the chamfer at the fore end of the attachment as shown in zone 3 of Figures (3.7) and (3.8) is also short. The analysis of zone 3 can therefore be omitted with very little loss in accuracy. In this case zone 2, which may be straight-parallel or straight-tapered, is extended to include zone 3 as shown by the hatched lines. Thus, P_2 and P_3 are synonymous.

The analytical procedures for the plug-attachments are similar to those for the Christopherson tubes, but they are described in

detail here to avoid confusion.

3.4.3.1 Straight-parallel plug-attachment

Applying equation (3.24) to a straight-parallel plug-attachment in zone 2 (which includes zone 3) and integrating between the limits $P = 0$ at $x = 0$ and $P = P_2 = P_3$ at $x = l_2$, and simplifying,

$$P_3 = -\frac{1}{\phi} \ln \left[1 - \frac{12\eta_0\phi l_2}{h_2^3} \left(\frac{U_2 h_2}{2} - q_2 \right) \right] \quad (3.62)$$

By the continuity of flow, the rates of lubricant flow are equal in each zone and described by equation (3.60). Furthermore, the velocity of the undrawn tube is unaltered. Thus, the subscripts for these terms are omitted, and upon substituting q_2 by equation (3.60), equation (3.62) becomes

$$P_3 = -\frac{1}{\phi} \ln \left[1 - \frac{6\eta_0\phi U l_2}{h_2^3} \cdot z \left(\frac{h_2}{z} - h_4 \right) \right] \quad (3.63)$$

where z is described by equations (3.58) and (3.59).

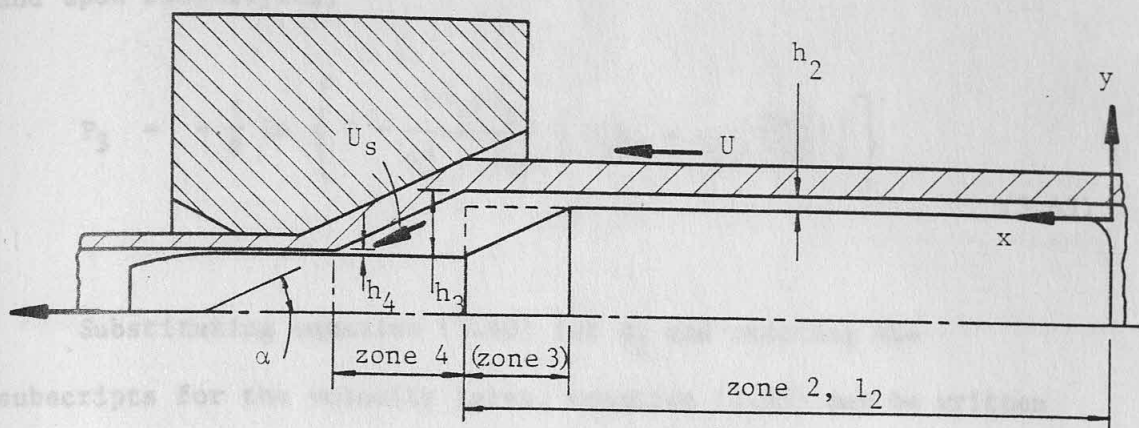
3.4.3.2 Straight-tapered plug-attachment

If zone 2 has a straight-tapered profile and h is the radial clearance at any point within this zone, then by simple geometry

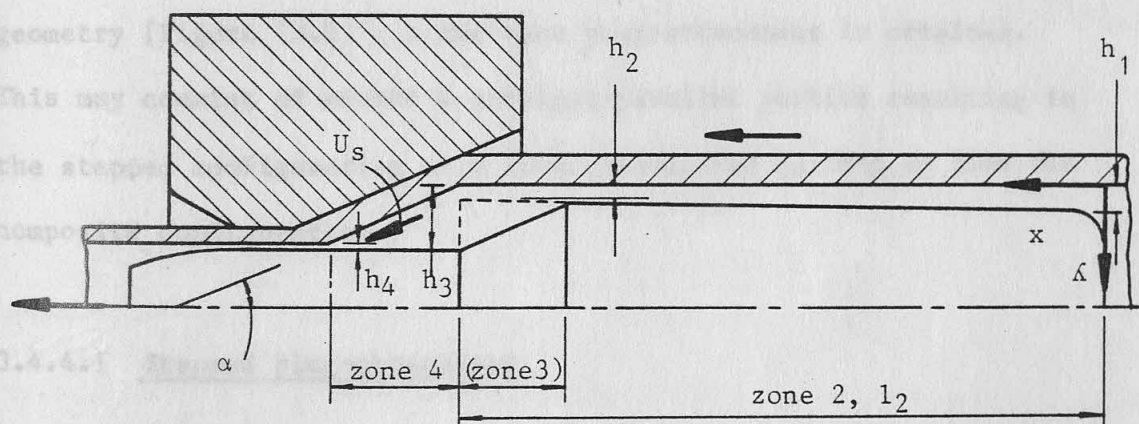
$$h = h_2 \left(1 + K - \frac{K}{l_2} x \right) \quad (3.64)$$

where $K = \frac{h_1 - h_2}{h_2}$ ie. $\frac{h_1}{h_2} = 1 + K$

Substituting equation (3.64) for h in equation (3.24) and



(a) Straight-parallel plug-attachment



(b) Straight-tapered plug-attachment

Figure (3.7) Analysis of plug-attachments

integrating between the limits $P = 0$ at $x = 0$ and $P = P_3$ at $x = l_2$ and upon simplifying,

$$P_3 = -\frac{1}{\phi} \ln \left\{ 1 - \frac{6\eta_0 \phi l_2}{h_2^3 (1+K)} \left[U_2 h_2 - q_2 \left(\frac{2+K}{1+K} \right) \right] \right\} \quad (3.65)$$

Substituting equation (3.60) for q_2 and omitting the subscripts for the velocity terms, equation (3.65) may be written

$$P_3 = -\frac{1}{\phi} \ln \left\{ 1 - \frac{3\eta_0 \phi U l_2}{h_2^3 (1+K)^2} \cdot z \cdot (2+K) \left[\frac{2(1+K)}{(2+K)} \cdot \frac{h_2}{z} - h_4 \right] \right\} \quad (3.66)$$

3.4.4 Analysis of two-zone plug-attachments

If zone 2 is extended to include zone 1 which is of a different geometry [Figure (3.8)], a two-zone plug-attachment is obtained. This may consist of either a straight-parallel portion resulting in the stepped configuration or a straight-tapered portion to form the composite configuration.

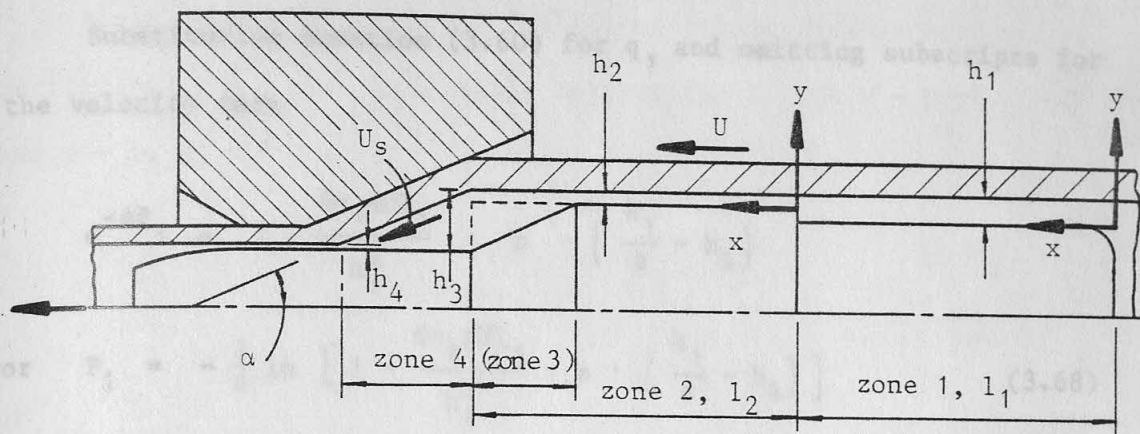
3.4.4.1 Stepped plug-attachment

Applying equation (3.24) to the straight-parallel portion in zone 1 and integrating between the limits $P = 0$ at $x = 0$ and $P = P_1$ at $x = l_1$,

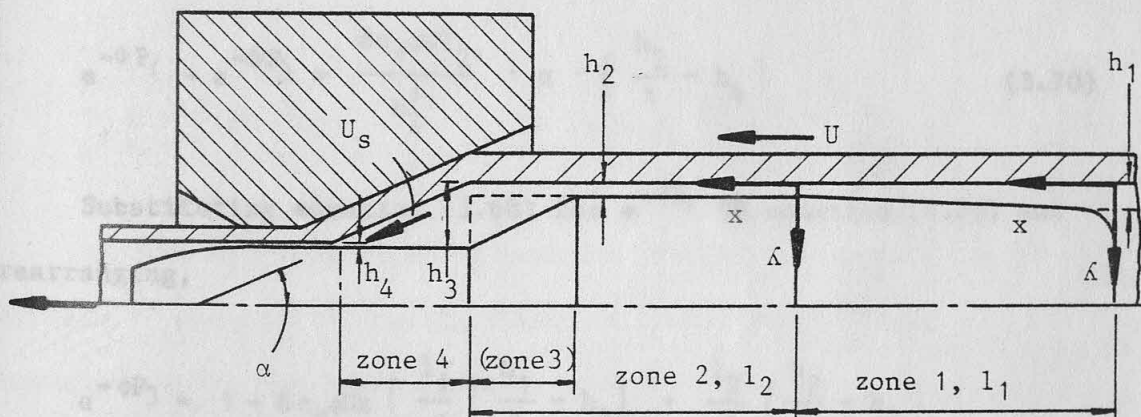
$$e^{-\phi P_1} = 1 - \frac{12\eta_0 \phi l_1}{h_1^3} \left(\frac{U_1 h_1}{2} - q_1 \right)$$

or

$$(3.67)$$



(a) Stepped plug-attachment



(b) Composite plug-attachment

Figure (3.8) Analysis of two-zone plug-attachments

$$P_1 = -\frac{1}{\phi} \ln \left[1 - \frac{12\eta_0 \phi l_1}{h_1^3} \left(\frac{U_1 h_1}{2} - q_1 \right) \right]$$

Substituting equation (3.60) for q_1 and omitting subscripts for the velocity term

$$e^{-\phi P_1} = 1 - \frac{6\eta_0 \phi U l_1}{h_1^3} \cdot z \cdot \left(\frac{h_1}{z} - h_4 \right)$$

$$\text{or } P_1 = -\frac{1}{\phi} \ln \left[1 - \frac{6\eta_0 \phi U l_1}{h_1^3} \cdot z \cdot \left(\frac{h_1}{z} - h_4 \right) \right] \quad (3.68)$$

Integrating equation (3.24) for zone 2 between the limits $P = P_1$ at $x = 0$ and $P = P_2$ at $x = l_2$,

$$-\frac{1}{\phi} e^{-\phi P_3} + \frac{1}{\phi} e^{-\phi P_1} = \frac{12\eta_0 l_2}{h_2^3} \left(\frac{U_2 h_2}{2} - q_2 \right) \quad (3.69)$$

Substituting equation (3.60) for q_2 and simplifying,

$$e^{-\phi P_1} - e^{-\phi P_3} = \frac{6\eta_0 \phi U l_2}{h_2^3} \cdot z \cdot \left(\frac{h_2}{z} - h_4 \right) \quad (3.70)$$

Substituting equation (3.68) for $e^{-\phi P_1}$ in equation (3.70) and rearranging,

$$e^{-\phi P_3} = 1 - 6\eta_0 \phi U z \left[\frac{1}{h_1^3} \left(\frac{h_1}{z} - h_4 \right) + \frac{1}{h_2^3} \left(\frac{h_2}{z} - h_4 \right) \right]$$

$$\text{or } P_3 = -\frac{1}{\phi} \ln \left\{ 1 - 6\eta_0 \phi U z \left[\frac{1}{h_1^3} \left(\frac{h_1}{z} - h_4 \right) + \frac{1}{h_2^3} \left(\frac{h_2}{z} - h_4 \right) \right] \right\} \quad (3.71)$$

3.4.4.2 Composite plug-attachment

Applying equations (3.24) and (3.64) to the straight-tapered portion in zone 1 and integrating between the limits $P = 0$ at $x = 0$ and $P = P_1$ at $x = l_1$,

$$e^{-\phi P_1} = 1 - \frac{6\eta_0 \phi l_1}{h_2^3 (1+K)} \left[U_1 h_2 - q_1 \left(\frac{2+K}{1+K} \right) \right]$$

or (3.72)

$$P_1 = -\frac{1}{\phi} \ln \left\{ 1 - \frac{6\eta_0 \phi l_1}{h_2^3 (1+K)} \left[U_1 h_2 - q_1 \left(\frac{2+K}{1+K} \right) \right] \right\}$$

Substituting equation (3.60) for q_1 and omitting subscripts for thickness h_2 at the plane of the end of sinking or at entry to the plug-tube interface. However, the complexity of the equation for h_2

$$e^{-\phi P_1} = 1 - \frac{3\eta_0 \phi U l_1}{h_2^3 (1+K)^2} \cdot z \cdot (2+K) \left[\frac{2(1+K)}{(2+K)} \cdot \frac{h_2}{z} - h_4 \right]$$

or

$$P_1 = -\frac{1}{\phi} \ln \left\{ 1 - \frac{3\eta_0 \phi U l_1}{h_2^3 (1+K)^2} \cdot z \cdot (2+K) \left[\frac{2(1+K)}{(2+K)} \cdot \frac{h_2}{z} - h_4 \right] \right\} \quad (3.73)$$

For the straight-parallel portion in zone 2, equation (3.70) applies. Hence substituting equation (3.73) for $e^{-\phi P_1}$ in equation (3.70) and rearranging,

$$e^{-\phi P_3} = 1 - 3\eta_0 \phi U z \left\{ \frac{1}{h_2^3} \cdot \frac{(2+K)}{(1+K)^2} \left[\frac{2(1+K)}{(2+K)} \cdot \frac{h_2}{z} - h_4 \right] + \frac{2l_2}{h_2^3} \left(\frac{h_2}{z} - h_4 \right) \right\}$$

Flow rate can be obtained by equation (3.60),

The flow chart for the general iterative procedure is illustrated in Figure (3.9) and the computer programme which was

or

$$P_3 = -\frac{1}{\phi} \ln \left\{ 1 - 3\eta_0 \phi U z \left\{ \frac{1}{h_2^3} \cdot \frac{(2+K)}{(1+K)^2} \left[\frac{2(1+K)}{(2+K)} \cdot \frac{h_2}{z} - h_4 \right] \right. \right. \right. \quad (3.74)$$

$$\left. \left. + \frac{21_2}{h_2^3} \left(\frac{h_2}{z} - h_4 \right) \right\} \right\}$$

3.5 SOLUTION OF THE HYDRODYNAMIC PRESSURE AND LUBRICANT FILM THICKNESS GENERATED BY THE PLUG-ATTACHMENTS

The analysis of the plug-attachments provided, in each case, two equations. One depicts the hydrodynamic pressure P_3 generated at the entry to the sink zone and the other gives the lubricant film thickness h_4 at the plane of the end of sinking or at entry to the plug-tube interface. However, the complexity of the equation for h_4 given by equation (3.52), prevents a direct solution for P_3 and h_4 . Consequently, an iterative technique with the aid of a digital computer was employed. An initial value of h_4 was estimated and used simultaneously to compute the corresponding values of P_3 from equation (3.61), which was derived using the analysis of the sink-zone, and those equations derived by the analyses of the plug-attachments. The values of P_3 obtained by the two different analyses were compared and the value of h_4 was adjusted until the computed hydrodynamic pressures were equal to within a 'set' tolerance. At this point the iteration was terminated and the value of P_3 is the hydrodynamic pressure generated by that particular plug-attachment. The validity of h_4 can be checked by substituting the value of P_3 into equation (3.52). The lubricant flow rate can be obtained by equation (3.60).

The flow chart for the general iterative procedure is illustrated in Figure (3.9) and the computer programme which was

3.6 APPLICATION TO TOOL DESIGN

Although the technique of pressurization is

relatively simple, of view much valuable time and effort is required to predict the most suitable and practical design of plug-attachment for a given set of drawing conditions.

dependent on the lubricant film thickness at the plug-tube interface is This, in turn, is a function of the amount of sinking, die semi-

angle, lubricant viscosity, undrawn tube velocity and the geometry of the plug attachment such as its length and the radial clearance or clearance provides.

ation is predetermined by the drawing schedule and thus will be treated as an independent variable. The same applies to the die

semi-angle since it is determined by the drawing schedule. The angle at which the total work including frictional work and redundant

work is minimal. It is possible to provide facilities to enhance the lubricant viscosity by using a lubricant cooling system.

However, it is assumed that there are no such provisions. Thus, for a given lubricant viscosity, the tool design problem treats the

undrawn tube velocity, which is proportional to the draw speed, the lubricant viscosity and the geometry of the plug-attachment as the

main variables. Under identical conditions, the hydrodynamic pressure

which could be generated is directly proportional to the draw speed, lubricant viscosity and the length of the attachment and inversely

proportional to the radial clearance which it provides.

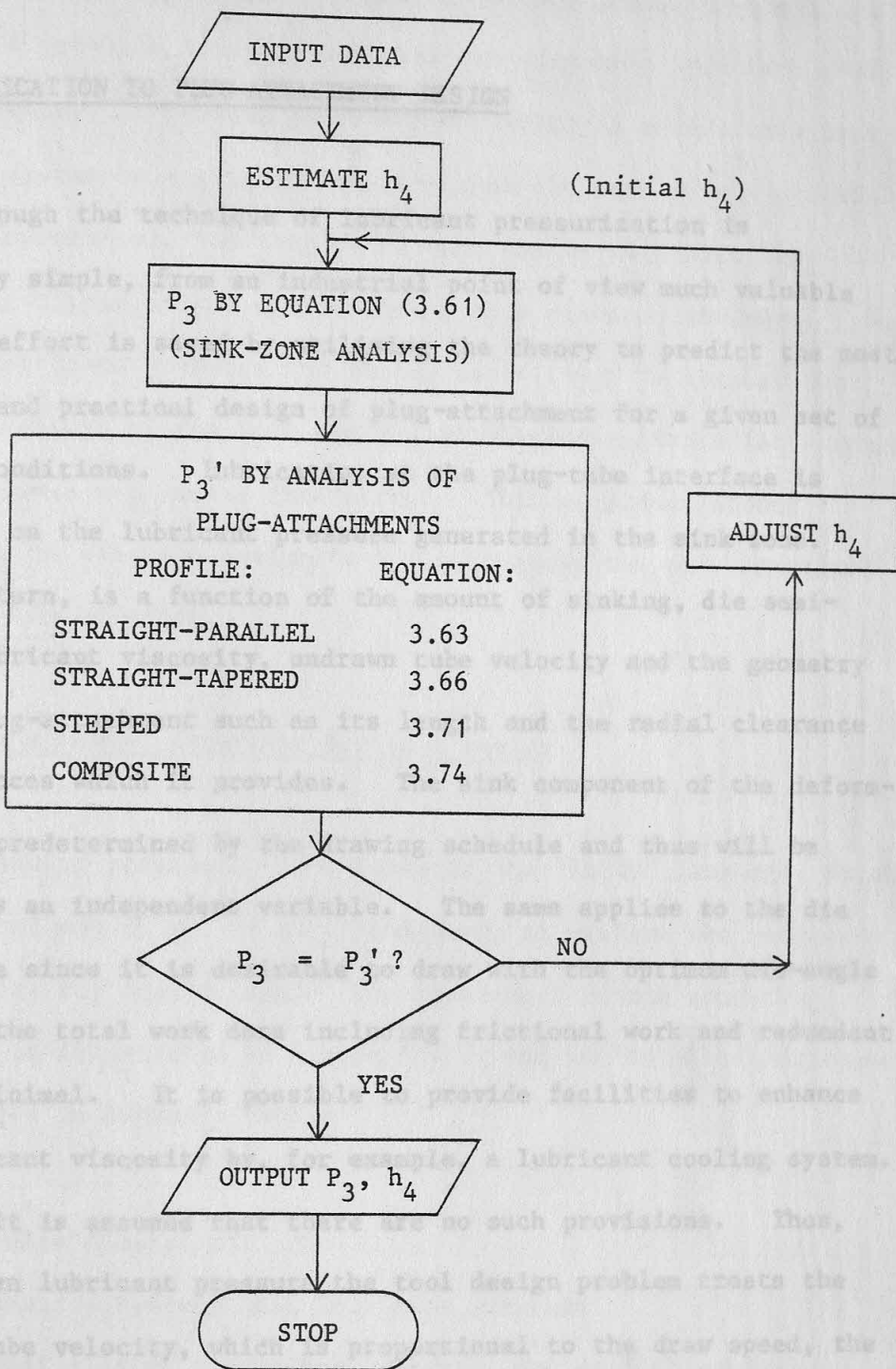


Figure (3.9) Computer flow-chart for the solution of hydrodynamic pressure and lubricant film thickness

written in the "FORTRAN" language is included in Appendix (A4).

3.6 APPLICATION TO PLUG-ATTACHMENT DESIGN

Although the technique of lubricant pressurization is relatively simple, from an industrial point of view much valuable time and effort is saved by utilising the theory to predict the most suitable and practical design of plug-attachment for a given set of drawing conditions. Lubrication at the plug-tube interface is dependent on the lubricant pressure generated in the sink-zone. This, in turn, is a function of the amount of sinking, die semi-angle, lubricant viscosity, undrawn tube velocity and the geometry of the plug-attachment such as its length and the radial clearance or clearances which it provides. The sink component of the deformation is predetermined by the drawing schedule and thus will be treated as an independent variable. The same applies to the die semi-angle since it is desirable to draw with the optimum die-angle at which the total work done including frictional work and redundant work is minimal. It is possible to provide facilities to enhance the lubricant viscosity by, for example, a lubricant cooling system. However, it is assumed that there are no such provisions. Thus, for a given lubricant pressure the tool design problem treats the undrawn tube velocity, which is proportional to the draw speed, the lubricant viscosity and the geometry of the plug-attachment as the main variables.

Under identical drawing conditions the hydrodynamic pressure which could be generated is directly proportional to the draw speed, lubricant viscosity and the length of the attachment and inversely proportional to the radial clearance which it provides.

Industrially it is desirable to have lubricant pressures which are as high as possible since friction at the plug-tube interface would then be lowest. However, an attachment which is excessively long and of diameter only slightly smaller than the bore of the undrawn tube is impractical, but this difficulty can be alleviated by drawing at higher speeds and/or with a more viscous lubricant. For a given lubricant pressure the theory is utilized to compute the required lengths of the four designs of plug-attachments for a range of draw speeds and radial clearances. This enables a direct comparison of the four designs and consequently the most practical design can be selected.

3.6.1 The computer programme for tool design

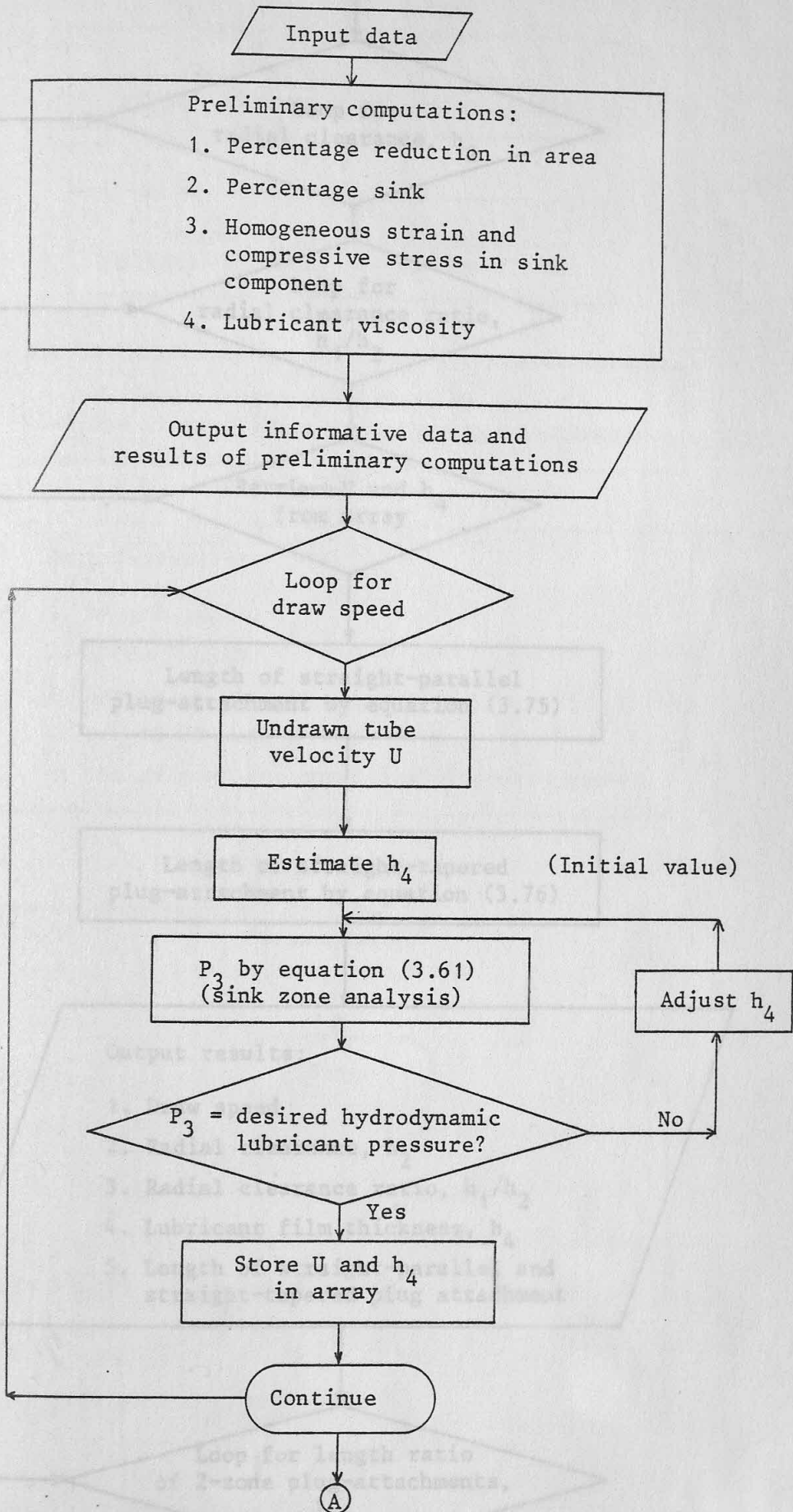
A computer programme was written in the "BASIC" language, which is ideal for use on a micro computer, to perform the necessary computations for tool design. The flow-chart of the computing procedure is illustrated in Figure (3.10) and the detailed programme is presented in Appendix (A4).

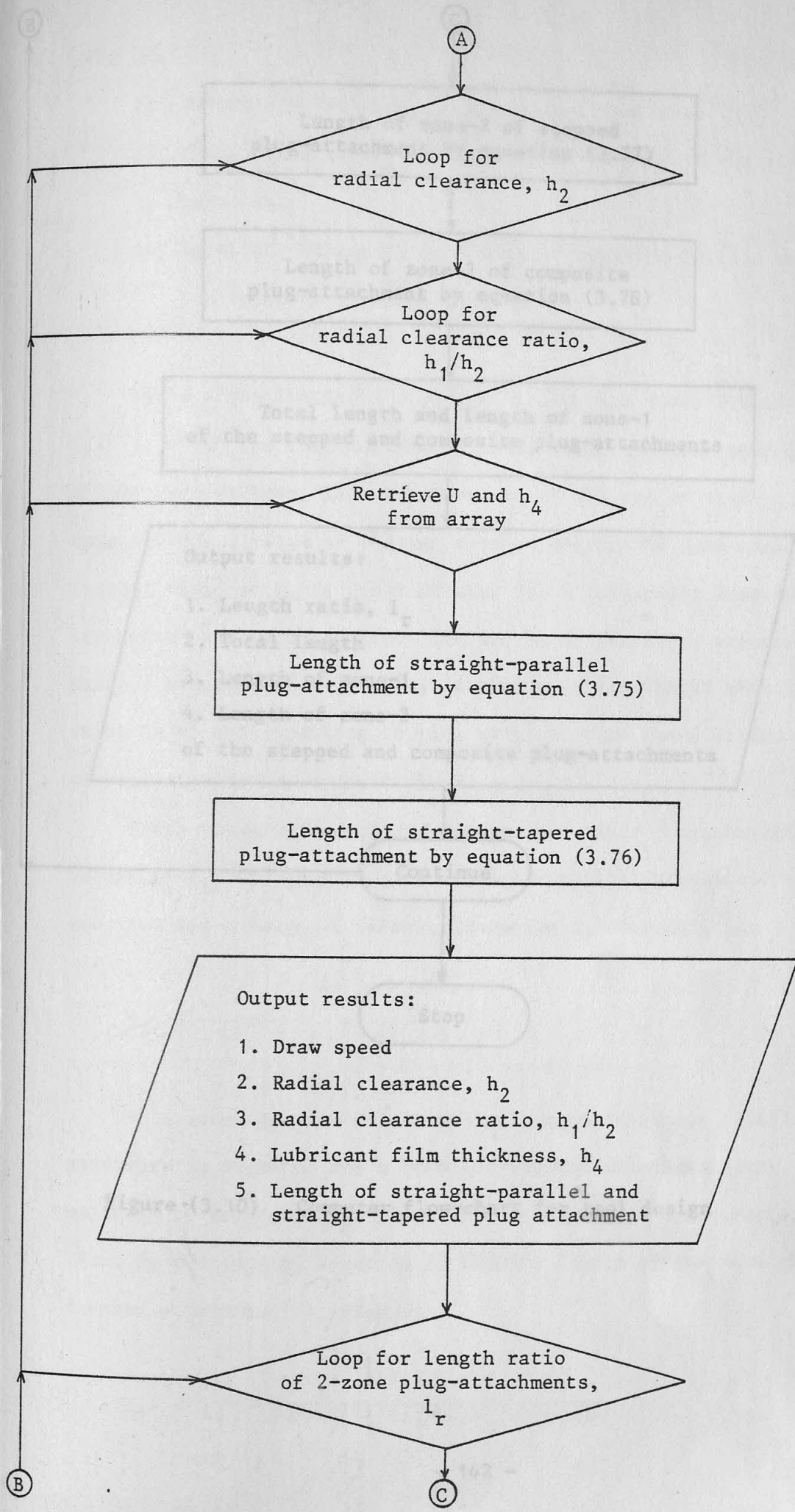
The input data consist of:

- 1) Desired hydrodynamic lubricant pressure
- 2) Initial tube dimensions (diameter and wall thickness)
- 3) Final tube dimensions (diameter and wall thickness)
- 4) Die semi-angle
- 5) Viscosity-pressure coefficient
- 6) Anticipated lubricant temperature

The relevant data are used to perform the preliminary computations

Figure (3.10) Computer flow-chart for tool design





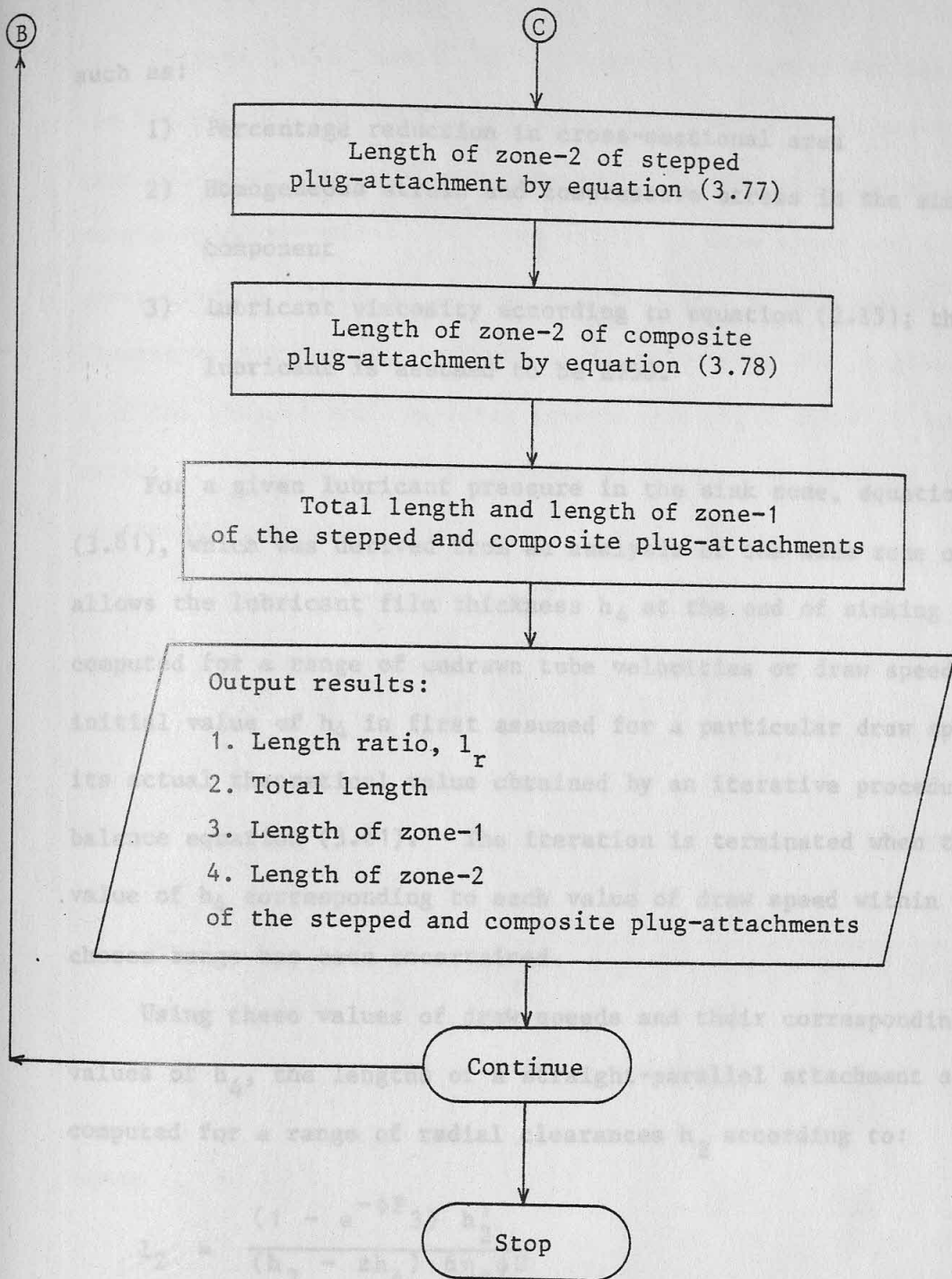


Figure (3.10) Computer flow-chart for tool design

such as:

- 1) Percentage reduction in cross-sectional area
- 2) Homogeneous strain and compressive stress in the sink component
- 3) Lubricant viscosity according to equation (2.15); the lubricant is assumed to be EP50.

For a given lubricant pressure in the sink zone, equation (3.61), which was derived from an analysis of the sink zone only, allows the lubricant film thickness h_4 at the end of sinking to be computed for a range of undrawn tube velocities or draw speeds. An initial value of h_4 is first assumed for a particular draw speed and its actual theoretical value obtained by an iterative procedure to balance equation (3.61). The iteration is terminated when the value of h_4 corresponding to each value of draw speed within the chosen range has been ascertained.

Using these values of draw speeds and their corresponding values of h_4 , the lengths of a straight-parallel attachment are computed for a range of radial clearances h_2 according to:

$$l_2 = \frac{(1 - e^{-\phi P_3}) h_2^3}{(h_2 - z h_4) 6 \eta_0 \phi U} \quad (3.75)$$

This equation is obtained by rearranging equation (3.63). The procedure is repeated for a straight-tapered attachment, but extended to consider the effect of the radial clearance ratio, h_1/h_2 . Thus, by rearranging equation (3.66) the length of the straight-tapered attachment is given by:

$$l_2 = \frac{(1 - e^{-\phi P_3})(1 + K)^2 h_2^3}{[2(1+K)h_2 - z(2+K)h_4](3\eta_0 \phi U)} \quad (3.76)$$

Figures (3.11) and (3.12) illustrate the equivalent lengths of the stepped and composite plug-attachments required to generate the same lubricant pressure when compared with that required by a single zone plug-attachment. The same values of draw speed and their corresponding values of h_4 , radial clearances h_2 and radial clearance ratios h_1/h_2 are used again to compute the lengths of zone 2 of the stepped and composite attachments for a range of length ratios, $l_r = l_2/l_1$. The relevant equations are obtained by rearranging equations (3.71) and (3.74). Thus,

$$l_2 = \frac{1 - e^{-\phi P_3}}{\left[\frac{1}{l_1 h_1^3} (h_1 - zh_4) + \frac{1}{h_2^3} (h_2 - h_4) \right] (6\eta_0 \phi U)} \quad \text{(Stepped)} \quad (3.77)$$

and

$$l_2 = \frac{1 - e^{-\phi P_3}}{\left\{ \frac{1}{l_1 h_2^3} \frac{(2+K)}{(1+K)^2} \left[\frac{2(1+K)}{(2+K)} h_2 - zh_4 \right] + \frac{2}{h_2^3} (h_2 - zh_4) \right\} (3\eta_0 \phi U)} \quad \text{(Composite)} \quad (3.78)$$

where $l_r = l_2/l_1$

If the overall length of the attachment is written

$$l_o = l_1 + l_2$$

then by simple substitution,

$$l_o = l_2 \left(1 + \frac{1}{l_r} \right) \quad (3.79)$$

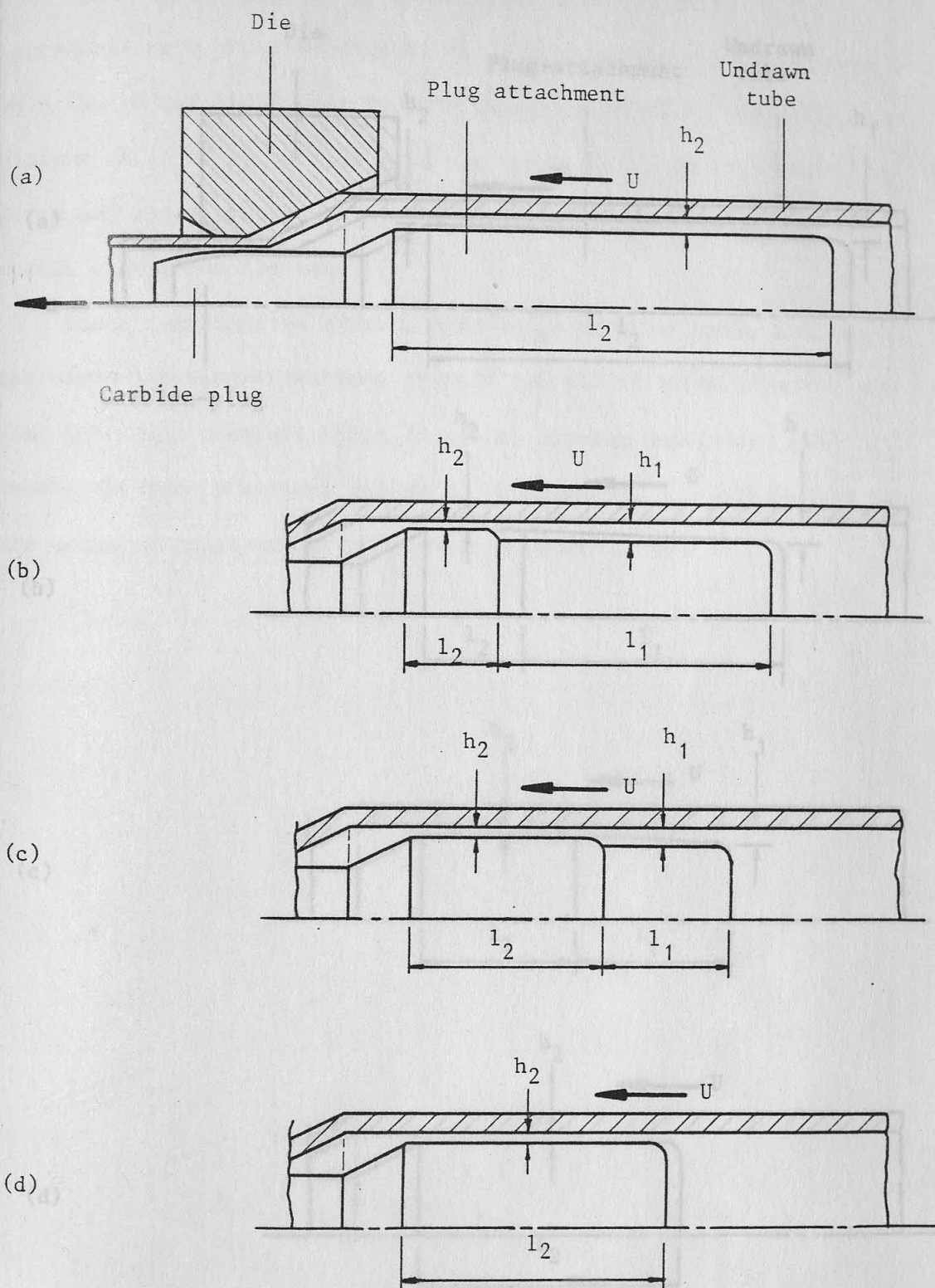


Figure (3.11) Equivalent lengths of a stepped plug-attachment to develop the same pressure on entry to the sink zone

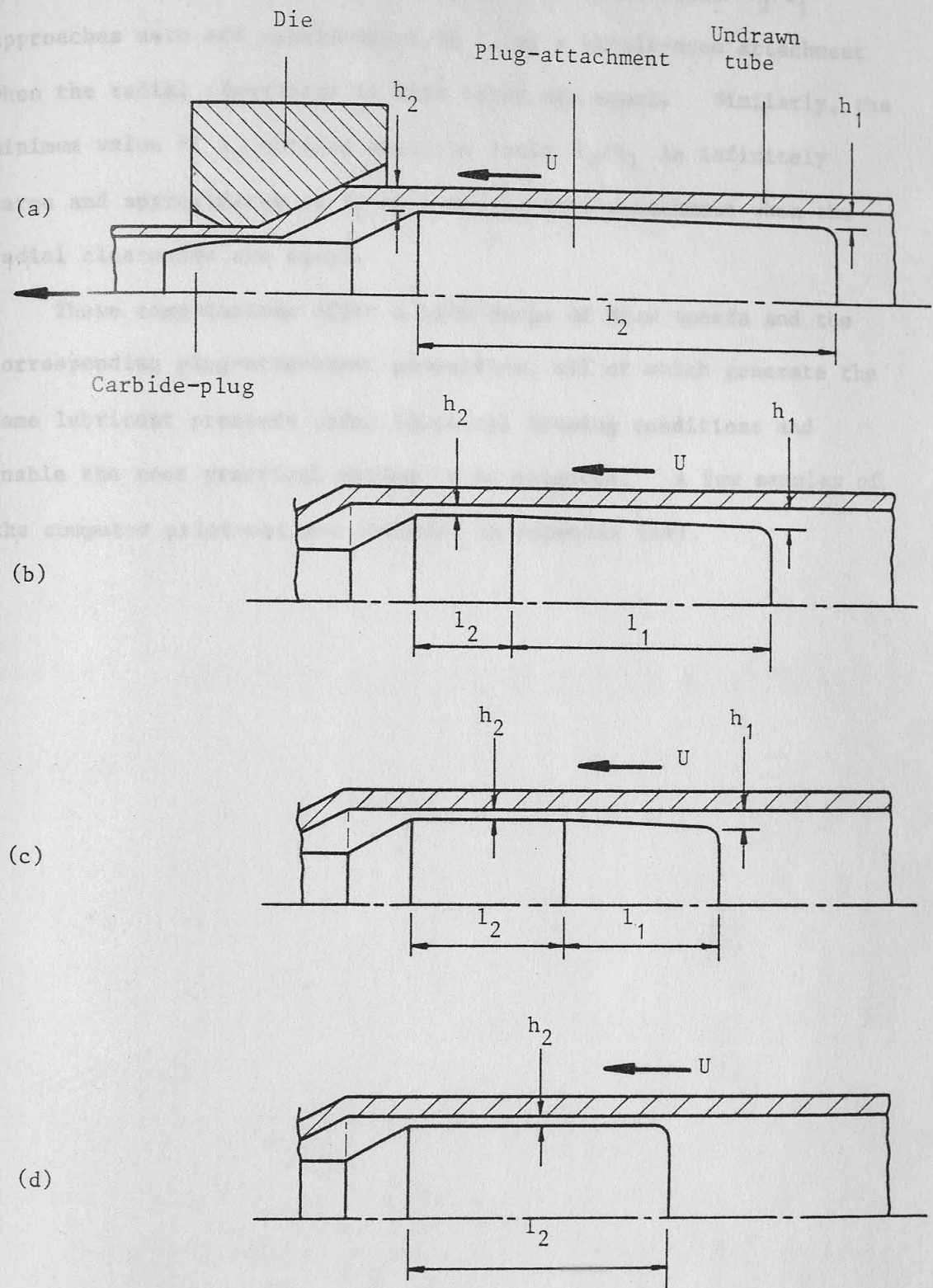


Figure (3.12) Equivalent lengths of a composite plug-attachment to develop the same pressure on entry to the sink zone

The maximum value of l_0 is obtained when the ratio l_2/l_1 approaches zero and approximates to l_2 of a single-zone attachment when the radial clearances in both cases are equal. Similarly, the minimum value of l_0 obtains when the ratio l_2/l_1 is infinitely large and approximates to l_2 of a single-zone attachment when the radial clearances are equal.

These computations offer a wide range of draw speeds and the corresponding plug-attachment geometries, all of which generate the same lubricant pressure under identical drawing conditions and enable the most practical design to be selected. A few samples of the computer print-out are included in Appendix (A4).

CHAPTER 4: DESCRIPTION OF EXPERIMENTAL EQUIPMENT AND MATERIALS

CHAPTER 4: DESCRIPTION OF EXPERIMENTAL EQUIPMENT AND MATERIALS

4.1 INTRODUCTION

The experimental investigation of the promotion of hydrodynamic lubrication in tube-drawing required the measurement of the draw force, plug force, lubricant pressure and draw speed. A description

CHAPTER 4: DESCRIPTION OF EXPERIMENTAL EQUIPMENT AND MATERIALS

"Talysurf" was used to measure the surface finish of the tubes before and after drawing since this also gives some indication of the effectiveness of lubrication, but it is not intended to describe such a standard instrument. In addition to these, descriptions of the experimental equipment and materials are given of the draw-bench, dies, plugs, tube material and lubricants.

4.2 THE DRAW-BENCH

The hydraulic draw-bench used in the present work had been used previously in the investigation of rod-drawing⁽⁷⁰⁾, section-drawing⁽⁷¹⁾ and polygonal tube-drawing on a fixed-plug⁽⁶⁵⁾. It has a drawing capacity of 30 tons with a 34 in stroke and a maximum draw speed of 15 ft min⁻¹. The specifications of the machinery are included in Appendix (A8).

4.3 LOAD CELLS

These load cells had been installed on the draw-bench and successfully used by previous investigators^(70,71,85). All that was required was some minor modifications such as re-wiring and re-calibration.

CHAPTER 4: DESCRIPTION OF EXPERIMENTAL EQUIPMENT AND MATERIALS

4.1 INTRODUCTION

The experimental investigation of the promotion of hydrodynamic lubrication in tube-drawing required the measurement of the draw force, plug force, lubricant pressure and draw speed. A description of the instruments used in these measurements is given here. A "Talysurf" was used to measure the surface finish of the tubes before and after drawing since this also gives some indication of the effectiveness of lubrication, but it is not intended to describe such a standard instrument. In addition to these, descriptions of the experimental equipment and materials are given of the draw-bench, dies, plugs, tube material and lubricants.

4.2 THE DRAW-BENCH

The hydraulic draw-bench used in the present work had been used previously in the investigation of rod-drawing⁽⁷⁰⁾, section-drawing⁽⁷¹⁾ and polygonal tube-drawing on a fixed-plug⁽⁸⁵⁾. It has a drawing capacity of 30 tonf with a 54 in stroke and a maximum draw speed of 15 ft min⁻¹. The specifications of the machinery are included in Appendix (A8).

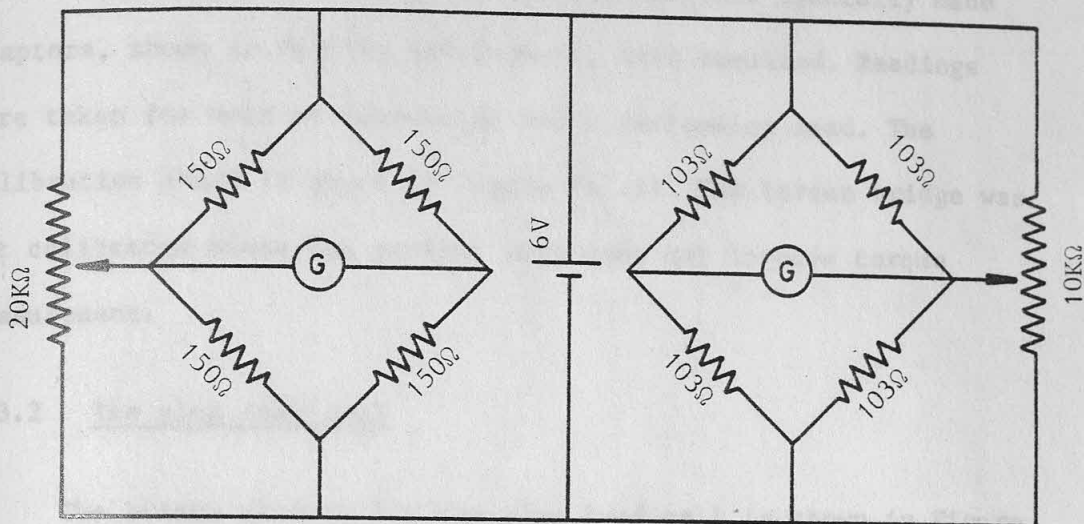
4.3 LOAD CELLS

These load cells had been installed on the draw-bench and successfully used by previous investigators(70,71,85). All that was required was some minor modifications such as re-wiring and re-calibration.

It is essential that the draw force and plug force are recorded continuously during drawing so that any changes in these parameters may be detected. Consequently the load cells for measuring these forces, which were supplied with a direct current, were connected to an ultra-violet beam recorder. Continuously screened cables avoided the cross-coupling effect. The bridge circuit of each load cell consisted of a set of metal foil straingauges from the same batch. However, owing to the inherent inequality in the resistance or tolerance, a trimming resistance was used for the initial bridge balance. A high degree of repeatability and accuracy is desirable in measuring the forces in order that compatible comparisons may be made when drawing conditions are altered. The testing machine used in the calibration of these load cells had been maintained according to B.S. 1610:1964 (Load verification of testing machines) and B.S. 5781:1979 (Specification for measurement and calibration systems).

4.3.1 The draw load cell

The draw load cell was mounted on the tag holder of the draw-bench. It was originally designed for measuring the rotational torque on the tag when determining the mean coefficient of friction using the rotating-die technique by previous investigators(70,71,85), in addition to the draw force. The combined bridge circuit of the load cell is shown in Figure (4.1). It is of the rod type and its detail drawings are shown in Figure (A6.1) of Appendix (A6).



Torque bridge

Force bridge

Figure (4.1) Circuit diagram of the tag load cells

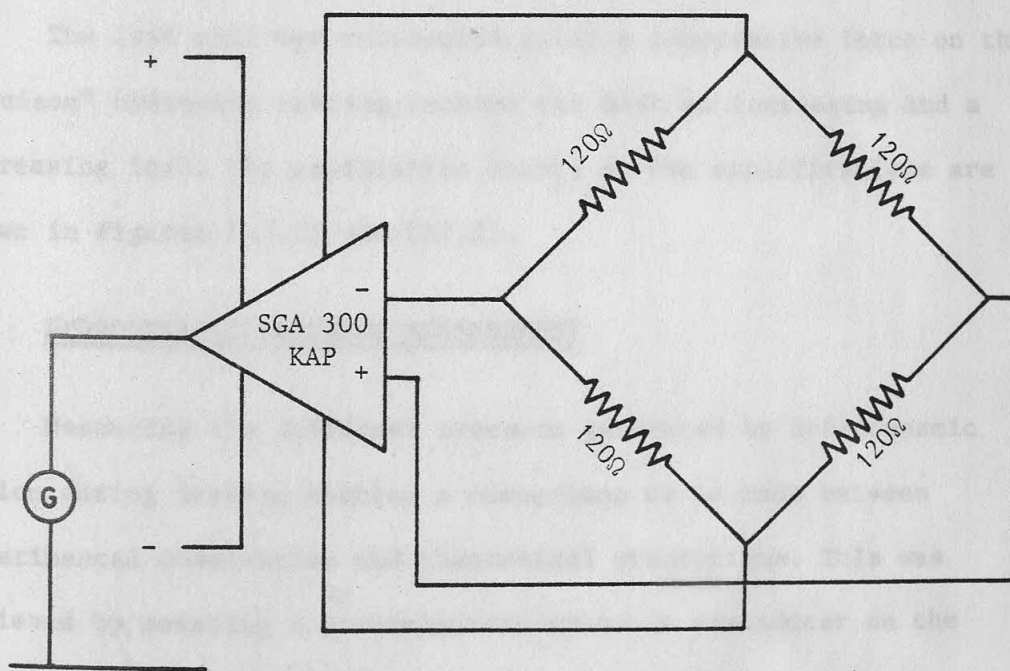


Figure (4.2) Circuit diagram of the plug load cell

The draw load cell was calibrated under a direct tensile force on a 50 tonf "Denison" hydraulic testing machine. Specially made adaptors, shown in Figures (A6.2-A6.4), were required. Readings were taken for both an increasing and a decreasing load. The calibration chart is shown in Figure (A7.1). The torque bridge was not calibrated since the present work does not involve torque measurement.

4.3.2 The plug load cell

The bridge circuit for the plug load cell is shown in Figure (4.2). The load cell was made according to the drawing shown in Figure (A6.5). The output signal of the bridge circuit was amplified by a "SGA 300 KAP" amplifier. This type of amplifier with a zero setting device provided a bridge supply which was virtually independent of the source. In addition, the device had potentiometers for zero, span and bridge supply voltage adjustments.

The load cell was calibrated under a compressive force on the "Denison" hydraulic testing machine for both an increasing and a decreasing load. The calibration charts at two amplifications are shown in Figures (A7.2) and (A7.3).

4.4 HYDRODYNAMIC PRESSURE MEASUREMENT

Measuring the lubricant pressure generated by hydrodynamic action during drawing enabled a comparison to be made between experimental observation and theoretical predictions. This was achieved by mounting a piezoelectric pressure transducer on the lubricant pressurizing device as described in Chapter 5.

The arrangement of the pressure transducer and its associated instrumentation are shown schematically in Figure (4.3). Its technical data are included in Appendix (A8.6). The measured pressure

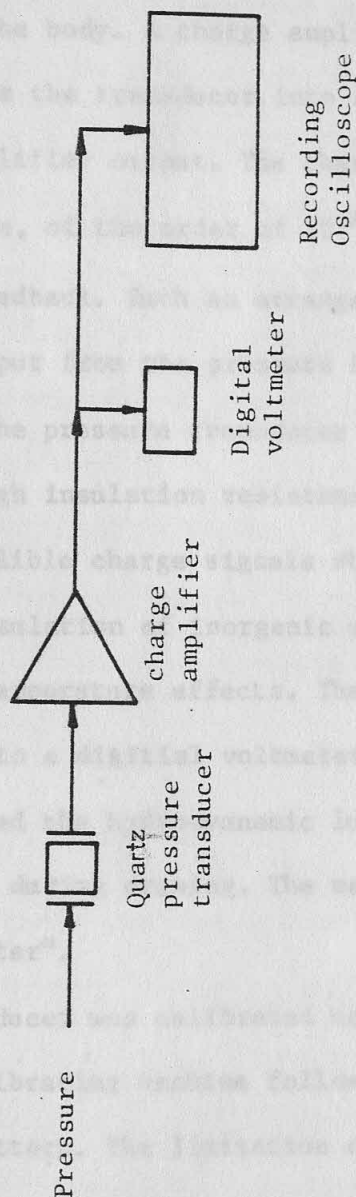


Figure (4.3) Schematic arrangement of the pressure transducer and instrumentation

acts through the diaphragm on the quartz crystal measuring element which transforms the pressure into an electrostatic charge. The stainless steel diaphragm is welded flush and hermetically sealed to the stainless steel transducer body. The quartz elements are mounted in a highly sensitive arrangement in the quartz chamber, which is welded hermetically to the body. A charge amplifier converts the electrostatic charge from the transducer into a proportional voltage on the low impedance amplifier output. The charge amplifier has a very high input impedance, of the order of $10^{15} \Omega$, and incorporates a capacitive negative feedback. Such an arrangement stabilizes the electrostatic charge output from the pressure transducer. A special coaxial cable connects the pressure transducer to the charge amplifier. This has an extremely high insulation resistance and low capacitance which generates only negligible charge signals when moved. A high-temperature resistant insulation of inorganic material and a jacket of glass fibre nullify temperature effects. The output from the amplifier was connected to a digital voltmeter and a recording oscilloscope. This enabled the hydrodynamic lubricant pressure to be recorded continuously during drawing. The mean pressure was deduced using a "Planimeter".

The pressure transducer was calibrated using a "Budenberg" hydrostatic pressure calibrating machine following an increasing and a decreasing load pattern. The limitation of the "Budenberg" tester was that the maximum permissible pressure was 2000 lbf in^{-2} . However, the maximum linearity error for the pressure transducer at any calibrated range was given by its manufacturer to be $\pm 0.8\%$. Thus, the calibration chart as shown in Figure (A7.4) is also valid at higher pressures.

4.5 DRAW SPEED MEASUREMENT

The control valve on the hydraulic draw-bench was calibrated to give draw speeds ranging from 0 to 15 ft min⁻¹. However, a constant draw speed of 15 ft min⁻¹ was used throughout the experimental programme. Since the hydrodynamic lubricant pressure generated at the entry to the metal deformation zone is also a function of the velocity of the undrawn tube, a more accurate speed check was obtained by measuring the draw speed manually. Two marks were made on the draw-bench at a known distance apart. The time taken for the draw carriage to travel this distance during drawing was measured using a stop-watch. The speed thus calculated was checked against the setting on the control valve and was found to be adequate. The velocity of the undrawn tube which was utilized to predict the theoretical hydrodynamic lubricant pressure generated was deduced on the basis of volume constancy, in conjunction with the percentage reduction in cross-sectional area of the tube.

4.6 DIES AND PLUGS

For reasons of economy, the dies and plugs used in the experimental work were provided by Fine Tubes Limited. Some of these tools are shown in Plate (4.1). These were industrial tools and therefore were not designed specially for experimental purposes. However, the usage of these tools was advantageous since they provided a useful assessment of the current tube-drawing practice. Initially four dies and five plugs were used. The appropriate combinations of which yielded nominal reductions in cross-sectional area of the tube of 45%, 40%, 35%, 30% and 25%. Four additional dies nominally having semi-angles of 12°, 10°, 8° and 6° were specially made for the determination of the optimum die semi-angle.



Plate (4.1) Dies and conventional plugs available for tube-drawing

The pertinent dimensions of these tools were measured and tabulated as shown in Table (4.1). To measure the profile of the dies such as die semi-angle, length of the land and of the conical portion, replicas were made using a mixture of "Acrulite, Microtech Type A" liquid and powder which combined to form a plastic when set. A releasing agent was applied on the die surface for ease of removing the replica from the die. It was found that by partitioning a thin longitudinal section of the die enabled a replica of the entire profile from the entry to the exit to be made in one piece without removal difficulties. These replicas were polished to a thickness of approximately 1 mm to avoid errors arising from parallax when they were projected on a "Nikon" profile projector where direct measurements were made. The 45° chamfer at the fore end of the plugs were measured with the aid of the profile projector also.

The effective diameters of the dies and plugs were measured on a "Universal Measuring Machine". Although the design drawing of the plugs specified a taper of 0.008 in per in, which is equivalent to an angular taper of 27.5 min, measurements taken at half inch intervals showed angular tapers ranging from 8 min to 21 min. These tools were not new. Thus, due to wear and subsequent polishing, deviations from the original dimensions are to be expected.

Following the completion of the preparatory experiments, dies of 12° semi-angle were used in conjunction with specially designed experimental plugs. For reasons discussed in Chapter 5, the conventional 45° chamfer at the fore end of the plugs was replaced by a curved profile. Also, the working portions of these plugs were parallel. The dimensions of these tools were measured by the methods described previously.

The dies were of 94% tungsten carbide and 6% cobalt and were made by sintering powders of approximately 1.5 micron. The plugs

Die Serial No.	Mean Diameter (in)	Mean angle (degree)	Land (in)	Depth of conical portion (in)	Plug Serial No.	Mean Diameter (in)	Chamfer (in)
804	0.803	29.89	0.063	-	650	0.652	0.0295
834	0.834	28.10	0.148	-	722	0.725	0.0345
896	0.896	30.38	0.115	-	677	0.677	0.055
865	0.864	26.58	0.138	-	700	0.700	0.0393
12	0.830	24.12	0.072	0.821	663	0.663	0.070
10	0.830	19.94	0.072	0.78			
8	0.832	15.84	0.045	1.17			
6	0.832	12.22	0.085	1.116			

Table (4.1) Dimensions of the tools used in the preparatory experiments.

were of 90% tungsten carbide and 10% cobalt and powders of approximately 3.5 micron were used in the sintering process. The surfaces of both the dies and plugs were polished with a diamond paste and had CLA values of approximately 3 micron. Typical design drawings of the dies and conventional plugs are shown in Figures (A6.6) and (A6.7) and those of the newly designed experimental plugs are given in Figure (5.17) of Chapter 5.

4.7 TOOLS FOR PROMOTING HYDRODYNAMIC LUBRICATION

These tools refer to Christopherson tubes and plug-attachments for promoting hydrodynamic lubrication at the die-tube and plug-tube interface respectively. Descriptions of these tools are given in Chapter 5 in the discussion on the experimental programme.

4.8 TUBE MATERIAL

Annealed austenitic stainless steel tubes were used in the drawing experiments. The material is of the AISI 347 type and has the following composition:

Cr	Ni	C	Nb	Mn
18%	11%	0.06%	0.7%	1.5%

This type of steel are used for general purposes requiring a good resistance against "weld-decay" and were suggested and provided by Fine Tubes Limited who have reported considerable lubrication problems when drawing such tubes.

Tension tests on full sections of the tube were carried out in order to determine the stress-strain relationship of the tube material. The specimens, plugged at the ends, were gripped between the jaws of a "Avery-Denison" hydraulic testing machine. The machine has a built-in extensometer and a servomechanism for plotting the load-elongation diagram. It has been calibrated according to B.S. 1610:1964.

The constitutive equation of the power law form $\sigma = \sigma' \epsilon^n$ (166,167) was re-written as:

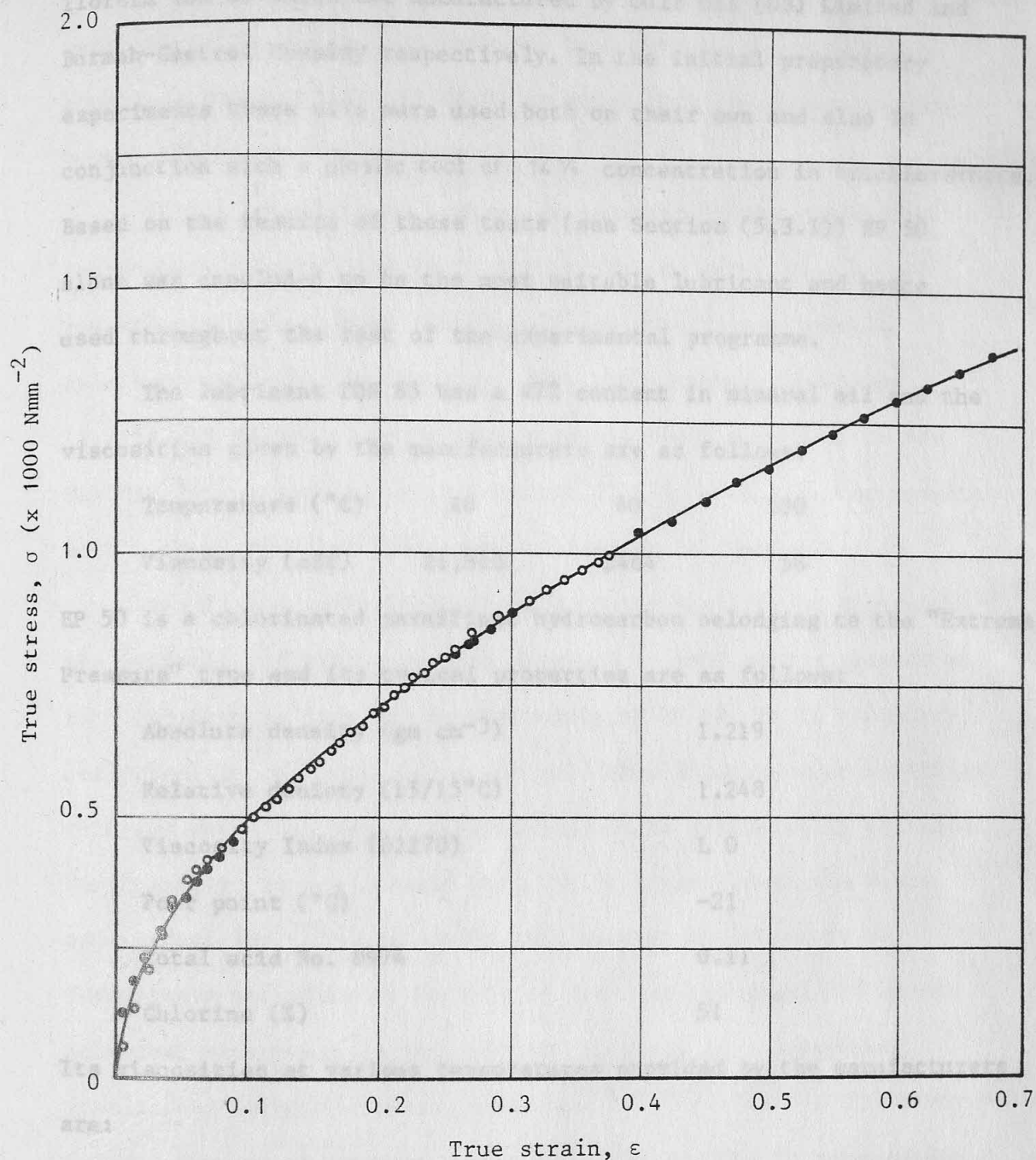
$$\ln(\sigma) = \ln(\sigma') + n \ln(\epsilon) \quad (4.1)$$

and thus used to express the stress-strain relation of the tube material. From the tension tests, if the graph of $\ln(\sigma)$ against $\ln(\epsilon)$ is plotted and the initial 5% plastic strain disregarded as non-representative, a reasonably straight line is obtained. The slope of the line gives the strain hardening exponent n which is numerically equal to the plastic instability strain(168); the value of σ' is obtained by extrapolating the same line to intersect the stress axis at unit strain. The true stress-strain curve for the tube material, reproduced from equation (4.1), is shown in Figure (4.4).

4.9 LUBRICANTS

Low friction and smooth drawing, combined with the ability to permit high reductions while preventing pick-up on the tool surfaces, are the primary requirements for tube-drawing lubricants. These factors are interrelated, for it has been shown⁽²⁰⁾ that pick-up increases very rapidly for quite small increases in base friction, while "die ringing", attributable to high stress concentrations at the point of entry of the tube into the die⁽¹⁶⁹⁾, is likely to be minimized when friction is low. In addition, the lubricants should be able to withstand the high localised temperatures and be readily removable so as not to stain the tube surface in any subsequent bright annealing operation.

Two viscous lubricating oils, recommended by their manufacturers for use in arduous metal working applications and currently used by Fine Tubes Limited, namely, EP 50 and TDN 85, were used in the present work. The trade names of these oils are EP Drawing Oil 50 and



- Experimental
- Theoretical, $\sigma = 1720 \epsilon^{0.5771} \text{ Nmm}^{-2}$
 $= 249542 \epsilon^{0.5771} \text{ lbf in}^{-2}$

Figure (4.4) Stress-strain relation of annealed tube material (Austenitic stainless steel, AISI 347)

Iloform TDN 85 which are manufactured by Gulf Oil (GB) Limited and Burmah-Castrol Company respectively. In the initial preparatory experiments these oils were used both on their own and also in conjunction with a plastic coat of 14% concentration in trichlorethane. Based on the results of these tests (see Section (5.3.1)) EP 50 alone was concluded to be the most suitable lubricant and hence used throughout the rest of the experimental programme.

The lubricant TDN 85 has a 47% content in mineral oil and the viscosities given by the manufacturers are as follows:

Temperature (°C)	20	40	100
Viscosity (cSt)	21,810	2464	58

EP 50 is a chlorinated paraffinic hydrocarbon belonging to the "Extreme Pressure" type and its typical properties are as follows:

Absolute density (gm cm ⁻³)	1.219
Relative density (15/15°C)	1.248
Viscosity Index (D2270)	L 0
Pour point (°C)	-21
Total acid No. D974	0.11
Chlorine (%)	51

Its viscosities at various temperatures provided by the manufacturers are:

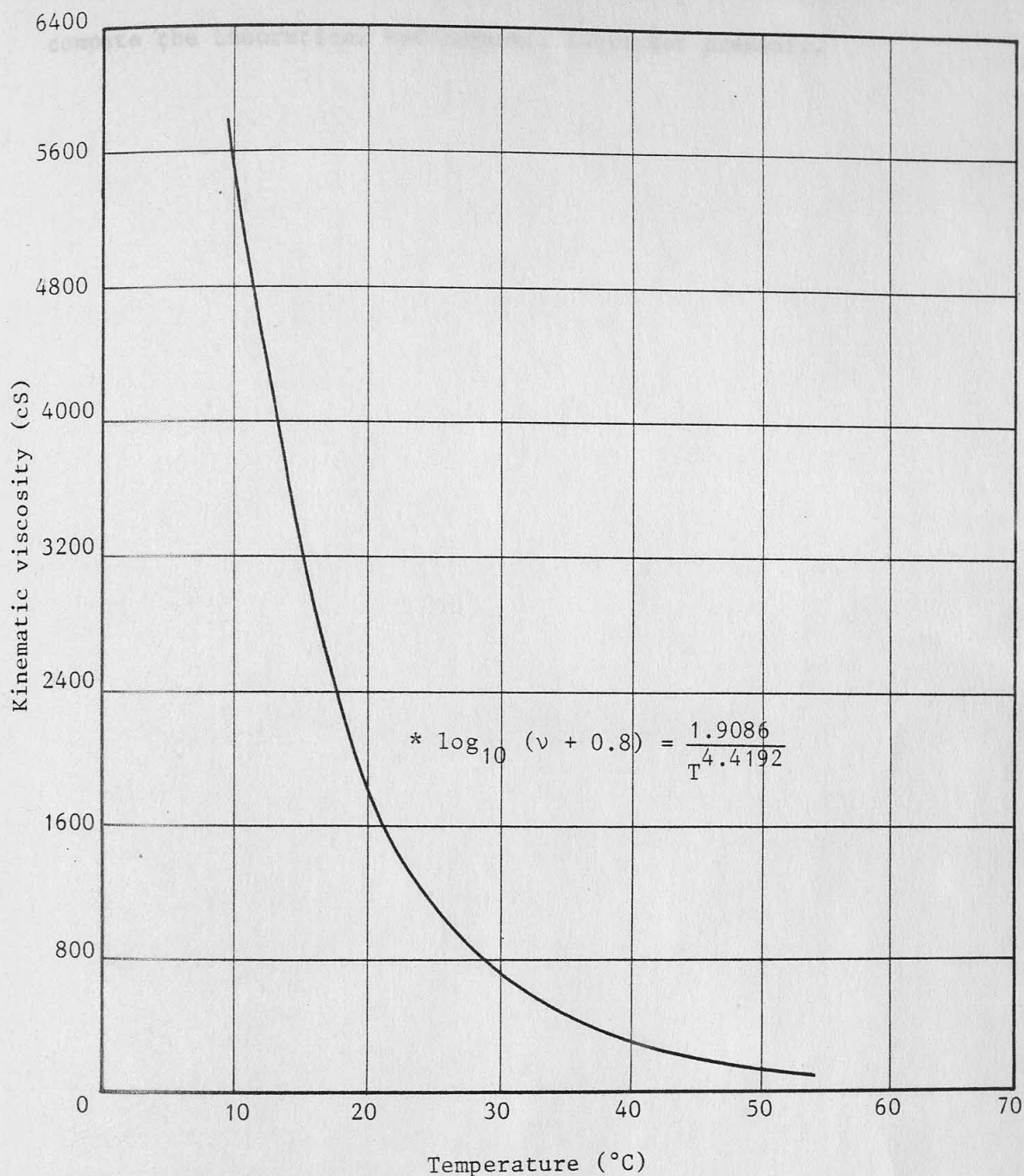
Temperature (°C)	20	40	50	100
Viscosity (cSt)	1880	282	135.7	12.95

The above information were entered on a "R.E.F.U.T.A.S." viscosity-temperature chart, from which the viscosities at other temperatures can be obtained conveniently. However, for a more accurate viscosity check, the viscosities of EP 50 at the above temperatures and at four other temperatures between 20°C and 50°C were measured using a "Cannon-Fenske No. 500" viscometer in accordance with B.S. 188:1957 (Determination of the viscosity of liquids). A

silicone fluid, "Dow Corning 200/1000 cS", which has a known viscosity variation with temperature was used to determine the viscometer constant. The results were found to agree with the data provided by the lubricant manufacturers.

It is convenient to express mathematically the viscosity-temperature relation for EP 50 rather than to refer to a viscosity-temperature chart. Among the empirical viscosity-temperature relations published in the literature and reviewed in Section (2.5.1), EP 50 was found to behave very closely according to the Walther⁽¹¹⁰⁾ proposal, as in equation (2.15), with c having a value of 0.8. The graphical illustration is shown in Figure (4.5.).

Due to the unavailability of both the facility to determine the variation of viscosity with pressure as well as the absence of such information from the manufacturers of EP 50, it is necessary, unfortunately, to assume from the published literature an empirical relation which has proven subsequently to be sufficiently reliable. Consequently, it was assumed that the lubricant obeys the Barus exponential law⁽¹⁰²⁾ $\eta = \eta_0 e^{\phi P}$; this assumption proved to be fortunately satisfactory in view of its simplicity and its almost universal acceptance, especially in the study of hydrodynamic lubrication in metal-forming processes^(5,6,7,91,93,94). The Burmah-Castrol Company who manufactures the lubricant TDN 85 recommended a value of ϕ equals $1.662 \times 10^{-4} \text{ in}^2 \text{ lbf}^{-1}$ for mineral oils. A survey of the hydrodynamic lubrication theories in the the metal-forming processes reviewed in Sections (2.3) and (2.4) revealed that the values ascribed to ϕ were between $1 \times 10^{-4} \text{ in}^2 \text{ lbf}^{-1}$ and $2 \times 10^{-4} \text{ in}^2 \text{ lbf}^{-1}$. These values appeared to be consistent with Neal's⁽¹⁷⁰⁾ recommendation that the viscosity of lubricating oils approximately doubles for every 5000 lbf in^{-2} increase in pressure. On this basis, it can be shown that ϕ approximates to $1.386 \times 10^{-4} \text{ in}^2 \text{ lbf}^{-1}$.



* v = Kinematic viscosity in centistokes

T = absolute temperature in degrees Rankine

Figure. (4.5) Viscosity-temperature relation of EP50

This value was used in the equations developed in Chapter 3 to compute the theoretical hydrodynamic lubricant pressure.

CHAPTER 5: EXPERIMENTAL PROGRAMME

5.1 INTRODUCTION

A systematic description of the experimental programme is presented in this chapter. This was designed to cover the practical aspects of the project as thoroughly as possible in the time available. It is composed of three sections, namely, the preparatory experiments, experiments with plug-attachments and experiments with Christopherson tubes. The preparatory experiments were investigative in nature and aimed at establishing a reference for the experiments on the promotion of hydrodynamic lubrication in the tube-drawing process. The basic drawing parameters, using industrial tooling and lubricants, such as the draw stress and plug force, the most suitable lubricant and the optimum die-angle or die semi-angle were assessed. Preparatory experiments with plug-attachments were conducted also to facilitate tool design and the establishment of a proper experimental technique for the main experiments. The experiments with Christopherson tubes and with plug-attachments were aimed at providing experimental data for comparison with the lubrication theories developed in Chapter 3 and also at observing the changes in the drawing process as a result of pressurizing the lubricant. In addition tests were carried out to investigate the possibility of drawing tubes in which the bore surfaces had not been treated

CHAPTER 5: EXPERIMENTAL PROGRAMME

5.1 INTRODUCTION

A systematic description of the experimental programme is presented in this chapter. This was designed to cover the practical aspects of the project as thoroughly as possible in the time available. It is composed of three sections, namely, the preparatory experiments, experiments with plug-attachments and experiments with Christopherson tubes. The preparatory experiments were investigative in nature and aimed at establishing a reference for the experiments on the promotion of hydrodynamic lubrication in the tube-drawing process. The basic drawing parameters, using industrial tooling and lubricants, such as the draw stress and plug force, the most suitable lubricant and the optimum die-angle or die semi-angle were assessed. Preparatory experiments with plug-attachments were conducted also to facilitate tool design and the establishment of a proper experimental technique for the main experiments. The experiments with Christopherson tubes and with plug-attachments were aimed at providing experimental data for comparison with the lubrication theories developed in Chapter 3 and also at observing the changes in the drawing process as a result pressurizing the lubricant. In addition tests were carried out to investigate the possibility of drawing tubes in which the bore surfaces had not been treated

either by pickling or by grit-blasting i.e. in the as-drawn surface condition, without the occurrence of metal transference or pick-up between the tube and the plug, when drawing with the proposed technique of bore lubrication. Current industrial practice necessitates bore surface treatment before drawing.

5.2 EXPERIMENTAL TECHNIQUE

In view of the wide scope of the experimental programme there are some variations in the experimental technique. A general description of the procedure is presented here and where appropriate references are made to the experiments concerned.

Before conducting the tests, both surfaces of the tubes were thoroughly cleaned with trichlorethane. The outside diameter and wall thickness of each tube were measured with a vernier caliper and a micrometer respectively. A code was etched on each tag to indicate the test number and the conditions under which the tests were carried out, e.g. draw speed, the lubricant used and percentage reduction in area. When a new batch of tubes was received, the external and internal surface finishes of a few tubes, selected at random from the batch, were obtained with a "Talysurf". These were considered to be representative of the particular batch. A few samples of these are shown in Figures (A6.13) and (A6.14). The external surfaces of the tubes were ground and the internal surfaces were grit-blasted. In a section of the experiments with plug-attachments, tubes which had been drawn were redrawn for a subsequent second pass. These tubes were annealed between the passes, but the surfaces were not treated. Thus, they were in the as-drawn surface condition and were much smoother than those which had received surface treatment.

The measuring instruments were switched on for about an hour before the actual usage so that they and the connecting circuits were allowed to stabilise. The bridges of both the draw load cell and the plug load cell were balanced and the zero was adjusted on the output of the u.v. recorder by adjusting the respective variable potentiometers connected to the load cells. When measuring the lubricant pressure, the charge amplifier, which was connected to the piezo-electric pressure transducer, was grounded just before the start of each draw in order to nullify any charge drift which might have occurred. The draw-bench was set at a draw speed of 15 ft min⁻¹ throughout the experimental programme. The actual speed was measured by observing the time elapsed for the draw carriage to traverse over a known distance.

Where lubrication included a plastic coating, as in some of the preparatory experiments, the coating was applied by dipping the tube into a cylindrical pipe filled with the plastic solution and allowed to drain. Lubricant was applied to the external surface of the tube with a brush. In the bore, the lubricant was applied by pouring it into the tube while rotating it slowly simultaneously so as to ensure that lubricant was deposited on its entire surface. When Christopherson tubes or plug-attachments were used, lubricant was applied also to these tools before they were positioned for the tests. A low pressure pneumatic cylinder supplied additional lubricant at the entry to the plug-attachments during drawing to ensure that ample lubricant was provided for the hydrodynamic action. A guide, having a diameter approximately equal to the bore of the undrawn tube was mounted on the plug-bar to prevent the undrawn tube from "wobbling" excessively relative to the plug. This was desirable since, in view of the small radial clearance, excessive "wobbling" could prevent a continuous flow of lubricant

and may result in a scoring of the surface of the Christopherson tubes or plug-attachments. The guide was made of a molybdenum disulphide impregnated nylon which combines rigidity with a degree of elasticity and has the added advantage in that molybdenum disulphide is a good solid lubricant. In these tests the ambient laboratory temperature was noted also in order that the lubricant viscosity may be deduced. Sealing at the joints between the plug and the attachment, and the pressure transducer and its mounting was achieved using lead washers. In addition a "Loctite" hydraulic seal was applied on the screw threads before tightening the mating components.

In the initial tests the plug-bar was adjusted such that the plug protruded from the land of the die by approximately $1/16$ in. This produced adverse effects and in the later tests effort was made to position the plug such that its end was in line with the down-stream end of the land of the die. The elongation of the plug-bar under a tensile load was accounted for.

For purposes of assessing the efficiency of the lubricants in the preparatory experiments, additional information was obtained by measuring the temperature of the tube with a thermo-couple immediately after drawing.

Residual lubricant remaining on the drawn tubes was removed using trichlorethane. The outside diameter and wall thickness of each drawn tube were measured. These measurements enabled the actual reduction in area and the homogeneous strain imposed on the tubes to be calculated. A section was sawn from each drawn tube and split and examined for possible surface defects such as pick-up and pitting corrosion. The surface finishes of both the external and internal surfaces were recorded with a "Talysurf". When Christopherson tubes or plug attachments were used, the traces of the draw force and/or plug force allowed the surface finish of different sections

of the same drawn tube undergoing differing force conditions to be observed. This was helpful since coarser surface finishes and lower forces are associated with better lubrication.

5.3 PREPARATORY EXPERIMENTS

These experiments were not aimed directly at achieving the objectives of the project, but rather, as the title implies, at establishing a reference for the experiments to be conducted to achieve these objectives. Thus, these experiments were designed to investigate or assess the basic drawing parameters as well as to establish an experimental technique for the experiments on the promotion of hydrodynamic lubrication. The results and observations made during the course of these preparatory experiments are discussed here in order that their relevance may be better appreciated. The results of these preparatory experiments are tabulated and presented in Tables (A2.1 - A2.6) of Appendix (A2).

The drawing tools and lubricants were of the design and type which are currently used in industrial practice. The tubes were of 347 stainless steel and were nominally 1.0 x 0.10 in (outside diameter x wall thickness) before drawing. The external surfaces of these tubes were ground and the internal surfaces were grit-blasted. These surface treatments are current industrial practice also. Tubes of the same nominal dimensions and surface conditions were used throughout these preparatory experiments so that the results were compatible.

5.3.1 Assessment of basic drawing parameters

The main objective of the series of tests described here was to assess the basic drawing parameters, with particular reference to the effects of friction and lubrication. Tubes were drawn at

at four reductions in area and using five lubricating systems. The reductions were 40%, 35%, 30% and 25%, and the lubricating systems were EP 50, TDN 85, 4% plastic solution in trichlorethane coating, EP 50 with a 14% plastic solution coating and TDN 85 with a 14% plastic solution coating. The drawing dies had a nominal semi-angle of 15°.

High frictional forces or insufficient lubrication at the tool-tube interfaces for a given amount of plastic straining are reflected by the draw force and the plug force. The plug force is the frictional force acting on the plug-tube interface since the plug is a cylinder and friction is the only force acting in the axial direction. The lubricant interposes between the interfaces a minute film of low strength which reduces the degree of metallic interaction and frictional heating. Thus, the draw force or draw stress, plug force, surface finish and temperature of the drawn tubes are indicative of the lubrication efficiency.

The tests were conducted in accordance with the relevant experimental procedure described in Section (5.2). Figure (5.1) shows the draw stress and the corresponding homogeneous strain imposed on the tubes for the five lubricating systems. Originally, these were plotted against the corresponding percentages reduction in area. However, since a close-pass draw regime did not prevail in these tube-drawing trials, a fractional reduction in area did not fully reflect the extent to which a tube had been deformed. Thus, the total homogeneous strain was obtained by summing the strains due to the draft and sink components of the deformation process according to:

$$\epsilon = \frac{\sqrt{3}}{2} \ln \frac{A_1}{A_S} + \ln \frac{t_1}{t_2} \quad (5.1)$$

Figure (5.2) was obtained by plotting the temperature of the drawn tubes against the homogeneous strain for the same lubricants.

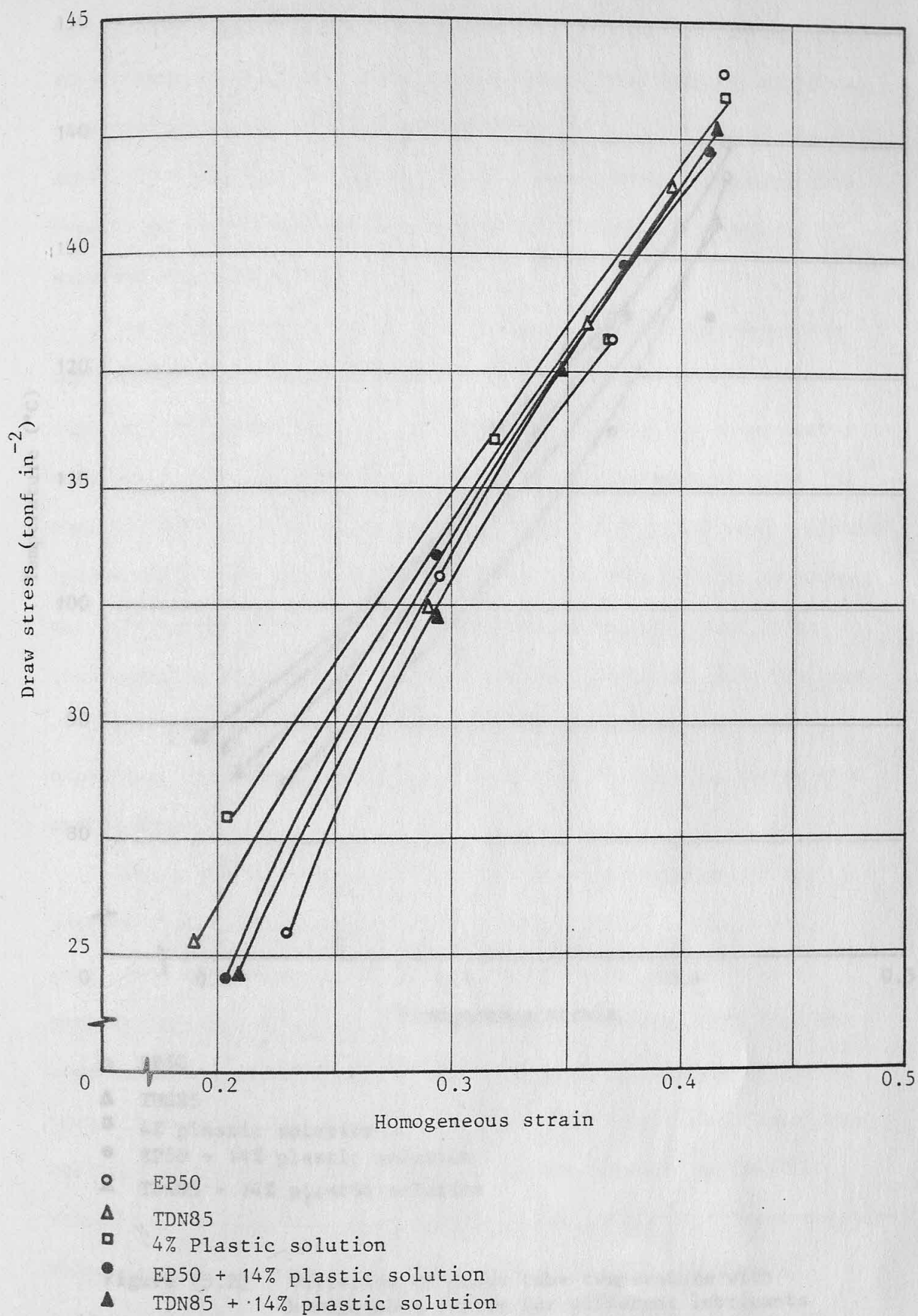


Figure (5.1) Variation of draw stress with homogeneous strain for different lubricants

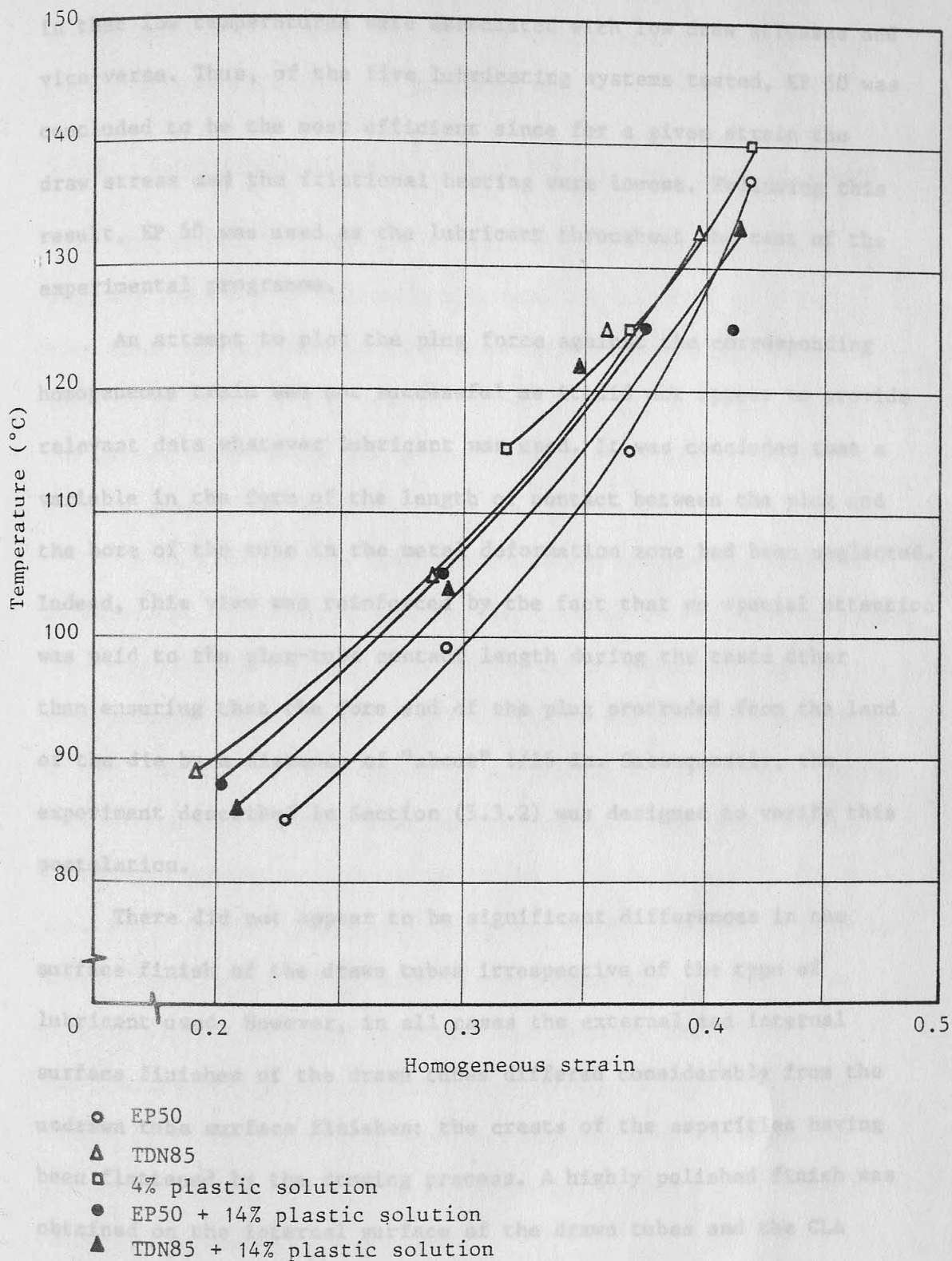


Figure (5.2) Variation of drawn tube temperature with homogeneous strain for different lubricants

It can be seen that the order of the curves in both graphs corroborate in that low temperatures were associated with low draw stresses and vice-versa. Thus, of the five lubricating systems tested, EP 50 was concluded to be the most efficient since for a given strain the draw stress and the frictional heating were lowest. Following this result, EP 50 was used as the lubricant throughout the rest of the experimental programme.

An attempt to plot the plug force against the corresponding homogeneous strain was not successful as it did not appear to provide relevant data whatever lubricant was used. It was concluded that a variable in the form of the length of contact between the plug and the bore of the tube in the metal deformation zone had been neglected. Indeed, this view was reinforced by the fact that no special attention was paid to the plug-tube contact length during the tests other than ensuring that the fore end of the plug protruded from the land of the die by a distance of "about" 1/16 in. Subsequently, the experiment described in Section (5.3.2) was designed to verify this postulation.

There did not appear to be significant differences in the surface finish of the drawn tubes irrespective of the type of lubricant used. However, in all cases the external and internal surface finishes of the drawn tubes differed considerably from the undrawn tube surface finishes; the crests of the asperities having been flattened by the drawing process. A highly polished finish was obtained on the internal surface of the drawn tubes and the CLA values ranged from 0.01 μm to 0.06 μm compared with a representative value of 0.25 μm before the tubes were drawn. On the external surface, the CLA values ranged from 0.12 μm to 1.3 μm compared with a representative value of 0.4 μm before drawing. These surfaces had a dull appearance and although the increase in CLA values could

be attributed partially to the surface extending or stretching during deformation, contributions to lubrication by hydrodynamic action at the die-entry was possible also.

5.3.2 Experiments on the effect of the plug-tube contact length

The effect on friction of the length of contact between the plug and the bore of the deforming tube was verified by drawing five tubes of the same initial dimensions at a nominal reduction in area using EP 50 as the lubricant. The same die and plug were used throughout these tests but in each case a different plug-tube contact length was used.

It is obvious that during the drawing process the plug-bar is subjected to an axial tensile load induced by friction. In order that the resulting elastic elongation may be taken into account when setting the plug-tube contact length, the elastic characteristic of the plug-bar was determined by subjecting it to a simple tension test within the elastic limit of its material. The tensile load - elongation property of the plug-bar is shown in Figure (5.3). The experience of the experiments described in the previous section has shown that the mean plug-force was approximately 0.7 tonf. The elastic elongation under this load was obtained from Figure (5.3) and subtracted from the predetermined contact length. The actual length of contact during drawing was deduced from the magnitude of the measured plug-force, its corresponding elongation, and the initial compensation under the mean load.

Figure (5.4) shows the variation of the plug-force and draw stress with the length of contact between the plug and the bore of the tube. It is seen that the plug force increased with the contact length and that the rate of increase became gradual and asymptotic as the plug protruded well beyond the land of the die.

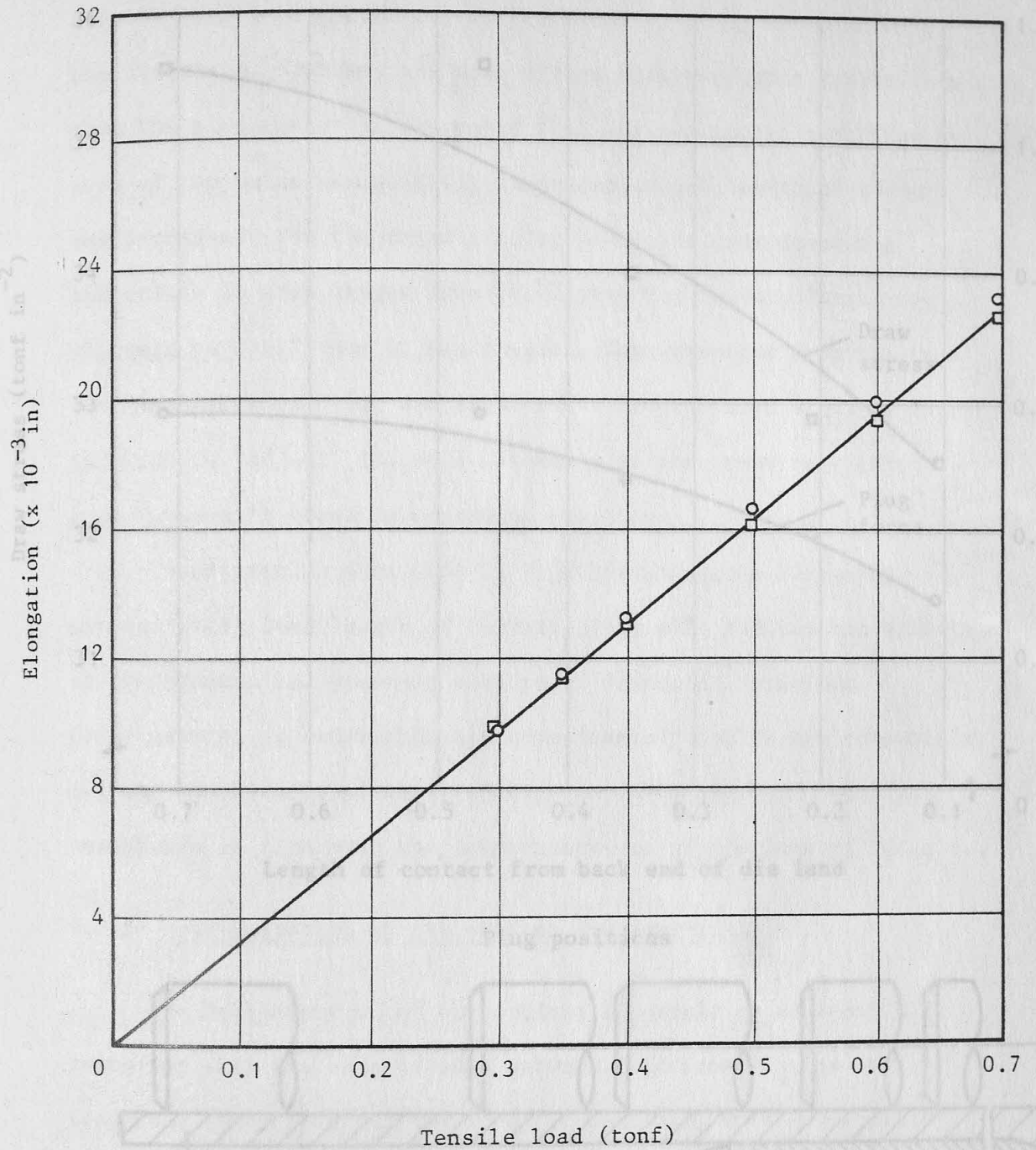


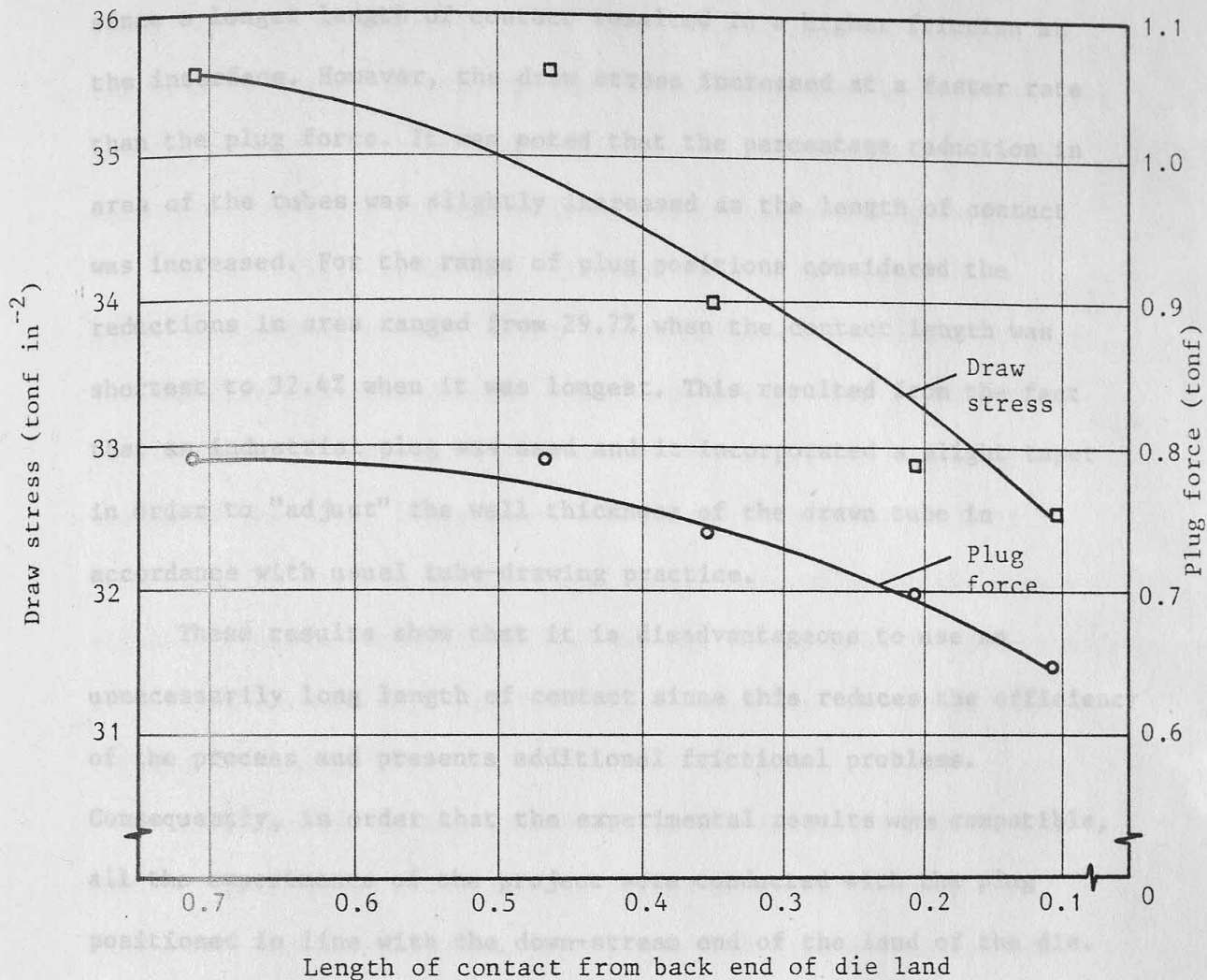
Figure (5.3) Calibration chart for the plug-bar

Material = 347 Stainless steel

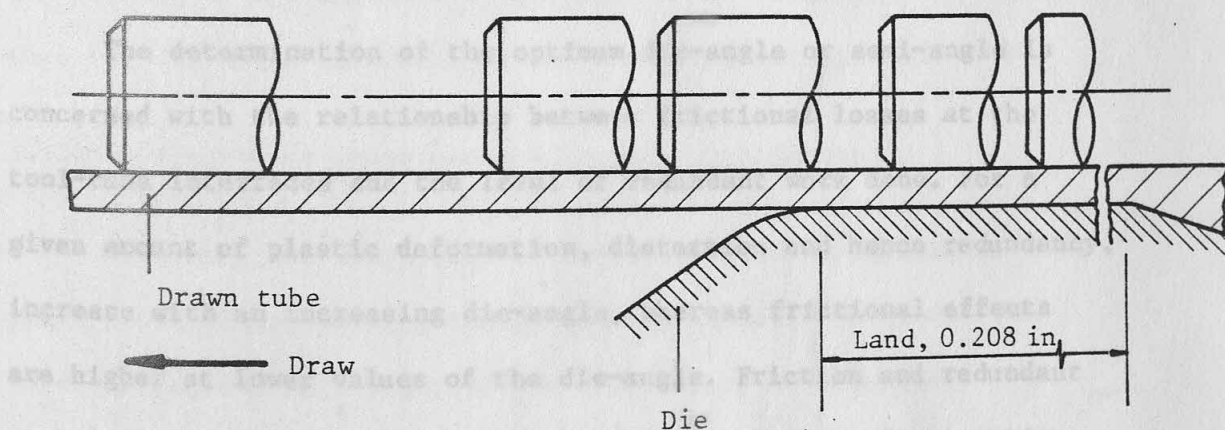
Reduction in area = 30%

Lubricant = EP50

Figure (3.4) Variation of plug force and draw stress with plug - 175 -



3.3.3 Determination of the Plug positions



Material = 347 Stainless steel

Reduction in area = 30%

Lubricant = EP50

Figure (5.4) Variation of plug force and draw stress with plug-tube contact length

The draw stress increased also with the contact length, as expected, since a longer length of contact resulted in a higher friction at the interface. However, the draw stress increased at a faster rate than the plug force. It was noted that the percentage reduction in area of the tubes was slightly increased as the length of contact was increased. For the range of plug positions considered the reductions in area ranged from 29.7% when the contact length was shortest to 32.4% when it was longest. This resulted from the fact that an industrial plug was used and it incorporated a slight taper in order to "adjust" the wall thickness of the drawn tube in accordance with usual tube-drawing practice.

These results show that it is disadvantageous to use an unnecessarily long length of contact since this reduces the efficiency of the process and presents additional frictional problems. Consequently, in order that the experimental results were compatible, all the experiments of the project were conducted with the plug positioned in line with the down-stream end of the land of the die.

5.3.3 Determination of the optimum die semi-angle

The determination of the optimum die-angle or semi-angle is concerned with the relationship between frictional losses at the tool-tube interfaces and the level of redundant work done. For a given amount of plastic deformation, distortion and hence redundancy, increase with an increasing die-angle, whereas frictional effects are higher at lower values of the die-angle. Friction and redundant work both increase the drawing load. Therefore, there is an optimum die-angle at which the total work done, including friction and work, is minimal.

The experimental programme consisted of drawing tubes nominally 1.0 x 0.10 in (outside diameter x wall thickness) at four reductions

in area using dies of 6° , 8° , 10° , 12° and 15° semi-angles. The tubes were lubricated with EP 50 since it had been established as the most efficient lubricant. The length of contact between the plug and the bore of the tube was consistent in each case, and set in accordance with the procedure described in the previous section.

Figure (5.5) shows the variation of draw stress with the total homogeneous strain, which was calculated using equation (5.1), for the five die semi-angles. These curves were used to plot the variation of draw stress with the die semi-angle for different values of the total homogeneous strain, as in Figure (5.6). It is seen that for a given strain there is an angle at which the draw stress is lowest; this is the optimum die semi-angle. For homogeneous strains of between 0.25 and 0.50 the optimum die semi-angle lies between 10° and 12° .

Furthermore, it was observed that the surface finish on the external surface of the tubes was duller in appearance and had higher CLA values when tubes were drawn with dies of smaller semi-angles. This is attributable to the fact that a contribution to lubrication by hydrodynamic action at the die entry is more pronounced when the die-angle is small, as was initially anticipated.

5.3.4 Preparatory experiments with plug-attachments

Following the completion of the preparatory experimental work using conventional drawing tools, the experimental programme was directed towards investigating the feasibility of promoting hydrodynamic lubrication of the bore by induced hydrodynamic action. It was proposed to fit an attachment, which provided a small radial clearance between itself and the bore of the undrawn tube, to a conventional plug. The motion of the tube and the viscosity of the lubricant draw the lubricant into the annular space so formed and

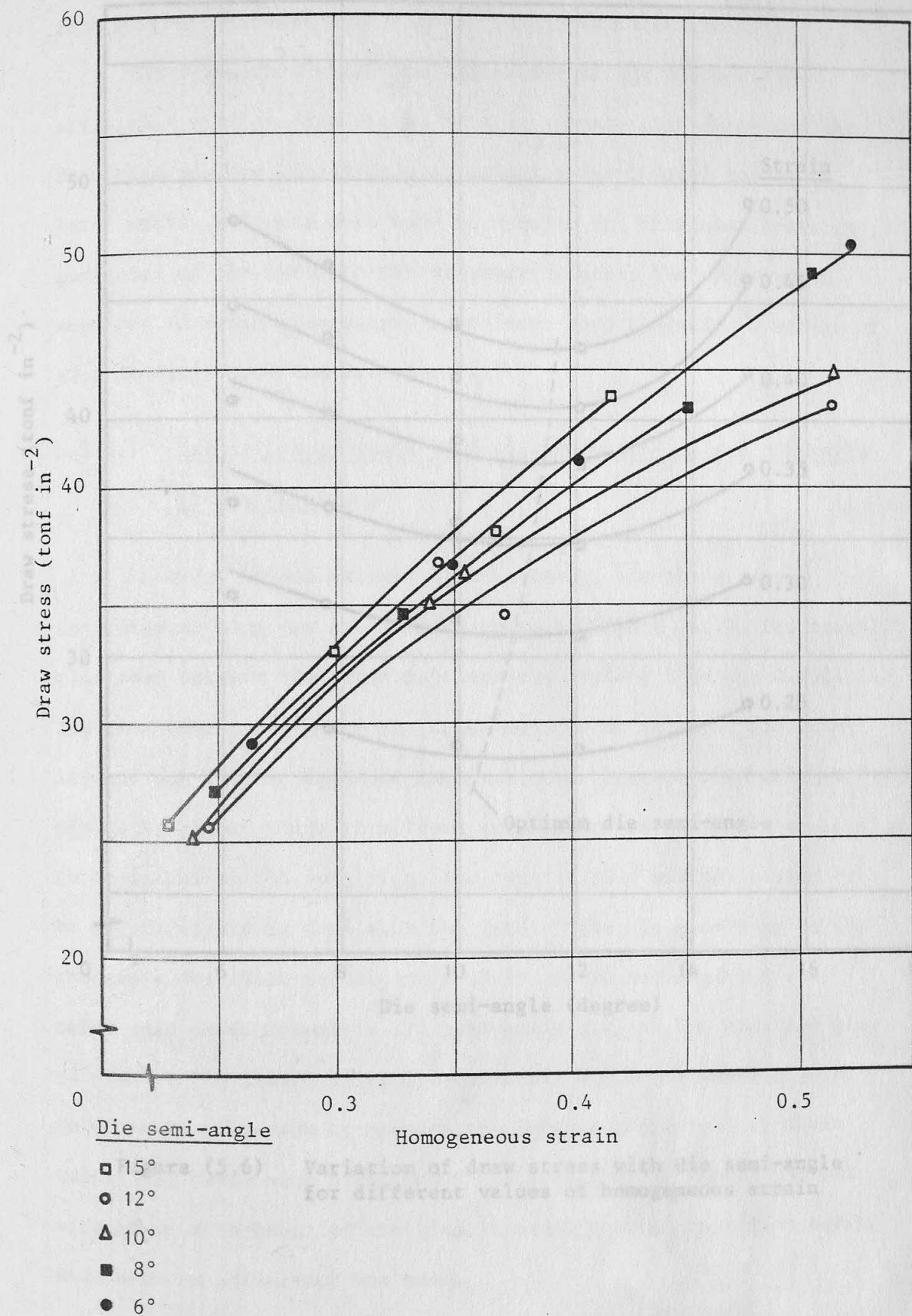


Figure (5.5) Variation of draw stress with homogeneous strain for different die semi-angles

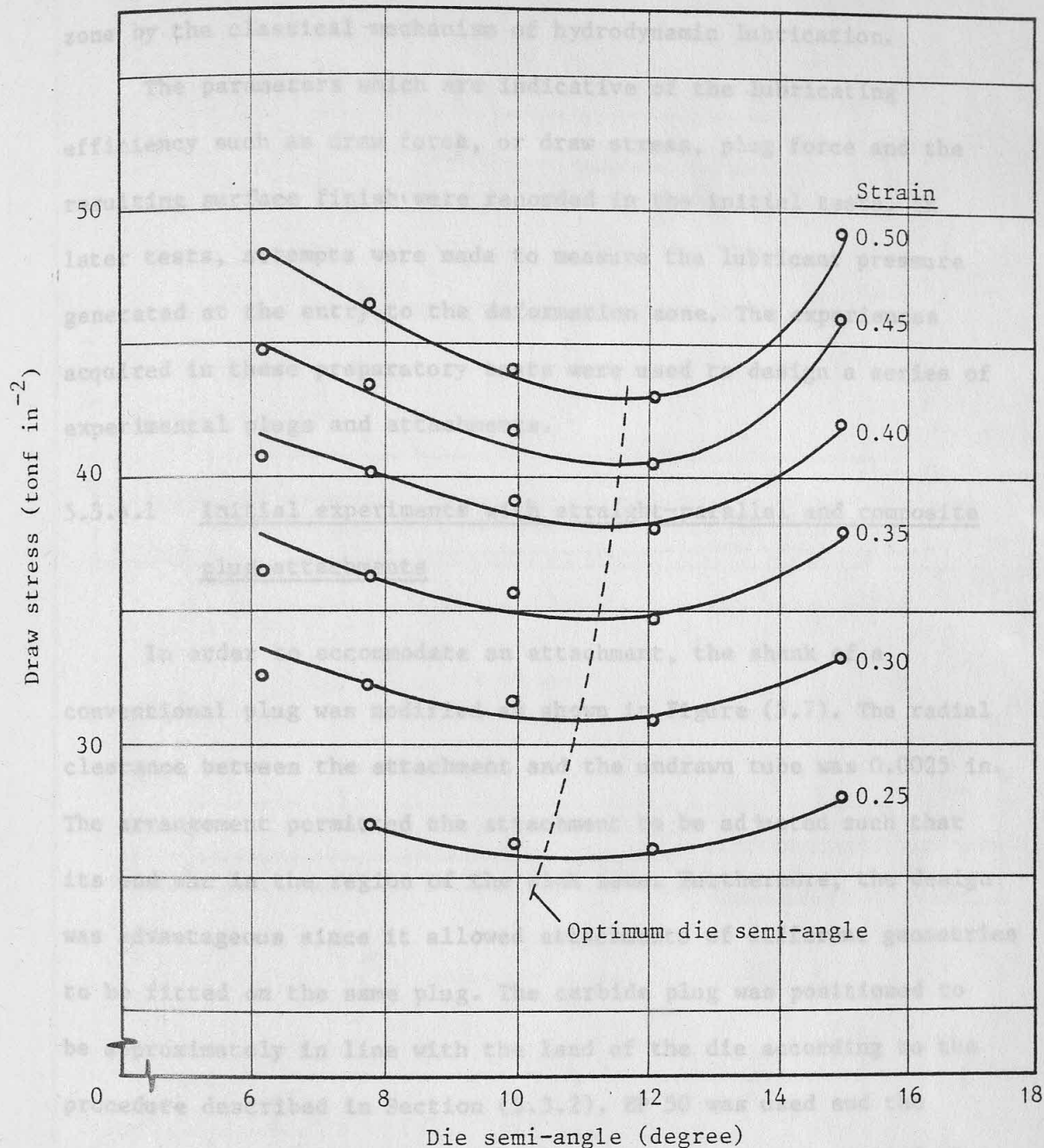


Figure (5.6) Variation of draw stress with die semi-angle for different values of homogeneous strain

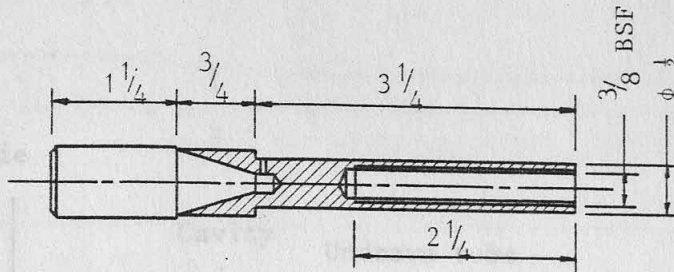
generates a high lubricant pressure at the entry to the deformation zone by the classical mechanism of hydrodynamic lubrication.

The parameters which are indicative of the lubricating efficiency such as draw force, or draw stress, plug force and the resulting surface finish were recorded in the initial tests. In later tests, attempts were made to measure the lubricant pressure generated at the entry to the deformation zone. The experiences acquired in these preparatory tests were used to design a series of experimental plugs and attachments.

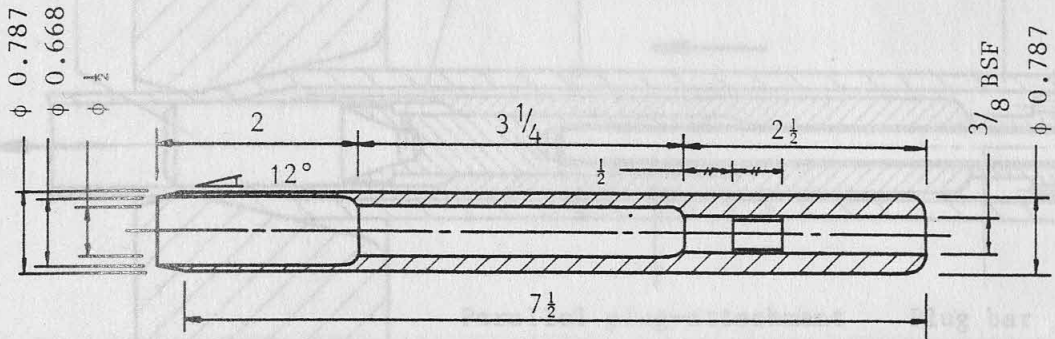
5.3.4.1 Initial experiments with straight-parallel and composite plug-attachments

In order to accommodate an attachment, the shank of a conventional plug was modified as shown in Figure (5.7). The radial clearance between the attachment and the undrawn tube was 0.0025 in. The arrangement permitted the attachment to be adjusted such that its end was in the region of the sink zone. Furthermore, the design was advantageous since it allowed attachments of different geometries to be fitted on the same plug. The carbide plug was positioned to be approximately in line with the land of the die according to the procedure described in Section (5.3.2). EP 50 was used and the tubes were drawn through a 12° semi-angle die and the modified plug to yield a 35% reduction or approximately 0.4 homogeneous strain. No attempts were made to measure the lubricant pressure in these tests. Two tubes were drawn under the same drawing conditions but without an attachment to the plug in order that a comparison may be made when an attachment was used.

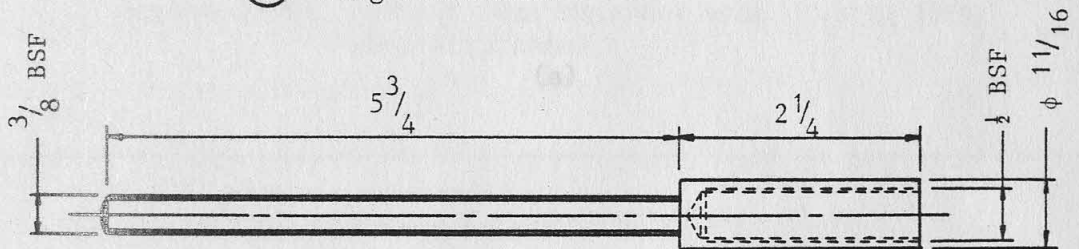
Five tubes were drawn successively with the straight-parallel attachment as shown in Figure (5.8), and typical traces of the drawn force and plug force shown in Figure (5.9) were obtained. The



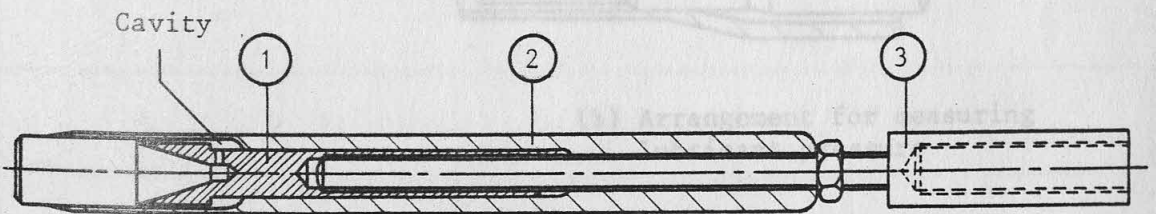
① Conventional plug with modified shank



② Plug attachment



③ Assembly screw



Assembly

Figure (3.8) Arrangement of the tools and pressure transducer in the preliminary experiments

Title	Plug attachment		
Scale	1:2	Dimension	Inches
Drawn	T B Lim	Material	Mild steel
Date	27.3.81	Figure	5.7

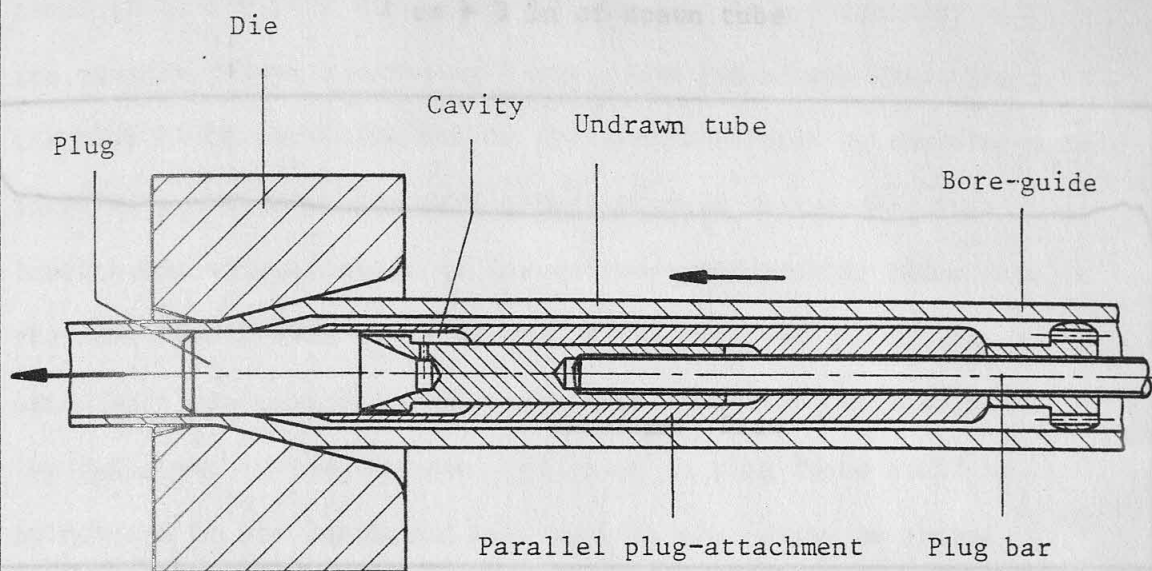
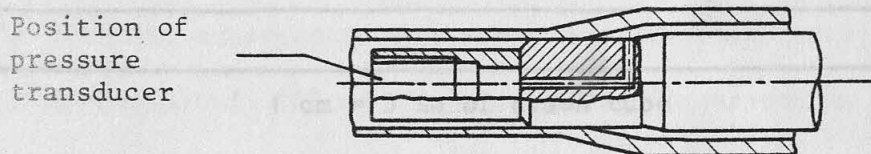


Figure (5.9) Force traces obtained when drawing with plug-attachment
(a)



(b) Arrangement for measuring lubricant pressure

Figure (5.8) Arrangement of the tools and pressure transducer in the preliminary experiments

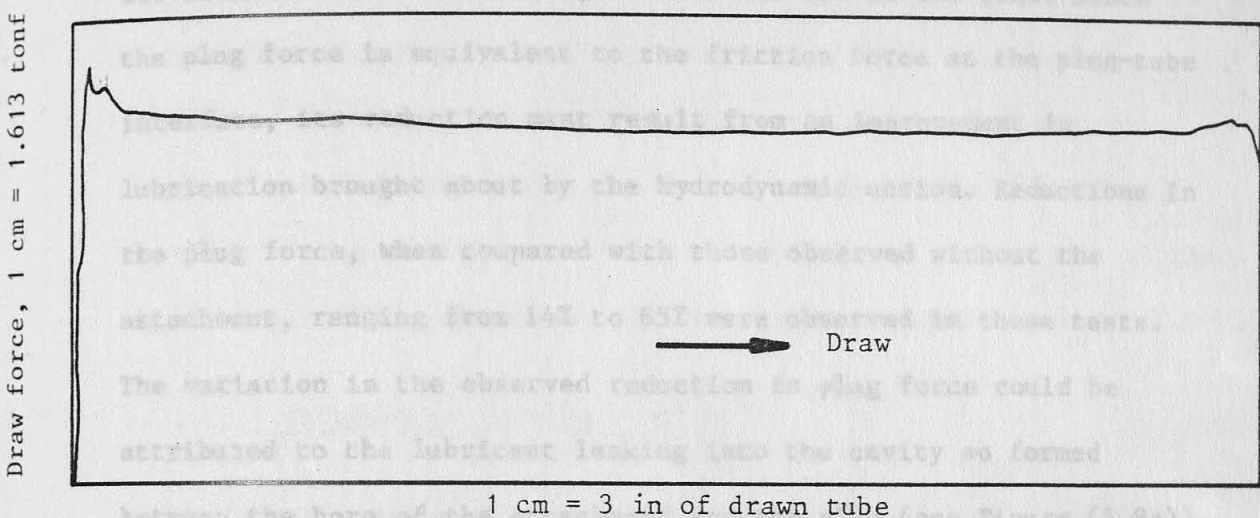
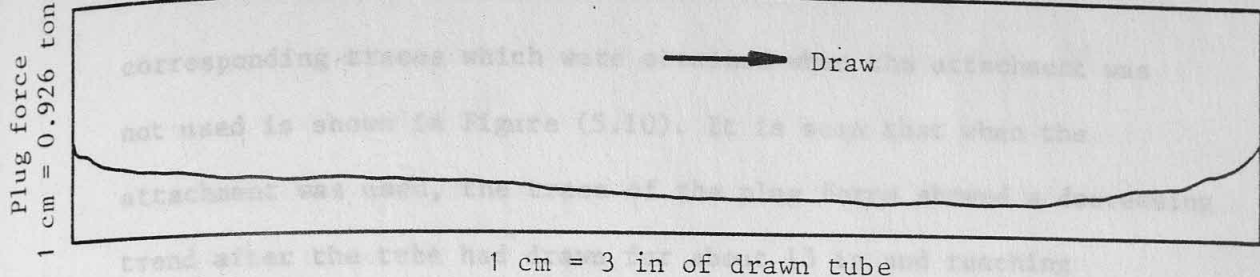


Figure (5.9) Force traces obtained when drawing with plug-attachment

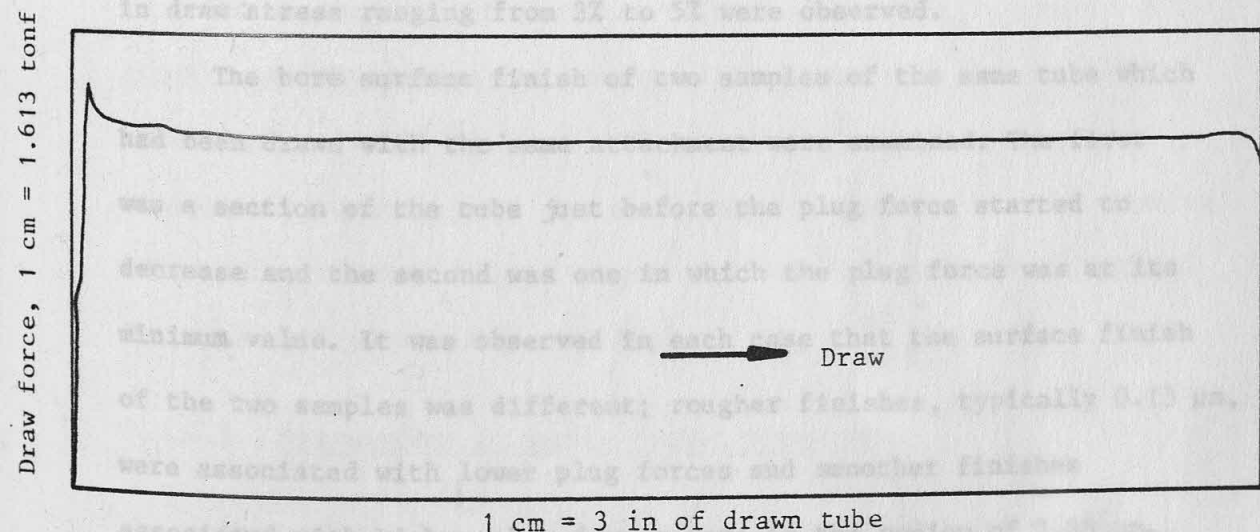
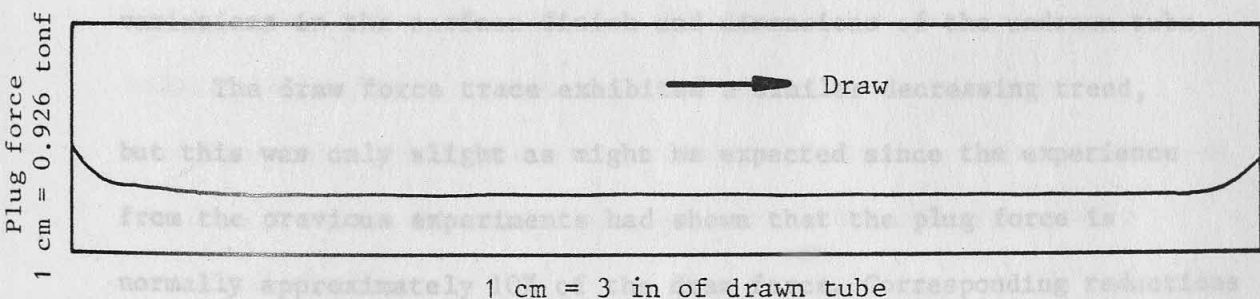


Figure (5.10) Force traces obtained when drawing without plug-attachment

corresponding traces which were obtained when the attachment was not used is shown in Figure (5.10). It is seen that when the attachment was used, the trace of the plug force showed a decreasing trend after the tube had drawn for about 13 in and reaching its minimum before increasing towards the end of the draw. Since the plug force is equivalent to the friction force at the plug-tube interface, its reduction must result from an improvement in lubrication brought about by the hydrodynamic action. Reductions in the plug force, when compared with those observed without the attachment, ranging from 14% to 65% were observed in these tests. The variation in the observed reduction in plug force could be attributed to the lubricant leaking into the cavity so formed between the bore of the attachment and the plug (see Figure (5.8a)), thus the highest lubricant pressure which could be generated was not likely to have been achieved. Other possible factors included variations in the surface finish and dimensions of the undrawn tube.

The draw force trace exhibited a similar decreasing trend, but this was only slight as might be expected since the experience from the previous experiments had shown that the plug force is normally approximately 10% of the draw force. Corresponding reductions in draw stress ranging from 2% to 5% were observed.

The bore surface finish of two samples of the same tube which had been drawn with the same attachment were examined. The first was a section of the tube just before the plug force started to decrease and the second was one in which the plug force was at its minimum value. It was observed in each case that the surface finish of the two samples was different; rougher finishes, typically $0.13\text{ }\mu\text{m}$, were associated with lower plug forces and smoother finishes associated with higher plug forces were in the region of $0.06\text{ }\mu\text{m}$. In addition, the smoother surface finish resembled that of tubes

which were drawn without the plug-attachment. These had CLA values of about $0.05 \mu\text{m}$. Typical bore surface finishes are illustrated in Figure (5.11). The representative bore surface finish of this batch of undrawn tubes was $1.0 \mu\text{m}$.

Observations, similar to these described above, obtained when a composite attachment was used. The ratio of the length of the parallel portion to that of the tapered portion was 1:2 and the angle of taper on the latter was 8 minutes. The radial clearance provided by the parallel portion was 0.0025 in as in the case of the straight-parallel attachment. The length of the attachment was 7.5 in.

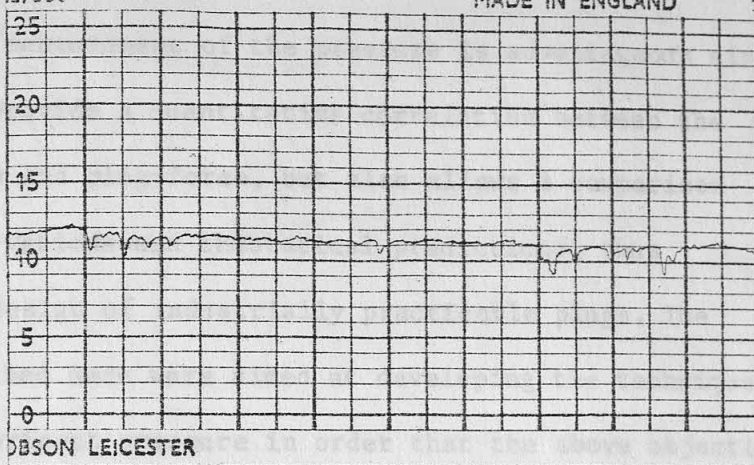
5.3.4.2 Elimination of plug chatter

The occurrence of plug chatter can be attributed to stick-slip friction arising from poor lubrication, i.e. from a lack of lubricant at the plug-tube interface or from the use of an ineffective lubricant, or both. Tests on the efficacy of the proposed method of inducing hydrodynamic lubrication of the plug-tube interface were therefore extended to the elimination of chatter by using a lubricant which is known to cause the plug to chatter when drawing with a conventional plug.

It was found that the conventional plug could be compelled to chatter by lubricating the plug-tube interface with a lubricant which contained 70% EP 50 and 30% paraffin. However, when the composite plug attachment was used under otherwise identical drawing conditions, chatter did not occur until the lubricant contained 60% EP 50 and 40% paraffin.

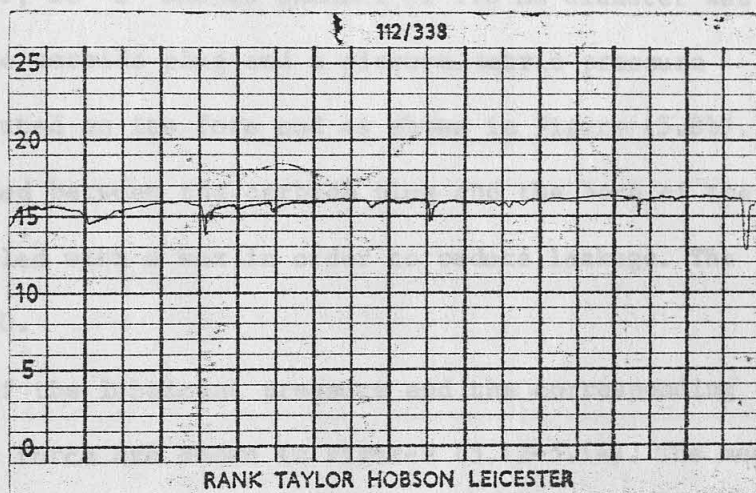
5.3.4.3 Measurement of hydrodynamic pressure

The experiments conducted so far suggest the existence of a high lubricant pressure at the entry to the metal deformation zone.



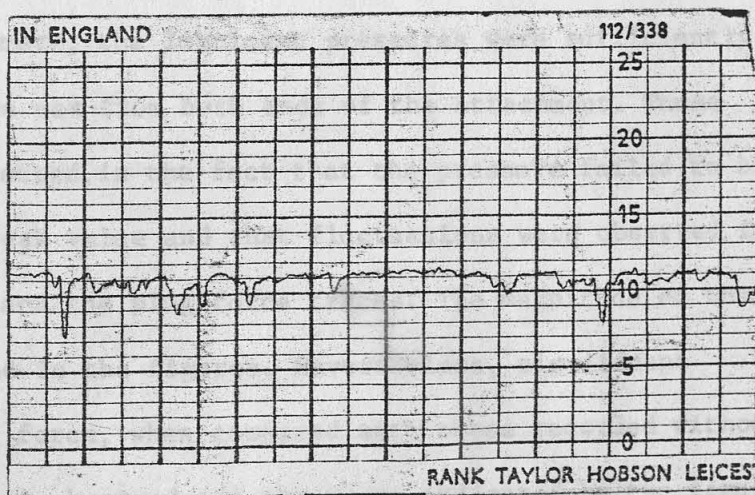
Scale = 100×10000 (L x H), $0.05 \mu\text{m}$ CLA

(a) Bore surface topography of tube drawn without plug-attachment



Scale = 100×10000 (L x H), $0.06 \mu\text{m}$ CLA

(b) Bore surface topography of tube drawn with plug-attachment; high plug force



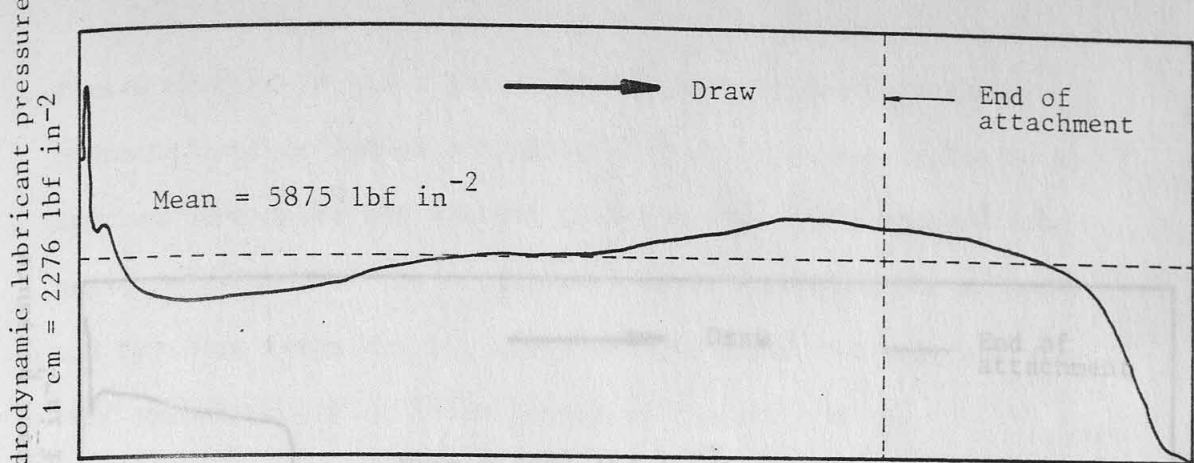
Scale = 100×10000 (L x H), $0.13 \mu\text{m}$ CLA

(c) Bore surface topography of tube drawn with plug-attachment; low plug force

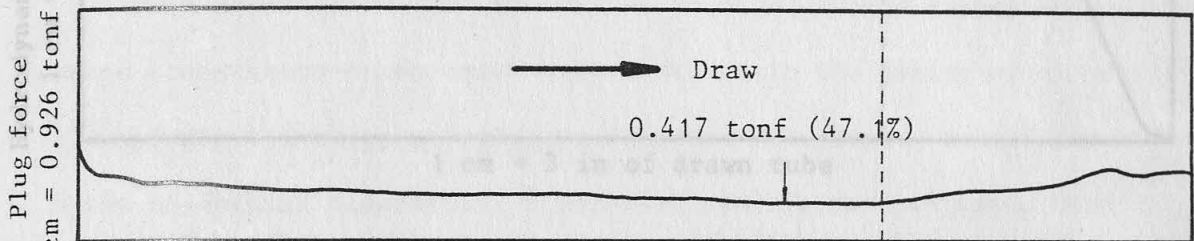
Figure (5.11) Bore surface topography of drawn tubes

However, a direct measurement of the pressure is advantageous since not only does it provide a quantitative correlation between the lubricant pressure and plug-force, but also allows a comparison experimental observations and theoretical predictions, thus facilitating the design of industrially practicable plugs. The experiments described here were aimed at developing the technique to measure the lubricant pressure in order that the above objectives may be achieved. The experiments were conducted with the plug, the 12° semi-angle die and the straight-parallel attachment used previously. However, an 'L' shaped channel of 1.0 mm diameter was spark-eroded in the carbide plug and a piezo-electric pressure transducer was mounted on its fore end as shown in Figure (5.8b). The cavity so formed between the carbide plug and the bore of the attachment was filled with a wax in order to reduce leakage. The lubricant was EP 50.

Three traces of the lubricant pressure and the corresponding traces of the plug force are shown in Figures (5.12-5.14). The mean pressures indicated in the figures were deduced using a "Planimeter". It is interesting to note that the rise of the lubricant pressure was almost instantaneous, i.e. it started as soon as drawing commenced. Furthermore, the lubricant pressures were sufficiently high to extrude the wax from both ends of the attachment. These leakages were reflected in the fact that the pressure failed to be sustained at the peak value and that fluctuations were observed in both the pressure and the plug force traces. The magnitude of these items are indicated in the figures. Nevertheless, significant reductions in plug force, when compared with those recorded without the attachment, were observed and these are indicated by the figures in parentheses. That low plug forces are associated with high hydrodynamic pressures in the lubricant is clearly illustrated by

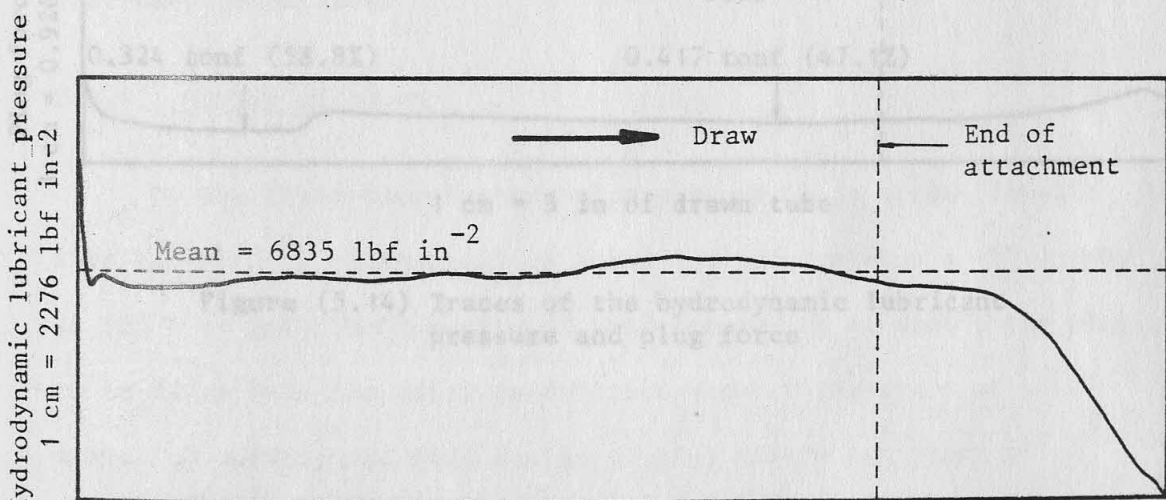


1 cm = 3 in of drawn tube

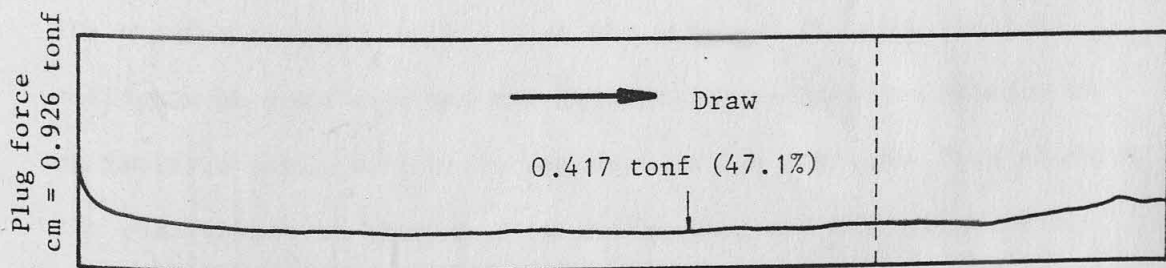


1 cm = 3 in of drawn tube

Figure (5.12) Traces of the hydrodynamic lubricant pressure and plug force



1 cm = 3 in of drawn tube



1 cm = 3 in of drawn tube

Figure (5.13) Traces of the hydrodynamic lubricant pressure and plug force

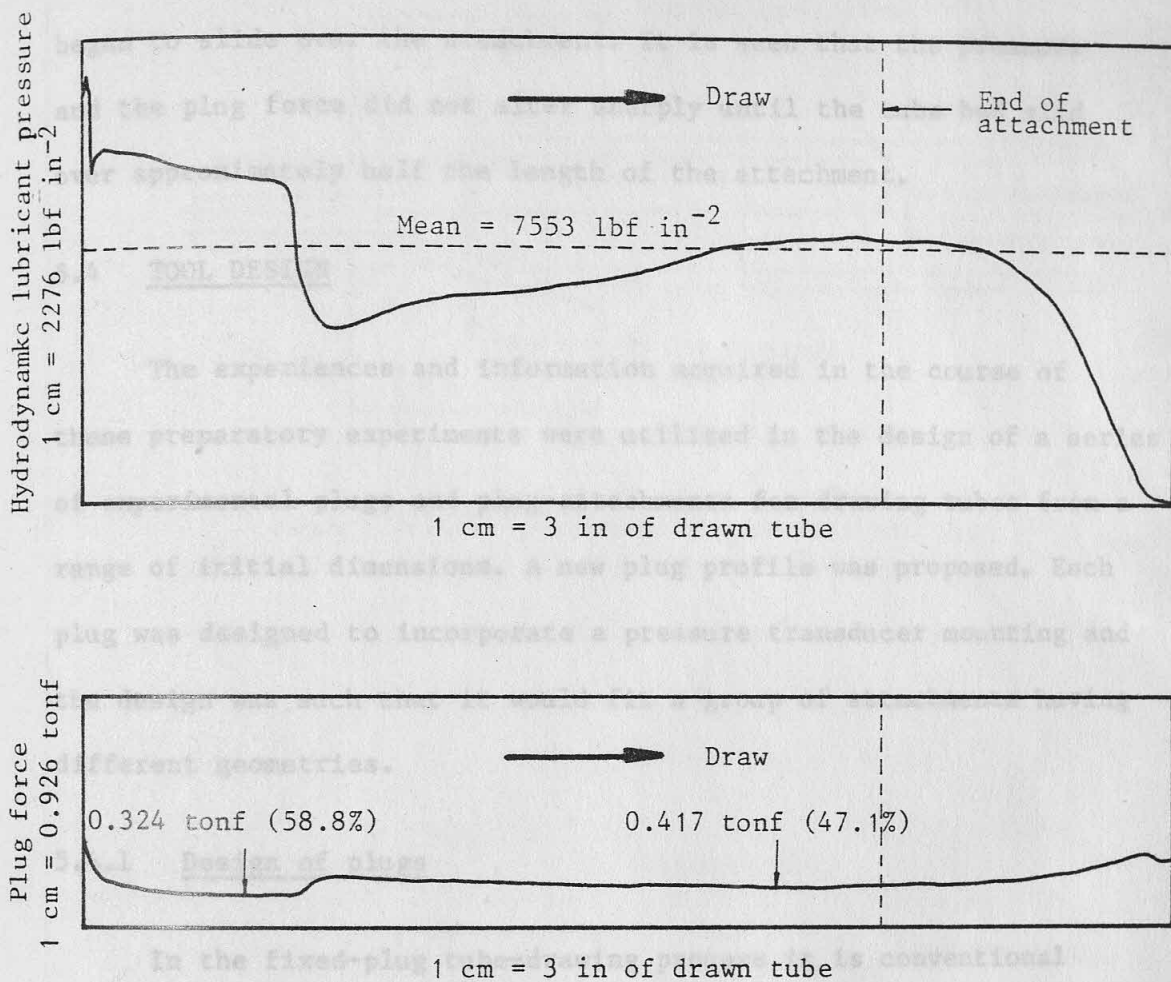


Figure (5.14) Traces of the hydrodynamic lubricant pressure and plug force

Figure (5.14), in which the distinctively different levels of pressure were reflected accordingly by the plug force. The vertical hatched line marks the instant when the end of the undrawn tube began to slide over the attachment. It is seen that the pressure and the plug force did not alter sharply until the tube had slid over approximately half the length of the attachment.

5.4 TOOL DESIGN

The experiences and information acquired in the course of these preparatory experiments were utilized in the design of a series of experimental plugs and plug-attachments for drawing tubes from a range of initial dimensions. A new plug profile was proposed. Each plug was designed to incorporate a pressure transducer mounting and the design was such that it would fit a group of attachments having different geometries.

5.4.1 Design of plugs

In the fixed-plug tube-drawing process it is conventional that the plug is cylindrical in shape and incorporates a 45° chamfer at its fore end. The function of this chamfer is to enable the plug to be drawn into the metal deformation zone at the start of the draw. The position of this design of plug before the start of drawing is shown in Figure (5.15). It is disadvantageous to have a sharp-edge contact between the bore surface of the undrawn tube and the chamfer of the plug since at the start of the draw the tube collapses on this edge and the high pressures involved results in an intimate metallic contact between the two surfaces. This enhances the possibility of pick-up between the plug and the tube, which, when initiated will propagate through the entire length of the drawn tube. Evidence of this occurrence can be seen by splitting

Position of initial
contact

Die

Conventional plug

Undrawn tube

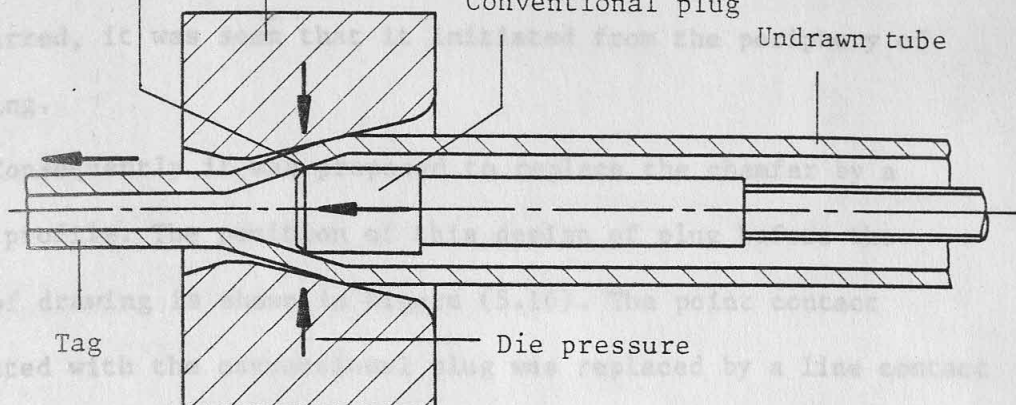


Figure (5.15) Position of conventional plug
at the start of drawing

Position of initial
contact

Die

Proposed plug

Undrawn plug

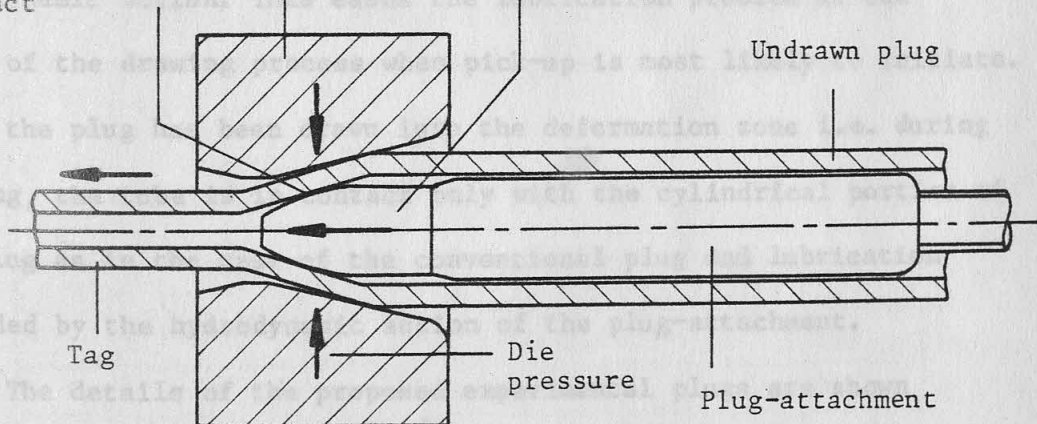
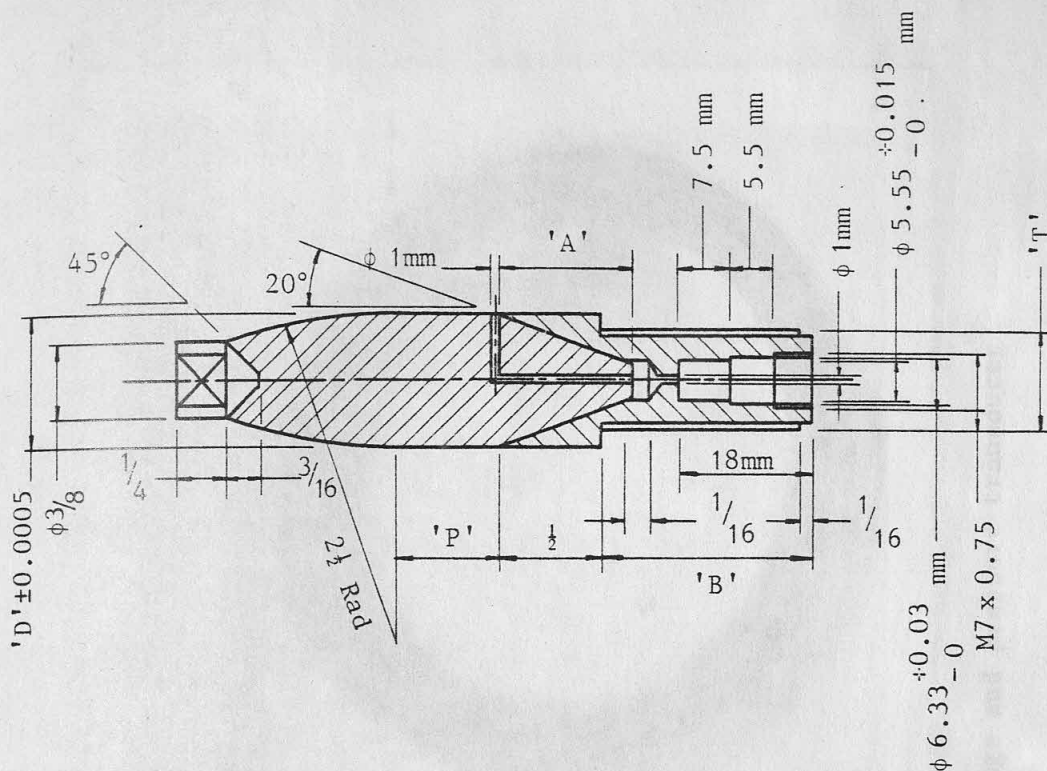


Figure (5.16) Position of proposed plug
at the start of drawing

the tagged end of the drawn tube where a distinctively highly polished ring was observed on the bore surface at the position where drawing initiated. Furthermore, in some instances when pick-up occurred, it was seen that it initiated from the periphery of this ring.

Consequently it was proposed to replace the chamfer by a curved profile. The position of this design of plug before the start of drawing is shown in Figure (5.16). The point contact associated with the conventional plug was replaced by a line contact between the curvature of the plug and the shoulder of the tag. This reduces the intimacy of the contact between the two surfaces as the tube collapses onto the plug at the start of drawing. Furthermore, since the plug is drawn almost instantaneously into the metal deformation zone, the high relative velocity between the tube and the plug together with the curvature of the plug provide conditions which are favourable for a better lubrication at this initial contact, by hydrodynamic action. This eases the lubrication problem at the start of the drawing process when pick-up is most likely to initiate. After the plug has been drawn into the deformation zone i.e. during drawing, the tube is in contact only with the cylindrical portion of the plug as in the case of the conventional plug and lubrication is aided by the hydrodynamic action of the plug-attachment.

The details of the proposed experimental plugs are shown in Figure (5.17) and Plate (5.1). Each plug is mounted on a shank which provides a mounting for the pressure transducer, where the diameter of the plug permits its usage. The 'L' shaped channel in the plug enables the pressure generated in the sink-zone to be measured.



Notes:

1. 3 off
2. Dimensions above are common in each case
3. Dimensions A, B, D, P, T are given separately below
4. Unspecified tolerance = ± 0.005 in
5. Surface finish on carbide plug = 1 to 3 micron

Plug No.	A	B	D	P	T
1	$\frac{5}{8}$	$1\frac{1}{16}$	0.646	0.5	$\frac{1}{2}$ BSF
2	$\frac{5}{8}$	$1\frac{1}{16}$	0.532	0.5	$\frac{1}{2}$ BSF
3*	$\frac{3}{8}$	$\frac{9}{16}$	0.438	0.4	$\frac{5}{16}$ BSF

* Channel in carbide plug and hole in mounting not required

Title	Experimental tube-drawing plug		
Scale	Full size	Dimension	Inches
Drawn	T B Lim	Material	Tungsten Carbide
Date	22.2.83	Figure	5.17



Plate (5.1) Experimental tube-drawing plugs and pressure transducer

5.4.2 Design of plug-attachments

The plug-attachments were designed with a view towards providing adequate experimental data for comparison with those predicted theoretically as well as minimising the number of plugs and attachments required, hence minimising the tooling costs. To meet these objectives, three attachments providing the same radial clearance between the attachment and the bore of the undrawn tube, but of different lengths, were designed to suit each plug. A range of radial clearances can be obtained by subsequently machining the attachments. The lengths which were planned for the experimental work were nominally 6 in, $7\frac{1}{2}$ in and 9 in, and the radial clearances ranged from 0.002 in to 0.007 in. The assembly of the plugs and the straight-parallel attachments are shown in Figure (5.18) and Plate (5.2).

Ideally, the plug and attachment should be made as an integral unit since experience in the preparatory experiments has shown that sealing, at the order of pressures encountered, can be a considerable problem. However, the designs described above reduce, for each plug size or each proposed reduction in area of the tube, the number of plugs required from three to just one; the three attachments of different lengths fit the same plug. The arrangement thus reduced the tooling cost. The details of the three plug-attachments associated with the three plugs sizes were shown in Figure (A6.8). The longitudinally through-hole along the axis of the attachment enabled the lead of the pressure transducer to be taken via the hollow plug-bar to the recording instrument. No such provisions were made for Attachment No. 3 since the size of the plug does not allow the pressure transducer to be used.

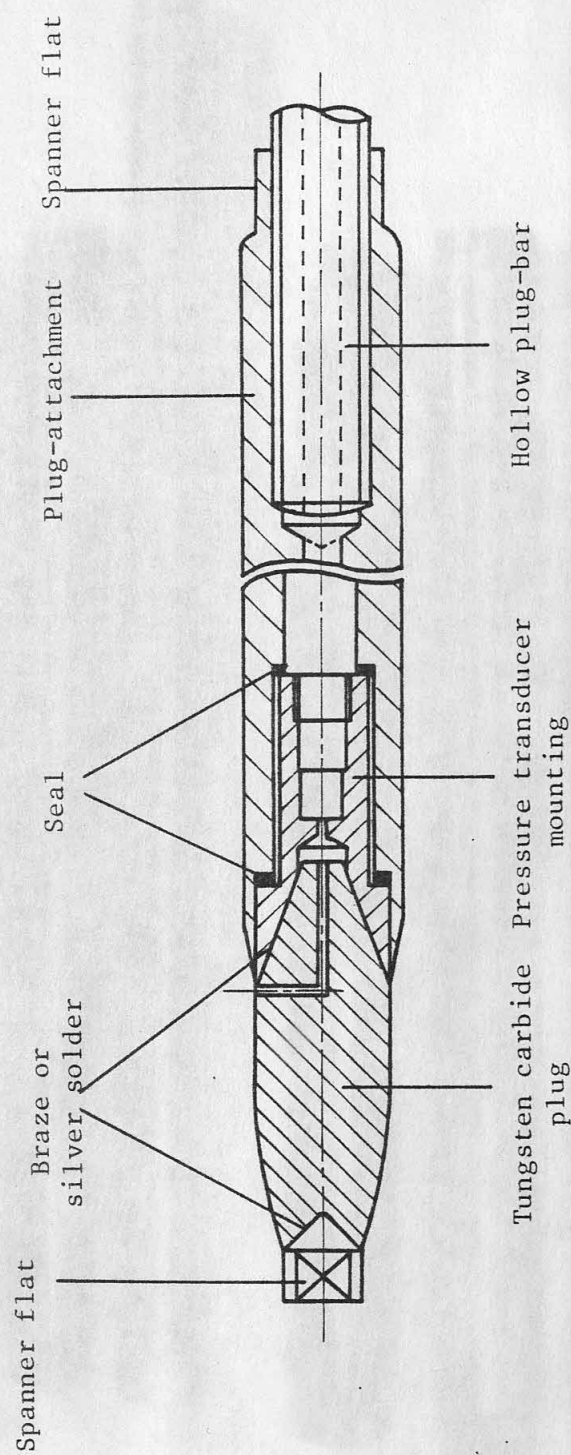
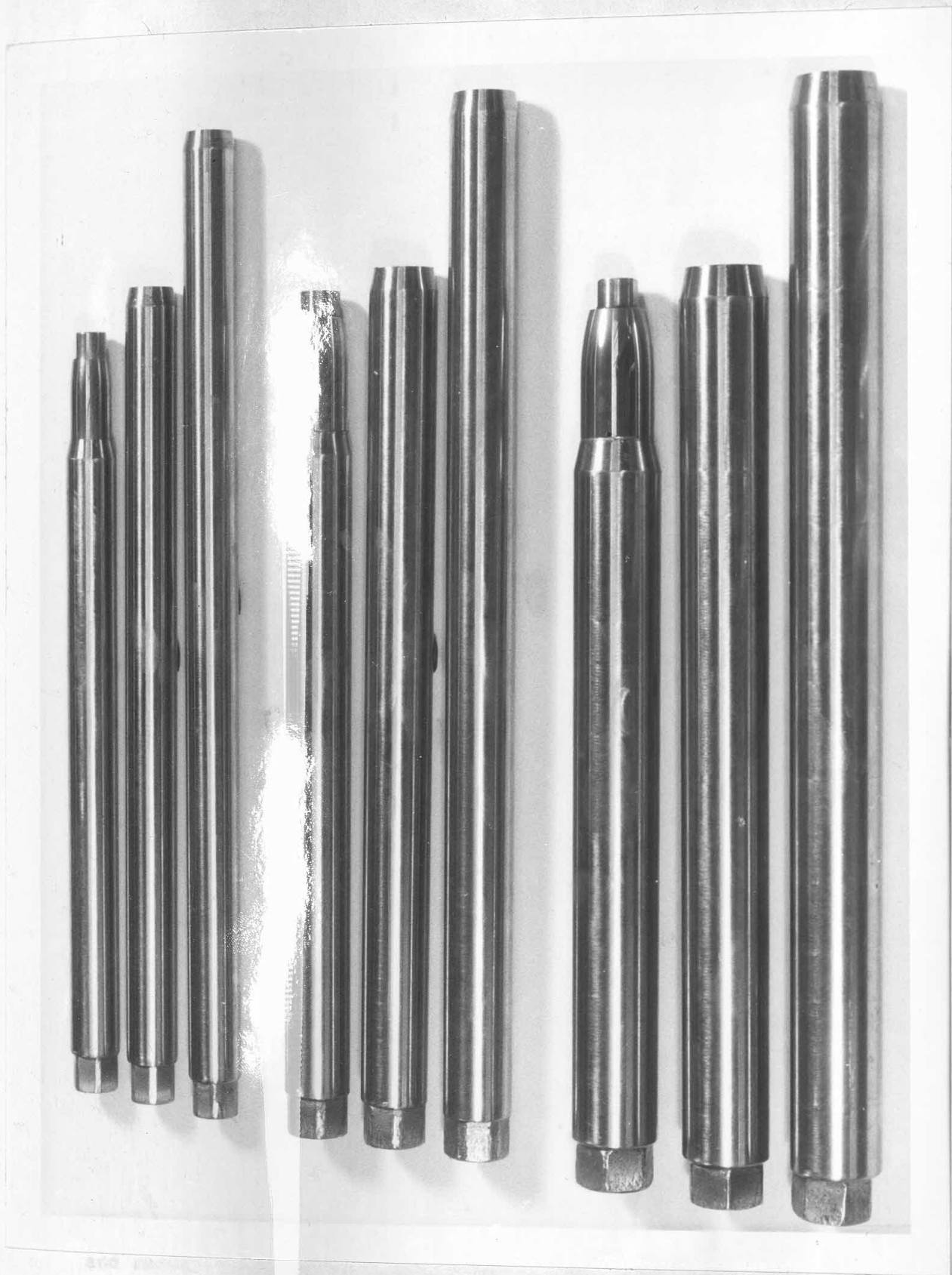


Figure (5.18) Assembly of the new plug and plug-attachment



5.5 EXPERIMENTS WITH NEW PLUGS AND PLUG-ATTACHMENTS

The tools were set up as shown in Figure (5.19) and Plate (5.3); while Plate (5.4) shows the arrangement when drawing with a conventional plug. The dies had a semi-angle of 12° which is approximately optimal for the range of homogeneous strains which were planned for in these tests. The length of contact between the parallel portion of the plug and tube in the metal deformation zone was set at a constant value in each set of tests. This enabled a compatible comparison between the plug force or friction force at this interface when attachments of different lengths, radial clearances or geometries were used.

The experimental programme was set out as illustrated by the flow chart in Figure (5.20) and the experiments were conducted in accordance with the relevant procedure described in Section (5.2). This was initiated by drawing tubes which had their external surfaces and internal surfaces ground and grit-blasted respectively. The tubes were nominally 1.0 x 0.10 in (outside diameter x wall thickness) and were drawn at approximately 30% reduction in area using Plug NO. 1 and Attachments No. 1 with an appropriate die. The lengths of the attachments were nominally 6, $7\frac{1}{2}$ and 9 inches. The initial radial clearance provided by these attachments was 0.004 in and subsequent clearances of 0.006 in and 0.007 in were obtained by progressively machining these attachments.

The tubes drawn by the first set of experiments were annealed and a second pass of 30% reduction in area were conducted using Plug No. 2 and Attachments No. 2 and an appropriate die. The same lengths and radial clearances of the attachments mentioned previously were used and the subsequent clearances were obtained by the same means. Both the external and internal surfaces of these tubes were not

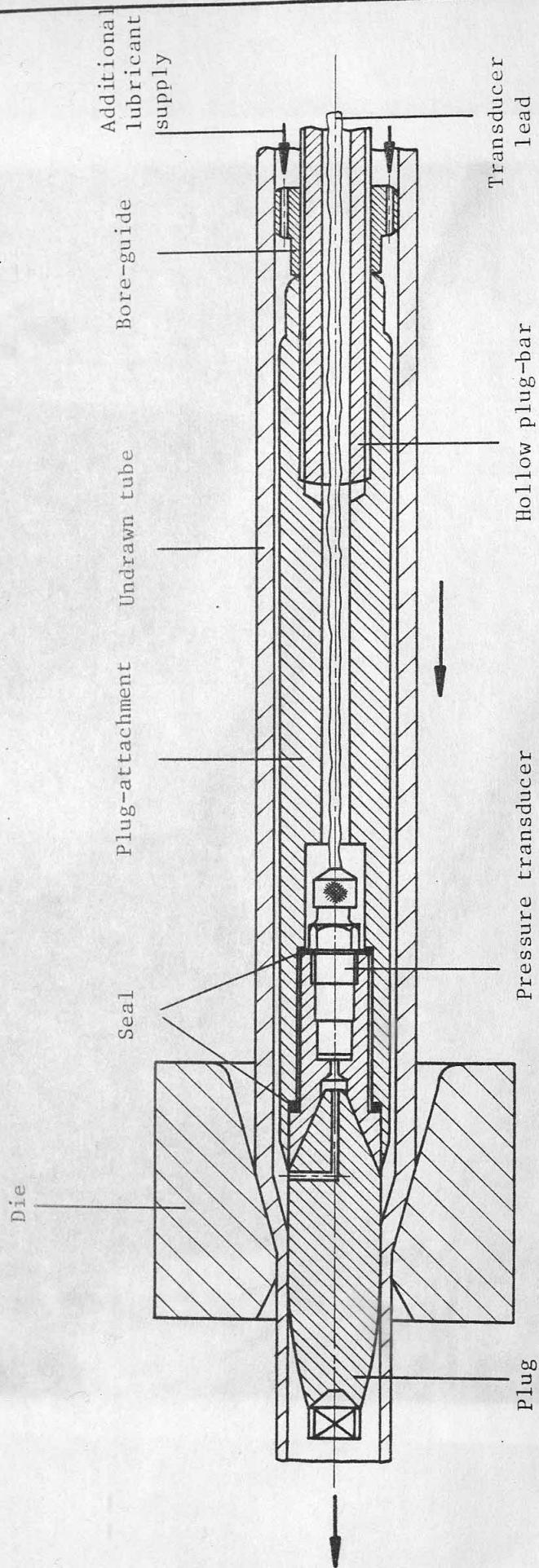


Figure (5.19) Experimental set-up for bore surface lubrication

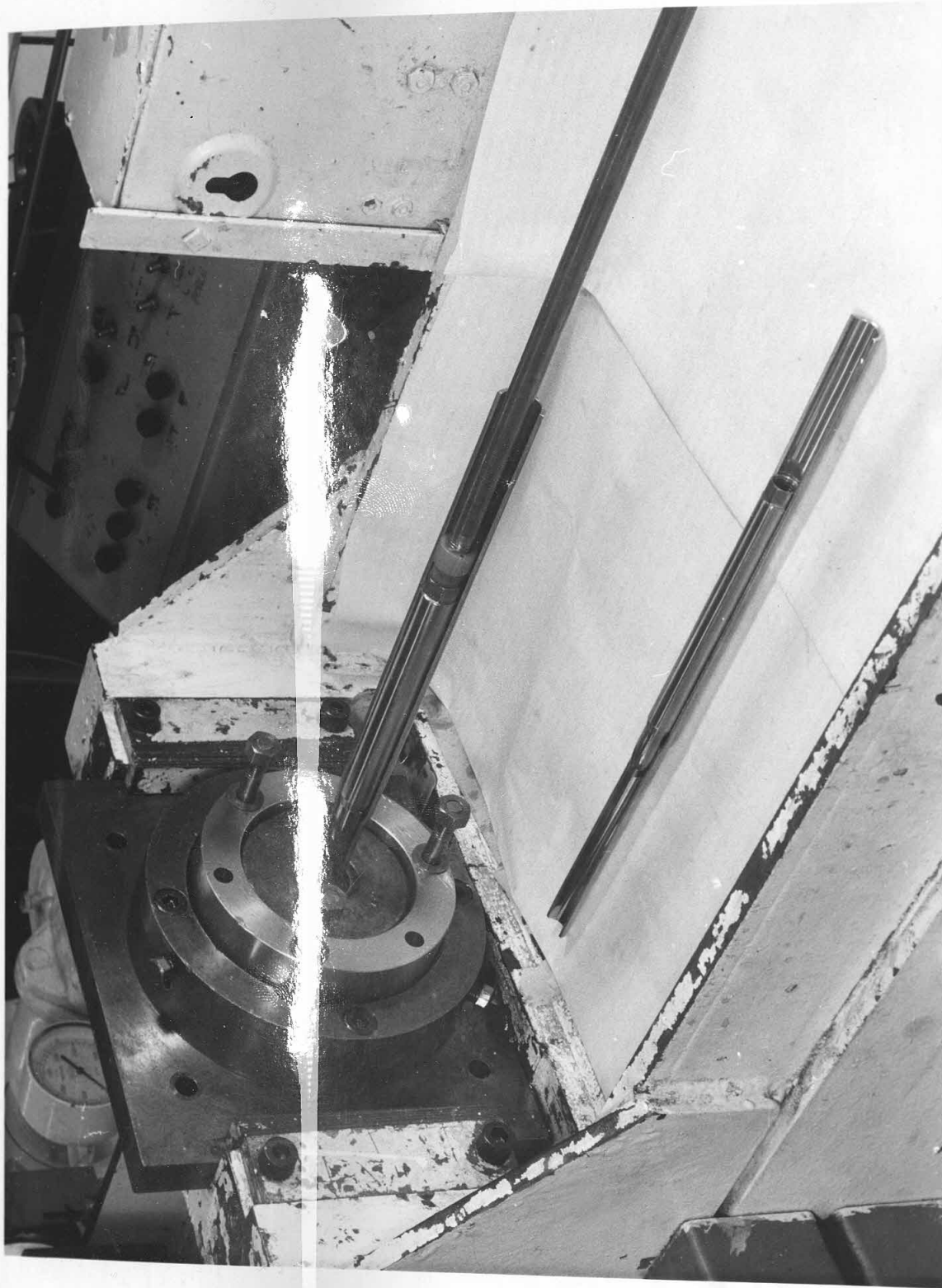


Plate (5.3) Arrangement of the plug-attachment technique during drawing

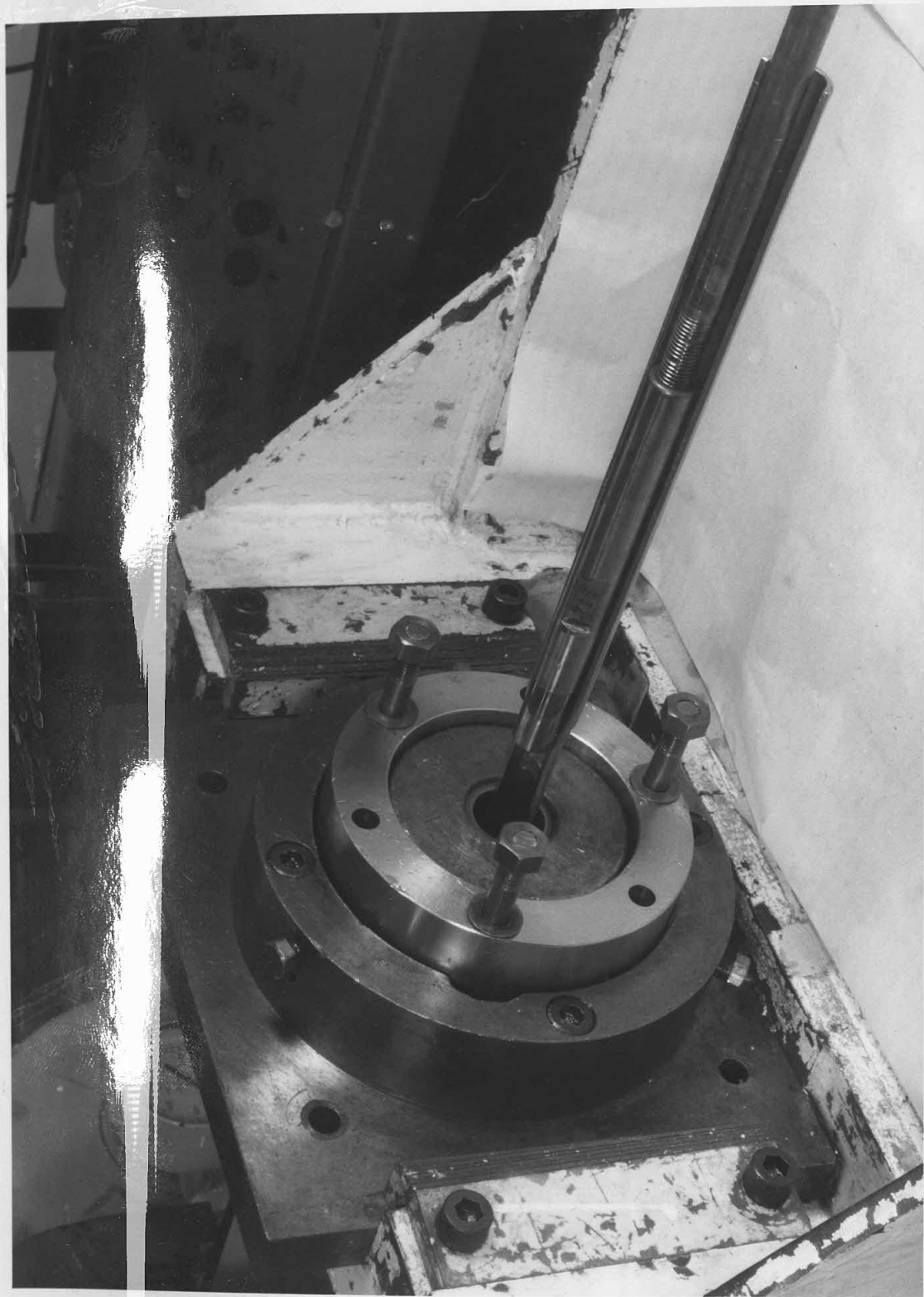


Plate (5.4) Arrangement of the plug in conventional tube-drawing practice

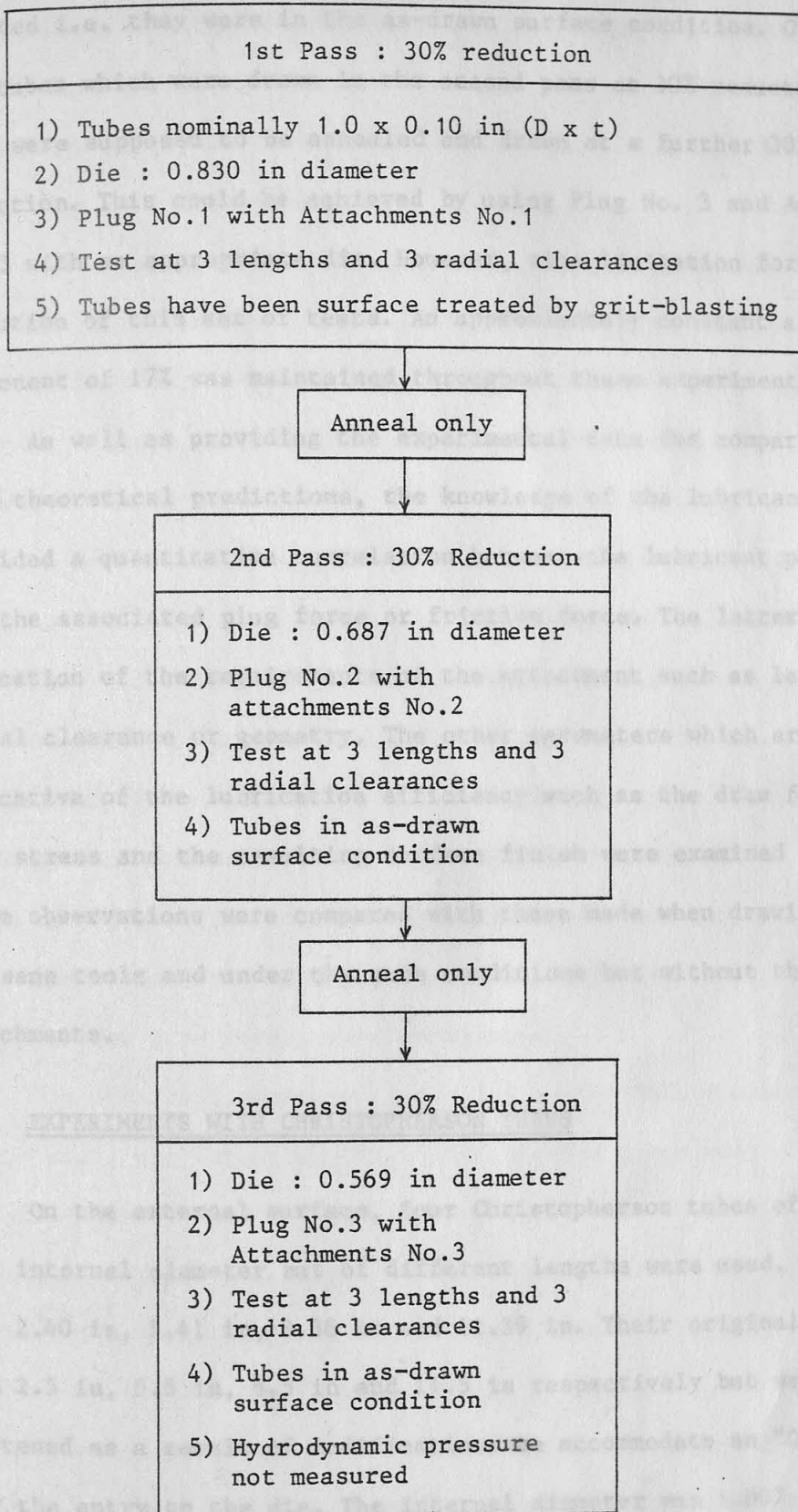


Figure (5.20) Experimental programme for straight-parallel plug-attachments

treated i.e. they were in the as-drawn surface condition. Originally the tubes which were drawn in the second pass at 30% reduction in area were supposed to be annealed and drawn at a further 30% reduction. This could be achieved by using Plug No. 3 and Attachments No. 3 with an appropriate die. However, time limitation forbade the execution of this set of tests. An approximately constant sink component of 17% was maintained throughout these experiments.

As well as providing the experimental data for comparison with theoretical predictions, the knowledge of the lubricant pressure provided a quantitative correlation between the lubricant pressure and the associated plug force or friction force. The latter gave an indication of the requirements of the attachment such as length, radial clearance or geometry. The other parameters which are indicative of the lubrication efficiency such as the draw force or draw stress and the resulting surface finish were examined also. These observations were compared with those made when drawing with the same tools and under the same conditions but without the plug-attachments.

5.6 EXPERIMENTS WITH CHRISTOPHERSON TUBES

On the external surface, four Christopherson tubes of the same internal diameter but of different lengths were used. These were 2.40 in, 5.41 in, 8.38 in and 11.39 in. Their original lengths were 2.5 in, 5.5 in, 8.5 in and 11.5 in respectively but were shortened as a result of modifications to accommodate an "O" ring near the entry to the die. The internal diameter was 1.007 in and was chosen to provide a radial clearance of 0.006 in between the Christopherson tubes and the external surface of the undrawn tubes. However, mid-way through the experimental work the original batch of tubes was exhausted and the external diameter of the tubes of

the subsequent batch was slightly smaller. Thus, the radial clearance in the experiments with these tubes was 0.007 in. The nominal dimensions of the tubes in both batches were 1.0 x 0.10 in (outside diameter x wall thickness).

The experiments were conducted according to the relevant procedure described in Section (5.2). The tools were set up as shown in Figure (5.21) and Plate (5.5); the detail drawings are shown in Figures (A6.9-A6.12). The same die and plug were used throughout these experiments. The former had a semi-die of 12° which is approximately optimal for a homogeneous strain of about 0.4 or a reduction in area of about 35% which were planned for in these tests. The plug was of the conventional design and incorporated a 45° chamfer at its fore-end since at the time when these experiments were conducted considerations had not yet been given to plug design. The length of contact between the plug and the bore of the tube in the metal deformation zone was maintained at a constant value in each draw. Hence frictional conditions at this interface, which influence the draw force, were consistent.

The lubricant pressures generated by the hydrodynamic action along the length of the Christopherson tubes were monitored by a pressure transducer and later compared with theoretical predictions. Where the length of the Christopherson tubes permitted, the pressure transducer was mounted at a distance of 0.91 in, 2.41 in, 3.41 in and 4.41 in from the die. However, for economic reasons, only one transducer was used. Thus, after each test it was necessary to seal the hole which had been drilled through the wall of the Christopherson tube and to drill a similar hole for the next measurement some distance from the previous position. This was repeated for each Christopherson tube until the lubricant pressures at the desired positions had been measured. The hole which had been

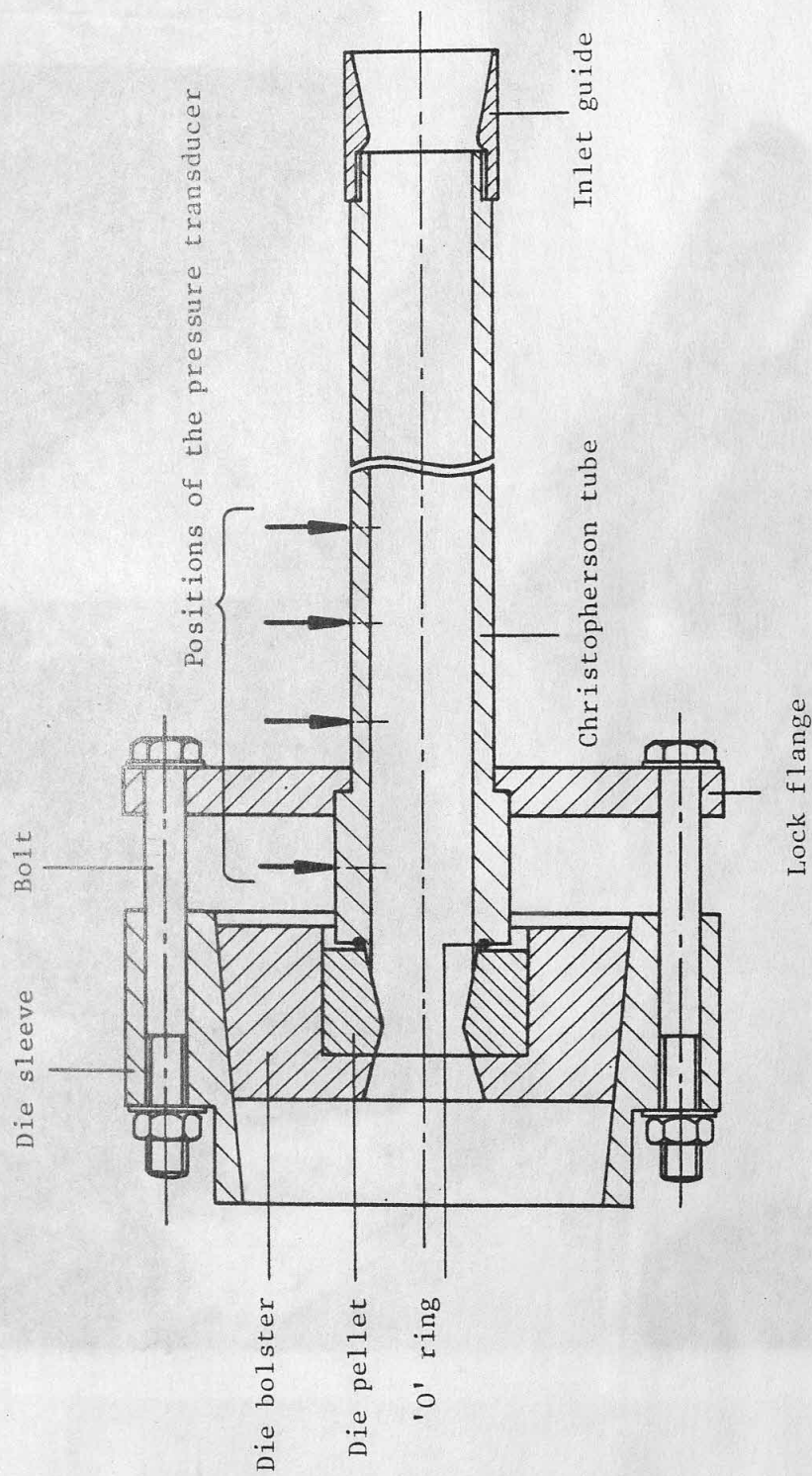


Figure (5.21) Experimental set-up for external surface lubrication

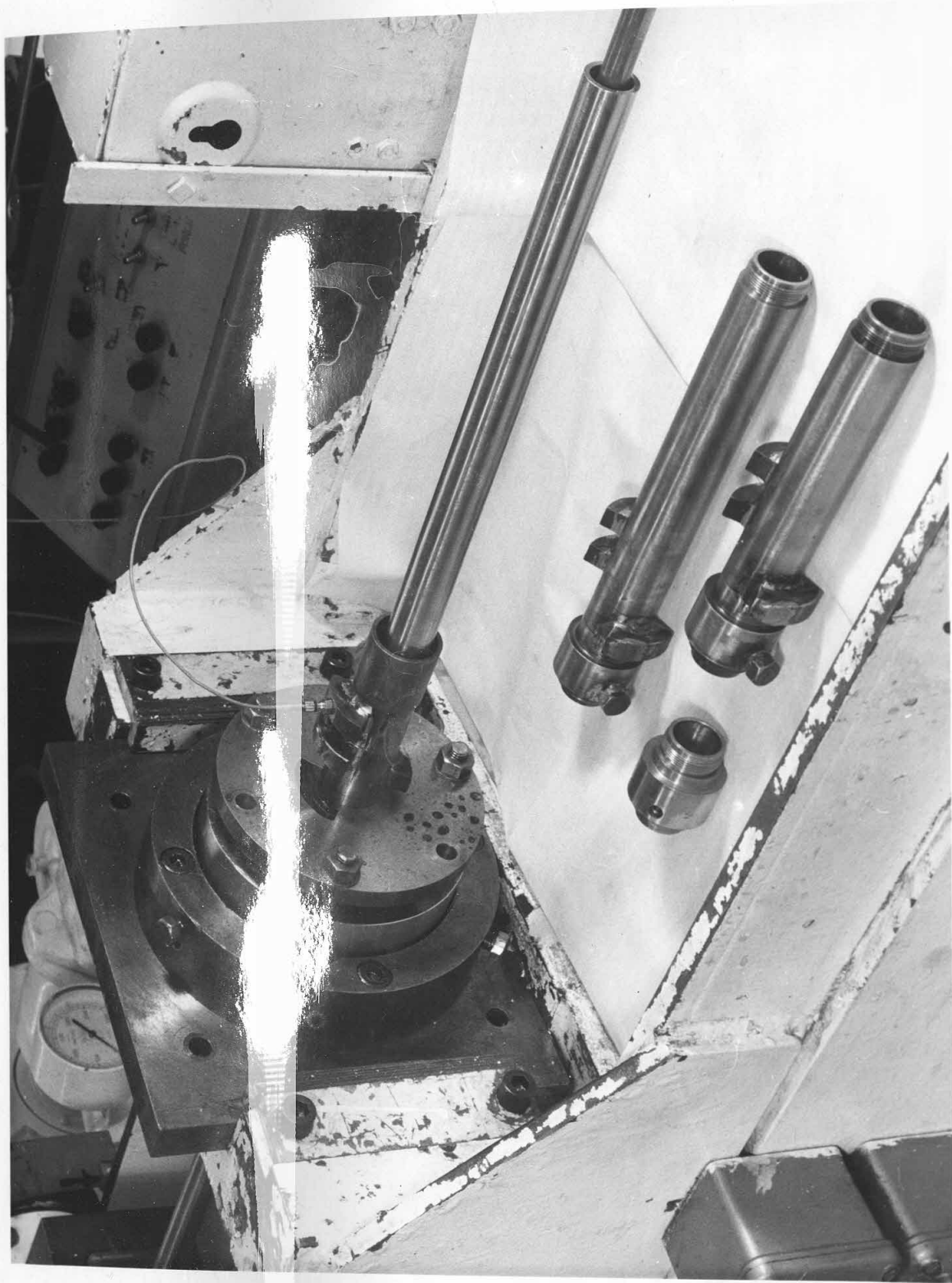


Plate (5.5) Experimental set-up of the Christopherson tube technique for external lubrication

used were sealed by brazing onto the Christopherson tube, a plug approximately the size of the hole and with its end filed to match the internal surface curvature of the Christopherson tube. Sealing at the pressure transducer mounting was by an annealed copper washer.

The draw force or draw stress and the resulting surface finish which are indicative of the lubrication efficiency were examined also. These were compared with the observations made when drawing with the same tools and under the same conditions but without the Christopherson tube.

CHAPTER 6: DISCUSSION OF RESULTS

CHAPTER 6: DISCUSSION OF RESULTS

6.1 INTRODUCTION

A comprehensive account of the experimental observations and a detailed discussion of the results, both experimental and theoretical, in the study of tool design and the prediction of hydrodynamic lubrication at the two tool-workpiece interfaces in tube-drawing are presented in this chapter.

CHAPTER 6: DISCUSSION OF RESULTS

The experimental results consist of the hydrodynamic lubricant pressures measured when drawing with Christopherian tubes of plug-attachments of different lengths and providing different radial clearances between themselves and the undrawn tube. Although unintended, the viscosity of the lubricant was altered as a result of climatic changes and these provided some indication of the influence of the lubricant viscosity on the pressure generation. The other results include the forces measured during drawing, in particular, the plug force which is the friction force at the plug-tube interface. The surface finish of the drawn tubes also is indicative of the lubrication efficiency. Relevant observations were made in the course of the experimental work. These observations together with some of those of the preparatory experiments, which have been discussed at some length in Chapter 5, are included here in order to present a clearer explanation.

CHAPTER 6: DISCUSSION OF RESULTS

6.1 INTRODUCTION

A comprehensive account of the experimental observations and a detailed discussion of the results, both experimental and theoretical, in the study of tool design and the promotion of hydrodynamic lubrication at the two tool-workpiece interfaces in tube-drawing are presented in this chapter.

The experimental results consist of the hydrodynamic lubricant pressure measured when drawing with Christopherson tubes or plug-attachments of different lengths and providing different radial clearances between themselves and the undrawn tube. Although unintended, the viscosity of the lubricant was altered as a result of climatic changes and these provided some indication of the influence of the lubricant viscosity on the pressure generation. The other results include the forces measured during drawing, in particular, the plug force which is the friction force at the plug-tube interface. The surface finish of the drawn tubes also is indicative of the lubrication efficiency. Relevant observations were made in the course of the experimental work. These observations together with some of those of the preparatory experiments, which have been discussed at some length in Chapter 5, are included here in order to present a clearer explanation.

For a given lubricant the lubrication at the tool-tube interfaces is a function of the lubricant pressure and the lubricant film thickness at the entry to the metal deformation zone. These, in turn, are dependent on the design of the Christopherson tube and the plug-attachment, and the drawing conditions such as the speed of drawing and the lubricant viscosity. Thus, the theoretical results are concerned with the influence of these factors on the generation of the lubricant pressure and the lubricant film thickness.

6.2 OBSERVATIONS

The experimental work on the plug-attachment technique for bore lubrication and the curve-profiled plug in tube-drawing proved to be highly successful. Hitherto, bore or plug-tube interface lubrication in current tube-drawing practice necessitates the roughening of the undrawn tube bore surface either by grit-blasting or pickling or some other processes⁽⁴⁴⁾ in order to entrap the lubricant. These surface treatment operations are necessary to avoid metallic transference or pick-up between the tube and the plug. The use of the curve-profiled plug in the present work reduced the degree of stress concentration between the plug and the tube at the start of drawing while maintaining a seal, thereby reducing the probability of the initiation of pick-up. The plug-attachment technique generated a high lubricant pressure at the entry to the metal deformation zone by hydrodynamic action. This pressure increased the flow of lubricant into the metal deformation zone thereby increasing the separation between the plug and the tube, and hence reducing friction. Using this technique stainless steel tubes in which the bore surface had not been roughened, i.e. in the as-drawn condition, but lubricated with oil alone were drawn successfully without the occurrence of pick-up; this would not otherwise have been possible. Even under these conditions significant reductions in the

plug force were observed as the lubricant pressure was increased. These observations are among the relevant observations which are discussed in a greater detail in the following sections.

6.2.1 The effect of the curve-profiled plug

The position of the conventional plug and that of the curve-profiled plug at the start of drawing have been illustrated in Figures (5.15) and (5.16). Evidence of the high stress concentration as the tube collapsed onto the chamfered edge of the conventional plug, before pulling it into the metal deformation zone, can be seen by an examination of the bore surface of the undrawn tube nearest to the tag. A highly polished ring, taking the shape of the 45° chamfer of the plug, was formed on the bore surface of the drawn tube. The formation of such a ring suggests that the lubricant film has been punctured. As the tube began to draw, friction between the plug and the tube was high increasing the risk of pick-up. Indeed, this view is reinforced by the observation that pick-up tended to initiate from the periphery of this ring, particularly when the plug was new since the edge of the chamfer was sharper. Further evidence of this phenomenon is exhibited by the trace of the plug force when drawing with a conventional plug irrespective of whether or not an attachment was used. Typical traces of the plug force are illustrated by Figures (5.9), (5.10), (5.12), (5.13), (5.14) and (6.1), where it is seen that the plug force is highest at the beginning of drawing.

The use of the curve-profiled plug introduced a larger and smoother area of contact between the curved portion of the plug and the shoulder of the tag. Thus, at the start of drawing, the tube collapsed onto the curved portion of the plug. Since the plug was drawn almost instantaneously into the metal deformation zone, the high change in the relative velocity between the tube and the plug

together with the curvature of the plug provided a high pressure lubricant wedge at the beginning of drawing. The effect of this lubricant wedge was reflected in the trace of the plug force. Figure (6.1) shows the trace of the plug force when a conventionally chamfered plug was used together with an attachment. It is seen that the plug force was highest at the start of drawing, indicating that friction was highest, before attaining a lower steady state value. Under otherwise identical conditions, Figure (6.2) was obtained when the curve-profiled plug was used together with an attachment. The effect of the lubricant wedge was to reduce the interfacial friction between the tube and the plug as indicated by the depression of the plug force trace at the early stages of the draw. The plug force then began to increase, showing that this localised improvement in lubrication was vitiated as drawing proceeded. Figure (6.3) shows the trace of the plug force of an identical draw after the plug load cell had been recalibrated at a higher amplification. It was noted that this improvement in lubrication at the early stages of drawing was not observed when the length of the shoulder of the tag was too short since the desirable lubricant wedge was not formed. This was because it was likely that the internal surface of the tube would be in contact with the edge of the plug.

An examination of the bore surface of the drawn tube nearest to the tag when the tube first collapsed onto the plug revealed that the type of highly polished ring associated with the conventionally chamfered plug was not obtained. Furthermore, the surface finish of the drawn tube at the end nearest to the tag exhibited a duller appearance for about half an inch when compared with the rest of the drawn tube. When the surface of a specimen was monitored on the "Talysurf", the section with the duller appearance had a CLA value of $0.2 \mu\text{m}$ while the rest of the tube measured $0.08 \mu\text{m}$. The CLA value

of the bore surface of the tube before drawing was 0.55 μm . These surface finishes are illustrated in Figure (6.4). Similar observations obtained when drawing tubes of which the bore surface had not been roughened. These observations corroborated well with the low plug force noted at the early stages of the draw.

Thus, the use of a curve-profiled plug has two important advantages. Firstly, it reduces the severity of the stress concentration when the tube first collapses onto the plug and secondly, it seals a high pressure lubricant wedge which improves lubrication by hydrodynamic action at the early stages of the draw. These observations were made both when the bore surfaces of the undrawn tubes had been roughened by grit-blasting and when they were in the as-drawn condition. The combined effect of these two features of the new plug is to reduce the risk of the occurrence of pick-up at the beginning of the drawing process.

6.2.2 Hydrodynamic lubricant pressure, plug force and draw stress

The pressure generated in the lubricant at the entry to the metal deformation zone by the lubricant pressurizing devices; namely the plug-attachment and the Christopherson tube, is seen to be directly proportional to the lengths of these devices and the lubricant viscosity and inversely proportional to the radial clearances which they provided. Since a constant draw speed of 15 ft min⁻¹ was used throughout the experimental work, the influence of draw speed on the pressure generation was not observed. However, the literature (4,5,6,8) suggests that a higher pressure would be generated when drawing at higher speeds.

The effect of the lubricant pressure on lubrication, or friction, is best illustrated by comparing the traces of the generated lubricant pressure with those of the plug force. When the lubricant was not

pressurized, as when a plug-attachment was not used, apart from the beginning and ending of the draw, the trace of the plug force was a straight line indicating that the friction at this interface was constant (Figure (5.10)). However, when the lubricant was pressurized with a plug-attachment the plug force was lower and varied inversely with the magnitude of the lubricant pressure. Three sets of lubricant pressure and plug force traces from the preparatory experimental work are shown in Figures (5.12), (5.13) and (5.14). As mentioned previously, the variation of the lubricant pressure was due to leakage and it is seen that the magnitude of the plug force matched inversely according to these variations. Figure (6.5) shows a set of the traces of the lubricant pressure, plug force and draw force when drawing with an attachment to the curve-profiled plug. The undulations in the lubricant pressure trace was due to the "wobbling" motion of the undrawn tube since a bore-guide was not used and there was no lubricant leakage. These undulations were suppressed significantly when a bore-guide was used. It is seen that the rise of the lubricant pressure was almost instantaneous, i.e. it started as soon as drawing commenced. This was because the annular space between the bore of the undrawn tube and plug unit was filled with lubricant and that a steady state condition had not yet been attained. Thus, as the drawing process continued the pressure proceeded towards a steady state regime accompanied simultaneously by a reverse flow of lubricant. This observation was verified by drawing the tube intermittently. The pressure and force traces of two such draws are shown in Figures (6.6) and (6.7). It is seen that when the draw was restarted after stopping the lubricant pressure rose, on each occasion, to its steady state value; the steady state condition had been attained already and was not vitiated. The stoppage time

was between 1 and 2 seconds. Additionally, the plug was drawn into the metal deformation zone at the start of drawing at a speed higher than that of the undrawn tube during the drawing process. This accounted partially for the almost instantaneous rise in the lubricant pressure when drawing first started. This rise in pressure is advantageous since it complements the action of the curve-profiled plug in reducing the risk of the occurrence of pick-up at the early stages of the draw.

It is clear that a high lubricant pressure increases the flow of lubricant into the metal deformation zone thereby increasing the separation of the plug and the tube and hence reducing the interfacial friction. Reductions in the plug force, when compared with those observed when the lubricant was not pressurized, ranging from 14% to 65% were observed in the preparatory experiments. Figure (6.8) was obtained by plotting the hydrodynamic lubricant pressure against the plug force when drawing tubes nominally of 1.0 x 0.10 in (outside diameter x wall thickness) at 30.6% reduction in area. The bore surface of these tubes had been roughened by grit-blasting. The line passing through the experimental points was obtained by the method of least squares. It is seen that the plug force varied inversely with the lubricant pressure. Pick-up did not occur in these tests. Figure (6.9) shows the variation of the percentage reduction in the plug force, when compared with those obtained without an attachment, with the lubricant pressure. The maximum and minimum percentage reduction observed were 24% and 4% respectively. Similar observation obtained when these tubes were annealed and drawn at a further 31.1% reduction in area. Both the bore and external surfaces of these tubes, however, were not roughened; they were in the as-drawn condition. The variation of plug force and lubricant pressure

is shown in Figure (6.10). It is seen that at pressures below about 500 lbf in⁻² pick-up occurred. Figure (6.11) illustrates the corresponding variation of the percentage reduction in plug force with the lubricant pressure. The reductions in plug force in this case were obtained by comparison with the highest plug force observed when pick-up did not occur since the occurrence of pick-up would render the plug force unrepresentative. Thus, reductions of between 12% and 41% were observed.

In contrast to the observations made on the influence of the lubricant pressure on the plug force, the observed draw stress when drawing the tubes in the first pass did not exhibit a decreasing trend with the increase in lubricant pressure. Such a trend was anticipated initially, since the draw stress is equivalent to the total work done per unit volume of the material deformed; it consists of the homogeneous work, redundant work and frictional work. Previous experience had shown the plug force or friction at the plug-tube interface to be approximately 10% of the draw force. This discrepancy could be attributed to the variation in the mechanical properties of the tube during heat treatment or when the tubes were straightened after annealing. However, the draw stress observed when drawing the tubes in the second pass exhibited a more orderly correlation with the lubricant pressure. This is illustrated in Figure (6.12).

In the experiments on the Christopherson tubes, the tubes were drawn at about 37% reduction in area and the pressure transducer was mounted consecutively at a distance of 0.91 in, 2.41 in, 3.41 in and 4.41 in from the die. Thus, the hydrodynamic lubricant pressures measured were those generated along the length of the Christopherson tubes rather than those generated by the Christopherson tubes at the entry to the die. A typical trace

of the lubricant pressure is shown in Figure (6.13). It is seen that the pressure attained a near steady state value after a length of the tube had been drawn; the almost instantaneous rise in the lubricant pressure from the start of drawing observed in the experiments on the plug-attachments was noticeably absent. The undulations in the pressure trace were due to the "wobbling" motion of the undrawn tube. The draw stresses observed in these tests were generally lower when a longer Christopherson tube was used. This implied that the longer Christopherson tubes, which generated higher lubricant pressures at the die entry, were more effective in reducing friction at the die-tube interface.

6.2.3 Surface finish

In the experiments on the plug-attachments the bore surface finish of each tube was recorded with a "Talysurf" before and after the tube had been drawn. This provided further indication on the lubrication efficiency. The literature (see Section (2.3)) has shown that the surface finish of the work has significant influences on lubrication during bulk plastic deformation.

The bore surface finish of the tubes drawn in the first pass had been roughened by grit-blasting. These had CLA values ranging from $0.25 \mu\text{m}$ to $1.3 \mu\text{m}$. Since friction at the plug-tube interface was seen to vary inversely with the generated lubricant pressure, the bore surface finish of the drawn tubes was initially expected to be rougher when the lubricant pressures were higher and vice-versa. This proved to be not the case since the wide variation in the original surface finish had rendered the experimental results incompatible. The observed lubricant pressure ranged from 257 lbf in^{-2} to 1488 lbf in^{-2} and within this range the drawn tubes had CLA values ranging from $0.1 \mu\text{m}$ to

0.2 μm . However, a more orderly correlation was obtained by plotting the plug force against the CLA values of the bore surface finish of the drawn tubes. This is illustrated in Figure (6.14); rougher surface finishes were associated with lower plug forces. The lowest CLA values of 0.08 μm and 0.09 μm were obtained when the attachment was not used. The corresponding plug forces were 0.682 tonf and 0.613 tonf.

Similar observations obtained when the tubes drawn in the first pass were annealed and re-drawn. Both surfaces of these tubes had not been roughened. Although the heat treatment resulted in the surface appearance being duller, no significant changes in the surface finish were noted when examined with a "Talysurf". Thus, the CLA values recorded after the tubes were drawn in the first pass and quoted above were valid. The lubricant pressure generated in these tests ranged from 229 lbf in⁻² to 3017 lbf in⁻² and the resultant CLA values ranged from 0.02 μm to 0.09 μm . When pick-up occurred the CLA values were found to be in the range 0.02 μm to 0.045 μm . Figure (6.15) shows the variation of the CLA values with the plug force observed in this group of tests.

The appearance of the bore surface of the tubes drawn in these two groups of tests were noted to be highly polished. However, by comparison they appeared to be duller when a higher lubricant pressure was generated. Figures (6.16-6.20) illustrate typical changes in the bore surface finish of the tubes as they were drawn through the first and second passes. It is seen that the surface asperities were severely flattened by the deformation process and were registered by the "Talysurf" only when very high magnifications were used.

The external surface of the tubes drawn in the experiments on the Christopherson tubes had been roughened by grinding and

had CLA values of between 0.4 μm and 0.6 μm . The tubes appeared to have a duller finish when drawn with a longer Christopherson tube. However, these tubes had similar surface topographies when examined with a "Talysurf" and did not appear to have significant differences in the CLA values. Typical CLA values recorded were in the range of 0.45 μm to 0.55 μm . In comparison with the bore surface of the tubes, it was noted that the external surface asperities were not flattened as severely. Typical surface finish observed in these tests are shown in Figure (6.21-6.25). As illustrated by Figure (6.22), it appeared that the surface asperities of the tube drawn without a Christopherson tube were flattened slightly more severely. Pick-up between the die and the tube did not occur throughout the experimental work, including those on the plug-attachments.

6.3 DISCUSSION OF THE EXPERIMENTAL RESULTS

The results of the experiments on the plug-attachments and those of the Christopherson tubes are discussed separately in the following sections.

6.3.1 Experimental results of plug-attachments

As noted previously, the experiments with plug-attachments consisted of drawing a batch of tubes at two passes. The tubes which had been drawn in the first pass were annealed but did not receive surface treatment prior to being drawn in the second pass. Thus, the objectives of the subsequent pass endeavoured to accumulate additional experimental results and at the same time explore the possibility of drawing stainless steel tubes without recourse to bore surface treatment such as grit-blasting or pickling. The following is the specification for the first pass:

1. Initial tube dimensions = 1.0 x 0.110 in (outside diameter x wall-thickness)
2. Final tube dimensions = 0.830 x 0.092 in (outside diameter x wall-thickness)
3. Initial tube external surface condition = ground
4. Initial tube internal surface condition = grit-blasted
5. Percentage sink = 17.2%
6. Percentage reduction in area = 30.6%

The following is the specification for the second pass:

1. Initial tube dimensions = 0.830 x 0.093 in (outside diameter x wall-thickness)
2. Final tube dimensions = 0.687 x 0.078 in (outside diameter x wall-thickness)
3. Initial tube external surface condition = as-drawn
4. Initial tube internal surface condition = as-drawn
5. Percentage sink = 17.6%
6. Percentage reduction in area = 31.1%

In addition, the following items were common to the two passes:

1. Draw speed = 15 ft min⁻¹
2. Lubricant = EP 50
3. Die semi-angle = 12°
4. Tube material = AISI 347 stainless steel

6.3.1.1 Length of the plug-attachments

The influence of the length of the plug-attachments on the lubricant pressure generation for a given radial clearance and lubricant viscosity observed in the first pass is shown in Figures (6.26 - 6.28) and that observed in the second pass is shown in

Figures (6.29 - 6.31). In each case the same scales were used in order that the influence of the radial clearance on the lubricant pressure may be more conspicuous.

The family of lighter lines are the theoretical results computed by equations (3.61) and (3.63) for different values of the lubricant viscosity as indicated. The experimental line in each set of tests was drawn through the experimental points obtained when drawing the tubes which provided a radial clearance nearest to the intended value. This is legitimate since variations in the wall-thickness of the undrawn tubes, which altered the radial clearance between the undrawn tubes and the plug-attachments, were observed. This effect was more pronounced with the tubes drawn in the first pass. It was for this reason that the two experimental points on the top right-hand side of Figure (6.26) were neglected when drawing the experimental line. It is apparent that the generated lubricant pressure was directly proportional to the length of the plug-attachment. Thus, for a given set of conditions the highest pressure was achieved with the longest attachment.

6.3.1.2 Radial clearance

Also apparent from Figures (6.26 - 6.31) is the influence of the radial clearance between the undrawn tube and the plug-attachment on the generation of the lubricant pressure. Apart from the differences in the laboratory ambient temperature, which altered the viscosity of the lubricant, the significance of which is discussed in the following section, it is seen that for a given length of the attachment the lubricant pressure varied inversely with the radial clearance. A more vivid illustration of this effect is obtained by plotting the observed lubricant pressure against the radial clearance for different lengths of the plug-attachment

as shown in Figures (6.32 - 6.34) for the tubes drawn in the first pass and in Figures (6.35 -6.37) for those drawn in the second pass.

As indicated in Figures (6.32 - 6.34), the laboratory ambient temperature at which the experimental points were obtained varied from 19°C to 23°C while those obtained for Figures (6.35 - 6.37) were at 19°C and 20°C. Thus, the experimental lines were drawn by visually compensating for the differences in the lubricant viscosity to be expected as a result of the variations in the temperature. These show clearly that the effect of an increasing radial clearance was to reduce the generated pressure in the lubricant.

In drawing the tubes in the second pass, the surfaces of which had not been treated, pick-up between the plug and the tube occurred when the lubricant pressure was below about 500 lbf in⁻². Thus, for the given drawing conditions the largest radial clearance to prevent pick-up was obtained by projecting from the pressure axis at 500 lbf in⁻² to intersect with the experimental line. The unshaded regions of Figures (6.35 -6.37) indicate the likely occurrence of pick-up. It is noted that the value of the "safe" radial clearance increases with the length of the plug-attachment.

6.3.1.3 Lubricant viscosity

Although no attempts were made to study experimentally, the influence of the lubricant viscosity on the generation of the lubricant pressure, climatic changes, which altered the viscosity of the lubricant, were noted to have a significant effect on the pressure generation. Under identical drawing conditions such as the draw speed, tools and tube sizes and the amount of plastic

deformation, the amount of heat conducted from the metal deformation zone to the plug-attachment and hence to the lubricant may be assumed to be equal. Thus, the laboratory ambient temperature may be used as an indication of the lubricant viscosity. With reference to Figures (6.27) and (6.28), it is seen that the pressures generated at a laboratory ambient temperature of 19°C by the plug-attachments providing a radial clearance of 0.007 in were higher than those observed when the ambient temperature and radial clearance were 23°C and 0.006 in respectively. This effect is more apparent in Figures (6.32 - 6.34) and was more pronounced with the longer plug-attachments. This observation shows that the lubricant viscosity and the radial clearance have opposing influences on the lubricant pressure generation.

6.3.2 Experimental results of Christopherson tubes

The tubes in the experiments with the Christopherson tubes were drawn with a conventional plug since at that time considerations had not yet been given to plug design. The internal diameter of the four Christopherson tubes was not altered in order to vary the radial clearance between them and the undrawn tubes. However, the tubes drawn in these experiments were from two different batches. These had slightly different dimensions and thus provided two different radial clearances.

In drawing tubes from the first batch the following details were recorded:

1. Initial tube dimensions = 0.997 x 0.107 in (outside diameter x wall-thickness)
2. Radial clearance = 0.006 in
3. Percentage sink = 14.7%
4. Percentage reduction in area = 36.3%

The following details were recorded in drawing tubes from the second batch:

1. Initial tube dimensions = 0.995 x 0.110 in (outside diameter x wall-thickness)
2. Radial clearance = 0.007 in
3. Percentage sink = 13.8%
4. Percentage reduction in area = 37.7%

In addition, the following items were common in each case:

1. Initial tube external surface condition = ground
2. Initial tube internal surface condition = grit-blasted
3. Final tube dimensions = 0.830 x 0.081 in (outside diameter x wall-thickness)
4. Draw speed = 15 ft min⁻¹
5. Lubricant = EP 50
6. Die semi-angle = 12°
7. Tube material = AISI 347 stainless steel

In the experiments with Christopherson tubes it was more convenient to mount the pressure transducer along the length of the Christopherson tubes rather than at the entry to the die. Thus, the lubricant pressures measured were those generated by the hydrodynamic action some distances away from the die. Figures (6.38 - 6.41) show the lubricant pressure generated by the same Christopherson tubes at four distances from the die. The influence of the length of the Christopherson tube on the lubricant pressure generation followed the same trend observed with the plug-attachments in that the lubricant pressure generated was directly proportional to the length of the Christopherson tube. It is seen that the lubricant pressures recorded were lower in magnitude at

distances farther from the die. Thus, the lubricant pressure at the die entry may be expected to be higher than those observed in these experiments.

The influences of the radial clearance and the lubricant viscosity on the pressure generation were not studied experimentally due to the lack of resources both in terms of time and material, and also because the main objective of the present work involves the development of a technique for the optimisation of lubrication of the bore in tube-drawing. The results accumulated in these experiments were not sufficient for a rational discussion on the influences of these two factors. However, since the mechanics of the lubricant pressure generation by the Christopherson tube technique and the plug-attachment technique are based on the same principles, the relevant discussions on the results of the experiments with plug-attachments also apply here.

6.4 DISCUSSION OF THE THEORETICAL RESULTS

The theoretical results computed by the theories developed in Chapter 3 are discussed in this section. The relevant equations were utilized to calculate the theoretical results under the experimental conditions described previously. These allowed a direct comparison between experimental observations and theoretical predictions and thus enabled the validity of the theories to be verified. In addition, the theories were applied to conditions other than those observed in the experimental work, in particular the two-zone plug-attachments or "Christopherson" tubes, in order to elucidate the influences of the various factors and also the potential of the techniques in promoting hydrodynamic lubrication.

6.4.1 Comparison between experimental and theoretical results

The lighter lines in Figures (6.26 - 6.37) for the experiments with the plug-attachments and those in Figures (6.38 - 6.41) for the experiments with the Christopherson tubes are the theoretical results computed by the relevant equations developed in Chapter 3 for different values of the lubricant viscosity. These values correspond to the viscosities of EP 50 at the indicated temperatures.

It is seen that in each set of experiments the trend of the experimental results corroborate very well with those of the theoretical results. For the experiments with the plug-attachments close agreement was found between the experimental and theoretical results at a value of the lubricant viscosity corresponding to a temperature of between 7°C and 8°C above the observed laboratory ambient temperature. However, for the experiments with the Christopherson tubes, this discrepancy between the theoretical lubricant viscosity and that observed at the laboratory ambient temperature was equivalent to a temperature difference of between 1°C and 2°C. These deviations from the theoretical results are attributable to the heat conducted from the metal deformation zone which reduced the viscosity of the lubricant. The theories, on the other hand, assume isothermal conditions and thus neglect thermal influences on the lubricant viscosity. Thus, since the plug was thermally isolated it is to be expected that the heat conducted to the attachment and hence to the lubricant in the annular space between the attachment and the undrawn tube would be higher than that conducted from the die to the lubricant when the external Christopherson tube was used. Indeed this view is reinforced by the observation that the plug-attachment was "warm" after drawing whereas the Christopherson tube remained "cool".

Space limitations coupled with the high pressures involved, which would present additional sealing problems, discouraged attempts to measure the lubricant temperature when drawing with the plug-attachment technique.

However, a successful attempt was achieved to measure the lubricant temperature in drawing with a Christopherson tube. The thermocouple, which was mounted at the same distance from the die as the pressure transducer, monitored a rise in the temperature of the lubricant of 1.4°C from the start of drawing until the undrawn tube had slid over the thermocouple. The traces of the lubricant temperature and pressure in this draw is shown in Figure (6.13).

A remarkably good agreement was found between the results predicted by the present theory and those recorded experimentally by Christopherson et al.⁽⁵⁾ in drawing mild steel wires. Figures (6.42 - 6.44) illustrate the results at draw speeds of up to 600 ft min^{-1} for three reductions in area.

Thus, in general the theories developed in Chapter 3 were found to be in good agreement with the experimental observations and can be used with good confidence to design industrially practicable tools.

The theoretical lubricant film thickness calculated at the end of sinking at four values of the lubricant temperature or lubricant viscosity corresponding to the conditions observed in the experiments with the plug-attachments are tabulated in Tables (A2.10), (A2.12), (A2.14), (A2.16), (A2.18) and (A2.20). Those calculated at the die entry corresponding to the conditions observed in the experiments with the Christopherson tubes are tabulated in Tables (A2.22), (A2.24), (A2.26) and (A2.28). The viscosity of EP 50 corresponding to the temperatures between 1°C and 30°C are tabulated in Table (A2.8). It can be deduced that

the lubricant film thickness is directly proportional to the viscosity of the lubricant and the length of the pressurizing devices and inversely proportional to the radial clearance which they provided. Thus, the lubricant film thickness varies proportionally with the lubricant pressure, as expected.

Under the experimental conditions observed when drawing tubes with the plug-attachments the theoretical lubricant film thickness at the end of sinking varied approximately from 0.5 μin to 1 μin . Although these are much thicker than the mono-molecular or several molecular layers associated with the boundary lubrication, the brightly polished internal surface of the drawn tubes and the occurrence of pick-up between the plug and the tube suggest that a full hydrodynamic lubrication regime at this interface had not been obtained. However, significant reductions in the plug force were noted and this together with the observation that the appearance of the drawn tubes were duller with the higher lubricant pressures, or the thicker lubricant film thickness, seem to suggest that a "quasi-hydrodynamic" lubrication regime had been established. The influence of increasing the draw speed, which is discussed in the following section, is to increase the lubricant pressure and the lubricant film thickness. Thus, further improvement to the lubrication at the plug-tube interface is to be expected when drawing at speeds above the experimental draw speed of 15 ft min⁻¹.

Christopherson et al.⁽⁵⁾ achieved full hydrodynamic lubrication in wire-drawing, the experimental lubricant pressures were shown to be in good agreement with those predicted by the present theory in Figures (6.42 -6.44). The lubricant film thickness at the die entry predicted by the present theory were found to range from 240 μin to 1180 μin corresponding

to a lubricant pressure range of $24640 \text{ lbf in}^{-2}$ to $41888 \text{ lbf in}^{-2}$ observed at draw speeds of between 200 ft min^{-1} and 600 ft min^{-1} . These results are tabulated in Table (A2.29). The lubricant film thickness predicted under the conditions observed when drawing tubes with the Christopherson tubes were found to be typically in the region of $2 \text{ } \mu\text{in}$. Thus, by comparison with those predicted when full hydrodynamic lubrication was known to have been obtained the lubricant film thickness predicted for the experiments with Christopherson tubes seem to suggest that the regime of lubrication at the die-tube interface was also one of "quasi-hydrodynamic".

6.4.2 Theoretical results of plug-attachments

The theoretical lubricant pressure generated at the entry to the sink zone and the lubricant film thickness at the end of sinking were calculated for the straight-parallel, straight-tapered, composite and stepped plug-attachments. These results are tabulated in Tables (A3.1 - A3.10) and illustrated graphically in Figures (6.45 - 6.61). Unless otherwise stated the following data were used in the calculations:

1. Initial tube dimensions = $1.0 \times 0.10 \text{ in}$ (outside diameter x wall-thickness)
2. Percentage sink = 15%
3. Percentage reduction in area = 35%
4. Die semi-angle = 12°
5. Draw speed = 100 ft min^{-1}
6. Lubricant viscosity = $3.503 \times 10^{-4} \text{ lbf s in}^{-2}$ (EP 50 at 20°C)
7. Radial clearance, $h_2 = 0.004 \text{ in}$
8. Radial clearance ratio, $h_1/h_2 = 1.5$

The radial clearance ratio, h_1/h_2 , applies to the straight-tapered,

composite and stepped plug-attachments. Thus, when $h_1/h_2 = 1.0$ the attachment has a straight-parallel profile.

In Figures (6.45-6.49) the calculated lubricant pressures for the straight-parallel and straight-tapered plug-attachments were plotted against the length of the attachment, radial clearance, lubricant viscosity, draw speed and the radial clearance ratio. The corresponding influences of these factors on the lubricant film thickness at the end of sinking are shown in Figures (6.50 - 6.54). An obvious feature of these illustrations is that both the lubricant pressure and the film thickness were of a magnitude much greater than those observed experimentally or calculated under the experimental conditions. Apart from the draw speed and the lubricant viscosity, which were maintained at constant values of 100 ft min^{-1} and $3.503 \times 10^{-4} \text{ lbf s in}^{-2}$, the other items listed above were compatible with those under the experimental conditions. The draw speed was about seven times, and the lubricant viscosity about twice that observed experimentally. This explains the differences in the order of the magnitude of the present theoretical calculations and those observed under experimental conditions and thus provides some indication of the significance of these two factors.

Figure (6.45) shows the variation of the theoretical lubricant pressure with the length of the plug-attachment for three values of the radial clearance, h_2 . Generally for a given length of the attachment the lubricant pressure is highest when the radial clearance is smallest. However, the situation can be reversed when the attachment exceeds a certain length. This effect is reflected in Figure (6.46) where it is seen that longer attachments tend to exhibit an optimum radial clearance at which the lubricant pressure is highest. Another interesting result is that with sufficiently long lengths of the attachment the straight-tapered design generates

a higher pressure than the straight-parallel design when the radial clearance h_2 in both cases are equal. An explanation for this effect may be found perhaps by a consideration of the design of journal bearings in which the lubricant pressure generation and hence the hydrodynamic lubrication is dependent on the geometry of the lubricant wedge so formed between the journal and the housing.

As noted previously the effect of an increasing radial clearance was to reduce the hydrodynamic lubricant pressure. The influence of the radial clearance on the lubricant pressure for three lengths of the plug-attachments is illustrated in Figure (6.46). For the range of clearances and lengths considered, it is seen that generally the straight-tapered attachment generates a lower pressure than the straight-parallel design. An optimum value of the radial clearance is exhibited by the longer attachments and diminishes with a decreasing length.

The lubricant pressure is directly proportional to the viscosity of lubricant and the draw speed as illustrated by Figures (6.47) and (6.48). Thus, for a given design of the plug-attachment a higher lubricant pressure can be generated either by using a more viscous lubricant or by drawing at a higher speed. Figure (6.49) shows the influence of the radial clearance ratio h_1/h_2 on the lubricant pressure at two values of the radial clearance h_2 for three lengths of the straight-tapered plug-attachment. The radial clearance ratio is a measure of the taper on the attachment. It is seen that the graphs exhibit an optimum value of the ratio h_1/h_2 for the longer attachments at the small value of the radial clearance h_2 .

Influences by these factors, on the generation of the lubricant film thickness at the end of sinking, follow closely the trends discussed above on the generation of the lubricant pressure as

evidenced by Figures (6.50 - 6.54). A logarithmic scale was used for the lubricant film thickness. These results correspond to the conditions under which the lubricant pressures discussed above were calculated. The theoretical lubricant film thickness can be seen to vary between 10 μin and 2000 μin . These values are compatible with those predicted by the present theory for the Christopherson tubes under the conditions in which Christopherson et al.⁽⁵⁾ obtained full hydrodynamic lubrication. However, these are seen to be generally much thicker than those quoted from the literature, tabulated in Tables (2.1) and (2.2), which considered conventional metal-forming processes, i.e. without lubricant pressurization. The measured lubricant film thickness in wire-drawing was found to be between 4 μin ⁽⁶²⁾ and 320 μin ⁽⁶⁴⁾ while those predicted by hydrodynamic lubrication theories were in the range 6 μin to 240 μin ^(93-96,99,98). Thus, under the conditions in which the present theoretical lubricant film thickness was calculated it may be concluded that lubrication at the plug-tube interface varied from a "quasi-hydrodynamic" to a full hydrodynamic regime.

It was seen earlier that the lubricant pressure, and hence the lubricant film thickness, bear a directly proportional relationship to the draw speed and the viscosity of the lubricant. Thus, it is convenient and useful to consolidate these two factors into one by taking their product and study its effect on the design of the plug-attachments. A lubricant viscosity of $3.503 \times 10^{-4} \text{ lbf s in}^{-2}$ and a draw speed of 100 ft min^{-1} at 35% reduction in area yields a product of $\eta_0 U = 4.554 \times 10^{-3} \text{ lbf in}^{-1}$ and it changes according to the manner in which the individual factors are altered.

Figures (6.55) and (6.56) show the influence of the product $\eta_0 U$ on the lubricant pressure for two lengths of the plug-attachment at four values of the radial clearance ratio h_1/h_2 . The trend of

these graphs is similar to those obtained when the lubricant pressure was plotted against the lubricant viscosity and draw speed as in Figures (6.47) and (6.48). It is seen that for the same value of $\eta_0 U$ the longer attachment generates a higher pressure. Conversely, to generate the same lubricant pressure the shorter attachment requires a higher draw speed or the use of a more viscous lubricant.

Figure (6.57) compares the lubricant pressures calculated for the four designs of plug-attachments when the value of $\eta_0 U$ is $0.001 \text{ lbf in}^{-1}$. The lengths of the two zones of the composite and the stepped attachments are equal, i.e. $l_2/l_1 = 1.0$. The radial clearance h_2 is 0.002 in and the radial clearance ratio h_1/h_2 is 1.5 . For the range of the length of the attachments considered, it is seen that for a given length, the lubricant pressure generated by the four designs of attachments in a decreasing order is straight-parallel, composite, stepped and straight-tapered. The explanation for this order can be found by a consideration of the overall radial clearance which these attachments provide. The straight-parallel attachment provides the smallest radial clearance and thus generates the highest pressure while the largest clearance is provided by the straight-tapered design which generates the lowest pressure. The radial clearance in zone 2 provided by the composite and the stepped attachments are equal. However, in zone 1 the composite attachment has a tapered profile which provides a smaller radial clearance when compared with that of the stepped attachment which has a parallel profile. Thus, the composite attachment generates a higher lubricant pressure. Judging from the trends of these graphs it appears that the order seen in Figure (6.57) would be altered when the length of the attachment is increased. This is attributable to the influences of the radial clearance and length of the attachment on the lubricant pressure generation as discussed previously.

The effect of other values of the product $\eta_0 U$ at other radial clearances and clearance ratios are shown in Figures (6.58 - 6.60). It is seen that the order of the graphs is the same as that described above. A higher value of the product $\eta_0 U$, i.e. a higher draw speed or a more viscous lubricant, has two significant effects. It enables the same lubricant pressure to be generated by a shorter plug-attachment and also allows the radial clearance and the radial clearance ratio to be increased. These two effects can be seen by a comparison of Figures (6.57 - 6.61).

The variation of the overall length and length ratio of the composite and the stepped attachments in generating a given lubricant pressure at different values of $\eta_0 U$ are summarised in Figure (6.61). At any value of $\eta_0 U$ it is seen that the required length of the composite attachment is shorter than that of the stepped attachment. Furthermore, the length of both attachments decreases as the length ratio is increased. The effect of increasing the length ratio is to increase the length of zone 2 which provides the smaller radial clearance.

6.4.3 Theoretical results of Christopherson tubes

Unless otherwise stated, the appropriate data used in the theoretical calculations for the plug-attachments were used again in the calculations for the straight-parallel, straight-tapered, composite and stepped Christopherson tubes. The results are tabulated in Tables (A3.11 - A3.21) and illustrated graphically in Figures (6.62 - 6.77).

It is seen that the influences of the length of the Christopherson tube, radial clearance, lubricant viscosity, draw speed and the radial clearance ratio on the generation of the lubricant pressure and the lubricant film thickness at the die entry are

similar to those observed for the plug-attachments. Thus, it is not intended nor is it desirable to repeat the discussion on the influences of these factors in this section unless necessary. Generally, the theoretical results obtained for the Christopherson tubes were of a greater magnitude than those obtained for the plug-attachments. This is attributable to the difference in the lubricant film geometries formed at the entry to the metal deformation zone between the undrawn tube and the Christopherson tube and that between the undrawn tube and the plug, as shown in Figures (3.1) and (3.6). In the case of the Christopherson tube the lubricant film is convergent in the die entry region whereas in the case of the plug-attachment there is an expansion in the lubricant geometry at the end of the attachment before it converges in the sink zone.

The influences of the various factors on the lubricant film thickness are summarised in Figures (6.67 - 6.69). The lubricant film thickness calculated under these conditions were found to be in the range associated with a hydrodynamic lubrication regime.

In Figures (6.70-6.73) the lubricant pressure is plotted against the product $\eta_0 U$ for the straight-parallel and straight-tapered Christopherson tubes of various lengths, radial clearances and radial clearance ratios. It is seen that the lubricant pressure increases with the value of $\eta_0 U$. An interesting feature of these illustrations is that as $\eta_0 U$ increases, a stage is reached at which the lubricant pressure generated by the straight-tapered Christopherson tube rises above that generated by the straight-parallel design. Further increments in $\eta_0 U$ result in the lubricant pressure attaining a peak value, equivalent to the yield stress of the tube material, before it decreases. The theoretical analysis limits the lubricant pressure to the yield stress of the tube material and does not account for pressures above this value.

Thus, at values of $\eta_0 U$ greater than that corresponding to the highest lubricant pressure the tube has deformed within the Christopherson tube. When this occurs the pressure to the right of the peak is therefore invalid. Experimentally, the occurrence of metal deformation, at values of the lubricant pressure above the yield stress of the work material, before the work enters the die had been reported by other workers (5,9,10,11) and it is on this principle that the technique of dieless wire-drawing (171) was developed recently. Within the valid regions of these figures, as in the case of the plug-attachments, the effect of a higher value of $\eta_0 U$ is to enable the same lubricant pressure to be generated with a shorter length of the Christopherson tube and allows the radial clearance and the radial clearance ratio to be increased.

Figures (6.74) and (6.75) compare the variation of the lubricant pressure with the product $\eta_0 U$ for the straight-parallel, composite and stepped Christopherson tubes at two length ratios. The variation of the lubricant pressure with the length of the four designs of Christopherson tubes at $\eta_0 U = 4.554 \times 10^{-3} \text{ lbf in}^{-1}$, equivalent to a draw speed of 100 ft min^{-1} at 35% reduction and a lubricant viscosity of $3.503 \times 10^{-4} \text{ lbf s in}^{-2}$, is shown in Figures (6.76) and (6.77). For short lengths of the Christopherson tubes, it is seen that these four designs generate a lubricant pressure in a decreasing order according to straight-parallel, composite, stepped and straight-tapered, which is identical to that observed for the plug-attachments. However, as was postulated previously, the order is altered as the length is increased. The peak lubricant pressure equivalent to the yield stress of the tube material is also evident in these illustrations and when it occurs, the pressure to its right is no longer valid.

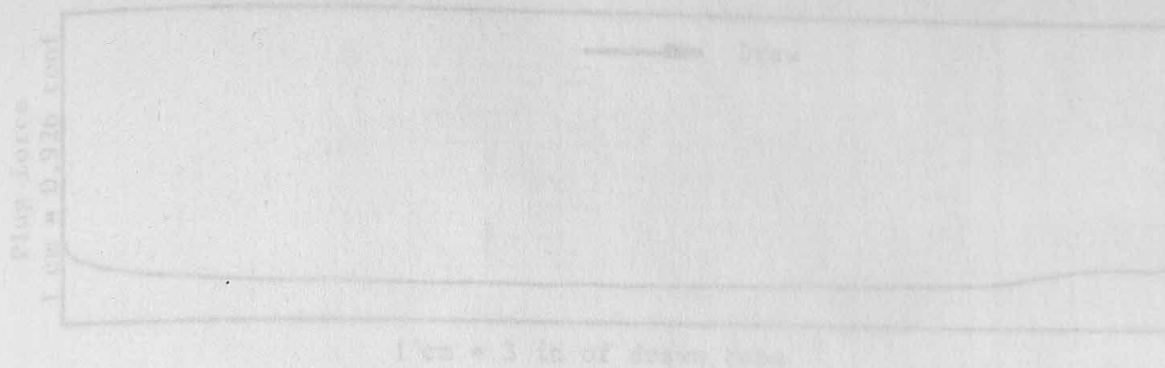
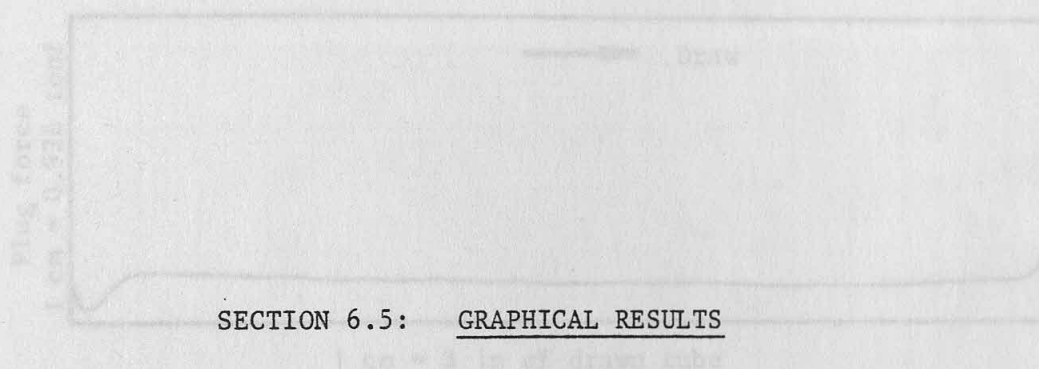


Figure (6.1) Trace of the plug force when drawing with conventional plug and plug-attachment



SECTION 6.5: GRAPHICAL RESULTS

Figure (6.2) Trace of the plug force when drawing with curve-profiled plug and plug-attachment

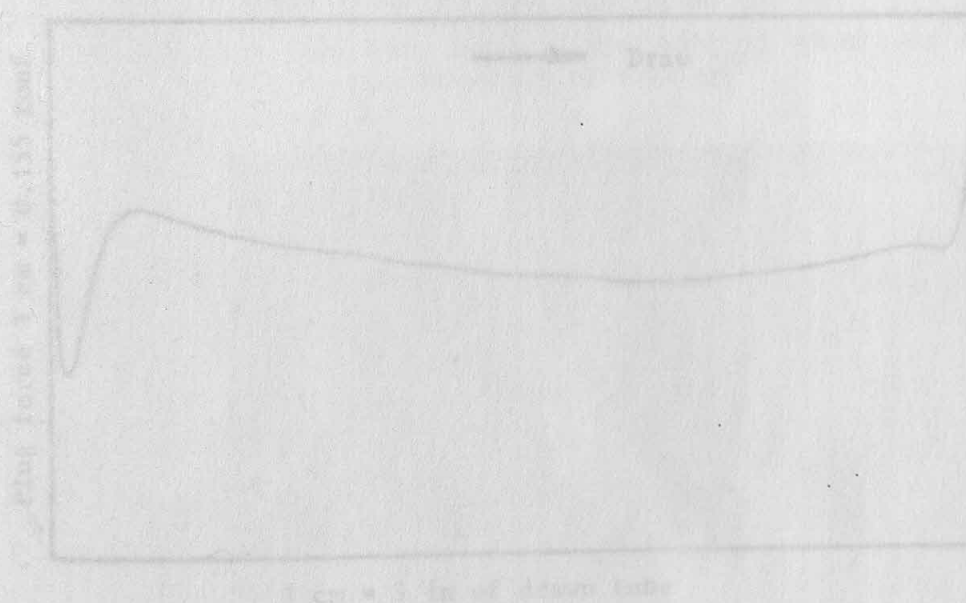
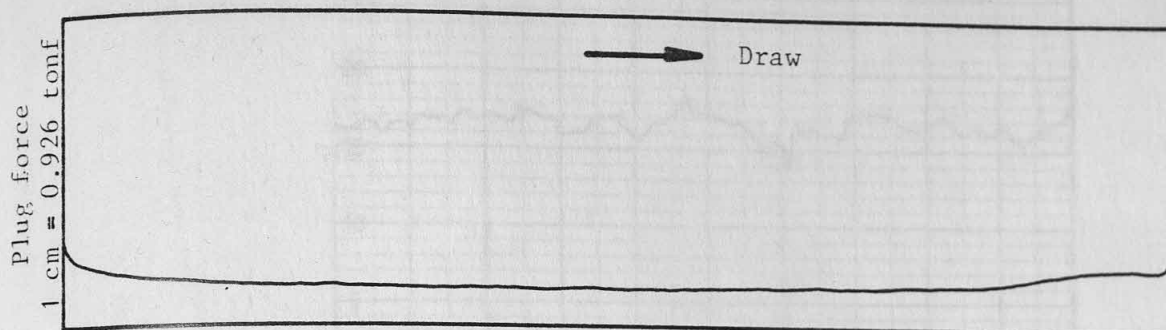
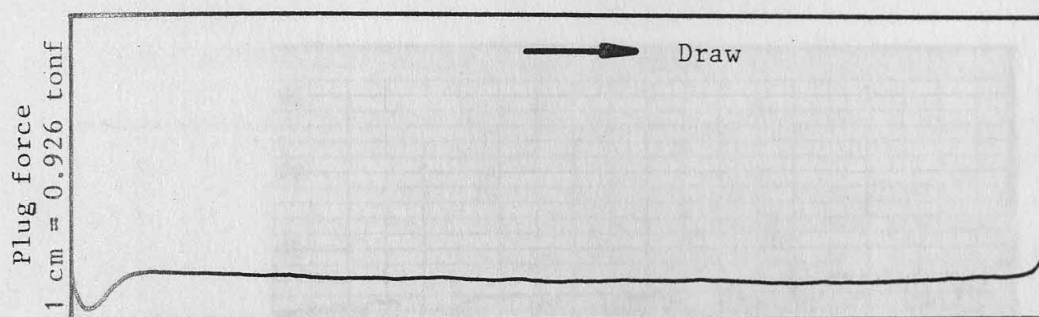


Figure (6.3) Trace of the plug force when drawing with cone-profiled plug and plug-attachment



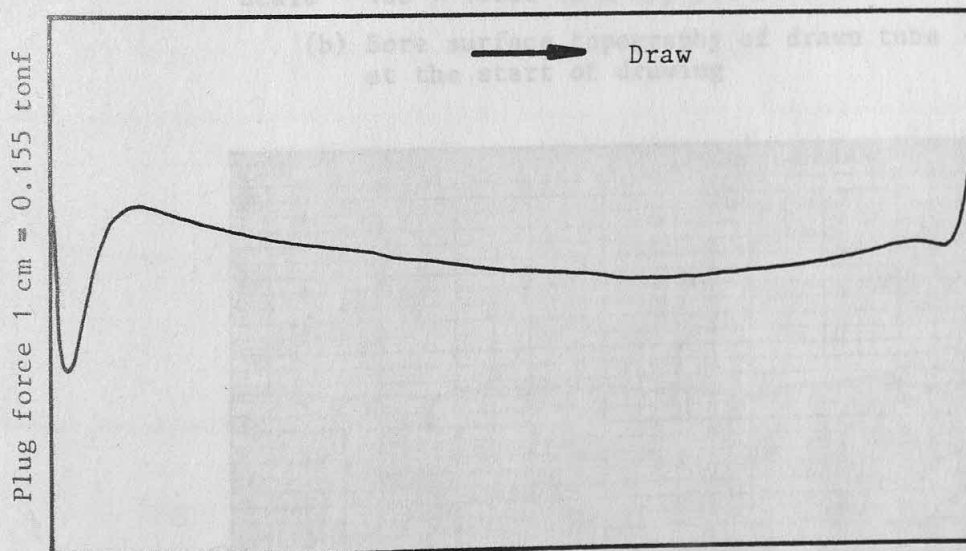
1 cm = 3 in of drawn tube

Figure (6.1) Trace of the plug force when drawing with conventional plug and plug-attachment



1 cm = 3 in of drawn tube

Figure (6.2) Trace of the plug force when drawing with curve profiled plug and plug-attachment



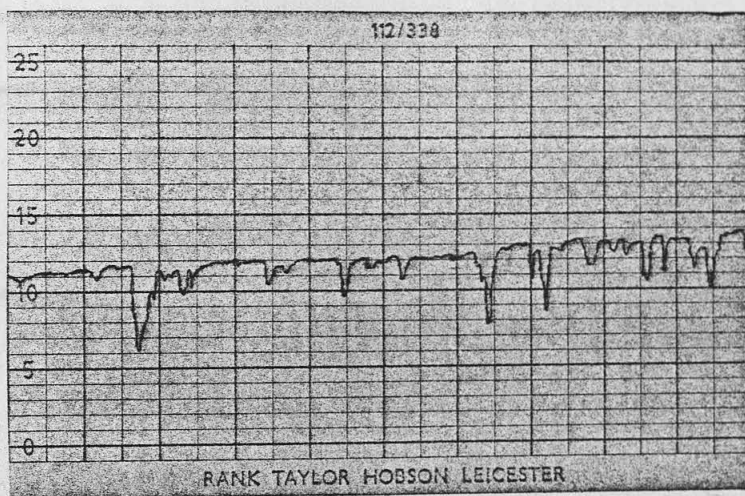
1 cm = 3 in of drawn tube

Figure (6.3) Trace of the plug force when drawing with curve-profiled plug and plug-attachment



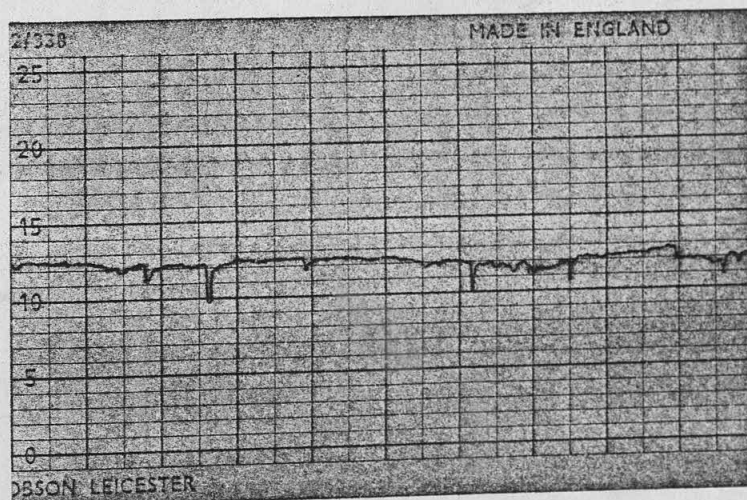
Scale = 100 x 2000 (L x H), 0.55 μ m CLA
 Surface condition = grit-blasted

(a) Initial tube bore surface topography



Scale = 100 x 10000 (L x H), 0.2 μ m CLA

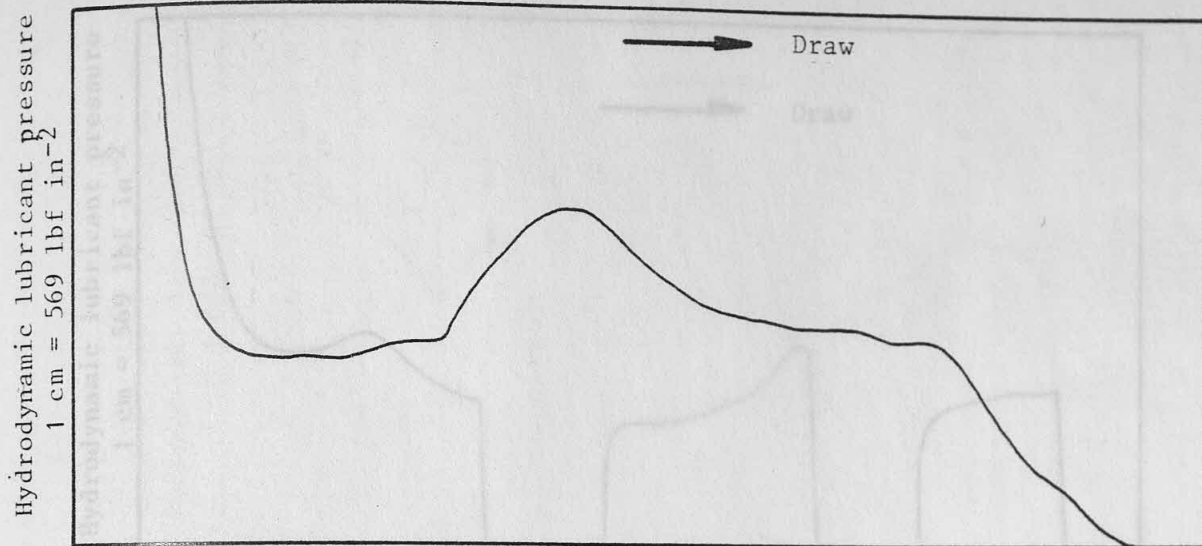
(b) Bore surface topography of drawn tube at the start of drawing



Scale = 100 x 10000 (L x H), 0.08 μ m CLA

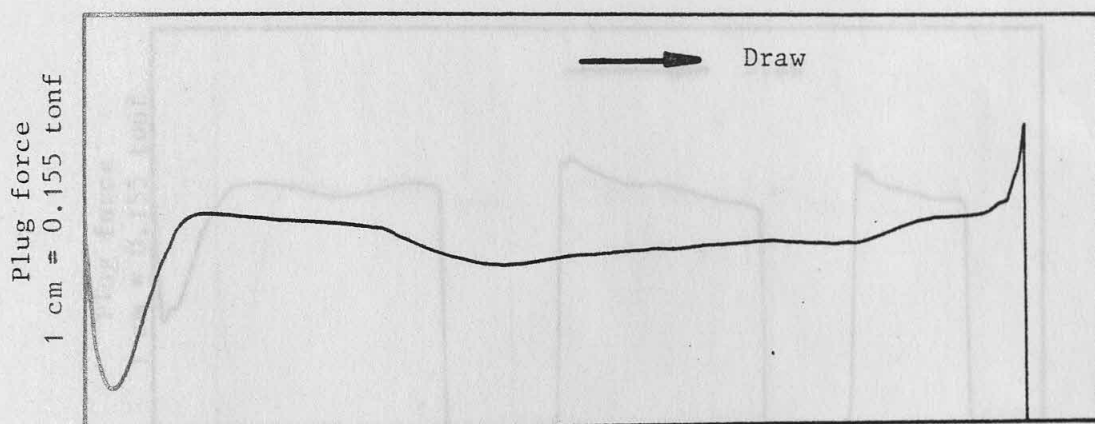
(c) Bore surface topography of drawn tube

Figure (6.4) Bore surface topographics of tube before and after drawing



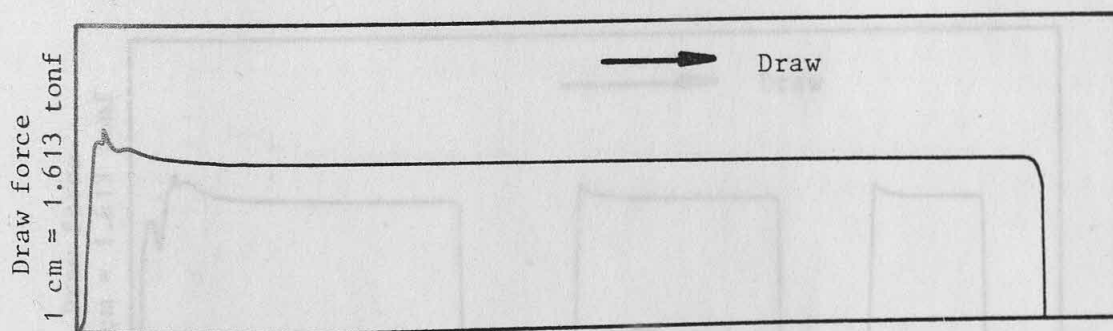
1 cm = 2.67 in of drawn tube

(a) Trace of the hydrodynamic lubricant pressure



1 cm = 3 in of drawn tube

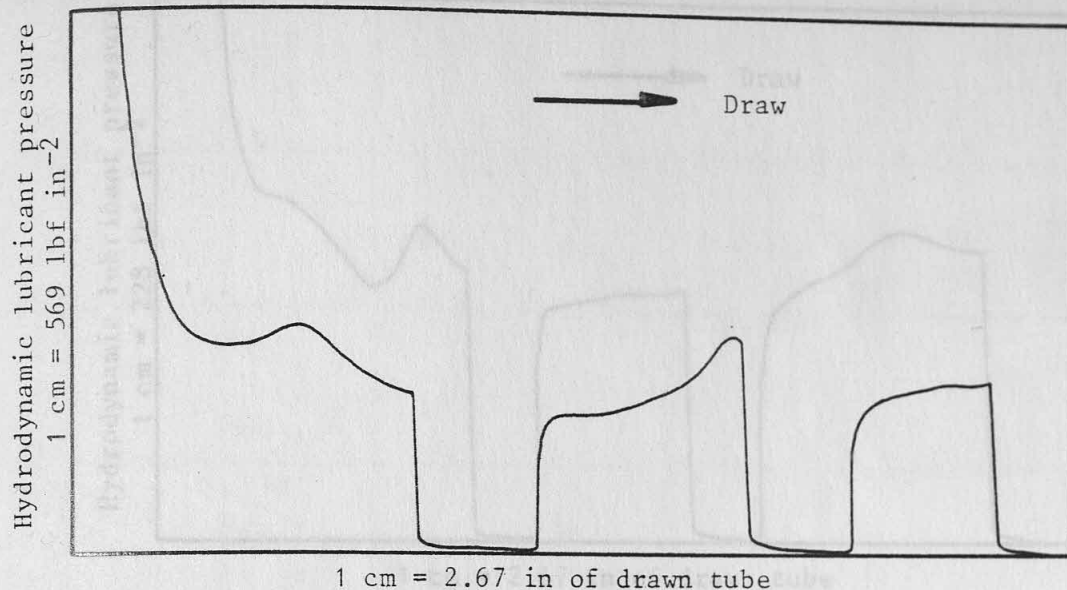
(b) Trace of the plug force



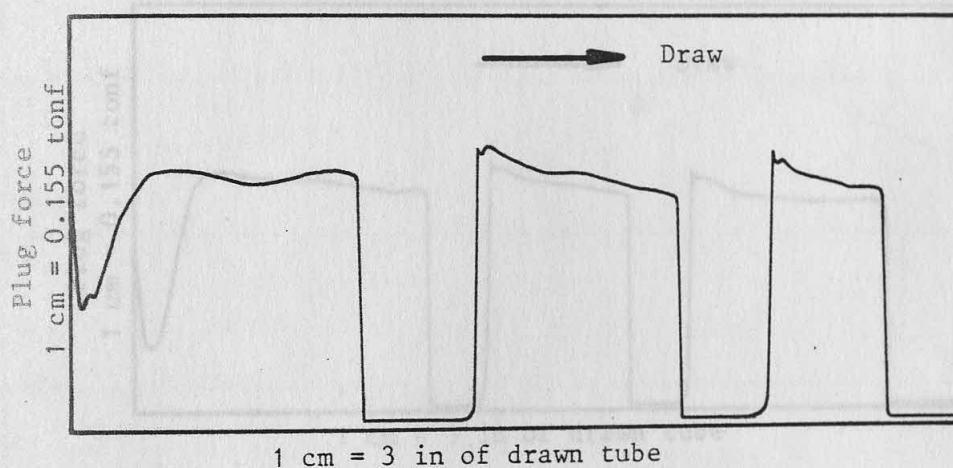
1 cm = 3 in of drawn tube

(c) Trace of the draw force

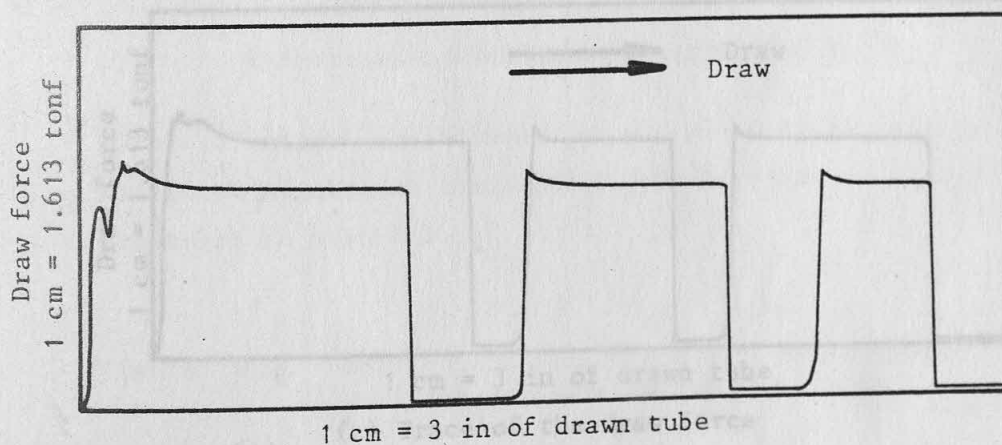
Figure (6.5) Hydrodynamic lubricant pressure and force traces in tube-drawing with the curve-profiled plug and plug-attachment



(a) Trace of the hydrodynamic lubricant pressure

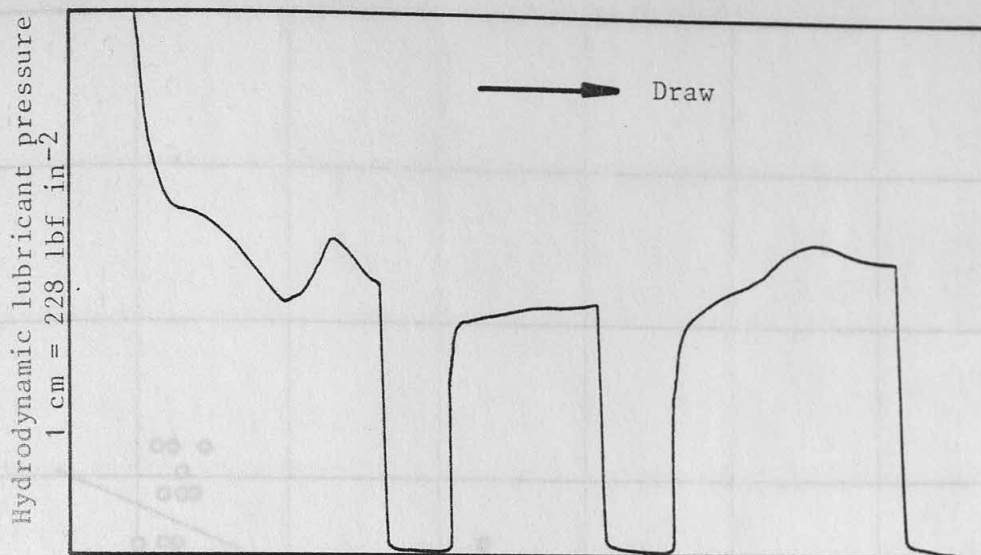


(b) Trace of the plug force



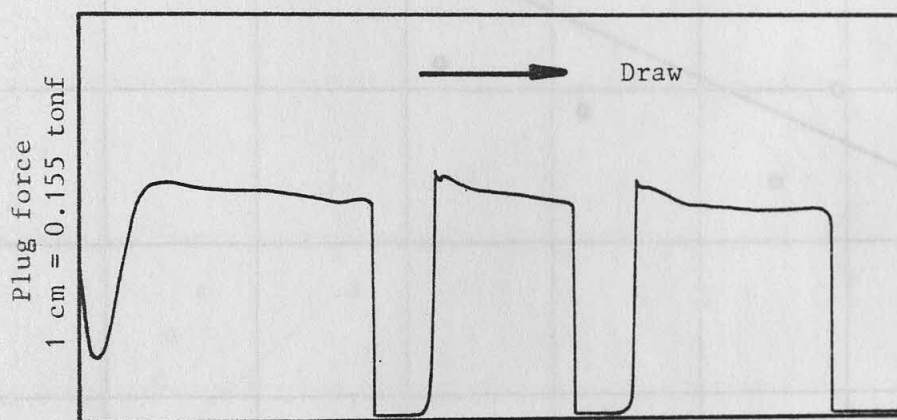
(c) Trace of the draw force

Figure (6.6) Hydrodynamic lubricant pressure and force traces in intermittent tube-drawing with the curve-profiled plug and plug-attachment



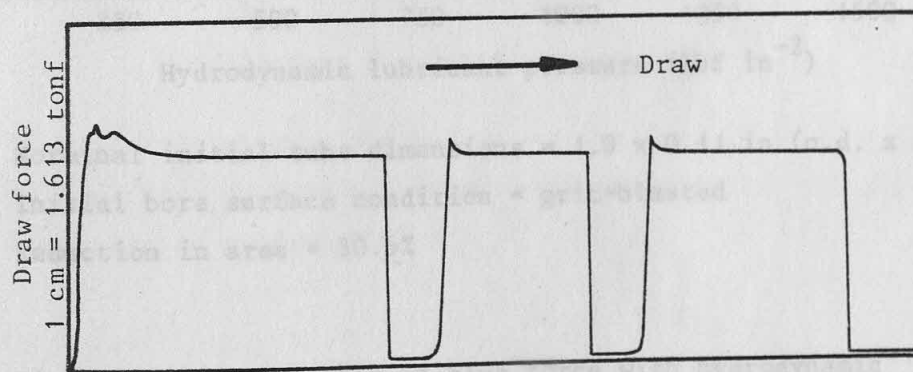
1 cm = 2.67 in of drawn tube

(a) Trace of the hydrodynamic lubricant pressure



1 cm = 3 in of drawn tube

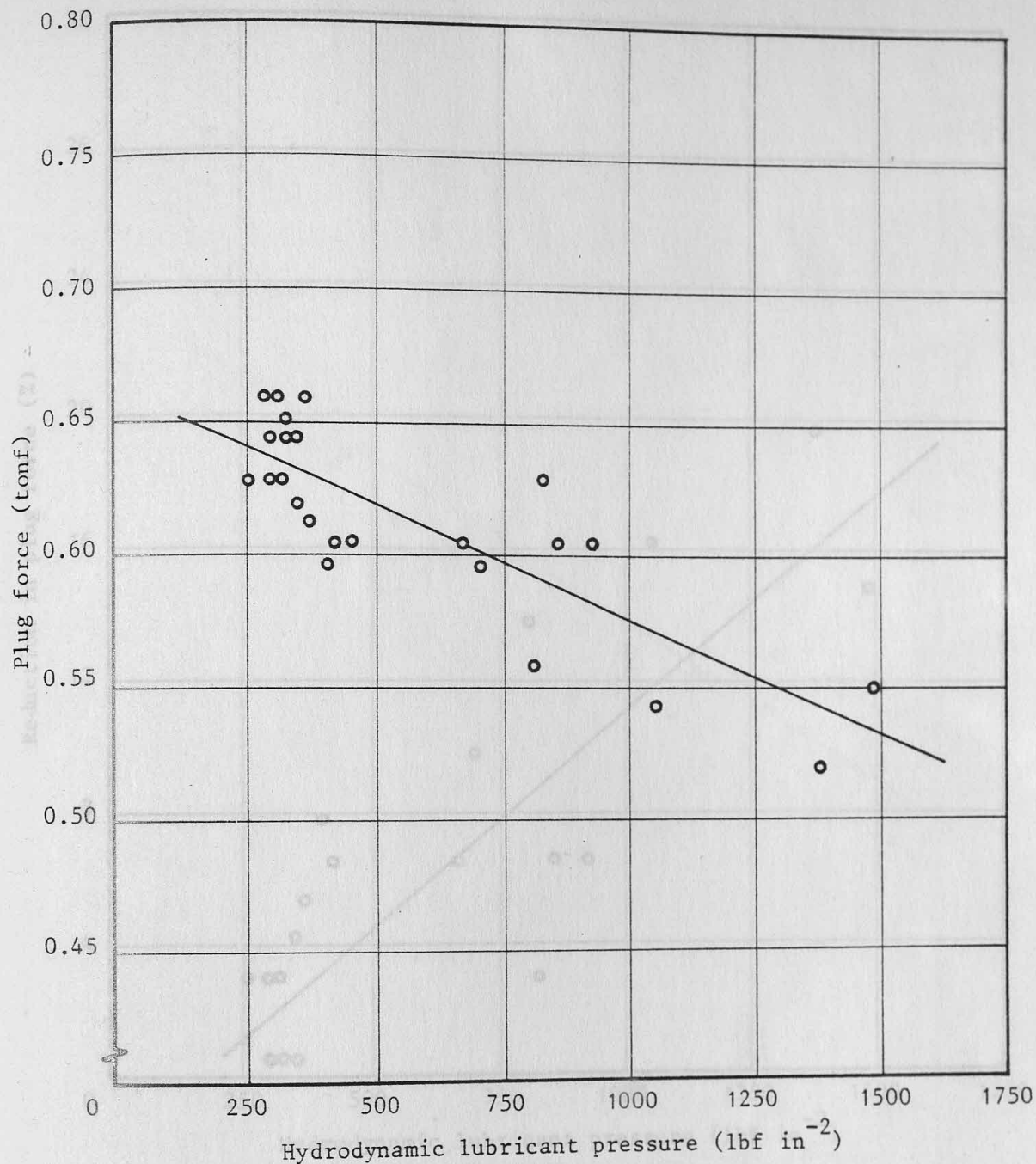
(b) Trace of the plug force



1 cm = 3 in of drawn tube

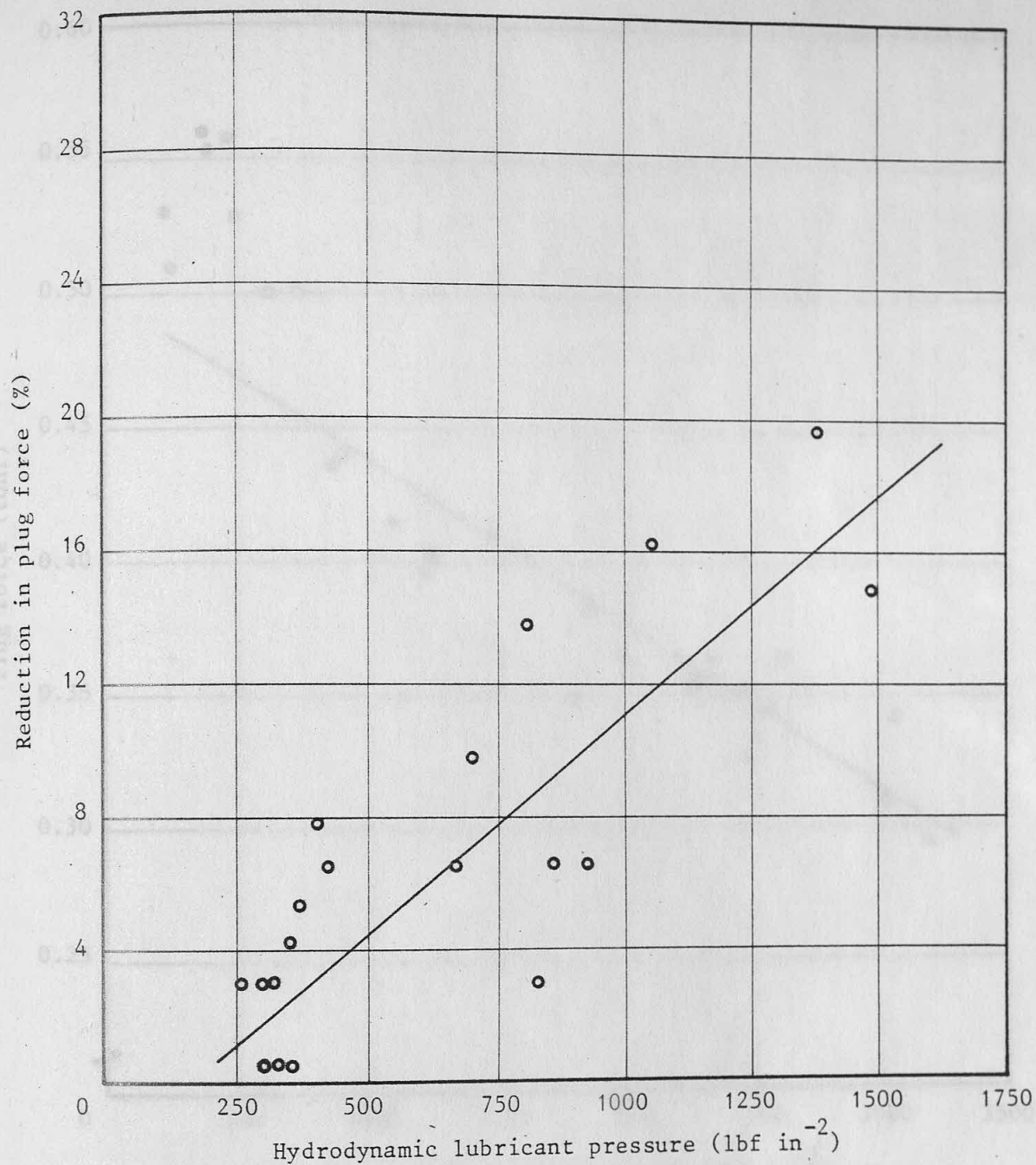
(c) Trace of the draw force

Figure (6.7) Hydrodynamic lubricant pressure and force traces in intermittent tube-drawing with the curve-profiled plug and plug-attachment



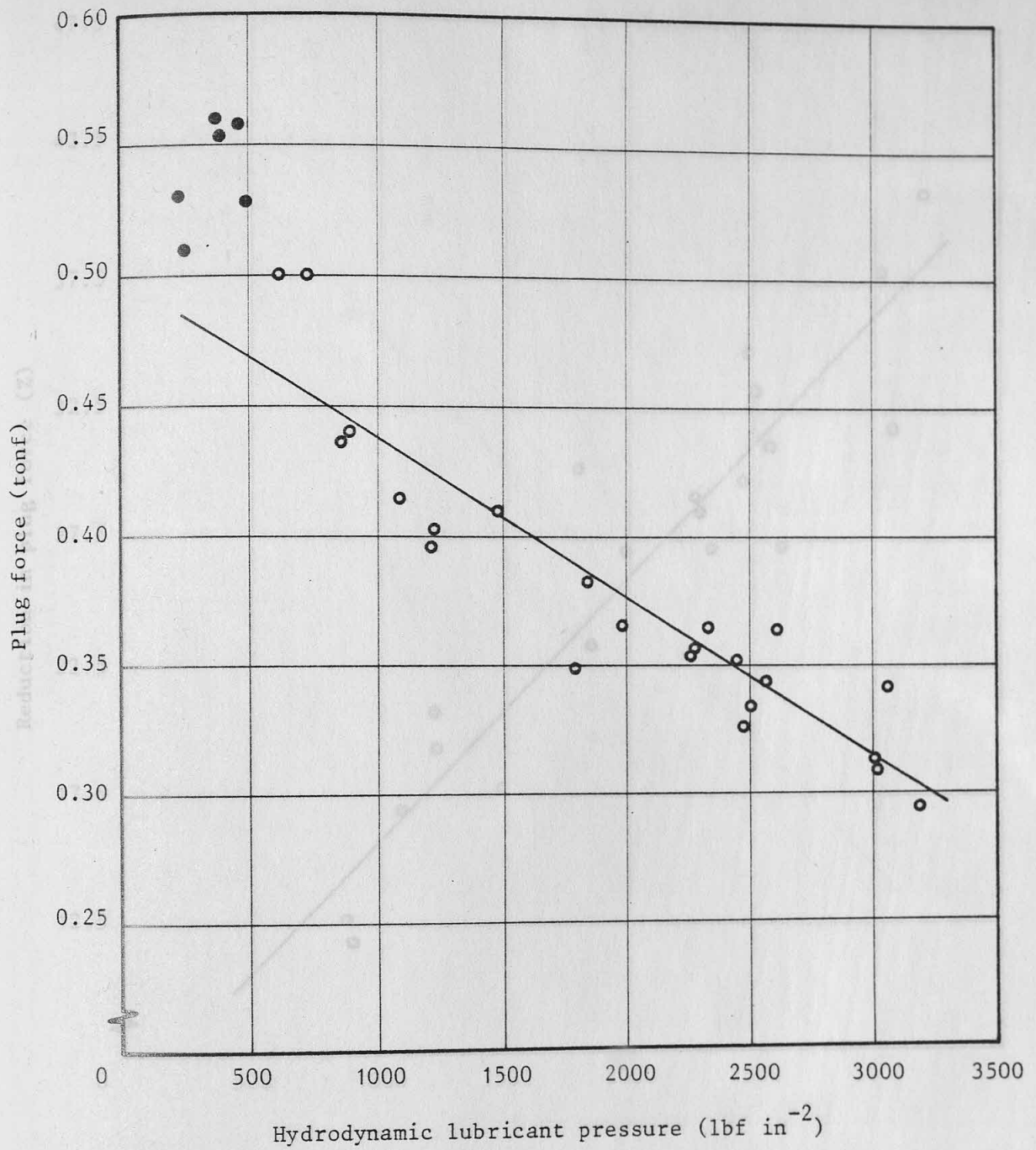
Normal initial tube dimensions = 1.0 x 0.11 in (o.d. x t)
 Initial bore surface condition = grit-blasted
 Reduction in area = 30.6%

Figure (6.8) Variation of plug force with hydrodynamic lubricant pressure in the first pass



Nominal initial tube dimensions = 1.0 x 0.11 in (o.d. x t)
 Initial bore surface condition = grit-blasted
 Reduction in area = 30.6%

Figure (6.9) Variation of percentage reduction in plug force with hydrodynamic lubricant pressure in the first pass



Nominal initial tube dimensions = 0.830 x 0.093 in (o.d. x t)

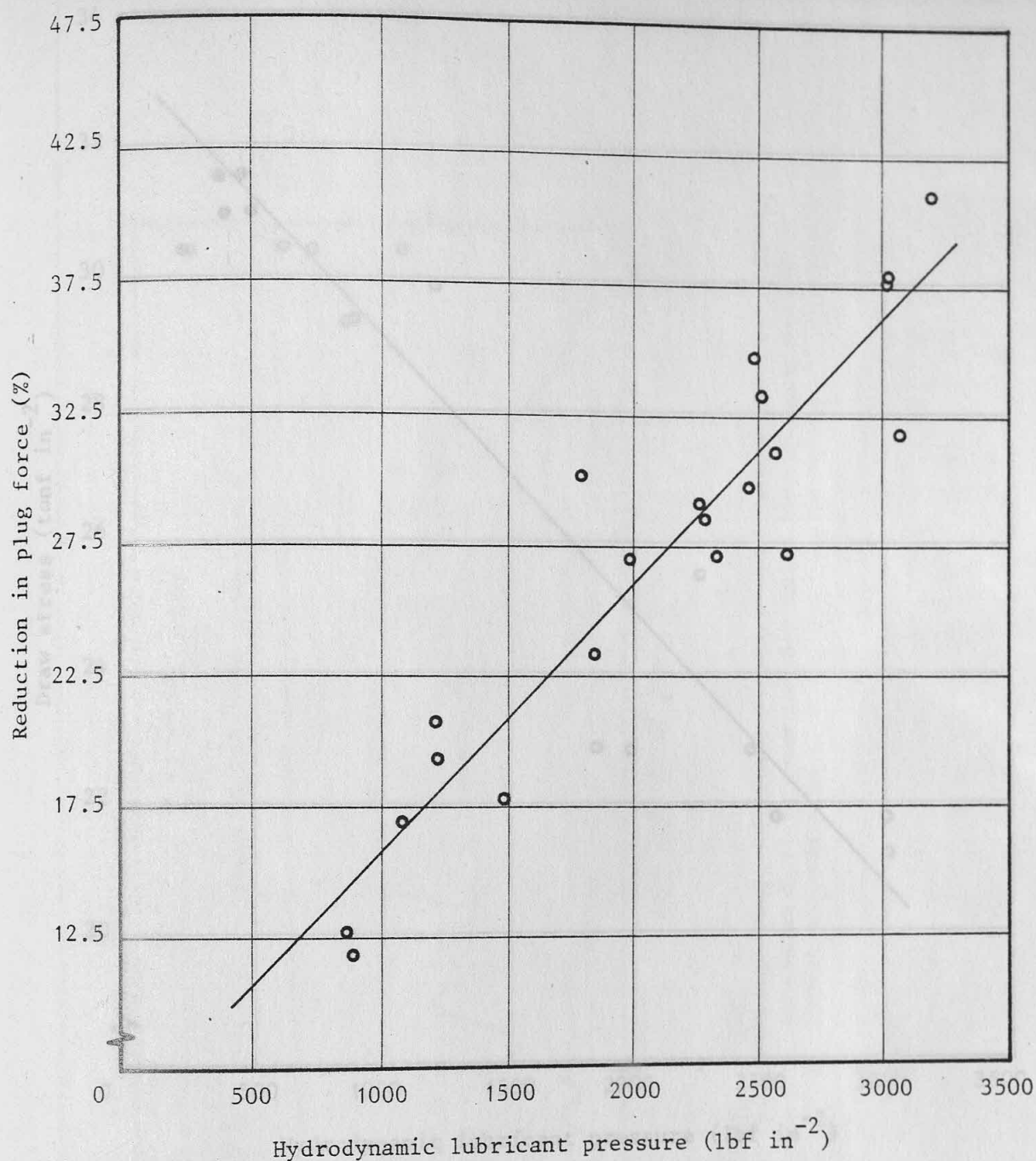
Initial bore surface condition = as-drawn

Reduction in area = 31.1%

● occurrence of pick-up

Figure (6.11) Variation of percentage reduction in plug

Figure (6.10) Variation of plug force with hydrodynamic lubricant pressure in the second pass



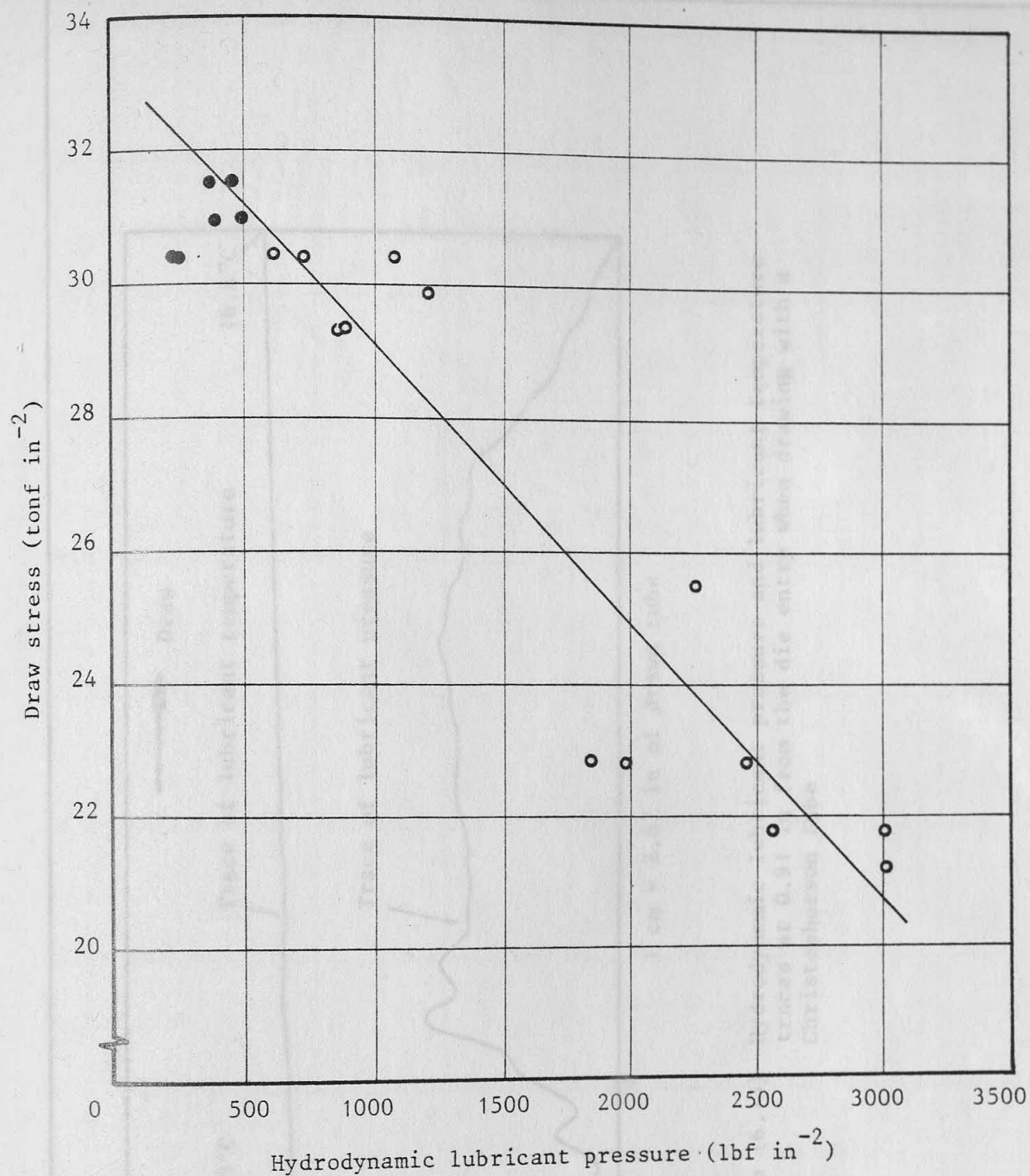
Nominal initial tube dimensions = 0.830 x 0.093 in (o.d. x t)

Initial bore surface condition = as-drawn

Reduction in area = 31.1%

● occurrence of pick-up

Figure (6.11) Variation of percentage reduction in plug force with hydrodynamic lubricant pressure in the second pass



Nominal initial tube dimensions = 0.830 x 0.093 in (o.d. x t)

Initial bore surface condition = as-drawn

Reduction in area = 31.1%

● occurrence of pick-up

Figure (6.12) Variation of draw stress with hydrodynamic lubricant pressure in the second pass

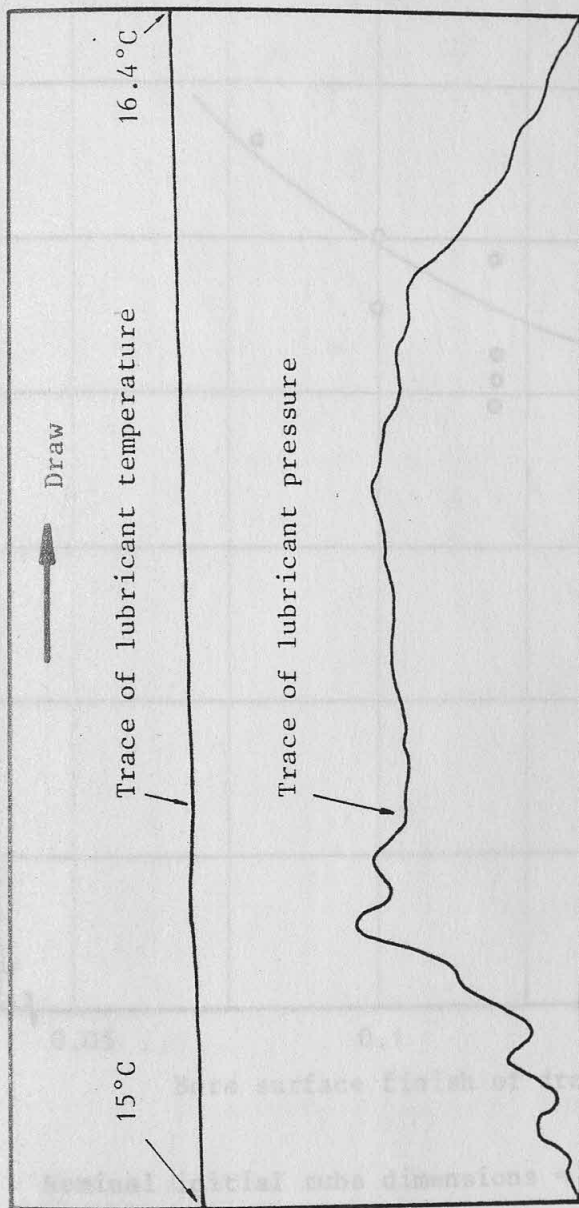
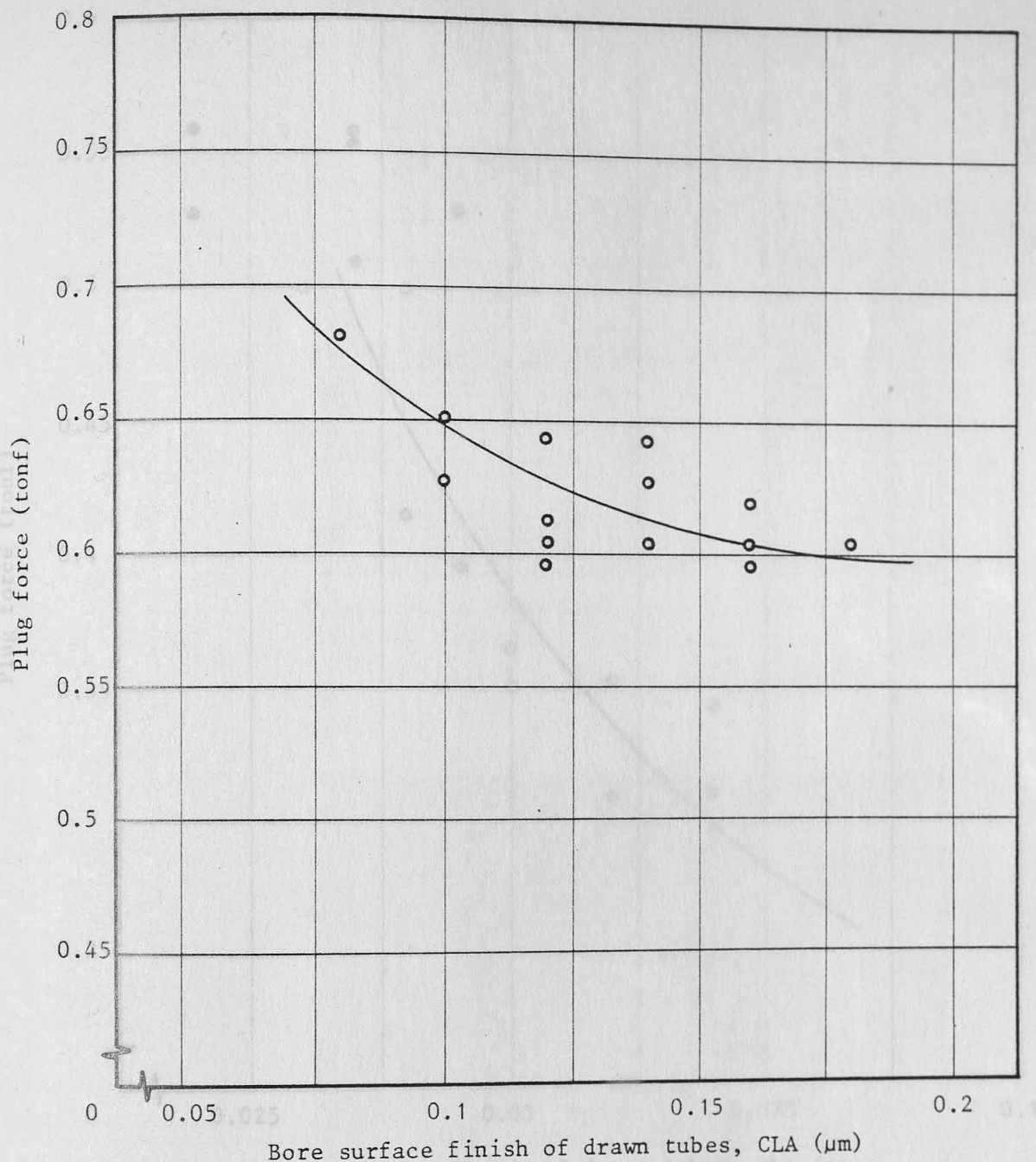


Figure (6.13) Hydrodynamic lubricant pressure and lubricant temperature traces at 0.91 in from the die entry when drawing with a Christopherson tube



Nominal initial tube dimensions = 1.0 x 0.11 in (o.d. x t)

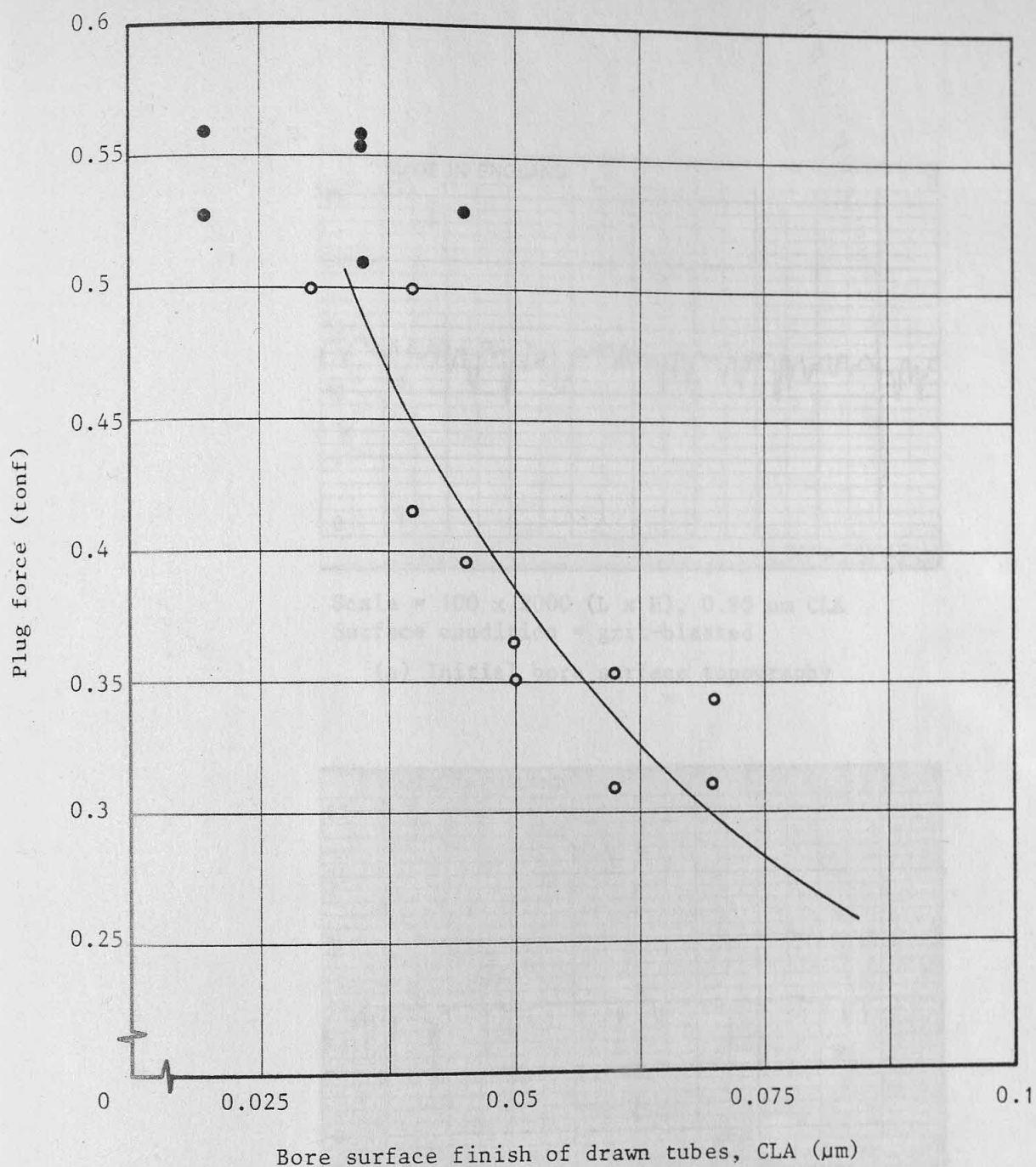
Initial bore surface condition = grit-blasted

Reduction in area = 30.6%

● occurrence of pick-up

Figure (6.14) Variation of the bore surface finish of the tubes drawn in the first pass with the plug force

Figure (6.15) Variation of the bore surface finish of the tubes drawn in the second pass with the plug force



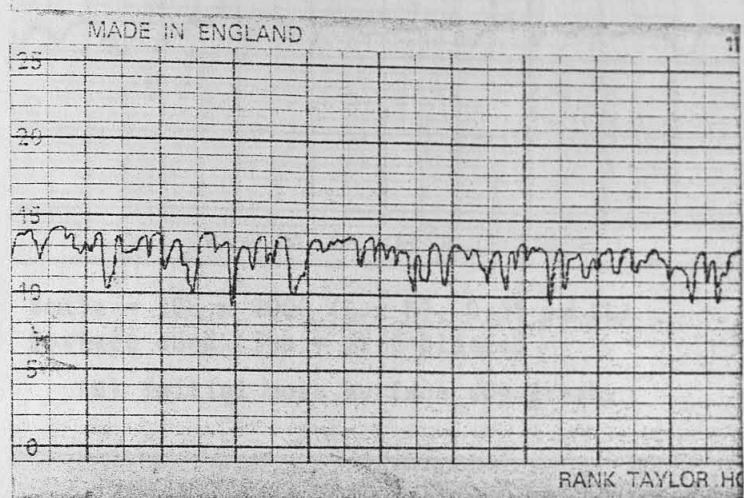
Nominal initial tube dimensions = 0.830 x 0.093 in (o.d. x t)

Initial bore surface condition = as-drawn

Reduction in area = 31.1%

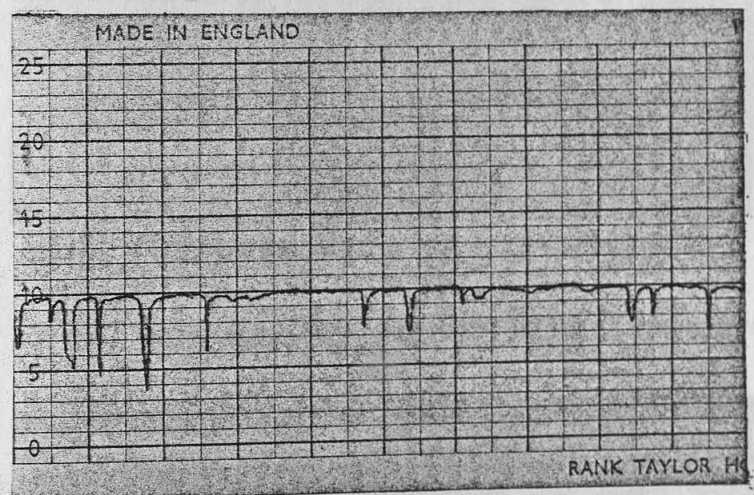
● occurrence of pick-up

Figure (6.15) Variation of the bore surface finish of the tubes drawn in the second pass with the plug force



Scale = 100 x 2000 (L x H), 0.95 μm CLA
 Surface condition = grit-blasted

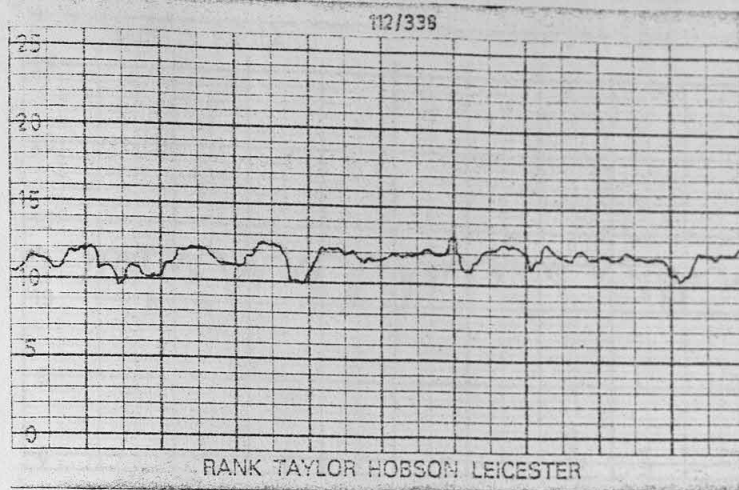
(a) Initial bore surface topography



Scale = 100 x 10000 (L x H), 0.08 μm CLA

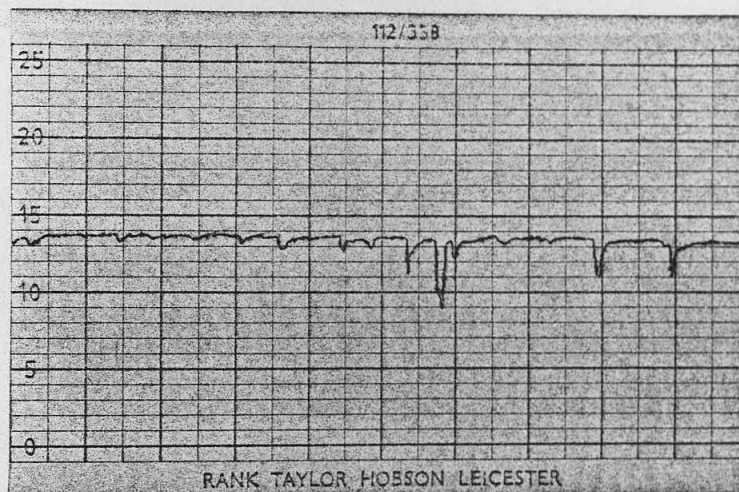
(b) Bore surface topography of tube drawn without plug-attachment

Figure (6.16) Bore surface topography of tube before and after drawing without plug-attachment



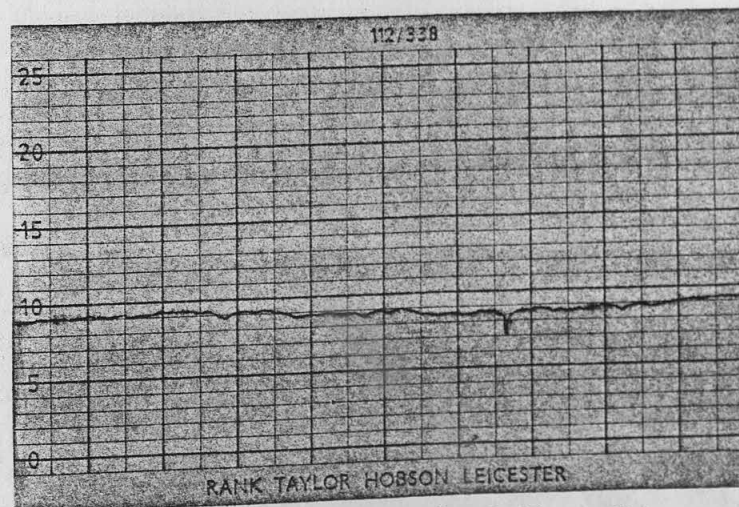
Scale = 100 x 2000 (L x H), 0.55 μm CLA
 Surface condition = grit-blasted

(a) Initial bore surface topography



Scale = 100 x 10000 (L x H), 0.1 μm CLA
 Lubricant pressure = 325 lbf in⁻²

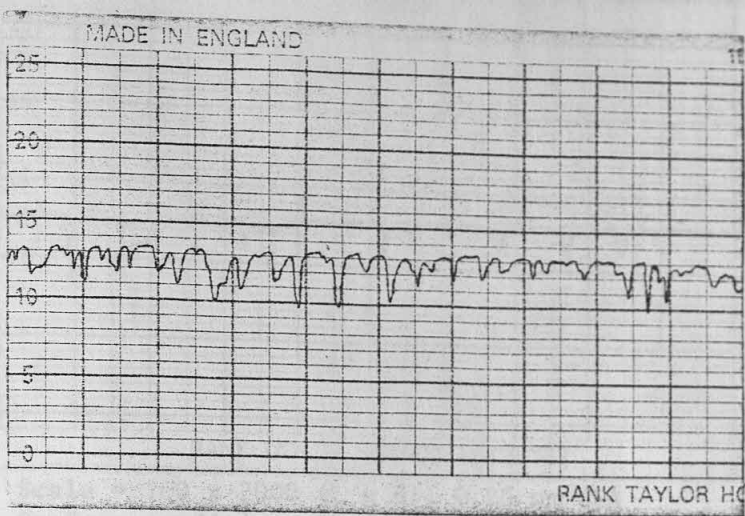
(b) Bore surface topography after first pass



Scale = 100 x 20000 (L x H), 0.02 μm CLA
 Lubricant pressure = 375 lbf in⁻²

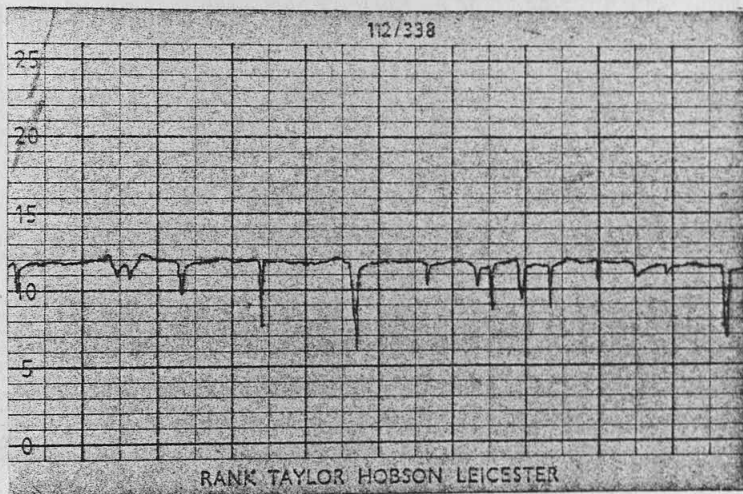
(c) Bore surface topography after second pass

Figure (6.17) Bore surface topography of tube before and after drawing with plug-attachment



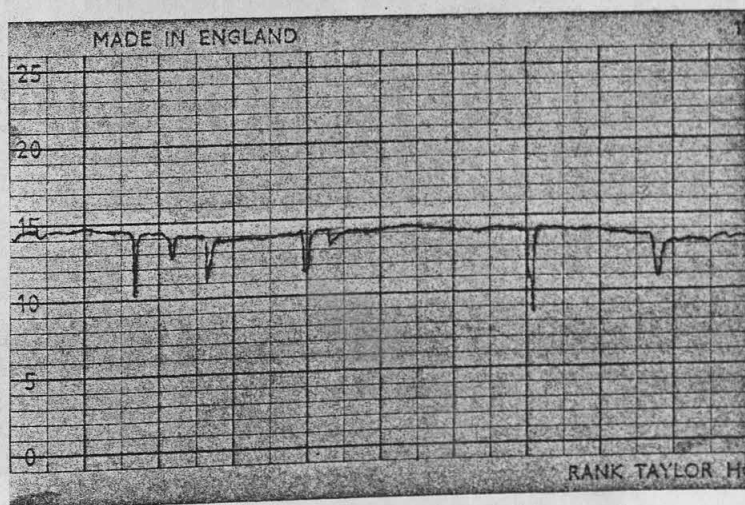
Scale = 100 x 2000 (L x H), 0.65 μm CLA
 Surface condition = grit-blasted

(a) Initial bore surface topography



Scale = 100 x 10000 (L x H), 0.14 μm CLA
 Lubricant pressure = 287 lbf in⁻²

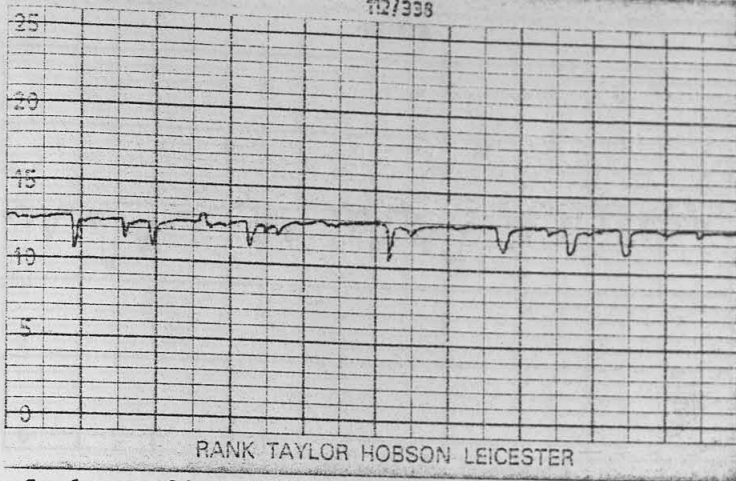
(b) Bore surface topography after first pass



Scale = 100 x 20000 (L x H), 0.04 μm CLA
 Lubricant pressure = 1080 lbf in⁻²

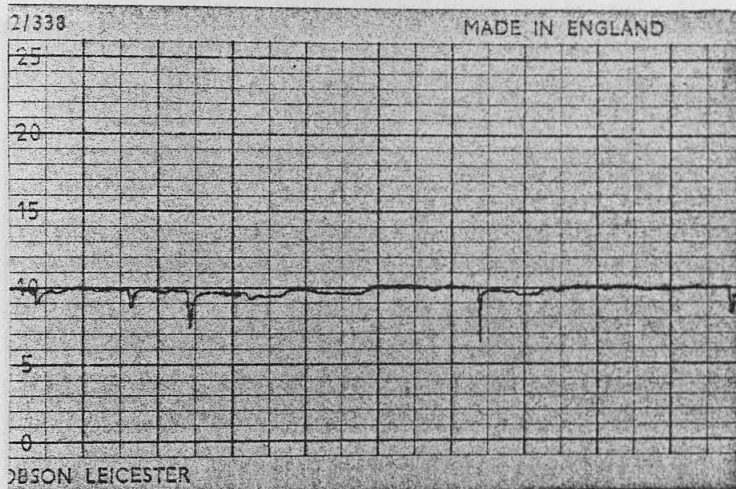
(c) Bore surface topography after second pass

Figure (6.18) Bore surface topography of tube before and after drawing with plug-attachment



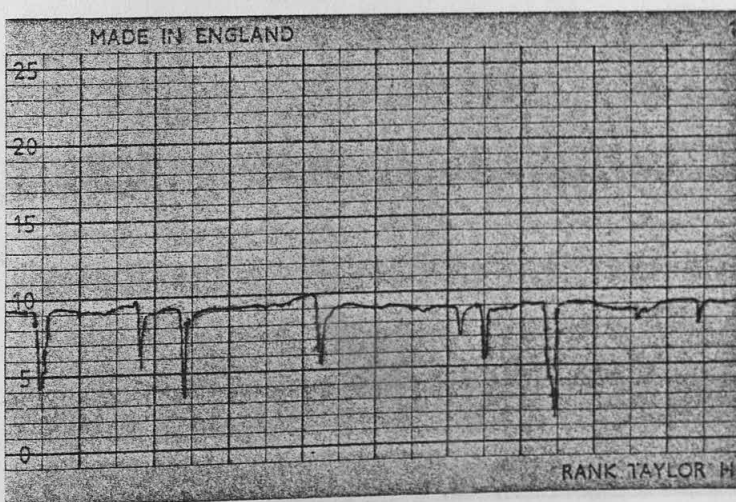
Scale = 100 x 2000 (L x H), 0.25 μm CLA
 Surface condition = grit-blasted

(a) Initial bore surface topography



Scale = 100 x 10000 (L x H), 0.16 μm CLA
 Lubricant pressure = 349 lbf in^{-2}

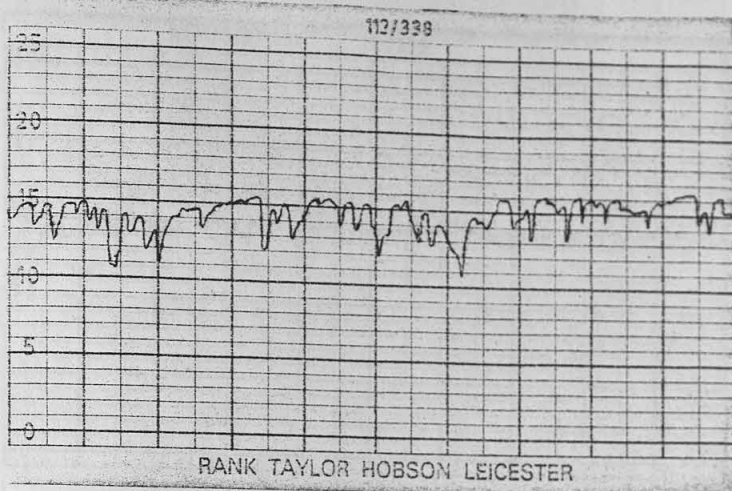
(b) Bore surface topography after first pass



Scale = 100 x 20000 (1 x H), 0.07 μm CLA
 Lubricant pressure = 3012 lbf in^{-2}

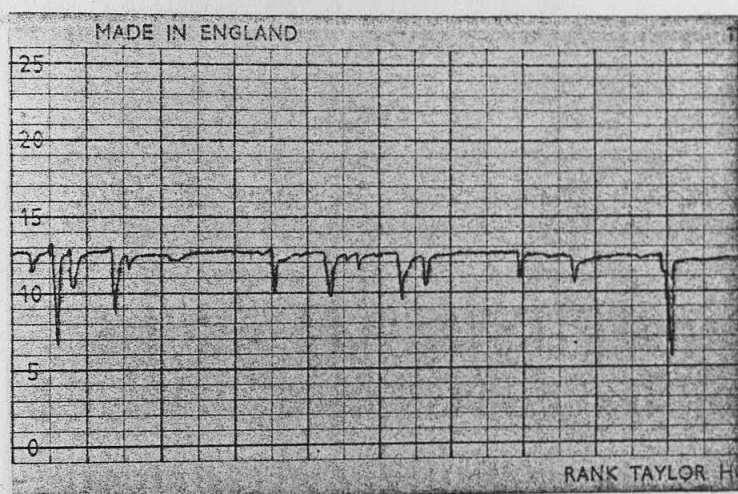
(c) Bore surface topography after second pass

Figure (6.19) Bore surface topography of tube before and after drawing with plug-attachment



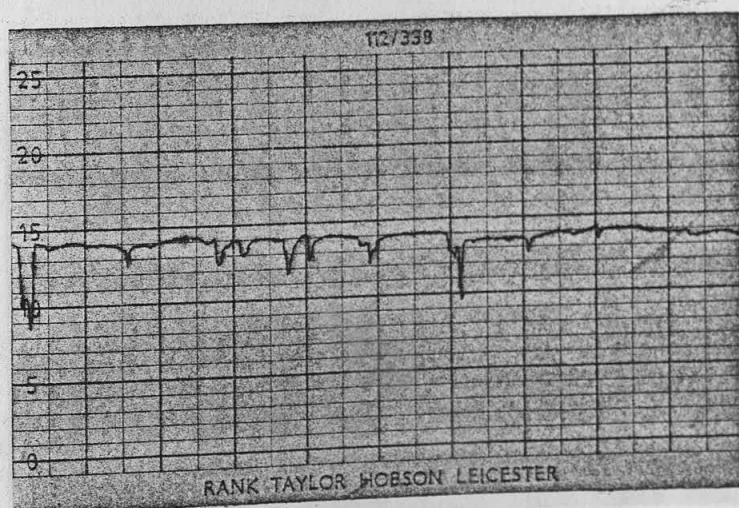
Scale = 100 x 2000 (L x H), 0.9 μm CLA
 Surface condition = grit-blasted

(a) Initial bore surface topography



Scale = 100 x 10000 (L x H), 0.18 μm CLA
 Lubricant pressure = 452 lbf in^{-2}

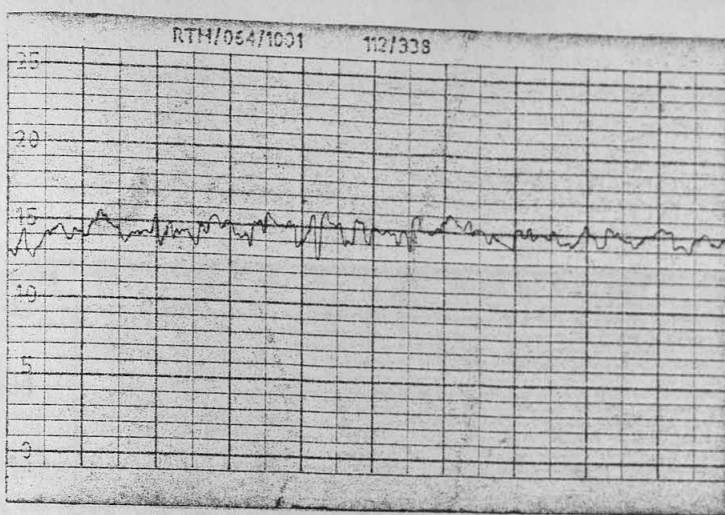
(b) Bore surface topography after first pass



Scale = 100 x 20000 (L x H), 0.09 μm CLA
 Lubricant pressure = 1846 lbf in^{-2}

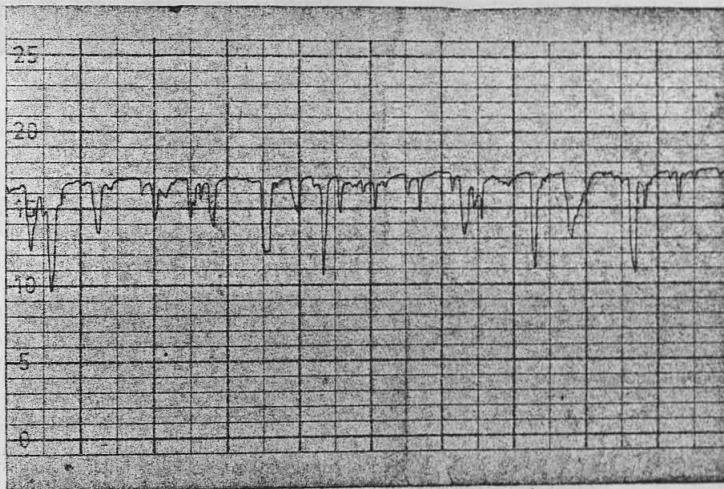
(c) Bore surface topography after second pass

Figure (6.20) Bore surface topography of tube before and after drawing with plug-attachment



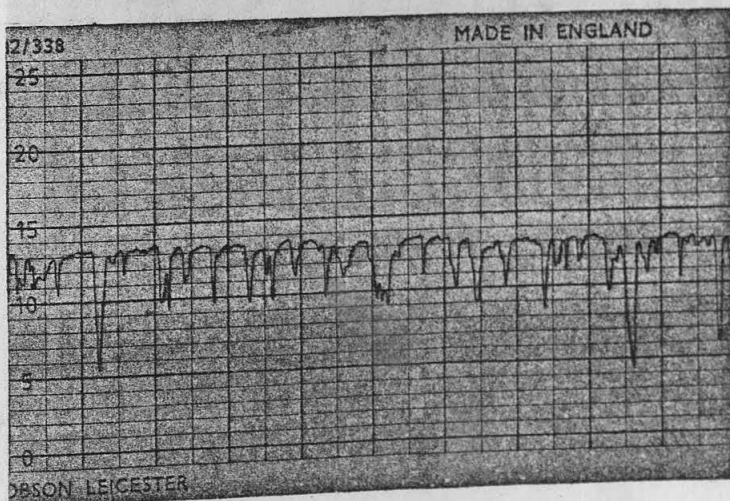
Scale = 100 x 2000 (L x H), 0.6 μ m CLA
 Surface condition = ground

Figure (6.21) Typical initial external surface topography of tube



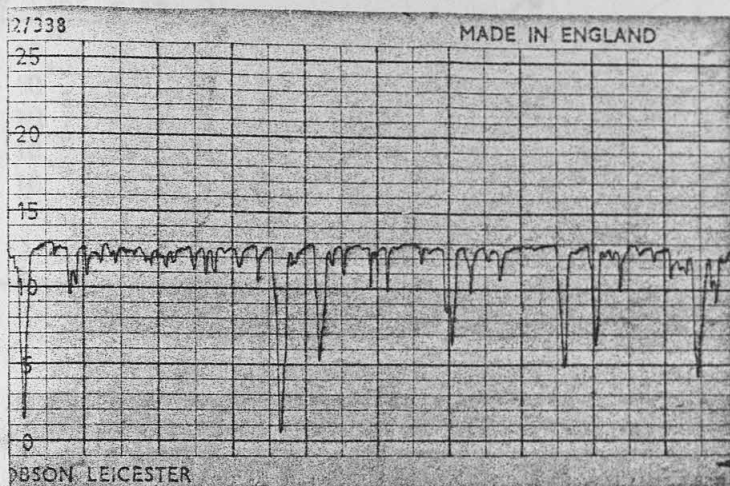
Scale = 100 x 5000 (L x H), 0.5 μ m CLA

Figure (6.22) Typical external surface topography of tube drawn without a Christopherson tube



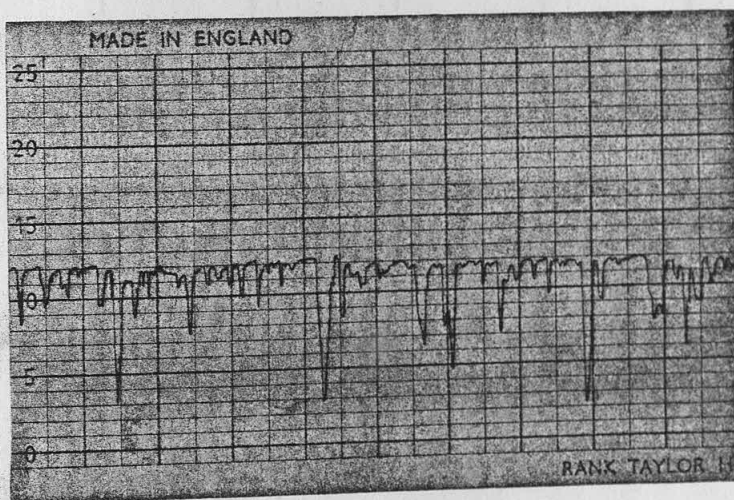
Scale = 100 x 5000 (L x H), 0.45 μ m CLA

Figure (6.23) External surface topography of tube drawn with a 2.4 in long Christopherson tube



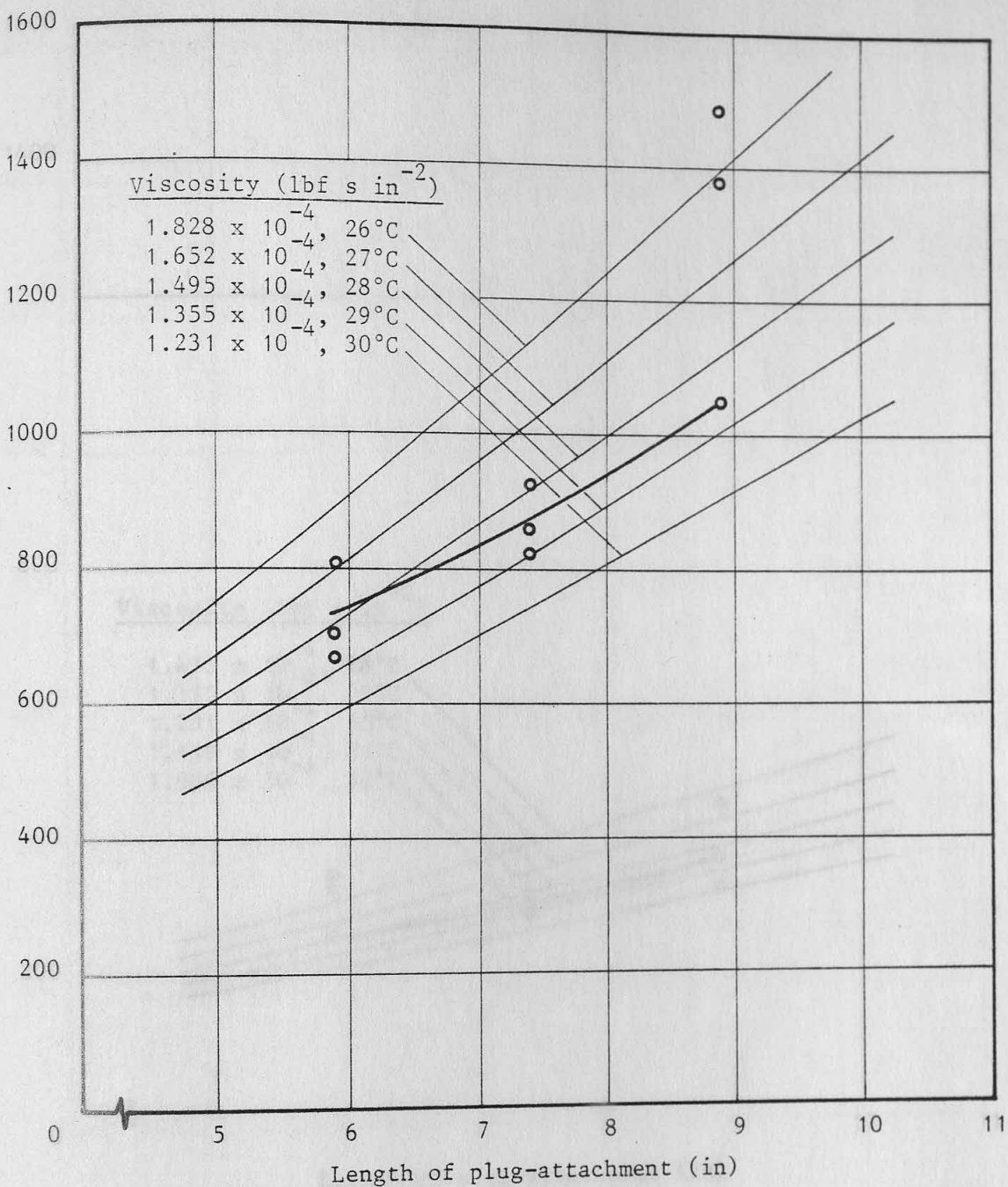
Scale = 100 x 5000 (L x H), 0.5 μ m CLA

Figure (6.24) External surface topography of tube drawn with a 5.4 in long Christopherson tube



Scale = 100 x 5000 (L x H), 0.55 μ m CLA

Figure (6.25) External surface topography of tube drawn with an 8.4 in long Christopherson tube



Mean radial clearance = 0.004 in

Laboratory ambient temperature = 21°C

Viscosity of EP50 at 21°C = 3.128 x 10⁻⁴ lbf s in⁻²

Reduction in area = 30.6%

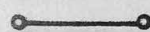
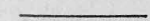
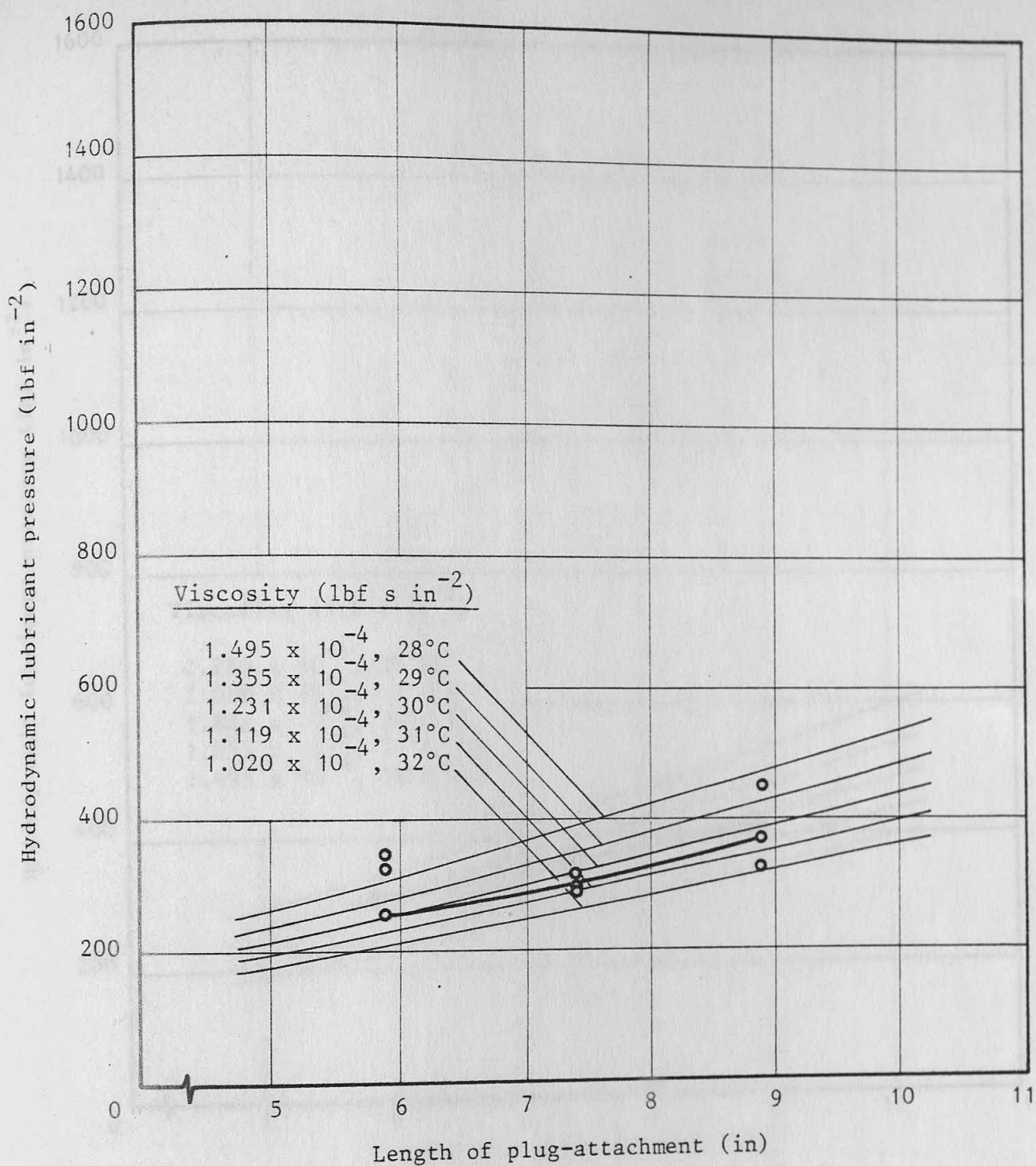
 Experimental results
 Theoretical results

Figure (6.26) Comparison between experimental and theoretical results for different lengths of straight-parallel plug-attachments



Mean radial clearance = 0.006 in

Laboratory ambient temperature = 23°C

Viscosity of EP50 at 23°C = 2.508×10^{-4} lbf s in⁻²

Reduction in area = 30.6%


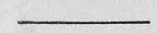
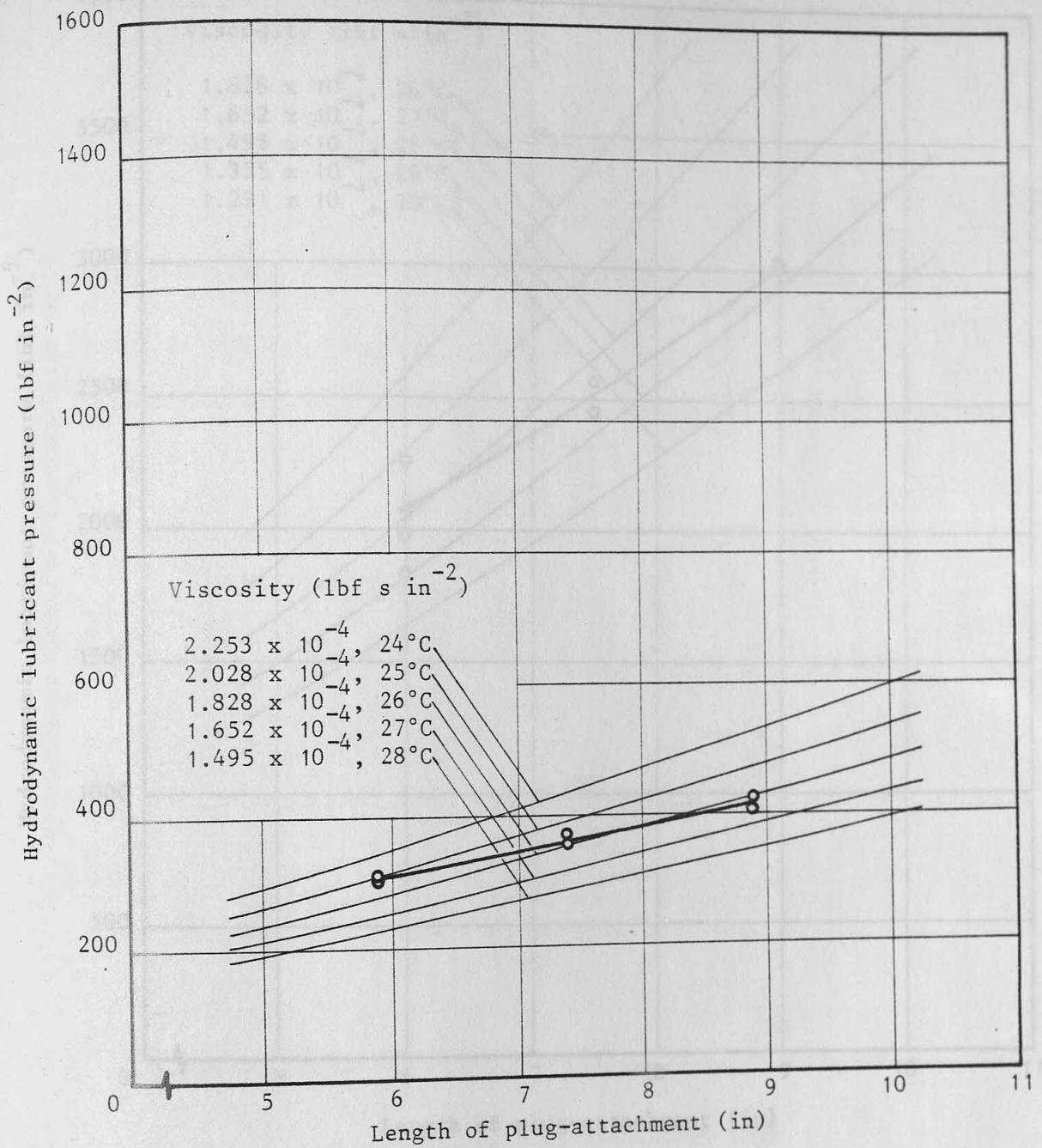
 Experimental results
 Theoretical results

Figure (6.27) Comparison between experimental and theoretical results for different lengths of straight-parallel plug-attachments



Mean radial clearance = 0.007 in

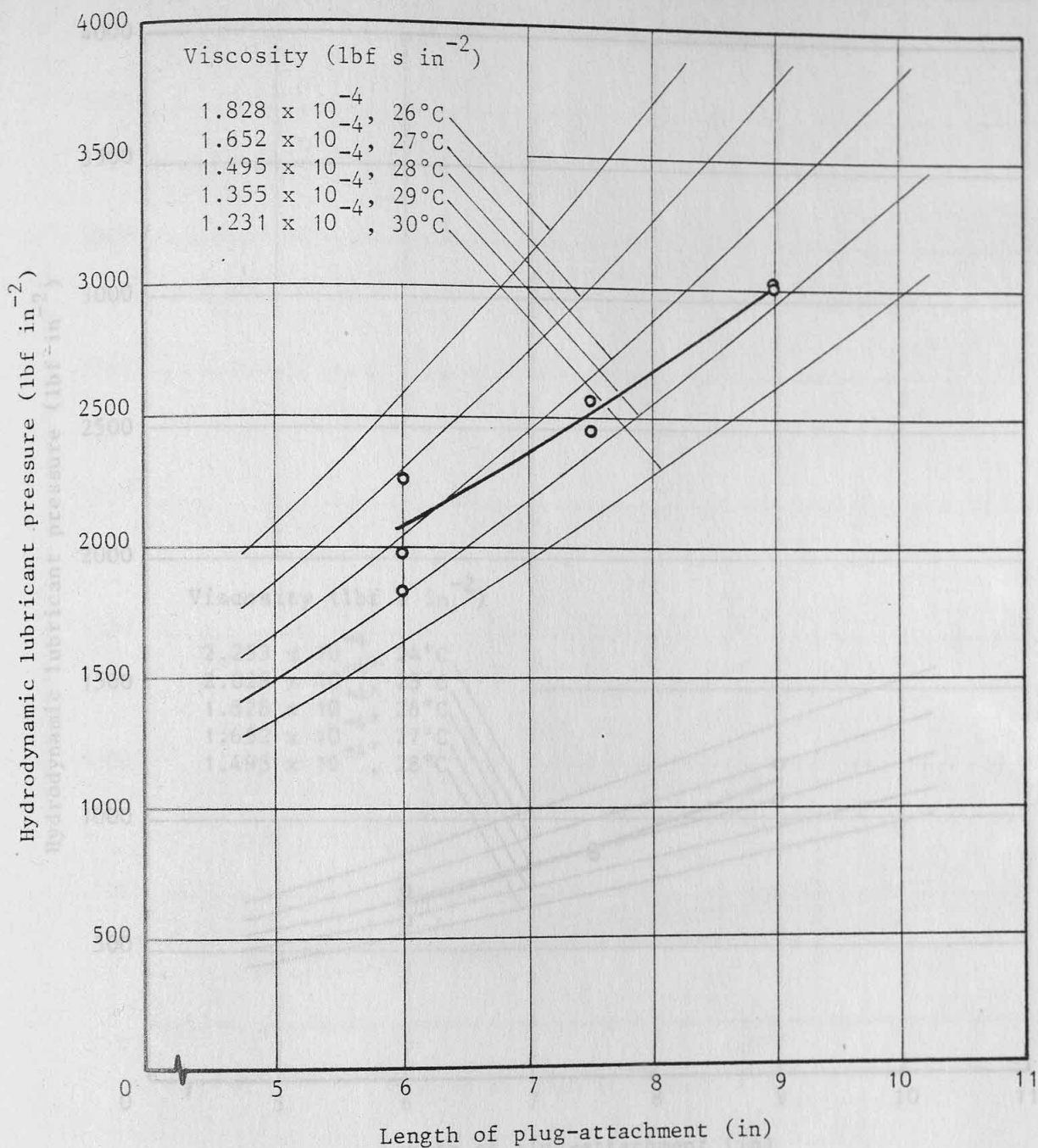
Laboratory ambient temperature = 19°C

Viscosity of EP50 at 19°C = 3.932×10^{-4} lbf s in⁻²

Reduction in area = 30.6%

—○— Experimental results
 — Theoretical results

Figure (6.28) Comparison between experimental and theoretical results for different lengths of straight-parallel plug-attachments



Mean radial clearance = 0.0025 in

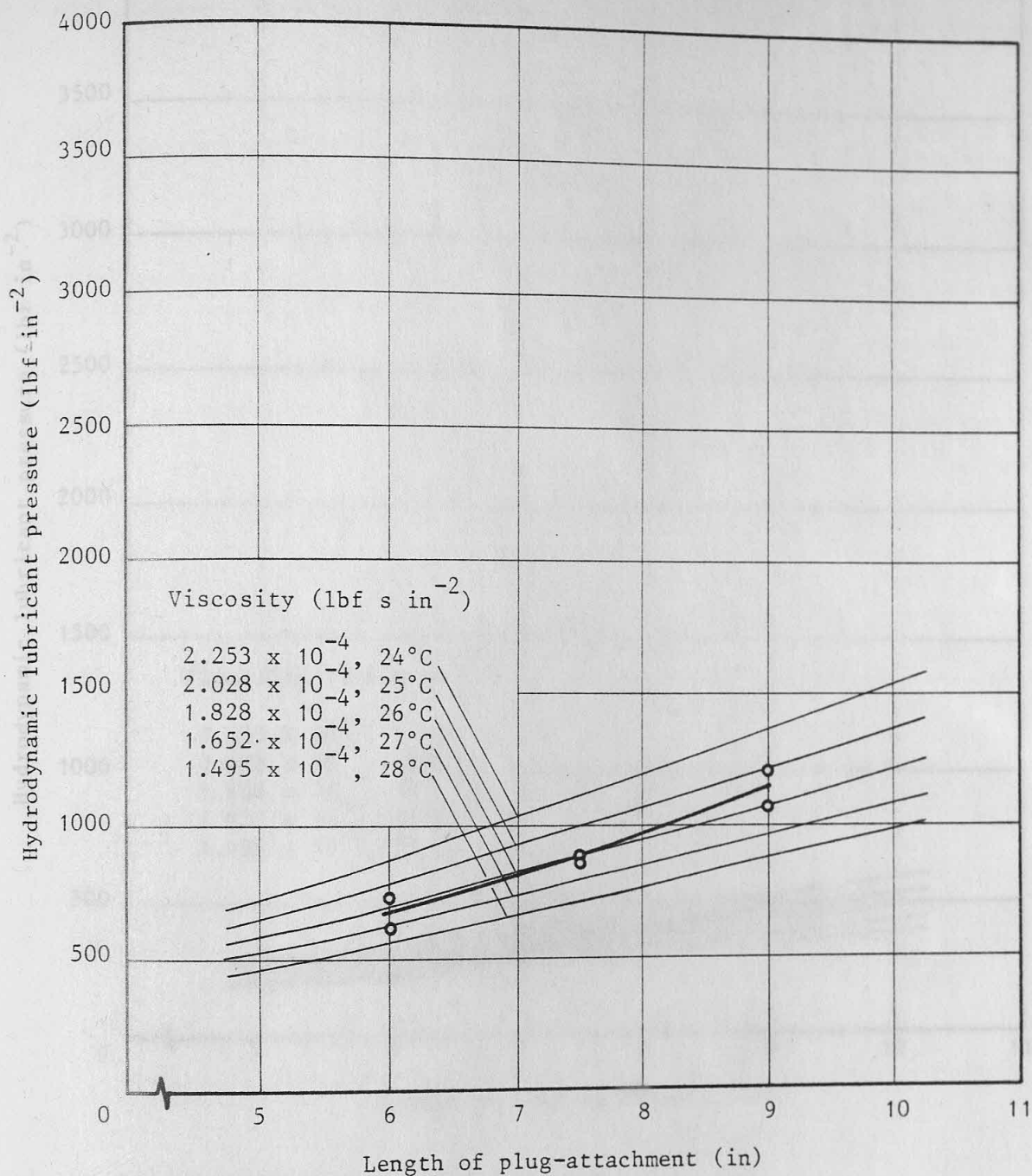
Laboratory ambient temperature = 20°C

Viscosity of EP50 at 20°C = 3.503×10^{-4} lbf s in⁻²

Reduction in area = 31.1%

○ — Experimental results
 — Theoretical results

Figure (6.29) Comparison between experimental and theoretical results for different lengths of straight-parallel plug-attachments



Mean radial clearance = 0.0045 in

Laboratory ambient temperature = 19°C

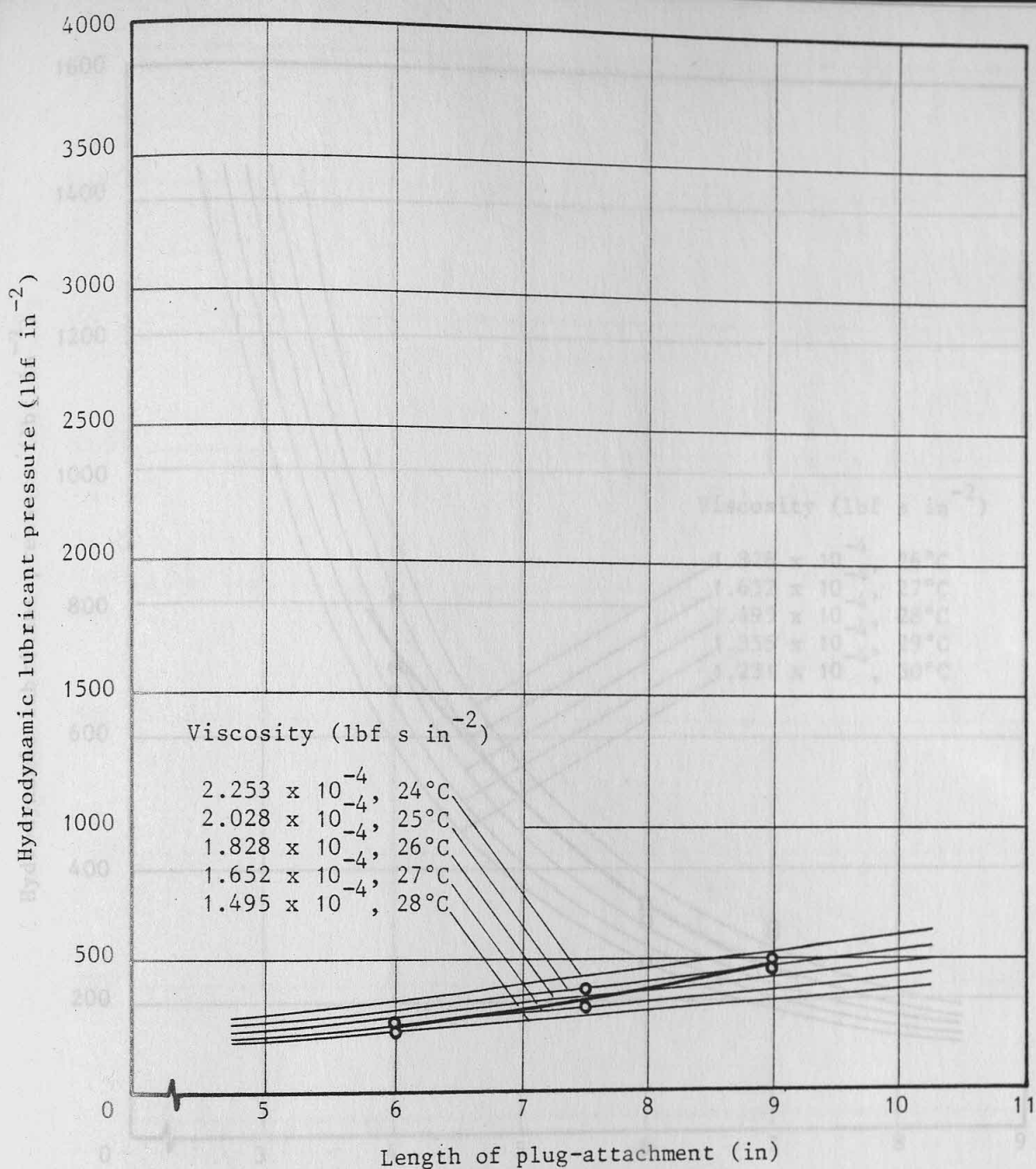
Viscosity of EP50 at 19°C = 3.932×10^{-4} lbf s in⁻²

Reduction in area = 31.1%

○—○ Experimental results

— Theoretical results

Figure (6.30) Comparison between experimental and theoretical results for different lengths of straight-parallel plug-attachments



Mean radial clearance = 0.007 in

Laboratory ambient temperature = 19°C

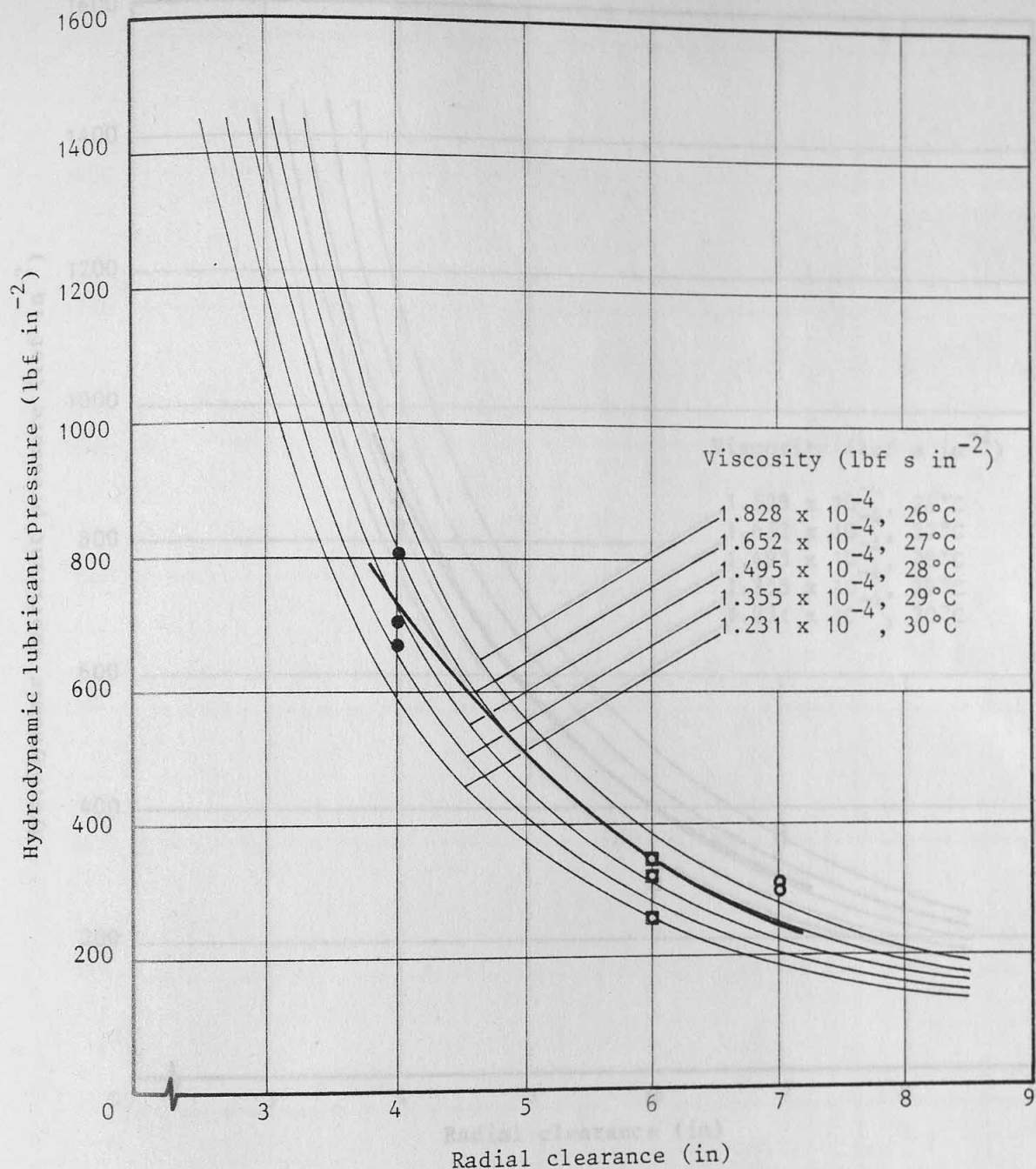
Viscosity of EP50 at 19°C = 3.932×10^{-4} lbf s in⁻²

Reduction in area = 31.1%

○—○ Experimental results
 — Theoretical results

Figure (6.31) Comparison between experimental and theoretical results for different lengths of straight-parallel plug-attachments

Figure (6.32) Comparison between experimental and theoretical results for different radial clearances



Length of plug-attachment = 5.9 in

Reduction in area = 30.6%

Laboratory ambient temperature

● 21°C

■ 23°C

○ 19°C

Viscosity of EP50 (lbf s in⁻²)

3.128×10^{-4}

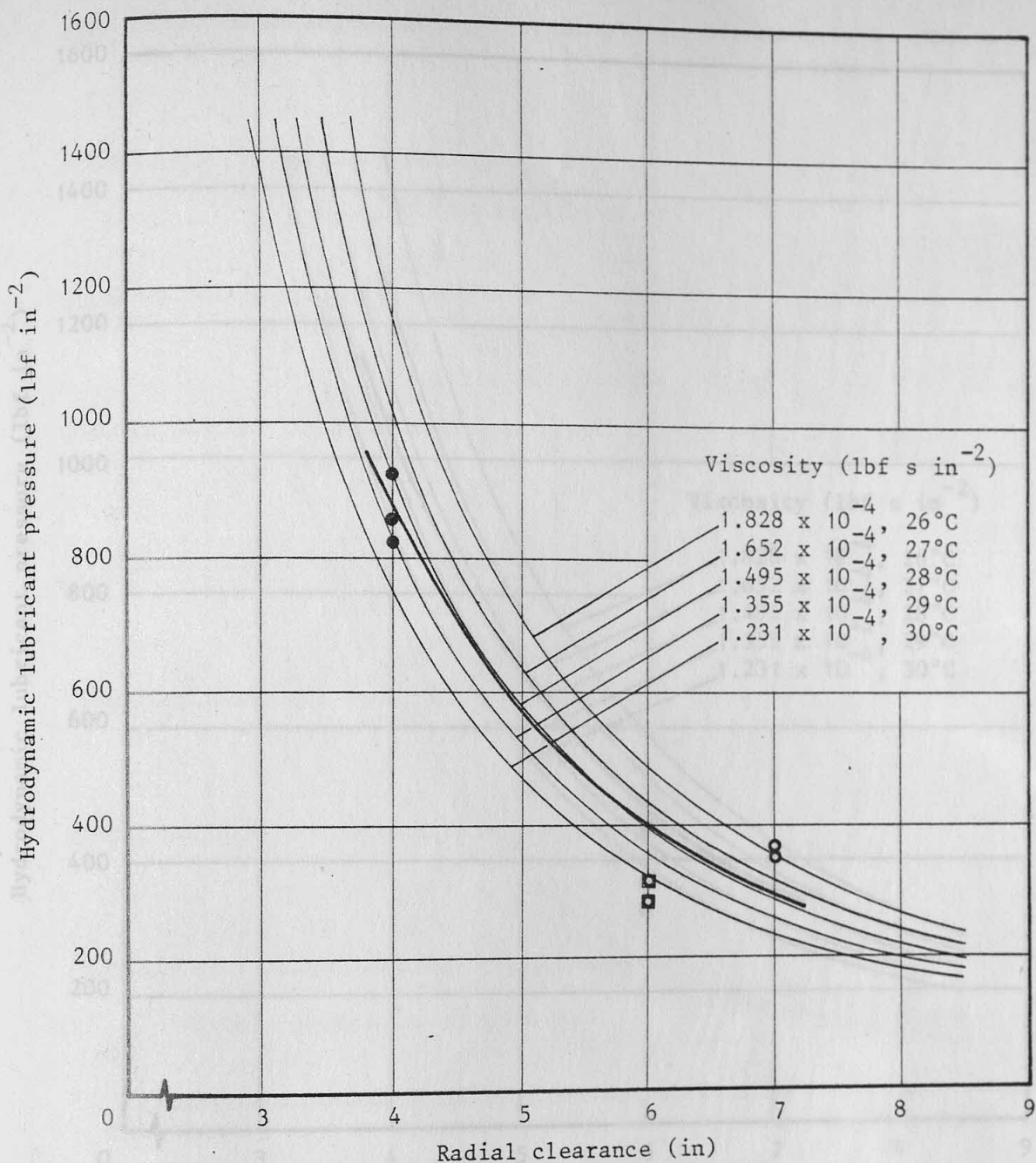
2.508×10^{-4}

3.932×10^{-4}

— Experimental results

— Theoretical results

Figure (6.32) Comparison between experimental and theoretical results for different radial clearances



Length of plug-attachment = 7.4 in

Reduction in area = 30.6%

Laboratory ambient temperature

Viscosity of EP50 (lbf s in⁻²)

● 21°C

3.128×10^{-4}

□ 23°C

2.508×10^{-4}

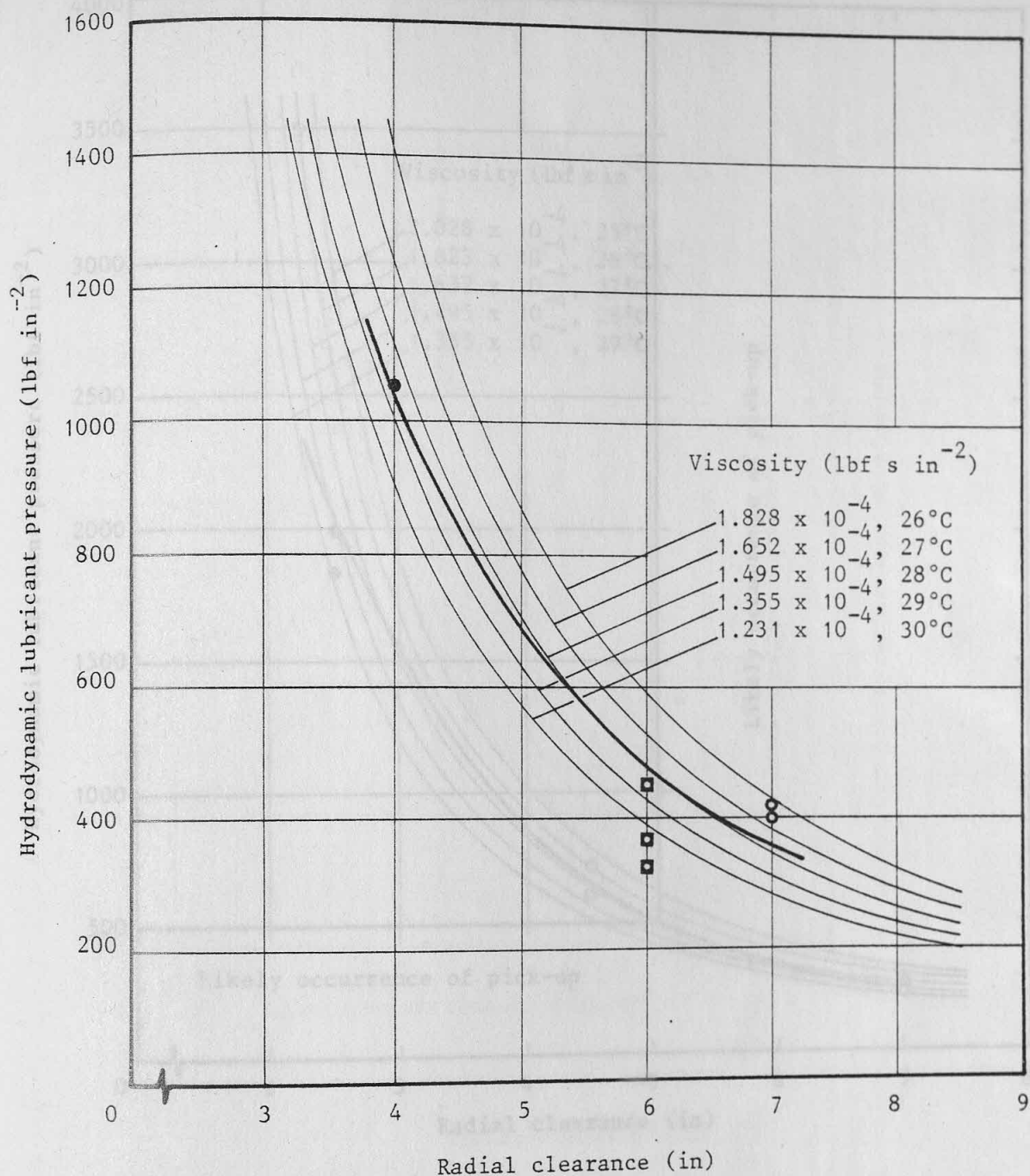
○ 19°C

3.932×10^{-4}

— Experimental results

— Theoretical results

Figure (6.33) Comparison between experimental and theoretical results for different radial clearances



Length of plug-attachment = 9 in

Reduction in area = 30.6%

Laboratory ambient temperature

Viscosity of EP50 (lbf s in⁻²)

● 21°C

3.128 x 10⁻⁴

■ 23°C

2.508 x 10⁻⁴

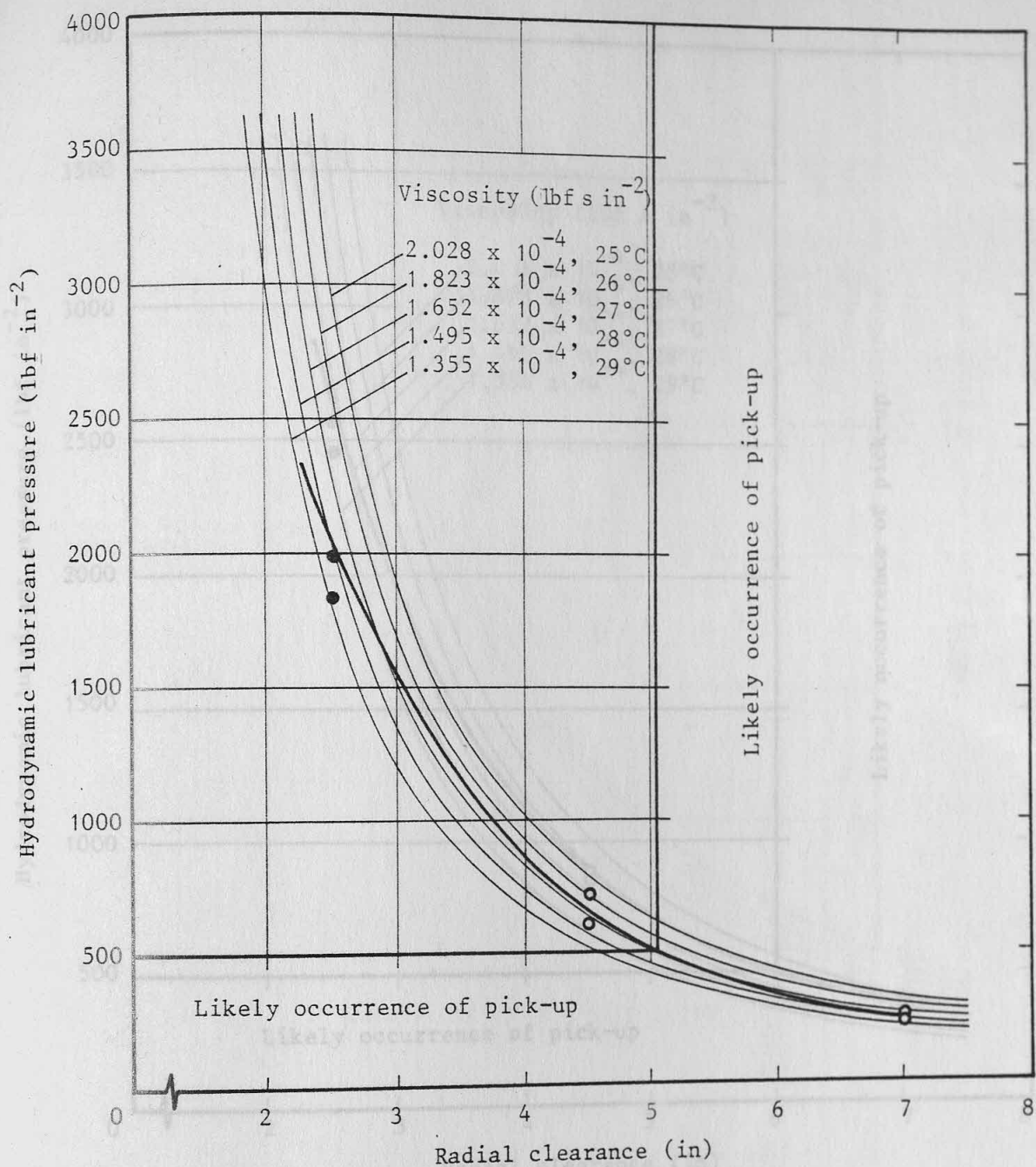
○ 19°C

3.932 x 10⁻⁴

— Experimental results

— Theoretical results

Figure (6.34) Comparison between experimental and theoretical results for different radial clearances



Length of plug-attachment = 6 in

Reduction in area = 31.1%

Laboratory ambient temperature

Viscosity of EP50 (lbf s in⁻²)

● 20°C

3.503×10^{-4}

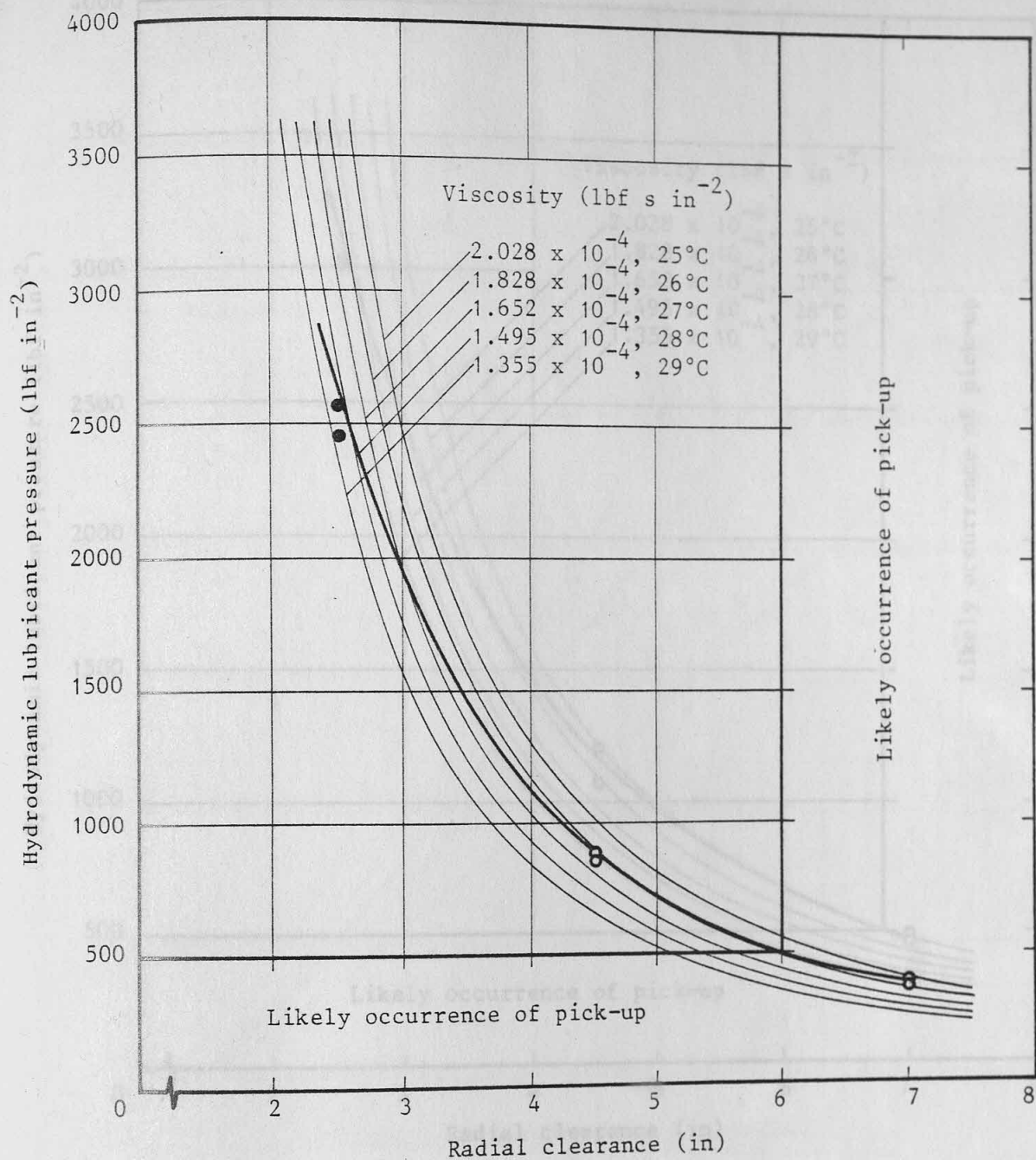
○ 19°C

3.932×10^{-4}

— Experimental results

— Theoretical results

Figure (6.35) Comparison between experimental and theoretical results for different radial clearances



Length of plug-attachment = 7.5 in

Reduction in area = 31.1%

Laboratory ambient temperature

Viscosity of EP50 (lbf s in⁻²)

● 20°C

3.503 x 10⁻⁴

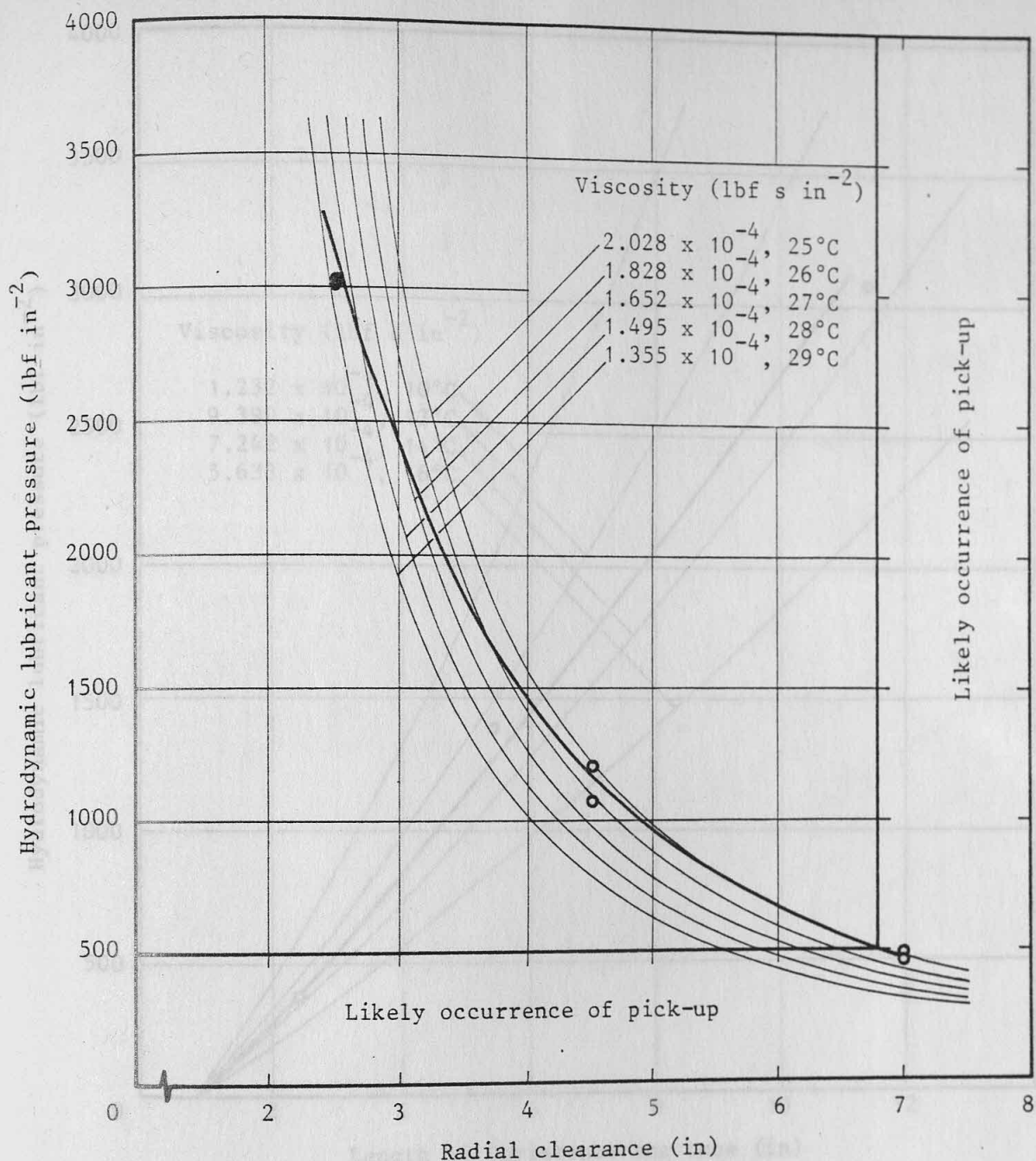
○ 19°C

3.932 x 10⁻⁴

— Experimental results

— Theoretical results

Figure (6.36) Comparison between experimental and theoretical results for different radial clearances



Length of plug-attachment = 9 in

Reduction in area = 31.1%

Laboratory ambient temperature

Viscosity of EP50 (lbf s in⁻²)

● 20°C

3.503×10^{-4}

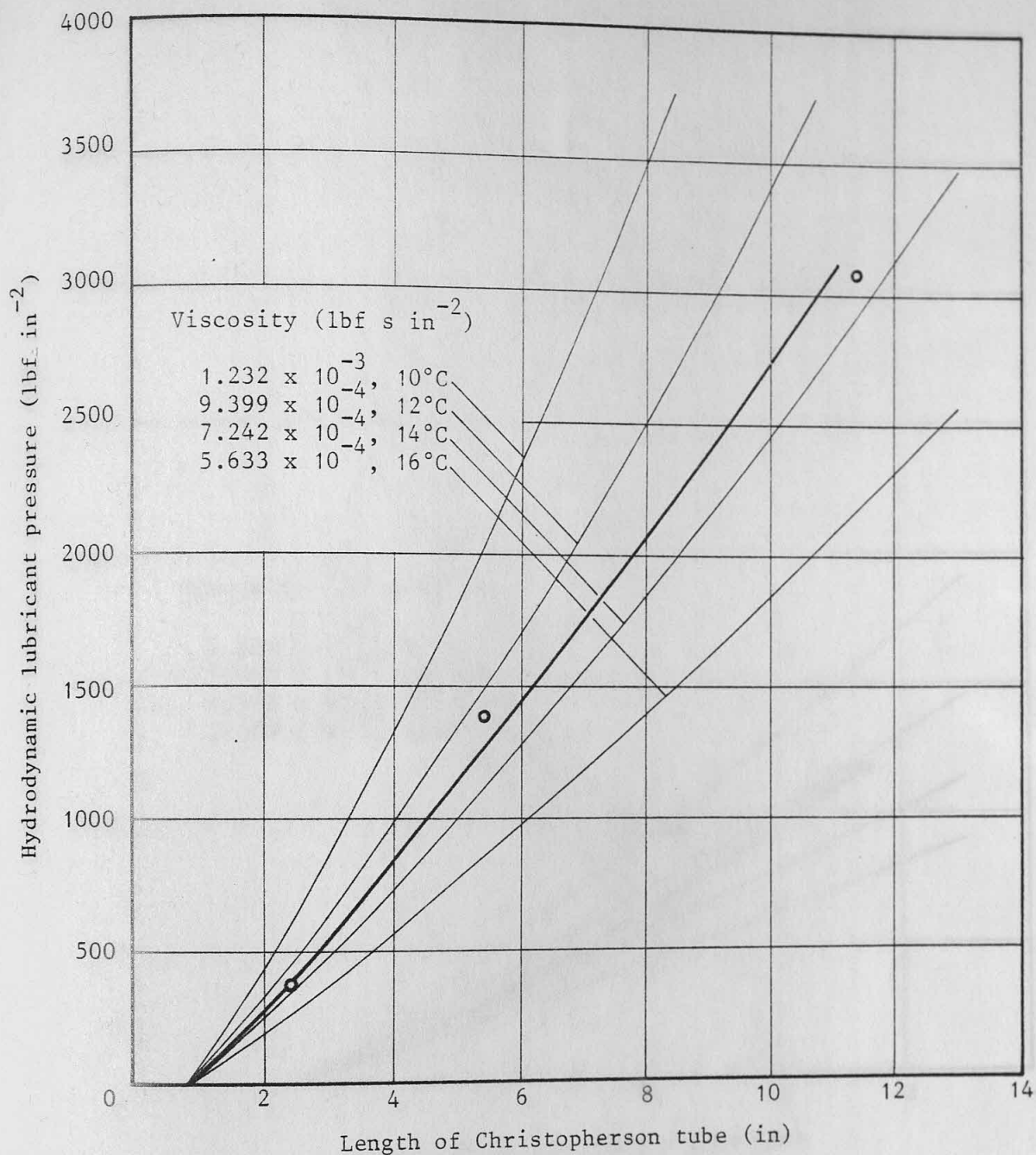
○ 19°C

3.932×10^{-4}

— Experimental results

— Theoretical results

Figure (6.37) Comparison between experimental and theoretical results for different radial clearances



Mean radial clearance = 0.006 in

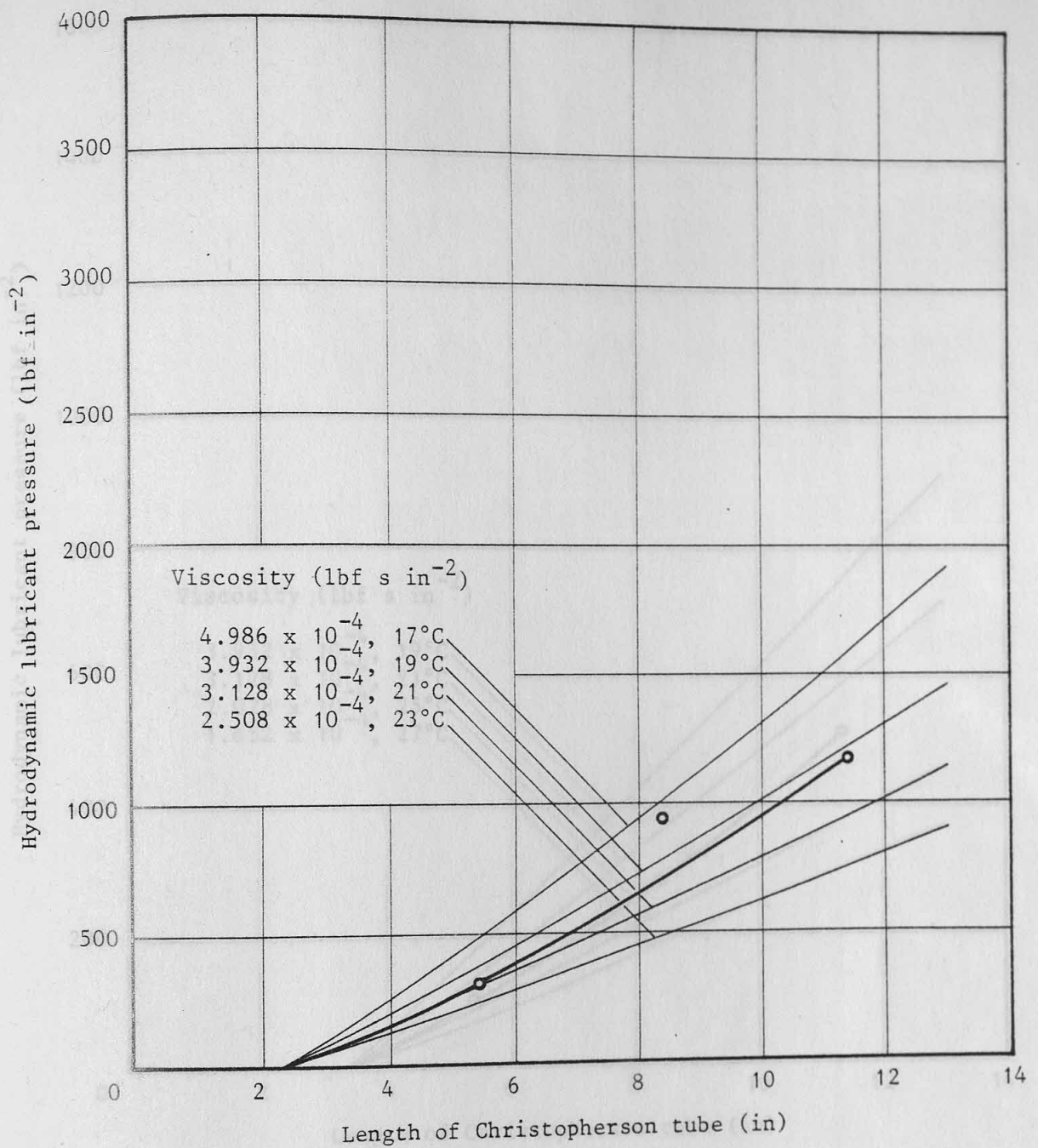
Laboratory ambient temperature = 12°C

Viscosity of EP50 at 12°C = 9.399×10^{-4} lbf s in⁻²

Reduction in area = 36.3%

○—○ Experimental results
 — Theoretical results

Figure (6.38) Comparison between experimental and theoretical lubricant pressures for different lengths of Christopherson tubes at 0.91 in from the die



Mean radial clearance = 0.006 in

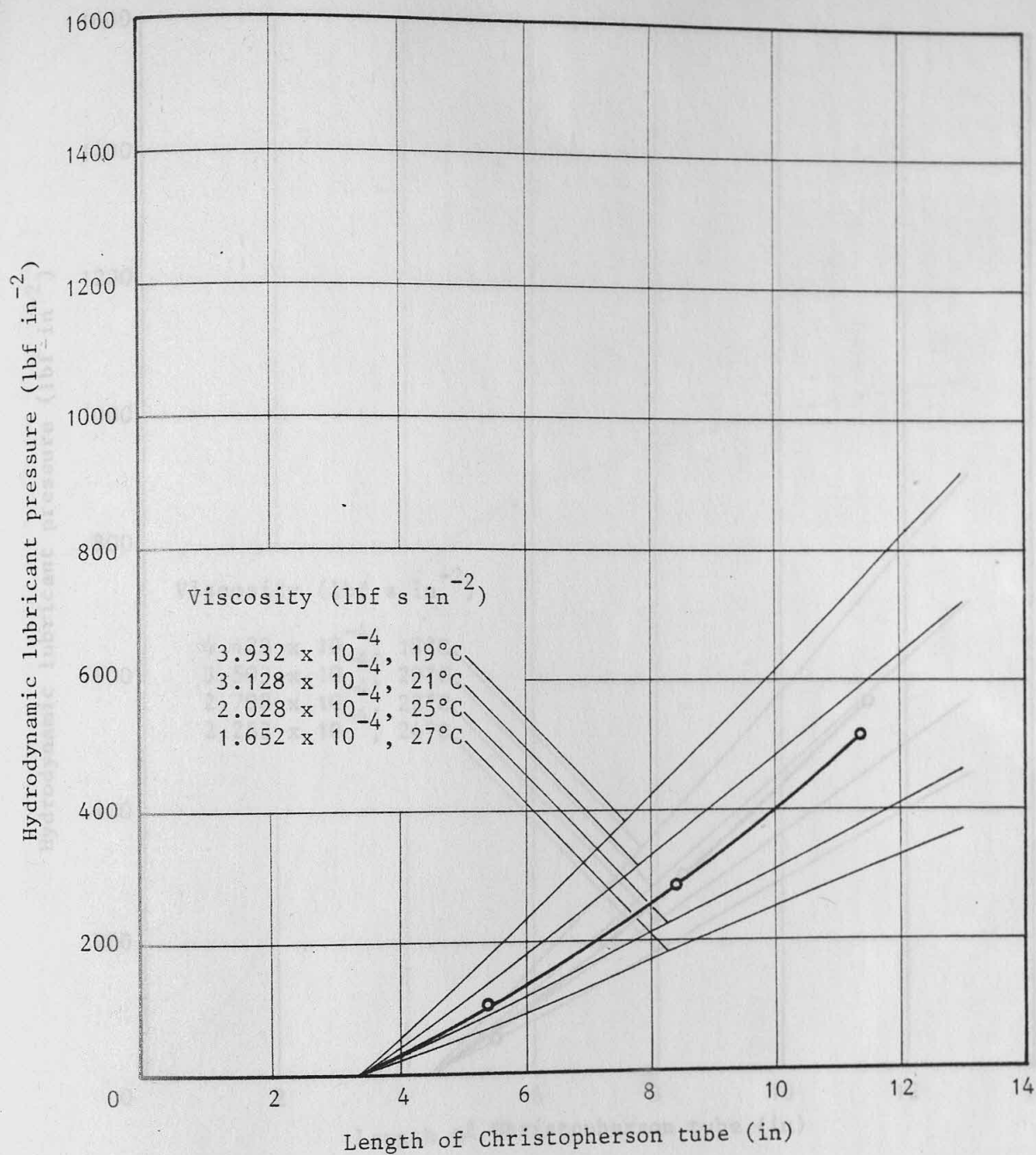
Laboratory ambient temperature = 17°C

Viscosity of EP50 at 17°C = 4.986×10^{-4} lbf s in⁻²

Reduction in area = 36.3%

—○— Experimental results
 — Theoretical results

Figure (6.39) Comparison between experimental and theoretical lubricant pressures for different lengths of Christopherson tubes at 2.41 in from the die



Mean radial clearance = 0.007 in

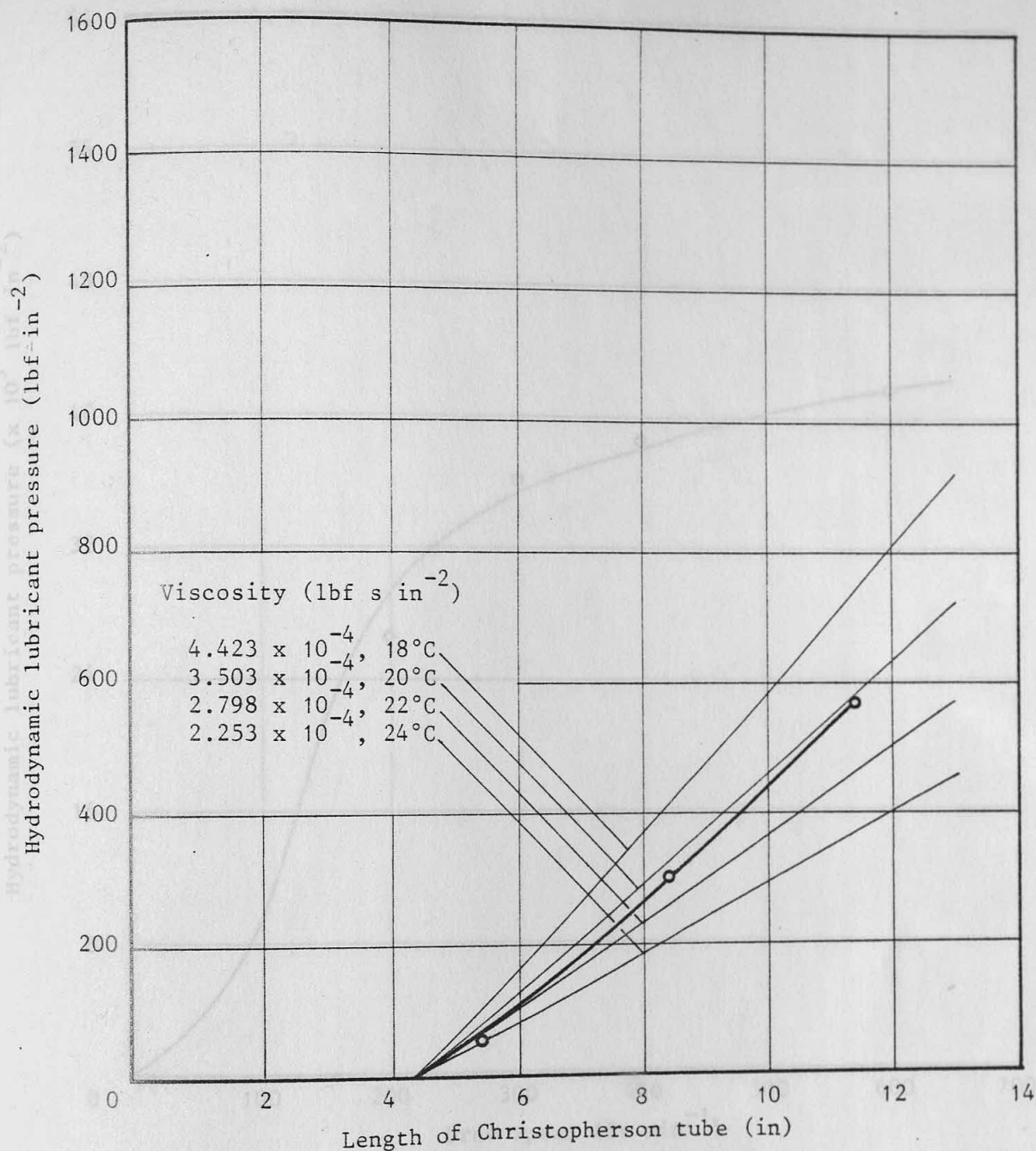
Laboratory ambient temperature = 21°C

Viscosity of EP50 at 21°C = 3.128 x 10⁻⁴ lbf s in⁻²

Reduction in area = 37.7%

—○— Experimental results
 — Theoretical results

Figure (6.40) Comparison between experimental and theoretical lubricant pressures for different lengths of Christopherson tubes at 3.41 in from the die



Radial clearance = 0.0015 in

Mean radial clearance = 0.007 in

Laboratory ambient temperature = 20°C

Viscosity of EP50 at 20°C = 3.503×10^{-4} lbf s in⁻²

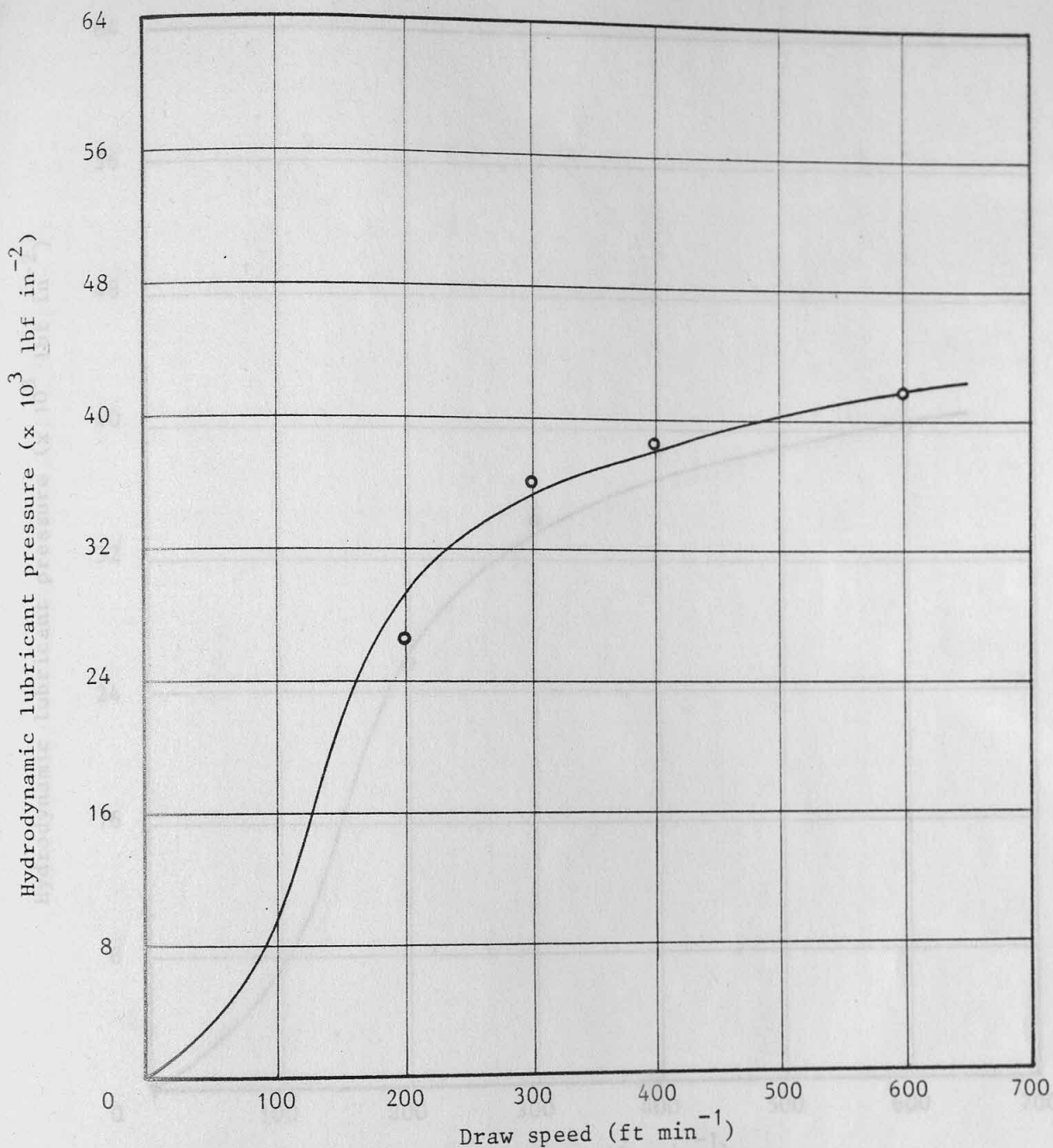
Reduction in area = 37.7%

—○— Experimental results

— Theoretical results

— Theoretical results by present theory

Figure (6.41) Comparison between experimental and theoretical lubricant pressures for different lengths of Christopherson tubes at 4.41 in from the die



Radial clearance = 0.0015 in

Length of Christopherson tube = 1.97 in (5 cm)

Initial wire diameter = 0.032 in

Final wire diameter = 0.030 in

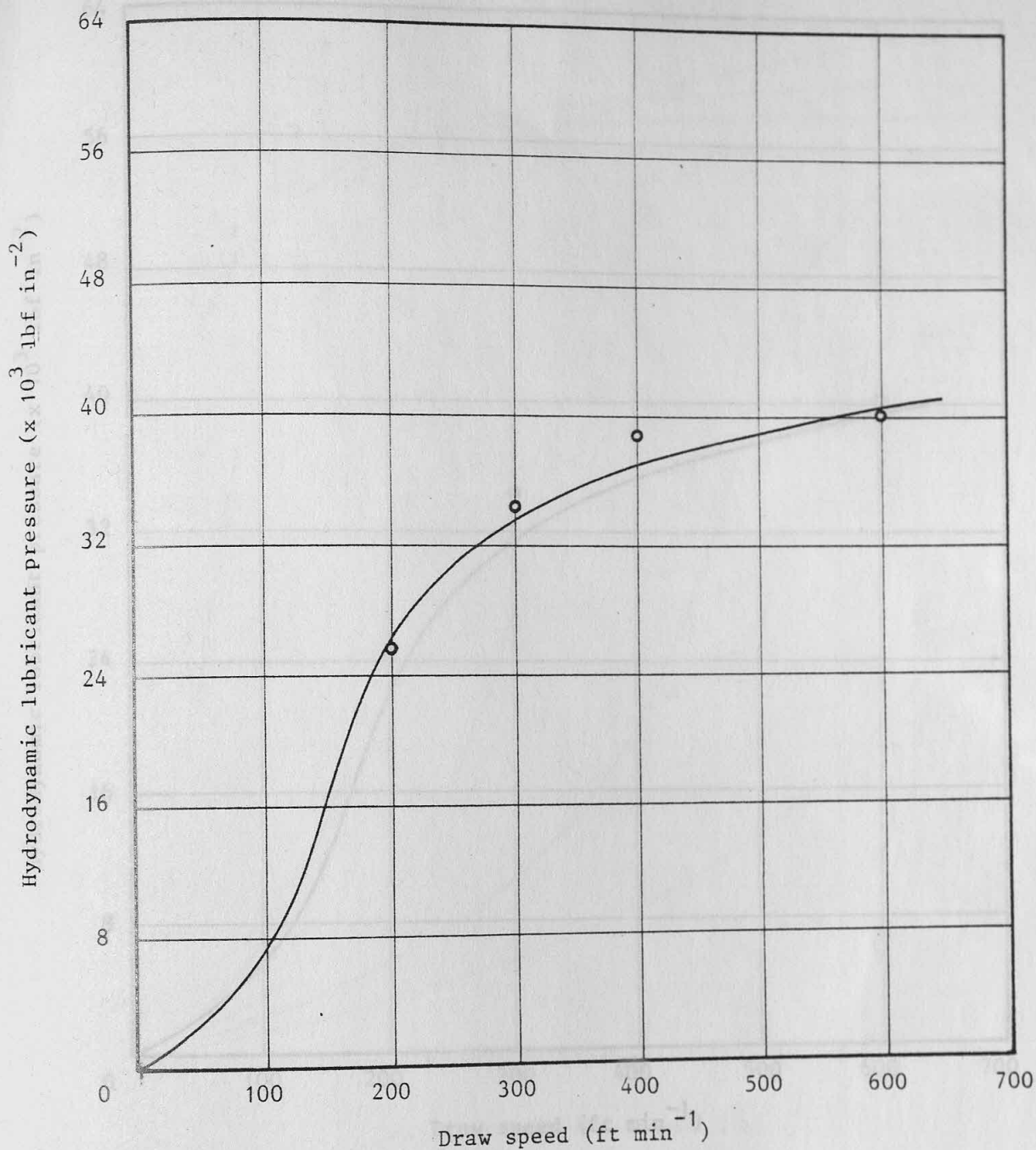
Reduction in area = 12.1%

Material = mild steel

○ Experimental results (after Christopherson et al^[5])

— Theoretical results by present theory

Figure (6.42) Comparison between theoretical results predicted by present theory with Christopherson et al's⁽⁵⁾ experimental results in wire-drawing



Radial clearance = 0.0015 in

Length of Christopherson tube = 1.97 (5 cm)

Initial wire diameter = 0.032 in

Final wire diameter = 0.028 in

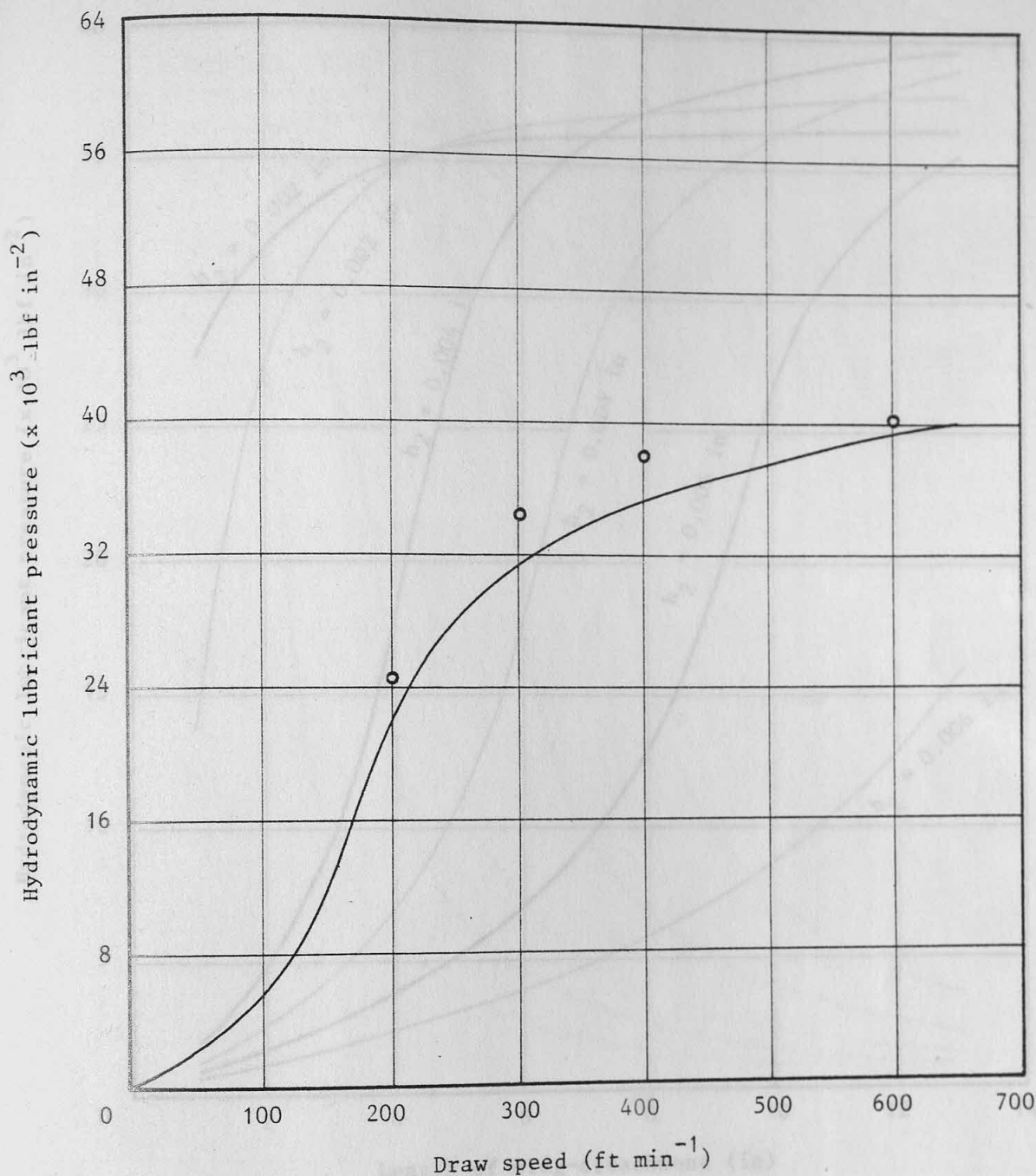
Reduction in area = 23.4%

Material = mild steel

○ Experimental results (after Christopherson et al^[5])

— Theoretical results by present theory

Figure (6.43) Comparison between theoretical results predicted by present theory with Christopherson et al's⁽⁵⁾ experimental results in wire-drawing



Radial clearance = 0.0015 in

Length of Christopherson tube = 1.97 in (5 cm)

Initial wire diameter = 0.012 in

Final wire diameter = 0.026 in

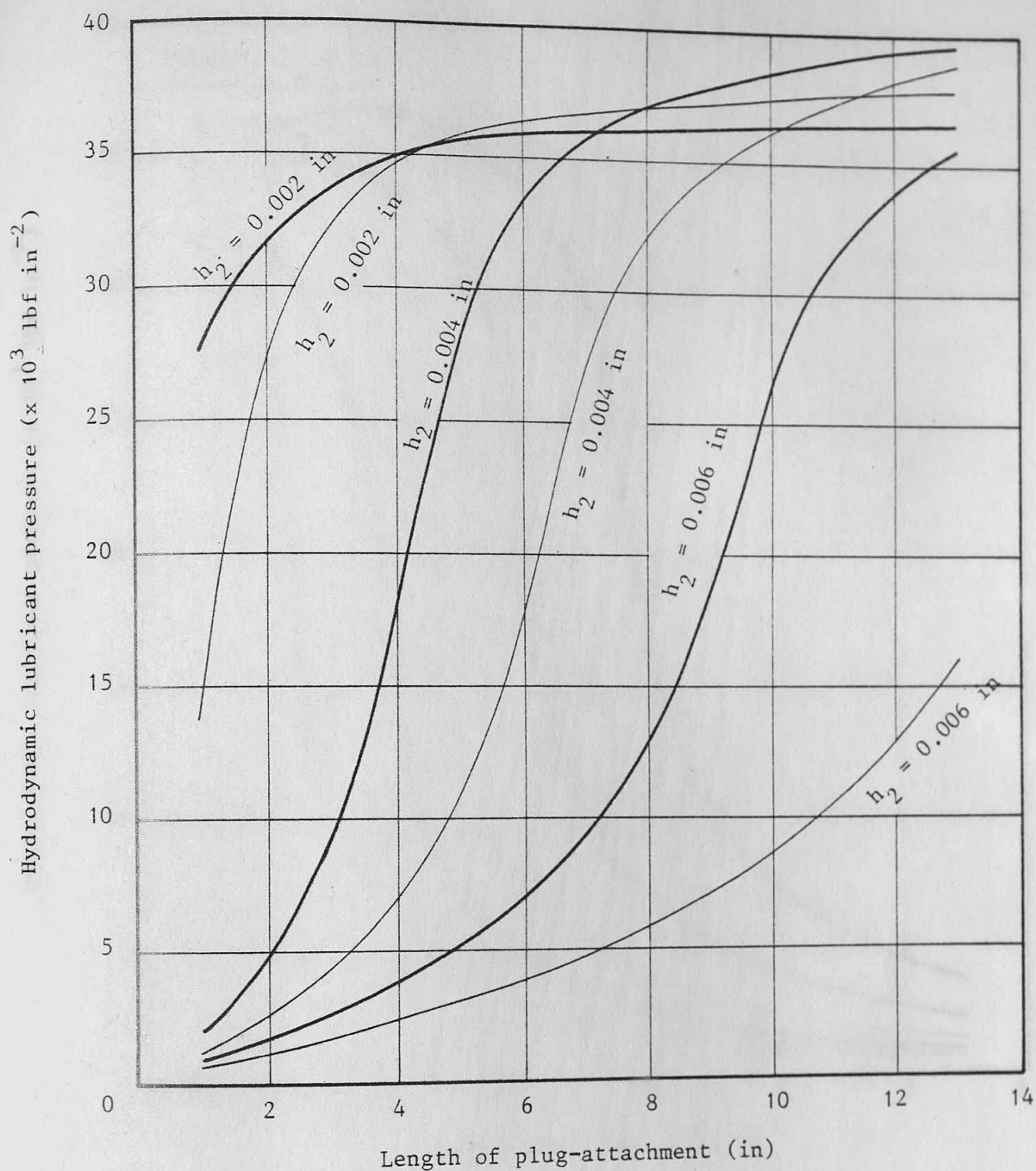
Reduction in area = 34%

Material = mild steel

• Experimental results (after Christopherson et al^[5])

— Theoretical results by present theory

Figure (6.44) Comparison between theoretical results predicted by present theory with Christopherson et al's (5) experimental results in wire-drawing



Draw speed = 100 ft min^{-1}

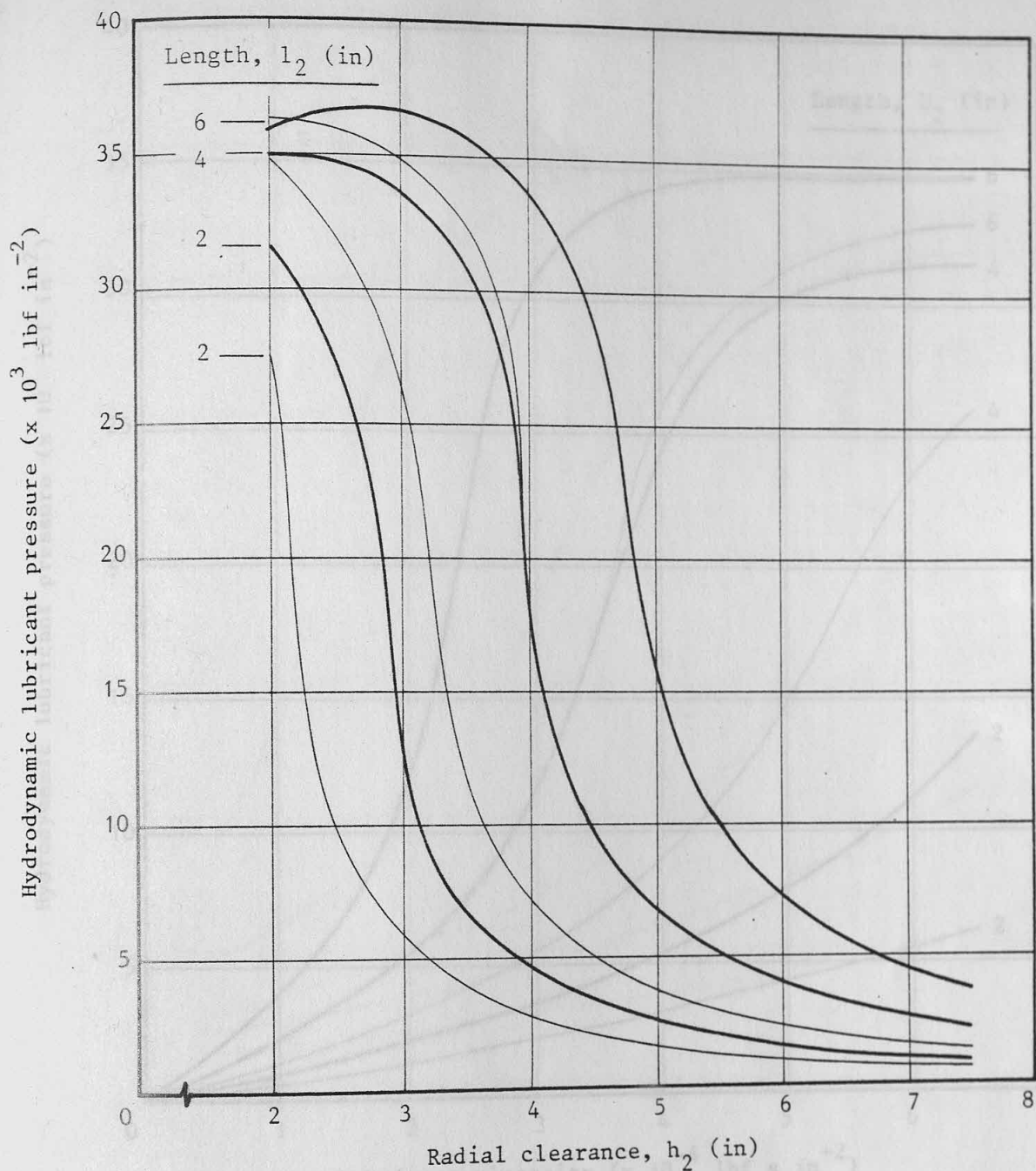
Lubricant viscosity = $3.503 \times 10^{-4} \text{ lbf s in}^{-2}$ (EP50 at 20°C)

Radial clearance ratio, $h_1/h_2 = 1.5$

— Straight-parallel

— Straight-tapered

Figure (6.45) Variation of theoretical hydrodynamic lubricant pressure with length for straight-parallel and straight-tapered plug attachments of different radial clearances



Draw speed = 100 ft min^{-1}

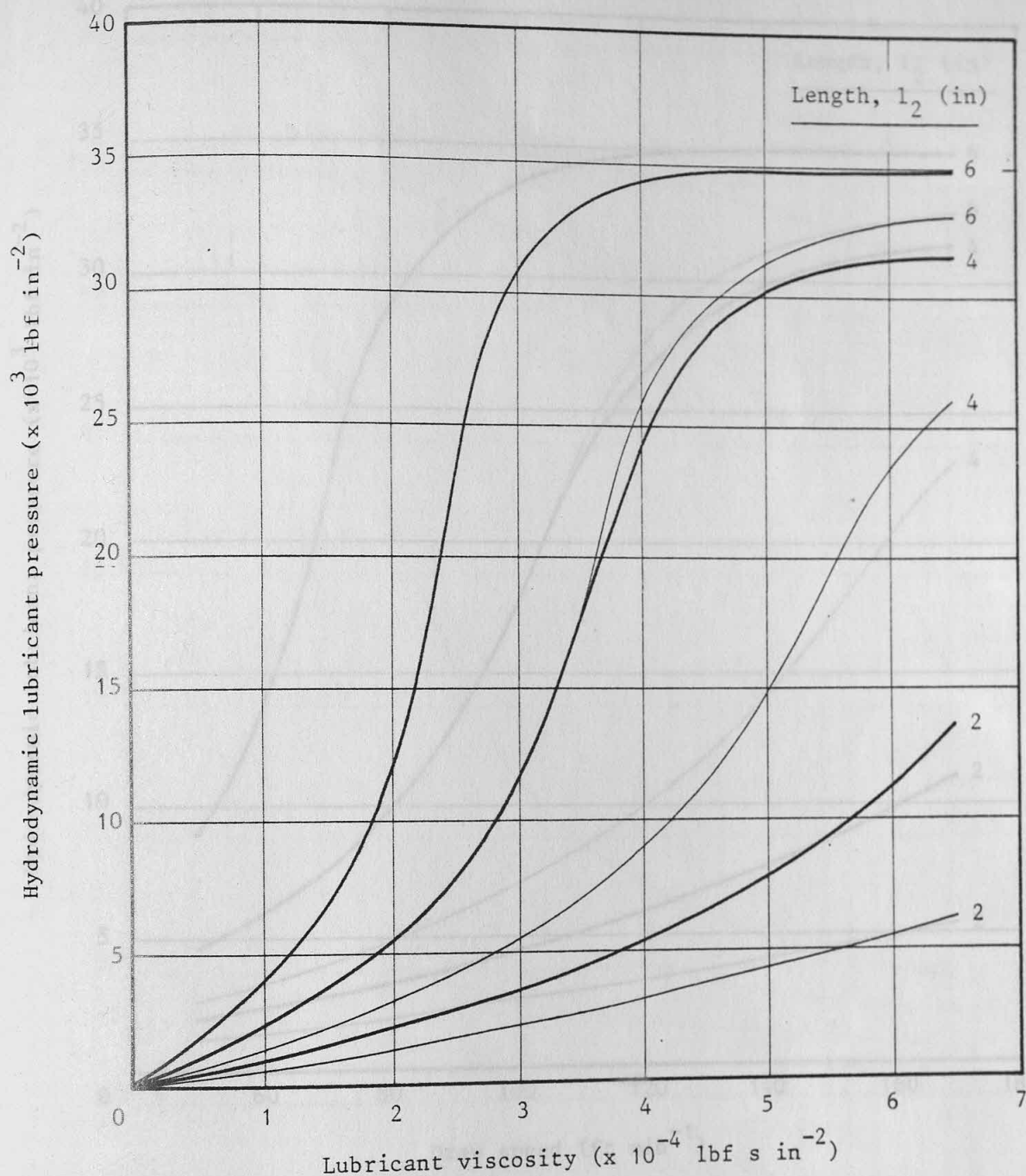
Lubricant viscosity = $3.503 \times 10^{-4} \text{ lbf s in}^{-2}$ (EP50 at 20°C)

Radial clearance ratio, $h_1/h_2 = 1.5$

— Straight-parallel

— Straight-tapered

Figure (6.46) Variation of theoretical hydrodynamic lubricant pressure with radial clearance for straight-parallel and straight-tapered plug-attachments of different lengths



Draw speed = 100 ft min⁻¹

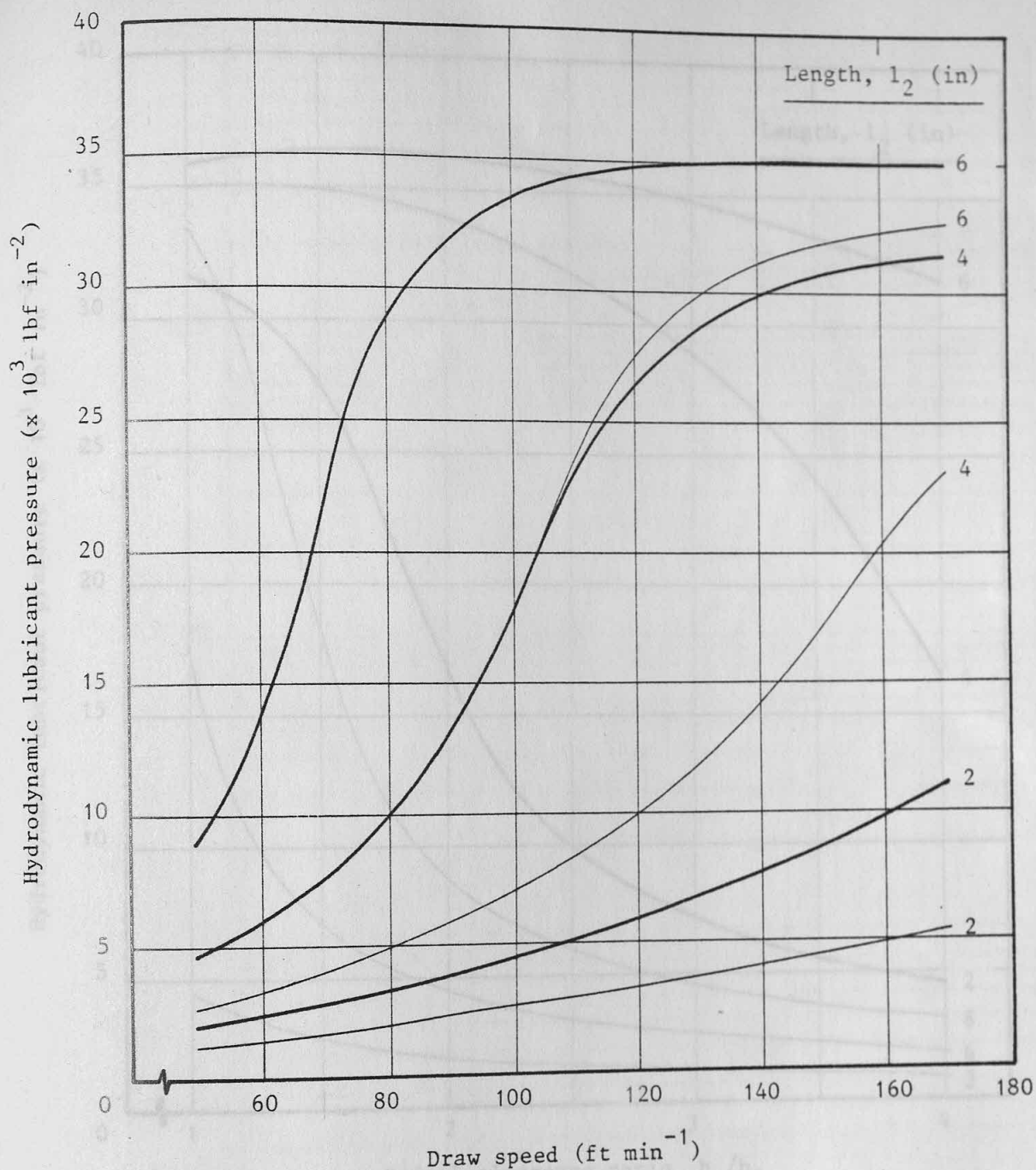
Radial clearance, $h_2 = 0.004$ in

Radial clearance ratio, $h_1/h_2 = 1.5$

— Straight-parallel

- - - Straight-tapered

Figure (6.47) Variation of theoretical hydrodynamic lubricant pressure with lubricant viscosity for straight-parallel and straight-tapered plug-attachments of different lengths



Lubricant viscosity = $3.503 \times 10^{-4} \text{ lbf s in}^{-2}$ (EP50 at 20°C)

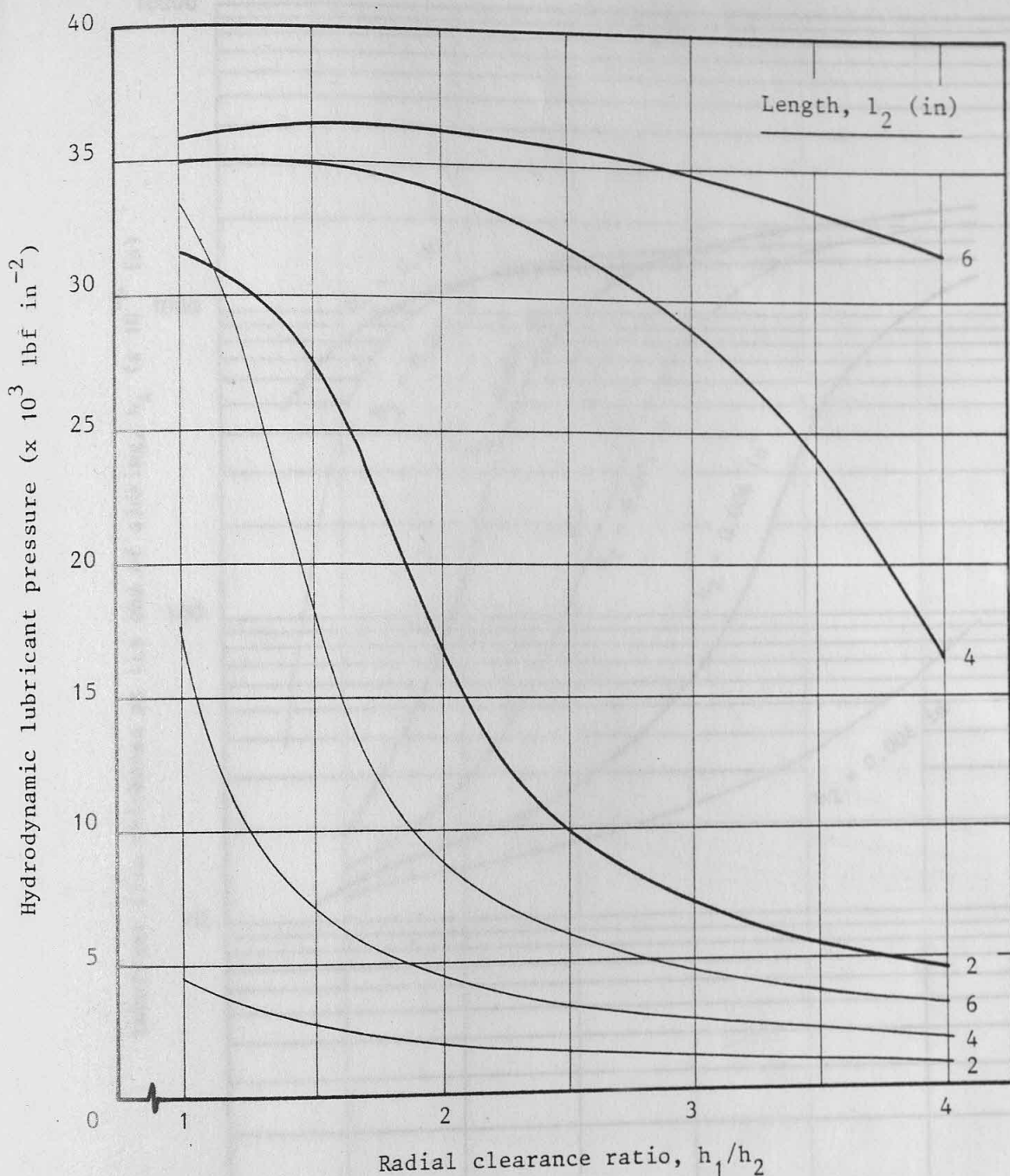
Radial clearance, $h_2 = 0.004 \text{ in}$

Radial clearance ratio, $h_1/h_2 = 1.5$

— Straight-parallel

- - - Straight-tapered

Figure (6.48) Variation of theoretical hydrodynamic lubricant pressure with draw speed for straight-parallel and straight-tapered plug-attachments of different lengths



* At $h_1/h_2 = 1.0$ the plug-attachment has a straight-parallel profile

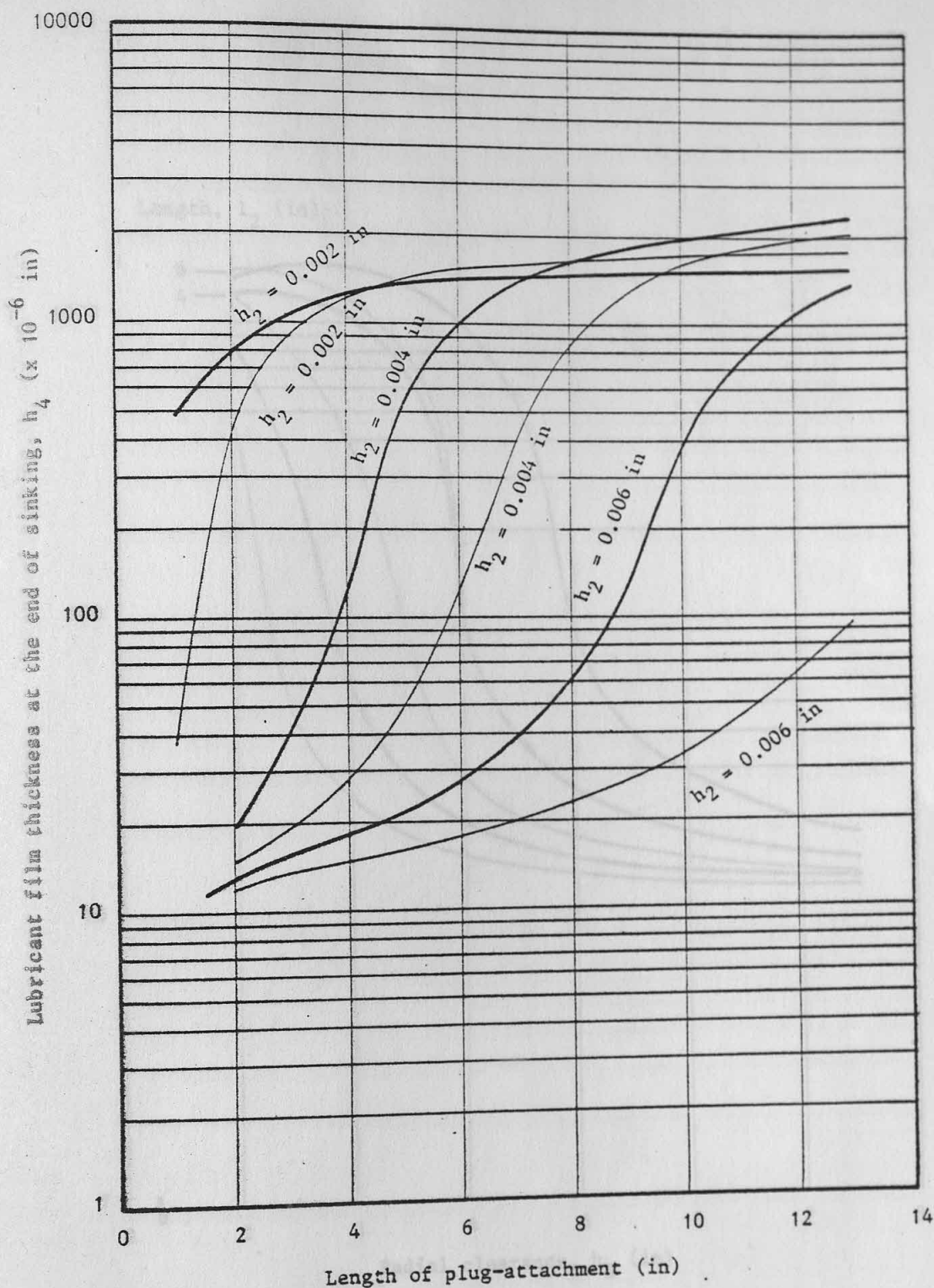
Draw speed = 100 ft min⁻¹

Lubricant viscosity = 3.503×10^{-4} lbf s in⁻² (EP50 at 20°C)

———— Radial clearance, $h_2 = 0.002$ in

———— Radial clearance, $h_2 = 0.004$ in

Figure (6.49) Variation of theoretical hydrodynamic lubricant pressure with radial clearance ratio for straight-parallel and straight-tapered plug-attachments of different lengths



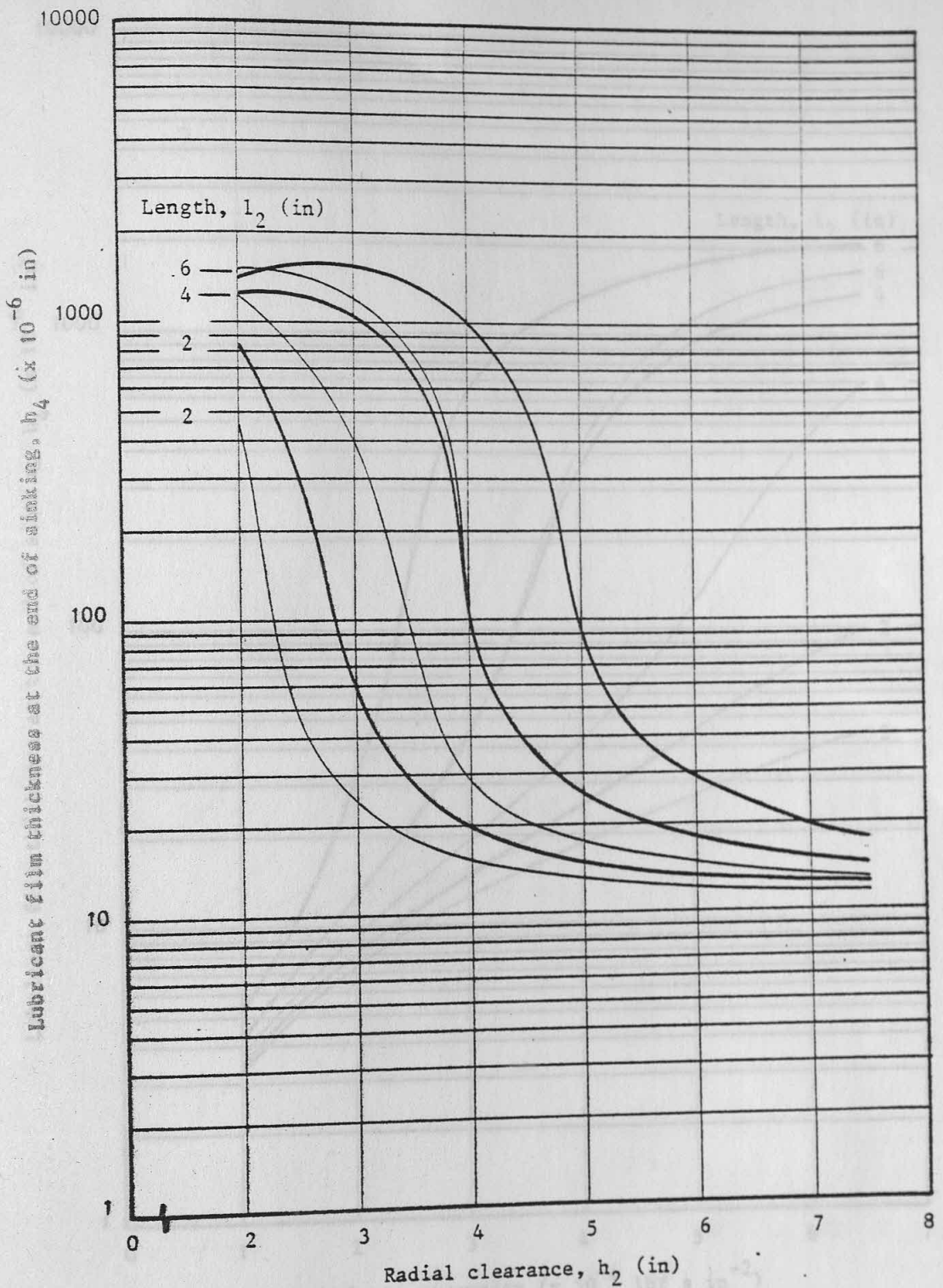
Draw speed = 100 ft min^{-1}

Lubricant viscosity = $3.503 \times 10^{-4} \text{ lbf s in}^{-2}$ (EP50 at 20°C)

Radial clearance ratio, $h_1/h_2 = 1.5$

————— Straight-parallel
 - - - Straight-tapered

Figure (6.50) Variation of theoretical lubricant film thickness at the end of sinking with length for straight-parallel and straight-tapered plug-attachments of different radial clearances



Draw speed = 100 ft min^{-1}

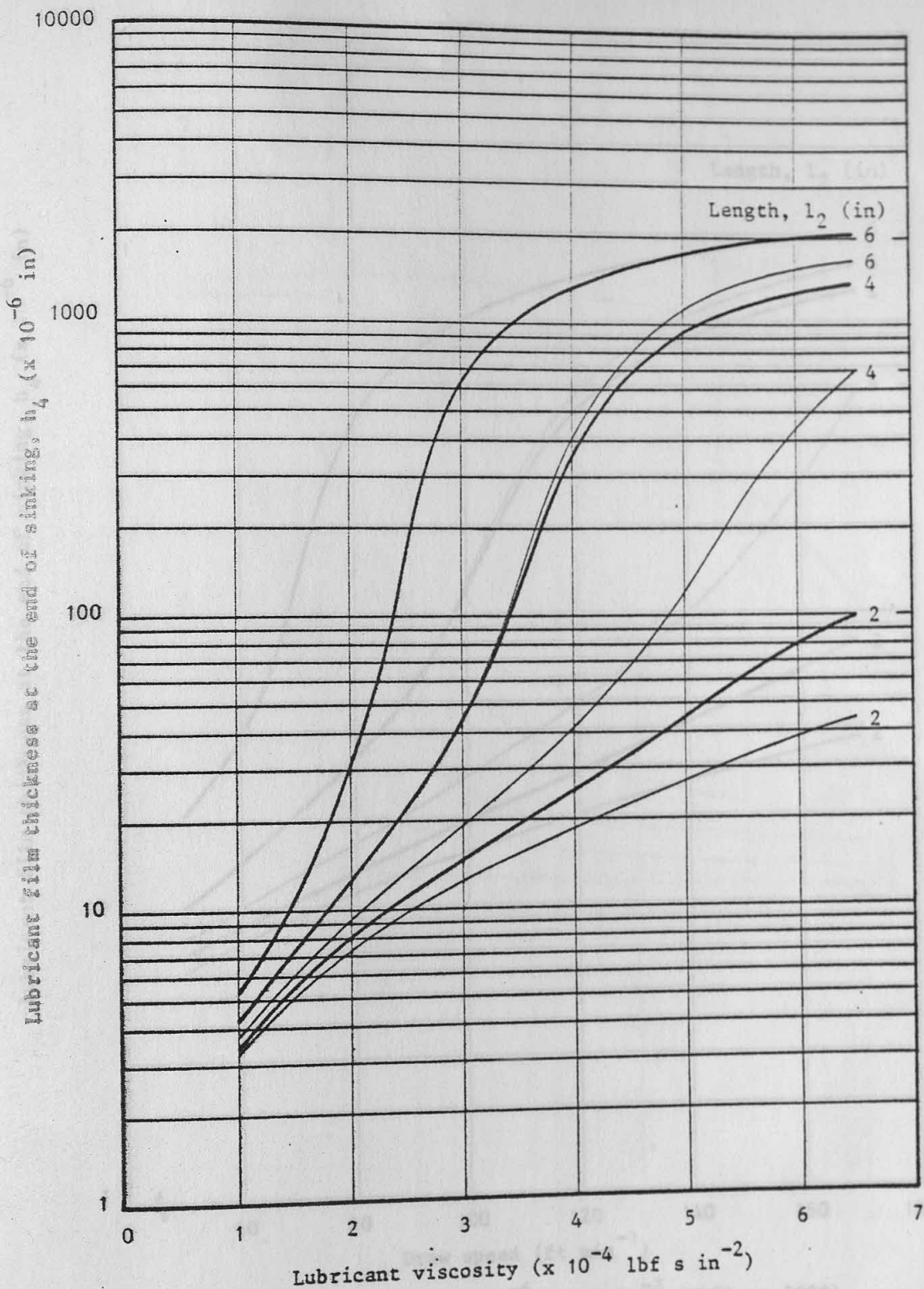
Lubricant viscosity = $3.503 \times 10^{-4} \text{ lbf s in}^{-2}$ (EP50 at 20°C)

Radial clearance ratio, $h_1/h_2 = 1.5$

— Straight-parallel

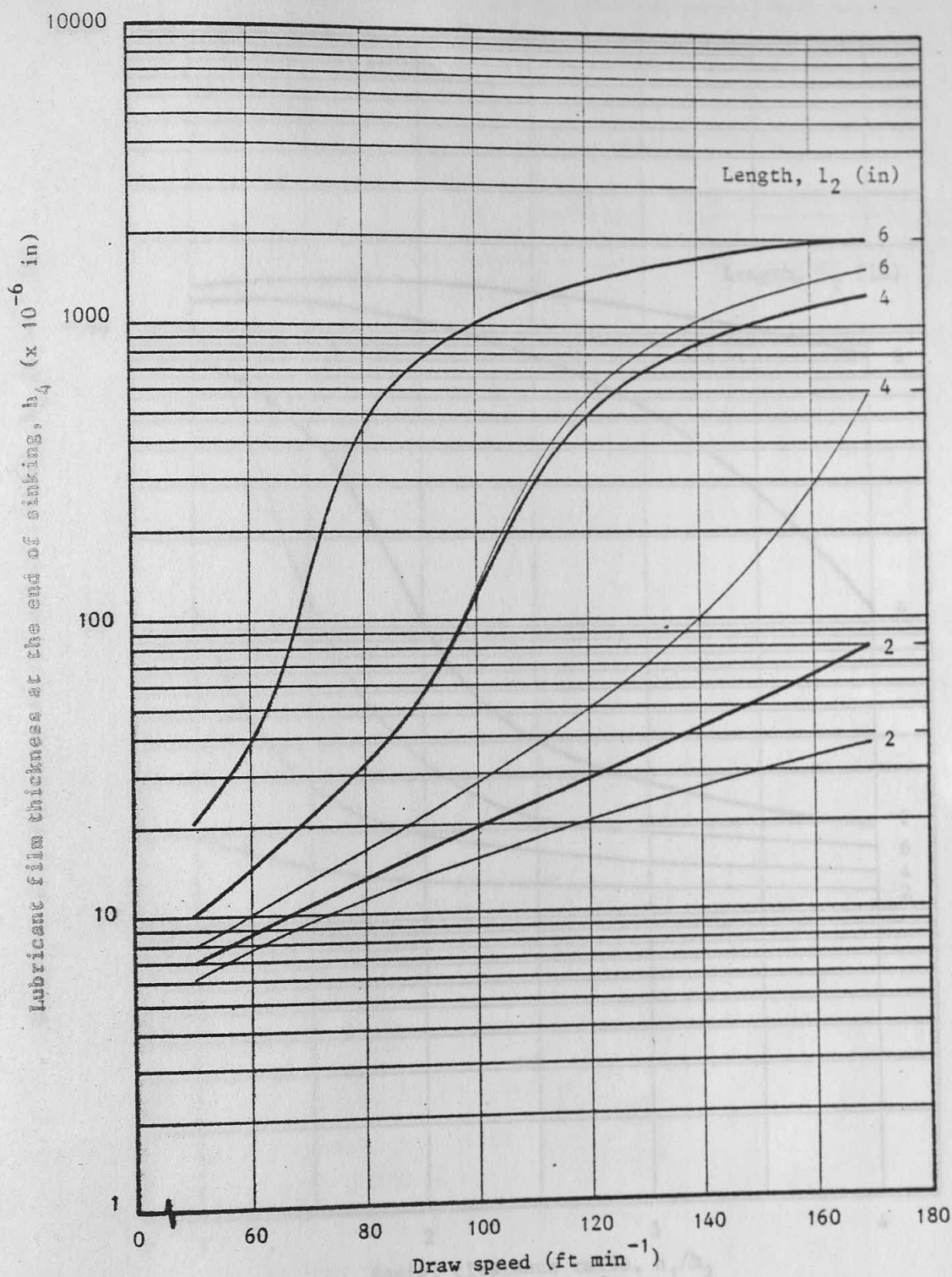
- - - Straight-tapered

Figure (6.51) Variation of theoretical lubricant film thickness at the end of sinking with radial clearance for straight-parallel and straight-tapered plug-attachments of different lengths



Draw speed = 100 ft min $^{-1}$
 Radial clearance, $h_2 = 0.004$ in
 Radial clearance ratio, $h_1/h_2 = 1.5$
 ——— Straight-parallel
 ——— Straight-tapered

Figure (6.52) Variation of theoretical lubricant film thickness at the end of sinking with lubricant viscosity for straight-parallel and straight-tapered plug-attachments of different lengths



Lubricant viscosity = 3.503×10^{-4} lbf s in $^{-2}$ (EP50 at 20°C)

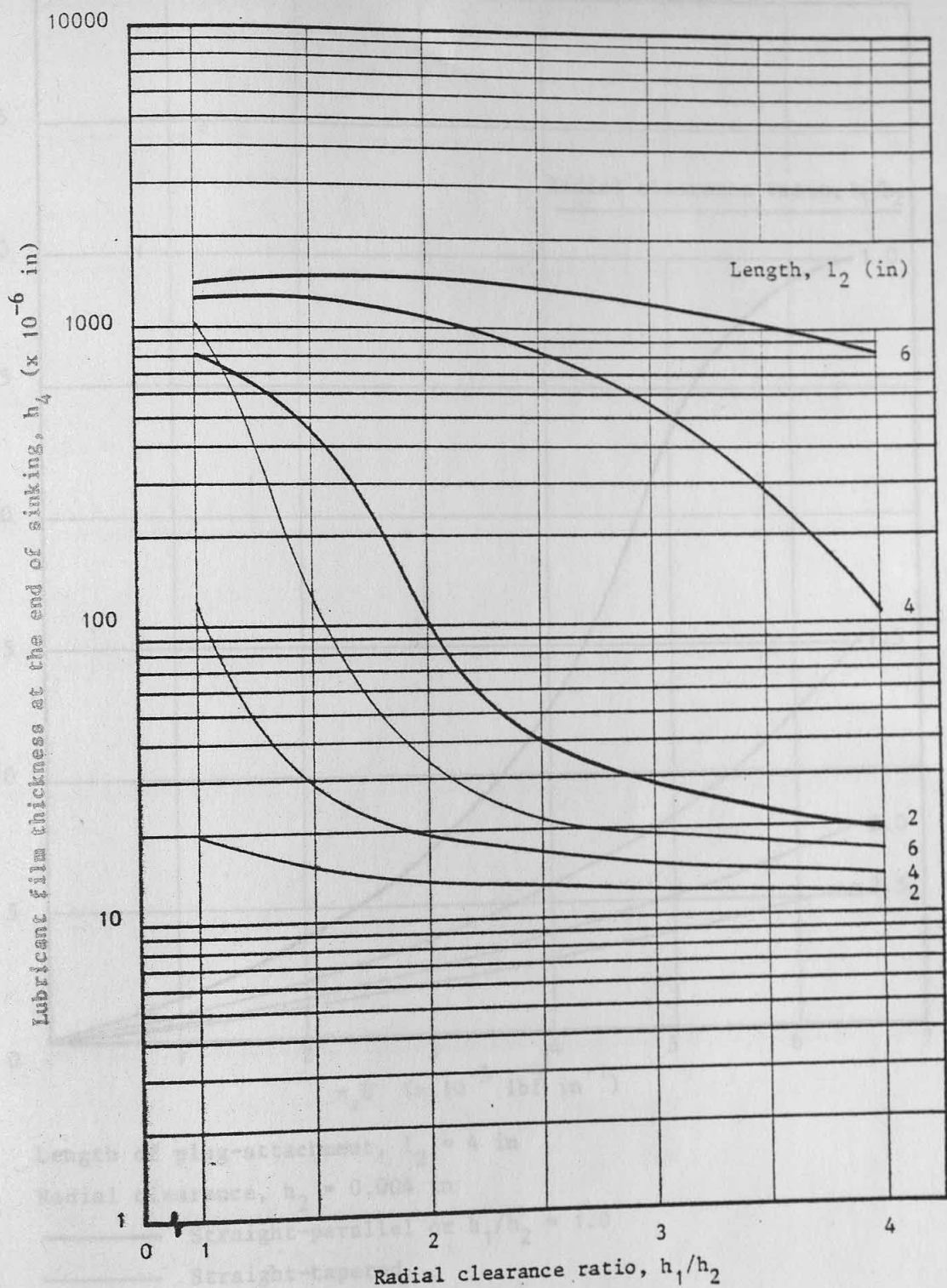
Radial clearance, $h_2 = 0.004$ in

Radial clearance ratio, $h_1/h_2 = 1.5$

— Straight-parallel

- - - Straight-tapered

Figure (6.53) Variation of theoretical lubricant film thickness at the end of sinking with draw speed for straight-parallel and straight-tapered plug-attachments of different lengths



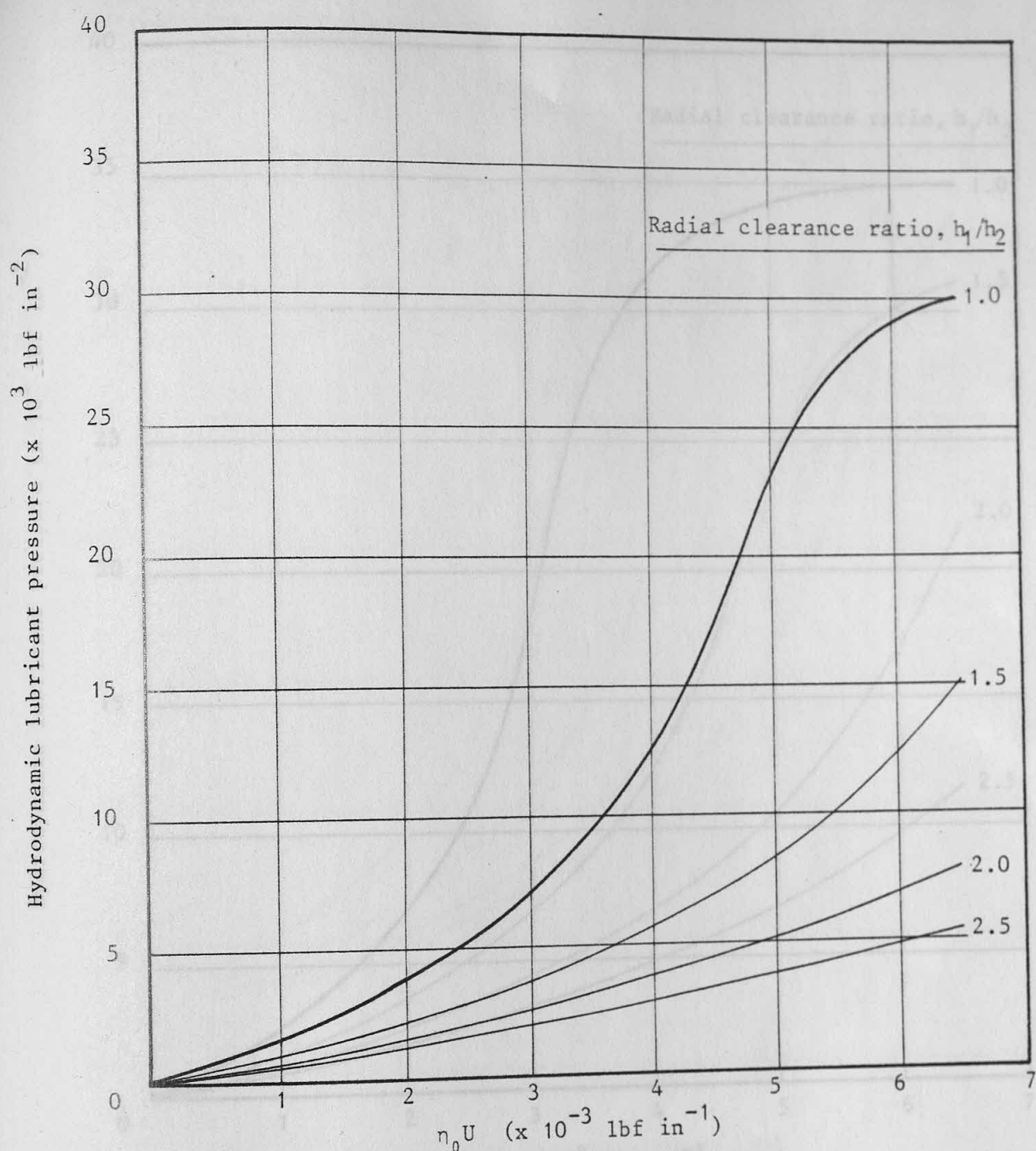
* At $h_1/h_2 = 1.0$ the plug-attachment has a straight-parallel profile
 Draw speed = 100 ft min^{-1}

Lubricant viscosity = $3.503 \times 10^{-4} \text{ lbf s in}^{-2}$ (EP50 at 20°C)

———— Radial clearance, $h_2 = 0.002 \text{ in}$

———— Radial clearance, $h_1 = 0.004 \text{ in}$

Figure (6.54) Variation of theoretical lubricant film thickness at the end of sinking with radial clearance ratio for straight-parallel and straight-tapered plug-attachments of different lengths



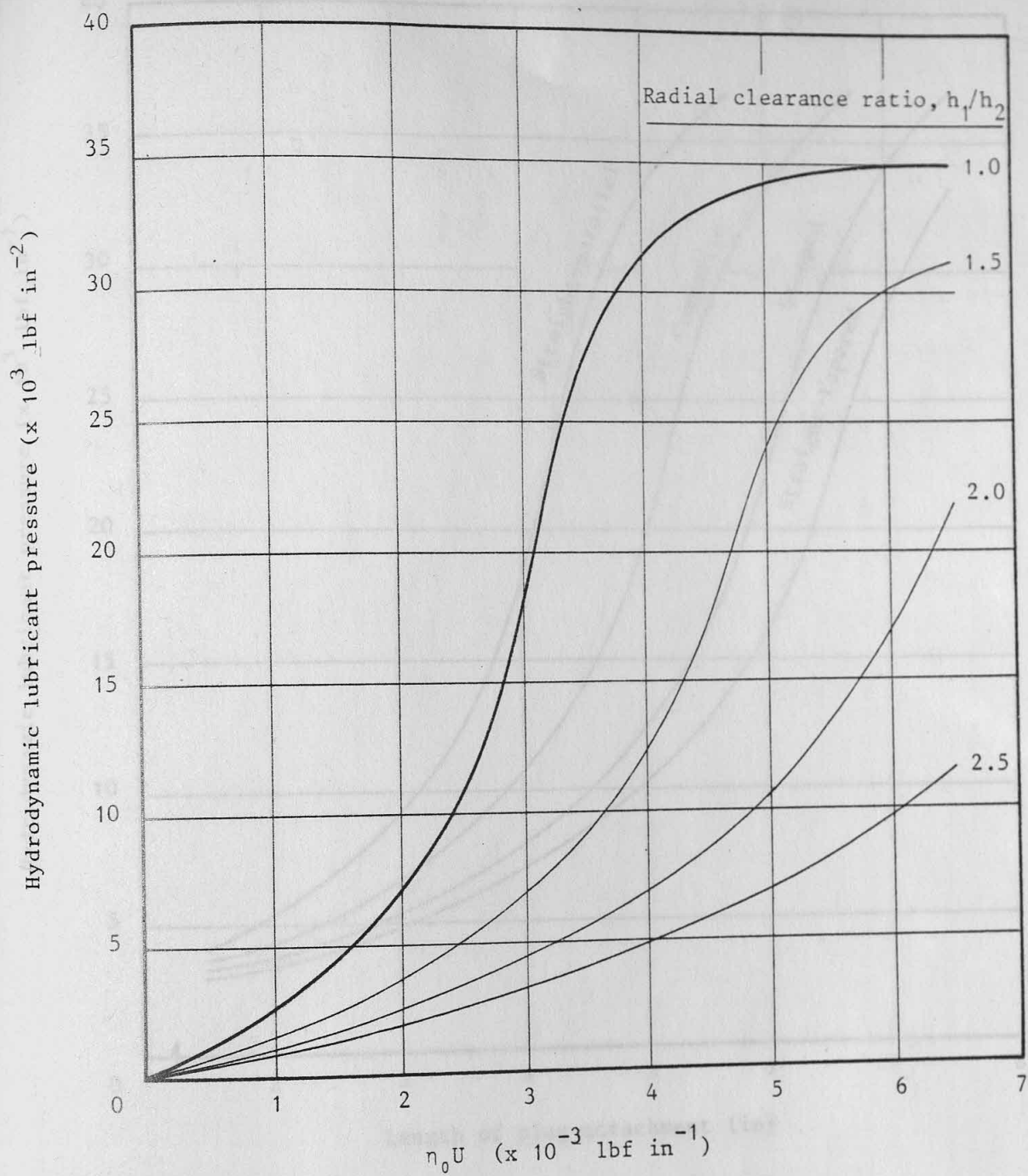
Length of plug-attachment, $l_2 = 4 \text{ in}$

Radial clearance, $h_2 = 0.004 \text{ in}$

— Straight-parallel or $h_1/h_2 = 1.0$

— Straight-tapered

Figure (6.55) Variation of theoretical hydrodynamic lubricant pressure for a 4 in straight-tapered plug-attachment with $\eta_0 U$ for different radial clearance ratios



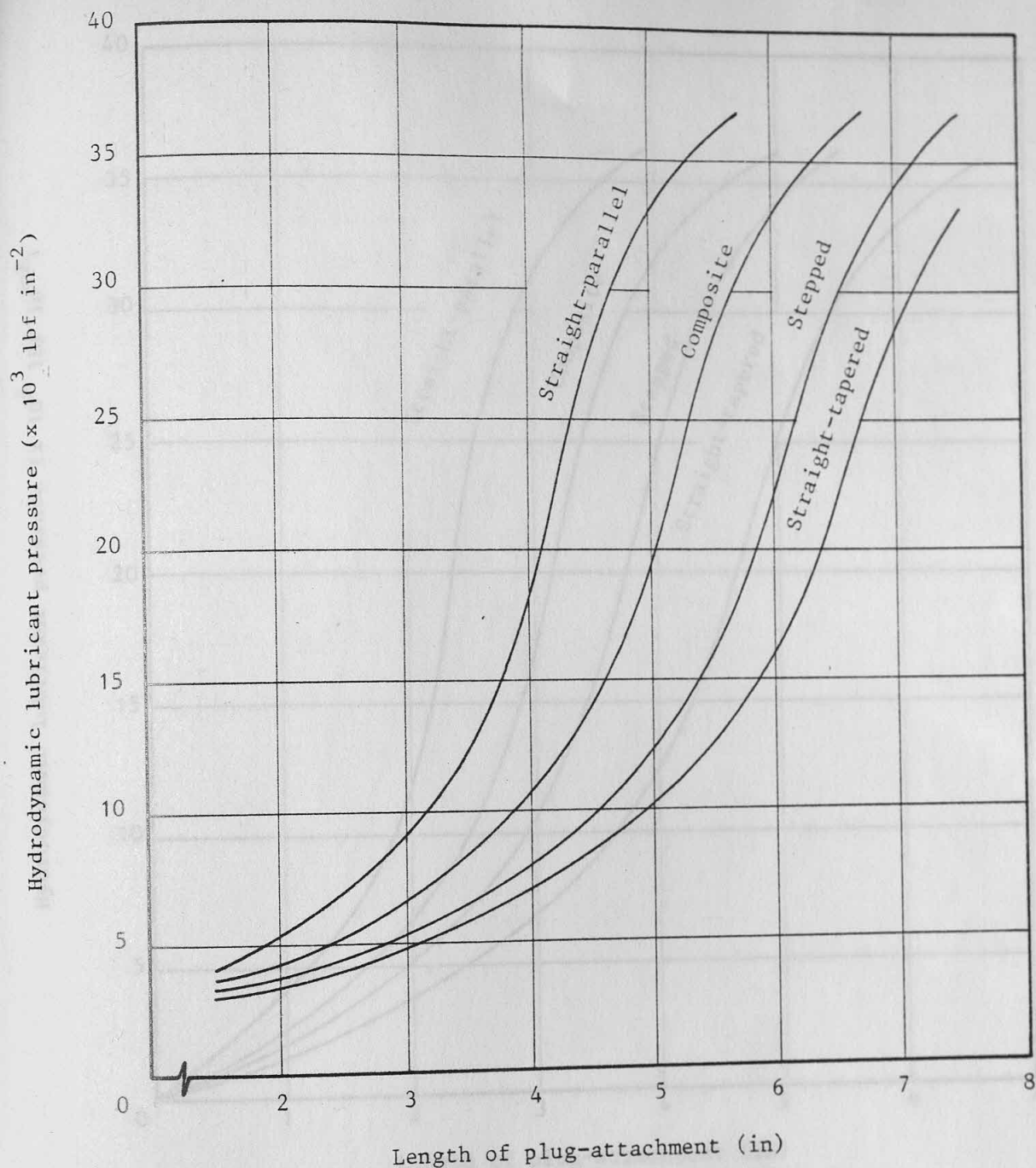
Length of plug-attachment, $l_2 = 6$ in

Radial clearance, $h_2 = 0.004$ in

———— Straight-parallel or $h_1/h_2 = 1.0$

———— Straight-tapered

Figure (6.56) Variation of theoretical hydrodynamic lubricant pressure for a 6 in straight-tapered plug-attachment with $\eta_0 U$ for different radial clearance ratios



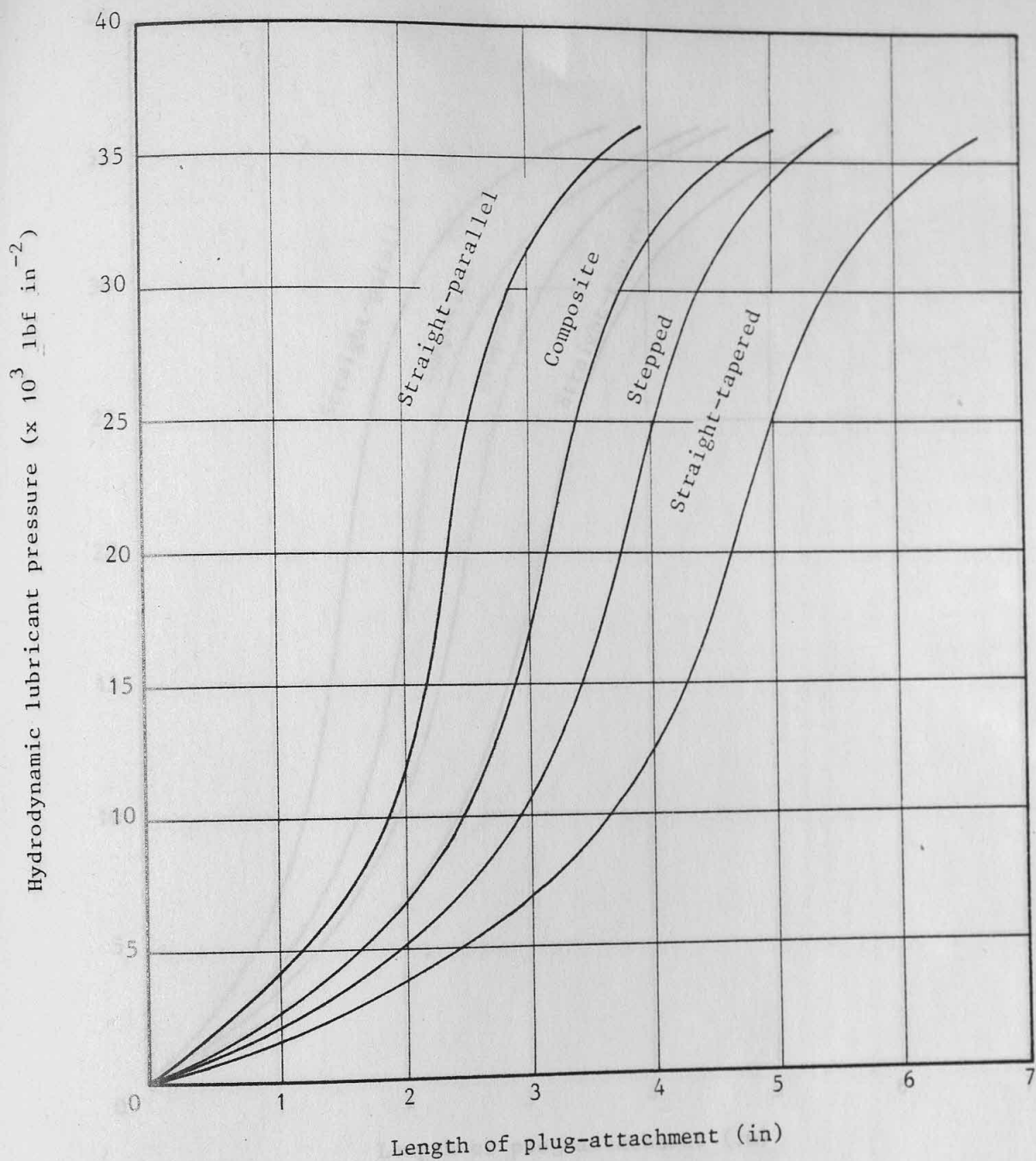
$$\eta_0 U = 0.001 \text{ lbf in}^{-1}$$

$$\text{Length ratio, } l_2/l_1 = 1.0$$

$$\text{Radial clearance, } h_2 = 0.002 \text{ in}$$

$$\text{Radial clearance ratio, } h_1/h_2 = 1.5$$

Figure (6.57) Variation of theoretical hydrodynamic lubricant pressure with length for four designs of plug-attachments



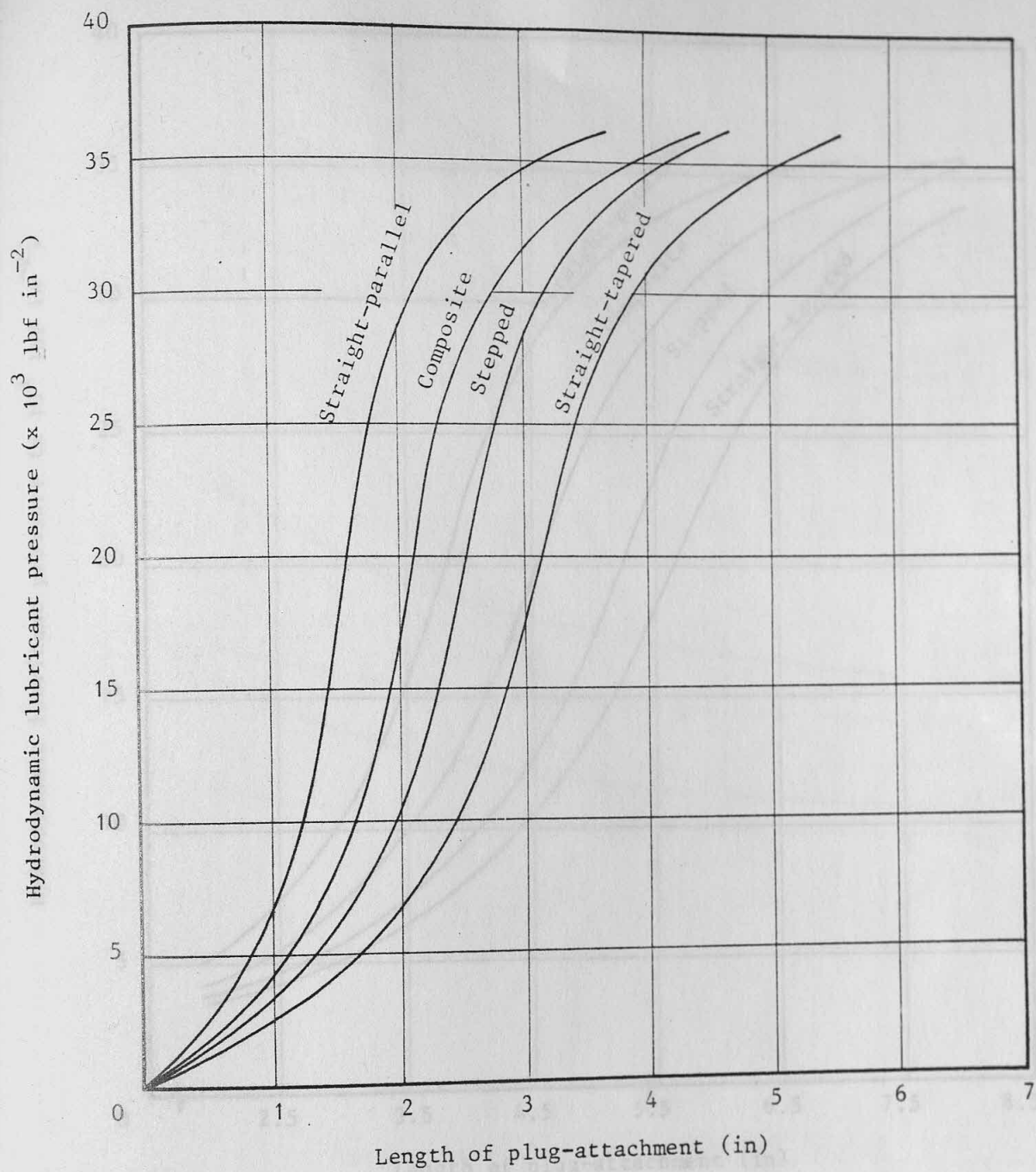
$$\eta_0 U = 0.002 \text{ lbf in}^{-1}$$

$$\text{Length ratio, } l_2/l_1 = 1.0$$

$$\text{Radial clearance, } h_2 = 0.002 \text{ in}$$

$$\text{Radial clearance ratio, } h_1/h_2 = 2.0$$

Figure (6.58) Variation of theoretical hydrodynamic lubricant pressure with length for four designs of plug-attachments



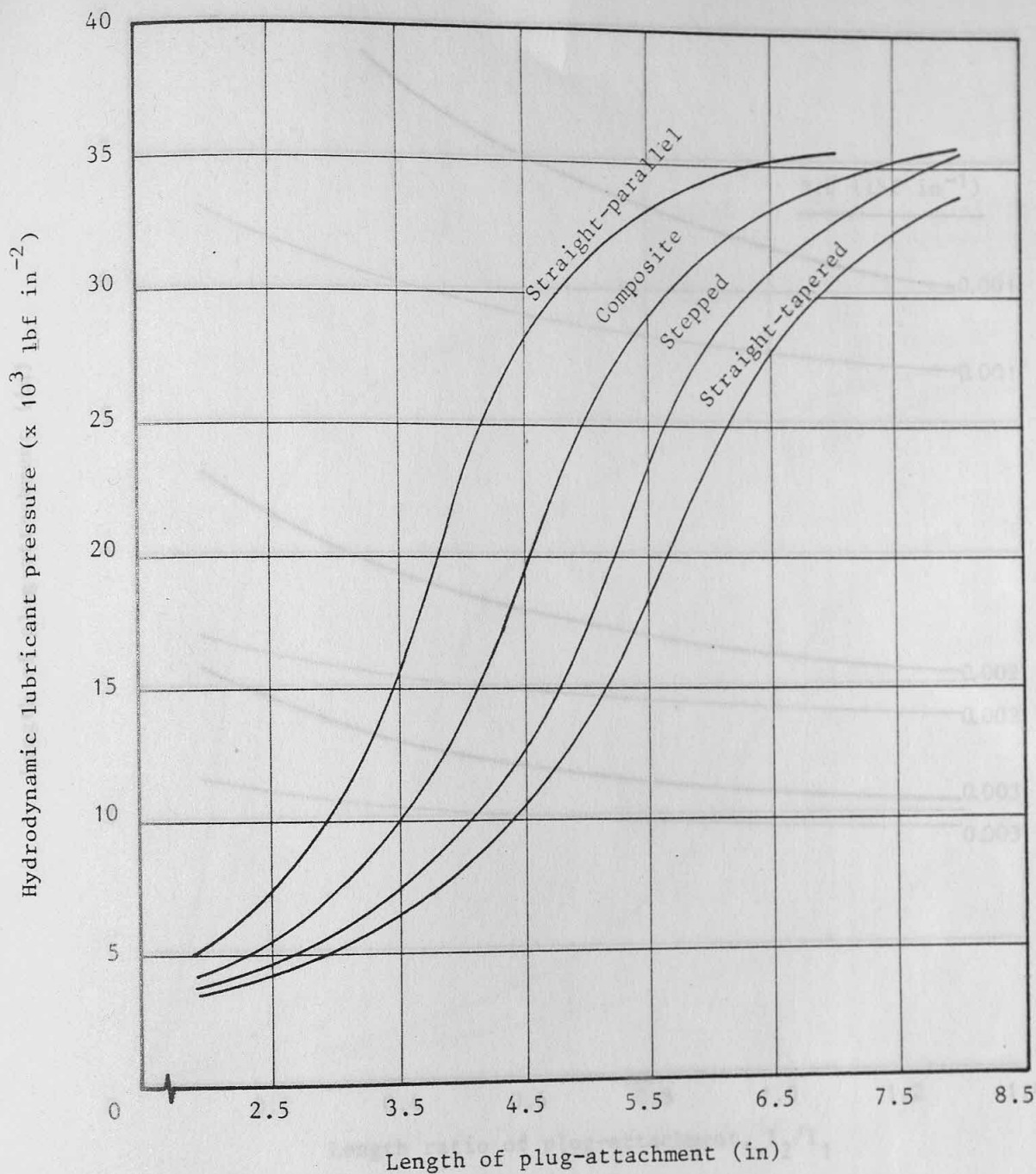
$$\eta_0 U = 0.003 \text{ lbf in}^{-1}$$

$$\text{Length ratio, } l_2/l_1 = 1.0$$

$$\text{Radial clearance, } h_2 = 0.002 \text{ in}$$

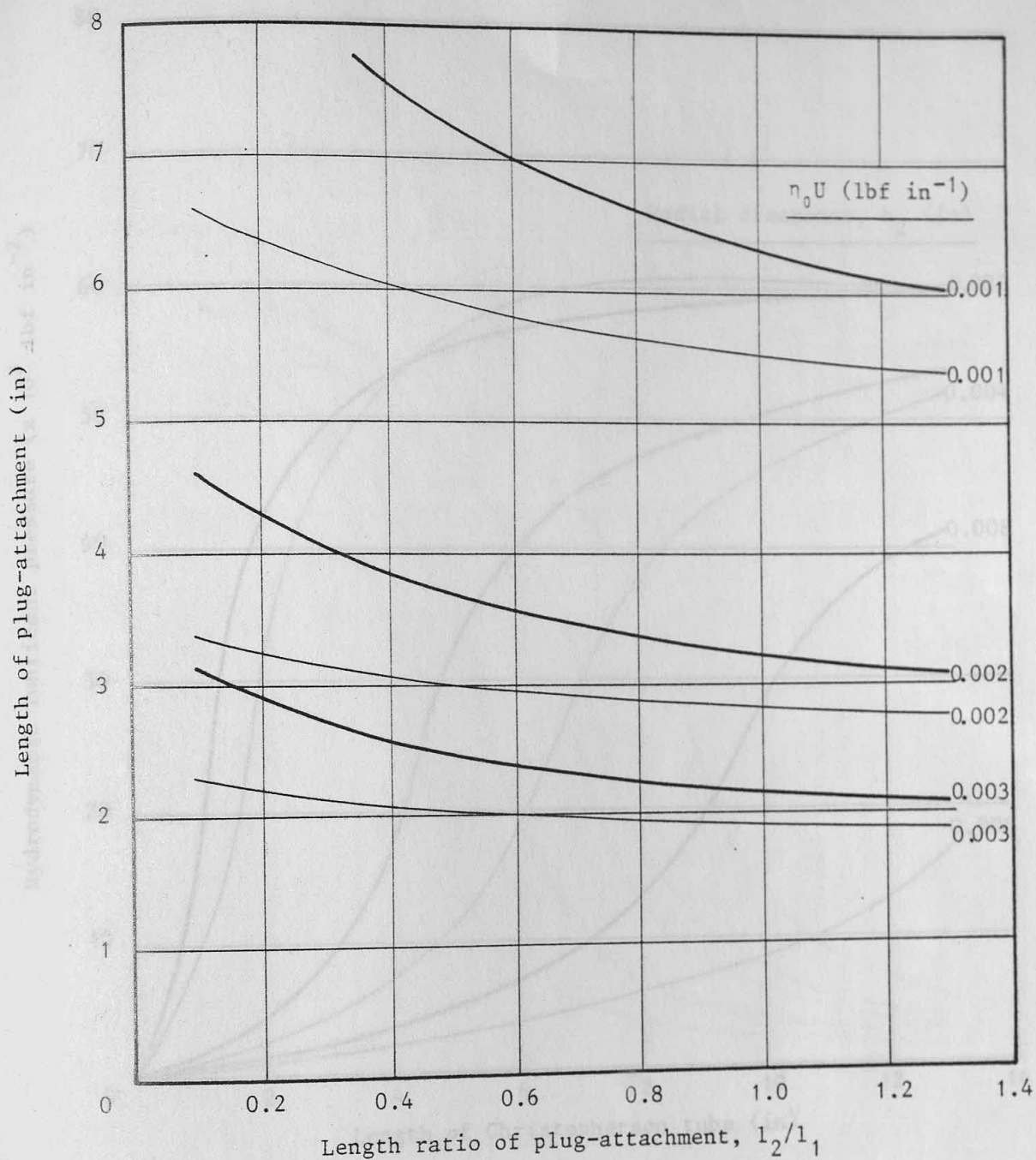
$$\text{Radial clearance ratio, } h_1/h_2 = 2.0$$

Figure (6.59) Variation of theoretical hydrodynamic lubricant pressure with length for four designs of plug-attachments



$\eta_0 U = 0.005 \text{ lbf in}^{-1}$
 Length ratio, $l_2/l_1 = 1.0$
 Radial clearance, $h_2 = 0.004 \text{ in}$
 Radial clearance ratio, $h_1/h_2 = 1.5$

Figure (6.60) Variation of theoretical hydrodynamic lubricant pressure with length for four designs of plug-attachments



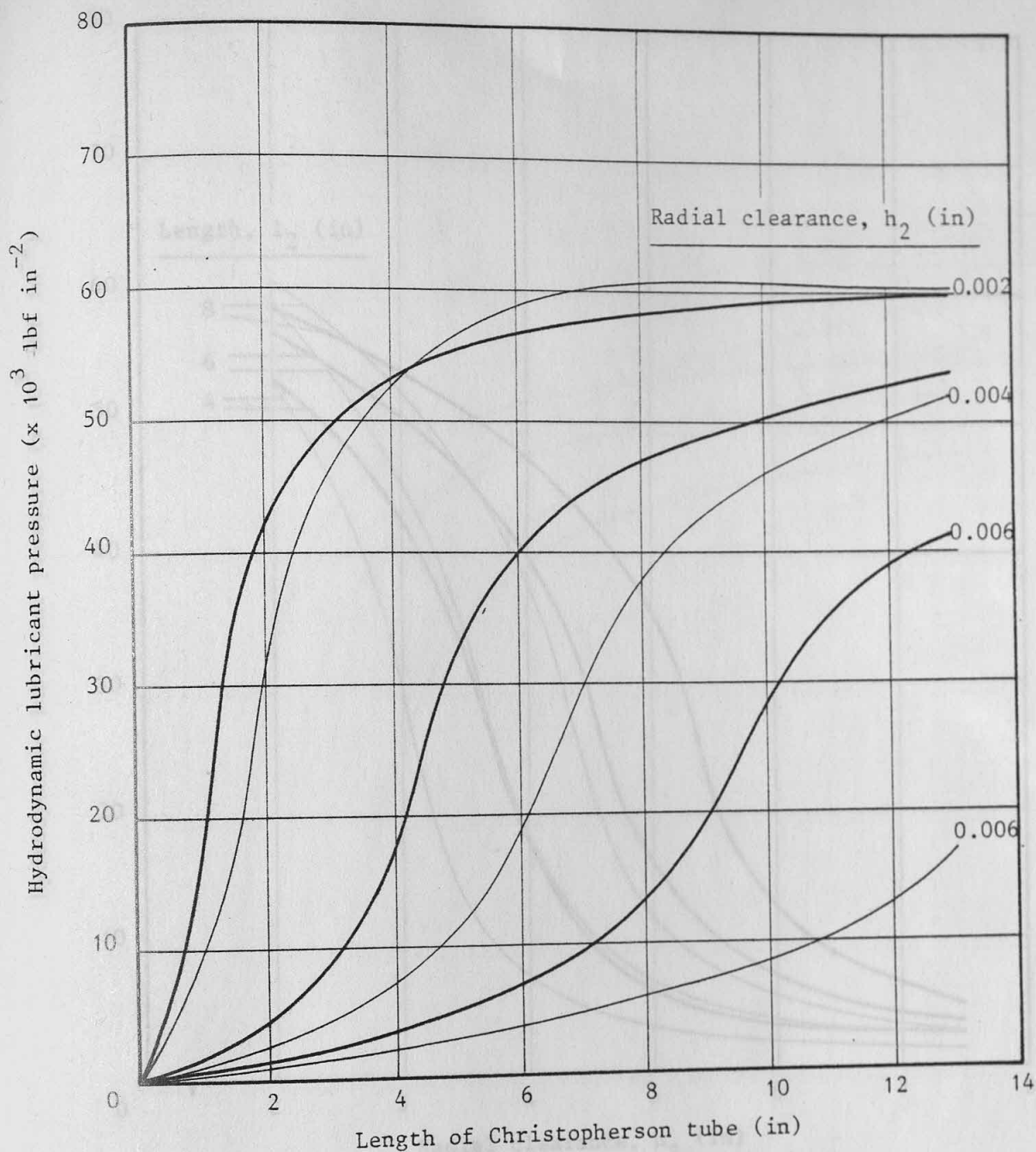
Radial clearance, $h_2 = 0.002$ in

Radial clearance ratio, $h_1/h_2 = 1.5$

— Stepped

- - - Composite

Figure (6.61) Variation of length with length ratio of the composite and stepped plug-attachments to generate a hydrodynamic lubricant pressure of 20000 lbf in $^{-2}$



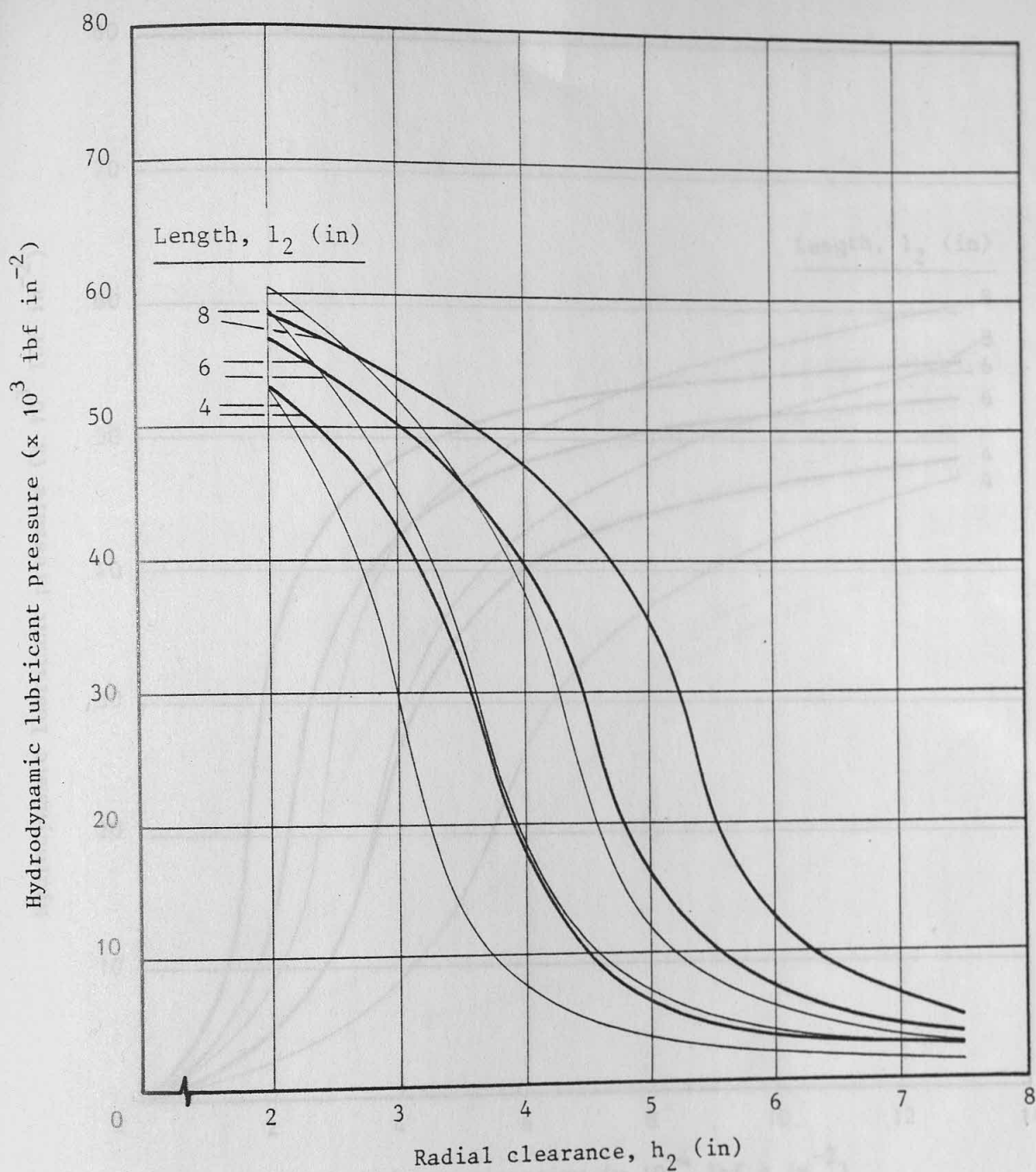
Draw speed = 100 ft min⁻¹

Lubricant viscosity = 3.503×10^{-4} lbf s in⁻² (EP50 at 20°C)

Radial clearance ratio, $h_1/h_2 = 1.5$

— Straight-parallel
 - - - Straight-tapered

Figure (6.62) Variation of theoretical hydrodynamic lubricant pressure with length for straight-parallel and straight-tapered Christopherson tube of different radial clearances



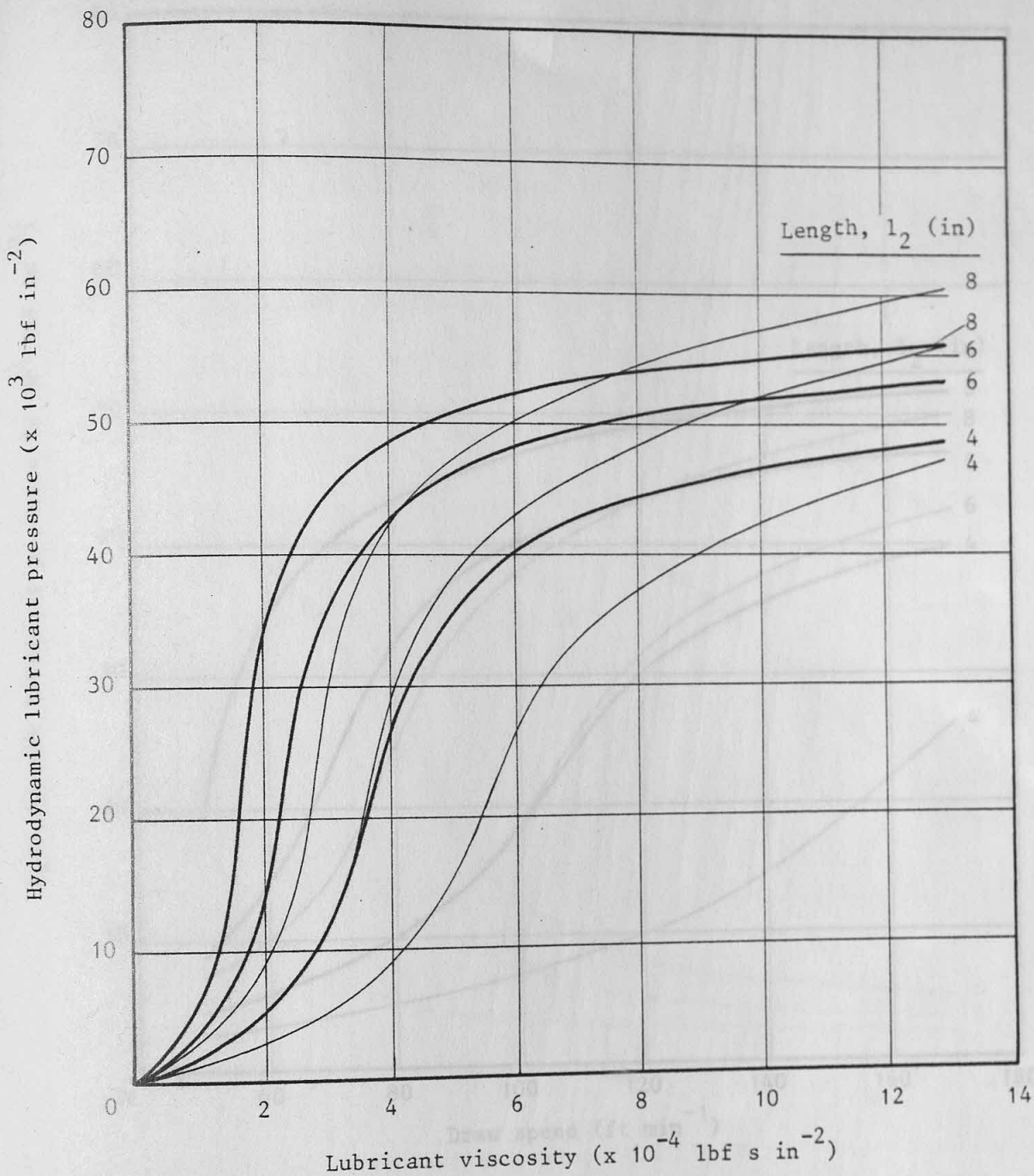
Draw speed = 100 ft min⁻¹

Lubricant viscosity = 3.503×10^{-4} lbf s in⁻² (EP50 at 20°C)

Radial clearance ratio, $h_1/h_2 = 1.5$

— Straight-parallel
 - - - Straight-tapered

Figure (6.63) Variation of theoretical hydrodynamic lubricant pressure with radial clearance for straight-parallel and straight-tapered Christopherson tubes of different lengths



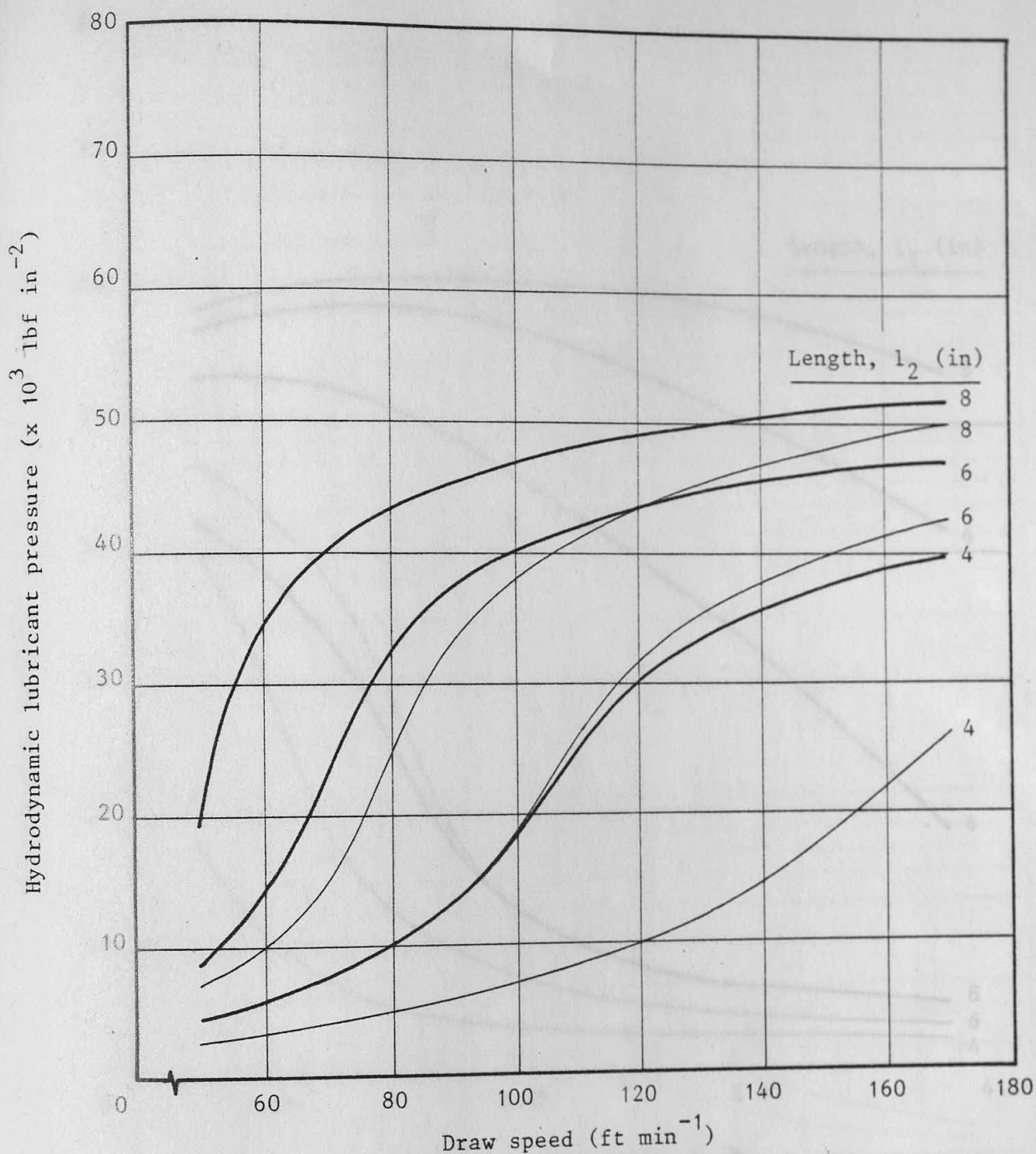
Draw speed = 100 ft min⁻¹

Radial clearance, $h_2 = 0.004$ in

Radial clearance ratio, $h_1/h_2 = 1.5$

— Straight-parallel
 - - - Straight-tapered

Figure (6.64) Variation of theoretical hydrodynamic lubricant pressure with lubricant viscosity for straight-parallel and straight-tapered Christopherson tubes of different lengths



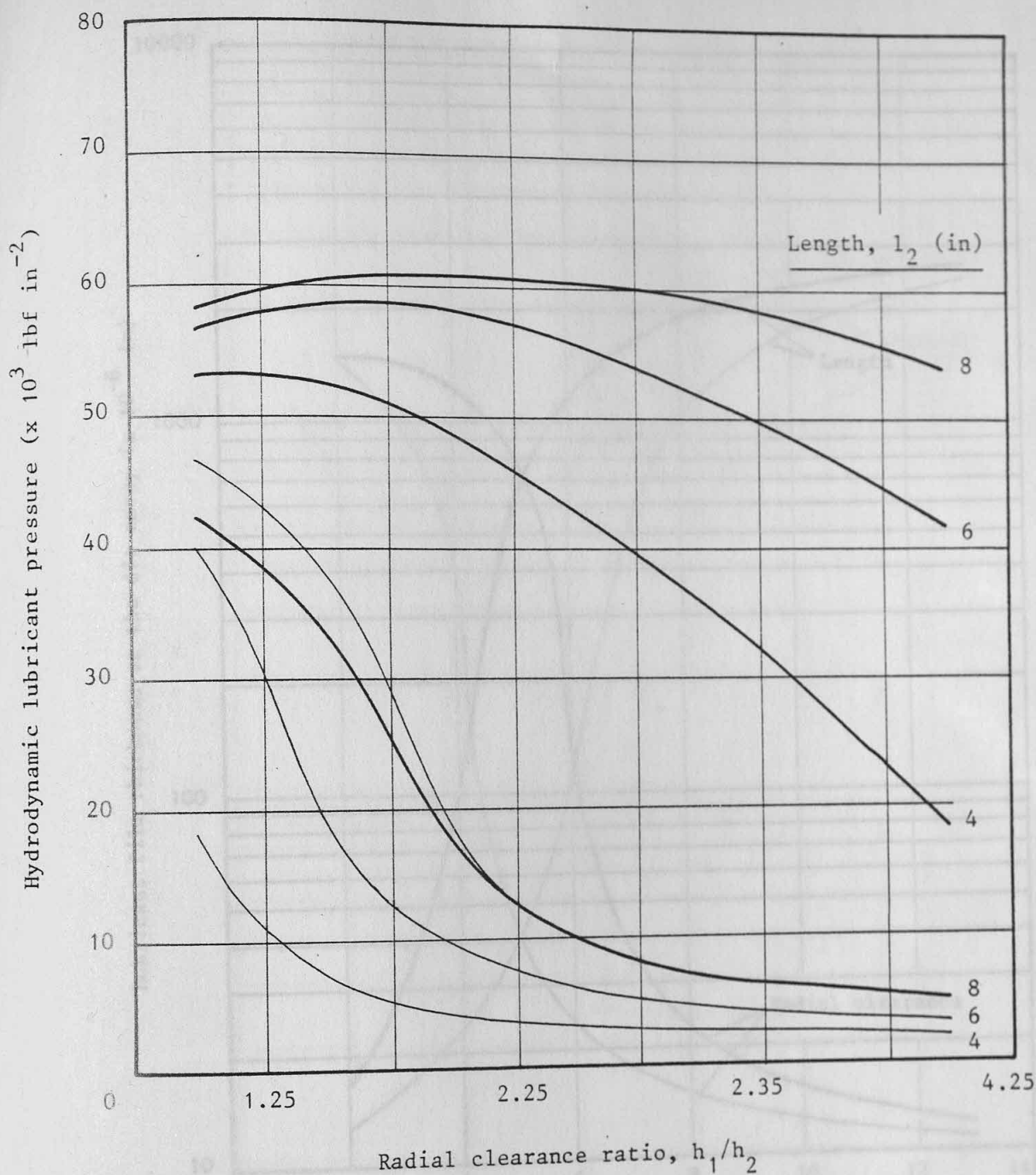
Lubricant viscosity = 3.503×10^{-4} lbf s in⁻² (EP50 at 20°C)

Radial clearance, $h_2 = 0.004$ in

Radial clearance ratio, $h_1/h_2 = 1.5$

— Straight-parallel
 - - - Straight-tapered

Figure (6.65) Variation of theoretical hydrodynamic lubricant pressure with draw speed for straight-parallel and straight-tapered Christopherson tubes of different lengths



* At $h_1/h_2 = 1.0$ the Christopherson tube has a straight-parallel profile

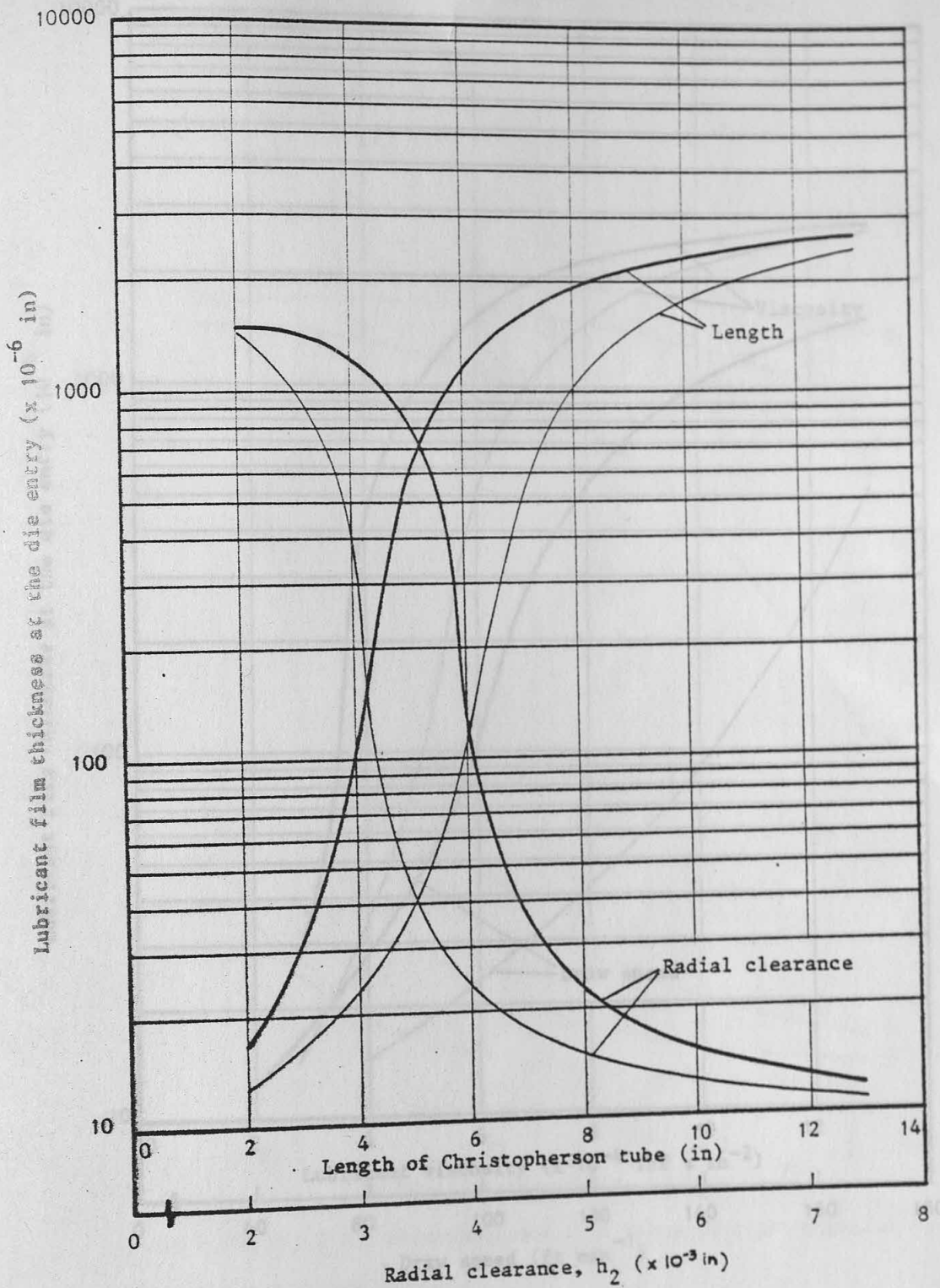
Draw speed = 100 ft min^{-1}

Lubricant viscosity = $3.503 \times 10^{-4} \text{ lbf s in}^{-2}$ (EP50 at 20°C)

———— Radial clearance, $h_2 = 0.002 \text{ in}$

———— Radial clearance, $h_2 = 0.004 \text{ in}$

Figure (6.66) Variation of theoretical hydrodynamic lubricant pressure with radial clearance ratio for straight-parallel and straight-tapered Christopherson tubes of different lengths



Draw speed = 100 ft min^{-1}

Lubricant viscosity = $3.503 \times 10^{-4} \text{ lbf s in}^{-2}$ (EP50 at 20°C)

Radial clearance ratio, $h_1/h_2 = 1.5$

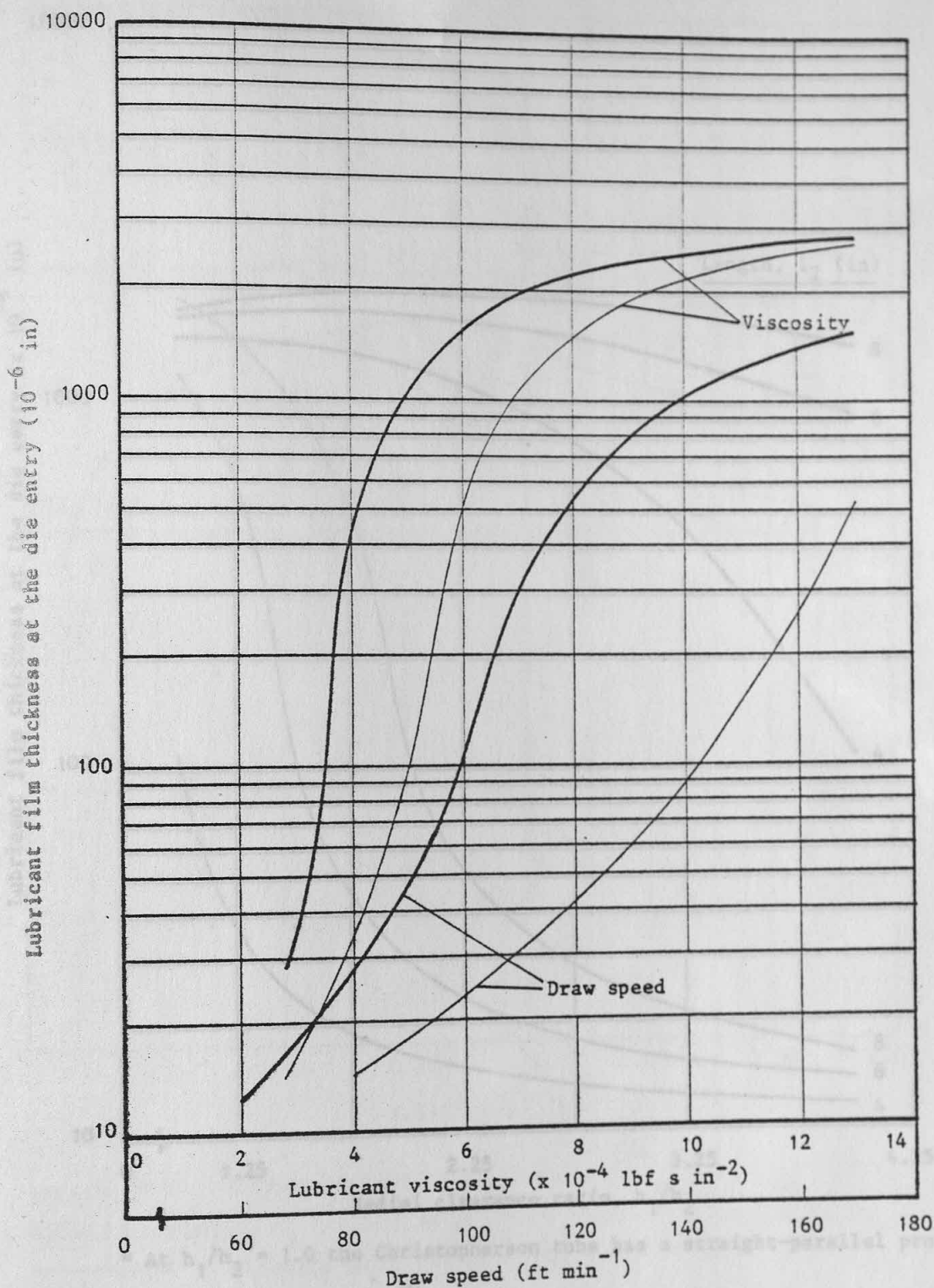
Radial clearance, $h_2 = 0.004 \text{ in}$

Length, $l_2 = 4 \text{ in}$

— Straight-parallel

— Straight-tapered

Figure (6.67) Variation of theoretical lubricant film thickness at the die entry with length and radial clearance for straight-parallel and straight-tapered Christopherson tubes



Draw speed = 100 ft min $^{-1}$

Lubricant viscosity = 3.503×10^{-4} lbf s in $^{-2}$ (EP50 at 20°C)

Radial clearance, $h_2 = 0.004$

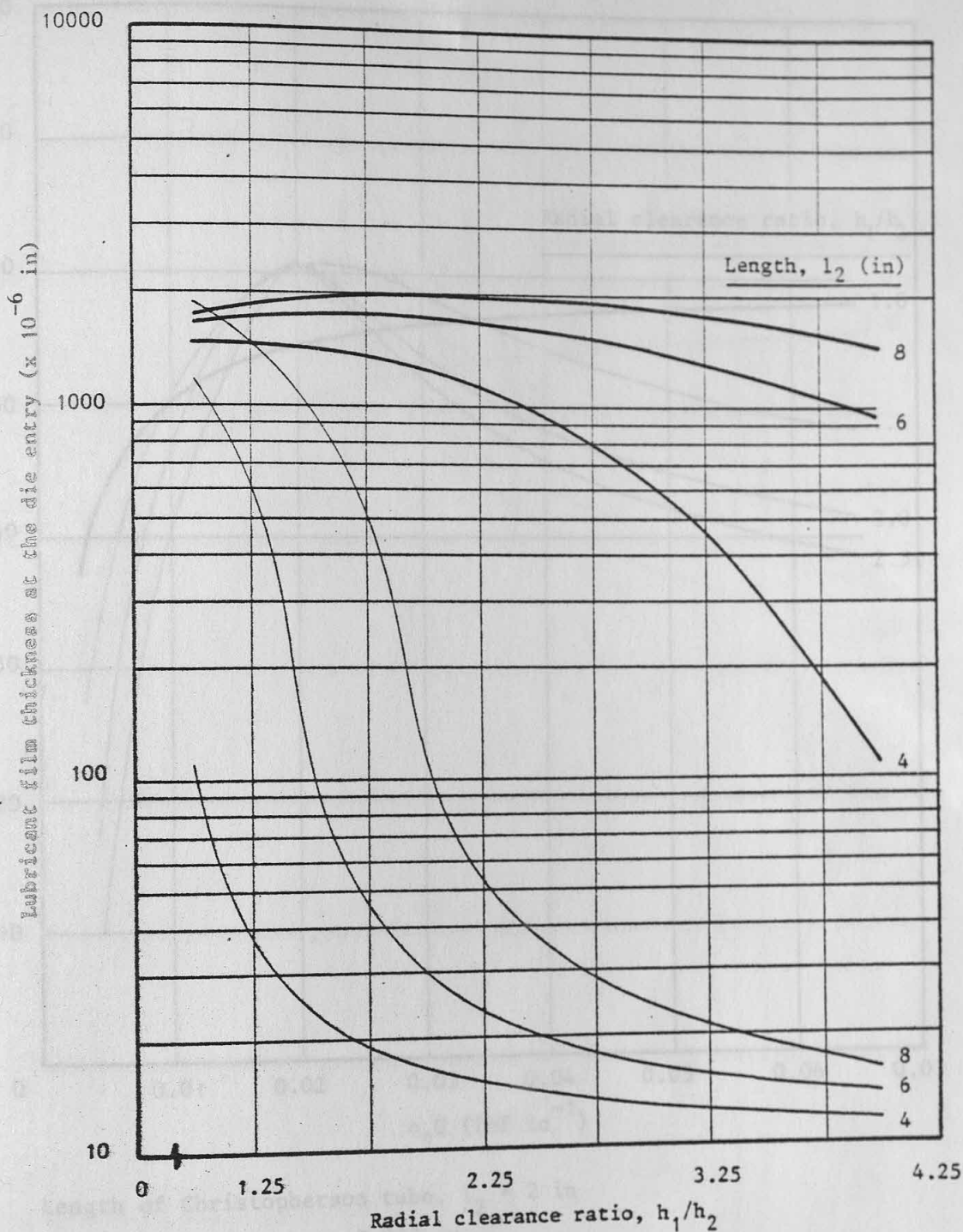
Radial clearance ratio, $h_1/h_2 = 1.5$

Length, $l_2 = 4$ in

— Straight-parallel

— Straight-tapered

Figure (6.68) Variation of theoretical lubricant film thickness at the die entry with lubricant viscosity and draw speed for straight-parallel and straight-tapered Christopherson tubes



* At $h_1/h_2 = 1.0$ the Christopherson tube has a straight-parallel profile

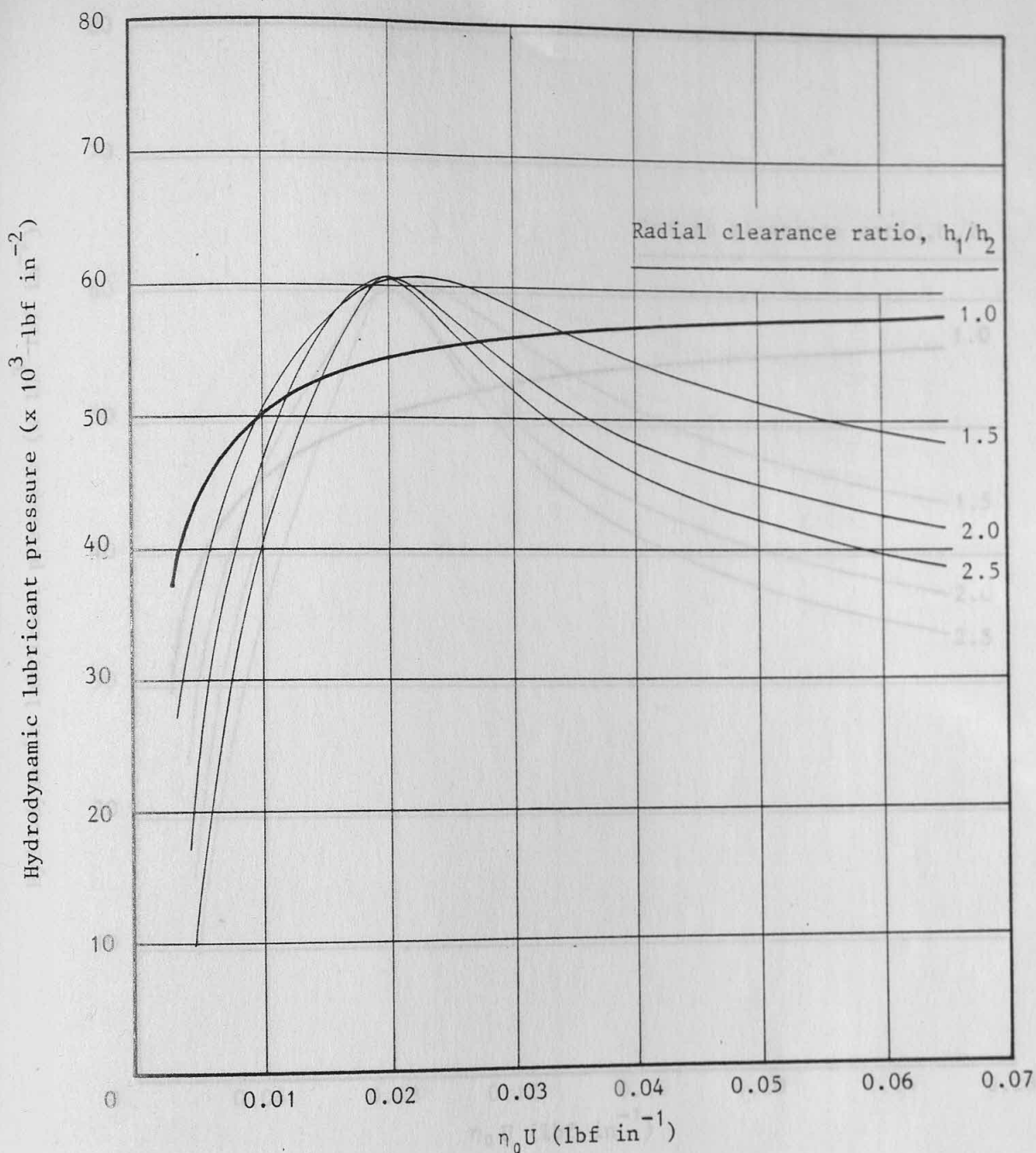
Draw speed = 100 ft min^{-1}

Lubricant viscosity = $3.503 \times 10^{-4} \text{ lbf s in}^{-2}$ (EP50 at 20°C)

———— Radial clearance, $h_2 = 0.002 \text{ in}$

----- Radial clearance, $h_2 = 0.004 \text{ in}$

Figure (6.69) Variation of theoretical lubricant film thickness at the die entry with radial clearance ratio for straight-tapered Christopherson tubes of different lengths



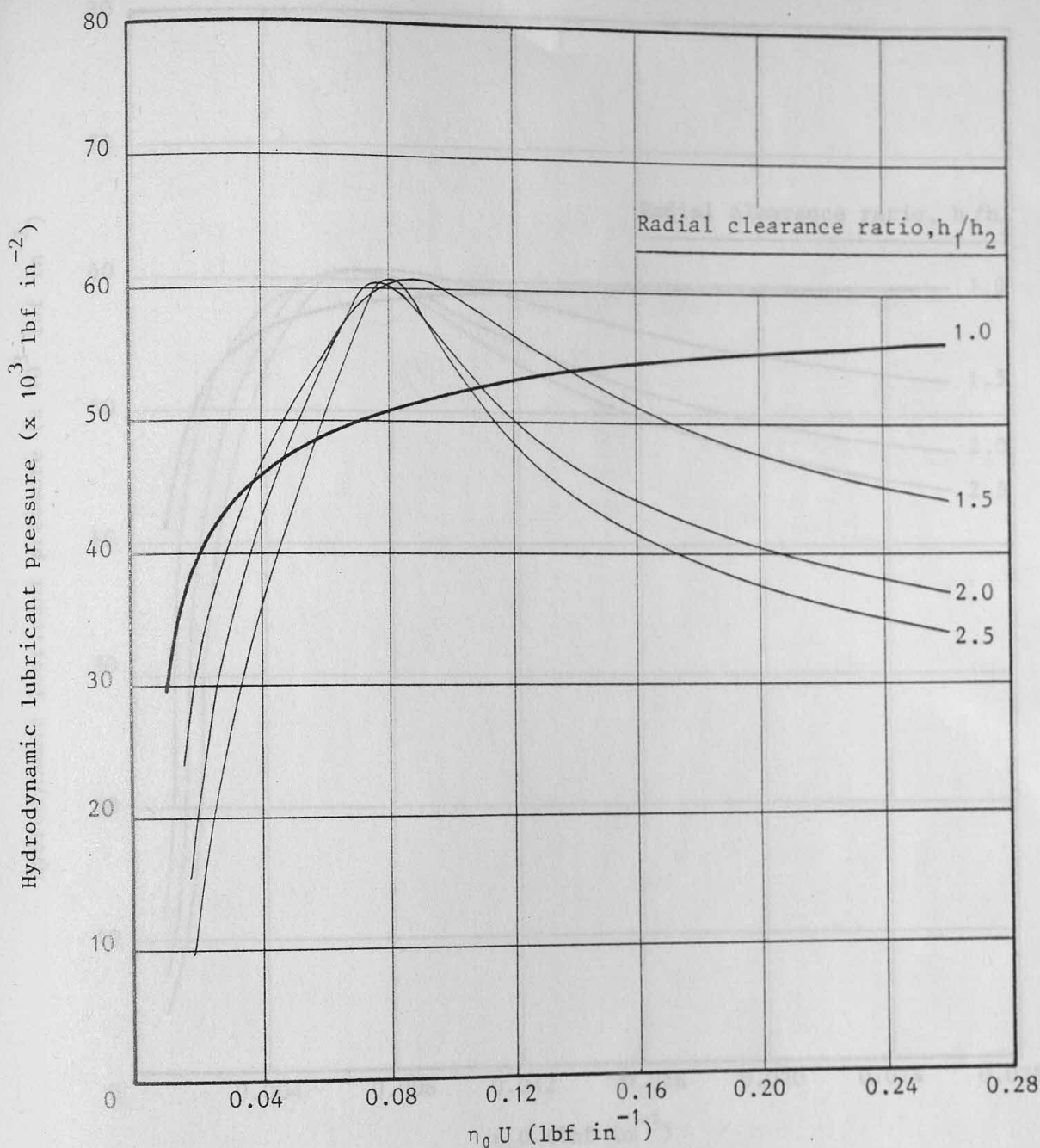
Length of Christopherson tube, $l_2 = 2 \text{ in}$

Radial clearance, $h_2 = 0.002 \text{ in}$

— Straight-parallel or $h_1/h_2 = 1.0$

— Straight-tapered

Figure (6.70) Variation of theoretical hydrodynamic lubricant pressure with $\eta_0 U$ for a 2 in straight-tapered Christopherson tube of different radial clearance ratios



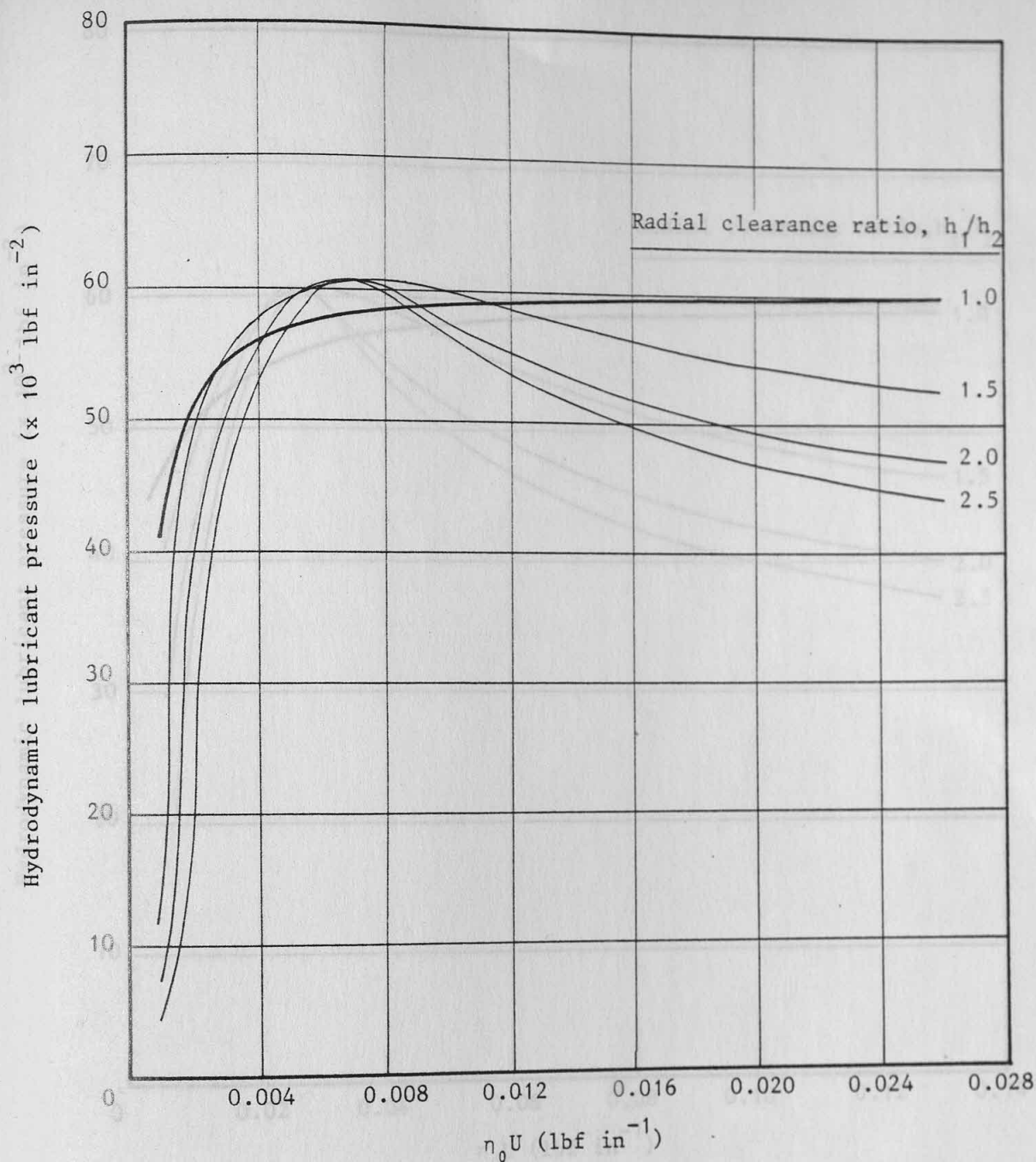
Length of Christopherson tube, $l_2 = 2 \text{ in}$

Radial clearance, $h_2 = 0.004 \text{ in}$

———— Straight-parallel or $h_1/h_2 = 1.0$

———— Straight-tapered

Figure (6.71) Variation of theoretical hydrodynamic lubricant pressure with $\eta_0 U$ for a 2 in straight-tapered Christopherson tube of different radial clearance ratios



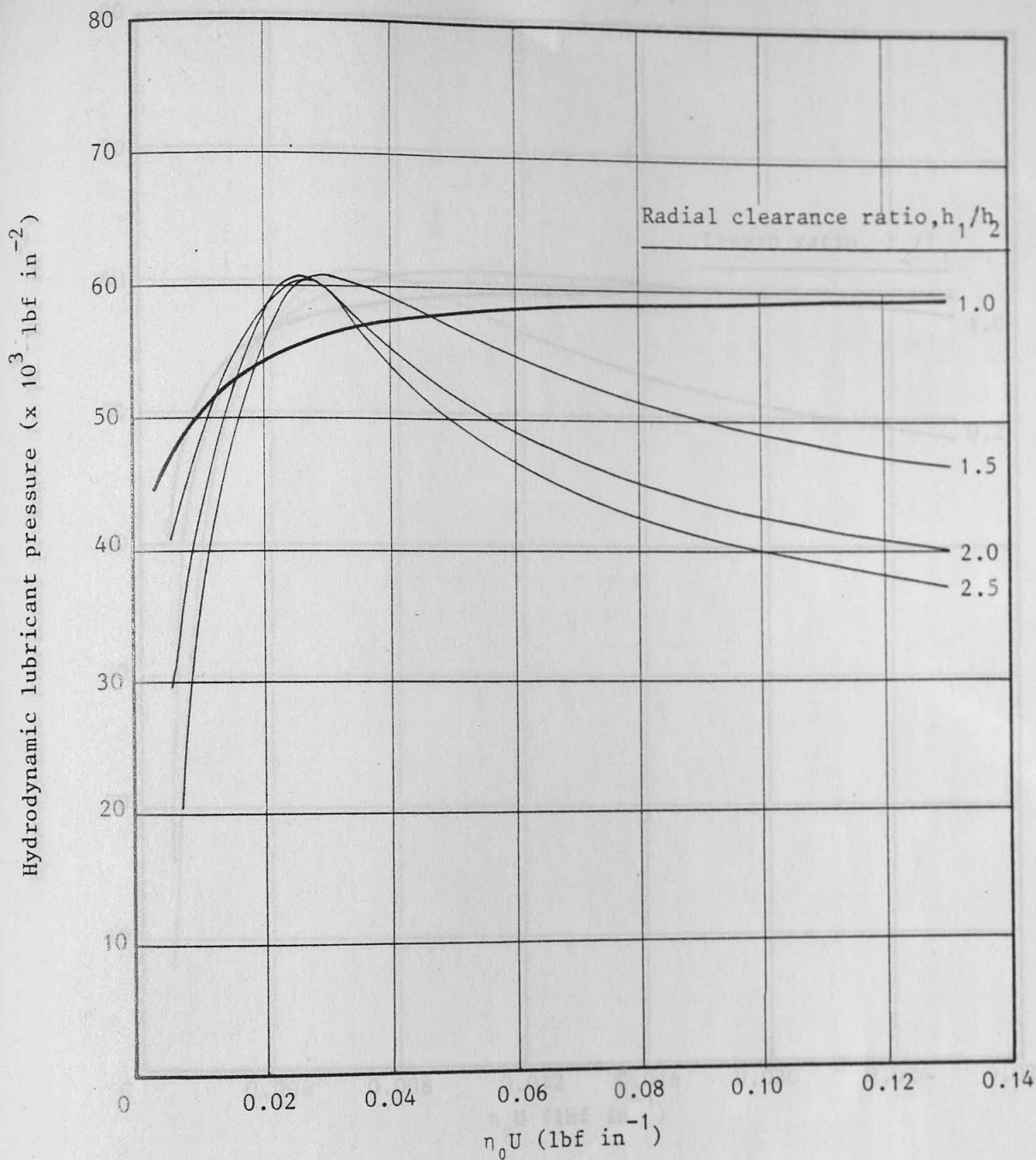
Length of Christopherson tube, $l_2 = 6 \text{ in}$

Radial clearance, $h_2 = 0.002 \text{ in}$

— Straight-parallel or $h_1/h_2 = 1.0$

— Straight-tapered

Figure (6.72) Variation of theoretical hydrodynamic lubricant pressure with $\eta_0 U$ for a 6 in straight-tapered Christopherson tube of different radial clearance ratios



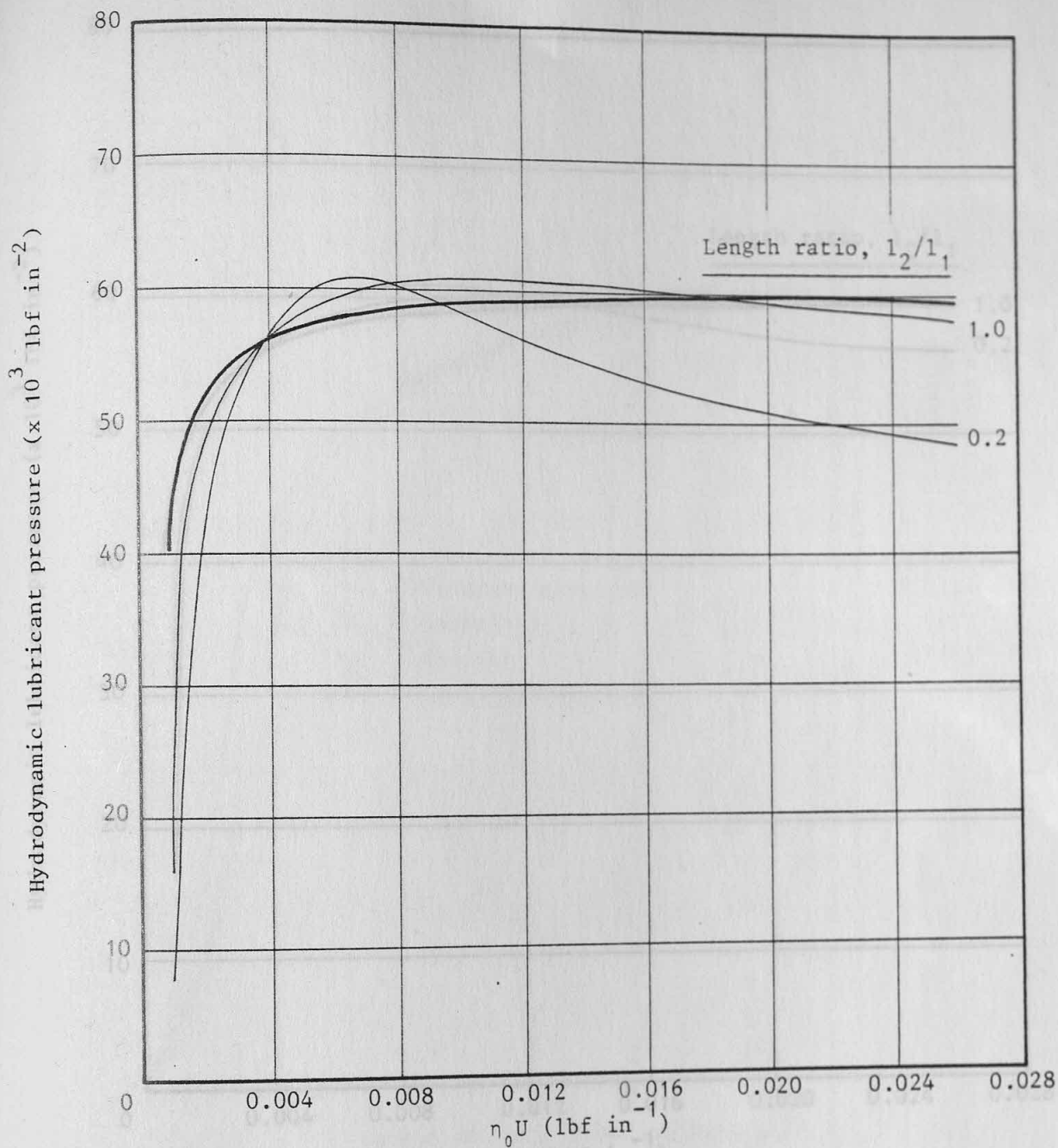
Length of Christopherson tube, $l_2 = 6 \text{ in}$

Radial clearance, $h_2 = 0.004 \text{ in}$

— Straight-parallel or $h_1/h_2 = 1.0$

— Straight-tapered

Figure (6.73) Variation of theoretical hydrodynamic lubricant pressure with $\eta_0 U$ for a 6 in straight-tapered Christopherson tube of different radial clearance ratios



Length of stepped Christopherson tube, $l_1 + l_2 = 6 \text{ in}$

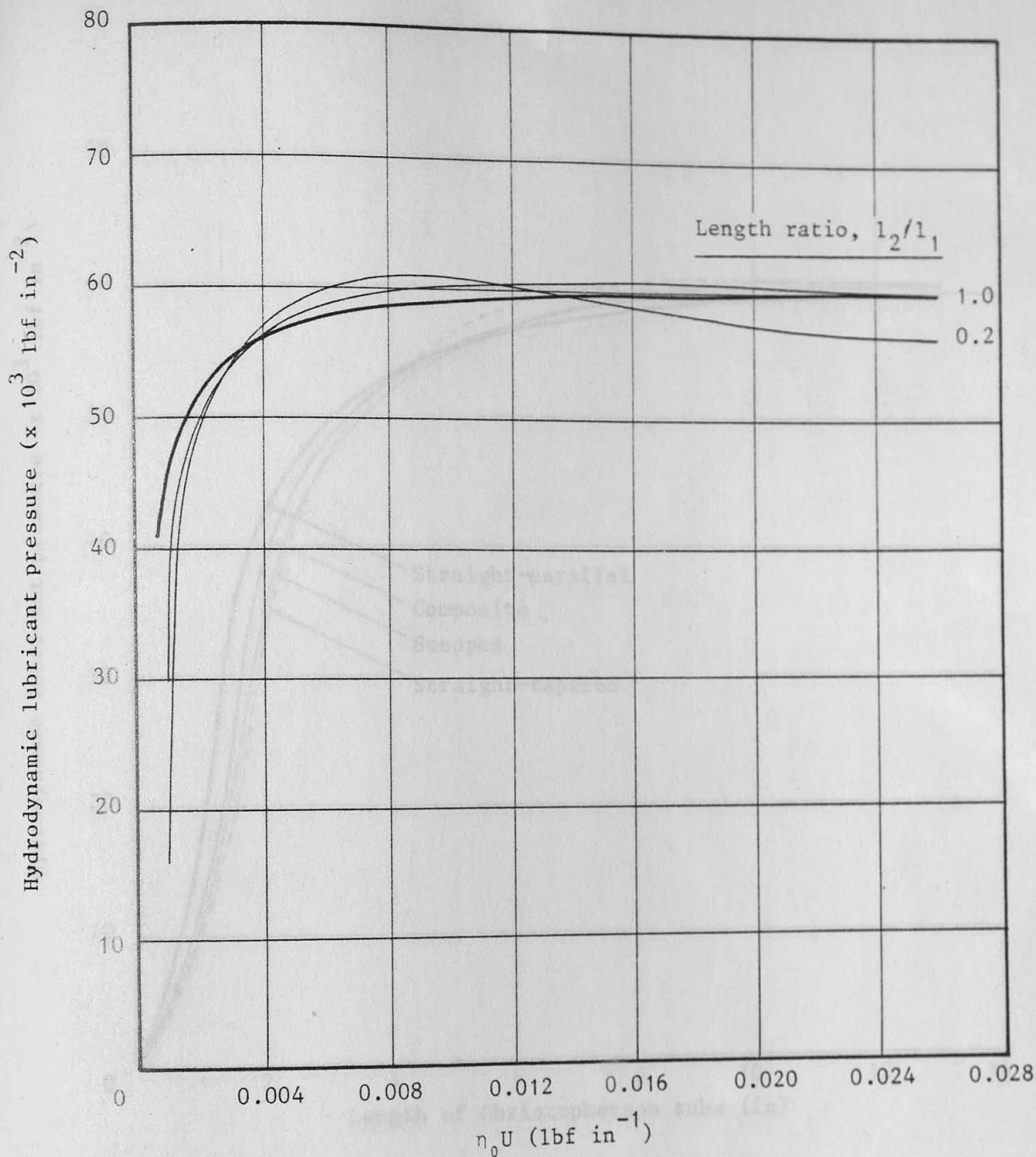
Radial clearance, $h_2 = 0.002 \text{ in}$

Radial clearance ratio, $h_1/h_2 = 1.5$

— Straight-parallel

— Stepped

Figure (6.74) Variation of theoretical hydrodynamic lubricant pressure with $\eta_0 U$ for a 6 in stepped Christopherson tube of different length ratios



Length of composite Christopherson tube, $l_1 + l_2 = 6$ in

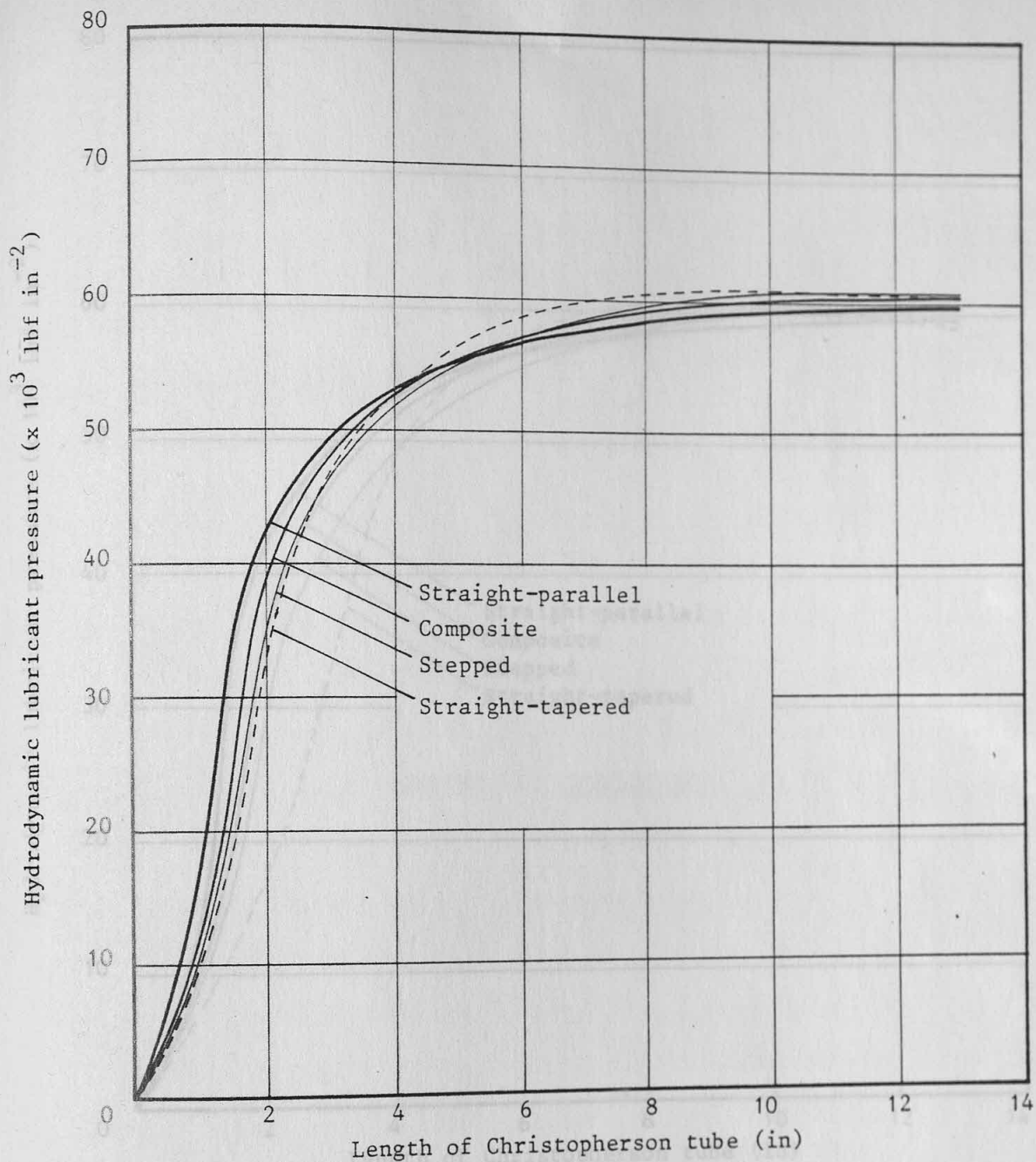
Radial clearance, $h_2 = 0.002$ in

Radial clearance ratio, $h_1/h_2 = 1.5$

— Straight-parallel

— Composite

Figure (6.75) Variation of theoretical hydrodynamic lubricant pressure with $\eta_0 U$ for a 6 in composite Christopherson tube of different length ratios



Draw speed = 100 ft min⁻¹

Lubricant viscosity = 3.503×10^{-4} lbf s in⁻² (EP50 at 20°C)

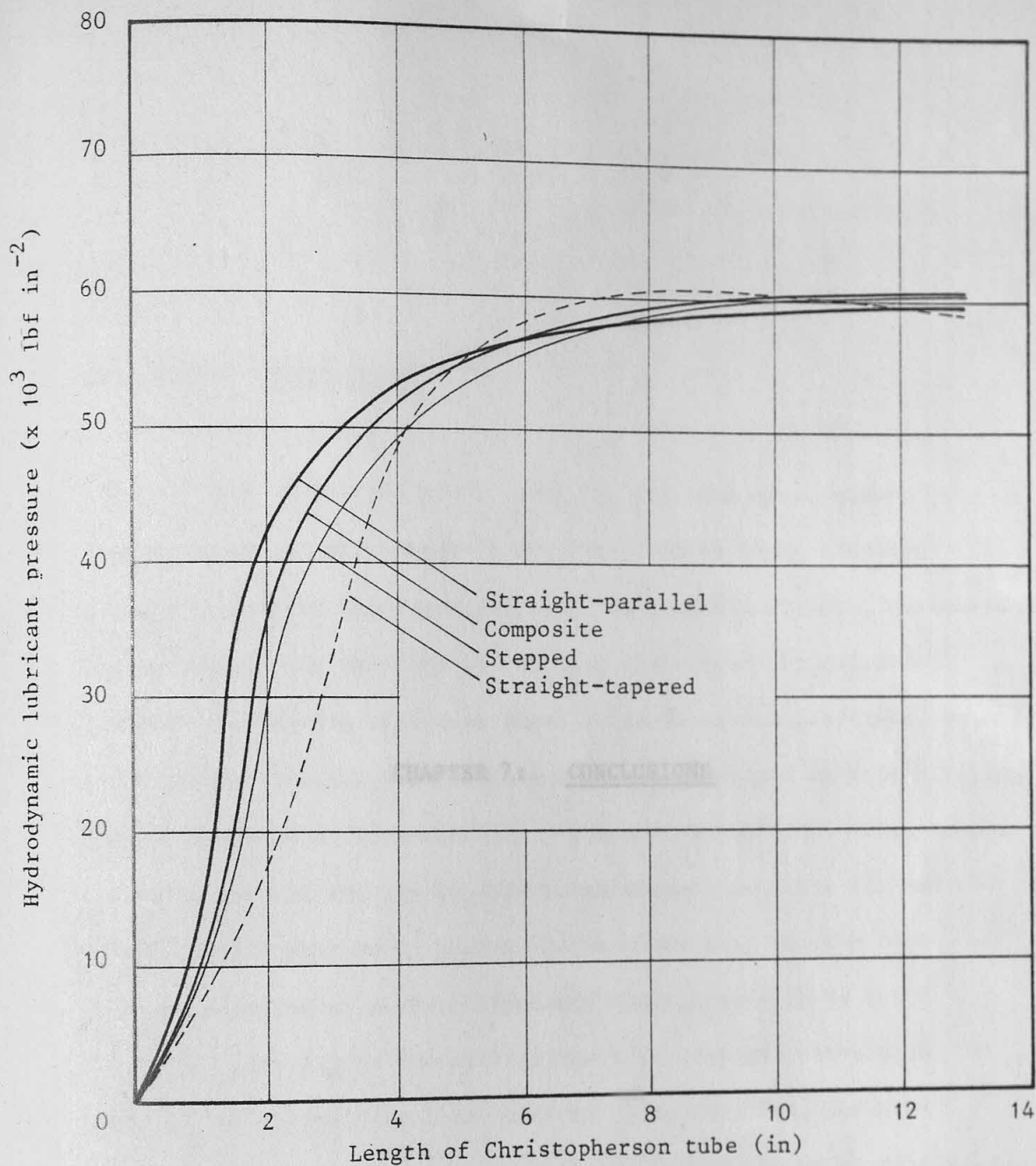
$\eta_0 U = 4.554 \times 10^{-3}$ lbf in⁻¹

Radial clearance, $h_2 = 0.002$ in

Radial clearance ratio, $h_1/h_2 = 1.5$

Length ratio, $l_2/l_1 = 1.0$

Figure (6.76) Variation of theoretical hydrodynamic lubricant pressure with length for four designs of Christopherson tubes



Draw speed = 100 ft min⁻¹

Lubricant viscosity = 3.503×10^{-4} lbf s in⁻² (EP50 at 20°C)

$\eta_0 U = 4.554 \times 10^{-3}$ lbf in⁻¹

Radial clearance, $h_2 = 0.002$ in

Radial clearance ratio, $h_1/h_2 = 2.0$

Length ratio, $l_2/l_1 = 1.0$

Figure (6.77) Variation of theoretical hydrodynamic lubricant pressure with length for four designs of Christopherson tubes

CHAPTER 7: CONCLUSIONS

A relatively simple and novel technique for bore lubrication, comprising of an attachment to a curve-profiled plug, has been developed for the tube-draw process. Using this technique, substantial reductions in the friction or the plug force of up to 65% were achieved in drawing stainless steel tubes using oil lubricant, both in which the initial surface condition was improved by grit-blasting and in as-drawn surface condition. The more significant achievement, however, was the ability to draw tubes of such material without the occurrence of chatter or pick-up between the plug and the tube, and without recourse to surface treatment operations such as grit-blasting, pickling or the application of a chemical conversion coating, which would not otherwise be possible. Thus, the new lubrication technique will reduce the production costs by eliminating the need for surface treatment and the related cleaning operations while ensuring efficient lubrication and a high product quality.

The curvature on the plug is desirable since it reduced the degree of stress concentration when the tube first collapsed onto it at the start of drawing and produced a condition of localized hydrodynamic lubrication as the plug was being drawn into the metal deformation zone. The combined effect of these actions was to reduce the risk of the occurrence of pick-up which was often seen to have

CHAPTER 7: CONCLUSIONS

A relatively simple and novel technique for bore lubrication, comprising of an attachment to a curve-profiled plug, has been developed for the tube-draw process. Using this technique, substantial reductions in the friction or the plug force of up to 65% were achieved in drawing stainless steel tubes using oil lubricant, both in which the initial bore surface had been roughened by grit-blasting and in as-drawn surface condition. The more significant achievement, however, was the ability to draw tubes of such material without the occurrence of chatter or pick-up between the plug and the tube, and without recourse to surface treatment operations such as grit-blasting, pickling or the application of a chemical conversion coating, which would not otherwise be possible. Thus, the new lubrication technique will reduce the production costs by eliminating the need for surface treatment and the related cleaning operations while ensuring efficient lubrication and a high product quality.

The curvature on the plug is desirable since it reduced the degree of stress concentration when the tube first collapsed onto it at the start of drawing and produced a condition of localised hydrodynamic lubrication as the plug was being drawn into the metal deformation zone. The combined effect of these actions was to reduce the risk of the occurrence of pick-up which was often seen to have

initiated from the point of initial contact between the plug and the tube when drawing with a conventionally chamfered plug.

The function of the plug-attachment was to generate a high pressure in the lubricant at the entry to the metal deformation zone by the classical mechanism of hydrodynamic lubrication. This pressure increased the flow of lubricant into the metal deformation zone and increased the separation of the plug and tube surfaces, thereby improving lubrication at this interface. Thus, the plug force and the draw stress were found to vary inversely with the lubricant pressure. The almost instantaneous rise of the lubricant pressure is advantageous since it eliminates the need for priming. The magnitude of the lubricant pressure was found to be directly proportional to the length of the attachment and the lubricant viscosity, and inversely proportional to the radial clearance between the attachment and the bore of the undrawn tube. The influence of the draw speed on the lubricant pressure was not investigated experimentally since a constant speed of 15 ft min^{-1} was used throughout the experimental work. This speed was much slower than the typical industrial speeds. However, the theoretical analysis showed that the lubricant pressure has a directly proportional relationship to the draw speed. In drawing the tubes with the bore surface in the as-drawn condition, i.e. in the second pass, pick-up occurred when the lubricant pressure was lower than about 500 lbf in^{-2} . Although the magnitude of this limiting pressure may be expected to vary with the size of the tube and the degree of plastic deformation desired, this minimum pressure at entry to the deformation zone may be obtained by an appropriate selection of the draw speed, lubricant, and practicable values of the length of the plug-attachment and the radial clearance which it provides. The use of a faster draw speed and/or a more viscous, and appropriate, lubricant would

therefore permit a relaxation of the practical restriction on the length and radial clearance of the plug-attachment.

A lustrous finish was produced on the bore surface of the drawn tubes, the CLA values of which decreased progressively with each subsequent pass. A batch of tubes which had been drawn at 30.6% reduction in area had a mean bore surface CLA value of $0.13\ \mu\text{m}$; the initial bore surface of these tubes had been roughened by grit-blasting and had a corresponding mean CLA value of $0.75\ \mu\text{m}$. When these tubes were annealed only but not roughened, and drawn at a further 31.1% reduction in area, the mean CLA value was reduced to $0.05\ \mu\text{m}$. The resulting surface finish was smoothest when the plug-attachment was not used or when pick-up had occurred. In general, the appearance of the bore surface was comparatively duller when the lubricant pressure was higher. The CLA values of the bore surface were found to possess a relationship with the lubricant pressure which was opposite to that observed for the plug force and the lubricant pressure, i.e. a higher lubricant pressure resulted in a lower plug force but a higher CLA value and vice-versa. Thus, these observations were corroborative and together with the lustrous surface finish suggest that the lubrication regime at the plug-tube interface was one of "quasi-hydrodynamic".

The theory of the plug-attachment predicted lubricant pressure trends in good agreement with experimental observations. The actual theoretical values, however, were higher by a magnitude equivalent to a lubricant viscosity difference corresponding to a change in the lubricant temperature of 7°C to 8°C . Thus, the theoretical lubricant pressures, at a value of the lubricant viscosity corresponding to a temperature of between 7°C and 8°C above the recorded laboratory ambient temperature, were in reasonably good agreement with the lubricant pressures observed experimentally.

This discrepancy occurred since the theory assumed isothermal conditions and hence neglected viscosity changes as a result of the heat conducted from the metal deformation zone, and aggravated by the propensity of the lubricant to change its viscosity rapidly with temperature changes. By compensating for this deficiency, i.e. by using a value of the lubricant viscosity corresponding to a temperature of about 8°C higher than the anticipated ambient temperature, therefore, the theory can be applied with confidence in the design of industrially suitable plug-attachments.

The theoretical results showed that the influences of the drawing conditions such as the draw speed and lubricant viscosity, and the geometry of the plug-attachment such as the length and radial clearance on the lubricant film thickness at the end of sinking are similar to those on the lubricant pressure. The lubricant film thickness, calculated under the experimental conditions and corresponding to the lubricant viscosities in which the theoretical lubricant pressures were within reasonable agreement with those observed experimentally, ranged typically from $0.5\text{ }\mu\text{in}$ to about $1\text{ }\mu\text{in}$. These were thicker than the mono-molecular or several molecular layers associated with boundary lubrication. However, these were much thinner in comparison with those found in the literature for other metal-forming processes in which hydrodynamic lubrication was known to have occurred. Consequently, these theoretical values of the lubricant film thickness, together with the observations made on the surface finish of the bore, the influences of the lubricant pressure on the friction or the plug force and the bore surface appearance, again suggest the occurrence of a "quasi-hydrodynamic" lubrication regime. While a lustrous bore surface finish is desirable, it was shown theoretically that lubricant film thickness of the order associated with a full hydrodynamic lubrication

regime can be achieved at higher values of the lubricant pressure, i.e. with higher draw speeds and more viscous lubricants, a longer length of the attachment and a smaller radial clearance. When this occurs the surface finish may be expected to "deteriorate".

Obviously, from an industrial point of view it is desirable to have a plug-attachment which is as short, and which provides a radial clearance as large as possible. Fortunately, the limiting lubricant pressure of about 500 lbf in^{-2} required for the elimination of the need for surface treatment and the occurrence of pick-up can be generated at a comparatively slow draw speed of 15 ft min^{-1} . Communications with tube-drawing industrialists had indicated that the shortest length of the plug-attachment, i.e. 6in, and the range of radial clearances used in the experimental work are within industrially acceptable limits. Thus, as mentioned earlier, at typical industrial draw speeds the practical restrictions on the dimensions of the attachment can be relaxed. However, further increments in the radial clearance can be made at the expense of a longer length, which is less likely to pose practical problems in this case, by the use of a composite or stepped plug-attachment as shown by the theoretical solutions for these attachments. On the other hand, it is desirable to have lubricant pressures which are as high as possible since friction would then be lowest. Thus, the final design of the plug-attachment demands a compromise among all the governing factors.

That pick-up between the die and the tube did not occur even when the external surface of the initial tube was not roughened or coated suggest that the existing lubrication system is adequate. This is attributable to the lubricant film geometry at the die entry which encouraged a contribution to lubrication by hydrodynamic action. Smaller die semi-angles, as in the experimental determination

of the optimum die semi-angle, resulted in the external surface of the drawn tubes having higher CLA values and duller appearances. Thus the contribution to lubrication by hydrodynamic action at the die entry was more pronounced when the die-angle was small. The use of a Christopherson tube, which generated a high lubricant pressure at the die entry as in the case of the plug-attachment, increased the flow of lubricant into the metal deformation zone and increased the separation of the die and tube surfaces, thereby improving lubrication at this interface. Observations on the surface finish similar to those made with the smaller die semi-angles obtained when the generated lubricant pressure was higher.

Allowing for the decrease in the viscosity of the lubricant as a result of the heat conducted from the metal deformation zone, the theoretical lubricant pressures were in good agreement with those observed experimentally. A temperature rise in the lubricant at 0.91 in from the die of 1.4°C was observed in one draw. The theoretical lubricant pressures at a value of the lubricant viscosity corresponding to a temperature of between 1°C and 2°C above the laboratory ambient temperature were in good agreement with the experimental lubricant pressures. Again, this discrepancy occurred since the theory assumed isothermal conditions. The corresponding lubricant film thickness at the die entry was found to be typically in the region of $2\text{ }\mu\text{in}$. Thus, it may be concluded that under the experimental conditions the lubrication regime was one of "quasi-hydrodynamic". The validity of the theory was reinforced by the good agreement between lubricant pressures predicted by the present theory and those measured by Christopherson et al.⁽⁵⁾ in drawing mild steel wires at speed of up to 600 ft min^{-1} .

The theoretical results showed that the influences of the drawing conditions and the geometry of the Christopherson tubes on

the generation of the lubricant pressure and lubricant film thickness were similar to those observed for the plug-attachments. Thus, a full hydrodynamic lubrication regime can be achieved at higher values of the lubricant pressures, i.e. with higher draw speeds and more viscous lubricants, a longer length of the Christopherson tube and a smaller radial clearance. It was noted that when these parameters were increased or reduced as the case may be, it is possible to generate lubricant pressures exceeding the yield stress of the tube material. When this occurs, the tube deforms within the Christopherson tube, i.e. before entering the die, and the theoretical pressures are no longer valid.

CHAPTER 31 SUGGESTIONS FOR FURTHER WORK

CHAPTER 8: SUGGESTIONS FOR FURTHER WORK

Close collaboration with the tube-drawing industry throughout the course of the research had meant that the new technique of bore lubrication had been developed with design considerations for an immediate industrial application. However, owing to the limitation of resources in terms of time, materials and experimental equipment, and the potential of the technology based on the principle of the present development, further work is suggested in the following directions:

The experimental draw speed of 15 ft min⁻¹ was the maximum speed available on the hydraulic draw bench. Further increase in the draw speed is expected to generate a higher hydrodynamic lubricant pressure, which was demonstrated experimentally and theoretically to be the governing factor of the efficacy of the plug-attachment technique. On the other hand, the accompanied increase in the energy dissipation as a result of plastic deformation work and friction work is likely to have a more pronounced effect on the lubricant viscosity, which in turn has an adverse influence on the pressure generation. Thus, an investigation of the optimum draw speed, at which the opposing effects of the draw speed and the accompanied reduction in the lubricant viscosity as a result of the work conducted from the metal deformation zone are balanced, is suggested.

CHAPTER 8: SUGGESTIONS FOR FURTHER WORK

Close collaboration with the tube-drawing industry throughout the course of the research had meant that the new technique of bore lubrication had been developed with design considerations for an immediate industrial application. However, owing to the limitation of resources in terms of time, materials and experimental equipment, and the potential of further contributions to the metal-forming technology based on the principle of the present development, further work is suggested in the following directions:

The experimental draw speed of 15 ft min^{-1} was the maximum speed available on the hydraulic draw bench. Further increase in the draw speed is expected to generate a higher hydrodynamic lubricant pressure, which was demonstrated experimentally and theoretically to be the governing factor of the efficacy of the plug-attachment technique. On the other hand, the accompanied increase in the energy dissipation as a result of plastic deformation work and friction work is likely to have a more pronounced effect on the lubricant viscosity, which in turn has an adverse influence on the pressure generation. Thus, an investigation of the optimum draw speed, at which the opposing effects of the draw speed and the accompanied reduction in the lubricant viscosity as a result of the heat conducted from the metal deformation zone are balanced, is suggested.

The lubricant, EP 50, used in the experiments on the plug-attachment was selected on the basis that it was the most effective lubricant among those tested when drawing with conventional tools. The viscosity of EP 50 is also known to be very susceptible to temperature changes. Investigations, therefore, should be extended to the use of chemically suitable lubricants, with a high viscosity and possessing a thermally stable viscosity or an isoviscous characteristic.

Another possibility of enhancing the lubricant pressure is with the aid of hydrostatic pressure in addition to the hydrodynamic pressure induced by the drawing action. However, practical problems, especially when the diameter of the initial tube is small are easily envisaged.

The experimental work considered only one nominal percentage reduction in area and two sizes of the initial tube. Since a higher productivity is also concerned with a higher reduction per pass, it would be beneficial to investigate the effect of increasing the percentage reduction in area per pass and with tubes of other sizes. Additionally, since the technique was successful when drawing tubes of stainless steel, which generally falls into the "difficult to draw" category, there are reasons to believe that it will work equally well, if not better, with tubes of other materials. Thus, further work in this direction is also recommended.

In order to facilitate a convenient selection of the proper design of the plug-attachment to suit any particular drawing schedule, it is suggested that a series of nomographs be designed for this purpose, relating such factors as the initial size of the tube, percentage reduction in area desired, lubricant viscosity and draw speed to the lubricant pressure required, and hence to the dimensions and design of the most practical attachment.

The incorporation of the curvature on the plug has been proven

to be desirable. Obviously, the efficacy of this curvature bears some geometrical relations with the diameter of the tag, and the length and curvature of its shoulder. However, the question of the optimal curvature or profile remains to be answered. Savings in the cost of the carbide plug may be achieved by replacing the curved portion with a less expensive material such as tool steel, since this part of the plug is non-functional once drawing has commenced. An investigation in these two features of the new plug should be carried out.

Following the success of the present work, the apparent extension is the application of this lubrication technique to the case of tube-drawing on a floating-plug. A research project in this area, funded by the Science and Engineering Research Council, to be conducted in the George Alexander Laboratory is about to commence and there is no doubt that more will be heard of this in the near future.

In recent years there has been a continuing and increasing interest in the application of ultra-sonic vibrations to the tools in metal-forming, particularly metal-drawing operations. The reported advantages arising from such vibrations are those of a reduced working load, higher reduction per pass, reduced friction and friction related problems, and improved surface finish. Thus, it would appear that further advantages can be achieved by the application of ultra-sonic vibrations to the plug-attachment in tube-drawing.

The isothermal theory for the plug-attachment could be extended to include thermal effects on the lubricant viscosity and hence its influence on the generation of the lubricant pressure and lubricant film thickness. While it is recognised that such an extension to the present theory would pose a difficult mathematical problem, the

theoretical solutions would certainly be more realistic. Furthermore, it would allow a direct comparison between the theoretical and experimental optimum draw speeds, mentioned earlier.

From an academic point of view it would be interesting to study the influence of the lubricant pressure on the mechanics of the deformation process. Obviously, friction at the plug-tube interface would be lower with a higher lubricant pressure. However, not so obvious is the effect of this pressure on the deforming tube, particularly in the sink zone. A theoretical analysis of this nature would then be able to predict directly the plug force and draw force or draw stress for a given lubricant pressure.

APPENDIX A-14 REPORTING PAPER
"HYDRODYNAMIC LUBRICATION IN
THE TUBE-DRAW PROCESS"

Presented at the "International conference for the
production and processing of ferrous and non-ferrous
tube, pipe and tube products"

International Tube Association
Tube Asia '82
Singapore

awarded Certificate of Merit

APPENDIX A1: SUPPORTING PAPER

"HYDRODYNAMIC LUBRICATION IN
THE TUBE-DRAW PROCESS"

Presented at the "International conference for the
production and processing of ferrous and non-ferrous
tube, pipe and tube products"

International Tube Association
Tube Asia '82
Singapore

Awarded Certificate of Merit

HYDRODYNAMIC LUBRICATION IN THE TUBE-DRAW PROCESS

T B Lim and D H Sansome

SYNOPSIS

There is a continuing and increasing interest in the promotion of high pressure lubricant films in wire-drawing generated by, for example, hydrodynamic action or external pressurisation, and this interest is extending to tube-drawing. The creation of high hydrodynamic pressure at the die entry is very much dependent on the design of the Christopherson tube used. The present paper endeavours to predict the conditions under which in tube-drawing a high pressure can be generated in the lubricant film at the die-tube interface, using the Christopherson tube technique developed in the wire-drawing process.

The influence on the generation of hydrodynamic pressure, of geometrical features of the Christopherson tube, such as its length and the radial clearance between it and the undrawn tube, and drawing conditions such as the speed of drawing and lubricant viscosity, are analysed. Christopherson tubes having geometrical features other than a straight or a parallel internal surface have been considered also. Consequently, the equations relating the pressure generated in the lubricant film to geometrical features have been developed.

There is very good agreement between the theoretical predictions and experimental observations. Using the equations the optimum design of a Christopherson tube can be found for the tube-draw process.

INTRODUCTION

Efficient lubrication is essential in metal drawing processes and indeed in any metal-working process, not only to combat the resistance produced by friction but also to minimise or eliminate redundant work and metal transference from one surface to the other. Metal transference causes surface damage to the workpiece and rapid wear of the tools. This is a most important factor affecting productivity and production costs. The presence of a sufficiently thick or tenacious lubricant film, separating the work from the tool or tools therefore alleviates this problem significantly.

In wire drawing, hydrodynamic lubrication was first achieved by Christopherson and Naylor⁽¹⁾ by supplying the lubricant to the die entry at an elevated pressure comparable with the yield stress of the wire material. They proposed a relatively simple and self-acting arrangement by sealing a tube of diameter only slightly larger than the wire diameter onto the inlet side of the die and supplying a viscous lubricant through the tube at atmospheric pressure. As the undrawn wire is drawn through the tube and into the die its motion generates, by viscous action, a high lubricant pressure at the die entry. Consequently the lubricant flow rate through the metal deformation zone is increased, thereby introducing a thick lubricant film between the wire and the die. This brings about significant reductions in the draw force and the die wear. Their theoretical analysis was confined to the hydrodynamic pressure generated and the lubricant flow within the inlet tube. This has since been extended, together with considerations of the lubrication conditions in the plastic deformation zone by Tattersall⁽²⁾ and Osterle and Dixon⁽³⁾. Tattersall improved on the inadequacy in Christopherson and Naylor's theory so that the lubricant flow can be predicted from entirely independent variables. This was expressed in terms of the thickness of the lubricant film remaining on the drawn wire which was then utilised to

viscosity of the lubricant, the length of the Christopherson tube and the radial clearance between it and the undrawn tube, are analysed. Christopherson tubes having geometrical features other than a straight or a parallel internal surface have been considered also. The equations developed enable theoretical predictions to be compared with the experimental results. Consequently the optimum design of a Christopherson tube can be found for the tube-draw process.

predict the hydrodynamic pressure generated. However, theoretical predictions require the use of an arbitrary constant in order that they are compatible with experimental observations. This constant was attributed to the eccentricity of the wire with respect to the tube during drawing. Using the work of Tattersall, Chu⁽⁴⁾ contributed to the works in this area by presenting practicable charts for the design of the Christopherson tube.

In the tube-draw process hydrodynamic lubrication at the die-tube interface can therefore be promoted by exactly the same principles. The present paper endeavours to predict the conditions under which a sufficiently high lubricant film pressure can be generated in tube-drawing at the die entry, using the above technique. A comprehensive theoretical analysis of the mechanics of hydrodynamic lubrication is presented in this paper. It considers first, the lubrication conditions at the die entry up to the entry to the plastic region and is then extended to include a Christopherson tube.

It is well known that Reynolds equation forms the basis of the theory of hydrodynamic lubrication. However, it contains two dependent variables: namely, the pressure generated and the lubricant flow rate per unit width, such that neither of which can be predicted without knowledge of the other. The idea of expressing the lubricant flow rate in terms of the thickness of the lubricant film remaining on the drawn tube is not favoured since the increase in the temperature of the drawn tube (often exceeding 150°C) causes much of the lubricant to be evaporated. Moreover, this difficulty is aggravated by the need to consider the lubricant remaining on the bore surface of the drawn tube. Consequently, a different approach is adopted in which equations relating the hydrodynamic pressure generated in the lubricant film to the independent variables are developed. The influences, on the generation of hydrodynamic pressure, of these variables such as the draw speed, the

NOTATION

B	$\frac{h_2 \tan \alpha}{6\eta_0 \phi u} \cdot C$	γ	Equivalent yield stress of tube material in plane strain
C	$e^{-\phi P_2} - e^{-\phi Y}$	γ	Co-ordinate perpendicular to drawing direction
E_1	$\frac{6\eta_0 \phi u_1}{h_2} \frac{1}{h_1}$	ϵ	Logarithmic strain in tube
E_2	$\frac{6\eta_0 \phi u_2}{h_2} \frac{1}{h_2}$	η	Viscosity of lubricant at any pressure P
h	Lubricant film thickness	η_0	Viscosity of lubricant at atmospheric pressure
h_m	Constant in integrated Reynolds equation (equals lubricant film thickness at maximum pressure)	σ	Mean axial stress in tube
k	$\frac{h_1}{h_2} - 1$	ϕ	Viscosity-pressure exponent
l	Length of Christopherson tube		
P	Lubricant film pressure		
q	Volume rate of lubricant flow per unit circumference of tube		
r	Radius of tube		
u	Velocity of undrawn tube		
W	$\frac{6\eta_0 \phi u}{h_2}$		
X	$\frac{6\eta_0 \phi u}{h_2}$		
x	Co-ordinate parallel to drawing direction		
x_d	Horizontal distance from die entry to the origin defined in Figure (1)		
x_p	Horizontal distance from plane of initiation of plastic deformation to the origin defined in Figure (1)		

Subscripts

1, 2, 3, Refer to conditions in the zones as shown in the figures.

THEORY

The following assumptions are made in the theoretical analysis:

1. The lubricant film thickness is sufficiently thin so that the one-dimensional Reynolds equation for a plane wedge can be applied.
2. The lubricant has Newtonian properties.
3. Isothermal conditions prevail.
4. The die remains rigid and the tube material is rigid plastic.
5. The undrawn tube travels concentrically with respect to the Christopherson tube.
6. The lubricant obeys the exponential viscosity - pressure law, $\eta = \eta_0 e^{\phi P}$

There are two variables which are directly indicative of the efficacy of the Christopherson tube; namely the pressure generated in the lubricant film and the volume rate of lubricant flow per unit circumference of the tube. These are the two unknown features of the Reynolds equation, which forms the basis of hydrodynamic lubrication. It is therefore advantages to develop equations, for tube-drawing, which can predict their magnitudes from entirely independent variables.

In the theoretical analysis three main zones are considered. These are the plastic deformation zone, the zone between the die entry and the entry to the plastic deformation zone, and the zone or zones comprising the Christopherson tube. The first task is to develop the equation depicting the lubricant film thickness at the entry to the plastic deformation zone. This is then integrated into the equation for the volume rate of lubricant flow. Since the continuity of flow demands that the rate of lubricant flow within the entire arrangement is constant, its knowledge therefore facilitates the development of an equation for the hydrodynamic pressure generated at the die entry. This equation permits the pressure to be predicted from entirely independent variables. Its

validity can be verified by comparing theoretical predictions with experimental observations.

Lubricant film thickness at entry to the plastic deformation zone

With reference to the origin chosen as in Figure (1), the integral form of Reynolds equation is

$$\frac{dP}{dx} = -6\eta_0 u_3 \left(\frac{h - h_m}{h^3} \right) \quad (1)$$

Taking into account the exponential viscosity-pressure relationship $\eta = \eta_0 e^{\phi P}$, this may be written as

$$e^{-\phi P} \frac{dP}{dx} = -6\eta_0 u_3 \left(\frac{h - h_m}{h^3} \right) \quad (2)$$

The film thickness at any point in the die entry region (zone 3) is given by

$$h = x \tan \alpha \quad (3)$$

Substituting this expression into equation (2) and upon integration it yields

$$P = -\frac{1}{\phi} \ln \left[\frac{6\eta_0 \phi u_3}{\tan \alpha} \left(-\frac{1}{x} + \frac{h_m}{2x^2 \tan \alpha} \right) - \phi A \right] \quad (4)$$

where A is the constant of integration.

The boundary conditions for this equation are $P = P_2$ at $x = x_d$.

Thus

$$A = \frac{1}{\phi} \left[\frac{6\eta_0 \phi u_3}{2 \tan \alpha} \left(-\frac{1}{x_d} + \frac{h_m}{2x_d^2 \tan \alpha} \right) - e^{-\phi P_2} \right] \quad (5)$$

and

$$P = -\frac{1}{\phi} \ln \left(\frac{6\eta_0 \phi u_3}{2 \tan \alpha} \left[\left(-\frac{1}{x} + \frac{h_m}{2x^2 \tan \alpha} \right) - \left(-\frac{1}{x_d} + \frac{h_m}{2x_d^2 \tan \alpha} \right) \right] + e^{-\phi P_2} \right) \quad (6)$$

If yielding initiates at a point where $x = x_p$ and $h = h_3$, the hydrodynamic pressure P can be equated to the yield stress of the tube material Y . Substituting these conditions into equation (6)

$$Y = -\frac{1}{\phi} \ln \left(\frac{6\eta_0 \phi u_3}{2 \tan \alpha} \left[\left(-\frac{1}{x_p} + \frac{h_m}{2x_p^2 \tan \alpha} \right) - \left(-\frac{1}{x_d} + \frac{h_m}{2x_d^2 \tan \alpha} \right) \right] + e^{-\phi P_2} \right) \quad (7)$$

This can be rearranged and written as

$$h_m = \frac{2 \tan \alpha (x_p x_d)}{(x_p + x_d)} + \frac{\tan^3 \alpha (x_p x_d)^2}{3\eta_0 \phi u_3 (x_p^2 - x_d^2)} \cdot C \quad (8)$$

where $C = (e^{-\phi P_2} - e^{-\phi Y})$

By equation (3), $x_d = \frac{h_2}{2}$ and $x_p = \frac{h_3}{2 \tan \alpha}$, hence

$$h_m = \frac{2h_2 h_3}{(h_2 + h_3)} + \frac{\tan \alpha (h_2 h_3)^2}{3\eta_0 \phi u_3 (h_2^2 - h_3^2)} \cdot C \quad (9)$$

The volume rate of flow, q , per unit circumference of the tube in terms of the pressure gradient $\frac{dp}{dx}$ is obtained by

$$q = \frac{uh}{2} + \frac{h^3}{12\eta} \frac{dp}{dx} \quad (10)$$

Substituting for $\frac{dp}{dx}$ as in equation (1), the volume rate of flow per unit circumference of the tube in the die entry zone is given by

$$q_3 = \frac{u h}{2} \quad (11)$$

The mean axial stress in the tube, the lubricant film pressure, and the yield stress of the tube material are related by the yield criterion

$$\sigma + P = Y \quad (12)$$

At the entry to the plastic deformation zone, the mean axial tensile stress in the tube is equal to the plastic work done per unit volume.

Thus

$$\sigma = \int_0^E Y \, d\epsilon, \quad \frac{d\sigma}{d\epsilon} = Y \quad (13)$$

From equations (12) and (13),

$$\frac{dp}{d\epsilon} = \frac{dY}{d\epsilon} - Y \quad (14)$$

In the plastic deformation zone

$$dx = dr \cot \alpha \quad (15)$$

$$d\epsilon = \frac{2dr}{r} \quad (16)$$

Hence
$$d\epsilon = \frac{2dx \tan \alpha}{r} \quad (17)$$

Substituting for $d\epsilon$ as in equation (17) and rearranging equation (14)

$$\frac{dp}{dx} = \left(\frac{r dy}{2 dx \tan \alpha} - y \right) \frac{2 \tan \alpha}{r} \quad (18)$$

when $\alpha=0$ as at the plane considered, $\frac{dp}{dx} = 0$. Hence the application of equation (10) for the volume rate of flow reduces to

$$q_3 = \frac{u_3 h_3}{2} \quad (19)$$

It follows from equations (11) and (19) that

$$h_m = h_3 \quad (20)$$

A good approximation to the lubricant film thickness at the entry to the plastic deformation zone can therefore be obtained by equating h_3 to h_m in equation (9). This can be simplified and rearranged as a quadratic in h_3

$$h_3^2 - h_3 \left(2h_2 + \frac{h_2^2 \tan \alpha}{3\eta_0 \phi u_3} \cdot C \right) + h_2^2 = 0 \quad (21)$$

Since the film thickness must take a positive value, it can be seen that the solution of this quadratic equation is

$$h_3 = h_2 \left\{ 1 + B \left(1 - \sqrt{1 + \frac{2}{B}} \right) \right\} \quad (22)$$

where $B = \frac{h_2 \tan \alpha}{6\eta_0 \phi u_3} \cdot C$

Alternatively equation (22) may be written

$$h_3 = \frac{h_2}{2B} \left(1 - \frac{1}{B} + \frac{5}{4B^2} - \frac{7}{4B^3} \dots \right) \quad (23)$$

It can be shown that typical values of B under practicable drawing conditions exceed 10^3 . These values are of considerable magnitude and hence equation (23) may be approximated to read

$$h_3 \approx \frac{3\eta_0 \phi u_3}{\tan \alpha \left(e^{-\phi P_2} - e^{-\phi Y} \right)} \quad (24)$$

It should be noted that P_2 in equation (24) is the lubricant film pressure at the die entry generated by the Christoperson tube.

Analysis of Christoperson tubes

The two basic shapes of the internal surface of the Christoperson tubes considered in the theoretical analysis are 1) parallel and 11) tapered. These are illustrated in zone 2 of Figure (2). The analysis is extended to include a parallel or tapered portion as shown in zone 1, thus forming a stepped or composite internal surface.

The origins of the co-ordinate systems are chosen at the beginning of each zone so that Reynolds equation for the lubricant film pressure gradient at any point, taking into account the increase in viscosity due

to pressure, can be written as

$$e^{-\phi P} \frac{dP}{dx} = \frac{12\eta_0}{h^3} \left(\frac{uh}{2} - q \right) \quad (25)$$

Hydrodynamic pressure generated by a parallel Christopherson tube

Applying this equation to a parallel Christopherson tube in zone 2

and integrating between the limits $x = 0$ and $x = l_2$,

$$e^{-\phi P_2} = 1 - \frac{12\eta_0 \phi l_2}{h_2^3} \left(\frac{u h_2}{2} - q_2 \right) \quad (26)$$

or

$$P_2 = -\frac{1}{\phi} \ln \left[1 - \frac{12\eta_0 \phi l_2}{h_2^3} \left(\frac{u h_2}{2} - q_2 \right) \right]$$

The continuity of flow demands that $q_2 = q_3$ and by equation (19), equation (26) may be simplified to read

$$e^{-\phi P_2} = 1 - \frac{6\eta_0 \phi l_2}{h_2^3} (h_2 - h_3) \quad (27)$$

the subscripts for the velocity terms are omitted since the velocity of the undrawn tube in these zones is unaltered. An equation depicting the pressure generated at the die entry can therefore be obtained by substituting equation (24) for h_3 in equation (27), viz.

$$e^{-\phi P_2} = 1 - \frac{6\eta_0 \phi l_2}{h_2^3} \left[h_2 - \frac{3\eta_0 \phi u}{\tan \alpha (e^{-\phi P_2} - e^{-\phi Y})} \right] \quad (28)$$

This can be rearranged as a quadratic in $e^{-\phi P_2}$ to give

$$e^{-\phi P_2} \left[\frac{6\eta_0 \phi l_2}{h_2^3} (e^{-\phi Y} + 1 - E_2) + (e^{-\phi Y} - e^{-\phi Y} - \frac{E_2^2 h_2}{2 l_2 \tan \alpha}) \right] = 0 \quad (29)$$

$$\text{where } E_2 = \frac{6\eta_0 \phi u l_2}{h_2^3}$$

The solution to this quadratic equation is

$$e^{-\phi P_2} = \frac{1}{2} \left\{ (e^{-\phi Y} + 1 - E_2) + \sqrt{(e^{-\phi Y} - 1)^2 + 2E_2(e^{-\phi Y} + \frac{E_2 h_2}{l_2 \tan \alpha} + \frac{E_2}{2} - 1)} \right\} \quad (30)$$

hence

$$P_2 = -\frac{1}{\phi} \ln \left\{ \frac{1}{2} \left[(e^{-\phi Y} + 1 - E_2) + \sqrt{(e^{-\phi Y} - 1)^2 + 2E_2(e^{-\phi Y} + \frac{E_2 h_2}{l_2 \tan \alpha} + \frac{E_2}{2} - 1)} \right] \right\} \quad (31)$$

In practice the yield stress of a metal is of a considerable magnitude. Therefore depending on the value of the viscosity-pressure exponent the term $e^{-\phi Y}$ may be insignificant. Under these conditions the pressure generated may be reduced without loss of accuracy to read

$$P_2 = -\frac{1}{\phi} \ln \left\{ \frac{1}{2} \left[(1 - E_2) + \sqrt{1 + 2E_2 \left(\frac{E_2 h_2}{l_2 \tan \alpha} + \frac{E_2}{2} - 1 \right)} \right] \right\} \quad (32)$$

Consider the case of a tapered Christopherson tube in zone 2. If h is the lubricant film thickness at any point within this zone, by simple geometry

$$\frac{h_1 - h_2}{x} = \frac{h_1 - h_2}{l_2} \quad (35)$$

$$h = h_2 \left(1 + k - \frac{k}{l_2} x \right) \quad (36)$$

$$\text{where } k = \frac{h_1 - h_2}{h_2} \quad \text{i.e. } \frac{h_1}{h_2} = 1 + k \quad (37)$$

Substituting equation (36) for h in equation (25), the pressure gradient of a tapered Christopherson tube is

$$e^{-\phi P_2} \frac{dP_2}{dx} = 12\eta_0 \left[\frac{u_2}{2h_2^2 (1+k - \frac{k}{l_2} x)^2} - \frac{q_2}{h_2^2 (1+k - \frac{k}{l_2} x)^3} \right] \quad (38)$$

Integrating between the limits $x = 0$ and $x = l_2$ and simplifying,

$$e^{-\phi P_2} = 1 - \frac{6\eta_0 \phi l_2}{h_2^2 (1+k)} \left[u_2 h_2 - q_2 \left(\frac{2+k}{1+k} \right) \right] \quad (39)$$

$$P_2 = -\frac{1}{\phi} \ln \left(1 - \frac{6\eta_0 \phi l_2}{h_2^2 (1+k)} \left[u_2 h_2 - q_2 \left(\frac{2+k}{1+k} \right) \right] \right)$$

Applying the conditions that $q_2 = q_3$ and $u_2 = u_3$, by equation (19), equation (39) may be simplified to read

Theoretical length and length-clearance ratio of the parallel Christopherson tube

Equation (28) shows that the hydrodynamic pressure generated at the die entry is proportional to the length of the Christopherson tube. Its length required to generate a desired pressure under a given set of drawing conditions can therefore be computed, viz.

$$l_2 = (1 - e^{-\phi P_2}) \left(W \left[1 - \frac{W h_2}{2 \tan \alpha (e^{-\phi P_2} - e^{-\phi Y})} \right] \right)^{-1} \quad (33)$$

$$\text{where } W = \frac{6\eta_0 \phi u}{h_2^2}$$

Alternatively for the purpose of tool design it may be more desirable to express the length-radial clearance ratio in terms of the other parameters. Hence

$$\frac{l_2}{h_2} = (1 - e^{-\phi P_2}) \left(X \left[1 - \frac{X}{2 \tan \alpha (e^{-\phi P_2} - e^{-\phi Y})} \right] \right)^{-1} \quad (34)$$

$$\text{where } X = \frac{6\eta_0 \phi u}{h_2}$$

$$e^{-\phi P_2} = 1 - \frac{6\eta_0 \phi u_1}{h_2^3 (1+k)} \left[h_2 - \frac{h_3}{2} \left(\frac{2+k}{1+k} \right) \right] \quad (40)$$

Hence the equation for the pressure generated at the die entry is obtained by substituting equation (24) for h_3 in equation (40),

$$e^{-\phi P_2} = 1 - \frac{6\eta_0 \phi u_1}{h_2^3 (1+k)} \left[h_2 - \frac{3\eta_0 \phi u_1}{2 \tan \alpha (e^{-\phi P_2} - e^{-\phi Y} \frac{2+k}{1+k})} \right] \quad (41)$$

As in the case of a parallel Christopherson tube the last equation can be rearranged as a quadratic in $e^{-\phi P_2}$ to give

$$e^{-\phi P_2} \left[\frac{2}{h_2^3} (e^{-\phi P_2} - e^{-\phi Y} \frac{2+k}{1+k}) \right] + \left[e^{-\phi Y} - e^{-\phi Y} \frac{E_2}{(1+k)} - \frac{E_2^2 h_2 (2+k)}{4 l_2^2 (1+k)^2 \tan \alpha} \right] = 0 \quad (42)$$

where, as before, $E_2 = \frac{6\eta_0 \phi u_1}{h_2^2}$

It is worth mentioning that when $(1+k) = 1$ i.e. $\frac{h_1}{h_2} = 1$, equation (42) reduces to equation (29) where the Christopherson tube is parallel.

The solution to this quadratic equation is

$$e^{-\phi P_2} = \frac{1}{2} \left((e^{-\phi Y} + 1 - \frac{E_2}{1+k}) \pm \sqrt{(e^{-\phi Y} - 1)^2 + \frac{2E_2}{(1+k)} \left[e^{-\phi Y} + \frac{E_2 h_2 (2+k)}{2 l_2^2 \tan \alpha (1+k)} + \frac{E_2}{2(1+k)} - 1 \right]} \right) \quad (43)$$

hence

$$P_2 = -\frac{1}{\phi} \ln \left[\frac{1}{2} \left((e^{-\phi Y} + 1 - \frac{E_2}{1+k}) \pm \sqrt{(e^{-\phi Y} - 1)^2 + \frac{2E_2}{(1+k)} \left[e^{-\phi Y} + \frac{E_2 h_2 (2+k)}{2 l_2^2 \tan \alpha (1+k)} + \frac{E_2}{2(1+k)} - 1 \right]} \right) \right] \quad (44)$$

It was mentioned previously that the value of the viscosity-pressure exponent may be such that the term $e^{-\phi Y}$ is insignificant. Hence,

$$P_2 = -\frac{1}{\phi} \ln \left[\frac{E_2}{2} \left((1 - \frac{E_2}{1+k}) \pm \sqrt{1 + \frac{2E_2}{1+k} \left(\frac{E_2 h_2 (2+k)}{2 l_2^2 \tan \alpha (1+k)} + \frac{E_2}{2(1+k)} - 1 \right)} \right) \right] \quad (45)$$

Theoretical length of a tapered Christopherson tube

The length of a tapered Christopherson tube required to generate a desired pressure at the die entry under a given set of drawing conditions can be computed from equation (41). This can be rearranged and simplified to give

$$l_2 = (1 - e^{-\phi P_2}) \left[\frac{W}{(1+k)} \left(1 - \frac{W h_2 (2+k)}{4(1+k) \tan \alpha (e^{-\phi P_2} - e^{-\phi Y})} \right) \right]^{-1} \quad (46)$$

where $W = \frac{6\eta_0 \phi u_1}{h_2^2}$

From this equation is calculated a tube which is longer by a factor of $(1+k)$ to generate the same pressure at the die entry when compared with a parallel tube.

Hydrodynamic pressure generated by a two-zone Christopherson tube

The analysis so far was confined to zone 2 where the Christopherson tube is either wholly parallel or tapered. This can be extended to include zone 1 (Figure 2) thus forming a two-zone Christopherson tube, in conjunction with the parallel portion in zone 2. This consists of either another parallel portion resulting in the stepped configuration or a tapered portion to form the composite configuration. Their relevance will be discussed in a later section.

The stepped Christopherson tube

This consists of a parallel portion in zone 1 in series with that in zone 2, but with a larger radial clearance. In this zone the analysis for a parallel Christopherson tube applies. Hence

$$P_1 = -\frac{1}{\phi} \ln \left[(e^{-\phi Y} + 1 - E_1) \pm \sqrt{(e^{-\phi Y} - 1)^2 + 2E_1(e^{-\phi Y} + \frac{E_1}{1} \tan \alpha + \frac{E_1}{2} - 1)} \right] \quad (47)$$

$$\text{where } E_1 = \frac{6\eta_0 \phi u_1}{h_1^2}$$

The pressure at the die entry is therefore the sum of P_1 and that described by equation (31). Hence

$$P_2 = P_1 - \frac{1}{\phi} \ln \left[(e^{-\phi Y} + 1 - E_2) \pm \sqrt{(e^{-\phi Y} - 1)^2 + 2E_2(e^{-\phi Y} + \frac{E_2}{1} \tan \alpha + \frac{E_2}{2} - 1)} \right] \quad (48)$$

The composite Christopherson tube

This consists of a tapered portion in zone 1 in series with a parallel portion in zone 2. The analysis for a tapered Christopherson tube applies. Hence

$$P_1 = -\frac{1}{\phi} \ln \left[(e^{-\phi Y} + 1 - \frac{E_1}{1+k}) \pm \sqrt{(e^{-\phi Y} - 1)^2 + \frac{2E_1}{(1+k)} (e^{-\phi Y} + \frac{E_1}{2} \tan \alpha(1+k) + \frac{E_1}{2(1+k)} - 1)} \right]$$

(49)

$$\text{where } E_1 = \frac{6\eta_0 \phi u_1}{h_2^2}$$

Thus the pressure generated at the die entry is the sum of P_1 and that described by equation (31). Hence

$$P_2 = P_1 - \frac{1}{\phi} \ln \left[(e^{-\phi Y} + 1 - E_2) \pm \sqrt{(e^{-\phi Y} - 1)^2 + 2E_2(e^{-\phi Y} + \frac{E_2}{1} \tan \alpha + \frac{E_2}{2} - 1)} \right] \quad (50)$$

$$\text{where } E_2 = \frac{6\eta_0 \phi u_2}{h_2^2}$$

Experimental Procedure

The tools used in the experimental work were set up as shown in Figure 3. The undrawn tube passed through a parallel Christopherson tube where the radial clearance was maintained at a constant value of 0.005 in. Four Christopherson tubes of the same internal diameter but of different lengths were used. These were 2.40 in, 5.41 in, 8.38 in and 11.39 in. Their original lengths were 2.5 in, 5.5 in, 8.5 in and 11.5 in respectively but were shortened as a result of modifications to accommodate an 'O' ring near the entry to the die. The same die and plug were used throughout and were made of tungsten carbide. The former had a semi-angle of 12.06° . The tubes drawn were of 347 stainless steel and had the same initial dimensions of 0.997 in outside diameter and 0.107 in wall thickness. The length of contact between the plug and the bore of the tube in the metal deformation zone was kept constant in each case draw. Hence the frictional conditions at this interface, which influence the draw force, were consistent. The lubricant used was a viscous chlorinated mineral oil; it was smeared onto the tube surfaces before each draw. A molybdenum disulphide impregnated nylon guide was mounted on the plug bar and took up a position in the bore of the undrawn tube in order to alleviate any undesired side movements during drawing. A mean draw speed of 15 ft min^{-1} was used.

The lubricant film pressures generated by the hydrodynamic action along the length of the Christopherson tubes were monitored by a piezoelectric pressure transducer. A thermocouple was mounted beside the pressure transducer with the hot junction immersed in the lubricant to monitor any temperature rise due to the heat conducted from the metal deformation zone and caused by viscous shear. An increase in the temperature is accompanied by a decrease in the viscosity of the lubricant and this could substantially reduce the pressure which would be generated. This procedure was discontinued when it became clear that the temperature

rise was small and had no apparent effect on the pressure.

Other parameters which are also indicative of the efficacy of the Christopherson tube in promoting hydrodynamic lubrication were also examined. These are the draw force or draw stress, which was measured by a load cell mounted on the carriage of the draw bench, and the surface finish produced, which was measured by a 'Tallysurf'. These are compared with the observations made when a tube was drawn with the same tools and under the same conditions but without the Christopherson tube.

Results and discussions

The results of these tests are presented in Table (1). The following items were common in each test and are recorded separately to avoid repetition:

1. Initial tube dimensions (od x t) = 0.997×0.107 in
2. Final tube dimensions (od x t) = 0.829×0.081 in
3. Mean draw speed = 15 ft min^{-1}
4. Percentage sink = 14.28%
5. Percentage reduction in area = 36.40%
6. Homogeneous strain = 0.377
7. Die semi-angle = 12.06°
8. Radial clearance between undrawn tube and Christopherson tube = 0.005 in
9. Lubricant = viscous chlorinated mineral oil
10. Tube material = 347 stainless steel
11. Mean yield stress of tube material in uniaxial tension
= $9.31 \times 10^4 \text{ lbf in}^{-2}$

In the absence of a knowledge of the viscosity-pressure exponent, ϕ , it was necessary to estimate its value. This was done by substituting the measured lubricant film pressure and the drawing conditions of a test into equation (28). The value of ϕ was estimated by numerical iteration and a value of $1.5 \times 10^{-5} \text{ in}^2 \text{ lbf}^{-1}$ was adopted in the theoretical calculations.

The lubricant film pressures measured and those predicted by equation (31) at a distance of 0.909 in from the die entry for four parallel Christopherson tubes of different lengths are presented in Figure (4). The pressure at the die entry can therefore be expected to be much higher. One distinct feature of the graph is the influence of temperature on the pressures generated. High temperatures reduce the viscosity of the lubricant thereby resulting in an adverse effect on the hydrodynamic action. This is substantiated by Figure (5) which shows the variation of the viscosity of the lubricant with temperature. With due consideration given to temperature and viscosity changes, Figure (4) shows that there is good agreement between theoretical predictions and experimental observations. It was thought that the experiments were conducted when the ambient temperatures were 12°C and 13°C . However, under the circumstances in which the temperature was measured (by a thermocouple and hence very sensitive to environmental changes eg. air circulation) the authors doubt the validity of the figures quoted. It is therefore very likely that the ambient temperature when drawing with the 2.40 in and 5.41 in Christopherson tubes was slightly higher than 12°C . The ambient temperature when drawing with the 11.39 in Christopherson tube was definitely higher than 12°C although it may not be exactly 13°C . Consequently this explains for the curve in the experimental graph.

A similar set of graphs are presented in Figure (6). The pressures concerned are those at a distance of 2.409 in from the die entry. It was expected that the pressures would be considerably lower than those

(1) Tube Number	(2) Length of Christopherson tube (in)	(3) Ambient temperature during drawing ($^\circ\text{C}$)	(4) Plug force (tonf)	(5) Draw force (tonf)	(6) Draw stress (tonf in ⁻²)	(7) Reduction in draw stress (%)	(8) Observed lubricant film pressure (lbf in ⁻²)	(9) Theoretical lubricant film pressure (lbf in ⁻²)
*874	-	15	0.74	7.42	38.98	-	-	-
Pressure transducer at 0.909 in from die entry								
S70a	2.40	13	0.74	7.18	37.72	3.23	355	440
S70b	2.40	12	0.74	7.18	37.72	3.23	376	480
S71	5.41	12	0.74	7.26	38.14	2.15	1385	1460
S72	8.38	15	0.69	7.02	36.88	5.39	1399	1885
S73a	11.39	14	0.74	7.34	38.56	1.08	-	2880
S73b	11.39	13	0.69	7.02	36.88	5.39	3079	3156
Pressure transducer at 2.409 in from die entry								
S75	5.41	17	0.69	7.26	38.14	2.18	308	630
S76	8.38	17	0.69	7.10	37.28	4.36	941	1255
S77	11.39	17	0.78	7.10	37.28	4.36	1171	1896

*Tube drawn without Christopherson tube

TABLE (1)

predicted and observed previously. It is apparent that the form of the graphs corroborate in both cases. The experiments were conducted within minutes of each other and consequently at the same ambient temperature. The experimental graph, which was obtained by the method of least squares, shows very good agreement with the theoretical graph at 21°C. For the reasons mentioned earlier it is postulated that the ambient temperature and hence the viscosity of the lubricant is in the vicinity of 21°C rather than the quoted 17°C.

The other distinctive features of these graphs are that the pressure generated is directly proportional to the length of the Christopherson tube and that the pressure gradient increases as the viscosity of the lubricant decreases. An increase in the lubricant film pressure increases the quantity of lubricant flowing through the metal deformation zone. This therefore reduces the friction at the die-tube interface and consequently reduces the draw force or the draw stress. The reduction in draw stress is defined as the difference between the draw stresses observed when drawing without and with a Christopherson tube, with the other factors being equal. The observed reduction in draw stress, expressed as a percentage of the draw stress observed when drawing without a Christopherson tube, corresponding to the length of the Christopherson tube used and hence the pressure generated are also shown in Figures (4) and (6). In both cases the highest reductions were observed with the longest Christopherson tube. These observations should ideally coincide but failed to do so as a result of the higher ambient temperature in the later experiments. These values range from 2.2% to 5.4% and when it is considered that friction is only a fraction of the draw force it will be realised that friction at the die surface has been reduced significantly.

It is common knowledge that hydrodynamic lubrication in metal working introduces a thick and tenacious lubricant film between the tool and work material interface. This results in a 'roughening' of the surface finish

of the worked material. In the present experiments it was observed that the surface finish of the drawn tubes became progressively rougher as the length of the Christopherson tube and hence the magnitude of the lubricant film pressure was increased.

Considerations for tool design and Christopherson tubes of other geometrical configurations

From the foregoing discussions it is apparent that hydrodynamic lubrication is associated with high lubricant film pressures. This is a function of the viscosity of the lubricant, speed of drawing and the length and radial clearance of the Christopherson tube as shown by equation (31) or (33). It will be useful to know how changes in the drawing conditions and the tool dimensions influence the hydrodynamic pressure generated. These are illustrated in Figure (7). For a given radial clearance it is seen that changes in the drawing conditions have a significant effect on the pressure gradient. For example, a pressure of 8000 lbf in⁻² will be generated at the die entry by a Christopherson tube 1.5 in long providing the radial clearance is 0.002 in when the reciprocal of the product $(\eta_0 u)^{-1}$ is 300 in lbf⁻¹. This product can represent a viscosity of 7×10^{-4} lbf s in⁻² when the velocity of the undrawn tube is about 4.8 in s⁻¹ or a draw speed of about 37 ft min⁻¹ at 35% reduction in area. When the viscosity is unaltered and the draw speed is changed such that the velocity of the undrawn tube is 2.0 in s⁻¹ i.e. $(\eta_0 u)^{-1} = 700$, then for a pressure of 8000 lbf in⁻² at the die entry a Christopherson tube 3.5 in long is required if the radial clearance is 0.002 in.

The influence of the radial clearance on pressure and the length requirement is even more significant. In the above example when the radial clearance is increased to 0.004 in with $(\eta_0 u)^{-1}$ remaining at 300 lbf in⁻¹, it will be seen that the length of the Christopherson tube

required is now 6 in in order to generate a pressure of 8000 lbf in⁻² at the die entry. Conversely it may be said that for a given length the Christopherson tube with a small radial clearance generates a much higher pressure at the die entry.

Due to this 'wedging' effect on the mechanism of pressure generation the die semi-angle also has a significant influence. This can be deduced from equation (33) which depicts the length of the Christopherson tube. It can be seen that the length required to generate a given pressure decreases as the die semi-angle decreases. However, it should be borne in mind that there is an optimum die semi-angle for a given percentage reduction in area. This is the angle at which the redundant work done in deformation and work done against friction are balanced, since a larger semi-angle increases the former but reduces the latter and vice-versa. For the tube material and the reduction in area considered in the theoretical and experimental work, a semi-angle of about 12° had been deduced previously.

Also shown in Figure (7) are two graphs which have been deduced theoretically under drawing conditions identical to those in the experimental work. The efficiency of the Christopherson tubes used is comparatively low and can be judged from the gradients of the graphs. This is attributable to the comparatively large radial clearance. However, even under these conditions the experimental observations suggest that a hydrodynamic lubrication regime has been introduced.

The radial clearance has proved to be a dominating factor in tool design. Consequently the introduction of a taper in the Christopherson tube, with other factors being equal, would reduce the magnitude of the pressure which could be generated by comparison with a parallel Christopherson tube. This is, of course, when the radial clearance at the end of the taper, i.e. the smaller end, is equal to the radial clearance of the parallel configuration. This effect is due to the

introduction of the the film thickness ratio $\frac{h_1}{h_2}$ i.e. (1+k) in equation (44) in the taper configuration and since this ratio is always larger than unity for a taper, it follows that the pressure generated will always be lower. A graphical illustration is presented in Figure (8). It is obvious that the pressure gradient decreases with increase in the film thickness ratio. An interesting feature in the illustration is that for a given pressure the required length of a tapered Christopherson tube is longer than that of a parallel tube by a factor equal to the film thickness ratio.

In practice situations may arise whereby the length and the radial clearance are limiting factors, eg. a long parallel Christopherson tube with a small radial clearance. Under these circumstances the desired pressure can be generated by employing a two zone Christopherson tube. This may consist of either two parallel portions in series, with the upstream portion providing a larger radial clearance, i.e. the stepped configuration or a parallel portion in series with a tapered portion, i.e. the composite configuration. The ratios of the lubricant film thickness and length of the two portions will play an important role in the pressure generation. A graphical illustration of their influences is presented in Figure (9) for four two zone Christopherson tubes with a 10 in overall length. These were deduced from equations (48) and (50). The pressure generated at the die entry decreases as the length ratio, $\frac{l_1}{l_2}$, is increased for both configurations. This is to be expected since a longer length is provided for the portion with a larger radial clearance. The stepped configuration generates a lower pressure since its radial clearance is larger.

CONCLUSIONS

A hydrodynamic theory for predicting the lubricant film pressure, using the Christopherson tube technique, has been developed for the tube-draw process. The theory predicts values of lubricant film pressure along the Christopherson tube in good agreement with those observed experimentally and extends to consider 'Christopherson' tubes having tapered, stepped and composite internal surfaces. Emphasis is placed on the hydrodynamic pressure generated at the die entry since hydrodynamic lubrication in the metal deformation zone is very much dependent on its magnitude. All other variables being equal the parallel Christopherson tube generates the highest pressure and hence is most efficient. However, the stepped and composite 'Christopherson' tubes can be useful when the required dimensions of a parallel tube become impractical.

The reduction of friction at the die-tube interface which is reflected by the observed reduction in draw stress and the 'roughening' of the surface finish of the drawn tubes indicate that a hydrodynamic lubrication regime can be introduced when the pressure at the die entry is only a fraction of the yield stress of the tube material. These range from about 320 lbf in^{-2} to 3760 lbf in^{-2} and were generated even by a relatively slow draw speed of 15 ft min^{-1} . The equivalent of the undrawn tube is approximately 9.5 ft min^{-1} or 1.9 in s^{-1} when drawing at 36.4% reduction in area. The changes in the lubrication regime may be first an improvement in boundary lubrication followed by a quasi-hydrodynamic regime and finally a full hydrodynamic regime as the pressure increases.

The hydrodynamic pressure is directly proportional to the length of the Christopherson tube, lubricant viscosity and velocity of the undrawn tube (which reflects on the draw speed) and inversely proportional to the die semi-angle and the radial clearance provided by the Christopherson

tube. Of these, the radial clearance has the most influence on the pressure. Using the equations developed the optimum design of a Christopherson tube can be found.

ACKNOWLEDGEMENTS

The authors would like to acknowledge the University of Aston in Birmingham and the Committee of Vice-Chancellors and Principals of the Universities of the United Kingdom (CVCP) for awarding one of the authors with a research scholarship, Fine Tubes Limited of Plymouth for providing the tools, tubes and lubricants, and last but not least Mrs Jeanette Neale for patiently typing the manuscript.

REFERENCES

- (1) CHRISTOPHERSON, D G and NAYLOR, H 'Promotion of fluid lubrication in wire-drawing' Proc. Instn. Mech. Engrs. 1955, 169, 643
- (2) TATTERSALL, G H 'Hydrodynamic lubrication in wire-drawing' Jnl. Mech. Engrg. Sci. 1961 3(No.4), 378
- (3) OSTERLE, J P and DIXON, J R 'Viscous lubrication in wire-drawing' Trans. American Soc. Lab. Engrs. 1962, 5, 233

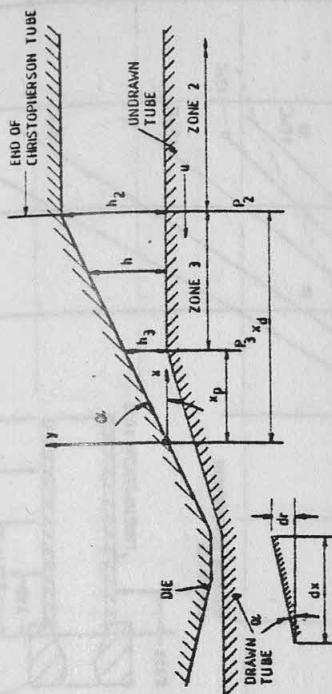


FIG (1)

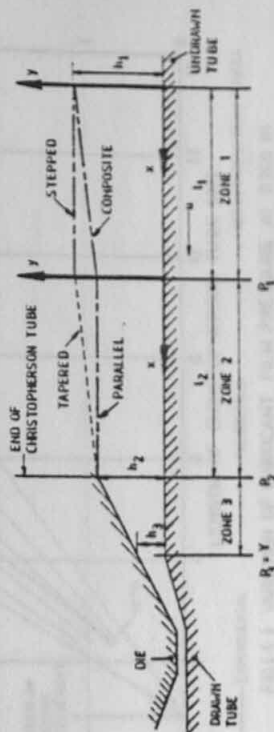


FIG (2)

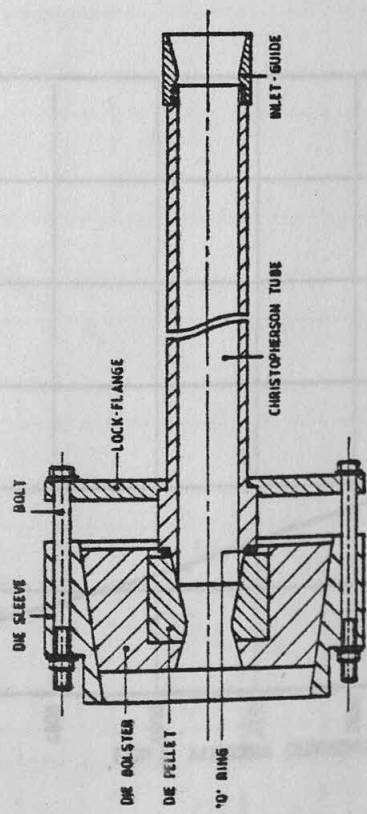


FIG (3) TOOL ARRANGEMENT

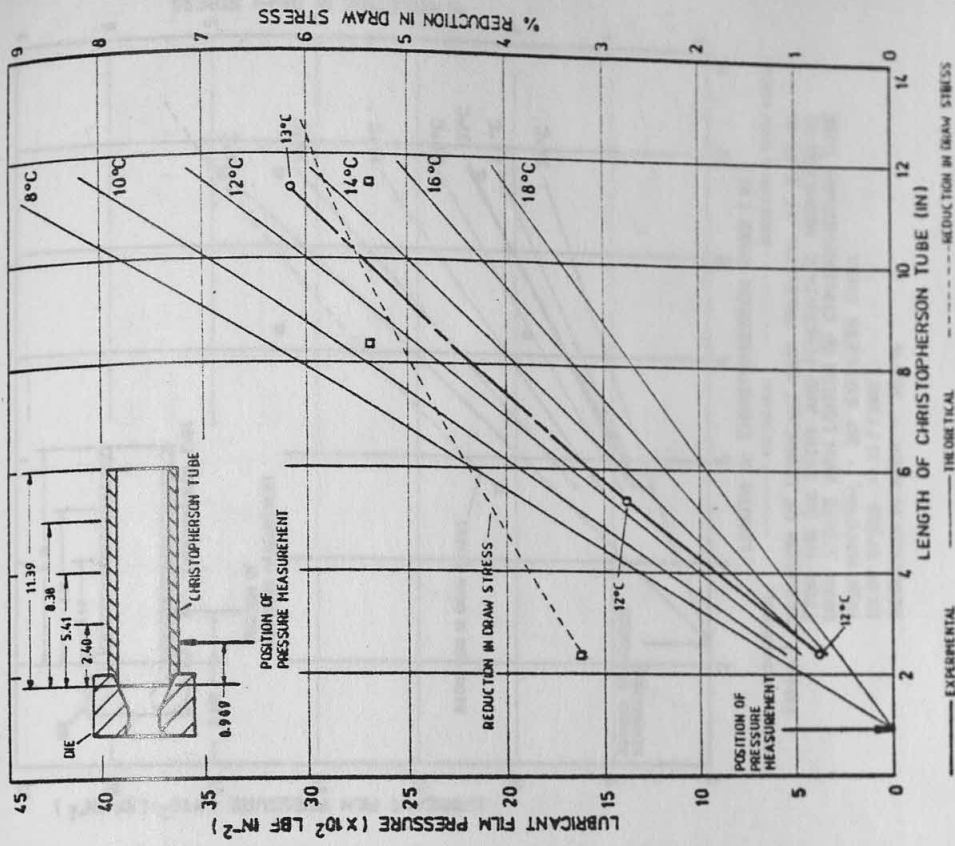


FIG (4) VARIATION OF LUBRICANT FILM PRESSURE AT 0.909 IN FROM THE DIE ENTRY AND PERCENTAGE REDUCTION IN DRAW STRESS WITH LENGTH OF CHRISTOPHERSON TUBE
TUBE MATERIAL : 347 STAINLESS STEEL
DRAW SPEED : 15 FT MIN⁻¹
REDUCTION IN AREA : 36.4 %

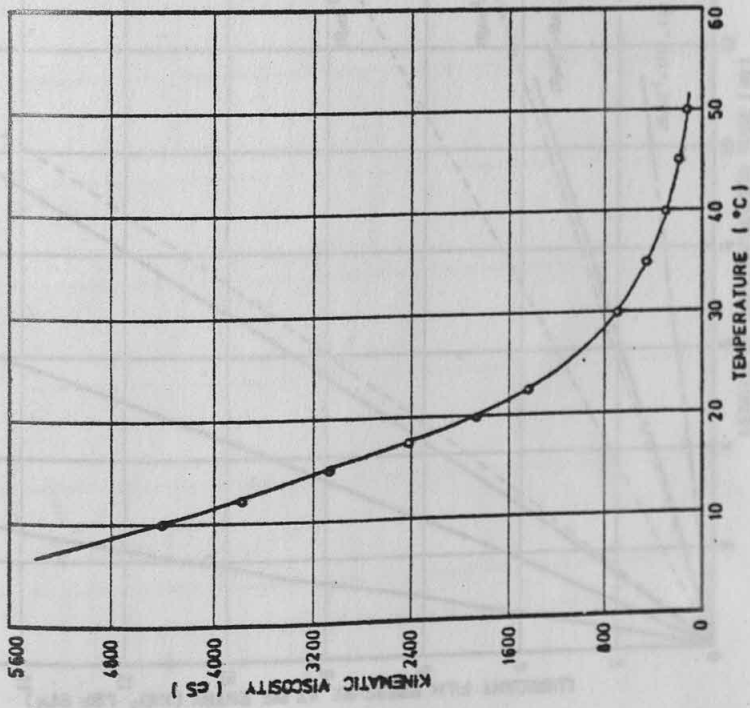
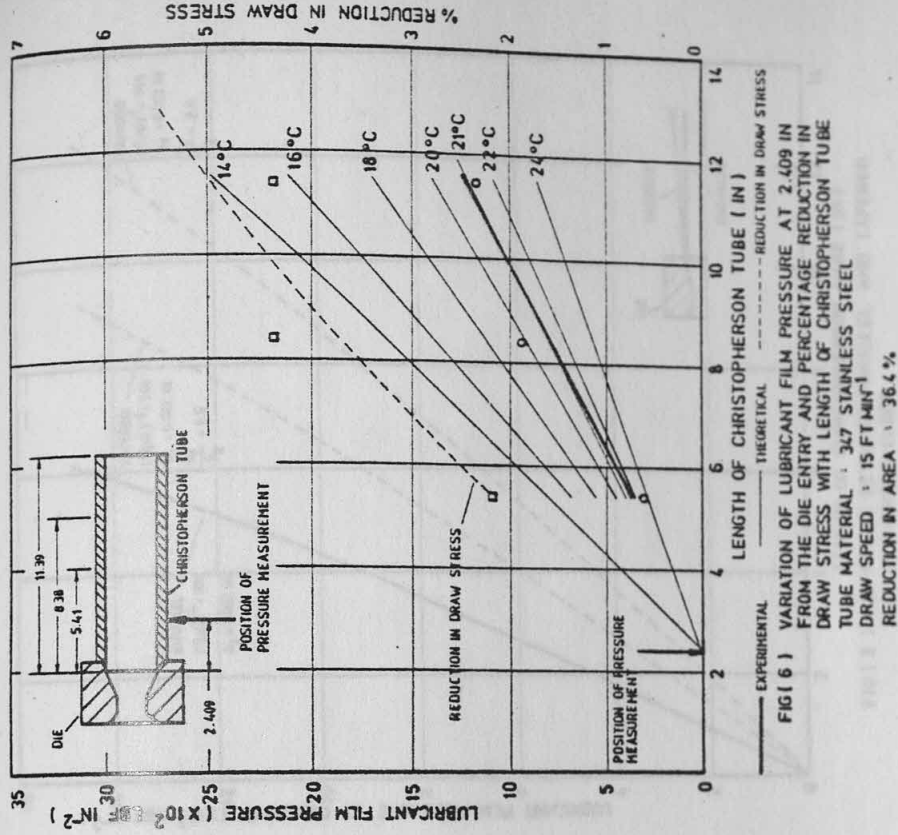
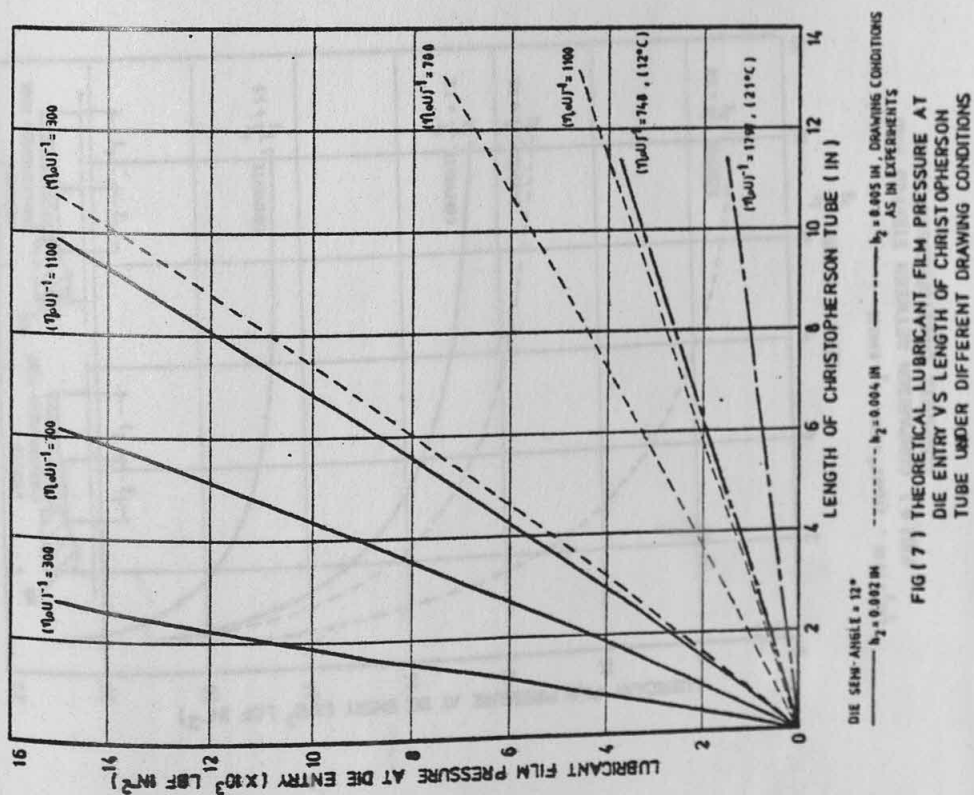
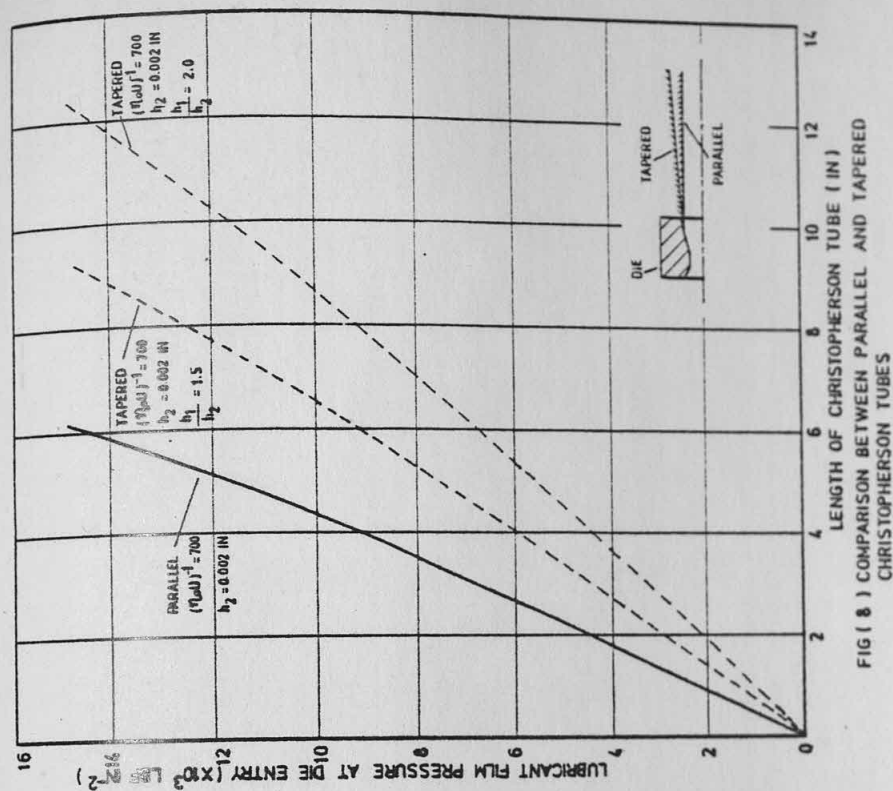
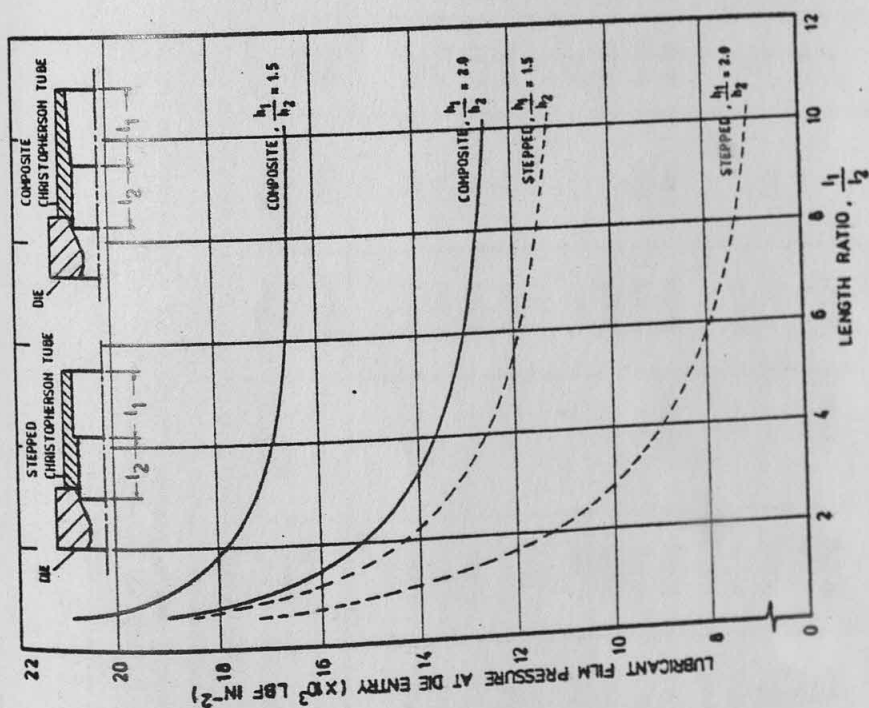


FIG 15) VISCOSITY-TEMPERATURE RELATIONSHIP FOR EP50







$l_1 l_2 = 10 \text{ IN}^2$, $(\pi \omega)^2 = 100$, $h_2 = 0.002 \text{ IN}$
 FIG (9) COMPARISON BETWEEN STEPPED AND COMPOSITE CHRISTOPHERSON TUBES

Draw speed = 15 ft min⁻¹
 Nominal die semi-angle = 15°
 Nominal initial tube dimensions = 1.0 x 0.10 in (outside diameter x wall-thickness)
 Initial tube external surface condition = ground
 Initial tube internal surface condition = grit-blasted
 Material = 347 stainless steel

Reduction in area (%)	Sink (%)	Total homo strain	Draw stress (tonf in ⁻²)	Plug force (tonf)	Tube temperature (°C)	Surface finish	
						Ext (μm)	Int (μm)
Lubricant = EP50							
40.2	17.5	0.388	43.8	0.556	137	0.2	0.025
36.3	14.3	0.364	38.2	0.602	115	0.25	0.025
32.6	11.7	0.288	33.1	0.741	99	0.12	0.03
25.8	7.9	0.230	25.4	0.694	85	0.08	0.05
Lubricant = TDN85							
38.7	17.5	0.397	41.5	0.556	133	0.2	0.025
35.6	14.5	0.355	38.5	0.694	125	0.23	0.01
30.0	11.6	0.282	32.3	0.648	105	0.085	0.05
22.4	8.5	0.190	25.3	0.648	89	0.12	0.06
Lubricant = 4% plastic in trichloroethylene							
40.2	17.5	0.419	43.4	0.648	140	1.5	0.03
36.2	14.3	0.364	38.2	0.556	125	0.9	0.02
32.2	11.4	0.316	36.0	-	115	0.85	0.03
23.6	8.6	0.204	27.8	0.787	-	0.8	0.035
Lubricant = EP50 + 14% plastic in trichloroethylene							
39.8	17.5	0.413	42.2	0.602	125	1.3	0.035
36.8	14.4	0.372	39.8	0.787	125	1.3	0.015
30.4	11.8	0.287	33.6	0.741	105	0.8	0.035
23.6	8.7	0.205	24.5	0.417	88	0.6	0.085
Lubricant = TDN85 + 14% plastic in trichloroethylene							
39.9	17.6	0.414	42.7	0.648	133	0.65	0.025
34.8	14.7	0.344	37.5	0.880	122	1.3	0.02
30.3	11.6	0.286	32.3	0.741	104	1.25	0.035
24.0	8.5	0.210	24.6	0.671	86	0.7	0.04

Table (A2.1) Assessment of basic drawing parameters using current industrial tools and lubricants

Draw speed = 15 ft min⁻¹
 Die semi-angle = 13.3°
 Lubricant = EP50
 Nominal initial tube dimensions = 1.0 x 0.10 in (outside diameter x wall-thickness)
 Initial tube external surface condition = ground
 Initial tube internal surface condition = grit-blasted
 Material = 347 stainless steel

Plug-tube contact length (in)	Draw stress (tonf in ⁻²)	Plug force (tonf)	Reduction in area (%)	Sink (Z)	Total homo strain	Surface finish	
						Ext (μm)	Int (μm)
0.102	32.6	0.65	29.7	11.3	0.285	0.32	0.04
0.206	32.9	0.69	30.8	11.2	0.299	0.20	0.03
0.351	34.0	0.74	31.0	11.5	0.302	0.15	0.035
0.465	35.6	0.79	31.7	11.4	0.311	0.25	0.02
0.711	35.6	0.79	32.4	11.4	0.321	0.23	0.035

Table (A2.2) Influence of plug-tube contact length on the draw stress and plug force

Draw speed = 15 ft min ⁻¹ Lubricant = EP50 Nominal initial tube dimension = 1.0 x 0.10 in (outside diameter x wall-thickness) Initial tube external surface condition = ground Initial tube internal surface condition = grit-blasted Material = 347 stainless steel						
Reduction in area (%)	Sink (%)	Total homogeneous strain	Draw stress (tonf in ⁻²)	Plug force (tonf)	Surface finish	
					External (μm)	Internal (μm)
Die semi-angle = 12.1°						
45.2	12.3	0.516	42.0	0.556	0.55	0.03
35.9	15.6	0.371	34.7	0.741	0.30	0.03
34.3	16.2	0.345	36.9	0.648	0.25	0.05
26.6	19.0	0.247	25.7	0.278	0.40	0.025
Die semi-angle = 10.0°						
44.8	12.4	0.516	45.0	0.671	0.25	0.03
34.2	16.2	0.354	36.2	0.810	0.30	0.025
33.0	16.6	0.338	35.2	0.694	0.21	0.03
25.4	19.4	0.240	25.2	0.324	0.25	0.025
Die semi-angle = 7.9°						
43.9	12.5	0.507	49.2	0.880	0.35	0.035
39.4	14.1	0.453	41.6	0.833	0.30	0.025
32.0	16.8	0.329	34.5	0.741	0.25	0.045
25.7	18.4	0.249	27.1	0.417	0.20	0.02
Die semi-angle = 6.1°						
44.7	12.4	0.524	51.3	1.019	0.60	0.035
37.1	15.0	0.405	41.1	0.880	0.50	0.025
33.2	16.3	0.350	36.4	0.833	0.50	0.045
27.0	18.5	0.269	28.5	0.509	0.50	0.04

Table (A2.3) Determination of the optimum die semi-angle

Draw speed = 15 ft min ⁻¹ Radial clearance, $h_2 = 0.0025$ in Die semi-angle = 12° Nominal sink = 15% Lubricant = EP50 Nominal initial tube dimensions = 1.0 x 0.10 in (outside diameter x wall-thickness) Initial tube external surface condition = ground Initial tube internal surface condition = grit-blasted Material = 347 stainless steel							
Reduction in area (%)	Total homogene- ous strain	Draw Stress (tonf in ⁻²)	Plug force (tonf)	Reduction in draw stress (%)	Reduction in plug force (%)	Internal surface finish at:	
						high plug force (μm)	low plug force (μm)
Straight-parallel plug-attachment, $l_2 = 7.5$ in							
*36.3	0.377	39.8	0.648	-	-	0.3	-
36.3	0.377	38.1	0.556	4.3	14.3	0.02	0.04
37.0	0.387	39.9	0.509	-	21.4	0.02	0.03
36.3	0.377	37.9	0.463	4.7	28.6	0.01	0.03
35.6	0.367	38.9	0.370	2.2	42.9	0.02	0.03
35.6	0.367	37.9	0.370	4.7	42.9	0.02	0.02
Composite plug-attachment, $l_1 + l_2 = 7.5$; $\frac{l_2}{l_1} = 0.5$; $\frac{h_1}{h_2} = 5.7$							
*36.4	0.378	38.1	0.602	-	-	0.05	-
36.4	0.378	36.5	0.214	4.4	64.5	0.10	0.15
36.4	0.378	37.3	0.278	2.2	53.8	0.06	0.13

* Tube drawn without plug-attachment

Table (A2.4) Preliminary results using the plug-attachment technique for bore lubrication

Draw speed = 15 ft min⁻¹

Die semi-angle = 12°

Lubricant : external surface = EP50

internal surface = EP50 plus paraffin

Nominal initial tube dimensions = 1.0 x 0.10 in (outside diameter x wall-thickness)

Initial tube external surface condition = ground

Initial tube internal surface condition = grit-blasted

Material = 347 stainless steel

Amount of paraffin in EP 50 (%)	Reduction in area (%)	Sink (%)	Total homogenous strain	Draw stress (tonf in ⁻²)	Plug force (tonf)
Conventional plug without attachment					
10	39.4	14.1	0.422	42.1	0.741
15	39.9	13.9	0.429	42.6	0.741
*20	39.9	13.9	0.429	43.0	0.833
20	36.4	14.8	0.378	38.1	0.556
*30	36.4	14.8	0.378	38.1	0.556
*30	36.4	14.8	0.378	39.0	0.556
Conventional plug with composite attachment, $l_1 + l_2 = 7.5$ in; $\frac{l_1}{l_2} = 0.5$; $\frac{h_1}{h_2} = 5.7$					
20	36.4	14.8	0.378	37.7	0.556
30	36.4	14.8	0.378	37.3	0.556
35	36.4	14.8	0.378	38.1	0.602
*40	36.4	14.8	0.378	39.0	0.648

* occurrence of chatter during drawing

Table (A2.5) Elimination of chatter using the plug-attachment technique for bore lubrication

Draw speed = 15 ft min⁻¹

Die semi-angle = 12°

Lubricant = EP50

Length of plug-attachment, $l_2 = 7.5$ in

Radial clearance, $h_2 = 0.0025$ in

Nominal initial tube dimensions = 0.995 x 0.110 in (outside diameter x wall-thickness)

Nominal final tube dimensions = 0.830 x 0.081 in (outside diameter x wall-thickness)

Reduction in area = 37.7%

Sink = 13.8%

Initial tube external surface condition = ground

Initial tube internal surface condition = grit-blasted

Material = 347 stainless steel

Hydrodynamic lubricant pressure		Draw stress (tonf in ⁻²)	Plug force (tonf)	Reduction in plug force (%)
Peak (lbf in ⁻²)	Mean (lbf in ⁻²)			
*	-	40.7	0.787	-
11041	5875	40.3	0.417	47.1
10244	6835	40.3	0.417	47.1
12634	7553	40.3	0.417 (0.324)	47.1 (58.8)

* tube drawn without attachment

Table (A2.6) Preliminary measurement of the hydrodynamic lubricant pressure generated by a straight-parallel plug-attachment

No.	Original surface finish, CLA (μm)	1st pass at 30.6% reduction		2nd pass at 31% reduction	
		Lubricant pressure (lbf in^{-2})	Plug force (tonf)	Surface finish, CLA (μm)	Surface finish, CLA (μm)
1	1.3	403	0.597	0.16	0.05
2	1.25	423	0.605	0.14	0.06
3	1.25	354	0.644	0.14	0.06
4	1.15	312	0.659	0.16	0.045
5	1.15	371	0.659	0.16	0.07
6	1.1	300	0.644	0.2	0.035
** 7	0.95	-	0.613	0.09	-
** 8	0.95	-	0.682	0.08	-
9	0.9	452	0.605	0.18	0.09
10	0.8	-	-	0.12	0.045
11	0.8	329	0.644	0.12	-
12	0.7	1379	0.520	0.12	-
13	0.7	1052	0.543	0.12	-
14	0.7	1488	0.551	0.14	0.06
15	0.65	287	0.659	0.14	0.04
16	0.65	370	0.613	0.12	0.04
17	0.6	318	0.628	0.1	0.05
18	0.6	297	0.628	0.14	-
19	0.6	860	0.605	0.16	0.06
20	0.58	704	0.597	0.12	0.04
21	0.55	927	0.605	0.12	-
22	0.55	670	0.605	0.12	-
23	0.55	325	0.651	0.1	0.02
24	0.55	257	0.628	0.14	0.02
25	0.5	810	0.558	0.12	0.035
26	0.45	826	0.628	0.14	0.035
27	0.3	-	-	0.14	0.03
28	0.25	349	0.620	0.16	0.05
					0.07

* Occurrence of pick-up

** Tube drawn without a plug-attachment

Table (A2.7) Hydrodynamic pressure, plug force and internal surface finish observed in tube-drawing with plug-attachments

Temperature ($^{\circ}\text{C}$)	Absolute dynamic viscosity (lbf s in^{-2})	Kinematic viscosity (cS)
1	4.787×10^{-3}	27076
2	4.068×10^{-3}	23008
3	3.468×10^{-3}	19614
4	2.965×10^{-3}	16772
5	2.543×10^{-3}	14385
6	2.188×10^{-3}	12374
7	1.887×10^{-3}	10676
8	1.633×10^{-3}	9236
9	1.417×10^{-3}	8013
10	1.232×10^{-3}	6971
11	1.075×10^{-3}	6080
12	9.399×10^{-4}	5316
13	8.240×10^{-4}	4661
14	7.242×10^{-4}	4096
15	6.379×10^{-4}	3608
16	5.633×10^{-4}	3186
17	4.986×10^{-4}	2820
18	4.423×10^{-4}	2501
19	3.932×10^{-4}	2224
20	3.503×10^{-4}	1981
21	3.128×10^{-4}	1769
22	2.798×10^{-4}	1583
23	2.508×10^{-4}	1419
24	2.253×10^{-4}	1274
25	2.028×10^{-4}	1147
26	1.828×10^{-4}	1034
27	1.652×10^{-4}	934
28	1.495×10^{-4}	845
29	1.355×10^{-4}	766
30	1.231×10^{-4}	696

Table (A2.8) The viscosity of EP50 at various temperatures

Mean radial clearance, $h_2 = 0.004$ in
Laboratory ambient temperature = 21°C (viscosity of EP50 = 3.128×10^{-4} lbf in $^{-2}$)
Draw speed = 15 ft min $^{-1}$
Die semi-angle = 12°
Nominal initial tube dimensions = 1.000 x 0.110 in (outside diameter x wall-thickness)
Nominal final tube dimensions = 0.830 x 0.092 in (outside diameter x wall-thickness)
Reduction in area = 30.6%
Sink = 17.2%
Initial tube bore surface condition = grit-blasted
Material = 347 stainless steel

Length, l_2 (in)	Experimental lubricant pressure at 21°C (lbf in $^{-2}$)	Theoretical lubricant pressure at:				Experimental plug force (tonf)	Experimental draw stress (tonf in $^{-2}$)
		27°C (lbf in $^{-2}$)	28°C (lbf in $^{-2}$)	29°C (lbf in $^{-2}$)	30°C (lbf in $^{-2}$)		
5	-	675	608	549	497	-	-
5.9	704	803	723	652	590	0.597	30.25
5.9	670	803	723	652	590	0.605	28.73
5.9	810	803	723	652	590	0.558	30.25
7.4	826	1022	919	830	748	0.628	29.11
7.4	860	1022	919	830	748	0.605	29.87
7.4	927	1022	919	830	748	0.605	29.49
8.9	1379	1248	1120	1008	909	0.520	29.49
8.9	1052	1248	1120	1008	909	0.543	30.25
8.9	1488	1248	1120	1008	909	0.551	29.49
10	-	1419	1272	1143	1030	-	-

Table (A2.9) Comparison between experimental and theoretical results for straight-parallel plug-attachments

Length, l_2 (in)	Theoretical lubricant film thickness, h_2 , at:			
	27°C ($\times 10^{-7}$ in)	28°C ($\times 10^{-7}$ in)	29°C ($\times 10^{-7}$ in)	30°C ($\times 10^{-7}$ in)
5	8.880	7.962	7.159	6.455
5.9	9.040	8.090	7.263	6.539
7.4	9.305	8.294	7.442	6.683
8.9	9.616	8.547	7.628	6.835
10	9.846	8.729	7.759	6.951

Table (A2.10) Theoretical lubricant film thickness at the end of sinking corresponding to the drawing conditions of Table (A2.9)

Mean radial clearance, $h_2 = 0.006$ in

Laboratory ambient temperature = 23°C (viscosity of EP50 = 2.508×10^{-4} lbf s in⁻²)

Draw speed = 15 ft min⁻¹

Die semi-angle = 12°

Nominal initial tube dimensions = 1.000 x 0.110 in (outside diameter x wall-thickness)

Nominal final tube dimensions = 0.830 x 0.092 in (outside diameter x wall-thickness)

Reduction in area = 30.6%

Sink = 17.2%

Initial tube bore surface condition = grit-blasted

Material = 347 stainless steel

Length, l_2 (in)	Experimental lubricant pressure at 23°C (lbf in ⁻²)	Theoretical lubricant pressure at:				Experimental plug force (tonf)	Experimental draw stress (tonf in ⁻²)
		29°C (lbf in ⁻²)	30°C (lbf in ⁻²)	31°C (lbf in ⁻²)	32°C (lbf in ⁻²)		
5	-	239	216	197	179	-	-
5.9	349	283	256	233	212	0.620	29.11
5.9	325	283	256	233	212	0.651	29.87
5.9	257	283	256	233	212	0.628	29.49
7.4	287	356	323	293	267	0.659	28.36
7.4	318	356	323	293	267	0.628	27.22
7.4	297	356	323	293	267	0.628	27.22
8.9	452	431	390	354	322	0.605	29.11
8.9	370	431	390	354	322	0.613	27.98
8.9	329	431	390	354	322	0.644	27.98
10	-	486	440	399	363	-	-

Table (A2.11) Comparison between experimental and theoretical results for straight-parallel plug-attachments

Length, l_2 (in)	Theoretical lubricant film thickness, h_4 , at:			
	29°C (x 10 ⁻⁷ in)	30°C (x 10 ⁻⁷ in)	31°C (x 10 ⁻⁷ in)	32°C (x 10 ⁻⁷ in)
5	6.858	6.208	5.633	5.120
5.9	6.899	6.243	5.661	5.143
7.4	6.954	6.301	5.708	5.182
8.9	7.042	6.360	5.744	5.222
10	7.096	6.404	5.793	5.252

Table (A2.12) Theoretical lubricant film thickness at the end of sinking corresponding to the drawing conditions of Table (A2.11)

Mean radial clearance, $h_2 = 0.007$ in Laboratory ambient temperature = 19°C (viscosity of EP50 = 3.932×10^{-4} lbf s in $^{-2}$) Draw speed = 15 ft min $^{-1}$ Die semi-angle = 12° Nominal initial tube dimensions = 1.000 x 0.110 in (outside diameter x wall-thickness) Nominal final tube dimensions = 0.830 x 0.092 in (outside diameter x wall-thickness) Reduction in area = 30.6% Sink = 17.2% Initial tube bore surface condition = grit-blasted Material = 347 stainless steel							
Length, l_2 (in)	Experimental lubricant pressure at 19°C (lbf in $^{-2}$)	Theoretical lubricant pressure at:				Experimental plug force (tonf)	Experimental draw stress (tonf in $^{-2}$)
		25°C (lbf in $^{-2}$)	26°C (lbf in $^{-2}$)	27°C (lbf in $^{-2}$)	28°C (lbf in $^{-2}$)		
5	-	263	237	213	193	-	-
5.9	312	311	280	253	228	0.659	29.11
5.9	300	311	280	253	228	0.644	29.11
7.4	354	393	353	318	287	0.644	27.22
7.4	371	393	353	318	287	0.659	27.22
8.9	403	475	427	385	347	0.597	26.84
8.9	423	475	427	385	347	0.605	26.09
10	-	536	481	433	391	-	-

Table (A2.13) Comparison between experimental and theoretical results for straight-parallel plug-attachments

Length, l_2 (in)	Theoretical lubricant film thickness, h_4 , at:			
	25°C ($\times 10^{-6}$ in)	26°C ($\times 10^{-7}$ in)	27°C ($\times 10^{-7}$ in)	28°C ($\times 10^{-7}$ in)
5	1.030	9.251	8.329	7.516
5.9	1.037	9.306	8.369	7.554
7.4	1.048	9.387	8.440	7.616
8.9	1.060	9.497	8.529	7.679
10	1.069	9.570	8.588	7.718

Table (A2.14) Theoretical lubricant film thickness at the end of sinking corresponding to the drawing conditions of Table (A2.13)

<p>Mean radial clearance, $h_2 = 0.0025$ in</p> <p>Laboratory ambient temperature = 20°C (viscosity of EP50 = 3.503×10^{-4} lbf s in⁻²)</p> <p>Draw speed = 15 ft min⁻¹</p> <p>Die semi-angle 12°</p> <p>Nominal initial tube dimensions = 0.830 x 0.093 in (outside diameter x wall-thickness)</p> <p>Nominal final tube dimensions = 0.687 x 0.078 in (outside diameter x wall-thickness)</p> <p>Reduction in area = 31.1%</p> <p>Sink = 17.4%</p> <p>Initial tube bore surface condition = as-drawn</p> <p>Material = 347 stainless steel</p>						
Length, l ₂ (in)	Experimental lubricant pressure at 20°C (lbf in ⁻²)	Theoretical lubricant pressure at:			Experimental plug force (tonf)	Experimental draw stress (tonf in ⁻²)
		27°C (lbf in ⁻²)	28°C (lbf in ⁻²)	29°C (lbf in ⁻²)	30°C (lbf in ⁻²)	
5	-	1858	1659	1488	1338	-
6	1846	2295	2043	1826	1638	22.82
6	1981	2295	2043	1826	1638	22.82
6	2263	2295	2043	1826	1638	25.54
7.5	2573	3004	2659	2365	2112	21.74
7.5	2458	3004	2659	2365	2112	22.82
9	3017	3790	3332	2947	2621	21.19
9	3012	3790	3332	2947	2621	21.74
10	-	4366	3818	3363	2980	-

Table (A2.15) Comparison between experimental and theoretical results for straight-parallel plug-attachments

Length, l ₂ (in)	Theoretical lubricant film thickness, h _d , at:			
	27°C (x 10 ⁻⁷ in)	28°C (x 10 ⁻⁷ in)	29°C (x 10 ⁻⁷ in)	30°C (x 10 ⁻⁷ in)
5	10.477	9.225	8.166	7.257
6	11.132	9.728	8.557	7.572
7.5	12.250	10.594	9.222	8.087
9	13.696	11.632	9.997	8.678
10	14.811	12.443	10.591	9.121

Table (A2.16) Theoretical film thickness at the end of sinking corresponding to the drawing conditions of Table (A2.15)

Mean radial clearance, $h_2 = 0.0045$ in Laboratory ambient temperature = 19°C (viscosity of EP50 = 3.932×10^{-4} lbf s in $^{-2}$) Draw speed = 15 ft min $^{-1}$ Die semi-angle = 12° Nominal initial tube dimensions = 0.830×0.093 in (outside diameter x wall-thickness) Nominal final tube dimensions = 0.687×0.078 in (outside diameter x wall-thickness) Reduction in area = 31.1% Sink = 17.4% Initial tube bore surface condition = as-drawn Material = 347 stainless steel						
Length, l_2 (in)	Experimental lubricant pressure at 19°C (lbf in $^{-2}$)	Theoretical lubricant pressure at:			Experimental plug force (tonf)	Experimental draw stress (tonf in $^{-2}$)
		25°C (lbf in $^{-2}$)	26°C (lbf in $^{-2}$)	27°C (lbf in $^{-2}$)		
5	-	649	583	524	-	-
6	620	786	705	634	0.500	30.43
6	726	786	705	634	0.500	30.43
7.5	890	997	893	802	0.440	29.34
7.5	859	997	893	802	0.436	29.34
9	1080	1214	1085	973	0.415	30.43
9	1217	1214	1085	973	0.396	29.89
10	-	1362	1217	1090	-	-

Table (A2.17) Comparison between experimental and theoretical results for straight-parallel plug-attachments

Length, l_2 (in)	Theoretical lubricant film thickness, h_4 , at:			
	25°C ($\times 10^{-7}$ in)	26°C ($\times 10^{-7}$ in)	27°C ($\times 10^{-7}$ in)	28°C ($\times 10^{-7}$ in)
5	10.878	9.702	8.709	7.825
6	11.087	9.885	8.842	7.930
7.5	11.395	10.146	9.032	8.081
9	11.742	10.403	9.268	8.274
10	12.009	10.590	9.419	8.394

Table (A2.18) Theoretical lubricant film thickness at the end of sinking corresponding to the drawing conditions of Table (A2.17)

<p>Mean radial clearance = 0.007 in</p> <p>Laboratory ambient temperature = 19°C (viscosity of EP50 = 3.932×10^{-4} lbf s in⁻²)</p> <p>Draw speed = 15 ft min⁻¹</p> <p>Die semi-angle = 12°</p> <p>Nominal initial tube dimensions = 0.830 x 0.093 in (outside diameter x wall-thickness)</p> <p>Nominal final tube dimensions = 0.687 x 0.078 in (outside diameter x wall-thickness)</p> <p>Reduction in area = 31.1%</p> <p>Sink = 17.4%</p> <p>Initial tube bore surface condition = as-drawn</p> <p>Material = 347 stainless steel</p>						
Length, l ₂ (in)	Experimental lubricant pressure at 19°C (lbf in ⁻²)	Theoretical lubricant pressure at:			Experimental plug force (tonf)	Experimental draw stress (tonf in ⁻²)
		25°C (lbf in ⁻²)	26°C (lbf in ⁻²)	27°C (lbf in ⁻²)	28°C (lbf in ⁻²)	
5	-	261	235	212	-	-
6	229	315	283	255	0.530	30.43
6	252	315	283	255	0.510	30.43
7.5	389	396	356	321	0.554	30.98
7.5	375	396	356	321	0.559	31.52
9	464	477	429	386	0.558	31.52
9	497	477	429	386	0.528	30.98
10	-	532	478	431	-	-

Table (A2.19) Comparison between experimental and theoretical results for straight-parallel plug-attachments

Length, l ₂ (in)	Theoretical lubricant film thickness, h ₄ , at:			
	25°C (x 10 ⁻⁷ in)	26°C (x 10 ⁻⁷ in)	27°C (x 10 ⁻⁷ in)	28°C (x 10 ⁻⁷ in)
5	10.309	9.262	8.340	7.526
6	10.371	9.323	8.390	7.567
7.5	10.503	9.417	8.466	7.617
9	10.622	9.514	8.544	7.692
10	10.703	9.579	8.597	7.734

Table (A2.20)

Theoretical lubricant film thickness at the end of sinking corresponding to the drawing conditions of Table (A2.19)

Position of pressure measurement = 0.91 in from die
 Radial clearance, h_2 = 0.006 in
 Laboratory ambient temperature = 12°C and 13°C (viscosity of EP50 = 9.399×10^{-4} and 8.240×10^{-4} lbf s in⁻² respectively)
 Draw speed = 15 ft min⁻¹
 Die semi-angle = 12°
 Nominal initial tube dimensions = 0.997 x 0.107 in (outside diameter x wall-thickness)
 Nominal final tube dimensions = 0.830 x 0.081 in (outside diameter x wall-thickness)
 Reduction in area = 36.3%
 Sink = 14.7%
 Initial tube external surface condition = ground
 Material = 347 stainless steel

Length, l_2 (in)	Experimental lubricant pressure at 12°C and 13°C (lbf in ⁻²)	Theoretical lubricant pressure at:				Experimental plug force (conf)	Experimental draw stress (tonf in ⁻²)
		10°C (lbf in ⁻²)	12°C (lbf in ⁻²)	14°C (lbf in ⁻²)	16°C (lbf in ⁻²)		
2.0	-	441	334	255	198	-	-
2.4	355 (13°C)	609	460	352	272	0.74	37.7
2.4	376 (12°C)	609	460	352	272	0.74	37.7
4.0	-	1327	989	750	577	-	-
5.4	1385 (12°C)	2018	1486	1117	854	0.74	38.1
7.0	-	2900	2100	1561	1184	-	-
9.0	-	4178	2948	2157	1620	-	-
11.4	3079 (13°C)	6085	4117	2945	2180	0.69	36.8
12.0	-	6652	4442	3156	2327	-	-

Table (A2.21) Comparison between experimental and theoretical lubricant pressure for straight-parallel Christopherson tubes at 0.91 in from the die

Length, l_2 (in)	Theoretical lubricant film thickness at die entry at:			
	10°C (x 10 ⁻⁶ in)	12°C (x 10 ⁻⁶ in)	14°C (x 10 ⁻⁶ in)	16°C (x 10 ⁻⁶ in)
2.0	5.137	3.809	2.876	2.204
2.4	5.265	3.879	2.916	2.228
4.0	5.849	4.188	3.087	2.326
5.4	6.478	4.501	3.253	2.419
7.0	7.385	4.921	3.468	2.536
9.0	8.951	5.571	3.778	2.698
11.4	12.000	6.619	4.234	2.923
12.0	13.112	6.946	4.365	2.985

Table (A2.22) Theoretical lubricant film thickness at the die entry corresponding to the drawing conditions of Table (A2.21)

Position of pressure measurement = 2.41 in from die Radial clearance, h_2 = 0.006 in Laboratory ambient temperature = 17°C (viscosity of EP50 = 4.986×10^{-4} lbf s in ⁻²) Draw speed = 15 ft min ⁻¹ Die semi-angle = 12° Nominal initial tube dimensions = 0.997 x 0.107 in (outside diameter x wall-thickness) Nominal final tube dimensions = 0.830 x 0.081 in (outside diameter x wall-thickness) Reduction in area = 36.3% Sink = 14.7% Initial tube external surface condition = ground Material = 347 stainless steel						
Length, l_2 (in)	Experimental lubricant pressure at 17°C (lbf in ⁻²)	Theoretical lubricant pressure at:			Experimental plug force (tonf)	Experimental draw stress (tonf in ⁻²)
		17°C (lbf in ⁻²)	19°C (lbf in ⁻²)	21°C (lbf in ⁻²)		
4.0	-	257	202	160	-	-
5.4	308	491	384	304	0.69	38.1
7.0	-	768	599	472	-	-
8.4	941	1020	792	623	0.69	37.3
10.0	-	1318	1019	799	-	-
11.4	1171	1590	1224	956	0.78	37.3
12.0	-	1710	1313	1025	-	-

Table (A2.23) Comparison between experimental and theoretical lubricant pressure for straight-parallel Christopherson tubes at 2.41 in from the die

Length, l_2 (in)	Theoretical lubricant film thickness at die entry at:			
	17°C (x 10 ⁻⁶ in)	19°C (x 10 ⁻⁶ in)	21°C (x 10 ⁻⁶ in)	23°C (x 10 ⁻⁶ in)
4.0	2.033	1.571	1.231	0.976
5.4	2.104	1.614	1.257	0.992
7.0	2.192	1.665	1.288	1.012
8.4	2.274	1.712	1.316	1.029
10.0	2.377	1.769	1.350	1.049
11.4	2.475	1.823	1.381	1.068
12.0	2.519	1.847	1.394	1.076

Table (A2.24) Theoretical lubricant film thickness at the die entry corresponding to the drawing conditions of Table (A2.23)

Position of pressure measurement = 3.41 in from die Radial clearance, h_2 = 0.007 in Laboratory ambient temperature = 21°C (viscosity of EP50 = 3.128×10^{-4} lbf s in ⁻²) Draw speed = 15 ft min ⁻¹ Die semi-angle = 12° Nominal initial tube dimensions = 0.995 x 0.110 in (outside diameter x wall-thickness) Nominal final tube dimensions = 0.830 x 0.081 in (outside diameter x wall-thickness) Reduction in area = 37.7% Sink = 13.8% Initial tube external surface condition = ground Material = 347 stainless steel						
Length, l_2 (in)	Experimental lubricant pressure at 21°C (lbf in ⁻²)	Theoretical lubricant pressure at:			Experimental plug force (tonf)	Experimental draw stress (tonf in ⁻²)
		19°C (lbf in ⁻²)	21°C (lbf in ⁻²)	25°C (lbf in ⁻²)		
4.0	-	53	42	27	-	-
5.4	105	181	144	93	0.65	37.7
7.0	-	331	262	169	-	-
8.4	286	464	366	235	0.74	37.3
10.0	-	619	488	313	-	-
11.4	514	757	596	381	0.69	37.3
12.0	-	818	643	410	-	-

Table (A2.25) Comparison between experimental and theoretical lubricant pressure for straight-parallel Christopherson tubes at 3.41 in from the die

Length, l_2 (in)	Theoretical lubricant film thickness at die entry at:			
	19°C ($\times 10^{-6}$ in)	21°C ($\times 10^{-6}$ in)	25°C ($\times 10^{-6}$ in)	27°C ($\times 10^{-6}$ in)
4.0	1.506	1.185	0.757	0.614
5.4	1.534	1.203	0.765	0.619
7.0	1.568	1.223	0.728	0.624
8.4	1.598	1.242	0.780	0.629
10.0	1.635	1.262	0.789	0.634
11.4	1.668	1.283	0.796	0.639
12.0	1.682	1.292	0.800	0.641

Table (A2.26)

Theoretical lubricant film thickness at the die entry corresponding to the drawing conditions of Table (A2.25)

Position of pressure measurement = 4.41 in from die
 Radial clearance, h_2 = 0.007 in
 Laboratory ambient temperature = 20°C (viscosity of EP50 = 3.503 lbf s in⁻²)
 Draw speed = 15 ft min⁻¹
 Die semi-angle = 12°
 Nominal initial tube dimensions = 0.995 x 0.110 in (outside diameter x wall-thickness)
 Nominal final tube dimensions = 0.830 x 0.081 in (outside diameter x wall-thickness)
 Reduction in area = 37.7%
 Sink = 13.8%
 Initial tube external surface condition = ground
 Material = 347 stainless steel

Length, l_2 (in)	Experimental lubricant pressure at 20°C (lbf in ⁻²)	Theoretical lubricant pressure at:				Experimental plug force (tonf)	Experimental draw stress (tonf in ⁻²)
		18°C (lbf in ⁻²)	20°C (lbf in ⁻²)	22°C (lbf in ⁻²)	24°C (lbf in ⁻²)		
5.0	-	60	47	38	30	-	-
5.4	64	101	80	64	51	0.74	37.7
7.0	-	267	211	168	135	-	-
8.4	302	416	327	260	209	0.74	37.7
10.0	-	589	463	367	294	-	-
11.4	570	745	583	462	370	0.69	36.8
12.0	-	812	636	503	402	-	-

Table (A2.27) Comparison between experimental and theoretical lubricant pressure for straight-parallel Christopherson tubes at 4.41 in from the die

Length, l_2 (in)	Theoretical lubricant film thickness at die entry at:			
	18°C (x 10 ⁻³ in)	20°C (x 10 ⁻⁶ in)	22°C (x 10 ⁻⁶ in)	24°C (x 10 ⁻⁶ in)
5.0	1.731	1.350	1.066	0.850
5.4	1.741	1.356	1.070	0.853
7.0	1.784	1.382	1.086	0.863
8.4	1.824	1.406	1.100	0.872
10.0	1.872	1.434	1.117	0.883
11.4	1.916	1.460	1.133	0.893
12.0	1.935	1.471	1.140	0.897

Table (A2.28) Theoretical lubricant film thickness at the die entry corresponding to the drawing conditions of Table (A2.27)

Outer speed = 100 ft/min tabular diameter = 5.01×10^{-4} in (0.50 at 2070) filer cone angle = 10° Reduction in area = 23% $\eta_{sp}/c = 1.0$ Initial tube diameter = 1.0×10^{-4} in (outside diameter is not tabulated)					
Length, l_0 (in)	Straight-parallel plug attachment		Straight-tapered plug attachment		
	Substrate pressure (lb/in ²)	Substrate thickness, h_0 (in)	Radial clearance ratio, $h_0/b_0 = 1.5$		Radial clearance ratio, $h_0/b_0 = 2$
			Substrate pressure (lb/in ²)	Substrate thickness, h_0 (in)	
1	1000	0.775×10^{-4}	2250	4.021×10^{-4}	1.267 $\times 10^{-4}$
2	1650	1.253×10^{-4}	3450	1.325×10^{-4}	1.054×10^{-4}
3	2000	1.425×10^{-4}	3630	1.505×10^{-4}	1.431×10^{-4}
4	2475	1.577×10^{-4}	3690	1.625×10^{-4}	1.672×10^{-4}
5	3000	1.737×10^{-4}	3700	1.714×10^{-4}	1.791×10^{-4}
10	3620	1.923×10^{-4}	3700	1.799×10^{-4}	1.876×10^{-4}
12	3630	1.931×10^{-4}	3700	1.799×10^{-4}	1.876×10^{-4}
Initial clearance, $h_0 = 0.006$ in					
1	1000	1.277×10^{-4}	2712	1.257×10^{-4}	6.375×10^{-5}
2	1650	1.382×10^{-4}	3117	1.366×10^{-4}	1.046×10^{-4}
3	2000	1.472×10^{-4}	3360	1.461×10^{-4}	1.197×10^{-4}
4	2475	1.545×10^{-4}	3516	1.541×10^{-4}	1.302×10^{-4}
5	3000	1.615×10^{-4}	3537	1.613×10^{-4}	1.366×10^{-4}
10	3620	1.707×10^{-4}	3530	1.696×10^{-4}	1.366×10^{-4}
12	3630	1.707×10^{-4}	3530	1.696×10^{-4}	1.366×10^{-4}
Initial clearance, $h_0 = 0.006$ in					
1	1000	1.253×10^{-4}	1680	1.253×10^{-4}	6.139×10^{-5}
2	1650	1.461×10^{-4}	2300	1.434×10^{-4}	1.036×10^{-4}
3	2000	1.611×10^{-4}	2720	1.584×10^{-4}	1.258×10^{-4}
4	2475	1.735×10^{-4}	2820	1.672×10^{-4}	1.406×10^{-4}
5	3000	1.824×10^{-4}	2820	1.824×10^{-4}	1.406×10^{-4}
10	3620	1.923×10^{-4}	2820	1.824×10^{-4}	1.406×10^{-4}
12	3630	1.931×10^{-4}	2820	1.824×10^{-4}	1.406×10^{-4}

Table A3.11 Comparison between straight-parallel and straight-tapered plug attachment at various lengths and initial clearances

Outer speed = 100 ft/min
 Substrate viscosity = 5.01×10^{-4} poise at 2070
 Filer cone angle = 10°
 Reduction in area = 23%
 $\eta_{sp}/c = 1.0$
 Initial tube diameter = 1.0×10^{-4} in (outside diameter is not tabulated)

Initial clearance, h_0 (in)	Straight-parallel plug attachment		Straight-tapered plug attachment		
	Substrate pressure (lb/in ²)	Substrate thickness, h_0 (in)	Radial clearance ratio, $h_0/b_0 = 1.5$		Radial clearance ratio, $h_0/b_0 = 2$
			Substrate pressure (lb/in ²)	Substrate thickness, h_0 (in)	
1	1000	1.195×10^{-4}	2000	4.001×10^{-4}	0.366
2	1650	1.470×10^{-4}	2600	1.302×10^{-4}	0.267
3	2000	1.626×10^{-4}	2720	1.577×10^{-4}	0.240
4	2475	1.697×10^{-4}	2740	1.813×10^{-4}	0.182
5	3000	1.754×10^{-4}	2740	1.819×10^{-4}	0.160
10	3620	1.826×10^{-4}	2740	1.819×10^{-4}	0.160
12	3630	1.826×10^{-4}	2740	1.819×10^{-4}	0.160
Initial clearance, $h_0 = 0.006$ in					
1	1000	1.253×10^{-4}	2000	1.253×10^{-4}	0.366
2	1650	1.461×10^{-4}	2600	1.434×10^{-4}	0.267
3	2000	1.611×10^{-4}	2720	1.584×10^{-4}	0.240
4	2475	1.735×10^{-4}	2820	1.672×10^{-4}	0.182
5	3000	1.824×10^{-4}	2820	1.824×10^{-4}	0.160
10	3620	1.923×10^{-4}	2820	1.824×10^{-4}	0.160
12	3630	1.931×10^{-4}	2820	1.824×10^{-4}	0.160
Initial clearance, $h_0 = 0.006$ in					
1	1000	1.253×10^{-4}	1680	1.253×10^{-4}	0.366
2	1650	1.461×10^{-4}	2300	1.434×10^{-4}	0.267
3	2000	1.611×10^{-4}	2720	1.584×10^{-4}	0.240
4	2475	1.735×10^{-4}	2820	1.672×10^{-4}	0.182
5	3000	1.824×10^{-4}	2820	1.824×10^{-4}	0.160
10	3620	1.923×10^{-4}	2820	1.824×10^{-4}	0.160
12	3630	1.931×10^{-4}	2820	1.824×10^{-4}	0.160

APPENDIX A3: TABULATED THEORETICAL RESULTS

Table A3.12 Comparison between straight-parallel and straight-tapered plug attachment at various lengths and initial clearances

APPENDIX A3: TABULATED THEORETICAL RESULTS

Draw speed = 100 ft min ⁻¹ Lubricant viscosity = 3.503 x 10 ⁻⁴ lbf s in ⁻² (EP50 at 20°C) Die semi-angle = 12° Reduction in area = 35% Sink = 15% Initial tube dimensions = 1.0 x 0.10 in (outside diameter x wall-thickness)									
Length, l ₂ (in)	Straight-parallel plug-attachment		Straight-tapered plug-attachment						
	Lubricant pressure (lbf in ⁻²)	Lubricant film thickness h ₂ (in)	Radial clearance ratio, h ₁ /h ₂ = 1.5		Radial clearance ratio, h ₁ /h ₂ = 2				
			Lubricant pressure (lbf in ⁻²)	Lubricant film thickness, h ₂ (in)	Lubricant pressure (lbf in ⁻²)	Lubricant film thickness, h ₂ (in)			
Radial clearance, h ₂ = 0.002 in									
2	31684	8.135 x 10 ⁻⁴	27457	4.601 x 10 ⁻⁴	16781	1.067 x 10 ⁻⁴			
4	34951	1.255 x 10 ⁻³	34852	1.239 x 10 ⁻³	33818	1.081 x 10 ⁻³			
6	35801	1.403 x 10 ⁻³	36339	1.505 x 10 ⁻³	36180	1.474 x 10 ⁻³			
8	36196	1.477 x 10 ⁻³	36993	1.639 x 10 ⁻³	37148	1.672 x 10 ⁻³			
10	36424	1.522 x 10 ⁻³	37362	1.719 x 10 ⁻³	37678	1.791 x 10 ⁻³			
12	36573	1.551 x 10 ⁻³	37599	1.772 x 10 ⁻³	38015	1.870 x 10 ⁻³			
Radial clearance, h ₂ = 0.004 in									
2	4589	1.977 x 10 ⁻⁵	2723	1.527 x 10 ⁻⁵	1941	1.371 x 10 ⁻⁵			
4	17650	1.202 x 10 ⁻⁴	7112	2.804 x 10 ⁻⁵	4598	1.980 x 10 ⁻⁵			
6	33452	1.029 x 10 ⁻³	18007	1.263 x 10 ⁻⁴	8797	3.541 x 10 ⁻⁵			
8	36884	1.616 x 10 ⁻³	32316	8.851 x 10 ⁻⁴	18203	1.297 x 10 ⁻⁴			
10	38424	1.971 x 10 ⁻³	36371	1.512 x 10 ⁻³	31124	7.546 x 10 ⁻⁴			
12	39315	2.208 x 10 ⁻³	38287	1.936 x 10 ⁻³	35589	1.365 x 10 ⁻³			
Radial clearance, h ₂ = 0.006 in									
2	1699	1.325 x 10 ⁻⁵	1087	1.218 x 10 ⁻⁵	800	1.170 x 10 ⁻⁵			
4	3921	1.803 x 10 ⁻⁵	2368	1.454 x 10 ⁻⁵	1700	1.326 x 10 ⁻⁵			
6	7129	2.811 x 10 ⁻⁵	3924	1.804 x 10 ⁻⁵	2728	1.528 x 10 ⁻⁵			
8	12844	6.195 x 10 ⁻⁵	5905	2.372 x 10 ⁻⁵	3926	1.804 x 10 ⁻⁵			
10	26100	3.827 x 10 ⁻⁴	8623	3.456 x 10 ⁻⁵	5360	2.200 x 10 ⁻⁵			
12	33933	1.097 x 10 ⁻³	12914	6.255 x 10 ⁻⁵	7145	2.817 x 10 ⁻⁵			

Table (A3.1) Comparison between straight-parallel and straight-tapered plug-attachments of various lengths and radial clearances

Draw speed = 100 ft min ⁻¹ Lubricant viscosity = 3.503 x 10 ⁻⁴ lbf s in ⁻² (EP50 at 20°C) Die semi-angle = 12° Reduction in area = 33% Sink = 15% Initial tube dimensions = 1.0 x 0.10 in (outside diameter x wall-thickness)									
Radial clear- ance, h ₂ (x 10 ⁻³ in)	Straight-parallel plug-attachment		Straight-tapered plug-attachment						
			Radial clearance ratio, h ₁ /h ₂ = 1.5		Radial clearance ratio, h ₁ /h ₂ = 2				
	Lubricant pressure (lbf in ⁻²)	Lubricant film thickness, h ₂ (in)	Lubricant pressure (lbf in ⁻²)	Lubricant film thickness, h ₂ (in)	Lubricant pressure (lbf in ⁻²)	Lubricant film thickness, h ₂ (in)			
Length of plug-attachment, l ₂ = 2 in									
2	31684	8.135 x 10 ⁻⁴	27458	4.601 x 10 ⁻⁴	16781	1.067 x 10 ⁻⁴			
3	12463	5.870 x 10 ⁻⁵	5869	2.360 x 10 ⁻⁵	3912	1.801 x 10 ⁻⁵			
4	4589	1.976 x 10 ⁻⁵	2723	1.527 x 10 ⁻⁵	1941	1.371 x 10 ⁻⁵			
5	2592	1.499 x 10 ⁻⁵	1623	1.312 x 10 ⁻⁵	1182	1.234 x 10 ⁻⁵			
6	1699	1.324 x 10 ⁻⁵	1087	1.217 x 10 ⁻⁵	800	1.170 x 10 ⁻⁵			
7	1208	1.238 x 10 ⁻⁵	783	1.166 x 10 ⁻⁵	579	1.135 x 10 ⁻⁵			
Length of plug-attachment, l ₂ = 4 in									
2	34951	1.255 x 10 ⁻³	34848	1.239 x 10 ⁻³	33818	1.081 x 10 ⁻³			
3	33593	1.050 x 10 ⁻³	26482	4.028 x 10 ⁻⁴	12646	6.027 x 10 ⁻⁵			
4	17651	1.202 x 10 ⁻⁴	7112	2.805 x 10 ⁻⁵	4598	1.980 x 10 ⁻⁵			
5	6650	2.633 x 10 ⁻⁵	3716	1.750 x 10 ⁻⁵	2595	1.501 x 10 ⁻⁵			
6	3921	1.802 x 10 ⁻⁵	2368	1.453 x 10 ⁻⁵	1700	1.326 x 10 ⁻⁵			
7	2660	1.512 x 10 ⁻⁵	1661	1.318 x 10 ⁻⁵	1209	1.238 x 10 ⁻⁵			
Length of plug-attachment, l ₂ = 6 in									
2	35801	1.403 x 10 ⁻³	36334	1.505 x 10 ⁻³	36180	1.474 x 10 ⁻³			
3	36543	1.547 x 10 ⁻³	34955	1.257 x 10 ⁻³	31013	7.436 x 10 ⁻⁴			
4	33459	1.029 x 10 ⁻³	18009	1.262 x 10 ⁻⁴	8797	3.541 x 10 ⁻⁵			
5	15855	9.380 x 10 ⁻⁵	6661	2.637 x 10 ⁻⁵	4351	1.913 x 10 ⁻⁵			
6	7129	2.811 x 10 ⁻⁵	3924	1.803 x 10 ⁻⁵	2728	1.528 x 10 ⁻⁵			
7	4475	1.945 x 10 ⁻⁵	2661	1.513 x 10 ⁻⁵	1899	1.363 x 10 ⁻⁵			

Table (A3.2) Comparison between straight-parallel and straight-tapered plug-attachments of various radial clearances and lengths

Draw speed = 100 ft min ⁻¹ Lubricant viscosity = 3.503 x 10 ⁻⁴ lbf s in ⁻² (EP50 at 20°C) Die semi-angle = 12° Reduction in area = 35% Sink = 15% Initial tube dimensions = 1.0 x 0.10 in (outside diameter x wall-thickness)					
Radial clearance ratio, h ₁ /h ₂	Radial clearance, h ₂ = 0.002 in		Radial clearance, h ₂ = 0.004 in		
	Lubricant pressure (lbf in ⁻²)	Lubricant film thickness, h _u (in)	Lubricant pressure (lbf in ⁻²)	Lubricant film thickness, h _u (in)	
Length of plug-attachment, l ₂ = 2 in					
* 1.0	31684	8.135 x 10 ⁻⁴	4589	1.976 x 10 ⁻⁵	
1.5	27457	4.601 x 10 ⁻⁴	2723	1.527 x 10 ⁻⁵	
2.0	16781	1.067 x 10 ⁻⁴	1941	1.369 x 10 ⁻⁵	
2.5	9850	4.095 x 10 ⁻⁵	1510	1.290 x 10 ⁻⁵	
3.0	7063	2.785 x 10 ⁻⁵	1235	1.242 x 10 ⁻⁵	
3.5	5546	2.258 x 10 ⁻⁵	1045	1.209 x 10 ⁻⁵	
Length of plug-attachment, l ₂ = 4 in					
* 1.0	34951	1.255 x 10 ⁻³	17651	1.202 x 10 ⁻⁴	
1.5	34852	1.239 x 10 ⁻³	7112	2.805 x 10 ⁻⁵	
2.0	33818	1.081 x 10 ⁻³	4598	1.978 x 10 ⁻⁵	
2.5	31965	8.447 x 10 ⁻⁴	3418	1.681 x 10 ⁻⁵	
3.0	28994	5.666 x 10 ⁻⁴	2725	1.527 x 10 ⁻⁵	
3.5	24022	2.883 x 10 ⁻⁴	2268	1.433 x 10 ⁻⁵	
Length of plug-attachment, l ₂ = 6 in					
* 1.0	35801	1.403 x 10 ⁻³	33459	1.029 x 10 ⁻³	
1.5	36339	1.505 x 10 ⁻³	18009	1.262 x 10 ⁻⁴	
2.0	36180	1.474 x 10 ⁻³	8797	3.538 x 10 ⁻⁵	
2.5	35801	1.368 x 10 ⁻³	6010	2.406 x 10 ⁻⁵	
3.0	34702	1.215 x 10 ⁻³	4601	1.979 x 10 ⁻⁵	
3.5	33463	1.031 x 10 ⁻³	3738	1.757 x 10 ⁻⁵	

* At h₁/h₂ = 1.0 the plug-attachment has a straight-parallel profile

Table (A3.5) Comparison of straight-tapered plug-attachments at various radial clearance ratios and lengths

Length of plug-attachment, $l_2 = 4$ in Radial clearance, $h_2 = 0.004$ in Die semi-angle = 12°			
Product ($\eta_0 U$) ($\times 10^{-3}$ lbf in $^{-1}$)	Lubricant pressure (lbf in $^{-2}$)	Lubricant film thickness at the end of sinking, h_u (in)	
* Radial clearance ratio, $h_1/h_2 = 1.0$			
1.366	2406	4.393×10^{-6}	
2.277	4607	9.933×10^{-6}	
3.188	7753	2.149×10^{-5}	
4.099	13116	5.793×10^{-5}	
5.009	22913	2.720×10^{-4}	
6.375	29826	8.763×10^{-4}	
Radial clearance ratio, $h_1/h_2 = 1.5$			
1.366	1512	3.879×10^{-6}	
2.277	2729	7.654×10^{-6}	
3.188	4188	1.311×10^{-5}	
4.099	6006	2.167×10^{-5}	
5.009	8404	3.690×10^{-5}	
6.375	14236	1.050×10^{-4}	
Radial clearance ratio, $h_1/h_2 = 2.0$			
1.366	1104	3.666×10^{-6}	
2.277	1945	6.863×10^{-6}	
3.188	2895	1.096×10^{-5}	
4.099	3986	1.640×10^{-5}	
5.009	5265	2.391×10^{-5}	
6.375	7710	4.266×10^{-5}	
Radial clearance ratio, $h_1/h_2 = 2.5$			
1.366	869	3.549×10^{-6}	
2.277	1512	6.464×10^{-6}	
3.188	2216	9.975×10^{-6}	
4.099	2996	1.429×10^{-5}	
5.009	3866	1.971×10^{-5}	
6.375	5398	3.099×10^{-5}	

* At h₁/h₂ = 1.0 the plug-attachment has a straight-parallel profile

Table (A3.6) Comparison of a 4 in straight-tapered plug-attachment at various values of (η₀U) and radial clearance ratios

Length of plug-attachment, $l_2 = 6$ in Radial clearance, $h_2 = 0.004$ in Die semi-angle = 12°			Lubricant film thickness at the end of sinking, h_4 (in)	
Product ($\eta_0 U$) ($\times 10^{-3}$ lbf in $^{-1}$)	Lubricant pressure (lbf in $^{-2}$)			
* Radial clearance ratio, $h_1/h_2 = 1.0$				
1.366	3997		5.473×10^{-6}	
2.277	8841		1.785×10^{-5}	
3.188	21743		1.482×10^{-4}	
4.099	32050		7.716×10^{-4}	
5.009	34199		1.243×10^{-3}	
6.375	34886		1.704×10^{-3}	
Radial clearance ratio, $h_1/h_2 = 1.5$				
1.366	2407		4.394×10^{-6}	
2.277	4611		9.935×10^{-6}	
3.188	7768		2.153×10^{-5}	
4.099	13217		5.876×10^{-5}	
5.009	23804		3.074×10^{-4}	
6.375	31133		1.043×10^{-3}	
Radial clearance ratio, $h_1/h_2 = 2.0$				
1.366	1726		3.997×10^{-6}	
2.277	3157		8.121×10^{-6}	
3.188	4935		1.454×10^{-5}	
4.099	7280		2.587×10^{-5}	
5.009	10680		5.055×10^{-5}	
6.375	20384		2.440×10^{-4}	
Radial clearance ratio, $h_1/h_2 = 2.5$				
1.366	1346		3.794×10^{-6}	
2.277	2406		7.322×10^{-6}	
3.188	3645		1.216×10^{-5}	
4.099	5135		1.922×10^{-5}	
5.009	6999		3.039×10^{-5}	
6.375	11064		6.782×10^{-5}	

* At $h_1/h_2 = 1.0$ the plug-attachment has a straight-parallel profile

Table (A3.7) Comparison of a 6 in straight-tapered plug-attachment at various values of ($\eta_0 U$) and radial clearance ratios

Initial tube dimensions = 1.0×0.10 in (outside diameter \times wall-thickness) Die semi-angle = 12° Reduction in area = 35% Sink = 153 Length ratio of plug-attachment, $l_2/l_1 = 1.0$				
Lubricant pressure (lbf in $^{-2}$)		Lubricant film thickness h_4 (in)	Required length of plug-attachment (in)	
			Parallel	Stepped
Product ($\eta_0 U$) = 0.001 lbf in $^{-1}$				
Radial clearance, $h_2 = 0.002$ in				
Radial clearance ratio, $h_1/h_2 = 1.5$				
5000	4.602×10^{-6}		2.41	3.61
10000	9.202×10^{-6}		3.63	5.43
15000	1.839×10^{-5}		4.25	6.37
20000	3.675×10^{-5}		4.61	6.89
25000	7.336×10^{-5}		4.87	7.25
30000	1.462×10^{-4}		5.18	7.65
35000	2.907×10^{-4}		5.76	8.35
Product ($\eta_0 U$) = 0.002 lbf in $^{-1}$				
Radial clearance, $h_2 = 0.002$ in				
Radial clearance ratio, $h_1/h_2 = 2.0$				
5000	9.202×10^{-6}		1.21	2.41
10000	1.839×10^{-5}		1.82	3.64
15000	3.674×10^{-5}		2.15	4.28
20000	7.334×10^{-5}		2.36	4.66
25000	1.461×10^{-4}		2.55	4.98
30000	2.902×10^{-4}		2.85	5.43
35000	5.730×10^{-4}		3.60	6.39
			1.61	1.93
			2.43	2.91
			2.86	3.42
			3.13	3.73
			3.37	3.99
			4.37	3.74
			4.60	5.18

Table (A3.8) Theoretical length of four designs of plug-attachments required to generate a given hydrodynamic lubricant pressure

Initial tube dimensions = 1.0 x 0.10 in (outside diameter x wall-thickness)

Die semi-angle = 12°

Reduction in area = 35%

Sink = 15%

Length ratio of plug-attachment, $l_2/l_1 = 1.0$

Lubricant pressure (lb/in^2)	Lubricant film thickness h_0 (in)	Required length of plug-attachment (in)		
		Parallel	Tapered	Composite
Product ($\eta_0 U$) = 0.003 lb/in^{-1}				
Radial clearance, $h_2 = 0.002$ in				
Radial clearance ratio, $h_1/h_2 = 2.0$				
5000	1.380×10^{-5}	0.81	1.61	1.08
10000	2.757×10^{-5}	1.22	2.43	1.63
15000	5.505×10^{-5}	1.45	2.88	1.93
20000	1.098×10^{-4}	1.61	3.16	2.13
25000	2.183×10^{-4}	1.78	3.43	2.35
30000	4.321×10^{-4}	2.12	3.90	2.74
35000	8.483×10^{-4}	3.17	5.08	3.91
Product ($\eta_0 U$) = 0.005 lb/in^{-1}				
Radial clearance, $h_2 = 0.004$ in				
Radial clearance ratio, $h_1/h_2 = 1.5$				
5000	2.298×10^{-5}	1.94	2.90	2.32
10000	4.589×10^{-5}	2.92	4.38	3.51
15000	9.155×10^{-5}	3.46	5.17	4.14
20000	1.822×10^{-4}	3.81	5.66	4.56
25000	3.611×10^{-4}	4.17	6.13	4.96
30000	7.104×10^{-4}	4.79	6.88	5.65
35000	1.379×10^{-3}	6.42	8.65	7.37
2.68				
4.04				
4.76				
5.22				
5.64				
6.29				
7.79				

Table (A3.9) Theoretical length of four designs of plug-attachments required to generate a given hydrodynamic lubricant pressure

Hydrodynamic lubricant pressure = 20000 lb/in^2

Radial clearance, $h_2 = 0.002$ in

Radial clearance ratio, $h_1/h_2 = 1.5$

Initial tube dimensions = 1.0 x 0.10 in (outside diameter x wall-thickness)

Die semi-angle = 12°

Reduction in area = 35%

Sink = 15%

Length ratio, l_2/l_1	Length of plug-attachment (in)		
	Composite	Stepped	Tapered
Product ($\eta_0 U$) = 0.001 lbf in ⁻¹			
0.2	6.36	8.53	4.61
0.4	6.03	7.60	
0.6	5.81	7.02	
0.8	5.65	6.63	
1.0	5.52	6.35	
1.2	5.42	6.14	
1.4	5.34	5.97	6.89
Product ($\eta_0 U$) = 0.002 lbf in ⁻¹			
0.2	3.24	4.33	2.36
0.4	3.08	3.86	
0.6	2.96	3.57	
0.8	2.88	3.37	
1.0	2.82	3.23	
1.2	2.78	3.12	
1.4	2.73	3.04	3.51
Product ($\eta_0 U$) = 0.003 lbf in ⁻¹			
0.2	2.20	2.94	1.61
0.4	2.09	2.62	
0.6	2.02	2.42	
0.8	1.96	2.29	
1.0	1.92	2.19	
1.2	1.89	2.12	
1.4	1.86	2.06	2.38

Table (A3.10) Variation of length and length ratio of the composite and stepped plug-attachments to generate a hydrodynamic lubricant pressure of 20000 lb/in^2

Draw speed = 100 ft min ⁻¹ Lubricant viscosity = 3.503×10^{-4} lbf s in ⁻² (EP50 at 20°C) Reduction in area = 35% Die semi-angle = 12°									
Radial clearance	Straight-parallel Christopherson tube			Straight-tapered Christopherson tube			Straight-tapered Christopherson tube		
	h ₂ (x10 ⁻³ in)	lubricant pressure (lbf in ⁻²)	film thickness at die entry (in)	h ₁ /h ₂ = 1.5	lubricant pressure (lbf in ⁻²)	film thickness at die entry (in)	h ₁ /h ₂ = 1.5	lubricant pressure (lbf in ⁻²)	film thickness at die entry (in)
length of Christopherson tube, l ₂ = 4 in									
2	53037	1.472x10 ⁻³	52568	1.450x10 ⁻³	48593	1.260x10 ⁻³			
3	42462	1.223x10 ⁻³	30317	4.403x10 ⁻⁴	12824	5.101x10 ⁻⁵			
4	18351	1.077x10 ⁻⁴	7136	2.370x10 ⁻⁵	4606	1.674x10 ⁻⁵			
5	6670	2.228x10 ⁻⁵	3721	1.484x10 ⁻⁵	2598	1.271x10 ⁻⁵			
6	3926	1.528x10 ⁻⁵	2370	1.233x10 ⁻⁵	1701	1.124x10 ⁻⁵			
7	2662	1.284x10 ⁻⁵	1662	1.119x10 ⁻⁵	1210	1.051x10 ⁻⁵			
length of Christopherson tube, l ₂ = 6 in									
2	56675	1.648x10 ⁻³	58797	1.767x10 ⁻³	58164	1.728x10 ⁻³			
3	49909	1.813x10 ⁻³	45546	1.465x10 ⁻³	37392	8.497x10 ⁻⁴			
4	40035	1.195x10 ⁻³	18666	1.123x10 ⁻⁴	8836	2.990x10 ⁻⁵			
5	16204	8.168x10 ⁻⁵	6678	2.230x10 ⁻⁵	4357	1.620x10 ⁻⁵			
6	7148	2.383x10 ⁻⁵	3929	1.529x10 ⁻⁵	2730	1.296x10 ⁻⁵			
7	4481	1.651x10 ⁻⁵	2663	1.285x10 ⁻⁵	1900	1.156x10 ⁻⁵			
length of Christopherson tube, l ₂ = 8 in									
2	58298	1.736x10 ⁻³	60548	1.925x10 ⁻³	60708	1.963x10 ⁻³			
3	53611	2.110x10 ⁻³	52217	1.997x10 ⁻³	47577	1.627x10 ⁻³			
4	46764	1.891x10 ⁻³	38095	1.018x10 ⁻³	18837	1.148x10 ⁻⁴			
5	35955	9.032x10 ⁻⁴	11685	4.428x10 ⁻⁵	6682	2.231x10 ⁻⁵			
6	12967	5.290x10 ⁻⁵	5915	2.011x10 ⁻⁵	3930	1.529x10 ⁻⁵			
7	6911	2.309x10 ⁻⁵	3824	1.508x10 ⁻⁵	2663	1.285x10 ⁻⁵			

Table (A3.12) Comparison between straight-parallel and straight-tapered Christopherson tubes of various radial clearances and lengths

Draw speed = 100 ft min ⁻¹ Lubricant viscosity = 3.503×10^{-4} lbf s in ⁻² (EP50 at 20°C) Reduction in area = 35% Die semi-angle = 12°									
Length, l ₂ (in)	Straight-parallel Christopherson tube			Straight-tapered Christopherson tube			Straight-tapered Christopherson tube		
	lubricant pressure (lbf in ⁻²)	film thickness at die entry (in)	lubricant pressure (lbf in ⁻²)	h ₁ /h ₂ = 1.5	lubricant pressure (lbf in ⁻²)	film thickness at die entry (in)	h ₁ /h ₂ = 2	lubricant pressure (lbf in ⁻²)	film thickness at die entry (in)
Radial clearance, h ₂ = 0.002 in									
2	42329	9.470x10 ⁻⁴	33455	5.176x10 ⁻⁴	17664	9.391x10 ⁻⁵			
4	53037	1.472x10 ⁻³	52568	1.450x10 ⁻³	48593	1.260x10 ⁻³			
6	56675	1.648x10 ⁻³	58797	1.767x10 ⁻³	58164	1.728x10 ⁻³			
8	58298	1.736x10 ⁻³	60548	1.925x10 ⁻³	60708	1.963x10 ⁻³			
10	59135	1.789x10 ⁻³	60745	2.020x10 ⁻³	60396	2.104x10 ⁻³			
12	59614	1.824x10 ⁻³	60520	2.083x10 ⁻³	59566	2.197x10 ⁻³			
Radial clearance, h ₂ = 0.004 in									
2	4600	1.673x10 ⁻⁵	2727	1.292x10 ⁻⁵	1943	1.160x10 ⁻⁵			
4	18351	1.077x10 ⁻⁴	7136	2.370x10 ⁻⁵	4606	1.674x10 ⁻⁵			
6	40035	1.195x10 ⁻³	18666	1.123x10 ⁻⁴	8836	2.990x10 ⁻⁵			
8	46764	1.891x10 ⁻³	38095	1.018x10 ⁻³	18837	1.148x10 ⁻⁴			
10	50539	2.312x10 ⁻³	45597	1.764x10 ⁻³	36181	8.575x10 ⁻⁴			
12	52992	2.593x10 ⁻³	50150	2.268x10 ⁻³	43938	1.587x10 ⁻³			
Radial clearance, h ₂ = 0.006 in									
2	1700	1.124x10 ⁻⁵	1088	1.033x10 ⁻⁵	800	9.926x10 ⁻⁶			
4	3926	1.528x10 ⁻⁵	2370	1.233x10 ⁻⁵	1701	1.124x10 ⁻⁵			
6	7148	2.383x10 ⁻⁵	3929	1.529x10 ⁻⁵	2730	1.296x10 ⁻⁵			
8	12967	5.290x10 ⁻⁵	5915	2.011x10 ⁻⁵	3930	1.529x10 ⁻⁵			
10	28501	4.072x10 ⁻⁴	8651	2.930x10 ⁻⁵	5367	1.864x10 ⁻⁵			
12	38849	1.270x10 ⁻³	13019	5.328x10 ⁻⁵	7160	2.387x10 ⁻⁵			

Table (A3.11) Comparison between straight-parallel and straight-tapered Christopherson tubes of various lengths and radial clearances

Draw speed = 100 ft min⁻¹

Radial clearance, $h_2 = 0.004$ in

Reduction in area = 35%

Die semi-angle = 12°

Viscosity, η , ($\times 10^{-4}$ lbf s in ⁻²)	Corresp. temperature of EP50 (°C)	Straight - parallel Christopherson tube		Straight - tapered Christopherson tube	
		lubricant pressure ₂ (lbf in ⁻²)	film thick- ness at die entry (in)	lubricant pressure ₂ (lbf in ⁻²)	film thick- ness at die entry (in)
length of Christopherson tube, $l_2 = 4$ in					
9.400	12	45836	2.429x10 ⁻³	41175	1.976x10 ⁻³
7.242	14	42781	1.962x10 ⁻³	34548	1.153x10 ⁻³
5.633	16	38760	1.385x10 ⁻³	22488	2.812x10 ⁻⁴
4.423	18	32316	6.922x10 ⁻⁴	11204	5.186x10 ⁻⁵
3.503	20	18351	1.077x10 ⁻⁴	7136	2.370x10 ⁻⁵
2.798	22	10030	2.821x10 ⁻⁵	5040	1.422x10 ⁻⁵
length of Christopherson tube, $l_2 = 6$ in					
9.400	12	51653	2.951x10 ⁻³	51203	2.912x10 ⁻³
7.242	14	49633	2.639x10 ⁻³	46670	2.352x10 ⁻³
5.633	16	47218	2.251x10 ⁻³	41478	1.658x10 ⁻³
4.423	18	44199	1.774x10 ⁻³	34078	8.208x10 ⁻⁴
3.503	20	40035	1.195x10 ⁻³	18666	1.123x10 ⁻⁴
2.798	22	32679	5.125x10 ⁻⁴	10055	2.831x10 ⁻⁵
length of Christopherson tube, $l_2 = 8$ in					
9.400	12	54720	3.213x10 ⁻³	56668	3.384x10 ⁻³
7.242	14	53246	2.979x10 ⁻³	53067	2.962x10 ⁻³
5.633	16	51496	2.688x10 ⁻³	49043	2.439x10 ⁻³
4.423	18	49389	2.329x10 ⁻³	44396	1.795x10 ⁻³
3.503	20	46764	1.891x10 ⁻³	38095	1.018x10 ⁻³
2.798	22	43245	1.362x10 ⁻³	24635	1.970x10 ⁻⁴
Radial clearance ratio $h_1/h_2 = 2$					
		lubricant pressure ₂ (lbf in ⁻²)		lubricant pressure ₂ (lbf in ⁻²)	
		film thickness at die entry (in)		film thickness at die entry (in)	
		Radial clearance ratio $h_1/h_2 = 1.5$		Radial clearance ratio $h_1/h_2 = 2$	
		lubricant pressure ₂ (lbf in ⁻²)		lubricant pressure ₂ (lbf in ⁻²)	
		film thickness at die entry (in)		film thickness at die entry (in)	
		Radial clearance ratio $h_1/h_2 = 1.5$		Radial clearance ratio $h_1/h_2 = 2$	
		lubricant pressure ₂ (lbf in ⁻²)		lubricant pressure ₂ (lbf in ⁻²)	
		film thickness at die entry (in)		film thickness at die entry (in)	
		Radial clearance ratio $h_1/h_2 = 1.5$		Radial clearance ratio $h_1/h_2 = 2$	
		lubricant pressure ₂ (lbf in ⁻²)		lubricant pressure ₂ (lbf in ⁻²)	
		film thickness at die entry (in)		film thickness at die entry (in)	
		Radial clearance ratio $h_1/h_2 = 1.5$		Radial clearance ratio $h_1/h_2 = 2$	
		lubricant pressure ₂ (lbf in ⁻²)		lubricant pressure ₂ (lbf in ⁻²)	
		film thickness at die entry (in)		film thickness at die entry (in)	
		Radial clearance ratio $h_1/h_2 = 1.5$		Radial clearance ratio $h_1/h_2 = 2$	
		lubricant pressure ₂ (lbf in ⁻²)		lubricant pressure ₂ (lbf in ⁻²)	
		film thickness at die entry (in)		film thickness at die entry (in)	
		Radial clearance ratio $h_1/h_2 = 1.5$		Radial clearance ratio $h_1/h_2 = 2$	
		lubricant pressure ₂ (lbf in ⁻²)		lubricant pressure ₂ (lbf in ⁻²)	
		film thickness at die entry (in)		film thickness at die entry (in)	
		Radial clearance ratio $h_1/h_2 = 1.5$		Radial clearance ratio $h_1/h_2 = 2$	
		lubricant pressure ₂ (lbf in ⁻²)		lubricant pressure ₂ (lbf in ⁻²)	
		film thickness at die entry (in)		film thickness at die entry (in)	
		Radial clearance ratio $h_1/h_2 = 1.5$		Radial clearance ratio $h_1/h_2 = 2$	
		lubricant pressure ₂ (lbf in ⁻²)		lubricant pressure ₂ (lbf in ⁻²)	
		film thickness at die entry (in)		film thickness at die entry (in)	
		Radial clearance ratio $h_1/h_2 = 1.5$		Radial clearance ratio $h_1/h_2 = 2$	
		lubricant pressure ₂ (lbf in ⁻²)		lubricant pressure ₂ (lbf in ⁻²)	
		film thickness at die entry (in)		film thickness at die entry (in)	
		Radial clearance ratio $h_1/h_2 = 1.5$		Radial clearance ratio $h_1/h_2 = 2$	
		lubricant pressure ₂ (lbf in ⁻²)		lubricant pressure ₂ (lbf in ⁻²)	
		film thickness at die entry (in)		film thickness at die entry (in)	
		Radial clearance ratio $h_1/h_2 = 1.5$		Radial clearance ratio $h_1/h_2 = 2$	
		lubricant pressure ₂ (lbf in ⁻²)		lubricant pressure ₂ (lbf in ⁻²)	
		film thickness at die entry (in)		film thickness at die entry (in)	
		Radial clearance ratio $h_1/h_2 = 1.5$		Radial clearance ratio $h_1/h_2 = 2$	
		lubricant pressure ₂ (lbf in ⁻²)		lubricant pressure ₂ (lbf in ⁻²)	
		film thickness at die entry (in)		film thickness at die entry (in)	
		Radial clearance ratio $h_1/h_2 = 1.5$		Radial clearance ratio $h_1/h_2 = 2$	
		lubricant pressure ₂ (lbf in ⁻²)		lubricant pressure ₂ (lbf in ⁻²)	
		film thickness at die entry (in)		film thickness at die entry (in)	
		Radial clearance ratio $h_1/h_2 = 1.5$		Radial clearance ratio $h_1/h_2 = 2$	
		lubricant pressure ₂ (lbf in ⁻²)		lubricant pressure ₂ (lbf in ⁻²)	
		film thickness at die entry (in)		film thickness at die entry (in)	
		Radial clearance ratio $h_1/h_2 = 1.5$		Radial clearance ratio $h_1/h_2 = 2$	
		lubricant pressure ₂ (lbf in ⁻²)		lubricant pressure ₂ (lbf in ⁻²)	
		film thickness at die entry (in)		film thickness at die entry (in)	
		Radial clearance ratio $h_1/h_2 = 1.5$		Radial clearance ratio $h_1/h_2 = 2$	
		lubricant pressure ₂ (lbf in ⁻²)		lubricant pressure ₂ (lbf in ⁻²)	
		film thickness at die entry (in)		film thickness at die entry (in)	
		Radial clearance ratio $h_1/h_2 = 1.5$		Radial clearance ratio $h_1/h_2 = 2$	
		lubricant pressure ₂ (lbf in ⁻²)		lubricant pressure ₂ (lbf in ⁻²)	
		film thickness at die entry (in)		film thickness at die entry (in)	
		Radial clearance ratio $h_1/h_2 = 1.5$		Radial clearance ratio $h_1/h_2 = 2$	
		lubricant pressure ₂ (lbf in ⁻²)		lubricant pressure ₂ (lbf in ⁻²)	
		film thickness at die entry (in)		film thickness at die entry (in)	
		Radial clearance ratio $h_1/h_2 = 1.5$		Radial clearance ratio $h_1/h_2 = 2$	
		lubricant pressure ₂ (lbf in ⁻²)		lubricant pressure ₂ (lbf in ⁻²)	
		film thickness at die entry (in)		film thickness at die entry (in)	
		Radial clearance ratio $h_1/h_2 = 1.5$		Radial clearance ratio $h_1/h_2 = 2$	
		lubricant pressure ₂ (lbf in ⁻²)		lubricant pressure ₂ (lbf in ⁻²)	
		film thickness at die entry (in)		film thickness at die entry (in)	
		Radial clearance ratio $h_1/h_2 = 1.5$		Radial clearance ratio $h_1/h_2 = 2$	
		lubricant pressure ₂ (lbf in ⁻²)		lubricant pressure ₂ (lbf in ⁻²)	
		film thickness at die entry (in)		film thickness at die entry (in)	
		Radial clearance ratio $h_1/h_2 = 1.5$		Radial clearance ratio $h_1/h_2 = 2$	
		lubricant pressure ₂ (lbf in ⁻²)		lubricant pressure ₂ (lbf in ⁻²)	
		film thickness at die entry (in)		film thickness at die entry (in)	
		Radial clearance ratio $h_1/h_2 = 1.5$		Radial clearance ratio $h_1/h_2 = 2$	
		lubricant pressure ₂ (lbf in ⁻²)		lubricant pressure ₂ (lbf in ⁻²)	
		film thickness at die entry (in)		film thickness at die entry (in)	
		Radial clearance ratio $h_1/h_2 = 1.5$		Radial clearance ratio $h_1/h_2 = 2$	
		lubricant pressure ₂ (lbf in ⁻²)		lubricant pressure ₂ (lbf in ⁻²)	
		film thickness at die entry (in)		film thickness at die entry (in)	
		Radial clearance ratio $h_1/h_2 = 1.5$		Radial clearance ratio $h_1/h_2 = 2$	
		lubricant pressure ₂ (lbf in ⁻²)		lubricant pressure ₂ (lbf in ⁻²)	
		film thickness at die entry (in)		film thickness at die entry (in)	
		Radial clearance ratio $h_1/h_2 = 1.5$		Radial clearance ratio $h_1/h_2 = 2$	
		lubricant pressure ₂ (lbf in ⁻²)		lubricant pressure ₂ (lbf in ⁻²)	
		film thickness at die entry (in)		film thickness at die entry (in)	
		Radial clearance ratio $h_1/h_2 = 1.5$		Radial clearance ratio $h_1/h_2 = 2$	
		lubricant pressure ₂ (lbf in ⁻²)		lubricant pressure ₂ (lbf in ⁻²)	
		film thickness at die entry (in)		film thickness at die entry (in)	
		Radial clearance ratio $h_1/h_2 = 1.5$		Radial clearance ratio $h_1/h_2 = 2$	
		lubricant pressure ₂ (lbf in ⁻²)		lubricant pressure ₂ (lbf in ⁻²)	
		film thickness at die entry (in)		film thickness at die entry (in)	
		Radial clearance ratio $h_1/h_2 = 1.5$		Radial clearance ratio $h_1/h_2 = 2$	
		lubricant pressure ₂ (lbf in ⁻²)		lubricant pressure ₂ (lbf in ⁻²)	
		film thickness at die entry (in)		film thickness at die entry (in)	
		Radial clearance ratio $h_1/h_2 = 1.5$		Radial clearance ratio $h_1/h_2 = 2$	
		lubricant pressure ₂ (lbf in ⁻²)		lubricant pressure ₂ (lbf in ⁻²)	
		film thickness at die entry (in)		film thickness at die entry (in)	
		Radial clearance ratio $h_1/h_2 = 1.5$		Radial clearance ratio $h_1/h_2 = 2$	
		lubricant pressure ₂ (lbf in ⁻²)		lubricant pressure ₂ (lbf in ⁻²)	
		film thickness at die entry (in)		film thickness at die entry (in)	
		Radial clearance ratio $h_$			

Table (A3.13) Comparison between straight-parallel and straight-tapered Christopherson tubes at various viscosities and lengths

Lubricant viscosity = 3.503×10^{-4} lbf s in ⁻² (EP50 at 20°C) Radial clearance, $h_2 = 0.004$ in Reduction in area = 35% Die semi-angle = 12°									
Draw Speed (ft min ⁻¹)	Straight-parallel Christopherson tube		Straight-tapered Christopherson tube		Straight-tapered Christopherson tube		Straight-tapered Christopherson tube		
	lubricant pressure (lbf in ⁻²)	film thickness at die entry (in)	lubricant pressure (lbf in ⁻²)	film thickness at die entry (in)	lubricant pressure (lbf in ⁻²)	film thickness at die entry (in)	Radial clearance ratio $h_1/h_2 = 1.5$	Radial clearance ratio $h_1/h_2 = 2$	film thickness at die entry (in)
length of Christopherson tube, $l_2 = 4$ in									
60	6028	1.226x10 ⁻⁵	3426	8.563x10 ⁻⁶	2406	7.438x10 ⁻⁶			
80	10063	2.838x10 ⁻⁵	5051	1.426x10 ⁻⁵	3424	1.140x10 ⁻⁵			
100	18351	1.077x10 ⁻⁴	7136	2.370x10 ⁻⁵	4606	1.674x10 ⁻⁵			
120	30167	5.337x10 ⁻⁴	10026	4.207x10 ⁻⁵	6014	2.433x10 ⁻⁵			
140	35604	1.004x10 ⁻³	14566	8.995x10 ⁻⁵	7748	3.589x10 ⁻⁵			
160	38661	1.372x10 ⁻³	22145	2.685x10 ⁻⁴	9991	5.543x10 ⁻⁵			
length of Christopherson tube, $l_2 = 6$ in									
60	13449	3.396 x 10 ⁻⁵	6033	1.227x10 ⁻⁵	3996	9.264x10 ⁻⁶			
80	32757	5.175x10 ⁻⁴	10089	2.848x10 ⁻⁵	6028	1.632x10 ⁻⁵			
100	40035	1.195x10 ⁻³	18666	1.123x10 ⁻⁴	8836	2.990x10 ⁻⁵			
120	43432	1.659x10 ⁻³	31714	6.280x10 ⁻⁴	13300	6.548x10 ⁻⁴			
140	45599	1.992x10 ⁻³	37766	1.199x10 ⁻³	21829	2.296x10 ⁻⁴			
160	47163	2.243x10 ⁻³	41357	1.642x10 ⁻³	30826	7.053x10 ⁻⁴			
length of Christopherson tube, $l_2 = 8$ in									
60	34631	5.089x10 ⁻⁴	10121	2.153x10 ⁻⁵	6035	1.227x10 ⁻⁵			
80	43274	1.367x10 ⁻³	24781	2.010x10 ⁻⁴	10101	2.853x10 ⁻⁵			
100	46764	1.891x10 ⁻³	38095	1.018x10 ⁻³	18837	1.148x10 ⁻⁴			
120	48877	2.242x10 ⁻³	43248	1.640x10 ⁻³	32653	6.907x10 ⁻⁴			
140	50350	2.493x10 ⁻³	46515	2.089x10 ⁻³	39124	1.328x10 ⁻³			
160	51457	2.681x10 ⁻³	48955	2.427x10 ⁻³	43108	1.822x10 ⁻³			

Table (A3.14) Comparison between straight-parallel and straight-tapered Christopherson tubes at various draw speeds and lengths

Draw speed = 100 ft min ⁻¹ Lubricant viscosity = 3.503 x 10 ⁻⁴ lbf s in ⁻² (EP50 at 20°C) Reduction in area = 35% Die Semi-angle = 12°				
Radial clearance ratio h ₁ /h ₂	Radial clearance, h ₂ = 0.002 in		Radial clearance, h ₂ = 0.004 in	
	lubricant pressure generated (lbf in ⁻²)	lubricant film thickness at die entry (in)	lubricant pressure generated (lbf in ⁻²)	lubricant film thickness at die entry (in)
Length of Christopherson tube, l ₂ = 4 in				
*1.0	53037	1.472 x 10 ⁻³	18351	1.077 x 10 ⁻⁴
1.5	52568	1.450 x 10 ⁻³	7136	2.370 x 10 ⁻⁵
2.0	48593	1.260 x 10 ⁻³	4606	1.674 x 10 ⁻⁵
2.5	42906	9.763 x 10 ⁻⁴	3423	1.422 x 10 ⁻⁵
3.0	36149	6.398 x 10 ⁻⁴	2728	1.293 x 10 ⁻⁵
3.5	27605	2.990 x 10 ⁻⁴	2270	1.213 x 10 ⁻⁵
Length of Christopherson tube, l ₂ = 6 in				
*1.0	56675	1.648 x 10 ⁻³	40035	1.195 x 10 ⁻³
1.5	58797	1.767 x 10 ⁻³	18666	1.123 x 10 ⁻⁴
2.0	58164	1.728 x 10 ⁻³	8836	2.990 x 10 ⁻⁵
2.5	55721	1.601 x 10 ⁻³	6023	2.034 x 10 ⁻⁵
3.0	51868	1.417 x 10 ⁻³	4609	1.675 x 10 ⁻⁵
3.5	47308	1.197 x 10 ⁻³	3743	1.487 x 10 ⁻⁵
Length of Christopherson tube, l ₂ = 8 in				
*1.0	58298	1.736 x 10 ⁻³	46764	1.891 x 10 ⁻³
1.5	60548	1.925 x 10 ⁻³	38095	1.018 x 10 ⁻³
2.0	60708	1.963 x 10 ⁻³	18837	1.148 x 10 ⁻⁴
2.5	60485	1.914 x 10 ⁻³	10083	3.545 x 10 ⁻⁵
3.0	59462	1.812 x 10 ⁻³	7148	2.373 x 10 ⁻⁵
3.5	57180	1.674 x 10 ⁻³	5592	1.917 x 10 ⁻⁵

* at h₁/h₂ = 1.0 the Christopherson tube has a straight-parallel internal profile

Table (A3.15) Comparison of straight-tapered Christopherson tubes at various radial clearance ratios and lengths

Length of Christopherson tube, $l_2 = 2$ in Radial clearance, $h_2 = 0.002$ in Die semi-angle = 12°			
Product ($\eta_0 U$) (lbf in $^{-1}$)	Lubricant pressure generated (lbf in $^{-2}$)	Lubricant film thickness at die entry (in)	
Radial clearance ratio, $h_1/h_2 = *1.0$			
0.01	50102	1.520×10^{-3}	
0.015	52737	1.680×10^{-3}	
0.02	54262	1.760×10^{-3}	
0.025	55278	1.808×10^{-3}	
0.03	56009	1.840×10^{-3}	
0.05	57643	1.904×10^{-3}	
Radial clearance ratio, $h_1/h_2 = 1.5$			
0.01	50523	1.535×10^{-3}	
0.015	57492	1.823×10^{-3}	
0.02	60587	1.967×10^{-3}	
0.025	60214	2.054×10^{-3}	
0.03	58366	2.112×10^{-3}	
0.05	51568	2.227×10^{-3}	
Radial clearance ratio, $h_1/h_2 = 2.0$			
0.01	46672	1.386×10^{-3}	
0.015	57143	1.812×10^{-3}	
0.02	60656	2.026×10^{-3}	
0.025	57315	2.154×10^{-3}	
0.03	53568	2.239×10^{-3}	
0.05	45082	2.411×10^{-3}	
Radial clearance ratio, $h_1/h_2 = 2.5$			
0.01	41132	1.145×10^{-3}	
0.015	53845	1.713×10^{-3}	
0.02	60759	1.999×10^{-3}	
0.025	56745	2.170×10^{-3}	
0.03	51985	2.285×10^{-3}	
0.05	42413	2.515×10^{-3}	

* At h₁/h₂ = 1.0 the Christopherson tube has a straight-parallel internal profile
 Table (A3.16) Comparison of a 2 in straight-tapered Christopherson tube at various values of (η₀U) and radial clearance ratios

Length of Christopherson tube, $l_2 = 2$ in Radial clearance, $h_2 = 0.004$ in Die semi-angle = 12°		
Product ($n_0 U$) (lbf in $^{-1}$)	Lubricant pressure generated (lbf in $^{-2}$)	Lubricant film thickness at die entry (in)
Radial clearance ratio, $h_1/h_2 = *1.0$		
0.04	45987	3.040×10^{-3}
0.06	49039	3.360×10^{-3}
0.08	50904	3.520×10^{-3}
0.10	52202	3.616×10^{-3}
0.14	53929	3.725×10^{-3}
0.20	55474	3.808×10^{-3}
Radial clearance ratio, $h_1/h_2 = 1.5$		
0.04	46471	3.072×10^{-3}
0.06	55254	3.646×10^{-3}
0.08	60418	3.935×10^{-3}
0.10	59707	4.108×10^{-3}
0.14	53620	4.306×10^{-3}
0.20	47650	4.454×10^{-3}
Radial clearance ratio, $h_1/h_2 = 2.0$		
0.04	42248	2.776×10^{-3}
0.06	54751	3.624×10^{-3}
0.08	60554	4.051×10^{-3}
0.10	54991	4.308×10^{-3}
0.14	46590	4.602×10^{-3}
0.20	40491	4.822×10^{-3}
Radial clearance ratio, $h_1/h_2 = 2.5$		
0.04	36489	2.301×10^{-3}
0.06	50397	3.426×10^{-3}
0.08	60759	3.997×10^{-3}
0.10	54175	4.341×10^{-3}
0.14	44230	4.735×10^{-3}
0.20	37681	5.031×10^{-3}

* At $h_1/h_2 = 1.0$ the Christopherson tube has a straight-parallel internal profile

Table (A3.17) Comparison of a 2 in straight-tapered Christopherson tube at various values of ($n_0 U$) and radial clearance ratios

Length of Christopherson tube, $l_2 = 6$ in Radial clearance, $h_2 = 0.002$ in Die semi-angle = 12°		
Product ($n_0 U$) (lbf in $^{-1}$)	Lubricant pressure generated (lbf in $^{-2}$)	Lubricant film thickness at die entry (in)
Radial clearance ratio, $h_1/h_2 = *1.0$		
0.002	51971	1.199×10^{-3}
0.004	56155	1.599×10^{-3}
0.006	57599	1.733×10^{-3}
0.008	58347	1.800×10^{-3}
0.012	59120	1.866×10^{-3}
0.020	59758	1.920×10^{-3}
Radial clearance ratio, $h_1/h_2 = 1.5$		
0.002	47801	9.592×10^{-4}
0.004	57613	1.680×10^{-3}
0.006	60439	1.919×10^{-3}
0.008	60662	2.039×10^{-3}
0.012	58783	2.160×10^{-3}
0.020	54778	2.256×10^{-3}
Radial clearance ratio, $h_1/h_2 = 2.0$		
0.002	39641	5.381×10^{-4}
0.004	56136	1.598×10^{-3}
0.006	60658	1.954×10^{-3}
0.008	59773	2.132×10^{-3}
0.012	55355	2.311×10^{-3}
0.020	49555	2.453×10^{-3}
Radial clearance ratio, $h_1/h_2 = 2.5$		
0.002	23937	9.831×10^{-5}
0.004	52715	1.427×10^{-3}
0.008	59646	2.142×10^{-3}
0.012	53802	2.380×10^{-3}
0.020	47091	2.571×10^{-3}

* at $h_1/h_2 = 1.0$ the Christopherson tube has a straight-parallel internal profile

Table (A3.18) Comparison of a 6 in straight-tapered Christopherson tube at various values of ($n_0 U$) and radial clearance ratios

Length of Christopherson tube, $l_2 = 6$ in Radial clearance, $h_2 = 0.004$ in Die semi-angle = 12°			Lubricant film thickness at die entry (in)
Product ($\eta_0 \dot{\gamma}$) (lbf in $^{-1}$)	Lubricant pressure generated (lbf in $^{-2}$)		
Radial clearance ratio, $h_1/h_2 = 1.0$			
0.02	54563		3.359×10^{-3}
0.025	55585		3.487×10^{-3}
0.03	56309		3.573×10^{-3}
0.04	57273		3.680×10^{-3}
0.08	58879		3.840×10^{-3}
0.12	59470		3.893×10^{-3}
Radial clearance ratio, $h_1/h_2 = 1.5$			
0.02	58425		3.646×10^{-3}
0.025	60377		3.877×10^{-3}
0.03	60731		4.031×10^{-3}
0.04	59079		4.223×10^{-3}
0.08	51552		4.512×10^{-3}
0.12	47419		4.608×10^{-3}
Radial clearance ratio, $h_1/h_2 = 2.0$			
0.02	58158		3.624×10^{-3}
0.025	60730		3.966×10^{-3}
0.03	59755		4.194×10^{-3}
0.04	55273		4.479×10^{-3}
0.08	45357		4.907×10^{-3}
0.12	40959		5.049×10^{-3}
Radial clearance ratio, $h_1/h_2 = 2.5$			
0.02	55500		3.425×10^{-3}
0.025	60412		3.883×10^{-3}
0.03	59808		4.188×10^{-3}
0.04	53916		4.570×10^{-3}
0.08	42647		5.143×10^{-3}
0.12	38049		5.335×10^{-3}

* At $h_1/h_2 = 1.0$ the Christopherson tube has a straight-parallel internal profile

Total length of Christopherson tube = 6 in Radial clearance, $h_2 = 0.002$ in Radial clearance ratio, $h_1/h_2 = 1.5$ Die semi-angle = 12°						
Product ($\eta_0 \dot{\gamma}$) ($\times 10^{-3}$ lbf in $^{-1}$)	Lubricant pressure generated (lbf in $^{-2}$)		Lubricant film thickness at die entry (in)			Stepped
	Parallel	Composite	Stepped	Parallel	Composite	
Length ratio, $l_2/l_1 = 1.0$						
2	51971	50504	48410	1.199×10^{-3}	1.113×10^{-3}	9.935×10^{-4}
4	56155	56691	56366	1.599×10^{-3}	1.628×10^{-3}	1.611×10^{-3}
6	57599	58875	59163	1.733×10^{-3}	1.799×10^{-3}	1.816×10^{-3}
8	58347	59914	60338	1.800×10^{-3}	1.885×10^{-3}	1.919×10^{-3}
12	59120	60679	60711	1.866×10^{-3}	1.971×10^{-3}	2.023×10^{-3}
16	59516	60734	60111	1.900×10^{-3}	2.014×10^{-3}	2.074×10^{-3}
20	59758	60514	59249	1.920×10^{-3}	2.040×10^{-3}	2.105×10^{-3}
Length ratio, $l_2/l_1 = 0.2$						
2	51971	44253	18214	1.199×10^{-3}	7.657×10^{-4}	4.676×10^{-5}
4	56155	56143	49962	1.599×10^{-3}	1.599×10^{-3}	1.291×10^{-3}
6	57599	60026	58581	1.733×10^{-3}	1.877×10^{-3}	1.783×10^{-3}
8	58347	60742	60704	1.800×10^{-3}	2.017×10^{-3}	2.030×10^{-3}
12	59120	58857	56147	1.866×10^{-3}	2.156×10^{-3}	2.276×10^{-3}
16	59516	56456	51995	1.900×10^{-3}	2.226×10^{-3}	2.400×10^{-3}
20	59758	54426	49096	1.920×10^{-3}	2.268×10^{-3}	2.474×10^{-3}

Table (A3.20) Comparison of three designs of a 6 in Christopherson tube at various values of ($\eta_0 \dot{\gamma}$) and length ratios

Table (A3.19) Comparison of a 6 in straight-tapered Christopherson tube at various values of ($\eta_0 \dot{\gamma}$) and radial clearance

Draw speed = 100 ft min ⁻¹ Lubricant viscosity = 3.503×10^{-4} lbf s in ⁻² (EP50 at 20°C) Radial clearance, $h_2 = 0.002$ in Length ratio, $l_2/l_1 = 1.0$ Reduction in area = 35% Die semi-angle = 12°				
Total length, $l_1 + l_2$ (in)	Lubricant pressure generated (lbf in ⁻²)		Lubricant film thickness at die entry (in)	
	Composite	Stepped	Composite	Stepped
Radial clearance ratio, $h_1/h_2 = 1.5$				
2	39247	35537	7.910×10^{-4}	6.111×10^{-4}
4	52869	51049	1.464×10^{-3}	1.415×10^{-3}
6	57484	57395	1.690×10^{-3}	1.686×10^{-3}
8	59343	59580	1.804×10^{-3}	1.821×10^{-3}
10	60140	60405	1.871×10^{-3}	1.903×10^{-3}
12	60499	60691	1.917×10^{-3}	1.957×10^{-3}
Radial clearance ratio, $h_1/h_2 = 2.0$				
2	36482	29864	6.556×10^{-4}	3.747×10^{-4}
4	51810	49093	1.414×10^{-3}	1.285×10^{-3}
6	57099	55643	1.670×10^{-3}	1.597×10^{-3}
8	59265	58580	1.798×10^{-3}	1.753×10^{-3}
10	60172	59886	1.875×10^{-3}	1.847×10^{-3}
12	60554	60452	1.926×10^{-3}	1.909×10^{-3}

Table (A3.21) Comparison between composite and stepped Christopherson tubes at various values of (η, μ) and radial clearance ratios

Vos 2.4

7 NOV 83 17:16:37

Terminal: 64

Pan = 7

$Pd_n = 7$

0012	TRACE 1	
0000	MASTER ATTACH	
0001	COMMON /BK1/R1, RP, Z, H2	
0002	COMMON /BK2/AV, VP, U, AR, P4	
0003	COMMON /BK6/PIE, T, S, SH, A1, RE	
0004		
0005	REAL K, J	C
0006	INTEGER AT, DB, L2, AD, P	
0007	PIE=3.14159264	
0008	VP=0.00013863	C
0009	VP - VISCOSITY PRESSURE COEFFICIENT.	
0010	D=1.0	
0011	C T - OUTSIDE DIAMETER OF UNDRAHN TUBE.	C
0012	T=0.10	
0013	T - WALL-THICKNESS OF UNDRAHN TUBE.	C
0014	DD=0.8345	
0015	DD - DIAMETER OF DIE.	C
0016	DP=0.68	
0017	DP - DIAMETER OF PLUG.	C
0018	RP=DP/2.0	
0019	RP - RADIUS OF PLUG.	C
0020	RI=(D-2.0*T)/2.0	
0021	RI - INSIDE RADIUS OF UNDRAHN TUBE.	C
0022	Z=RI/RP	
0023	S=249542.0	
0024	S - STRENGTH COEFFICIENT IN STRESS-STRAIN	C
0025	SH=0.9571	
0026	SH - STRAIN HARDENING CONSTANT IN STRESS-STRAIN	C
0027	A1=PIE*(D**2-(D-2.0*T)**2)/4.0	
0028	A1 - AREA OF UNDRAHN TUBE	C
0029		

0030	C	A2=PIE*(DD*62-DE*62)/4.0
0031		A2 - AREA OF DRAWN TUBE
0032	C	RA=1.0-(A2/A1)
0033		RA - REDUCTION IN AREA
0034	C	RE=100.0*RA
0035		RE - % REDUCTION IN AREA
0036	C	SK=(1.0-(DP/(D-2.0*T)))*100.0
0037		SK - % SINK
0038	C	DS - DRAW SPEED
0039		DS - DIE SEMI-ANGLE IN DEGREES
0040	C	AT - AMBIENT TEMPERATURE IN DEGREE CENTIGRADE
0041		H2 - RADIAL CLEARANCE
0042	C	CR - RADIAL CLEARANCE RATIO, H1/H2
0043		READ(1.10) DS,AD,H2,CR
0044	10	FORMAT(210,2F0.0)
0045		DO 20 I=10,30.2
0046		AT=1
0047		CALL FIND (AT,AD,CR,DS,L2,RA)
0048	20	CONTINUE
0049		READ (1.30) AT,DS,AD,CR
0050	30	FORMAT (310,F0.0)
0051		DO 40 N=2.8
0052		H2=N/1000.0
0053		CALL FIND (AT,AD,CR,DS,L2,RA)
0054	40	CONTINUE
0055		READ (1.50) AT,AD,H2,CR
0056	50	FORMAT (210,2F0.0)
0057		DO 60 L=50,200,10
0058		DS=L
0059		CALL FIND (AT,AD,CR,DS,L2,RA)
0060	60	CONTINUE
0061		READ (1.70) AT,DS,H2,CR
0062	70	FORMAT (210,2F0.0)
0063		DO 80 M=8,13
0064		AD=M
0065		CALL FIND (AT,AD,CR,DS,L2,RA)
0066	80	CONTINUE
0067		READ (1.90) AT,DS,AD,H2
0068	90	FORMAT (310,F0.0)
0069		DO 100 P=15.40.5
0070		CR=P/10.0
0071		CALL FIND (AT,AD,CR,DS,L2,RA)
0072	100	CONTINUE
0073		WRITE(2,99)
0074	99	FORMAT(//////,40X,'***** END OF PROGRAM *****')
0075		STOP
0076		END

END OF SEGMENT, LENGTH 241, NAME ATTACH

0077	TRACED
0078	SUBROUTINE FIND (AT,AD,CR,DS,L2,RA)
0079	REAL J,K,LLIM,XLIN
0080	INTEGER AT,AD,DS,L2
0081	COMMON /BK1/R1,RP,Z,H2,KERR
0082	COMMON /BK2/AV,VP,U,AR,P4
0083	COMMON /BK3/H4,PPA,E3
0084	

```

COMMON /BKA/HB,PTA,Q3
COMMON /BK6/PIE,T,S,SA,A1,BE

C
AR=(PIE/180.0)*RAD
C
AR - DIE SEMI-ANGLE IN RADIANS
AS=PIE*(12.0*(RP+7/COS(AR))**2-(2.0*RP)**2)/A.0
C
AS - AREA OF TUBE AFTER SINKING.
SN=ALOG(A1/AS)
P4=S*(BN**SH)
RT=1.8*AT+.492.0
RT - AMBIENT TEMPERATURE IN CENTIGRADE.
V1=10.0**(12.55-4.4192*ALOG(RT)/ALOG(10.0))
V2=10.0**(V1)-0.8
AV=0.000001768*V2
U=(1.0-RA)*DS*12.0/60.0
K=CR-1.0
H1=H2*(1.0+K)
WRITE (2,101)
101 FORMAT (//////////'/,/,/)
WRITE (2,102) AT,V2,AV
102 FORMAT (10X,'AMBIENT TEMP. = ',12.5X,'K. VISCOSITY = ',F7.1,5X,
'Z.D. VISCOSITY = ',E16.5)
WRITE (2,103) RE,DB,U
103 FORMAT (10X,'REDUCTION = ',F4.1,5X,'DRAW SPEED = ',13.5X,
'ZENTRY SPEED = ',F5.2)
WRITE (2,104) H2,H1
104 FORMAT (10X,'SMALL CLEARANCE = ',F5.3,
'LSX,LARGE CLEARANCE = ',F5.3)
WRITE (2,105) AD,CR
105 FORMAT (10X,'DIE SEMI-ANGLE = ',12.
'LSX,CLEARANCE RATIO = ',F3.1,/)
DO 99 I=2,14,2
L2=1
E3=H2/I-H2**3/(6.0*AV*VP*US*L2**2)
19 IF (E3.GT.0.0) GO TO 21
E3=E3+2.0*ABB(E3)
GO TO 19
21 H4=E3
C
KERR=O
C* INITIALISE JSIGN2
JSIGN2=1
XLIM=O.OOI
ICOUNT=O
22 ICOUNT=ICOUNT+1
CALL PARA(X,L2)
C* IN CASE E5 IS GREATER THAN OR EQUAL TO 1
IF(KERR.EQ.1) OLDDH=H4
IF(KERR.EQ.251) H4=OLDDH
IF(KERR.EQ.251) XLIM=XLIM/10.0
C
IF(KERR.NE.501) GOTO B01
H4=OLDDH
JSIGN2=-1
XLIM=O.OOI
B01 IF(KERR.EQ.751) XLIM=XLIM/10.0
IF(KERR.EQ.751) H4=OLDDH
C* ERROR EXISTS IF KERR=1000
IF(KERR.LE.1000) GOTO 25
144

```

```

0145 WRITE(2,903) L2
0146 FORMAT(' *** ERROR * PARA: INVALID E5 *** L2 = ',I4//)
0147 GOTO 99
C
0148 IF(KERR.NE.0) GOTO 23
0149 JSION2=X/ABS(X)
0150
C
0151 WRITE DEBUG OUTPUT
C
0152 WRITE(2,901) JCOUNT, X, H4, JSION2
0153 FORMAT(1H1, ' DEBUG * PARA : JCOUNT=',I6,4X,
0154 &'X = ',F15.7, ' H4 = ',E16.5, ' JSION2 = ',I2)
C
0155 IF(ABS(X).LT.1.0) GOTO 62
0156 IF(JCOUNT.EQ.1) GOTO 23
0157
C
0158 IF(JSION1.EQ.JSION2) GOTO 23
0159
C
0160 XLIM=XLIM/10.0
0161 H4=H4+JSION2*XLIM*H4
0162 JSION1=JSION2
0163 GOTO 22
C
0164
0165 O3=2.0*(1+K)*H2/((2.0+K)*Z)-H2**3*(1+K)**2
0166 & /13*AV*VP*U*L2*Z*(2.0+K))
0167 IF (O3.GT.0.0) GOTO 32
0168 O3=O3+2.0*ABS(O3)
0169 GO TO 33
0170
0171 H6=O3
0172
C
0173 C* RESET THE VALUE OF JSION2 TO BE 1 FOR TAPA
0174 JSION2=1
0175 XLIM=0.001
0176 JCOUNT=0
0177 KERR=0
0178 JCOUNT=JCOUNT+1
0179 CALL TAPA(K,L2,J)
0180
C* IN CASE O5 IS GREATER THAN OR EQUAL TO 1
0181 IF(KERR.EQ.1) OLDH6=H6
0182 IF(KERR.EQ.251) H6=OLDH6
0183 IF(KERR.EQ.251) XLIM=XLIM/10.0
C
0184 IF(KERR.NE.501) GOTO 811
0185 H6=OLDH6
0186 JSION2=-1
0187 XLIM=0.001
0188 IF(KERR.EQ.751) XLIM=XLIM/10.0
0189 IF(KERR.EQ.751) H6=OLDH6
0190
C** ERROR EXISTS IF KERR=1000
0191 IF(KERR.LE.1000) GOTO 341
0192 WRITE(2,904) L2
0193 FORMAT(' *** ERROR * TAPA: INVALID O5 *** L2 = ',I4//)
0194 GOTO 99
C
0195 IF(KERR.NE.0) GOTO 35
0196 JSION2=J/ABS(J)
C
0197
C
0198 WRITE DEBUG OUTPUT
C
0199 WRITE(2,902) JCOUNT, J, H6, JSION2
0200 FORMAT(1H1, ' DEBUG * TAPA : JCOUNT=',I6,4X,
0201 &'J = ',F15.7, ' H6 = ',E16.5, ' JSION2 = ',I2)
0202
C
0203
0204

```

0205	IF(ABS(J).LT.1.0) GO TO 37	
0206	IF(JCOUNT.EQ.1) GO TO 38	
0207	IF(JBION1.EQ.JBION2) GO TO 38	
0208	JLIM=JLIM/10.0	
0209	H6=H6+JBION2*JLIM*H6	
0210	JBION1=JBION2	
0211	GO TO 34	
C		
37	IPPA=INT(PPA)	
0212	IPTA=INT(PTA)	
0213	HP=H4	
0214	HT=H6	
0215	WRITE (2,38) L2,IPPA,IPTA,HP,HT	
0216	FORMAT (10X,'L2= ',I3.5X,'PPA= ',I6.5X,'PTA= ',I6.5X,'HP= ',E16.5,	
0217	38	
0218	5X,'HT= ',E16.5)	
0219	99 CONTINUE	
0220	RETURN	
0221	END	
0222		
(END OF SEGMENT, LENGTH 570, NAME FIND	
(
(TRACE 0	
0223	SUBROUTINE PARA (X,L2)	
0224	INTEGER L2	
0225	COMMON /BK1/R1,RP,Z,H2,KERR	
0226	COMMON /BK2/AV,VP,U,AR,P4	
0227	COMMON /BK3/H4,PPA,E3	
0228	H3=R1-RP	
0229	G1=1.0*RP/H3	
0230	G2=1.0*RP/H4	
0231	B1=1.0/VP*ALOG(G1/G2)	
0232	B2=ALOG(G2/G1)	
0233	B3=1.0/H3-1.0/H4	
0234	B4=1.0/H4-1.0/H3	
0235	B5=(RP/2.0)*(1.0/H3+2-1.0/H4+2)	
0236	B6=H4-(B2+(RP*B3))/(B1+B4+B5)	
0237	B7=6.0*AV*VP*U*(H3+RP)	
0238	B8=B7*(B1+B4+B5)/(RP+2*TAN(AR))	
0239	P3=-(1.0/VP*ALOG(B6*B8*EXP(-(VP*P4))))	
0240	E1=6.0*AV*VP*U*L2*Z/H2+3	
0241	E2=H2/Z-H4	
0242	E3=E1+E2	
0243	IF((E3.EQ.1.0).OR.(E3.GT.1.0)) GO TO 28	
0244	KERR=0	
0245	PPA=-(1.0/VP*ALOG(1.0-E1+E2))	
0246	X=PPA-P3	
0247	GO TO 29	
0248	28 KERR=KERR+1	
0249	29 RETURN	
0250	END	
0251		
0252		
(END OF SEGMENT, LENGTH 212, NAME PARA	
(
(TRACE 0	
0253		
0254		

```

0255 SUBROUTINE TAPA (K,L2,J)
0256 INTEGER L2
0257 REAL K,J
0258 COMMON /BK1/R1,RP,Z,H2,KERR
0259 COMMON /BK2/AV,VP,U,AR,P4
0260 COMMON /BK4/H6,PTA,O3
0261 H3=R1-RP
0262 M1=1.0+RP/H3
0263 M2=1.0+RP/H6
0264 Q1=1.0/VP*ALOG(M1/M2)
0265 Q2=ALOG(M2/M1)
0266 Q3=1.0/H3-1.0/H6
0267 Q4=1.0/H6-1.0/H3
0268 Q5=RP/2.0*(1.0/H3**2-1.0/H6**2)
0269 Q6=H6-(Q2+(RP*Q3))/(Q1+Q4+Q5)
0270 Q7=6.0*AV*VP*U*(H3+RP)
0271 Q8=Q7*(Q1+Q4+Q5)/(RP**2*TAN(AR))
0272 P3=-(1.0/VP*ALOG(Q6*Q8*EXP(-(VP*P4))))
0273 Q1=3.0*AV*VP*U*L2*(2.0+K)/(H2**3*(1.0+K)**2)
0274 Q2=2.0*(1.0+K)*H2/((2.0+K)*Z)-H6
0275 Q5=Q1*Q2
0276 IF((Q5.EQ.1.0).OR.(Q5.GT.1.0)) GO TO 53
0277 KERR=O
0278 PTA=-(1.0/VP*ALOG(1.0-Q1*Q2))
0279 J=PTA-P3
0280 GO TO 54
0281 53 KERR=KERR+1
0282 54 RETURN
0283 END

```

END OF SEGMENT, LENGTH 236, NAME TAPA

0284 FINISH

END OF COMPILATION - NO ERRORS

S/C SUBFILE : 33 BUCKETS USED
CONSOLIDATED BY XPCX 12H DATE 07/11/83 TIME 17/07/01

*SHORTLIST

*IN ED (FORTSEMCOMP)

*LIB ED (SUBGROUPRFA.SUBROUTINES)

*WORK ED (FORTHORFILE)

PROGRAM FXXX
EXTENDED DATA (22AM)
COMPACT PROGRAM (DBM)
CORE 6912

EOF.

Computer programme for tool design (BASIC)

```

10 ! THIS IS A PROGRAMME FOR TOOL DESIGN AND COMPUTES THE REQUIRED
20 ! LENGTHS OF THE FOUR DESIGNS OF PLUG-ATTACHMENTS TO GENERATE A
30 ! GIVEN HYDRODYNAMIC LUBRICANT PRESSURE IN THE SINK ZONE AT
40 ! DIFFERENT VALUES OF THE DRAW SPEED AND RADIAL CLEARANCE.
50 !
60 !
70 !
80 DIM H4(99),DS(99),U(99),PSK(99),PD(99)
90 SEMIANGLE=12
100 ! THE SEMI-ANGLE IS IN DEGREES
110 VP=.00013863
120 ! VP - VISCOSITY PRESSURE COEFFICIENT IN (IN2 LBF-1)
130 Y=60760
140 ! Y - YIELD STRESS OF TUBE MATERIAL IN (LBF IN-2)
150 S=249542
160 ! S - STRENGTH CONSTANT IN STRESS-STRAIN EQUATION (LBF IN-2)
170 N=.5571
180 ! N - STRAIN HARDENING CONSTANT IN STRESS-STRAIN EQUATION
190 !
200 !
210 ! INPUT DATA IN IMPERIAL UNITS
220 !
230 !
240 DISP "ENTER THE HYDRODYNAMIC LUBRICANT PRESSURE TO BE GENERATED"
250 INPUT P3
260 DISP "ENTER INITIAL TUBE DIMENSIONS - OUTSIDE DIAMETER AND WALL THICKNESS"
270 INPUT D,T
280 DISP "ENTER FINAL TUBE DIMENSIONS - OUTSIDE DIAMETER AND WALL THICKNESS"
290 INPUT DD,TT
300 DISP "ENTER ANTICIPATED AMBIENT TEMPERATURE IN DEGREE CENTIGRADE"
310 INPUT AT
320 !
330 !
340 ! PRELIMINARY COMPUTATIONS
350 !
360 !
370 A1=PI *(D^2-(D-2*T)^2)/4
380 ! A1 - CROSS SECTIONAL AREA OF INITIAL TUBE
390 A2=PI *(DD^2-(DD-2*TT)^2)/4
400 ! A2 - CROSS SECTIONAL AREA OF FINAL TUBE
410 RA=(1-A2/A1)*100
420 ! RA - PERCENTAGE REDUCTION IN CROSS SECTIONAL AREA
430 SK=(1-(DD-2*TT)/(D-2*T))*100
440 ! SK - PERCENTAGE SINK
450 RP=(DD-2*TT)/2
460 ! RP - RADIUS OF PLUG
470 RI=(D-2*T)/2
480 ! RI - INSIDE RADIUS OF INITIAL TUBE
490 Z=RI/RP
500 AR=PI /180*SEMIANGLE
510 ! AR - THE SEMI-ANGLE IN RADIANS
520 AS=PI *((2*(RP+T/COS (AR)))^2-(2*RP)^2)/4
530 ! AS - AREA OF TUBE AFTER SINKING
540 STRAIN=LOG (A1/AS)
550 P4=S*STRAIN^N

```

```

560 COMPAT=AT+8
570 ! ADD 8 DEGREES CENTIGRADE TO AMBIENT TEMPERATURE TO COMPENSATE FOR
580 ! HEAT CONDUCTED FROM METAL DEFORMATION ZONE
590 RT=1.8*COMPAT+492
600 ! RT - AMBIENT TEMPERATURE IN DEGREES RANKINE
610 V1=10^(12.55-4.4192*LOG (RT)/LOG (10))
620 V2=10^V1-.8
630 AV=.0000001768*V2
640 ! AV - VISCOSITY OF LUBRICANT (EP 50) IN (LBF S IN^-2)
650 !
660 !
670 !                                     END OF PRELIMINARY COMPUTATIONS
680 !
690 !
700 !
710 !
720 !                                     OUTPUT INFORMATIVE DATA AND RESULTS OF PRELIMINARY COMPUTATIONS
730 !
740 !
750 PRINT USING 880 ; "HYDRODYNAMIC LUBRICANT PRESSURE=",P3,"LBF IN^-2"
760 PRINT USING 890 ; "INITIAL TUBE DIMENSIONS=",D," X ",T,"IN (O.D. X T)"
770 PRINT USING 900 ; "FINAL TUBE DIMENSIONS=",DD," X ",TT,"IN (O.D. X T)"
780 PRINT USING 910 ; "PERCENTAGE REDUCTION IN AREA=",RA,"%"
790 PRINT USING 920 ; "PERCENTAGE SINK=",SK,"%"
800 PRINT USING 930 ; "ANTICIPATED AMBIENT TEMPERATURE=",AT,"DEGREE CENTIGRADE"
810 PRINT USING 940 ; "LUBRICANT VISCOSITY (EP 50)=",AV,"LBF S IN^-2"
820 PRINT USING 950 ; "DIE SEMI-ANGLE=",SEMIANGLE,"DEGREE"
830 PRINT
840 PRINT
850 PRINT USING 960 ; "*****"
860 PRINT
870 PRINT
880 IMAGE 3X,33A,4D
890 IMAGE 3X,25A,Z.DDD,3A,Z.DDD
900 IMAGE 3X,23A,Z.DDD,3A,Z.DDD
910 IMAGE 3X,30A,DD.DD
920 IMAGE 3X,17A,DD.DD
930 IMAGE 3X,33A,DD
940 IMAGE 3X,29A,D.DDDE
950 IMAGE 3X,16A,DD
960 IMAGE 3X,57A
970 !
980 !
990 ! NUMERICAL ITERATION TO COMPUTE H4 USING EQUATION (3.61) BY SINK ZONE
1000 ! ANALYSIS AT DIFFERENT VALUES OF THE DRAW SPEED
1010 !
1020 !
1030 FOR I=1 TO 5
1040 DS(I)=I*10
1050 U(I)=(1-RA/100)*DS(I)*12/60
1060 H4(I)=.000001
1070 ! THIS IS THE INITIAL ESTIMATE OF H4
1080 LIM=.1
1090 COUNT=0
1100 COUNT=COUNT+1

```

```

1110 GOSUB 1260
1120 DISP I,PD(I),H4(I)
1130 SIGN2=PD(I)/ABS (PD(I))
1140 IF ABS (PD(I))<1 THEN GOTO 1210
1150 IF COUNT=1 THEN GOTO 1180
1160 IF SIGN1=SIGN2 THEN GOTO 1180
1170 LIM=LIM/5
1180 H4(I)=H4(I)+SIGN2*LIM*H4(I)
1190 SIGN1=SIGN2
1200 GOTO 1100
1210 NEXT I
1220 GOTO 1500
1230 !
1240 ! START OF SUBROUTINE
1250 !
1260 H3=RI-RP
1270 G1=1+RP/H3
1280 G2=1+RP/H4(I)
1290 B1=1/RP*LOG (G1/G2)
1300 B2=LOG (G2/G1)
1310 B3=1/H3-1/H4(I)
1320 B4=1/H4(I)-1/H3
1330 B5=RP/2*(1/H3^2-1/H4(I)^2)
1340 B6=H4(I)-(B2+RP*B3)/(B1+B4+B5)
1350 B7=6*AV*U(I)*VP*(H3+RP)
1360 B8=B7*(B1+B4+B5)/(RP^2*TAN (AR))
1370 PSK(I)=-((1/VP*LOG (B6*B8+EXP (-(VP*P4))))
1380 PD(I)=P3-PSK(I)
1390 RETURN
1400 !
1410 ! END OF SUBROUTINE
1420 !
1430 !
1440 ! COMPUTATIONS FOR THE REQUIRED LENGTHS OF THE FOUR DESIGNS OF
1450 ! PLUG-ATTACHMENTS AT DIFFERENT VALES OF THE RADIAL CLEARANCE
1460 !
1470 !
1480 ! LOOP FOR DIFFERENT VALUES OF THE RADIAL CLEARANCE, H2
1490 !
1500 FOR H2=.002 TO .01 STEP .001
1510 !
1520 ! LOOP FOR DIFFERENT VALUES OF THE RADIAL CLEARANCE RATIO, CR=H1/H2
1530 !
1540 FOR CR=1.5 TO 2.5 STEP .5
1550 K=CR-1
1560 H1=H2*(1+K)
1570 !
1580 ! RETRIEVE UNDRAWN TUBE VELOCITY, U, AND CORRESPONDING VALUE OF H4
1590 ! FROM ARRAY
1600 !
1610 FOR I=1 TO 5
1620 L2P=(1-EXP (-(VP*P3)))*H2^3/((H2-Z*H4(I))*(6*AV*U(I)*VP))
1630 ! L2P - LENGTH OF STRAIGHT-PARALLEL PLUG-ATTACHMENT
1640 ! USING EQUATION (3.75)
1650 T1=(1-EXP (-(VP*P3)))*(1+K)^2*H2^3

```

```

1660 T2=(2*(1+K)*H2-Z*(2+K)*H4(I))*(3*AV*U(I)*VP)
1670 L2T=T1/T2
1680 ! L2T - LENGTH OF STRAIGHT-TAPERED PLUG-ATTACHMENT
1690 ! USING EQUATION (3.76)
1700 !
1710 !
1720 ! OUTPUT RESULTS
1730 !
1740 !
1750 PRINT USING 1840 ; "DRAW SPEED=",DS(I),"FT MIN^-1"
1760 PRINT USING 1850 ; "RADIAL CLEARANCE, H2=",H2,"IN"
1770 PRINT USING 1860 ; "RADIAL CLEARANCE RATIO, H1/H2=",CR
1780 PRINT USING 1870 ; "LUBRICANT FILM THICKNESS, H4=",H4(I),"IN"
1790 PRINT
1800 PRINT USING 1880 ; "LENGTH OF STRAIGHT-PARALLEL PLUG-ATTACHMENT=",L2P,"IN"
1810 PRINT USING 1890 ; "LENGTH OF STRAIGHT-TAPERED PLUG-ATTACHMENT=",L2T,"IN"
1820 PRINT
1830 PRINT
1840 IMAGE 3X,12A,DD
1850 IMAGE 3X,22A,D.DDD
1860 IMAGE 3X,31A,D.D
1870 IMAGE 3X,29A,D.DDDDE
1880 IMAGE 3X,45A,DD.DD
1890 IMAGE 3X,43A,DD.DD
1900 !
1910 !
1920 ! COMPUTATION OF THE LENGTHS OF THE TWO-ZONE PLUG-ATTACHMENTS
1930 !
1940 !
1950 ! LOOP FOR DIFFERENT VALUES OF THE LENGTH RATIO, LR= L2/L1
1960 !
1970 FOR LR=.5 TO 1.5 STEP .5
1980 T3=1-EXP(-(VP*P3))
1990 T4=(1/(LR*H1^3))*(H1-Z*H4(I))+1/H2^3*(H2-H4(I))*(6*AV*U(I)*VP)
2000 T5=(2+K)/(LR*H2^3*(1+K)^2)*(2*(1+K)*H2/(2+K)-Z*H4(I))
2010 T6=(T5+2*(H2-Z*H4(I))/H2^3)*(3*AV*U(I)*VP)
2020 L2S=T3/T4
2030 ! L2S - LENGTH OF ZONE 2 OF STEPPED PLUG-ATTACHMENT
2040 ! USING EQUATION (3.77)
2050 L2C=T3/T6
2060 ! L2C - LENGTH OF ZONE 2 OF COMPOSITE PLUG-ATTACHMENT
2070 ! USING EQUATION (3.78)
2080 TLS=L2S/LR+L2S
2090 ! TLS - TOTAL LENGTH OF STEPPED PLUG-ATTACHMENT
2100 L1S=TLS-L2S
2110 ! L1S - LENGTH OF ZONE 1 OF STEPPED PLUG-ATTACHMENT
2120 TLC=L2C/LR+L2C
2130 ! TLC - TOTAL LENGTH OF COMPOSITE PLUG-ATTACHMENT
2140 L1C=TLC-L2C
2150 ! L1C - LENGTH OF ZONE 1 OF COMPOSITE PLUG-ATTACHMENT
2160 !
2170 !
2180 ! OUTPUT RESULTS
2190 !
2200 !

```

```

2210 PRINT USING 2270 ; "LENGTH RATIO OF TWO-ZONE PLUG-ATTACHMENT, LR=L2/L1=",LR
2220 PRINT USING 2280 ; "COMPOSITE (IN)","STEPPED (IN)"
2230 PRINT USING 2290 ; "TOTAL LENGTH",TLC,TLs
2240 PRINT USING 2300 ; "LENGTH OF ZONE 1",L1C,L1s
2250 PRINT USING 2310 ; "LENGTH OF ZONE 2",L2C,L2s
2260 PRINT
2270 IMAGE 3X,52A,D.D
2280 IMAGE 24X,14A,6X,12A
2290 IMAGE 3X,12A,13X,DD.DD,15X,DD.DD
2300 IMAGE 3X,16A,9X,DD.DD,15X,DD.DD
2310 IMAGE 3X,16A,9X,DD.DD,15X,DD.DD
2320 NEXT LR
2330 PRINT
2340 PRINT
2350 PRINT USING 2360 ; ".....
.. "
2360 IMAGE 3X,57A
2370 PRINT
2380 PRINT
2390 NEXT I
2400 PRINT
2410 NEXT CR
2420 PRINT
2430 NEXT H2
2440 PRINT
2450 PRINT
2460 PRINT " ***** END OF PROGRAMME *****"
2470 END

```

LENGTH RATIO OF TWO-ZONE PLUG-ATTACHMENT, LR=L2/L1= 1.0		
	COMPOSITE (IN)	STEPPED (IN)
TOTAL LENGTH	3.73	4.31
LENGTH OF ZONE 1	1.87	2.15
LENGTH OF ZONE 2	1.87	2.15

LENGTH RATIO OF TWO-ZONE PLUG-ATTACHMENT, LR=L2/L1= 1.0		
	COMPOSITE (IN)	STEPPED (IN)
TOTAL LENGTH	3.89	4.80
LENGTH OF ZONE 1	1.44	1.80
LENGTH OF ZONE 2	2.45	3.00

Sample of the computer print-out

HYDRODYNAMIC LUBRICANT PRESSURE= 500 LBF IN⁻²
INITIAL TUBE DIMENSIONS= 0.830 X 0.093 IN (O.D. X T)
FINAL TUBE DIMENSIONS= 0.687 X 0.078 IN (O.D. X T)
PERCENTAGE REDUCTION IN AREA= 30.70 %
PERCENTAGE SINK= 17.55 %
ANTICIPATED AMBIENT TEMPERATURE= 20 DEGREE CENTIGRADE
LUBRICANT VISCOSITY (EP 50)= 1.495E-004 LBF S IN⁻²
DIE SEMI-ANGLE= 12 DEGREE

DRAW SPEED= 20 FT MIN⁻¹
RADIAL CLEARANCE, H2= .004 IN
RADIAL CLEARANCE RATIO, H1/H2= 1.5
LUBRICANT FILM THICKNESS, H4=1.0537E-006 IN

LENGTH OF STRAIGHT-PARALLEL PLUG-ATTACHMENT= 3.11 IN

LENGTH OF STRAIGHT-TAPERED PLUG-ATTACHMENT= 4.66 IN

LENGTH RATIO OF TWO-ZONE PLUG-ATTACHMENT, LR=L2/L1= .5
COMPOSITE (IN) STEPPED (IN)
TOTAL LENGTH 4.00 4.94
LENGTH OF ZONE 1 2.67 3.29
LENGTH OF ZONE 2 1.33 1.65

LENGTH RATIO OF TWO-ZONE PLUG-ATTACHMENT, LR=L2/L1= 1.0
COMPOSITE (IN) STEPPED (IN)
TOTAL LENGTH 3.73 4.31
LENGTH OF ZONE 1 1.87 2.15
LENGTH OF ZONE 2 1.87 2.15

LENGTH RATIO OF TWO-ZONE PLUG-ATTACHMENT, LR=L2/L1= 1.5
COMPOSITE (IN) STEPPED (IN)
TOTAL LENGTH 3.59 4.00
LENGTH OF ZONE 1 1.44 1.60
LENGTH OF ZONE 2 2.15 2.40

.....

Sample of the computer print-out

HYDRODYNAMIC LUBRICANT PRESSURE= 1000 LBF IN⁻²
 INITIAL TUBE DIMENSIONS= 0.830 X 0.093 IN (O.D. X T)
 FINAL TUBE DIMENSIONS= 0.687 X 0.078 IN (O.D. X T)
 PERCENTAGE REDUCTION IN AREA= 30.70 %
 PERCENTAGE SINK= 17.55 %
 ANTICIPATED AMBIENT TEMPERATURE= 20 DEGREE CENTIGRADE
 LUBRICANT VISCOSITY (EP 50)= 1.495E-004 LBF S IN⁻²
 DIE SEMI-ANGLE= 12 DEGREE

DRAW SPEED= 30 FT MIN⁻¹
 RADIAL CLEARANCE, H2= .004 IN
 RADIAL CLEARANCE RATIO, H1/H2= 2.0
 LUBRICANT FILM THICKNESS, H4=1.6939E-006 IN

LENGTH OF STRAIGHT-PARALLEL PLUG-ATTACHMENT= 4.01 IN

LENGTH OF STRAIGHT-TAPERED PLUG-ATTACHMENT= 8.02 IN

LENGTH RATIO OF TWO-ZONE PLUG-ATTACHMENT, LR=L2/L1= .5

	COMPOSITE (IN)	STEPPED (IN)
TOTAL LENGTH	6.01	8.02
LENGTH OF ZONE 1	4.01	5.34
LENGTH OF ZONE 2	2.00	2.67

LENGTH RATIO OF TWO-ZONE PLUG-ATTACHMENT, LR=L2/L1= 1.0

	COMPOSITE (IN)	STEPPED (IN)
TOTAL LENGTH	5.34	6.41
LENGTH OF ZONE 1	2.67	3.21
LENGTH OF ZONE 2	2.67	3.21

LENGTH RATIO OF TWO-ZONE PLUG-ATTACHMENT, LR=L2/L1= 1.5

	COMPOSITE (IN)	STEPPED (IN)
TOTAL LENGTH	5.01	5.73
LENGTH OF ZONE 1	2.00	2.29
LENGTH OF ZONE 2	3.01	3.44

.....

Sample of the computer print-out

HYDRODYNAMIC LUBRICANT PRESSURE= 1500 LBF IN⁻²
INITIAL TUBE DIMENSIONS= 0.830 X 0.093 IN (O.D. X T)
FINAL TUBE DIMENSIONS= 0.687 X 0.078 IN (O.D. X T)
PERCENTAGE REDUCTION IN AREA= 30.70 %
PERCENTAGE SINK= 17.55 %
ANTICIPATED AMBIENT TEMPERATURE= 20 DEGREE CENTIGRADE
LUBRICANT VISCOSITY (EP 50)= 1.495E-004 LBF S IN⁻²
DIE SEMI-ANGLE= 12 DEGREE

DRAW SPEED= 40 FT MIN⁻¹
RADIAL CLEARANCE, H2= .004 IN
RADIAL CLEARANCE RATIO, H1/H2= 1.5
LUBRICANT FILM THICKNESS, H4=2.4204E-006 IN

LENGTH OF STRAIGHT-PARALLEL PLUG-ATTACHMENT= 4.36 IN

LENGTH OF STRAIGHT-TAPERED PLUG-ATTACHMENT= 6.54 IN

LENGTH RATIO OF TWO-ZONE PLUG-ATTACHMENT, LR=L2/L1= .5
COMPOSITE (IN) STEPPED (IN)
TOTAL LENGTH 5.61 6.93
LENGTH OF ZONE 1 3.74 4.62
LENGTH OF ZONE 2 1.87 2.31

LENGTH RATIO OF TWO-ZONE PLUG-ATTACHMENT, LR=L2/L1= 1.0
COMPOSITE (IN) STEPPED (IN)
TOTAL LENGTH 5.23 6.04
LENGTH OF ZONE 1 2.62 3.02
LENGTH OF ZONE 2 2.62 3.02

LENGTH RATIO OF TWO-ZONE PLUG-ATTACHMENT, LR=L2/L1= 1.5
COMPOSITE (IN) STEPPED (IN)
TOTAL LENGTH 5.03 5.61
LENGTH OF ZONE 1 2.01 2.24
LENGTH OF ZONE 2 3.02 3.36

.....

Sample of the computer print-out

HYDRODYNAMIC LUBRICANT PRESSURE= 2000 LBF IN⁻²
INITIAL TUBE DIMENSIONS= 0.830 X 0.093 IN (O.D. X T)
FINAL TUBE DIMENSIONS= 0.687 X 0.078 IN (O.D. X T)
PERCENTAGE REDUCTION IN AREA= 30.70 %
PERCENTAGE SINK= 17.55 %
ANTICIPATED AMBIENT TEMPERATURE= 20 DEGREE CENTIGRADE
LUBRICANT VISCOSITY (EP 50)= 1.495E-004 LBF S IN⁻²
DIE SEMI-ANGLE= 12 DEGREE

DRAW SPEED= 50 FT MIN⁻¹
RADIAL CLEARANCE, H2= .004 IN
RADIAL CLEARANCE RATIO, H1/H2= 2.0
LUBRICANT FILM THICKNESS, H4=3.2422E-006 IN

LENGTH OF STRAIGHT-PARALLEL PLUG-ATTACHMENT= 4.50 IN

LENGTH OF STRAIGHT-TAPERED PLUG-ATTACHMENT= 9.00 IN

LENGTH RATIO OF TWO-ZONE PLUG-ATTACHMENT, LR=L2/L1= .5
COMPOSITE (IN) STEPPED (IN)
TOTAL LENGTH 6.75 9.00
LENGTH OF ZONE 1 4.50 6.00
LENGTH OF ZONE 2 2.25 3.00

LENGTH RATIO OF TWO-ZONE PLUG-ATTACHMENT, LR=L2/L1= 1.0
COMPOSITE (IN) STEPPED (IN)
TOTAL LENGTH 6.00 7.20
LENGTH OF ZONE 1 3.00 3.60
LENGTH OF ZONE 2 3.00 3.60

LENGTH RATIO OF TWO-ZONE PLUG-ATTACHMENT, LR=L2/L1= 1.5
COMPOSITE (IN) STEPPED (IN)
TOTAL LENGTH 5.63 6.43
LENGTH OF ZONE 1 2.25 2.57
LENGTH OF ZONE 2 3.38 3.86

.....

APPENDIX A5: THEORETICAL ANALYSIS OF TUBE-DRAWING - AN UPPER-BOUND APPROACH

Adopting Johnson's⁽¹²⁾ proposal of using straight lines as velocity discontinuities, a kinematically admissible velocity field is assumed for the deformation process. Johnson⁽¹²⁾, however, considered plane strain extrusion and rolling processes and assumed that the deforming metal acted between these lines as a rigid body. Loke⁽⁸⁴⁾ adopted this model and accounted for circumferential straining in the analysis of bimetal tube-drawing on a floating-plug. In the present analysis it is proposed to consider, also, both the circumferential and the thickness straining in the deformation process.

APPENDIX A5: THEORETICAL ANALYSIS OF TUBE-DRAWING
- AN UPPER-BOUND APPROACH

The proposed straight line velocity discontinuities are shown in Figure (A5.1). Plastic work is dissipated by shearing across the velocity discontinuities AB and CD, and by friction at the tool-work interfaces ADE and CF. Further work is dissipated in the deformation zone due to circumferential and thickness straining, causing an increase in the velocity of the material in this zone. In zone I the undrawn tube travels in a direction parallel to the drawing axis. In zone II the material flows approximately at an angle α to the drawing axis and accelerates due to circumferential and thickness straining.

APPENDIX A5: THEORETICAL ANALYSIS OF TUBE-DRAWING - AN UPPER-BOUND

APPROACH

Adopting Johnson's⁽¹²⁾ proposal of using straight lines as velocity discontinuities, a kinematically admissible velocity field is assumed for the deformation process. Johnson⁽¹²⁾, however, considered plane strain extrusion and coining processes and assumed that the deforming metal moved between these lines as a rigid body. Loke⁽⁸⁴⁾ adopted this method and accounted for circumferential straining in the analysis of bimetal tube-drawing on a floating-plug. In the present analysis it is proposed to consider, also, both the circumferential and the thickness straining in the deformation process.

The proposed straight line velocity discontinuities are shown in Figure (A5.1). Plastic work is dissipated by shearing across the velocity discontinuities AB and CD, and by friction at the tool-work interfaces ADE and CF. Further work is dissipated in the deformation zone due to circumferential and thickness straining, causing an increase in the velocity of the material in this zone. In zone 1 the undrawn tube travels in a direction parallel to the drawing axis. In zone 2 the material flows approximately at an angle α to the drawing axis and accelerates due to circumferential and thickness straining.

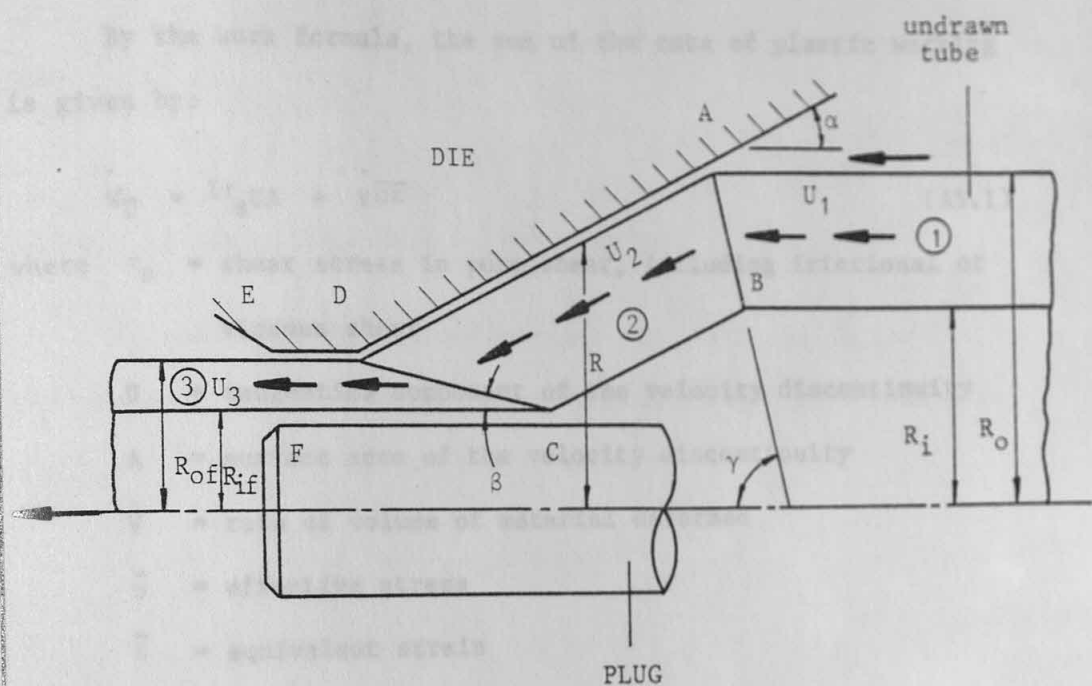


Figure (A5.1) Proposed straight line velocity discontinuities

$U_3 = \text{Draw speed}$

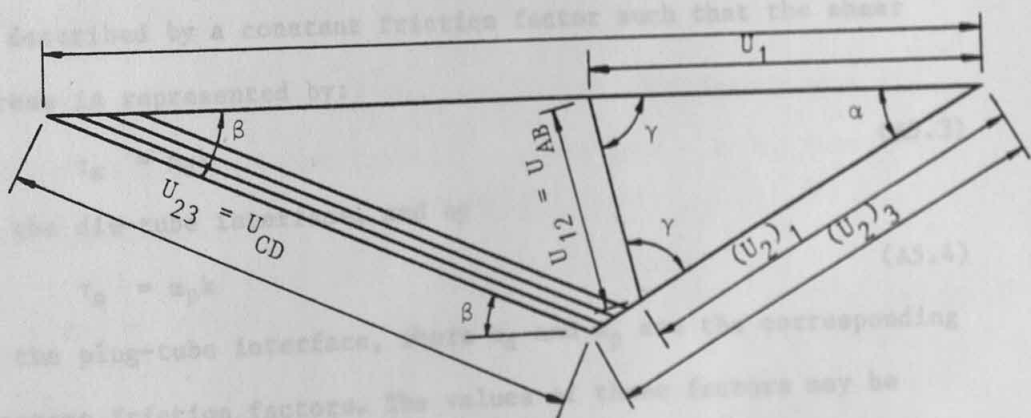


Figure (A5.2) Hodograph associated with Figure (A5.1)

A5.1 BASIC CONSIDERATIONS

By the work formula, the sum of the rate of plastic working is given by:

$$\dot{W}_T = \Sigma \tau_s UA + \dot{V} \bar{\sigma} \bar{\epsilon} \quad (A5.1)$$

where τ_s = shear stress in pure shear, including frictional or viscous shear

U = tangential component of the velocity discontinuity

A = surface area of the velocity discontinuity

\dot{V} = rate of volume of material deformed

$\bar{\sigma}$ = effective stress

$\bar{\epsilon}$ = equivalent strain

In the above equation:

$$\tau_s = k \quad (A5.2)$$

where k is the shear yield stress of the material in pure shear when considering shearing across a velocity discontinuity within the material. For simplicity shearing at the tool-work interfaces is described by a constant friction factor such that the shear stress is represented by:

$$\tau_s = m_d k \quad (A5.3)$$

at the die-tube interface, and by

$$\tau_s = m_p k \quad (A5.4)$$

at the plug-tube interface, where m_d and m_p are the corresponding constant friction factors. The values of these factors may be expected to vary inversely with the hydrodynamic pressure generated by, for example, a Christopherson tube or a plug-attachment at the entry to the deformation zone. However, it is not proposed to include the evaluations of the values of m_d and m_p in equation (A5.1), when drawing under different lubrication conditions.

Using the von Mises' yield criterion:

$$\bar{\sigma} = \sqrt{3} k \quad (A5.5)$$

and

$$k = \frac{Y}{2} \quad (A5.6)$$

where Y is the yield stress of the material.

In analysing the circumferential and thickness in the deformation zone the cylindrical co-ordinate (R, Z, θ) system is used. The equivalent strain can be written:

$$\bar{\epsilon} = \frac{2}{\sqrt{3}} (\epsilon_R^2 + \epsilon_R \epsilon_\theta + \epsilon_\theta^2)^{\frac{1}{2}} \quad (A5.7)$$

or

$$d\bar{\epsilon} = \frac{2}{\sqrt{3}} (d\epsilon_R^2 + d\epsilon_R d\epsilon_\theta + d\epsilon_\theta^2)^{\frac{1}{2}}$$

where $d\epsilon_R = \frac{dt}{t}$ and $d\epsilon_\theta = \frac{dc}{c}$ (A5.8)

t and c being the wall thickness and circumference of the tube respectively.

The circumference of the tube in the deformation zone at any radius R (see Figure (A5.1)) is given by $c = 2\pi R$. Hence using equation (A5.8),

$$d\epsilon_\theta = \frac{dR}{R} \quad (A5.9)$$

Hence, in the direction of drawing,

$$\epsilon_\theta = \int_{R_{of}}^{R_o} \frac{dR}{R} = \ln\left(\frac{R_o}{R_{of}}\right) \quad (A5.10)$$

If it is assumed that the wall thickness does not alter during sinking, the strain in draft, by (A5.8), is given by

$$\begin{aligned}\epsilon_R &= \int_{t_2}^{t_1} \frac{dt}{t} \\ &= \ln \left(\frac{t_1}{t_2} \right)\end{aligned}\quad (A5.11)$$

where t_1 and t_2 are the initial and final wall thickness respectively. With reference to Figure (A5.1),

$$t_1 = R_o - R_i \quad \text{and} \quad t_2 = R_{of} - R_{if} \quad (A5.12)$$

Hence,

$$\epsilon_R = \ln \frac{R_o - R_i}{R_{of} - R_{if}} \quad (A5.13)$$

The equivalent strain $\bar{\epsilon}$ described by equation (A5.7) is now completely defined by equations (A5.10) and (A5.13).

From equation (A5.1) it is clear that the total rate of plastic working consists of the rate of working in shearing across velocity discontinuities; including those at the tool-work interfaces which may be characterised by boundary or hydrodynamic lubrication described by a constant friction factor, and in internal deformation. These components will be considered in turn.

A5.2 PLASTIC WORKING ACROSS INTERNAL VELOCITY DISCONTINUITIES

The rate of plastic working across a discontinuity is given by the first term on the right-hand side of equation (A5.1), viz.,

$$\dot{W} = \tau_s U A \quad \text{or} \quad \dot{W} = k U A \quad (A5.14)$$

Referring to Figure (A5.1) the rate of working across discontinuity

AB is given by:

$$\dot{W}_{AB} = k U_{12} A_{AB} \quad (A5.15)$$

$$A_{AB} = \pi \frac{(R_o^2 - R_i^2)}{\sin \gamma} \quad (A5.16)$$

By the volume constancy,

$$\pi (R_o^2 - R_i^2) U_1 = \pi (R_{of}^2 - R_{if}^2) U_3 \quad (A5.17)$$

$$\text{or } U_1 = \frac{U_3 (R_{of}^2 - R_{if}^2)}{(R_o^2 - R_i^2)}$$

where U_1 and U_3 are the velocity of the undrawn and drawn tube respectively.

From the hodograph in Figure (A5.2) using the sine rule,

$$U_{12} = \frac{\sin \alpha}{\sin \gamma} U_1 \quad (A5.18)$$

Substituting for U_1 as in equation (A5.17),

$$U_{12} = U_3 \frac{\sin \alpha}{\sin \gamma} \cdot \frac{(R_{of}^2 - R_{if}^2)}{(R_o^2 - R_i^2)} \quad (A5.19)$$

Substituting for U_{12} and A_{AB} in equation (A5.15),

$$\dot{W}_{AB} = k U_3 \frac{\sin \alpha}{\sin \gamma} \cdot \frac{(R_{of}^2 - R_{if}^2)}{(R_o^2 - R_i^2)} \cdot \frac{\pi (R_o^2 - R_i^2)}{\sin \gamma} \quad (A5.20)$$

$$= \pi k U_3 (R_{of}^2 - R_{if}^2) \frac{\sin \alpha}{\sin^2 \gamma}$$

The rate of working across discontinuity CD is given by:

$$\dot{W}_{CD} = k U_{23} A_{CD} \quad (A5.21)$$

From Figure (A5.1),

$$A_{CD} = \frac{\pi (R_{of}^2 - R_{if}^2)}{\sin \beta} \quad (A5.22)$$

From the hodograph in Figure (A5.2), using the sine rule,

$$U_{23} = U_3 \frac{\sin \alpha}{\sin (\pi - \beta - \alpha)} \quad (A5.23)$$

Substituting for U_{23} and A_{CD} in equation (A5.21),

$$\begin{aligned}\dot{W}_{CD} &= kU_3 \frac{\sin \alpha}{\sin [\pi - (\beta + \alpha)]} \cdot \frac{\pi(R_{of}^2 - R_{if}^2)}{\sin \beta} \\ &= \pi kU_3 \frac{(R_{of}^2 - R_{if}^2) \sin \alpha}{\sin \beta \sin (\beta + \alpha)}\end{aligned}\quad (A5.24)$$

A5.3 PLASTIC WORKING DUE TO INTERNAL DEFORMATION (CIRCUMFERENTIAL AND THICKNESS STRAINING)

The rate of plastic working in deformation is given by the second term on the right-hand side of equation (A5.1) viz.,

$$\dot{W}_P = \dot{V} \bar{\sigma} \bar{\epsilon} \quad (A5.25)$$

The rate of volume of material deformed per unit time is given by:

$$\begin{aligned}\dot{V} &= \pi(R_o^2 - R_i^2) U_1 \\ &= \pi(R_{of}^2 - R_{if}^2) U_3\end{aligned}\quad (A5.26)$$

by volume constancy.

Hence, substituting \dot{V} as in equation (A5.26), $\bar{\sigma}$ as in equation (A5.5) and $\bar{\epsilon}$ as in equation (A5.7) into equation (A5.25),

$$\dot{W}_P = 2\pi k U_3 (R_{of}^2 - R_{if}^2) (\epsilon_R^2 + \epsilon_R \epsilon_\theta + \epsilon_\theta^2)^{\frac{1}{2}} \quad (A5.27)$$

where by equation (A5.10), $\epsilon_\theta = \ln (R_o/R_f)$ and by equation (A5.13), $\epsilon_R = \ln (R_o - R_i)/(R_{of} - R_{if})$

A5.4 PLASTIC WORKING ACROSS SURFACE VELOCITY DISCONTINUITIES (TOOL-WORK INTERFACES)

Substituting $\tau_s = m_d k$ as in equation (A5.3) into equation (A5.14) the rate of working across the conical portion of the die-tube interface is given by:

$$\dot{W}_{AD} = m_d k U_2 A_{AD} \quad (A5.28)$$

Referring to Figure (A5.1), for a small change dR in R , the incremental area of the die-tube interface dA is given by:

$$dA = \frac{2 \pi R dR}{\sin \alpha} \quad (A5.29)$$

Hence,

$$A_{AD} = \int_{R_{of}}^{R_o} \frac{2 \pi R dR}{\sin \alpha} \quad (A5.30)$$

The velocity U_2 along the die-tube interface changes due to the acceleration in zone 2. If $(U_2)_1$ is the velocity along the interface at A, the velocity at any point whose distance from the drawing axis is R , is given by:

$$U_2 R = (U_2)_1 R_o \quad (A5.31)$$

assuming volume constancy.

From the hodograph in Figure (A5.2), by simple trigonometry

$$(U_2)_1 = U_1 \text{ at AD} \quad (A5.32)$$

Substituting for U_1 as in equation (A5.17) into equation (5.31),

$$U_2 R = U_3 \frac{(R_{of}^2 - R_{if}^2)}{(R_o^2 - R_1^2)} R_o \quad (A5.33)$$

Thus equation (A5.28) may be written, substituting for A_{AD} as in equation (A5.30),

$$\dot{W}_{AD} = m_d k \int_{R_{of}}^{R_o} U_2 \frac{2 \pi R dR}{\sin \alpha} \quad (A5.34)$$

Substituting for $U_2 R$ as in equation (A5.33),

$$\dot{W}_{AD} = m_d k \int_{R_{of}}^{R_o} \frac{2 \pi}{\sin \alpha} \cdot U_3 R_o \frac{(R_{of}^2 - R_{if}^2)}{(R_o^2 - R_1^2)} dR \quad (A5.35)$$

$$= 2 \pi m_d k U_3 R_o \frac{(R_o - R_{of}) (R_{of}^2 - R_{if}^2)}{\sin \alpha (R_o^2 - R_{if}^2)} \quad (A5.35)$$

The rate of working across the discontinuity DE i.e. at the die-tube interface corresponding to the land of the die is given by:

$$\dot{W}_{DE} = m_d k U_3 A_{DE} \quad (A5.36)$$

assuming the same friction factor m_d .

Referring to Figure (A5.1),

$$A_{DE} = 2 \pi R_{of} L_d \quad (A5.37)$$

where L_d is the length of the land of the die.

Thus, substituting for A_{DE} in equation (A5.36) by equation (A5.37),

$$\dot{W}_{DE} = 2 \pi m_d k U_3 R_{of} L_d \quad (A5.38)$$

Substituting $\tau_s = m_p k$ as in equation (A5.4) into equation (A5.14), the rate of working across the discontinuity CF i.e. at the plug-tube interface, is given by:

$$\dot{W}_{CF} = m_p k U_3 A_{CF} \quad (A5.39)$$

Referring to Figure (A5.1),

$$A_{CF} = 2 \pi R_{if} L_p \quad (A5.40)$$

where L_p is the length of contact between the plug and the tube.

Thus substituting for A_{CF} in equation (A5.39) by equation (A5.40),

$$\dot{W}_{CF} = 2 \pi m_p k U_3 R_{if} L_p \quad (A5.41)$$

A5.5 RATE OF WORKING BY THE DRAW BENCH

The rate of working by the external pull is given by

$$\dot{W}_{\text{ext.}} = \sigma \pi (R_{\text{of}}^2 - R_{\text{if}}^2) U_3 \quad (\text{A5.42})$$

where σ is the draw stress. Equating the external rate of working to the total rate of working in plastic flow,

$$\begin{aligned} \dot{W}_{\text{ext.}} &= \dot{W}_T \\ &= \dot{W}_{\text{AB}} + \dot{W}_{\text{CD}} + \dot{W}_P + \dot{W}_{\text{AD}} + \dot{W}_{\text{DE}} + \dot{W}_{\text{CF}} \end{aligned} \quad (\text{A5.43})$$

as in equations (A5.42), (A5.20), (A5.24), (A5.27), (A5.35), (A5.38) and (A5.41) respectively.

Substituting the appropriate equations into equation (A5.43),

$$\begin{aligned} \sigma \pi (R_{\text{of}}^2 - R_{\text{if}}^2) U_3 &= \pi k U_3 (R_{\text{of}}^2 - R_{\text{if}}^2) \frac{\sin \alpha}{\sin^2 \gamma} \\ &+ \pi k U_3 \frac{(R_{\text{of}}^2 - R_{\text{if}}^2) \sin \alpha}{\sin \beta \sin (\beta + \alpha)} \\ &+ 2 \pi k U_3 (R_{\text{of}}^2 - R_{\text{if}}^2) (\epsilon_R^2 + \epsilon_R \epsilon_\theta + \epsilon_\theta^2)^{\frac{1}{2}} \\ &+ 2 \pi m_d k U_3 R_o \frac{(R_o - R_{\text{of}})(R_{\text{of}}^2 - R_{\text{if}}^2)}{\sin \alpha (R_o^2 - R_{\text{if}}^2)} \\ &+ 2 \pi m_d k U_3 R_{\text{of}} L_d + 2 \pi m_p k U_3 R_{\text{if}} L_p \end{aligned} \quad (\text{A5.44})$$

Dividing by $\pi (R_{\text{of}}^2 - R_{\text{if}}^2) U_3$,

$$\begin{aligned} \sigma &= k \frac{\sin \alpha}{\sin^2 \gamma} + k \frac{\sin \alpha}{\sin \beta \sin (\beta + \alpha)} \\ &+ 2 k (\epsilon_R^2 + \epsilon_R \epsilon_\theta + \epsilon_\theta^2)^{\frac{1}{2}} + 2 m_d k R_o \frac{(R_o - R_{\text{of}})}{\sin \alpha (R_o^2 - R_{\text{if}}^2)} \end{aligned}$$

$$+ 2m_d k R_{of} L_d \frac{1}{(R_{of}^2 - R_{if}^2)} + 2m_p k R_{if} L_p \frac{1}{(R_{of}^2 - R_{if}^2)} \quad (A5.45)$$

Dividing equation (A5.45) by $2k$,

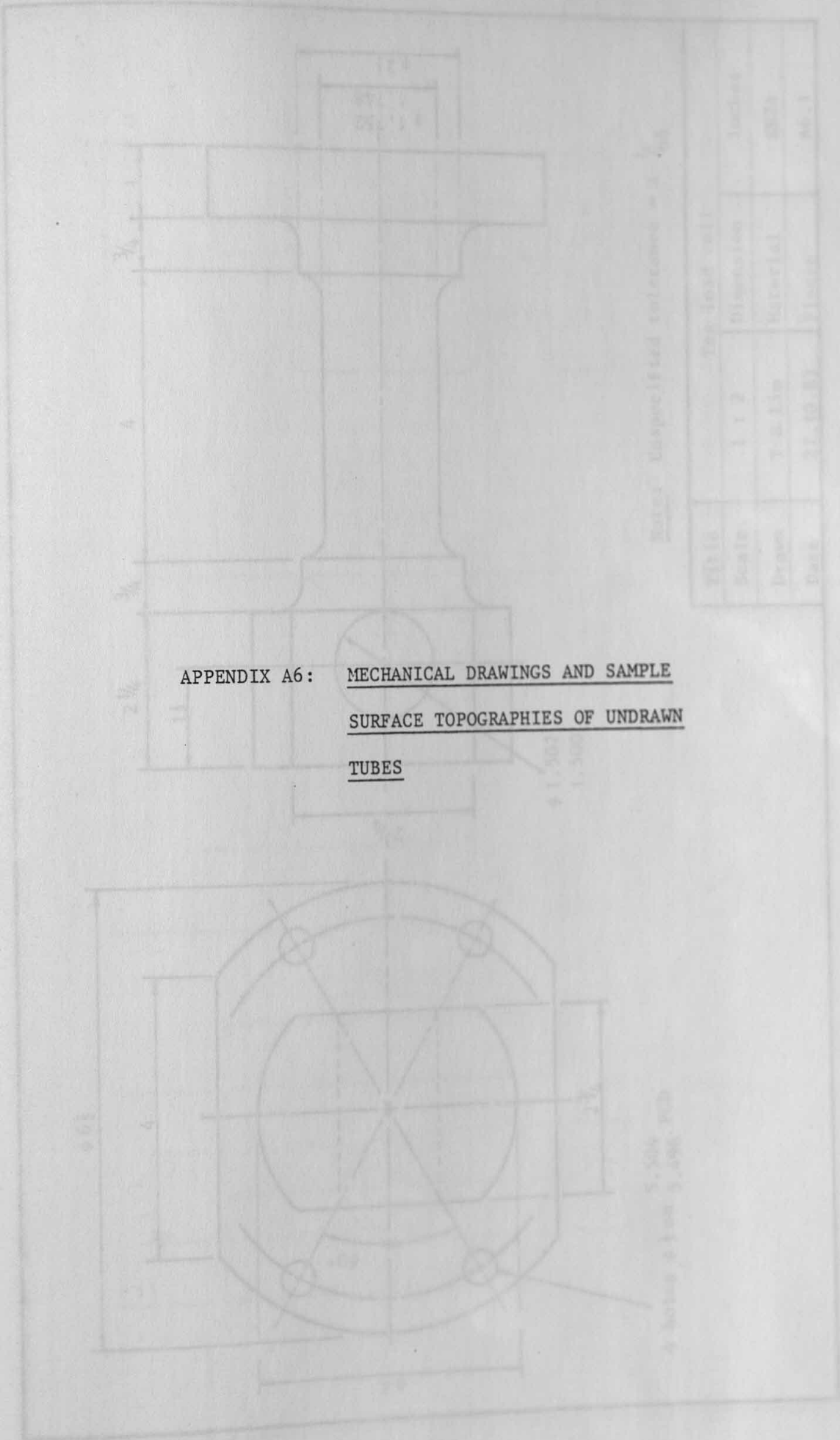
$$\frac{\sigma}{2k} = \frac{\sin \alpha}{2 \sin^2 \gamma} + \frac{\sin \alpha}{2 \sin \beta \sin (\beta + \alpha)} + (\epsilon_R^2 + \epsilon_R \epsilon_\theta + \epsilon_\theta^2)^{\frac{1}{2}}$$

$$+ m_d R_o \frac{(R_o - R_{of})}{\sin \alpha (R_o^2 - R_i^2)}$$

$$+ m_d R_{of} L_d \frac{1}{(R_{of}^2 - R_{if}^2)} + m_p R_{if} L_p \frac{1}{(R_{of}^2 - R_{if}^2)} \quad (A5.46)$$

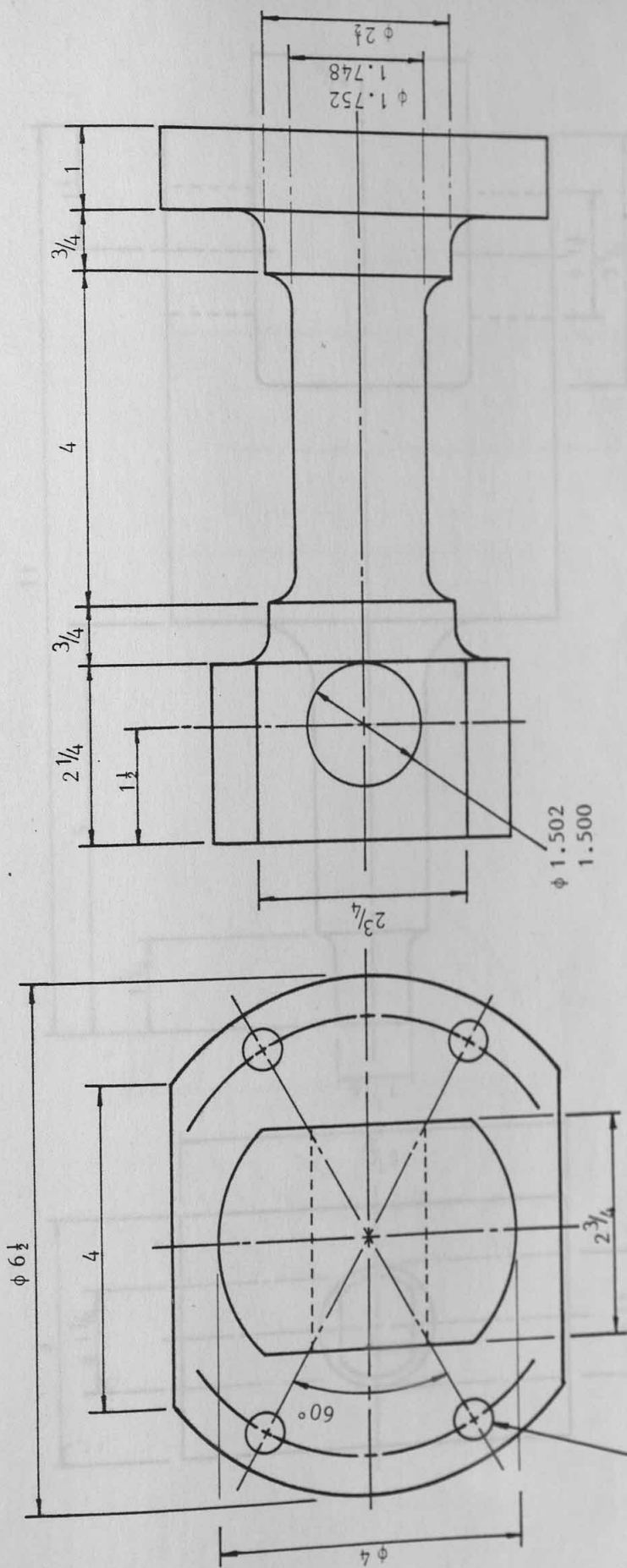
Since by equation (A5.6) $k = Y/2$, equation (A5.46) is also equal to σ/Y .

The upper bound solution for a given set of drawing conditions can be obtained by optimising the angles β and γ which give the minimum draw stress.



Notes: Unspecified tolerances are ± 0.005

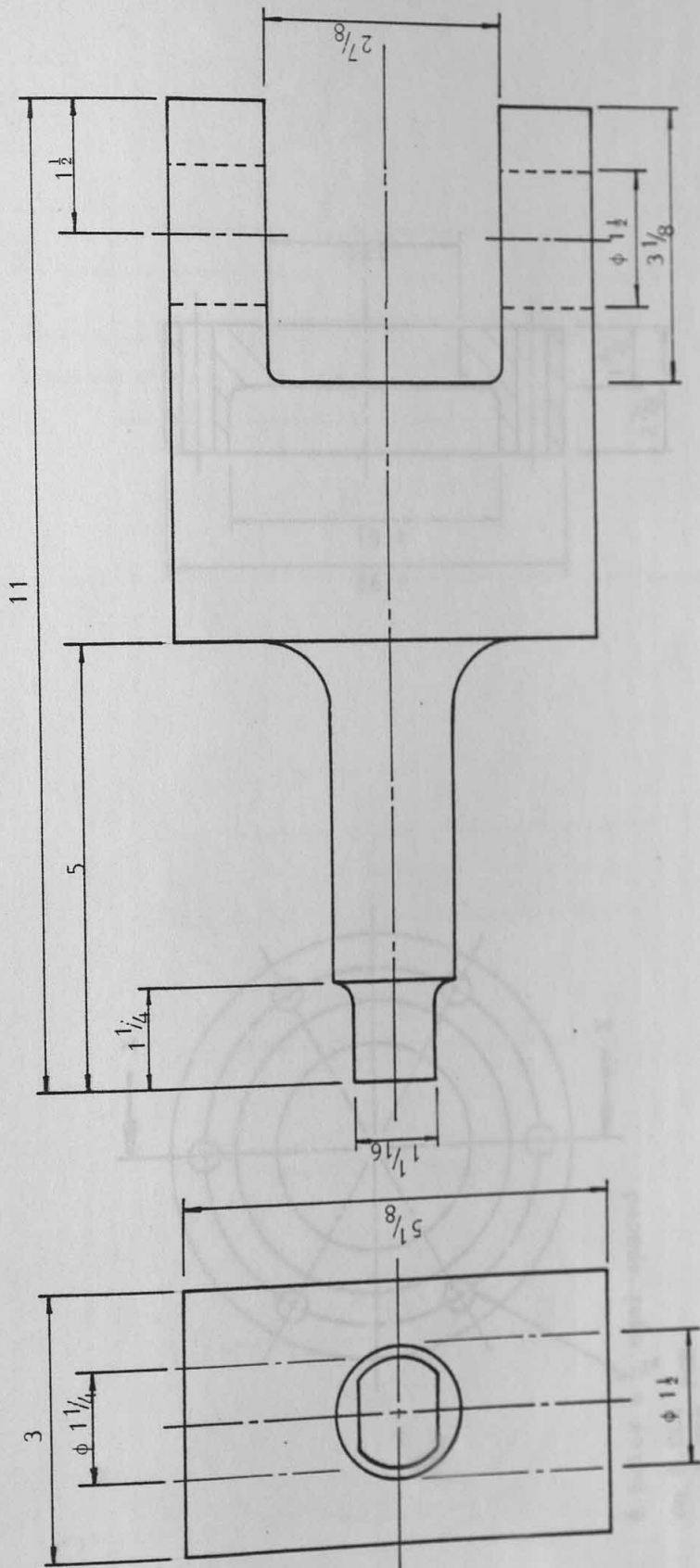
Field	The last cell		
Scale	1	2	100000
Drawn	Material		100000
Drawn	Material		100000



4 holes $\phi 1$ on 5.496 PCD

Note: Unspecified tolerance = $\pm \frac{1}{64}$

Title		Tag load cell	
Scale	1 : 2	Dimension	Inches
Drawn	T B Lim	Material	EN24
Date	27.10.83	Figure	A6.1

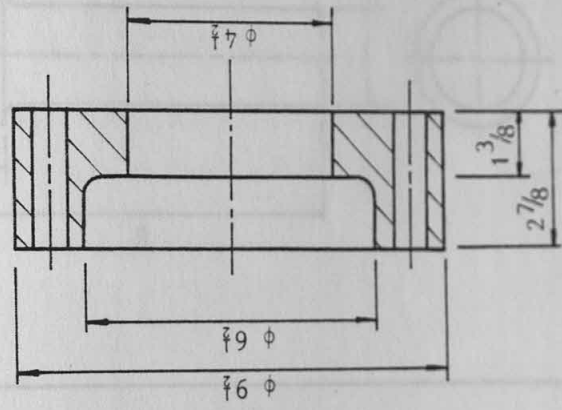


Note: General tolerance = $\pm \frac{1}{64}$

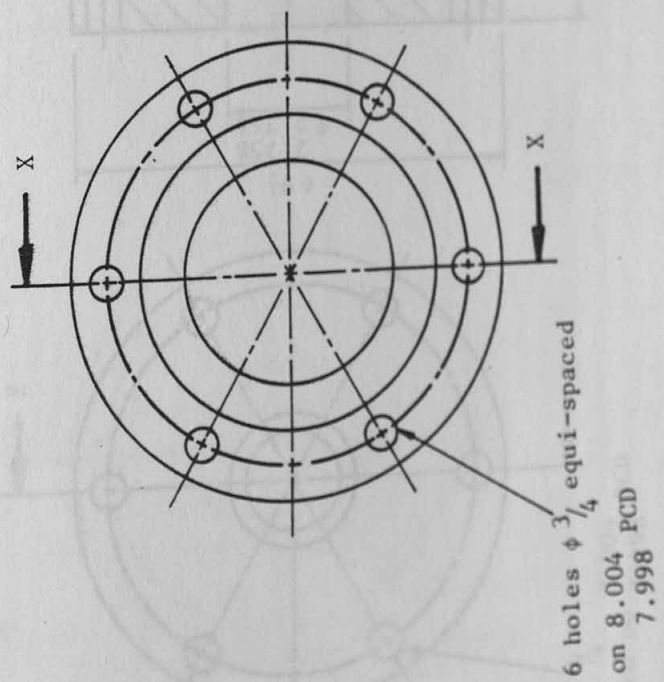
Tag load cell calibrating adaptor			
Title	Scale	1 : 2	Inches
Drawn	T B Lim	Material	EN24
Date	27.10.83	Figure	A6.2

Component B

2.758
7.268



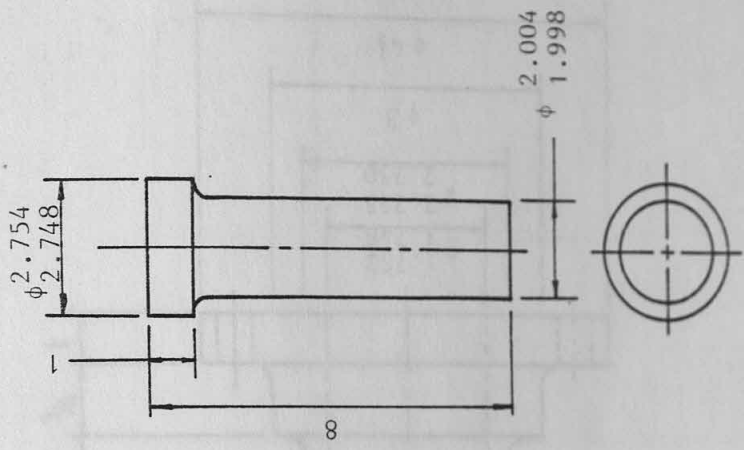
Component A



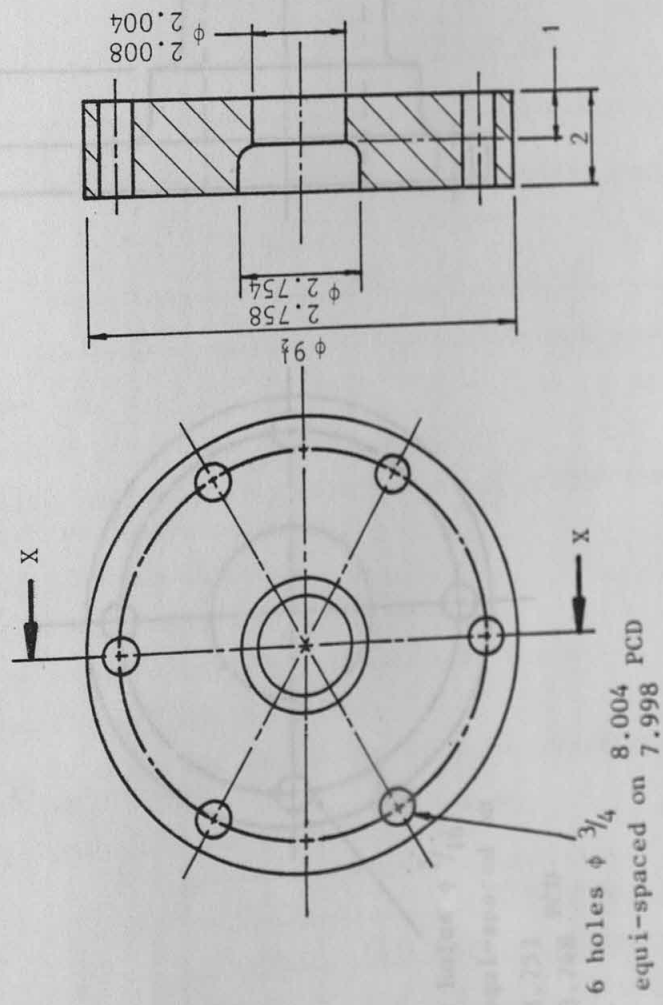
Note: General tolerance = $\pm \frac{1}{64}$

Title	Tag load cell - Denison adaptor		
	Scale	Dimension	Inches
Drawn	T B Lim	Material	Mild Steel
Date	27.10.83	Figure	A6.3

Component B

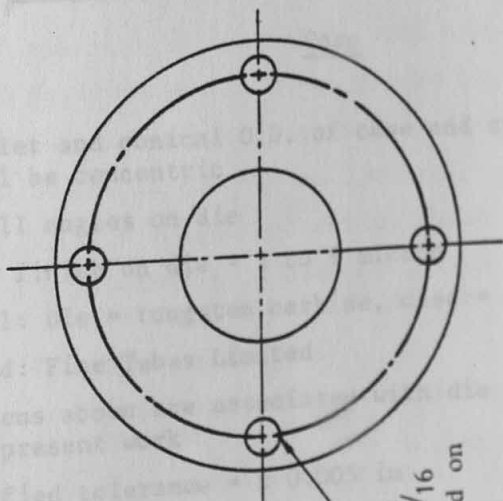
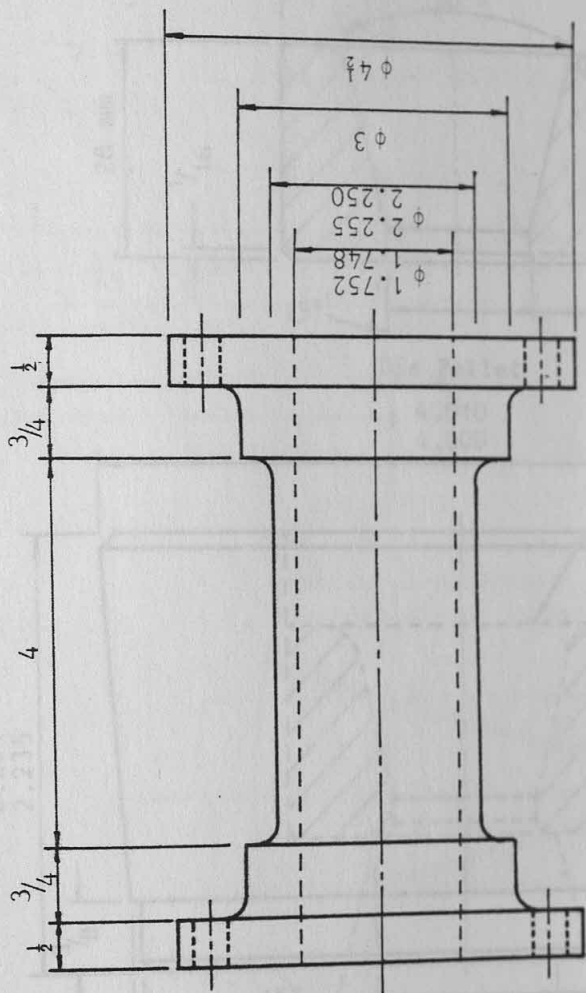


Component A



Note: Unspecified tolerance = $\pm \frac{1}{64}$

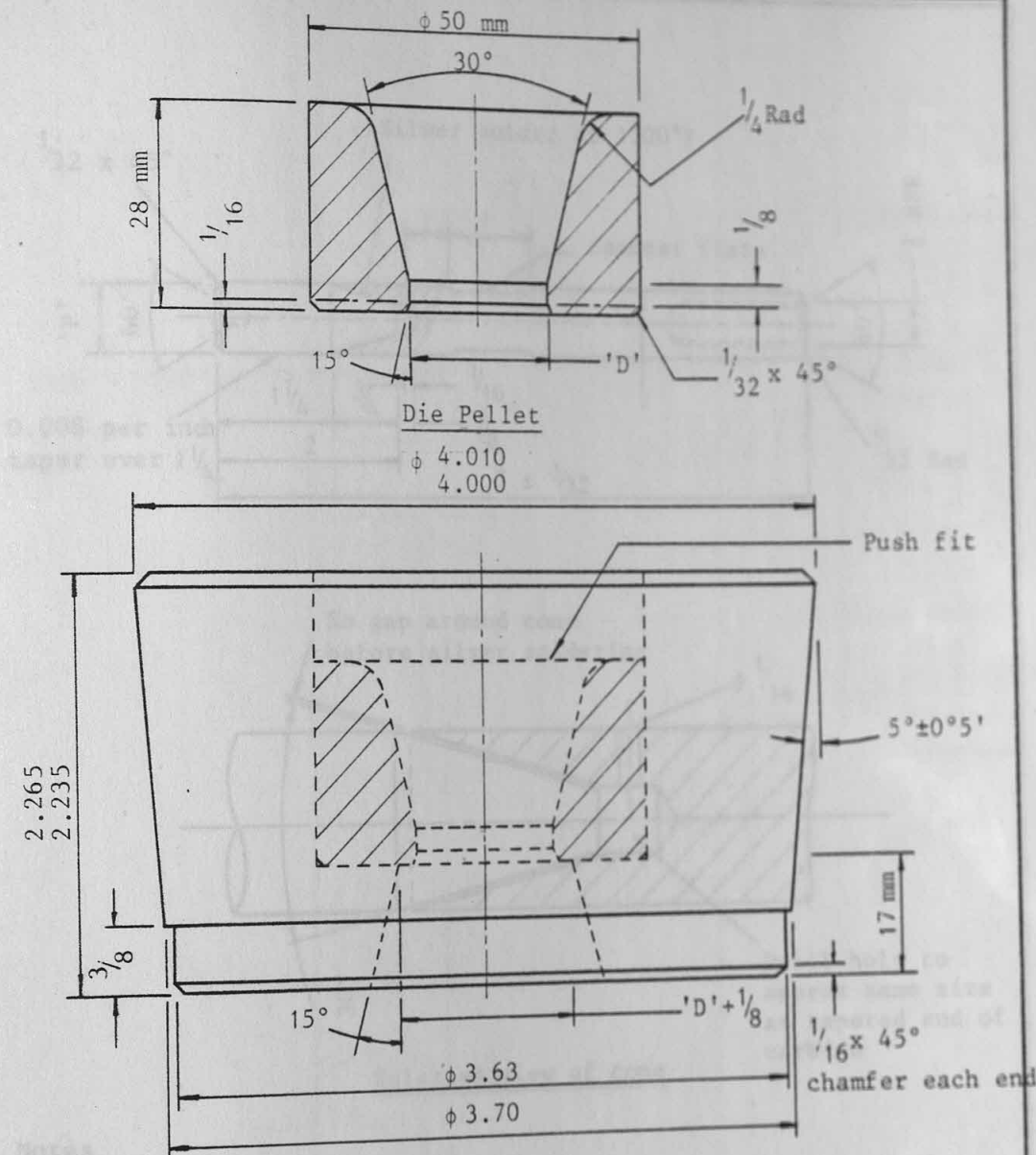
Tag load cell - Denison adaptors			
Title	Scale	Dimension	Inches
Drawn	1 : 4		
Date	T B Lim	Material	Mild Steel
	27.10.83	Figure	A6.4



4 holes $\phi 7/16$
equi-spaced on
3.752 PCD
3.748

Note: Unspecified tolerance = $\pm 1/64$

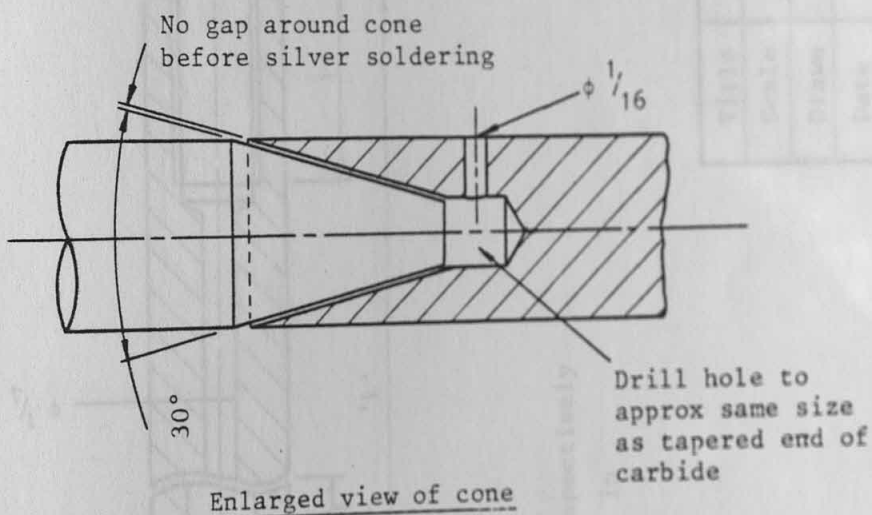
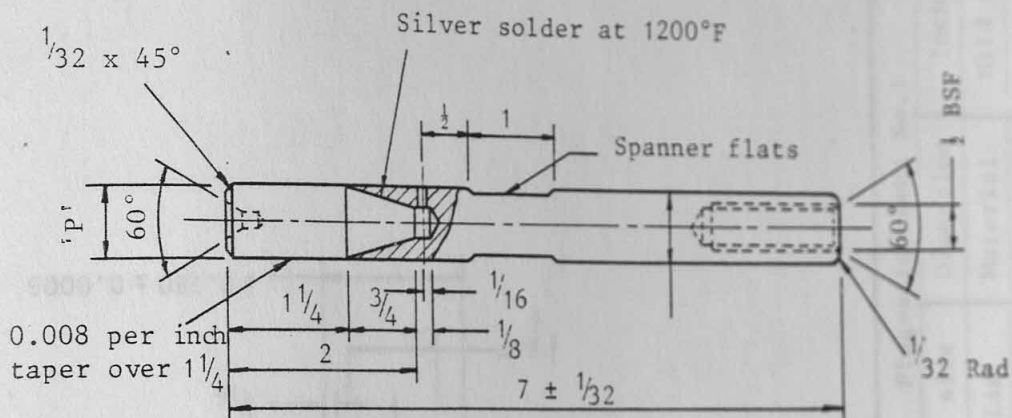
Plug load cell			
Title	1 : 2	Dimension	Inches
Scale	T B Lim	Material	EN24
Drawn	27.10.83	Figure	A6.5



Note:

1. Die pellet and conical O.D. of case and cylindrical O.D. of case must all be concentric
2. Blend all angles on die
3. Surface finish on die = 1 to 6 micron
4. Material: Die = tungsten carbide, case = steel
5. Designed: Fine Tubes Limited
6. Dimensions above are associated with die diameters 'D' used in the present work
7. Unspecified tolerance = ± 0.005 in

Tube-drawing die			
Title	Full size	Dimension	Inches
Scale	T B Lim	Material	As above
Drawn	8.7.83	Figure	A6.6
Date			



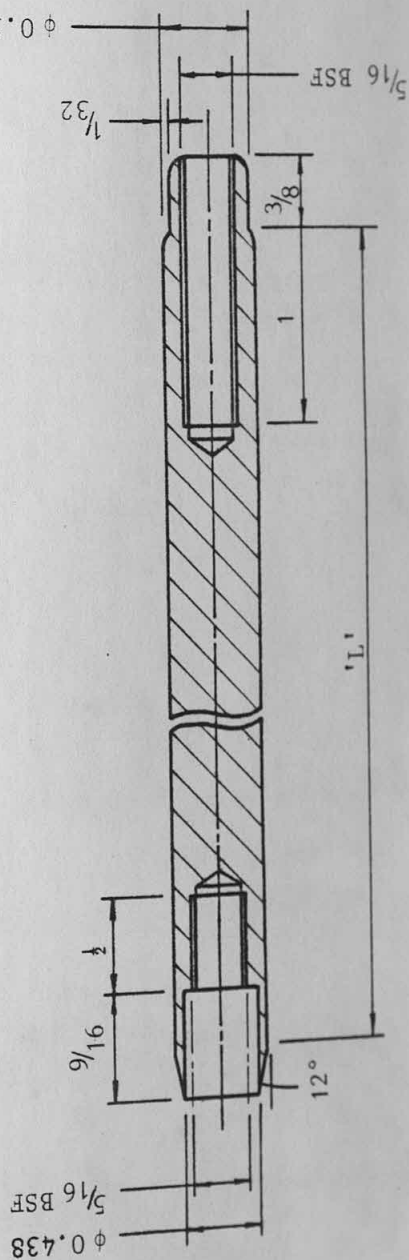
Notes

1. O.D. of nib must be concentric with centres to within 0.005 in
2. Conical position of nib to be ground but not polished
3. Nib to be free from porosity and surface defects
4. Surface finish on nib = 1 to 3 micron
5. Material: nib = tungsten carbide, shank = high tensile steel
6. When silver soldering carbide nib to be spring loaded on end to avoid excessive thickness of solder in joint
7. Design: Fine Tubes Limited
8. Dimensions above are associated with the plug diameters 'P' used in the present work
9. Unspecified tolerance = ± 0.005 in

Tube-drawing plug			
Title	1 : 2	Dimension	Inches
Scale	T B Lim	Material	as above
Drawn	8.7.83	Figure	A6.7
Date			



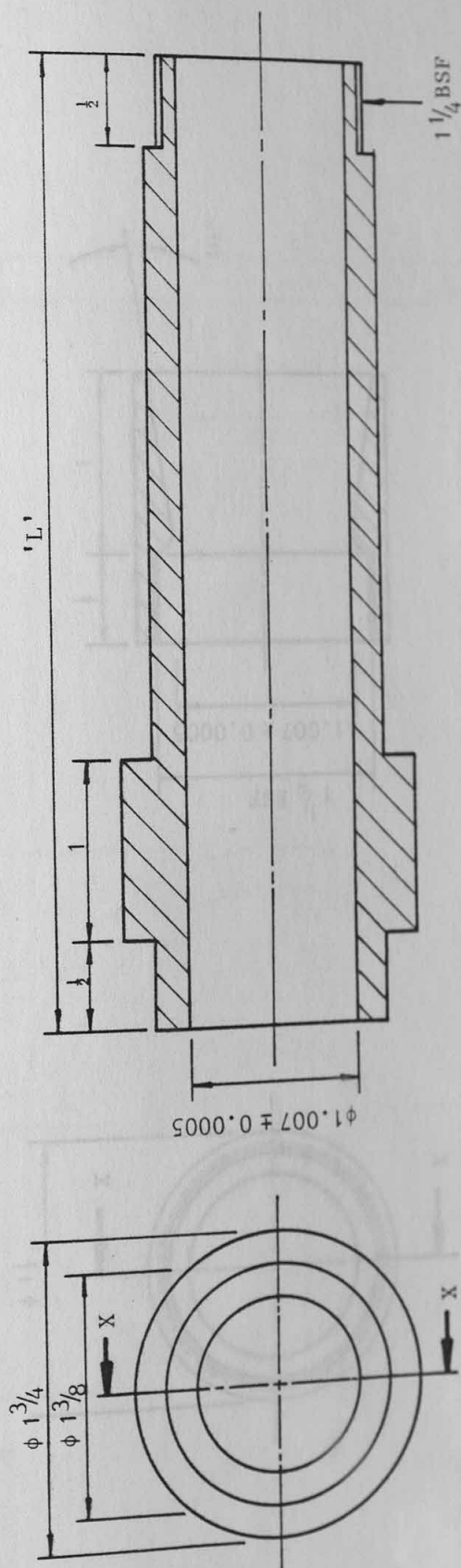
- | Title | Plug-attachment No. 1 | | |
|-------|-----------------------|-----------|------------|
| Scale | Full size | Dimension | Inches |
| Drawn | T B Lim | Material | Mild steel |
| Date | 22.2.83 | Figure | A6.8a |



Notes:

1. 3 off with L = 6, 7½, 9 inch respectively
2. Unspecified tolerance = ± 0.005 in
3. Surface finish: ground

Plug-attachment No. 3			
Title	Full size	Dimension	Inches
Scale	T B Lim	Material	Mild steel
Drawn	22.2.83	Figure	A6.8c

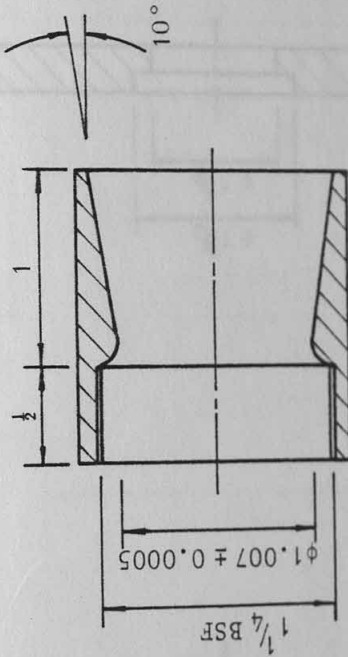
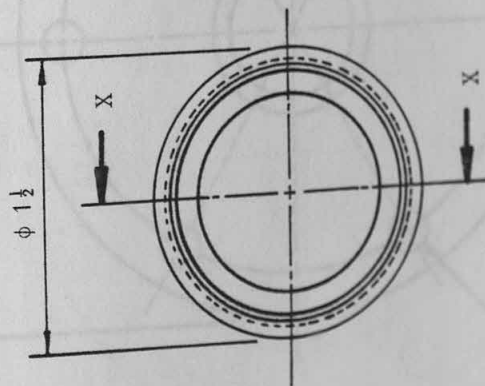


Notes:

1. 4 off with L = 2.5, 5.5, 8.5, 11.5 inch respectively
2. Unspecified tolerance = ± 0.005 in

3. Hardened and tempered (50 Rockwell C)

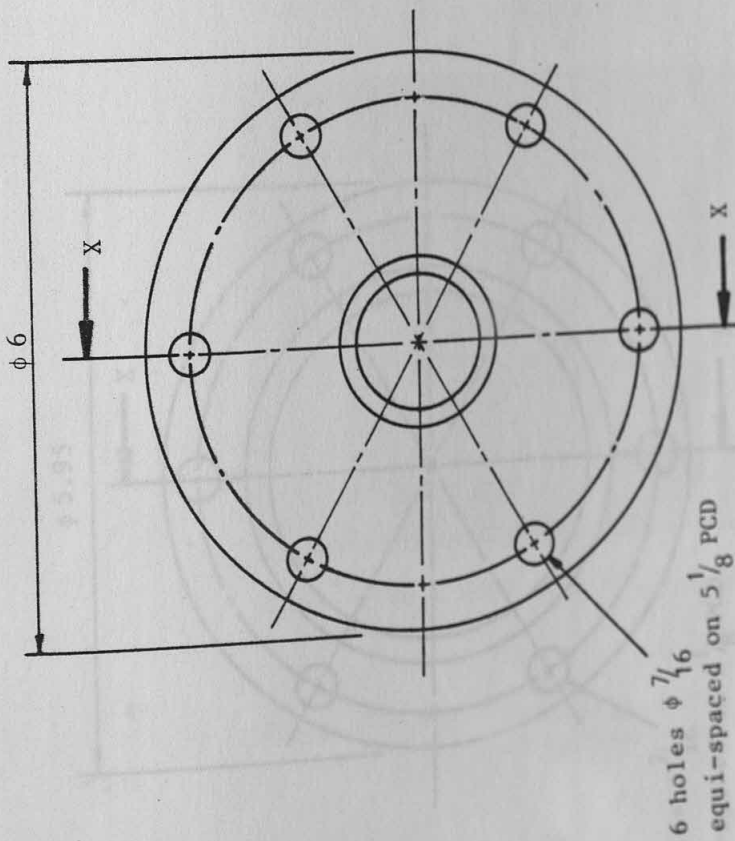
Title	Christopherson tube		
	Full size	Dimension	Inches
Scale	T B Lim	Material	Mild steel
Drawn	9.6.81	Figure	A6.9
Date			



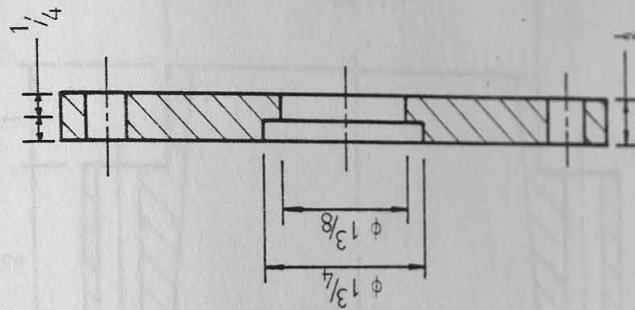
Notes:

1. Unspecified tolerance = ± 0.005 in
2. Hardened and tempered (50 Rockwell)

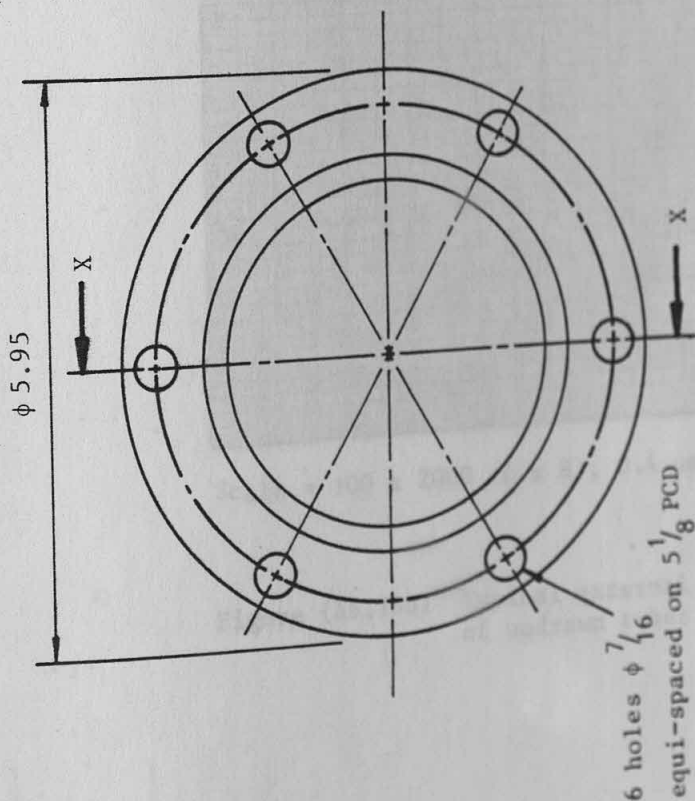
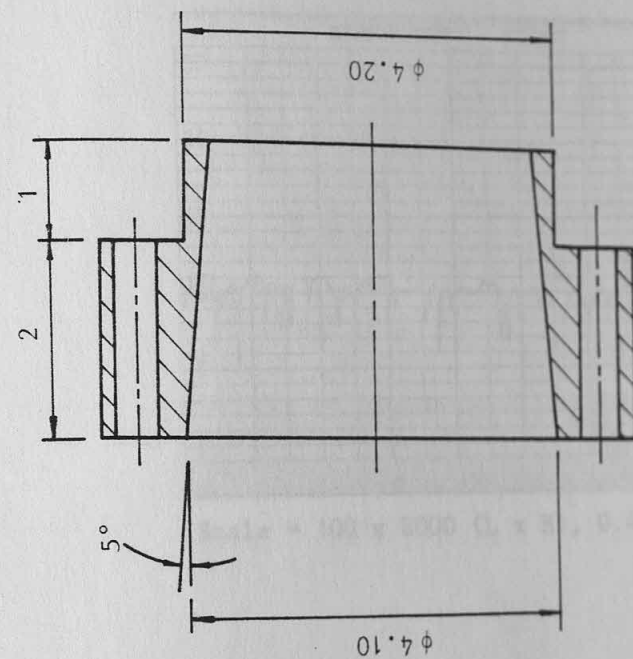
Title	Inlet-guide		
	Full size	Dimension	Inches
Scale	T B Lim	Material	EN24
Drawn	9.6.81	Figure	A6.10
Date			



Note:
General tolerance = ± 0.005 in



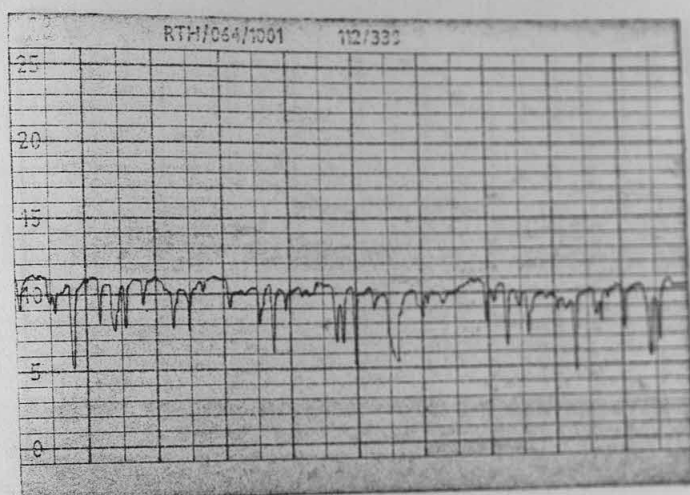
Title	Lock-flange		
	1 : 2	Dimension	Inches
Scale	T B Lim	Material	Mild steel
Drawn	9.6.81	Figure	A6.11
Date			



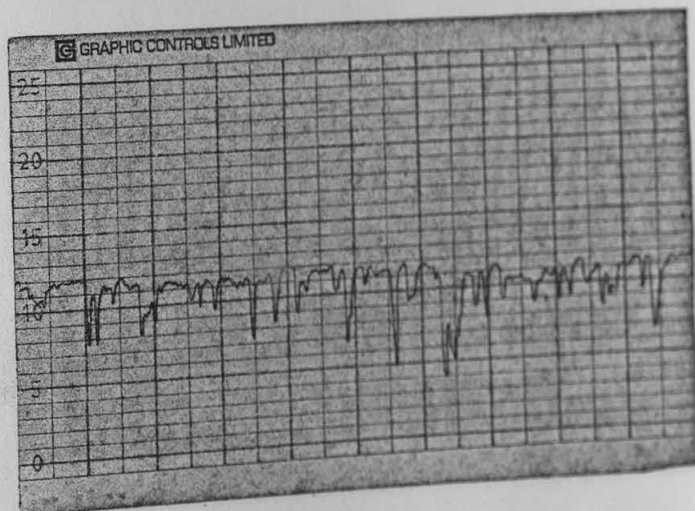
Note:

General tolerance = ± 0.005 in

Title			
Die sleeve			
Scale	1 : 2	Dimension	Inch
Drawn	T B Lim	Material	Mild steel
Date	2.12.80	Figure	A6.12

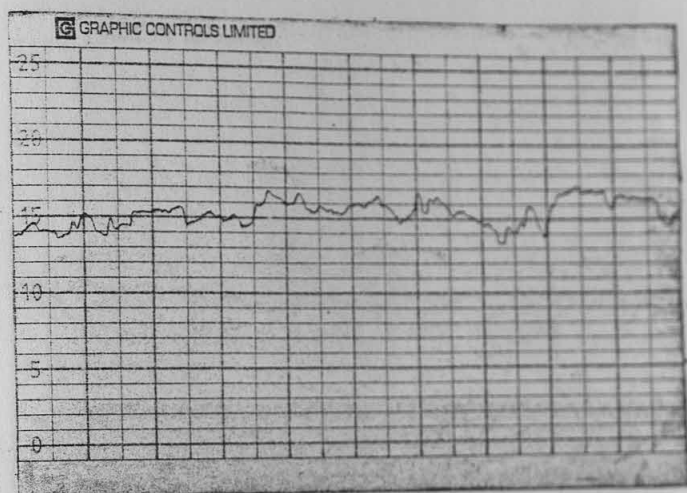


Scale = 100 x 2000 (L x H), 0.4 μ m CLA

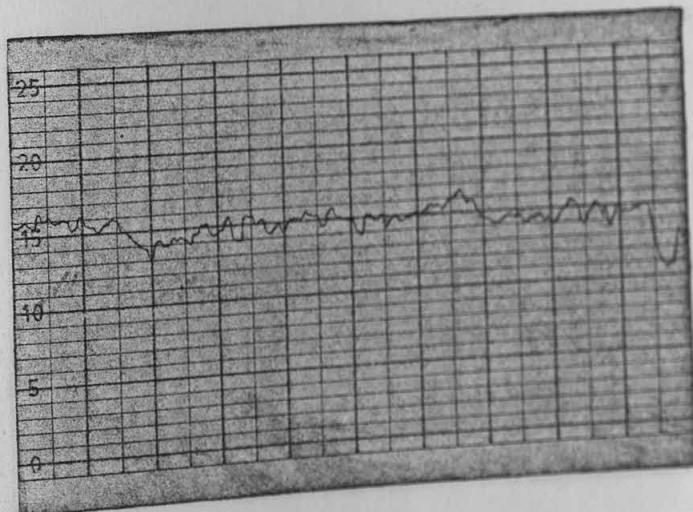


Scale = 100 x 2000 (L x H), 0.4 μ m CLA

Figure (A6.13a) Typical external surface topographies of undrawn tubes

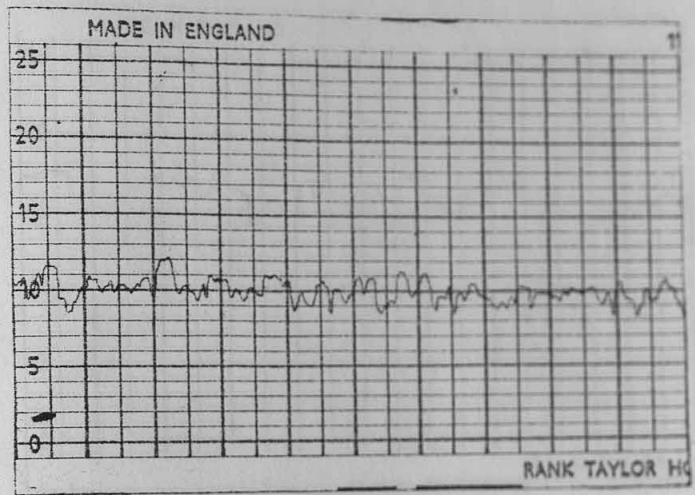


Scale = 100 x 5000 (L x H), 0.25 μ m CLA

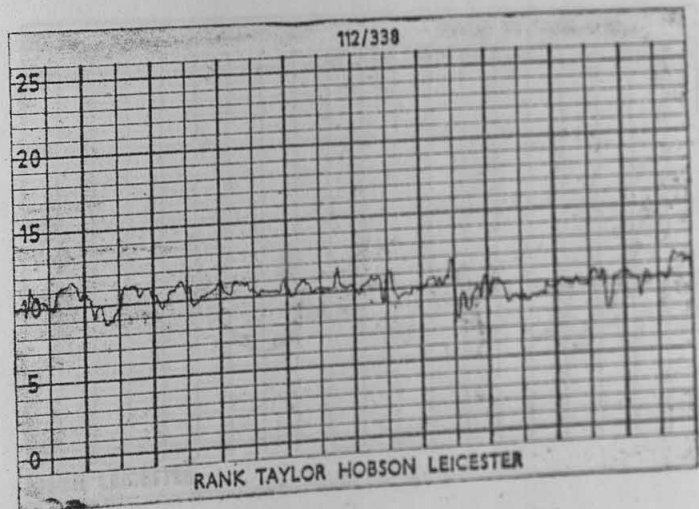


Scale = 100 x 5000 (L x H), 0.25 μ m CLA

Figure (A6.13b) Typical bore surface topographies of undrawn tubes

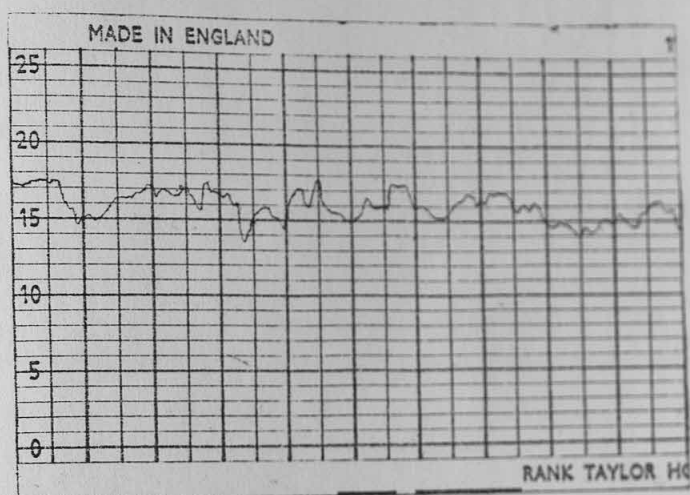


Scale = 100 x 2000 (L x H), 0.6 μm CLA



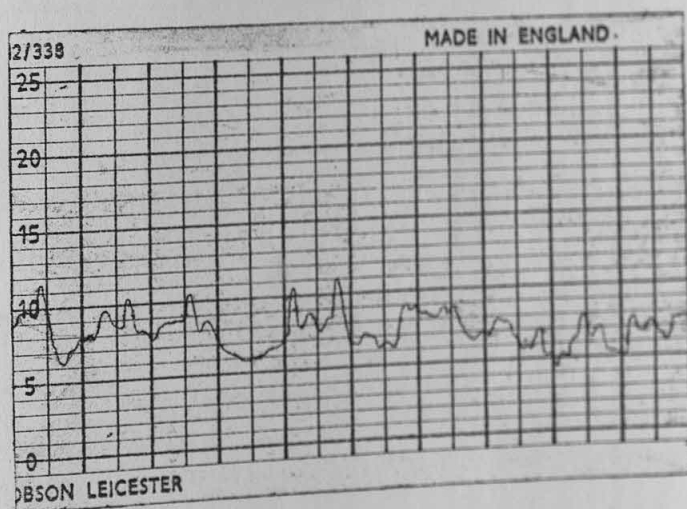
Scale = 100 x 2000 (L x H), 0.5 μm CLA

Figure (A6.14a) Typical external surface topographies of undrawn tubes



Scale = 100 x 2000. (L x H), 1.0 μ m CLA

APPENDIX A7: CALIBRATION CHARTS



Scale = 100 x 2000 (L x H), 1.0 μ m CLA

Figure (A6.14b) Typical bore surface topographies of undrawn tubes

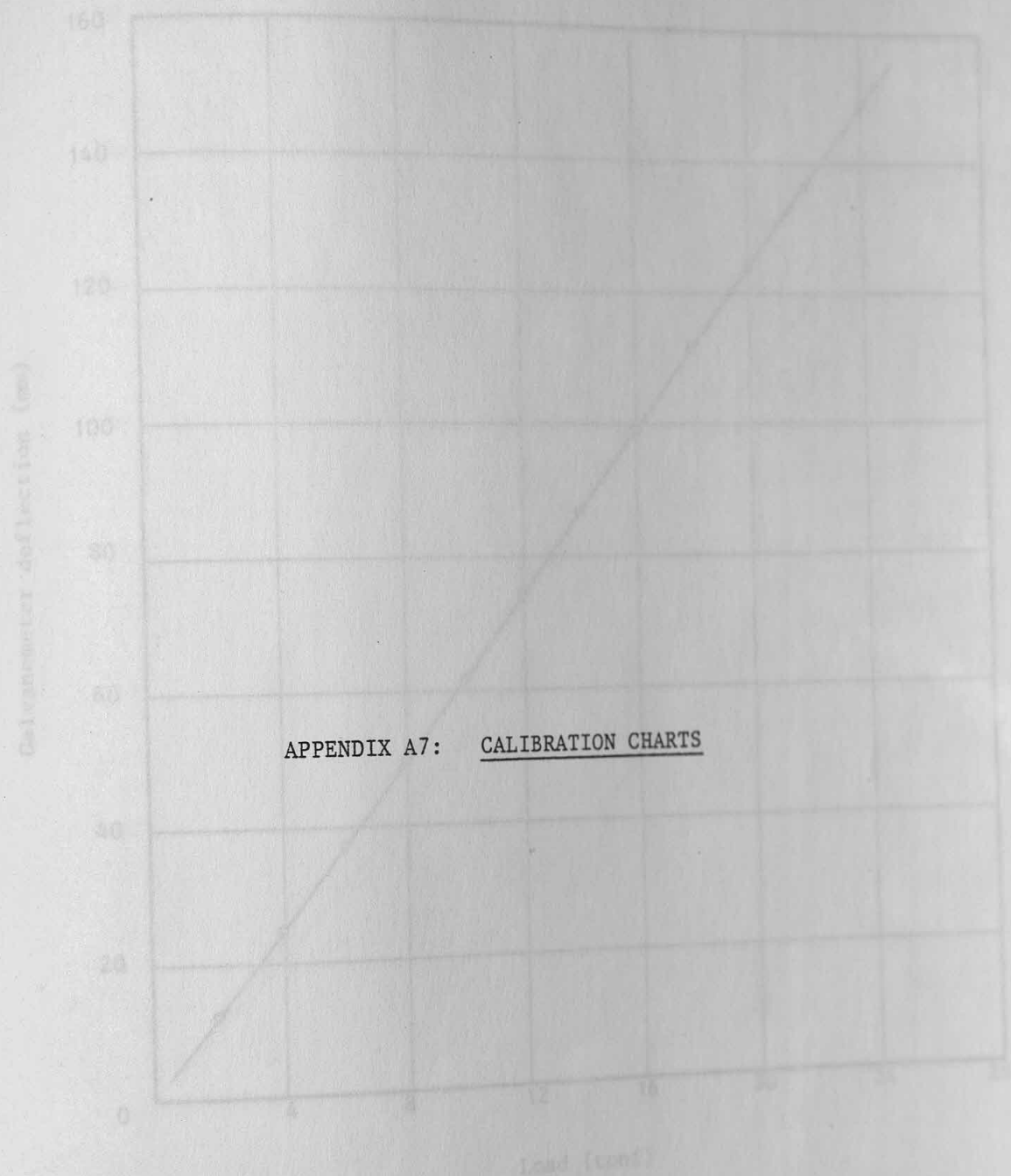


Figure A7.1 Calibration chart of the load cell
at the bag holder

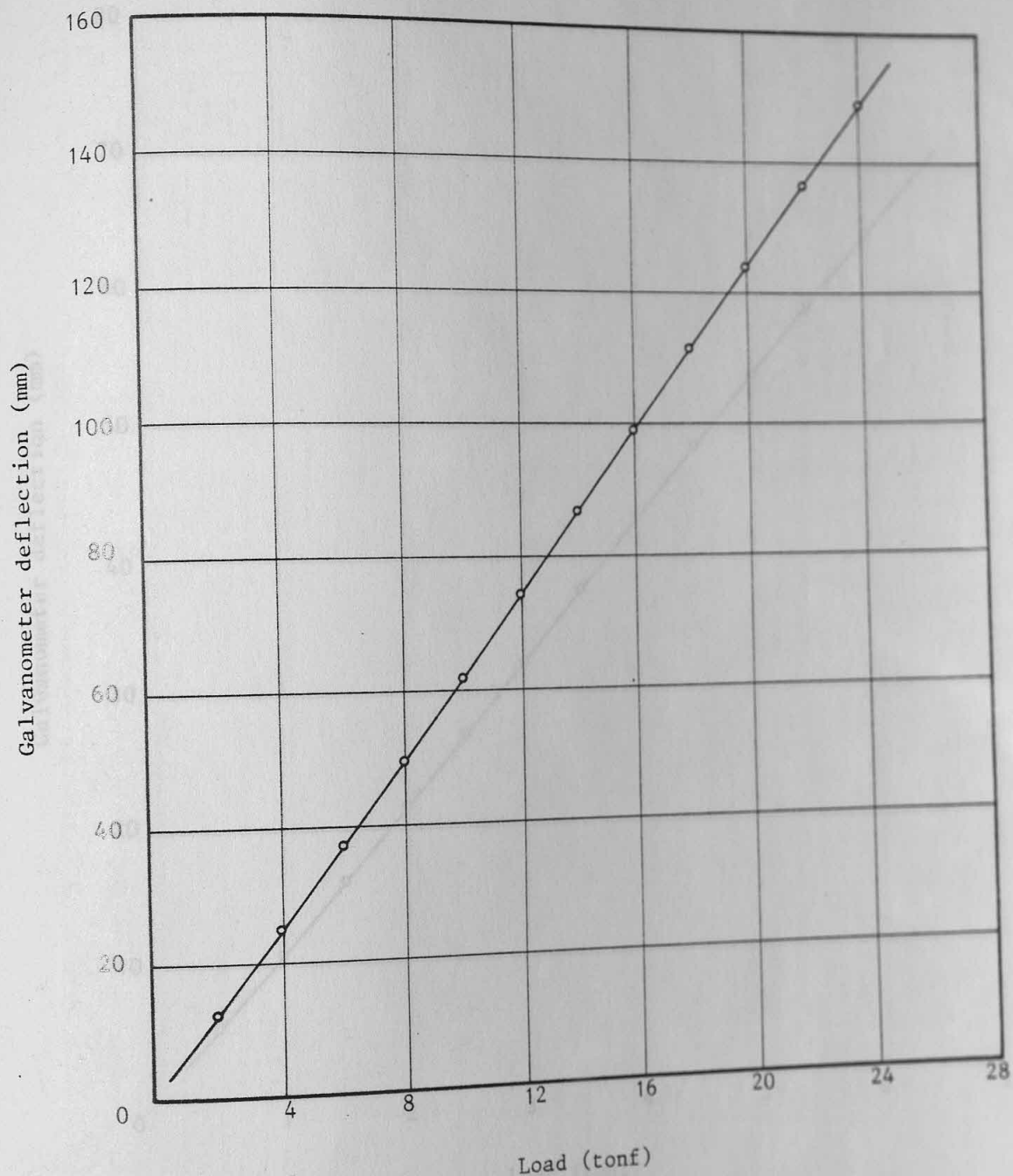


Figure (A7.1) Calibration chart of the load cell at the tag holder

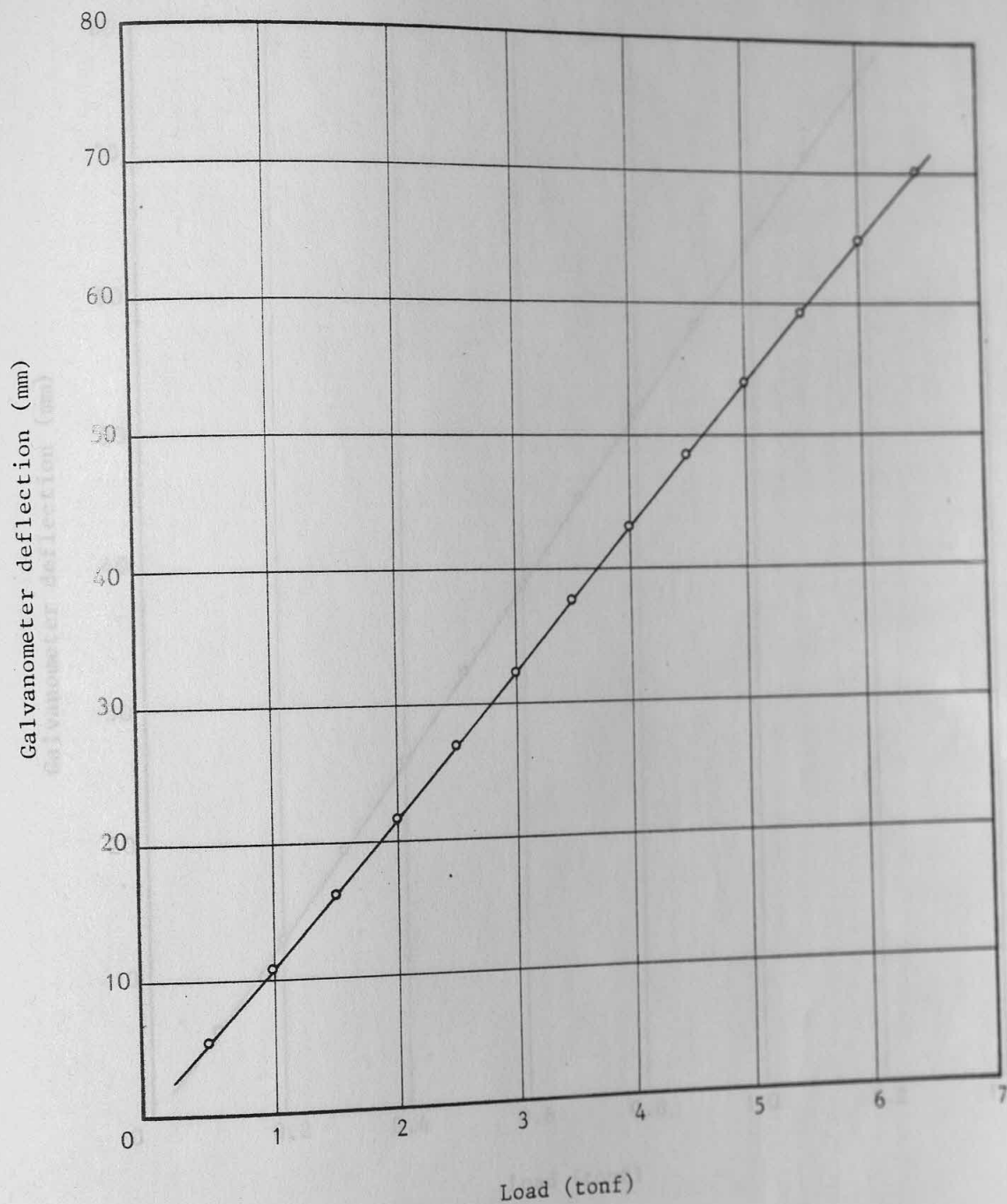


Figure (A7.2) Calibration chart of the plug load cell

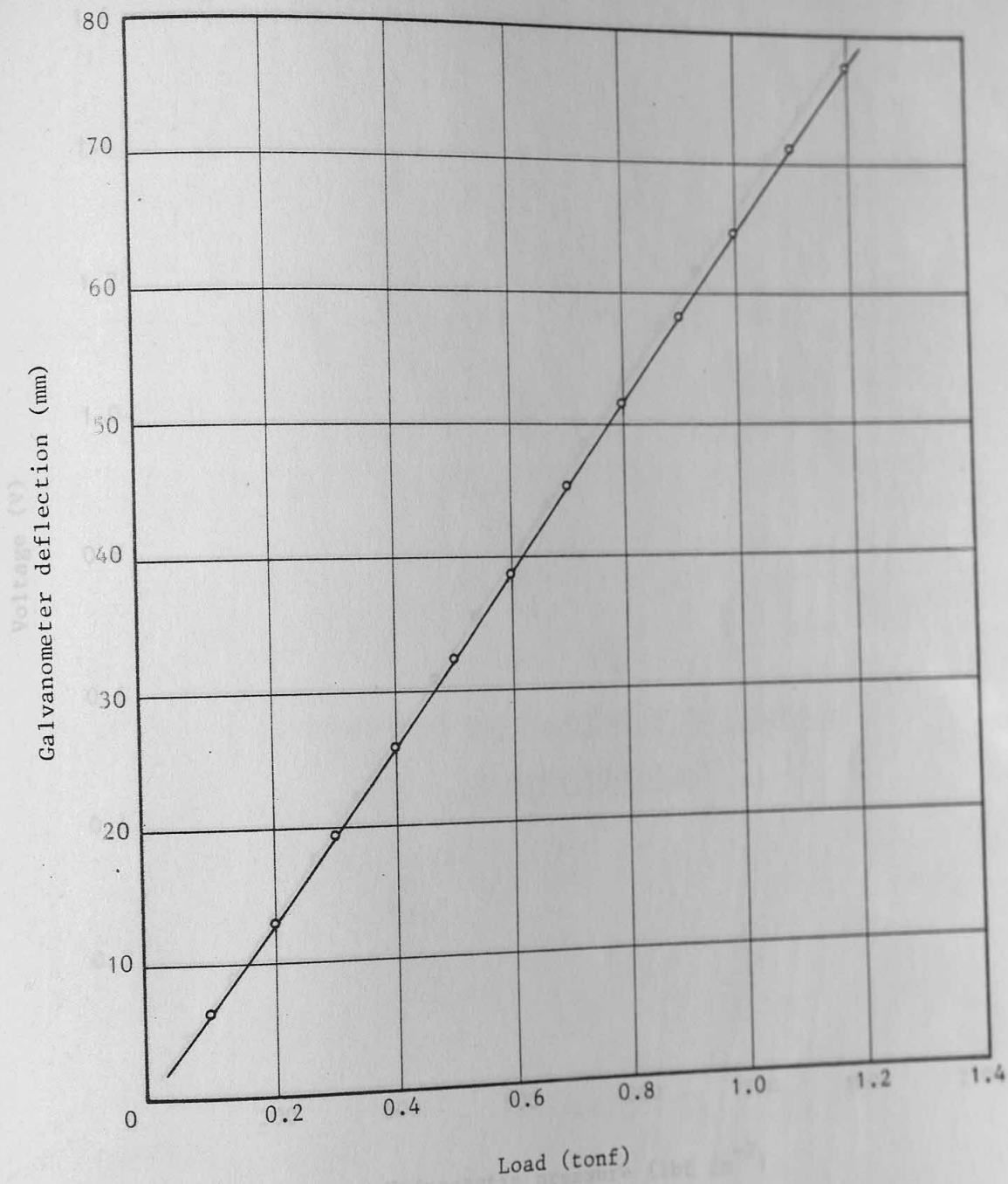


Figure (A7.3) Calibration chart of the plug load cell

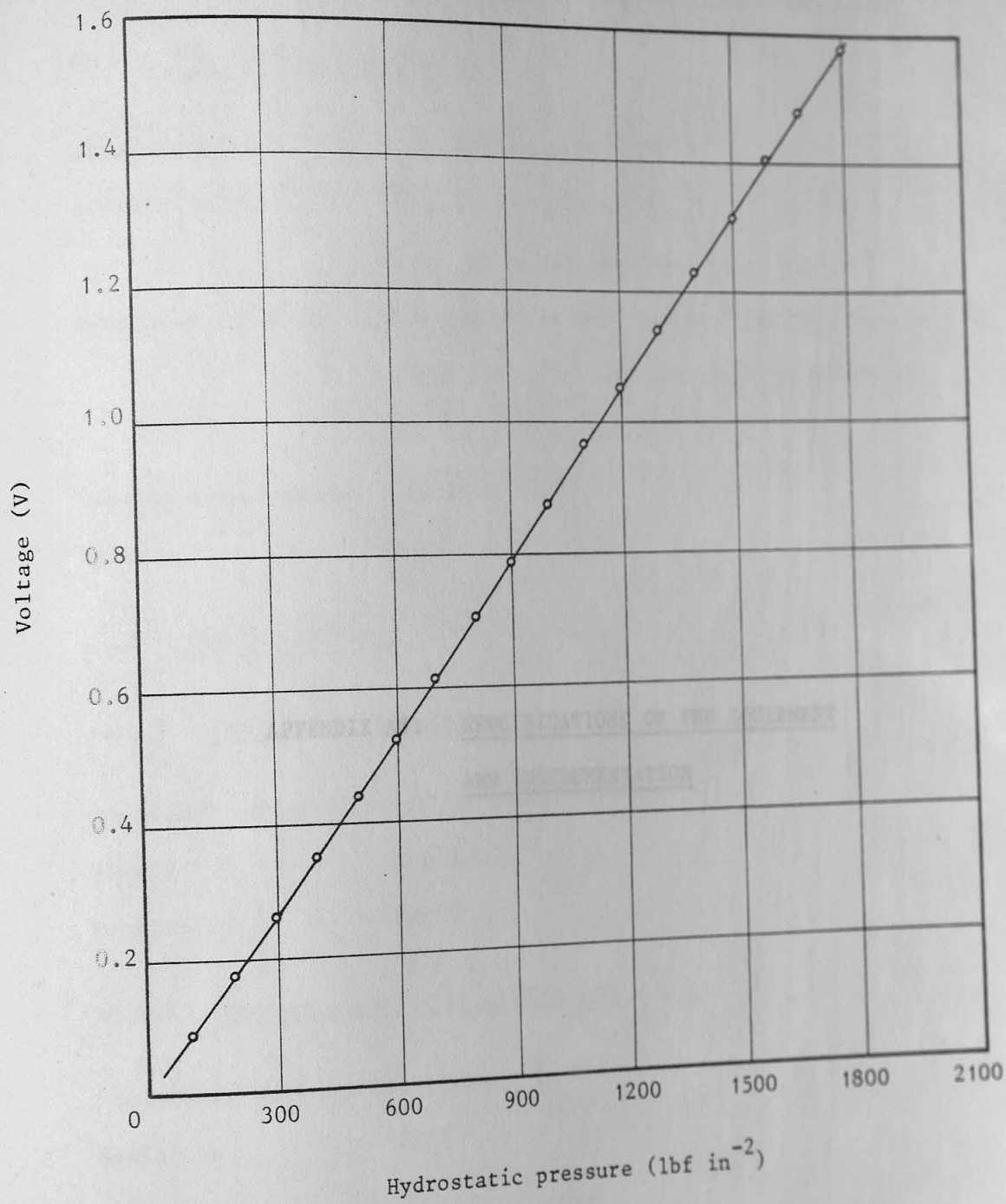


Figure (A7.4) Calibration chart of the pressure transducer

A8.1 THE HYDRAULIC CRAM-SUCK

Manufacturer: Brookes Limited

Primary driver: 3-phase induction motor

40 hp, 50 hp and 1000 rev min⁻¹

Hydraulic delivery: 25.1 g min⁻¹ at 1000 rev min⁻¹ and a pressure of 100 lbf in⁻²; maximum working pressure of 2000 lbf in⁻² at 30 tons

Nominal speed range: 0 to 15 ft min⁻¹

Stroke: 34 in

A8.2 TESTING MACHINES

A8.2.1 Load **APPENDIX A8: SPECIFICATIONS OF THE EQUIPMENT AND INSTRUMENTATION**

"Denison" universal hydraulic

Model: Type DCJ

Machine No: 822404

A8.2.2 Pressure Transducer calibration

"Hidenberg" hydrostatic pressure tester

Serial No: 3213

A8.2.3 Tension test on tube material

"Avery-Denison" testing machine

Type: 2153

Machine No: 30941

Maximum capacity: 500 lb

A8.3 METROLOGY EQUIPMENT

A8.1 THE HYDRUALIC DRAW-BENCH

Manufacturer: Brookes Limited

Primary drive: 3-phase induction motor
40 hp, 50 hz and 1440 rev min⁻¹

Hydraulic delivery: 25.2 g min⁻¹ at 1440 rev min⁻¹ and a pressure
of 100 lbf in⁻²; maximum working pressure of
2000 lbf in⁻² at 30 tonf

Nominal speed range: 0 to 15 ft min⁻¹

Stroke: 54 in

A8.2 TESTING MACHINES

A8.2.1 Load cells calibration

"Denison" universal hydraulic testing machine

Model: 7104 DCJ

Machine No: E62404

A8.2.2 Pressure transducer calibration

"Budenberg" hydrostatic pressure tester

Serial No: 3215

A8.2.3 Tension test on tube material

"Avery-Denison" testing machine

Type: 7152

Machine No: 30941

Maximum capacity: 600 kN

A8.3 METROLOGY EQUIPMENT

A8.3.1 Measurement of surface finish

"Talysurf" Model 4

Manufacturer: Rank Precision Industries Limited, England.
Complete with a) recorder, b) electronic unit, c) gear box and stand.

A8.3.2 Inspection of tool profiles

"Nikon" profile projector

Manufacturer: Nippon Kogaku, Japan
Model: Shadowgraph 5A
Serial No: 2368

A8.3.3 Measurement of tool dimensions

"Universal measuring machine"

Manufacturer: Societe Genevoise D'Instruments de Physique,
Switzerland.
Type: MU-214B
Serial No: 745

A8.3.4 Measurement of mean lubricant pressure

"OTT" Compensating Polar Planimeter

Type: 17
No: 83286

A8.4 PRESSURE TRANSDUCER

Manufacturer: Kistler Instrumente AG, Switzerland
Model: 601H

A detail description of its technical data is given in Appendix
(A8.6).

A8.5 DATA RECORDING ACCESSORIES

Charge amplifier

Manufacturer: Kistler Instrumente AG, Switzerland

Model: 568, SN 2004

Recording
Oscilloscope: "Meledec"

Manufacturer: Meledec Limited, England

Model: M-Scope, FOR-4

No. of Channels: 4

Digital Voltmeter: Digital Multimeter

Model: DMM3

Voltage supply: "Farnell L30 BT" stabilised power source,
0 to 30 volts d.c. and 1 amp. maximum

Bridge amplifier: "SGA 300 KAP"; provides supply voltage
virtually independent of the source voltage;
potentiometers for zero, span and bridge
supply adjustments

Ultra-violent
beam recorder:

"Oscillograph" Model 3006

Manufacturer: Southern Electronics Limited,
England.

15 channels

Paper speed: 0.4 - 10 in sec⁻¹ or in min⁻¹

Pressure Transducer

601H

max. measuring range	at*	0-1000
calibrated partial ranges: 10%	at*	0-100
1%	at*	0-10
resolution	at*	0.002
max. pressure	at*	1200
sensitivity	pC/at	16
force-sensitivity	pC/kp	125
resonant frequency	kHz	130
rise-time	μs	3
linearity (max. error for each calibrated range)	±%	0.8
insulation resistance	Ω	10 ¹⁴
capacity	pF	5
acceleration sensitivity	at/g	0.001
temperature coefficient	-%/°C	0.01
working-temperature range	°C	-150+240
shock and vibration	g	15'000
weight	g**	1.7

* 1 at = kp cm⁻² = 14.22 lbf in⁻² = 0.981 Bar = 735.56 Torr

** 1 g = 0.001 kg = 0.03527 oz.

1. James, D & Baynes, J E
"Use of chemical conversion coatings to facilitate wire-drawing and cold-chamber operations"
Technology in Iron and Steel Works,
The Iron and Steel Inst., 1963, pp 13-37
2. Lancaster, P R & Rowe, C W
"Experimental study of the influence of lubrication upon cold-drawing under approximately plane-strain conditions at low speeds"
Proc Instn Mech Engrs, 1963-64, 177, Pt 1 No 1, pp 67-68
3. Lancaster, P R & Rowe, C W
"A comparison of boundary lubrication under light and heavy loads"
Wear, 1964-69, 2, pp 425-437
4. Christopherson, D G, Baynes, J & Mills, J
"Some observations on conditions of lubrication in wire-drawing dies"
J Instn Petrol, 1961, 50, pp 100-105

LIST OF REFERENCES

5. Christopherson, D G & Baynes, J
"Examination of fluid lubrication in wire-drawing"
Proc Instn Mech Engrs, 1955, 159, pp 643-651
6. Christopherson, D G
"Hydrodynamic lubrication in wire-drawing"
J Mech Engr Sci, 1961, 2, No 4, pp 176-183
7. Lee, J P & J
"Theory of lubrication applied to pressure die-casting in wire-drawing"
Proc Instn Mech Engrs, 1962-67, 181, Pt 1 D, pp 105-111
8. Gosselin, J R & Dixon, J R
"Viscous lubrication in wire-drawing"
Trans ASME, 1961, 83, pp 153-161
9. Davies, J S
"A method for continuous wire-drawing aided by externally applied hydrostatic oil pressure"
J Instn Mech Engrs, 1964-65, 183, pp 123-125
10. Davies, J S & Gosselin, J R
"The process of feeding lubricant to the deformation zone in wire-drawing"
Proc Instn Mech Engrs, March 1962, pp 137-139

REFERENCES

1. James, D & Haynes, J E
'Use of chemical conversion coatings to facilitate wire-drawing and cold-forging operations'
Tribology in iron and steel works,
The Iron and Steel Inst, 1969, pp 55-57
2. Lancaster, P R & Rowe, G W
'Experimental study of the influence of lubrication upon cold-drawing under approximately plane-strain conditions at low speeds'
Proc Instn Mech Engrs, 1963-64, 178, Pt 1 No 3, pp 69-86
3. Lancaster, P R & Rowe, G W
'A comparison of boundary lubricants under light and heavy loads'
Wear, 1958-59, 2, pp 428-437
4. Christopherson, D G, Naylor, H & Wells, J
'Some observations on conditions of lubrication in wire-drawing dies'
J Inst Petroleum, 1954, 40, pp 295-298
5. Christopherson, D G & Naylor, H
'Promotion of fluid lubrication in wire-drawing'
Proc Instn Mech Engrs, 1955, 169, pp 643-653
6. Tattersall, G H
'Hydrodynamic lubrication in wire-drawing'
J Mech Engg Sci, 1961, 3, 4, pp 378-393
7. Chu, P S Y
'Theory of lubrication applied to pressure nozzle design in wire-drawing'
Proc Instn Mech Engrs, 1966-67, 181 Pt 3 0, pp 104-111
8. Osterle, J F & Dixon, J R
'Viscous lubrication in wire-drawing'
Trans ASLE, 1962, 5, pp 233-241
9. Butler, L H
'A method for continuous wire-drawing aided by externally generated hydrostatic oil pressure'
J Inst Metals, 1964-65, 93, pp 123-125
10. Moseev, V F & Korostilin, A A
'New method of feeding lubricant to the deformation zone in wire-drawing'
Stal' in English, March 1962, pp 237-239

11. Middlemiss, A
'Hydrodynamic lubrication for drawing steel wire'
Proc Conf on Tribology in iron and steel works,
The Iron and Steel Inst, September 1969, pp 47-54
12. Johnson, W
'Estimation of upper bound loads for extrusion and coining
operations'
Proc Instn Mech Engrs, 1959, 173, pp 61-72
13. Tomlinson, G A
'A molecular theory of friction'
Phil Mag, 1929, 7, pp 905-939
14. Bowden, F P & Tabor, D
'The friction and lubrication of solids'
Clarendon Press, 1950
15. Cameron, A
'Principles of hydrodynamic lubrication'
Longman, 1966
16. Hardy, W B
'Collected works'
Cambridge University Press, 1936
17. Edwards, C M & Halling, J
'An analysis of the plastic interaction of surface asperities
and its relevance to the value of the coefficient of friction'
J Mech Engg Sci, 1968, 10, No 2, pp 101-110
18. Edwards, C M & Halling, J
'Experimental study of the plastic interaction of model
surface asperities during sliding'
J Mech Engg Sci, 1968, 10, NO 2, pp 121-132
19. Moore, D F
'Principles and application of tribology'
Pergamon Press, 1975
20. Rabinowicz, E & Tabor, D
'Metallic transfer between sliding metals: An Autoradiographic
study'
Proc Roy Soc, (A), 1951, 208, pp 455-475
21. Bowden, F P & Hughes, T P
'The friction of clean metals and the influence of absorbed
gases. The temperature coefficient of friction'
Proc Roy Soc, (A), 1939, 72, pp 263-279

22. Bowden, F P & Young, J E
'Friction of clean metals and the influence of absorbed films'
Proc Roy Soc, (A), 1951, 208, pp 311-325

23. Whitehead, J R
'Surface deformation and friction of metals at light loads'
Proc Roy Soc, (A), 1950, 201, pp 109-124

24. Wilson, R
'Influence of oxide films on metallic friction'
Proc Roy Soc, (A), 1952, 212, pp 450-452

25. Rabinowicz, E
'Friction and lubrication in metal processing'
Trans ASME, 1966, pp 90

26. Rabinowicz, E
'The role of surface energy of adhesion in metalworking'
J Inst Metals, 1967, 95, pp 321-326

27. Shaw, P E & Leavey, E W L
'Friction of dry solids in vacuo'
Phil Mag, Series 7, 1930, 10, pp 809-822

28. Coffin, L F
Lubrication Engineer, 1956, 12, pp 50

29. Ernst, H & Merchant, M E
Proc Special Summer Conf on Friction and Surface Finish, MIT,
1940, pp 76.
Quoted by Ref (135)

30. Welsh, N C
'Frictional heating and its influence on the wear of steel'
J Appl Phys, 1957, 28, pp 960-968

31. Bowden, F P & Ridler, K E W
'The surface temperature of sliding metals. The temperature
of lubricated surfaces'
Proc Roy Soc, (A), 1936, 154, pp 640-656

32. Bowden, F P & Thomas, P H
'The surface temperature of sliding solids'
Proc Roy Soc, (A), 1954, 223, pp 29-40

33. Kingsbury, A
'Experiments on the friction of screws'
Trans ASME, 1896, 17, pp 96-116
Quoted by Ref (50)

34. Fuller, D D
'Theory and practice of lubrication for engineers'
Chapman and Hall, 1956, pp 342-373
35. Burwell, J T
'The role of surface chemistry and profile in boundary lubrication'
J SAE, 1942, 50, pp 450
36. Hardy, W B & Doubleday, I
'Boundary lubrication - the paraffin series'
Proc Roy Soc, (A), 1921, 100, pp 550-574
37. Campbell, W E
'Boundary lubrication'
Bell Lab Record, August 1932, 10, pp 406-411
38. Bowden, F P & Moore, A C
'Physical and chemical adsorption of long chain compounds on radioactive metals'
Trans Faraday Soc, 1951, 47, pp 900-907
39. Bowden, F P & Tabor, D
'Mechanism of friction and lubrication in metal-working'
J Inst Petroleum, 1954, 40, pp 243-253
40. Gregory, J N
'The lubrication of metals by compounds containing chlorine'
J Inst Petroleum, 1948, 34, pp 670-676
41. Greenhill, E B
'The lubrication of metals by compounds containing sulphur'
J Inst Petroleum, 1948, 34, pp 659-669
42. Boyd, J & Robertson, B P
'The friction properties of various lubricants at high pressure'
Trans ASME, 1945, 67, pp 51-56
43. Loh, N H
'The mechanics of drawing wire at elevated temperatures'
PhD Thesis, University of Aston, 1983
44. Perry, A L H
'Lubricants for tube and bar drawing'
J Inst Petroleum, 1954, 40, pp 319-324

45. Tower, B
'First report on friction experiments'
Proc Inst Mech Engrs, (a) 1883, pp 632-659 (b) 1884, pp 29-35
'Second report on friction experiments'
Proc Inst Mech Engrs, 1885, pp 58-70
46. Reynolds, O
'On the theory of lubrication and its application to Mr
Beauchamp Tower's experiments, including an experimental
determination of the viscosity of olive oil'
Phil Trans Roy Soc, London, 1886, 177, Pt 1, pp 157-234
47. Martin, H M
'The lubrication of gear teeth'
Engineering, London, 1916, 102, pp 119-121
48. Grubin, A N & Vinogradova, I E
'Central Scientific Research Inst for Tech and Mech Engg,
Book No 30, Moscow, 1949
(DSIR Translation No 337), Quoted by Ref (49)
49. Dowson, D & Higginson, G R
'Elasto-hydrodynamic lubrication'
Pergamon Press, 1966
50. Hersey, M D
'Theory and research in lubrication: Foundation for future
developments'
John Wiley and Sons, 1966, pp 105
51. Dowson, d & Higginson, G R
'A numerical solution to the elastohydrodynamic problem'
J Mech Engg Sci, 1959, 1, 1, pp 6-15
52. Cheng, H S & Sternlicht, B
'A numerical solution for the pressure, temperature and film
thickness between two infinitely long, lubricated rolling and
sliding cylinders, under heavy load'
ASME, Paper No 64, 1964, Quoted by Ref (49)
53. Crook, A W
'The lubrication of rollers'
Phil Trans Roy Soc, (A), 1958, 250, pp 387-409
'The lubrication of rollers, II: Film thickness with relation
to viscosity and speed'
Phil Trans Roy Soc, (A), 1961, 254, pp 234-258

54. Lewicki, W
'Hydrodynamic lubrication of roller bearings'
Engineer, London, 1954, 197, pp 920-922
'Some physical aspects of lubrication in roller bearings and gears'
Engineer, London, 1955, 200, pp 212-215
55. El-Sisi, & Shawki, G S A
'Measurement of oil-film thickness between discs by electrical conductivity'
Trans ASME, J Basic Engg (D), 1960, 82, pp 12-18
56. Sibley, L B & Orcutt, F K
'Elastohydrodynamic lubrication of rolling contact surfaces'
Trans ASLE, 1961, 4, pp 234
57. Ford, H
'The role of friction in metal-working processes'
J Inst Petroleum, 1954, 40, 370, pp 291-294
58. Wistreich, J G
'The fundamentals of wire-drawing'
Met Rev, 1958, 3, 10, pp 97-142
59. Whitton, P W & Ford, H
'Surface friction and lubrication in cold strip rolling'
Proc Instn Mech Engrs, 1955, 169, pp 123-133
60. Baron, H G & Thompson, F G
'Friction in wire-drawing'
J Inst Metals, 1951, 78, pp 415-462
61. Lancaster, P R & Smith, B F
'High speed wire-drawing'
Wire Ind, November 1974, pp 933-937
62. Ranger, A E & Wistreich, J G
'Study of lubrication in wire-drawing by an electrical method'
J Inst Petroleum, 1954, 40, 370, pp 308-314
63. Isupov, V F, Smetanina, A I & Mashura, G P
'The thickness of the oil film in the drawing of rods'
Stal' in English, December 1967, pp 1042-1043
64. Lancaster, P R
'A review of hydrodynamic lubrication in wire-drawing'
Wire Ind, August 1976, pp 627-629

65. Fowler, T & Lancaster, P R
'A discussion of the factors which determine the limiting speed in wire-drawing operations'
Tech Conf on Advances in Steel Wire Production
British Independent Steel Producers Association, 1982,
pp 23(4) - 31(4)
66. Lim, T B
Unpublished report on lubrication in tube-drawing
University of Aston, 1982
67. Butler, L H
'The effect of interposed lubricants on the surface deformation of metals during plastic working'
J Inst Metals, 1959-60, 88, pp 337-343
68. Butler, L H
'The effect of lubricants on the growth of surface-contact areas during plastic deformation of metals'
J Inst Metals, 1960-61, 89, pp 116-123
69. Butler, L H
'The influence of base-lubricant viscosity and boundary additions on surface contact and friction during metal deformation'
J Inst Metals, 1960-61, 89, pp 449-455
70. Rothman, D
'An investigation of shear stress distribution by die-rotation'
PhD Thesis, University of Aston, 1970
71. Basily, B B
'The mechanics of section-drawing'
PhD Thesis, University of Aston, 1976
72. Pearsall, G W & Backofen, W A
'Frictional boundary conditions in plastic compression'
Trans ASME, J Engg Ind, 1963, 85, pp 68-76
73. Thomsen, E G, Yang, C T & Kobayashi, S
'Plastic deformation in metal processing'
Macmillan, 1965
74. Hockett, J E
'Note: On coefficient of friction measurements'
Int J Mech Sci, 1967, 9, pp 233-236

75. Wistreich, J G
'Investigation of the mechanics of wire-drawing'
Proc Instn Mech Engrs, 1955, 169, pp 654-665
76. MacLellan, G D S
"Some friction effects in wire-drawing"
J Inst Metals, 1952-53, 81, pp 1-13
77. MacLellan, G D S
'A critical survey of wire-drawing theory'
J Iron Steel Inst, 1948, 158, pp 347-356
78. Rothman, D & Sansome, D H
'An investigation of rod-drawing with die rotation'
Int J MTDR, 1970, 10, pp 179-192
79. Linicus, W & Sachs, G
'Spanlose Formung der Metalle'
Mitt Dt Mater Anst, 1931, 16, pp 36-67
80. Schroeder, W & Webster, D A
'Press-forging thin-sections: Effect of fiction, area, and thickness on pressures required'
J Appl Mech, 1949, 16, pp 289-294
81. Basily, B B & Sansome, D H
'Determination of the mean coefficient of friction in the direct drawing of section rods from round bars'
Proc Int MTDR Conf, 1976, 17, pp 475-481
82. Evans, W & Avitzur, B
'Measurement of friction in drawing, extrusion and rolling'
Trans ASME, J Lub Tech, January 1968, 90, pp 70-80
83. Lunt, R W & MacLellan, G D S
'An extension of wire-drawing theory, with special reference to the contributions of K B Lewis'
J Inst Metals, 1946, 72, pp 65-96
84. Loke, S K
'Force determination of bimetal tube drawing on a mandrel or floating plug'
PhD Thesis, University of Aston, 1979
85. wa Muriuki, M
'The mechanics of drawing polygonal tube from round on a cylindrical plug'
PhD Thesis, University of Aston, 1981

86. Blazynski, T Z & Cole, I M
'An investigation of the plug drawing process'
Proc Instn Mech Engrs, 1960, 174, 28, pp 797-804
87. Young, M J R & Meadows, B J
'Prediction of axial stress in tube-drawing using a fixed plug'
J Iron Steel Inst, September 1970, pp 813-818
88. Avitzur, B
'Metal-forming: processes and analysis'
McGraw Hill, 1968
89. Smith, D J & Bramley, A N
'A theoretical study of tube-drawing with a floating plug'
Proc Int MTDR Conf, 1972, 13, pp 501-508
90. Pugh, H L D
'The application of hydrostatic pressure to metal working
Part I: Extrusion'
Nat Engg Lab, December 1967, Report No 334
91. Hillier, M J
'A hydrodynamic model of hydrostatic extrusion'
Int J Prod Res, 1966, 5, 2, pp 171-181
92. Avitzur, B
'Analysis of wire-drawing and extrusion through conical dies
of large cone angle'
Trans ASME, J Engg Ind, (B), 1964, 86, pp 304-316
93. Wilson, W R D & Walowit, J A
'An isothermal hydrodynamic lubrication theory for hydrostatic
extrusion and drawing process with conical dies'
Trans ASME, J Lub Tech, 1971, 93, pp 69-74
94. Bloor, S M, Dowson, D & Parsons, B
'An elasto-plasto-hydrodynamic lubrication analysis of the
plane strain drawing process'
J Mech Engg Sci, 1970, 12, 3, pp 178-190
95. Dowson, D, Parsons, B & Lidgitt, P J
'An elasto-plasto-hydrodynamic lubrication analysis of the
wire-drawing process'
Instn Mech Engrs Symp on elastohydrodynamic lubrication,
1972, pp 97-106

96. Snidle, R W, Parsons, B & Dowson, D
'An elasto-plasto-hydrodynamic lubrication analysis of the hydrostatic extrusion process including the effects of strain hardening and redundant deformation'
Instn Mech Engrs Symp on elastohydrodynamic lubrication, 1972, pp 107-117
97. Lancaster, P R
'A review of hydrodynamic lubrication in wire-drawing Part II'
Wire Ind, August 1976, pp 627-629
98. Kudo, H, Tsubouchi, M, Takada, H & Okamura, K
'An investigation into plasto-hydrodynamic lubrication with a cold sheet-drawing test'
Ann CIRP, 1982, 31, 1, pp 175-179
99. Wilson, W R D & Mahdavian, S M
'Hydrodynamic lubrication of hydrostatic extrusion'
Trans ASME, J Lub Tech, 1976, 98, pp 27-31
100. Wilson, W R D
'The film thickness variation in the work zone of hydrodynamically lubricated continuous deformation process'
Trans ASME, J Lub Tech, 1973, 95, pp 541-543
101. Mahdavian, S M, & Wilson, W R D
'Lubricant flow in a plastohydrodynamic work zone'
Trans ASME, J Lub Tech, 1976, 98, pp 16-21
102. Barus, C
'Isothermals, isopiestic and isometrics relative to viscosity'
American J Sci, 1893, 45, 3, pp 87-96
103. MacLellan, G D S & Cameron, A
British Patent No 566 434
104. Fogg, B & Dafila, K
'Externally pressurized lubrication in the drawing of thin walled cylindrical components'
Ann CIRP, 1975, 24, pp 179-184
105. Duffing, G
Zeitschrift fur angewandte mathematik and mechanik, 1924, 4, pp 296. Quoted by Ref. (50)
106. Slotte, K F
'On the internal friction of liquids'
Ofvers of Finska Vetensk Soc Forhandl, 1890, 32, pp 116-149
Quoted by Ref. (50)

107. Herschel, W H
'The change in viscosity of oils with the temperature'
Ind Engg Chem, 1922, 14, pp 715-723
108. Vogel, H
'Die Bedeutung der temperatur abh ngigkeit der viskosit t
f.d. Beurteilung von Oelen'
Zeitschrift angew chem, 1922, 35, pp 561-563
Quoted by Ref. (50)
109. Cameron, A
'The isothermal and adiabatic compressibilities of oil'
J Inst Petroleum, 1945, 31, pp 421-427
110. Walther, C
'Uber die answertung von viskosit tsangaben'
World Petroleum Cong Lon, 1933, Proc 2 (1934), pp 419-420
Quoted by Ref. (50)
111. Blott, J F T & Verver, C G J
'Methods for expressing the viscosity-temperature relationship
of lubricating oils'
J Inst Petroleum, 1952, 38, pp 196-249
112. Cornelliissen, J & Waterman, H I
'The viscosity temperature relationship of liquids'
Chem Engg Sci, 1955, 4, pp 238-246
113. Roelands, C J A, Vlugter, J C & Waterman, H I
'The viscosity-temperature-pressure relationship of lubricating
oils and its correlation with chemical constitution'
Trans ASME, J Basic Engg, 1963, 85, pp 601-610
114. Bridgeman, P W
'The effect of pressure on the viscosity of forty-three pure
liquids'
Proc American Acad Arts Sci, 1926, 61, pp 57-99
Quoted by Ref. (119)
115. Hersey, M D
'Theory of the torsion and rolling ball viscosimeters and
their use in determining the effect of pressure on viscosity'
J Washington Acad Sci, 1916, 6, pp 525-530
116. Needs, S J
'Influence of pressure on film viscosity in heavily-loaded
bearings'
Trans ASME, 1938, 60, pp 347-358

117. Bradbury, D, Mark, M & Kleinschmidt, R V
'Viscosity and density of lubricating oils from 0 to 150,000
Psig and 32°F to 425°F'
Trans ASME, 1951, 73, pp 667-676
118. Galvin, G D, Naylor, H & Wilson, A R
'The effect of pressure and temperature on some properties of
fluids of importance in elastohydrodynamic lubrication'
Proc Instn Mech Engrs, 1963-64, 178, Pt 3N, pp 283-290
119. Hersey, M D & Hopkins, R F
'Viscosity of lubricants under high pressure'
Mech Engg, 1945, 67, pp 820-824
120. Hersey, M D & Shore, H
'Viscosity of lubricants under pressure'
Mech Engg, 1928, 50, pp 221-232
Quoted by Ref. (50)
121. Hyde, J H
'On the viscosities and compressibilities of liquids at high
pressures'
Proc Roc Soc, London, (A), 1920, 97, pp 240-259
122. Dow, R B
'The effects of pressure and temperature on the viscosity of
lubricating oils'
J Appl Phys, 1937, 8, pp 367-372
123. Thomas, B W, Ham, W R & Dow R B
'Viscosity-pressure characteristics of lubricating oils'
Ind Engg Chem, 1939, 31, 10, pp 1267-1270
124. Chu, P S Y & Cameron, A
'Pressure viscosity characteristics of lubricating oils'
J Inst Petroleum, 1962, 48, 461, pp 147-155
125. Clark, O H
'Prediction of lubricating oil viscosities at high pressures'
Trans ASME, 1956, 78, pp 905-908
126. Hersey, M D & Hopkins, R F
'Viscosity of lubricants under pressure'
ASME, 1954, pp 87
Quoted by Ref (50)
127. Sternlicht, B
'Influence of oil pressure and temperature on oil viscosity
in thrust bearings'
Trans ASME, 1958, 80, pp 1108-1112

128. Appledoorn, J K
'A simplified viscosity-pressure-temperature equation'
J SAE, 1963, 71, pp 108
Quoted by Ref (50)
129. Sachs, G
Zeit Ang Math Mech, 1927, 7, pp 235-236
130. Davies, E A & Dokos, S J
'The theory of wire-drawing'
J Appl Mech, 1944, 11, pp A193-A198
131. Wistreich, J G
'An investigation of back-pull wire-drawing as an industrial technique'
J Iron Steel Inst, November 1949, pp 316-330
132. Shield, R T
'Plastic flow in a converging conical channel'
J Mech Phys Solids, 1955, 3, pp 246-258
133. Korber, F & Eichinger, A
'Die Grundlagen der bildamen Verformung'
Mitt K W Inst Eisenforsch, 1940, 22, pp 57
134. Johnson, W & Sowerby, R
Wire Ind, 1969, 36, pp 137-144, 249-256
135. Shaw, M S, Stableford, W H & Sansome, D H
'Critical review of drawing with particular reference to lubrication'
Int J MTDR, 1970, 10, pp 203-212
136. Hill, R
'The mathematical theory of plasticity'
Clarendon Press, 1950
137. Hill, R & Tupper, S J
'A new theory of plastic deformation in wire-drawing'
J Iron Steel Inst, 1948, 159, pp 353-359
138. Green, A P & Hill, R
'Calculations on the influence of friction and die geometry in sheet drawing'
J Mech Phys Solids, 1953, 1, pp 31-36
139. Pawelski, O
Arch Eisenhuttenwesen, 1961, 8, pp 513

140. Kudo, H
'Some analytical and experimental studies of axisymmetric cold forging and extrusion'
I: Int J Mech Sci, 1960, 2, pp 102-127
II: Int J Mech Sci, 1961, 3, pp 91-117
141. Kobayashi, S
'Upper bound solutions of axisymmetric forming problems'
I: Trans ASME, May 1964, pp 122-126
II: Trans ASME, November 1964, pp 326-332
142. Atkins, A G & Caddell, R M
'The incorporation of work hardening and redundant work in rod-drawing analyses'
Int J Mech Sci, 1968, 10, pp 15-28
143. Yang, C T
'On the mechanics of wire-drawing'
Trans ASME, (B), 1961, 83, pp 523-530
144. Parsons, B, Taylor, R & Cole, B N
'High speed drawing of metals: A first report'
Proc Instn Mech Engrs, 1965-66, 180, Pt 3I, pp 230-240
145. Atkins, A G & Caddell, R M
'The influence of redundant work when drawing rods through conical dies'
Trans ASME, (B), 1968, 90, pp 411-418
146. Johnson, R W & Rowe, G W
'Redundant work in drawing cylindrical stock'
J Inst Metals, 1968, 96, pp 97-105
147. Siebel, E
'The application to shaping processes of Hencky's Laws of equilibrium'
J Iron Steel Inst, 1947, 155, pp 526-534
148. Sachs, G, Lubahn, J D & Tracy, D P
'Drawing thin-walled tubing with a moving mandrel through a single stationary die'
J Appl Mech, December 1944, 11, pp A199-A210
149. Sachs, G & Baldwin, W M
'Stress analysis of tube sinking'
Trans ASME, 1946, 68, pp 655-662
150. Swift, H W
'Stress and strains in tube-drawing'
Phil Mag, Series (7), September 1949, 40, 308, pp 883-902

151. Chung, S Y & Swift, H W
'A theory of tube sinking'
J Iron Steel Inst, 1952, 170, pp 29-36
152. Blazynski, T Z & Cole, I M
'An investigation of the sinking and mandrel drawing processes'
Proc Instn Mech Engrs, 1963-64, 178, Pt 1 No 33, pp 894-905
153. Green, A P
'Plane strain theory of drawing'
Proc Instn Mech Engrs, 1960, 174, 31, pp 847-864
154. Johnson, W & Mellor, P B
'Engineering plasticity'
Van Nostrand Reinhold, London, 1973
155. Johnson, W, Sowerby, R & Haddow, J B
'Plane-strain slip-line fields - theory and bibliography'
Edward Arnold, 1970
156. Prager, W & Hodge, P G
'Theory of perfectly plastic solids'
Willey, N Y, 1951
157. Hill, R
'A theoretical analysis of the stresses and strains in
extrusion and piercing'
J Iron Steel Inst, 1948, 158, pp 177-185
158. Alexander, J M
'Discussion on extrusion, coining, plastic bending and
stretching'
Proc Instn Mech Engrs, 1959, 173, pp 85-87
159. Avitzur, B
'Analysis of wire-drawing and extrusion through conical dies
of small cone angles'
Trans ASME, (B), 1963, 85, pp 89-96
160. Avitzur, B
'Tube sinking and expanding'
Trans ASME, (B), 1965, 87, pp 71-79
161. Avitzur, B
'Flow through converging dies with hydrodynamic lubrication
treated as an adiabatic process'
Proc Int MTDR Conf, 1976, 17, pp 445-451

162. Thompson, P J, Odgen, H O & Butterworth, N A
'An apparent strain analysis of orthogonal cutting'
Int J MTDR, 1969, 9, pp 97-116
163. Pugh, H L I D
'Redundant work and friction in the hydrostatic extrusion of
pure aluminium and an aluminium alloy'
J. Mech Engg Sci, 1964, 6, 4, pp 362-370
164. Majors, H J R
'Studies in cold-drawing-Pt 3, Determination of friction
coefficient'
Trans ASME, 1955, 78, pp 79-87
165. Trozera, T A
'On non-homogeneous work for wire-drawing'
Trans ASME, 1964, 57, pp 309-323
166. Vivian, A C
'Essential metallurgy for engineers'
Pitman, London, 1948
167. Erasmus, L A
'The significance of tensile test results'
Metallurgia and Metal Forming, 1975, 42, pp 94-99
168. Gensamer, M
'The yield point in metals'
Trans AIMME, 1938, 128, pp 104-117
169. Wistreich, J G
'Ring in wire-drawing dies'
J Iron Steel Inst, 1951, 167, pp 162-164
170. Neale, M J
'Tribology Handbook'
Butterworths, 1973
171. Symmons, G R, Hashmi, M S J & Parvinmehr, H
'Plasto-hydrodynamic, dieless wire-drawing: theoretical
treatment and experimental results'
Metals Soc, Developments in the drawing of metals, May 1983
(Pre-print), pp 54-62